

# **Rare-Earth-Metal Alkyl Complexes in Isoprene Polymerization**

---

## **Seltenerdmetall-Alkyl-Komplexe in der Isopren- Polymerisation**

### **Dissertation**

der Mathematisch-Naturwissenschaftlichen Fakultät  
der Eberhard Karls Universität Tübingen  
zur Erlangung des Grades eines  
Doktors der Naturwissenschaften  
(Dr. rer. nat.)

vorgelegt von  
Dipl.-Chem. Dominic Diether  
aus Reutlingen

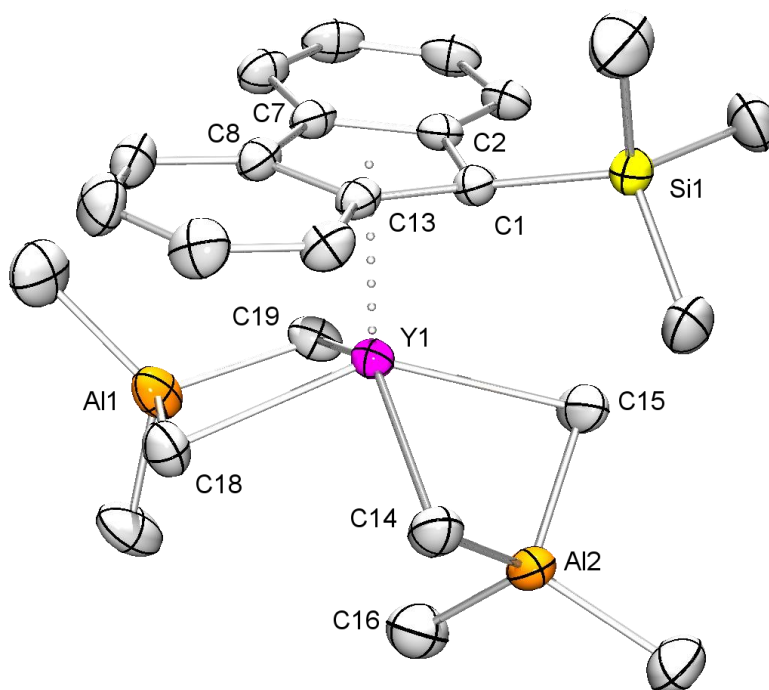
Tübingen  
2019

Gedruckt mit Genehmigung der Mathematisch-Naturwissenschaftlichen Fakultät der  
Eberhard Karls Universität Tübingen.

Tag der mündlichen Qualifikation:	01.10.2019
Dekan:	Prof. Dr. Wolfgang Rosenstiel
1. Berichterstatter:	Prof. Dr. Reiner Anwander
2. Berichterstatter:	Dr. Peter Sirsch

# Rare-Earth-Metal Alkyl Complexes in Isoprene Polymerization

Dominic Diether





“Wenn ich nun einzelnes von unseren Arbeiten erzähle, so bitte ich Sie freundlichst, sich an jene berühmte Rede von HELMHOLTZ zu erinnern, wo er schildert, wie ganz anders und meist wieviel weniger imponierend der Werdegang einer Erfindung im Laboratorium sich abspielt, als er nachher in der endgültigen Publikation des Forschers erscheint. So wird Ihnen vielleicht auch das, was wir chemisch getan, einfach und folgerichtig scheinen, während es doch in Wahrheit nur das Fazit aus vielen Irrtümern und Mißerfolgen ist.”

FRITZ HOFMANN

F. Hofmann, *Angew. Chem.* **1912**, 25, 1462–1467.



## Preface

The following PhD thesis consists of a survey about developments in Ziegler-Natta polymerization, the use of bis(alkyl) rare-earth-metal (half-)sandwich- and pincer complexes in polymerization reactions during 2015 to 2018, a summary of the main results, and the scientific papers published during this thesis.

The work has been carried out at the Institut für Anorganische Chemie of the Eberhard Karls Universität Tübingen, Germany, during the period from September 2015 to July 2019 under the supervision of **Prof. Dr. Reiner Anwander**. In October and November 2018 I was afforded the opportunity to stay in the laboratory of **Prof. Dr. Charlotte Williams** at Oxford University. There I was able to learn more about the polymerization of functional monomers.

Parts of the thesis have been presented as posters at national and international conferences. The research conducted in this thesis has been funded by the Deutsche Forschungsgemeinschaft (DFG, AN238/14-2) and Bridgestone Japan.





## Acknowledgements

First of all, I like to thank my research supervisor **Prof. Dr. Reiner Anwander** for giving me the opportunity to accomplish my thesis in the interesting field of polymerization reactions. With your patience and kind way you supported me and made this work a success. Many thanks for letting me attend national and international conferences to present my work and furthermore for giving me the opportunity to have an outstanding research trip to the University of Oxford. To **Prof. Dr. Charlotte Williams** at the University of Oxford I am also very grateful for having me in her laboratory and giving me the opportunity to deepen my knowledge about polymers.

A special thanks to **Dr. Cäcilia Maichle-Mössmer** for teaching me the secrets of single crystal X-ray crystallography. It was a pleasure to benefit from your extraordinary competence and it diversified my everyday work even more.

Without the support of the NMR Team **Dr. Klaus Eichele** and **Kristina Strohmaier**, the invaluable EA measurements by **Wolfgang Bock**, and the support in polymer analytics by **Daniela Kauling** and **Felix Thol** this work would not have been possible. Especially **Elke Niquet**, **Tobias Wolf**, **Heinz-Jürgen Kolb**, and **Jenny Steinhilber** are responsible for keeping the laboratory running and for everyday support.

Many thanks to every current and former coworker of the Anwander AG, **Uwe Bayer**, **Dr. Christoph Stuhl**, **Dr. Benjamin Wolf**, **Denis Burghardt**, **Damir Barisic**, **Verena Birkelbach**, **Lorenz Bock**, **Martin Bonath**, **Dennis Buschmann**, **Felix Kracht**, **Dr. Nicole Dettenrieder**, **Dr. Jochen Friedrich**, **Christoph Hollfelder**, **Dr. Lars Jende**, **Markus Katzenmayer**, **Dr. Dorothea Schädle**, **Dr. Andreas Krenzer**, **Lars Kuckuk**, **Dr. Yucang Liang**, **Dr. Leilei Luo**, **Eric Moinet**, **Jakob Lebon**, **Alexandros Mortis**, **Theresa Rieser**, **Dr. David Schneider**, **Tassilo Berger**, **Andrea Sonström**, **Dr. Tatiana Spallek**, **Georgios Spiridopolous**, **Dr. Renita Thim**, **Simon Trzmiel**, **Dr. Daniel Werner** and **Dr. Ning Yuan** for the nice atmosphere during the last years.

It was an extraordinary honor to study with **Marius Bayer** and **Tobias Zweiböhmer**. It has been a great time exhausting boundaries.

I am very grateful for my parents **Thomas** and **Anne Diether**. Only because of your generous support throughout the whole time I was able to accomplish this. Also my sisters **Helen** and **Yvonne** for having a great childhood.

Last but not least I want to thank my wife **Svenja Diether** for all of her support and love. Emotional and subject related you have been an immense help.

# Contents

<b>Preface</b>	<b>III</b>
<b>Acknowledgements</b>	<b>V</b>
<b>Contents</b>	<b>VI</b>
<b>Abbreviations</b>	<b>VII</b>
<b>Abstract</b>	<b>IX</b>
<b>Zusammenfassung</b>	<b>X</b>
<b>Publications and Personal Contribution</b>	<b>XII</b>
<b>Objective of the Thesis</b>	<b>XV</b>
<b>A Ziegler-Type Polymerization Reactions</b>	<b>1</b>
1 Ziegler-Natta Polymerization	2
1.1 Heterogeneous Ziegler-Natta Polymerization	3
1.2 Homogenous Ziegler-Natta Polymerization	6
2 Isoprene and Isoprene Polymerization	8
3 Rare-Earth-Metal (Half-)Sandwich (Bis)Alkyl Complexes	9
3.1 Half-Sandwich Complex Promoted Polymerization Reactions	14
3.2 Sandwich Complex Promoted Polymerization Reactions	23
4 Pincer Complexes	26
<b>B Summary of the Main Results</b>	<b>33</b>
1 Synthesis of Rare-Earth-Metal Indenyl and Fluorenyl Complexes	34
2 Synthesis of Pincer-Like Rare-Earth-Metal Complexes	39
3 Isoprene Polymerization with Rare-Earth-Metal Alkyl Complexes	42
<b>C Unpublished Results</b>	<b>47</b>
<b>D Bibliography</b>	<b>53</b>
<b>Publications I - III</b>	<b>63</b>
<b>Appendix</b>	

## Abbreviations

A	alkaline metal	Et	ethyl
A	$[\text{Ph}_3\text{C}][\text{B}(\text{C}_6\text{F}_5)_4]$	FG	functional group
B	$[\text{PhNMe}_2\text{H}][\text{B}(\text{C}_6\text{F}_5)_4]$	Flu	fluorenyl
C	$\text{B}(\text{C}_6\text{F}_5)_3$	Flu <sup>R</sup>	substituted fluorenyl
Cp	cyclopentadienyl	Flu <sup>Si</sup>	trimethylsilyl fluorenyl
Cp*	pentamethylcyclopentadienyl	Flu <sup>tBu</sup>	di(tertbutyl) fluorenyl
Cp'	2,3,4,5-tetramethylcyclopentadienyl-trimethylsilane	GPC	gel permeation chromatography
Cp <sup>R</sup>	substituted cyclopentadienyl	HDPE	high density polyethylene
CHD	cyclohexadiene	Ind	indenyl
D	dimethylaluminum chloride	Ind <sup>Et</sup>	ethyl indenyl
DEVP	diethyl vinylphosphonate	Ind <sup>R</sup>	substituted indenyl
DMB	1,4-dimethoxybenzene	Ind <sup>Si</sup>	trimethylsilyl indenyl
DSC	differential scanning calorimetry	IPOx	2-isopropylene-2-oxazolin
DRIFTS	diffuse reflectance infrared fourier transform spectroscopy	IR	infrared
E	diethylaluminum chloride	LDPE	low density polyethylene
EA	elemental analysis	Ln	rare-earth metal (Sc, Y, La-Lu)
equiv	equivalent	MAO	methylalumoxane
		MCP	methylenecyclopentene
		Me	methyl

Me <sub>2</sub> pz	dimethyl pyrazolyl
MHD	3-methylenehepta-1,6-diene
NBA	norbornadiene
NMR	nuclear magnetic resonance
PDI	polydispersity index
Ph	phenyl
R	alkyl or benzyl substituent
TMA	trimethylaluminum
TIBA	<i>triisobutyl</i> aluminum

## Abstract

Alkylaluminum complexes supported by cyclopentadienyl ligands ( $\text{Cp}^{\text{R}}$ ) have played a pivotal role in advancing rare-earth-metal chemistry. These various complexes already compile a huge library of hydrocarbyl compounds to reveal interesting and diverse reactivities like terminal alkyl formation via donor (ether) induced alkylaluminum cleavage and cluster formation upon addition of chlorinating agents. Probably the most interesting feature is the high activity of the respective  $\text{Cp}^{\text{R}}$  half-sandwich complexes in polymerization reactions, in particular 1,3-diene polymerization. By expanding the library of alkylaluminum half-sandwich rare-earth-metal complexes to fluorenyl and indenyl derivatives, the assessment of any ancillary ligand-implied structure-reactivity (polymerization) changes should be feasible.

A major difference compared to the  $\text{Cp}^{\text{R}}$  derivatives was already detected for the synthesis of the fluorenyl and indenyl (half-)sandwich complexes. While rare-earth-metal  $\text{Cp}^{\text{R}}$  half-sandwich bis(aluminate) complexes are usually obtained according to a protonolysis reaction, employing Ln alkyls and cyclopentadiene, this was not feasible for the indenyl and fluorenyl congeners. Therefore, salt-metathesis protocols were applied, using  $\text{Ln}(\text{AlMe}_4)_3$  and a sodium or potassium salt of indene and fluorene, respectively. The catalyst formation reaction via addition of common polymerization cocatalysts such as  $[\text{Ph}_3\text{C}][(\text{C}_6\text{F}_5)_4]$ ,  $[\text{PhNMe}_2\text{H}][\text{B}(\text{C}_6\text{F}_5)_4]$ , and  $\text{B}(\text{C}_6\text{F}_5)_3$ , revealed that indenyl half-sandwich complexes are activated similarly to the  $\text{Cp}^{\text{R}}$  half-sandwich complexes, whereas fluorenyl complexes can undergo ancillary ligand abstraction. Having established a comprehensive library of cyclopentadienyl, pentadienyl, indenyl, and fluorenyl half-sandwich complexes it was possible to investigate the influence of the supporting ligand on the performance in isoprene polymerization. Furthermore, the implications of the central metal for the polymerization could be determined by the half-sandwich complexes  $\text{Flu}^{\text{Si}}\text{Ln}(\text{AlMe}_4)_2$  ( $\text{Ln} = \text{Y}, \text{La}, \text{Nd}, \text{Lu}$ ). It was also revealed that complex  $\text{IndLa}(\text{AlMe}_4)_2$  promotes the living polymerization of isoprene.

The treatment of the homoleptic rare-earth-metal methylaluminates with 2-(6-methyl-2-pyridyl)-1,1-diphenyl-ethanol result in tandem protonolysis C–H bond activation reactions affording pincer-type complexes. The importance of the ionic radii of the rare-earth metal is revealed by engaging in single or double C–H bond activation. The produced complexes are not only active in the isoprene polymerization reaction, but feature interesting examples with respect to atropisomerism and chirality.

## Zusammenfassung

Seltenerdmetall-Alkylaluminat-Verbindungen welche durch Cyclopentadienyl-Liganden ( $\text{Cp}^{\text{R}}$ ) stabilisiert werden, haben wesentlich zur Weiterentwicklung der Seltenerdmetall Chemie beigetragen. Die erhaltenen Komplexe umfassen bereits eine große Bibliothek an Hydrocarbyl-Verbindungen, welche interessante und auch diverse Reaktivitäten aufweisen, wie die Bildung von terminalen Alkylen, durch Donor (Ether)-induzierter Alkylaluminatspaltung, oder die Bildung von Clustern mittels Chlorierungsreagenzien. Die wohl interessanteste Eigenschaft der  $\text{Cp}^{\text{R}}$ -Halbsandwich-Komplexe ist deren Performance in der 1,3-Dien-Polymerisation. Durch die Erweiterung der Alkylaluminat-Halbsandwich-Seltenerdmetall-Bibliothek um die Fluorenyl- und Indenyl-Derivate, konnte eine Einschätzung der Veränderung des additiven Liganden und dessen implizierter Strukturaktivität (Polymerisation) ermöglicht werden.

Ein gravierender Unterschied zu den  $\text{Cp}^{\text{R}}$ -Derivaten der Halbsandwich-Komplexe wurde schon bei der Synthese der Fluorenyl und Indenyl Halbsandwich-Komplexe festgestellt. Während die Seltenerdmetall- $\text{Cp}^{\text{R}}$ -Halbsandwich-Bis(aluminat)-Komplexe über eine Protonolysereaktion mittels Ln-Alkylen und Cyclopentadien zugänglich waren, war dies für die Indenyl- und Fluorenyl-Derivate nicht möglich. Daher wurden Salzmetathese-Protokolle, unter Verwendung von  $\text{Ln}(\text{AlMe}_4)_3$  und eines Natrium- oder Kalium-Indenyl- bzw. Fluorenyl-Salzes, angewendet. Der aktive Katalysator wurde durch die Verwendung von üblichen Kokatalysatoren wie  $[\text{Ph}_3\text{C}][(\text{C}_6\text{F}_5)_4]$ ,  $[\text{PhNMe}_2\text{H}][\text{B}(\text{C}_6\text{F}_5)_4]$  und  $\text{B}(\text{C}_6\text{F}_5)_3$  erhalten. Es zeigte sich, dass die Indenyl-Halbsandwich-Komplexe in gleicher Weise aktiviert werden wie  $\text{Cp}^{\text{R}}$ -Halbsandwich-Komplexe, wohingegen bei den Fluorenyl-Komplexen eine Ligandenabstraktion auftreten kann. Durch die Etablierung einer umfassenden Bibliothek an Cyclopentadienyl-, Pentadienyl-, Indenyl- und Fluorenyl-Halbsandwich-Komplexen war es möglich den Einfluss dieser Zuschauer-Liganden auf die Isoprenpolymerisation zu untersuchen. Mit dem Halbsandwich-Komplexen  $\text{Flu}^{\text{Si}}\text{Ln}(\text{AlMe}_4)_2$  ( $\text{Ln} = \text{Y}, \text{La}, \text{Nd}, \text{Lu}$ ) ließ sich zudem der Einfluss des Zentralmetalls auf die Polymerisation nachweisen. Eine lebende Polymerisation von Isopren konnte unter Verwendung von  $\text{IndLa}(\text{AlMe}_4)_2$  bewiesen werden.

Pincer-ähnliche Komplexe wurden bei der Umsetzung eines homoleptischen Seltenerdmetall-Methylaluminats mit 2-(6-Methyl-2-pyridyl)-1,1-diphenyl-ethanol über eine Protonolyse-C-H

–Bindungsaktivierungs-Reaktionsfolge erhalten. Das Vorliegen einer einfachen oder doppelten C–H-Bindungsaktivierung war abhängig vom Ionenradius des Seltenerdmetalls. Die erhaltenen Komplexe sind nicht nur aktiv in der Isoprenpolymerisation, sondern weisen auch interessante Eigenschaften hinsichtlich Atropisomerie und Chiralität auf.

## Publications and Personal Contribution

This thesis is based on the following scientific papers. In the text they will be referred to by the roman numerals.

**Paper I** Fluorenyl Half-Sandwich Bis(tetramethylaluminate) Complexes of the Rare-Earth Metals: Synthesis, Structure, and Isoprene Polymerization  
D. Diether, K. Tyulyunov, C. Maichle-Mössmer, R. Anwander  
*Organometallics* **2017**, *36*, 4649–4659.  
<https://doi.org/10.1021/acs.organomet.7b00543>

**Paper II** Implications of Indenyl Substitution for the Structural Chemistry of Rare-Earth-Metal (Half-)Sandwich Complexes and Performance in Living Isoprene Polymerization  
D. Diether, C. Maichle-Mössmer, R. Anwander  
*Organometallics* **2019**, *38*, 3007–3017  
<https://doi.org/10.1021/acs.organomet.9b00344>

**Paper III** Rare-Earth Metal-Induced (Double) C–H Bond Activation of a Pyridyl-Functionalized Alkoxy Ligand: Formation of  $[\text{ONC}]^{-(2-)}$  Pincer-Type Ligands and Implications for Isoprene Polymerization  
D. Diether, M. Meermann-Zimmermann, K. Törnroos, C. Maichle-Mössmer, R. Anwander  
*Manuscript*

Paper with contribution to polymerization reactions, polymer analytics and structural characterization. These publications are not attached to this thesis.

**Paper IV** 1,3-Diene Polymerization Mediated by Homoleptic Tetramethylaluminates of the Rare-Earth Metals  
C. O. Hollfelder, L. N. Jende, D. Diether, T. Zelger, R. Stauder, C. Maichle-Mössmer, R. Anwander  
*Catalysts* **2018**, *8*, 61–82.

**Paper V** Trimethylscandium  
D. Barisic, D. Diether, C. Maichle-Mössmer, R. Anwander  
*J. Am. Chem. Soc.* **2019**, *141*, 13931–13940.



**Paper I:** Fluorenyl Half-Sandwich Bis(tetramethylaluminate) Complexes of the Rare-Earth Metals: Synthesis, Structure, and Isoprene Polymerization

All reactions and analyses described were planned and conducted by myself. Analyses include  $^1\text{H}$ -,  $^{13}\text{C}\{^1\text{H}\}$ -,  $^1\text{H}$ - $^{13}\text{C}$  HSQC-,  $^1\text{H}$ - $^1\text{H}$  COSY NMR spectroscopic methods, DRIFT spectroscopy, GPC, DSC and sample preparation for elemental analyses. The synthesis of  $[\text{Flu}^{\text{Si}}\text{Y}(\text{AlMe}_4)\text{Cl}]_2$  and  $[\text{Flu}^{\text{Si}}\text{YCl}_2]_6$  were conducted by Konstantin Tyulyunov, during his Bachelor thesis, under my supervision. Publication writing was also done by me.

Structural analyses by single-crystal X-ray diffraction were done by Cécilia Maichle-Mössmer and me.

**Paper II:** Implications of Indenyl Substitution for the Structural Chemistry of Rare-Earth-Metal (Half-)Sandwich Complexes and Performance in Living Isoprene Polymerization

All reactions and analyses described were planned and conducted by myself. Analyses include  $^1\text{H}$ -,  $^{13}\text{C}\{^1\text{H}\}$ -,  $^{29}\text{Si}$ ,  $^1\text{H}$ - $^{13}\text{C}$  HSQC-,  $^1\text{H}$ - $^1\text{H}$  COSY NMR spectroscopic methods, DRIFT spectroscopy, GPC, DSC and sample preparation for elemental analyses.

Structural analyses by single-crystal X-ray diffraction were done by Cécilia Maichle-Mössmer and me.

**Paper III:** Rare-Earth Metal-Induced (Double) C–H Bond Activation of a Pyridyl-Functionalized Alkoxy Ligand: Formation of  $[\text{ONC}]^{-(2-)}$  Pincer-Type Ligands and Implications for Isoprene Polymerization

All reactions described were planned and conducted by M. Meermann-Zimmermann and myself. Analyses by  $^1\text{H}$ -,  $^{13}\text{C}\{^1\text{H}\}$ -, and  $^1\text{H}$  VT NMR spectroscopic methods, DRIFT spectroscopy, GPC, DSC and sample preparation for elemental analyses were conducted by myself.

Structural analyses by single-crystal X-ray diffraction were done by Karl Törnroos, Cäcilia Maichle-Mössmer and me.

**Paper IV:** 1,3-Diene Polymerization Mediated by Homoleptic Tetramethylaluminates of the Rare-Earth Metals

C. O. Hollfelder and L. N. Jende designed the isoprene and butadiene polymerization experiments. C. O. Hollfelder, L. N. Jende, T. Zelger, R. Stauder, and myself conducted the isoprene and butadiene polymerization reactions. Reactor design and reactions for ethylene polymerization were designed and conducted by me. The analyses of polyisoprene and polybutadiene were done by all authors.  $^1\text{H}$ -,  $^{13}\text{C}\{^1\text{H}\}$ -NMR, and DSC analyses for polyethylene were done by me. GPC analyses for polyethylene were performed by Malvern.

**Paper V:** Trimethylscandium

Reactions, analytics of the complexes and writing were done by D. Barisic. The analysis of the obtained polymers (DSC/GPC) and determination of decomposition temperature were done by me. Structural analyses by single-crystal X-ray diffraction were done by Cäcilia Maichle-Mössmer and me.

## Objective of the Thesis

The main objective of this thesis is to access rare-earth-metal alkyl complexes. Fluorenyl and indenyl half-sandwich complexes provided new ancillary ligands for the application in isoprene polymerization. Thereby the different influences of these precatalysts on the microstructure of the resulting polyisoprene can be identified.

Furthermore, the synthesis of post metallocene alkyl complexes and their performance in isoprene polymerization shall be assessed.

**Chapter A** of this thesis gives a brief overview of the historical development of Ziegler-Natta Catalysts, considering both homo- and heterogeneous catalytic system. This is followed by an overview of the synthesis of rare-earth-metal (half-)sandwich alkyl complexes and their application as polymerization catalysts from 2015 to 2018. Moreover, the thesis gives a brief overview on the synthesis of rare-earth-metal pincer alkyl complexes and their use in polymerization reactions from 2015 to 2018.

**Chapter B** covers the main results of this thesis. In particular, the following aspects are emphasized:

- Synthesis of (half-)sandwich rare-earth-metal alkyl complexes.
- Synthesis of pincer rare-earth-metal alkyl complexes.
- Activation reaction for isoprene polymerization.
- Isoprene polymerization promoted by half-sandwich and rare-earth-metal pincer alkyl complexes.



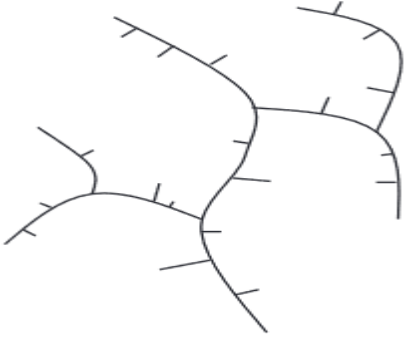

**A**

**Ziegler-Type  
Polymerization Reactions**

# 1 Ziegler-Natta Polymerization

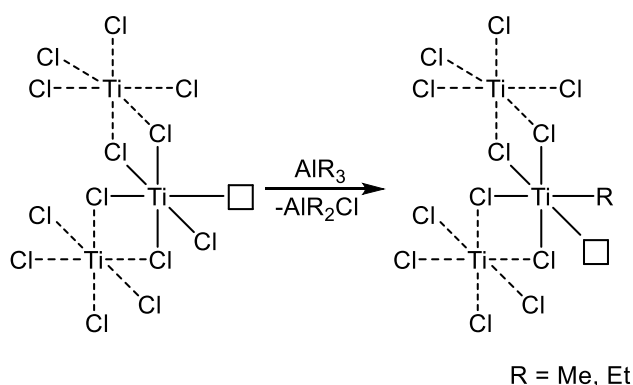
In 1953, the Philips Petroleum company reported on the PHILIPS catalyst.<sup>[1]</sup> Herein, chromium oxide, immobilized on a silica surface, is able to polymerize ethylene at 30 bar and 200 °C. The polymerization of ethylene was already known since 1938 and used on an industrial scale.<sup>[2]</sup> Applying 3000 MPa of pressure and temperatures of 300 °C, the conditions were rather harsh. The resulting polyethylene is a low density polyethylene (LDPE, Table 1). At the same time as the Philips Petroleum Company, ZIEGLER also succeeded in the ethylene polymerization.<sup>[3,4]</sup> Polyethylene is accomplished by ZIEGLER's titanium catalysts at atmospheric pressure and ambient temperature yielding high density polyethylene (HDPE) (Table 1). ZIEGLER also noticed the differences of the already known polyethylene to his new polyethylene and referred to it as "das neue Polyäthylen".<sup>[5]</sup>

**Table 1.** Properties of LDPE and HDPE adopted from MCDANIEL.<sup>[6]</sup>

	<b>LDPE</b>	<b>HDPE</b>
architecture		
branching	highly branched, long and short branches	little to no branching, short branches
density	0.915 – 0.935	0.935 – 0.975
Production in 2008 [10 <sup>6</sup> kg year <sup>-1</sup> ]	18	30
polymerization	radical	Ziegler-Natta catalyst, Phillips catalyst

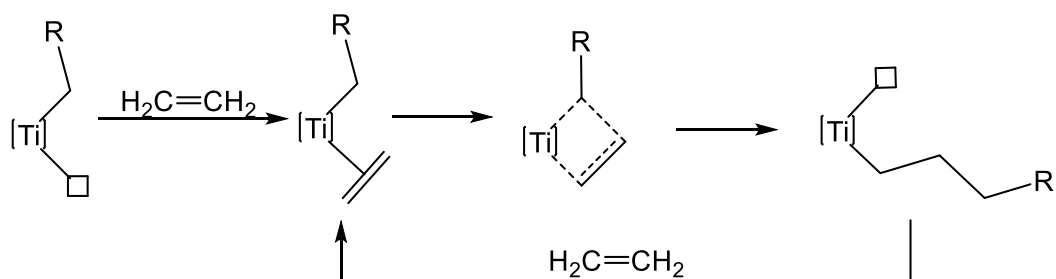
### 1.1 Heterogeneous Ziegler-Natta Polymerization

The heterogeneous ZIEGLER-NATTA catalyst is formed by the addition of trimethylaluminum or triethylaluminum to titanium(IV) tetrachloride in petrol to afford the active titanium(III) trichloride.<sup>[7]</sup> NATTA *et al.* analyzed the different modifications of the resulting  $\text{TiCl}_3$ . The study revealed that the  $\delta$ -modification is the most active modification for ethylene polymerization.<sup>[8]</sup> After controversial discussions concerning the reaction mechanism,<sup>[9-14]</sup> ARLMAN and COSSEE were able to identify the activation mechanism and the chain propagation pathway for the ZIEGLER-NATTA polymerization in 1963.<sup>[15-17]</sup> In the solid state, titanium centers are coordinated octahedrally by six chlorido ligands, while titanium centers at the surface have a lower coordination number and therefore accessible sites for reactions. The surface titanium centers are activated by alkylaluminum reagents, substituting a chlorido ligand for an alkyl group and forming a free coordination site (Scheme 1).



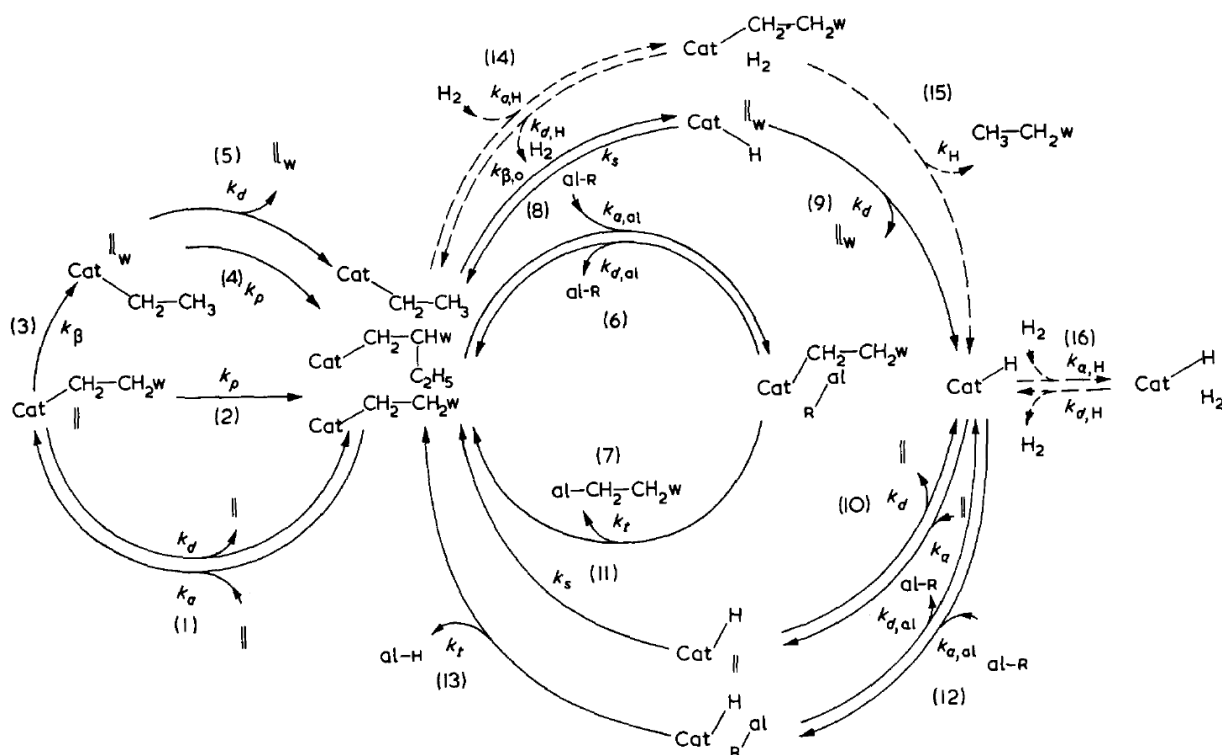
**Scheme 1.** Formation of the active site in trivalent titanium chloride.

This titanium alkyl species with an additional free coordination site allows the polymerization of  $\alpha$ -olefins. The  $\alpha$ -olefin can coordinate to the free coordination site and subsequently insert into the titanium alkyl bond. Thereby, forming a titanium alkyl group and again a free coordination site (Scheme 2).



**Scheme 2.** Chain propagation mechanism according to COSSEE and ARLMAN.

This mechanistic scheme indicates that the system is not restricted to ethylene polymerization. In fact, ZIEGLER's system is highly versatile and therefore valuable for industrial processes. The range of polymer properties can be widely varied, by copolymerization with other  $\alpha$ -olefins.<sup>[18–20]</sup> Additionally, the chain length of the polymer is adjusted by hydrogen gas over a wide range.<sup>[21]</sup> The reaction parameters can be tuned with regard to the active catalyst, olefinic monomer, aluminum alkyl, hydrogen pressure, and temperature. Mechanistic details of the ZIEGLER-NATTA catalysis are depicted in Scheme 3, as previously illustrated by BÖHM.<sup>[22]</sup>



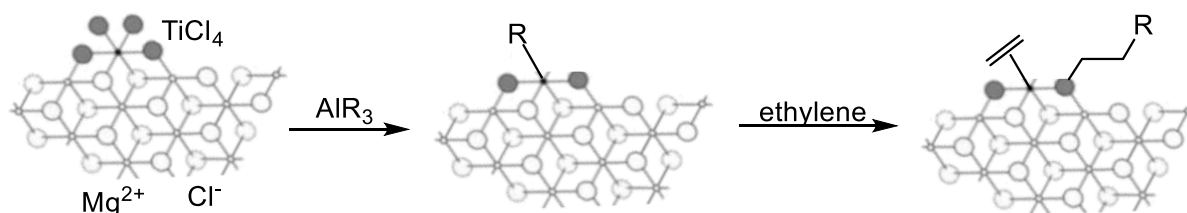
**Scheme 3.** Reaction pathways in the Ziegler-Natta polymerization, adopted from BÖHM *et al.*<sup>[22]</sup>

Due to reasons of simplicity, the titanium catalyst is depicted as 'Cat', ethylene as ||, and the polymer chain with 'w'. Step (1) and (2) correspond to the polymerization mechanism of ARLMAN and COSSEE shown in Scheme 2. Reaction step (3) is rather a minor side-reaction, including the  $\beta$ -H elimination of the growing polymer chain and transfer to the coordinated ethylene. The polymer chain herein, can dissociate (5) or insert into the titanium alkyl bond resulting in a branched polymer (4). The proportion of insertion (2) to  $\beta$ -H elimination (3) is  $10^4$ :1, showing the low influence of the  $\beta$ -H elimination.<sup>[23]</sup> The chain transfer capacity of alkylaluminum is shown for the reaction steps (6) and (7). Pathway (8) and (9) describe a  $\beta$ -H



elimination, yielding a titanium hydride species. This hydride species can be converted into an alkyl complex by substitution with an alkylaluminum compound (12, 13), or by coordination and insertion of ethylene (10, 11). The titanium hydride species also formed by hydrogen coordination and subsequent transfer onto the polymer (14, 15). The hydrogen concentration is crucial for the activity of the catalyst. The equilibrium of reaction (16) describes the state of an active and a dormant catalytic species. As already mentioned for the mechanism of COSSEE and ARLMAN the mechanism shown in Scheme 3 can also be adopted onto other  $\alpha$ -olefins or copolymerization reactions.

The shortcoming of the first ZIEGLER-NATTA systems was the low activity. This is mainly attributed to the few active titanium centers at the surface compared to the total amount of titanium in the solid particle. To compensate this,  $\text{TiCl}_4$  was immobilized on the surface of  $\text{MgCl}_2$ .<sup>[24,25]</sup> This is possible, due to similar structural motifs (cell parameters, ionic radii) of  $\delta\text{-TiCl}_3$  and  $\delta\text{-MgCl}_2$ .<sup>[26]</sup> After the immobilization of  $\text{TiCl}_4$  onto the  $\text{MgCl}_2$  surface, alkylaluminum reagents reduce the titanium centers and exchange the chlorido by alkyl ligands. At this active center, the polymerization can take place (Scheme 4). It was indicated, that the increase of activity is due to the higher quantity of active titanium centers at the surface.<sup>[27]</sup>



**Scheme 4.** Polymerization of ethylene by immobilized  $\text{TiCl}_4$  on  $\text{MgCl}_2$ , adopted from BÖHM.<sup>[26]</sup>

Beside the polymerization of ethylene, NATTA also investigated the polymerization reaction of different higher  $\alpha$ -olefins. Herein, he noticed various different physical properties of polymers consisting of the same monomer. He was able to attribute this to the difference in tacticity of the polymers.<sup>[18,28-30]</sup> The different types of tacticity in polymers of higher  $\alpha$ -olefins is shown in Figure 1. The tacticity can be subdivided into three general microstructures. In isotactic polymers, all of the substituents R are located on the same site of the polymer chain. For syndiotactic polymers the substituents R occupy alternating sites of the polymer chain. The distribution of R in atactic polymers is random along the polymer chain.

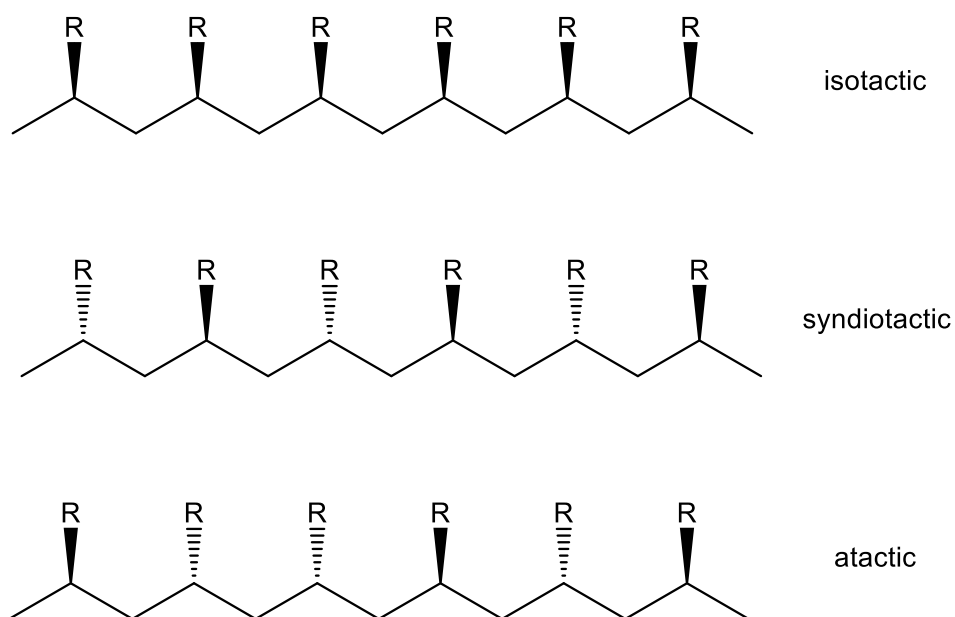


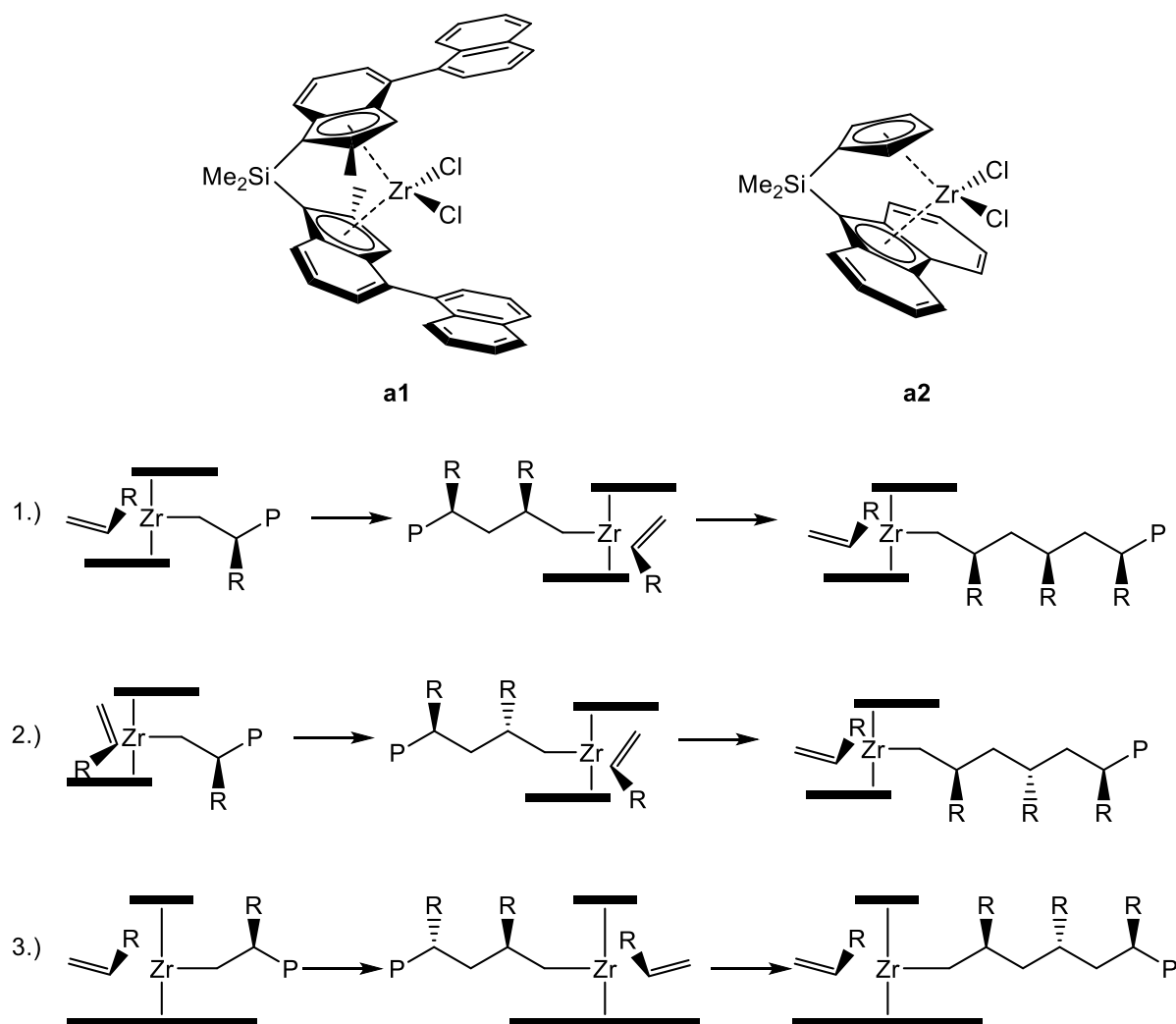
**Figure 1.** Different tacticities in higher  $\alpha$ -olefins.

## 1.2 Homogenous Ziegler-Natta Polymerization

Already NATTA<sup>[31,32]</sup> and BRESLOW<sup>[33,34]</sup> noticed that soluble bis(cyclopentadienyl) titanium complexes are excellent alternatives to the heterogeneous  $\text{TiCl}_4$  catalysts. Upon activation with bis(alkyl) aluminum chloride,  $\text{Cp}_2\text{TiCl}_2$  is a good catalyst for the polymerization of ethylene. Methylalumoxane (MAO) as a cocatalyst, especially for zirconium-based cyclopentadienyl complexes gained attention, due to the good performance as a cocatalyst. The activation of precatalysts by MAO is similar to the utilization of alkylaluminum reagents in heterogeneous Ziegler-Natta systems. MAO substitutes a chlorido by an alkyl group and generates a free coordination site. Thereby a cationic zirconium complex is generated and  $[\text{R-MAO}]^+$  features the corresponding weakly coordinating counterion. Since MAO poses not a distinct composition it is not feasible for a stoichiometric reaction. Therefore, borate and borane cocatalysts ( $[\text{Ph}_3\text{C}][(\text{C}_6\text{F}_5)_4]$  (**A**),  $[\text{PhNMe}_2\text{H}][\text{B}(\text{C}_6\text{F}_5)_4]$  (**B**), and  $\text{B}(\text{C}_6\text{F}_5)_3$  (**C**) feature a distinct composition to conduce stoichiometric activation for an improved insight into to polymerization reaction.

Tacticity control was significantly improved using *ansa*-metallocene complexes. Herein, the tacticity of the polymer is predetermined by the symmetry of the complex. For the polymerization of propylene SPALECK, for instance, synthesized a highly active  $\text{C}_2$ -symmetric

zirconium catalyst (**a1**).<sup>[35]</sup> Due to the  $C_2$ -symmetry of the catalyst, highly isotactic polypropylene is obtained. Considering the steric constraints, and the precoordination of the olefin, as depicted in Scheme 5, entry 1.), is preferred over the coordination as displayed in approach 2.). For comparison, **a2** a  $C_s$ -symmetric complex (mirror plane within the molecule) affords highly syndiotactic polymers.<sup>[36]</sup> The switch of coordination site by the polymer chain, as shown in Scheme 5, approach 3.), is responsible for the high syndiotacticity of the polymer.



**Scheme 5.** Control of tacticity by *ansa*-zirconocene catalysts, adopted from JANIÁK.<sup>[37]</sup>

## 2 Isoprene and Isoprene Polymerization

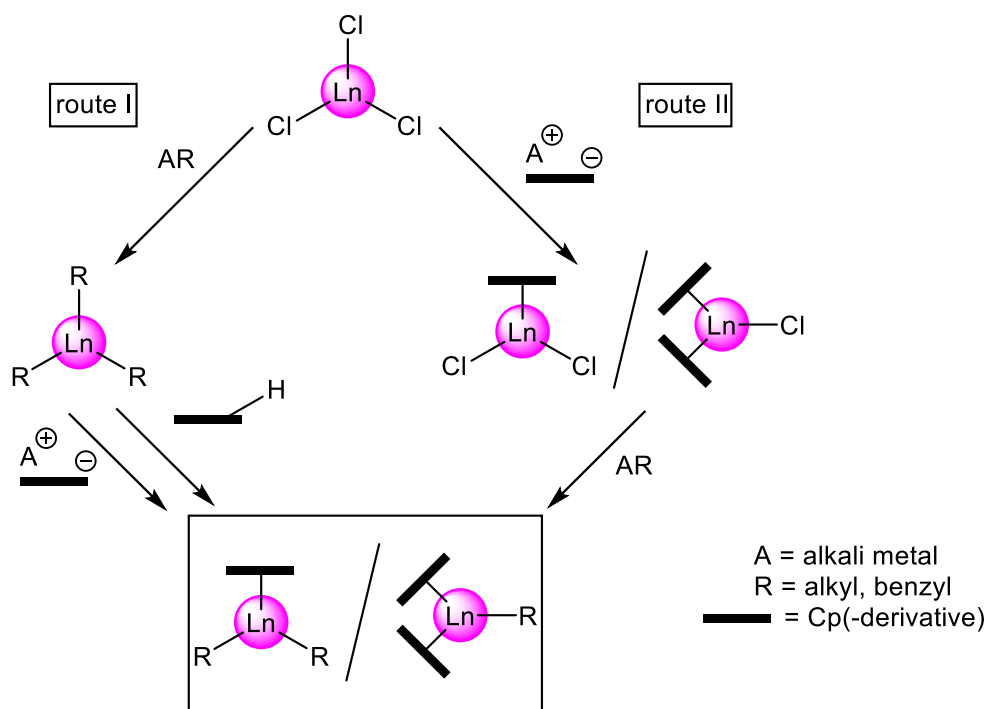
Polyisoprene is probably the polymer exploited earliest by mankind. Mesoamerican peoples have used saps of *havea brasiliensis* already 1600 B.C. For example, they used rubber balls for an ancient ball game.<sup>[38,39]</sup> Through the discovery of America, the knowledge of natural rubber was transferred to Europe. The invention of the vulcanization by GOODYEAR in 1939 increased the applicability and demand for natural rubber significantly.<sup>[40]</sup>

Already in 1911 a review about different butadienes and possible polymers of these dienes was published by HARRIES.<sup>[41]</sup> This shows how much effort was put into the understanding of the polymerization. WILLIAMS was the first to discover isoprene by dry distillation of natural rubber.<sup>[42]</sup> Afterward, HOFMANN isolated isoprene from stone coal in larger quantities and succeeded in polymerizing it, in 1909, by heating isoprene with egg albumin over several weeks.<sup>[43,44]</sup> By the invention of the Buna process, BOCK and TSCHUNKUR increased the polymerization activities with dienes significantly.<sup>[45]</sup> In 1929, they synthesized the butadiene styrene copolymer known as BunaS.<sup>[46]</sup>

Compared to the Buna process, the upcoming ZIEGLER-NATTA catalysts showed better selectivities for isoprene polymerization.<sup>[47-49]</sup> Fabrication of polyisoprene based on lanthanide catalysts was patented by Union Carbide Corporation.<sup>[50]</sup> Herein, they describe the use of a binary system consisting of lanthanum or cerium halide complexes coordinated by a bidentate chelating ligand (e.g. salicylaldehyde, 2-(methylamino)phenol, 2-hydroxyquinoline) and an alkylaluminum agent.<sup>[50]</sup> In the 1980s, companies like Bayer and Anic (later Eni) concentrated their research on neodymium(III) carboxylates<sup>[51]</sup> and neodymium(III) alcoholates<sup>[52]</sup> and started to use them in large scale.

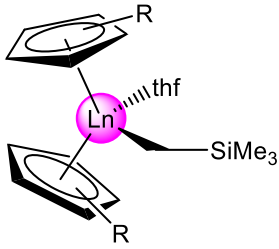
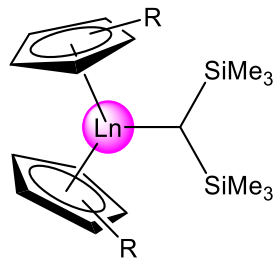
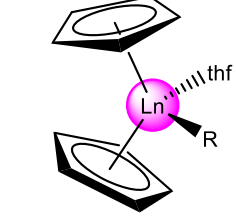
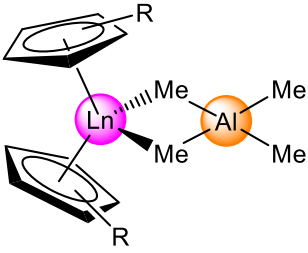
### 3 Rare-Earth-Metal (Half-)Sandwich (Bis)Alkyl Complexes

In the quest for new catalysts in the coordination polymerization, the knowledge of titanium and zirconium was transferred to the rare-earth metals. The need of a metal alkyl group adjacent to a free coordination site changed the design of the complexes, due to the oxidation state of +3 for the lanthanides. Therefore, especially the half-sandwich complexes gained attention in polymerization reactions. The first rare-earth-metal half-sandwich complex  $\text{Cp}^*\text{La}[\text{CH}(\text{SiMe}_3)_2]_2(\text{thf})$  was isolated in 1989.<sup>[53]</sup> The synthesis of (half-)sandwich complexes proceeds usually by salt metathesis or protonolysis reactions. Whereby the sequence of the different reaction steps can differ, as displayed in Scheme 6. The most widely used starting material is  $\text{LnCl}_3$ . Applying a salt metathesis protocol using  $\text{ACp}^{\text{R}}$  (A = alkali metal) the coordination of the  $\text{Cp}^{\text{R}}$  group can be achieved, yielding a bis(chloride) or bis( $\text{Cp}^{\text{R}}$ ) complexes. By a subsequent salt metathesis reaction with  $\text{AR}$  (R = alkyl, benzyl) the corresponding (half-)sandwich complex is obtained (Scheme 6, route II). This procedure was used for the synthesis of the first half-sandwich complex  $\text{Cp}^*\text{La}[\text{CH}(\text{SiMe}_3)_2]_2(\text{thf})$ <sup>[53]</sup> or the synthesis of dibenzyl complexes  $(\text{C}_5\text{Me}_4\text{SiMe}_3)\text{Sc}(\text{CH}_2\text{Ph})_2(\text{thf})$ ,  $(\text{C}_5\text{Me}_4\text{SiMe}_3)\text{Sc}(\text{CH}_2\text{Ph})_2(\text{thf})$ , and  $(\text{C}_5\text{Me}_5)\text{Gd}(\text{CH}_2\text{Ph})_2(\text{thf})$ .<sup>[54,55]</sup> The full potential of this synthetic route is displayed in the synthesis of sandwich complexes, shown in Table 2.

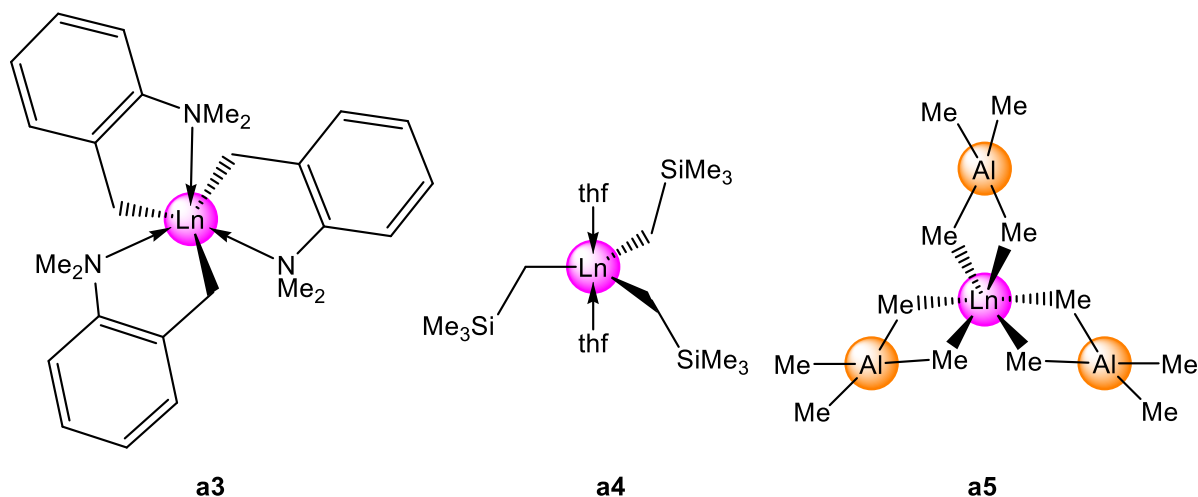


**Scheme 6.** General synthetic scheme of rare-earth-metal (half-)sandwich complexes.

**Table 2.** Synthesis of rare-earth-metal sandwich complexes according to route II.

	$\text{Y},^{[56]} \text{La},^{[57]} \text{Nd},^{[57,58]}$ $\text{Sm},^{[57]} \text{Lu}^{[57]}$	$\text{C}_5\text{Me}_5$
	$\text{Y},^{[60,61]} \text{Ce},^{[62]} \text{Nd},^{[61]} \text{Sm}^{[61]}$ $\text{Y},^{[63]} \text{Nd},^{[63]} \text{Sm}^{[63]}$	$\text{C}_5\text{Me}_5$ $\text{C}_5\text{Me}_4\text{Et}$
	$\text{Yb}^{[64]}$ $\text{Lu}^{[59]}$	$\text{CH}_3$ $\text{CH}_3, \text{C}_2\text{H}_5, \text{C}_4\text{H}_9, \text{C}(\text{CH}_3)_3,$ $\text{CH}_2\text{C}(\text{CH}_3)_3, \text{CH}_2\text{C}_6\text{H}_5$
	$\text{Sc},^{[65]} \text{Y},^{[65]} \text{Gd},^{[65]} \text{Dy},^{[65]}$ $\text{Ho},^{[65]} \text{Er},^{[65]} \text{Tm},^{[65]} \text{Yb}^{[65]}$	$\text{C}_5\text{H}_5$

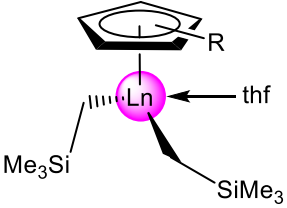
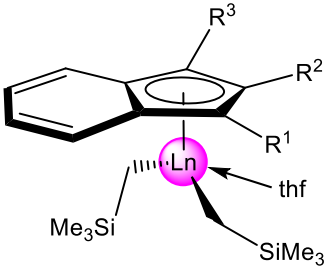
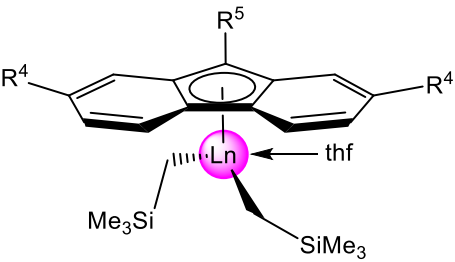
For the synthesis of the trialkyl rare-earth-metal species ( $\text{LnR}_3$ ), a salt metathesis reaction with AR (e.g.  $\text{LiCH}_2\text{SiMe}_3$  or lithium *N,N*-dimethyl-*o*-toluidine) and  $\text{LnCl}_3$  can be used (Scheme 6, route I).<sup>[66–69]</sup> These trialkyl rare-earth-metal complexes are suitable precursors for different (half-) sandwich complexes. Commonly used trialkyl rare-earth-metal complexes (**a3–a5**) are compiled in Figure 2.



**Figure 2.** Most widely used homoleptic trialkyl rare-earth-metal complexes.

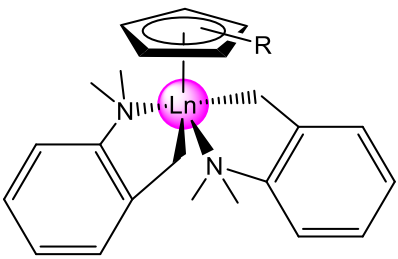
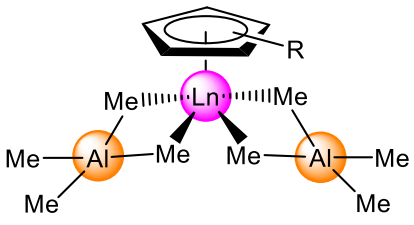
In order to obtain the corresponding (half-)sandwich complex, a subsequent protonolysis- or salt metathesis reaction is conducted. However, the latter seems less viable, since it is rather rare in literature. This latter route is mainly applied for the synthesis of tetramethylaluminate rare-earth-metal pentadienyl, fluorenyl, and indenyl (half-)sandwich complexes.<sup>[70–73]</sup> The protonolysis reaction of  $\text{LnR}_3$  with  $\text{HCp}^{\text{R}}$  instead of a salt metathesis reaction is the most widely used synthesis strategy for half-sandwich complexes. Examples of corresponding half-sandwich complexes isolated by this protocol are depicted in Table 3.

**Table 3.** Synthesis of half-sandwich complexes according to route I.

	Sc	$C_5H_5$ , <sup>[74]</sup> $C_5Me_5$ , <sup>[74]</sup> $C_5H_4Me$ , <sup>[74]</sup> $C_5HMe_4$ , <sup>[74]</sup> $C_5Me_4SiMe_3$ , <sup>[74,75]</sup> $C_5Me_4SiMe_2Ph$ , <sup>[76]</sup> $C_5Me_4(SiMe_2C_6F_5)$ , <sup>[77]</sup> $1,3-(SiMe_3)_2C_5H_3$ <sup>[78]</sup>
	$Y$ , <sup>[75,79]</sup> $Gd$ , <sup>[75]</sup> $Tb$ , <sup>[75]</sup> $Dy$ , <sup>[75]</sup> $Ho$ , <sup>[75]</sup> $Er$ , <sup>[75]</sup> $Tm$ , <sup>[75]</sup> $Yb$ , <sup>[75]</sup> $Lu$ <sup>[75,80]</sup>	$C_5Me_4SiMe_3$
	Sc	$Ind^R$ : $R^1=SiMe_3$ , $R^2=R^3=R^4=R^5=H$ ; $R^1=R^3=SiMe_3$ , $R^2=R^4=R^5=H$ ; $R^1=SiMe_3$ , $R^2=Me$ , $R^3=R^4=R^5=H$ ; $R^1=SiMe_3$ , $R^3=Me$ , $R^2=R^4=R^5=H$ ; $R^1=SiMe_2H$ , $R^2=R^3=R^4=R^5=H$ ; $R^1=R^3=SiMe_3$ , $R^2=Me$ , $R^4=R^5=H$ . <sup>[81]</sup>  $Flu^R$ : $R^4=R^5=H$ ; $R^4=tBu$ , $R^5=H$ ; $R^4=H$ , $R^5=SiMe_3$ , $R^4=tBu$ , $R^5=SiMe_3$ . <sup>[82]</sup>
	$Y$ , <sup>[75]</sup> $Dy$ , <sup>[75]</sup> $Lu$ <sup>[75,83]</sup>	$Ind^R$ : $R^1=R^3=SiMe_3$ , $R^2=R^4=R^5=H$ .



**Table 3** continued. Synthesis of half-sandwich complexes according to route I.

	Sc $C_5Me_5$ , <sup>[84]</sup> $C_5Me_4H$ , <sup>[85]</sup> $C_5Me_4SiMe_3$ <sup>[85]</sup>
	Y $C_5Me_5$ , <sup>[84]</sup> $C_5Me_4H$ , <sup>[84]</sup> $C_5Me_4SiMe_3$ , <sup>[84]</sup> $C_5Me_4Et$ , <sup>[84]</sup> $C_5(4-nBu-C_6H_4)_5$ <sup>[86]</sup>
	La, <sup>[73]</sup> Ce, Pr, Nd, Sm $C_5Me_4(SiMe_3)$ <sup>[75]</sup>
	Dy, Nd, Tm $C_5(4-nBu-C_6H_4)_5$ <sup>[86]</sup>
	La, Nd $C_5Me_5$ , <sup>[87]</sup> $C_5Me_4H$ , <sup>[88]</sup> $C_5Me_4SiMe_3$ , <sup>[89]</sup> $1,3-(SiMe_3)_2C_5H_3$ , <sup>[89]</sup> $1,2,4-(CMe_3)_3C_5H_2$ <sup>[89]</sup>
	Sm $C_5HMe_4$ , <sup>[88]</sup> $C_5Me_4SiMe_3$ , <sup>[89]</sup> $1,3-(SiMe_3)_2C_5H_3$ , <sup>[89]</sup> $1,2,4-(CMe_3)_3C_5H_2$ <sup>[89]</sup>
	Y, Lu $C_5Me_5$ , <sup>[87]</sup> $C_5HMe_4$ , <sup>[88]</sup> $C_5Me_4SiMe_3$ , <sup>[89]</sup> $1,3-(SiMe_3)_2C_5H_3$ <sup>[89]</sup>

---

### 3.1 Half-Sandwich Complex Promoted Polymerization Reactions

The isolation of the first structurally characterized rare-earth metal  $\text{Cp}^{\text{R}}$  half-sandwich complex ligated by two further alkyl moieties was a major breakthrough.<sup>[53]</sup> In the past 30, years extraordinary research efforts were made to develop new bis(alkyl) half-sandwich complexes to obtain further insight into these catalytic systems. A structural search on SciFinder® for  $\text{Cp}^{\text{R}}\text{LnR}_2$  ( $\text{Ln} = \text{Sc}, \text{Y}, \text{La-Lu}$ ;  $\text{R} = \text{any C moiety bonded to Ln}$ ) revealed 17,885 structural hits (as of March 2019). These complexes are not only of interest in academia, but also for industrial applications. Therefore, more than 930 patents on this kind of complexes were found on SciFinder®. Due to their variability for applications in different reactions, there is a great demand for those complexes. Such half-sandwich complexes are known for their use in C–H bond activation,<sup>[90–92]</sup> alkyne dimerization<sup>[93]</sup> or hydrocarbonation,<sup>[94]</sup> but most importantly for their application in polymerization reactions.<sup>[95–98]</sup>

Due to the huge research interest and great variability in application, this chapter will only focus on  $\text{Cp}^{\text{R}}$  bis(alkyl) half-sandwich complexes which have been used in polymerization reactions and have been published between 2015 and 2018. Constrained geometry complexes have not been included in this chapter. Review articles covering the years before 2015 have been published previously.<sup>[95–105]</sup> The literature is organized according to the  $\text{Cp}^{\text{R}}$  ligand and the alkyl moiety which has been used. Complexes discussed in this chapter are summarized in Figure 3. Polymers discussed in this chapter are depicted in Figure 4 and Figure 5.

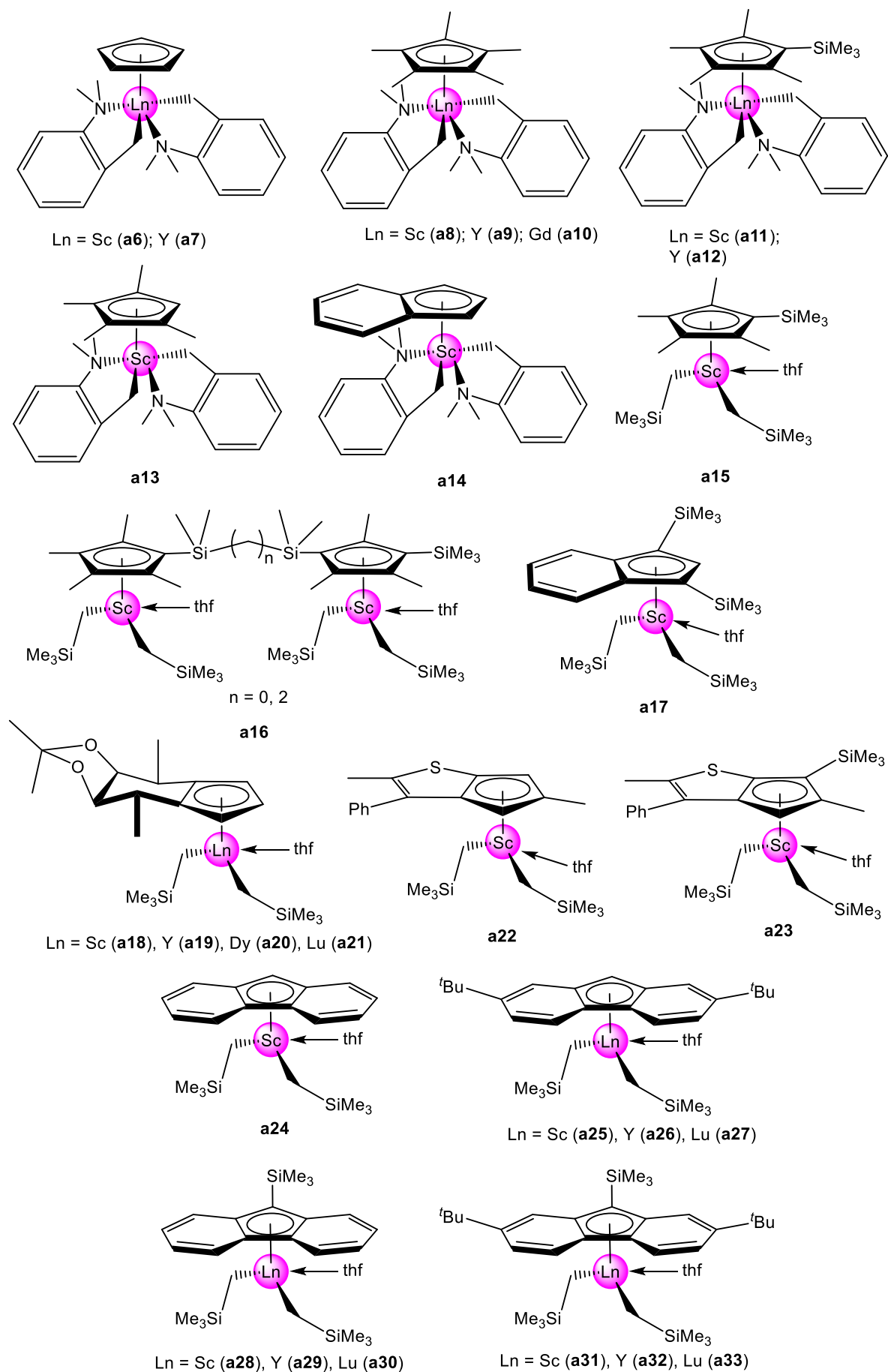
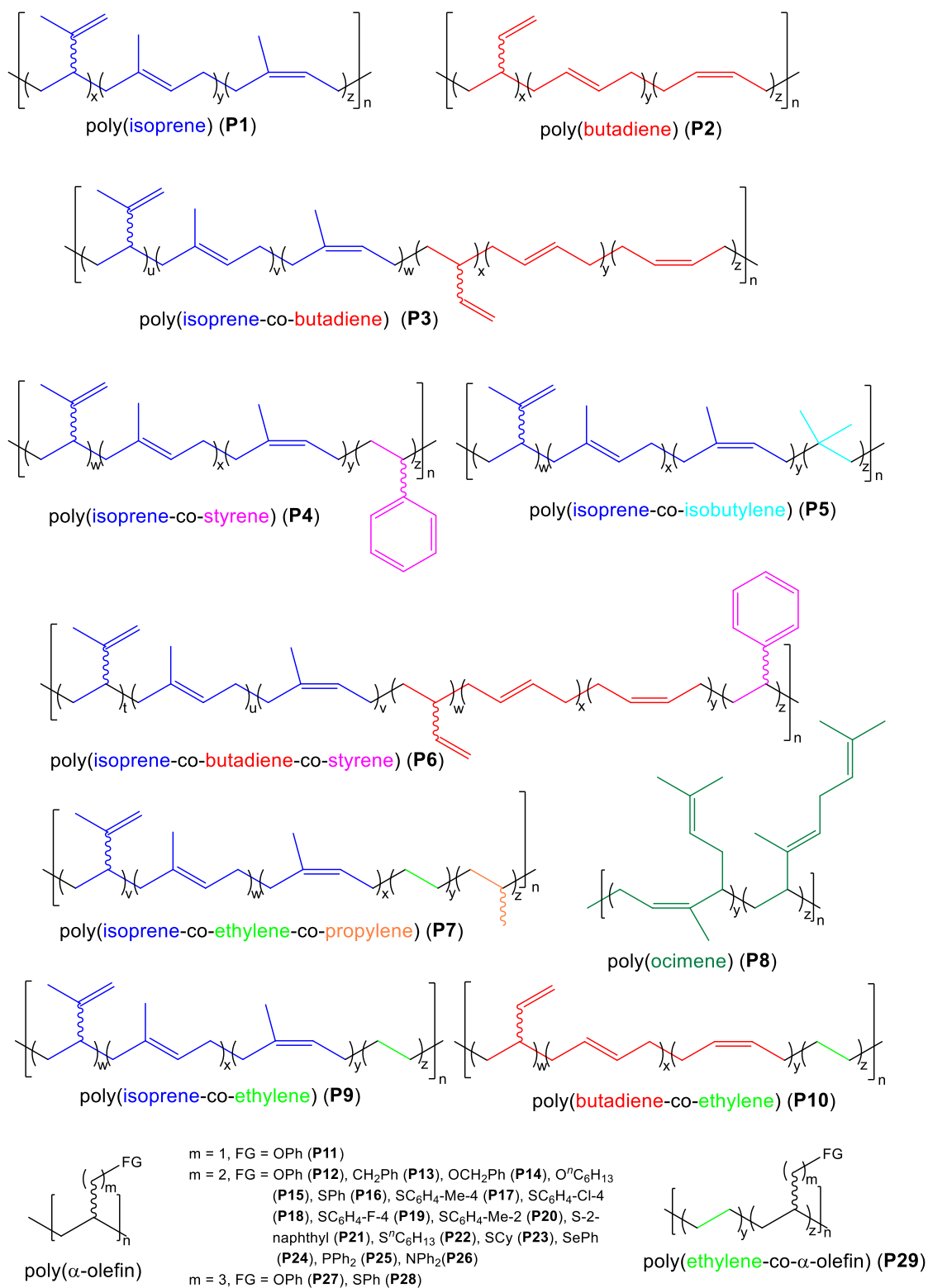
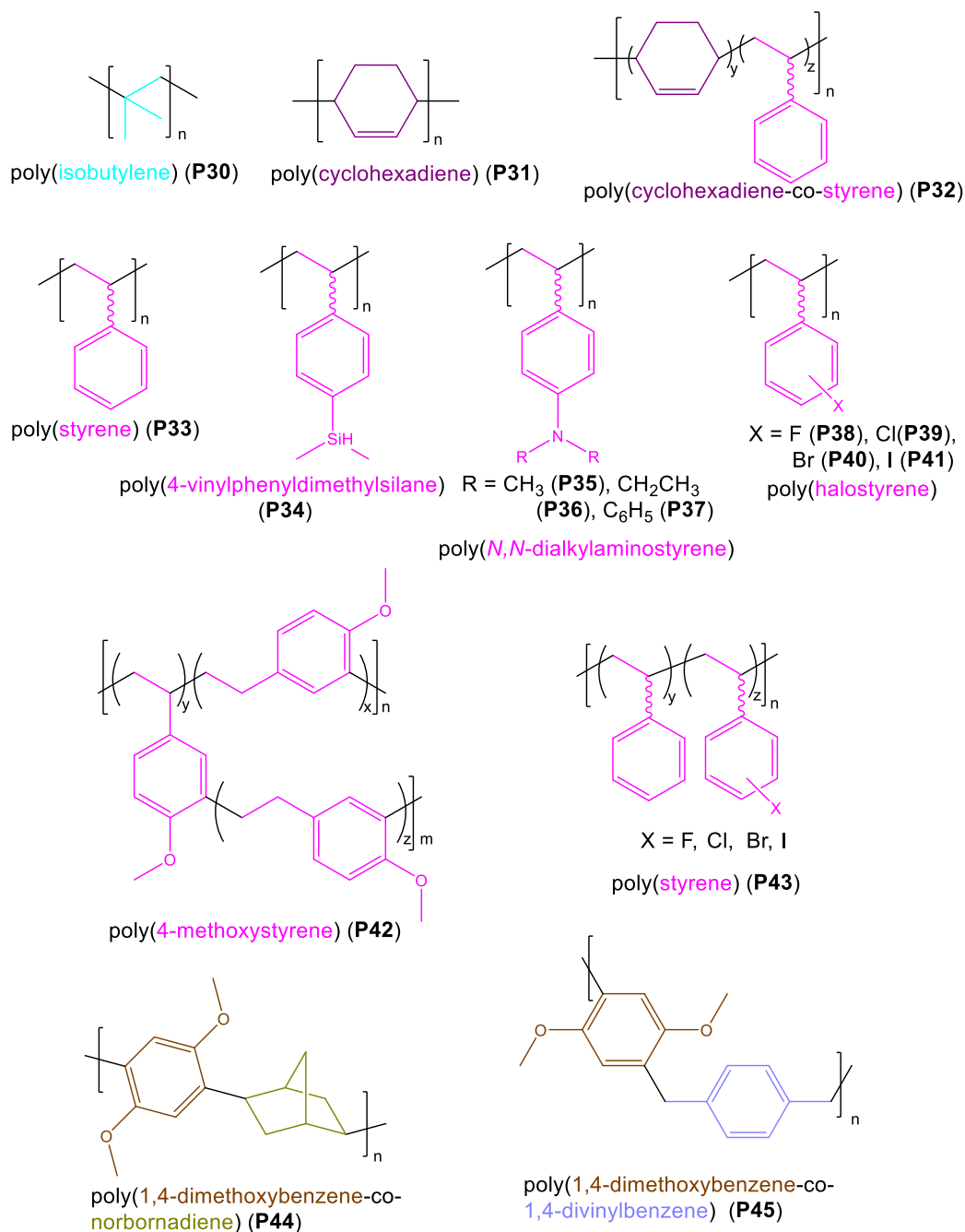


Figure 3. Half-sandwich complexes active as precatalysts in polymerization reactions.



**Figure 4.** (Co-)polymers obtained by polymerization with half-sandwich complexes.

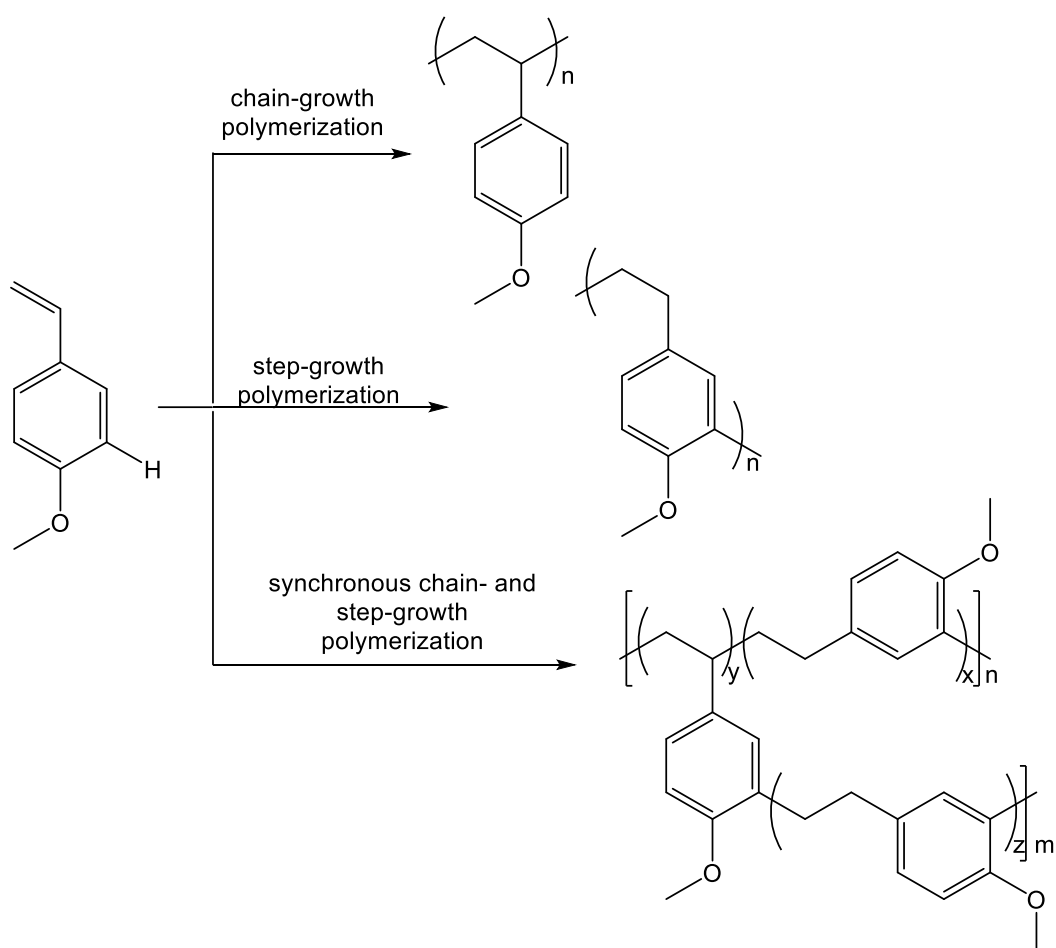


**Figure 5.** (Co-)polymers obtained by polymerization with half-sandwich complexes.

HOU and his group were able to polymerize 1,3-butadiene (**P2**) and styrene (**P33**) using CpSc(CH<sub>2</sub>C<sub>6</sub>H<sub>4</sub>NMe<sub>2</sub>-*o*)<sub>2</sub> (**a6**) in combination with cocatalyst **A**. The copolymerization of 1,3-butadiene with isoprene (**P3**) and isoprene with styrene (**P4**) was also successful. **a6** was highly selective for *cis*-1,4-polyisoprene (up to 97%) and *cis*-1,4-polybutadiene (up to 94%) with a narrow molecular weight distribution of 1.18 – 1.40. Additionally, the terpolymerization of styrene, 1,3-butadiene, and isoprene (**P6**) was achieved for the first time,

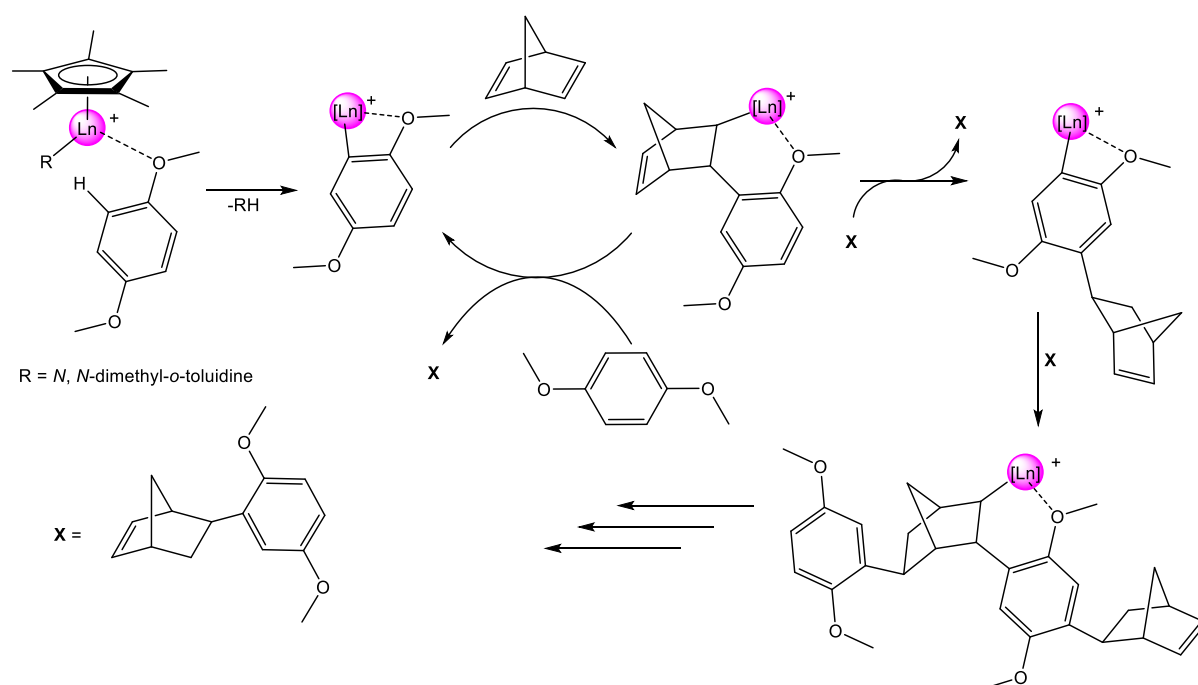
maintaining the high *cis* selectivity for isoprene and butadiene (up to 98%, and 96%, respectively) in addition to atactic polystyrene blocks.<sup>[106]</sup>

The corresponding permethylated ligand used in complexes  $\text{Cp}^*\text{Ln}(\text{CH}_2\text{C}_6\text{H}_4\text{NMe}_2\text{-}o)_2$  ( $\text{Ln} = \text{Sc}$  (**a8**),  $\text{Y}$  (**a9**),  $\text{Gd}$ (**a10**)), was applied for the simultaneous chain-growth and step-growth polymerization (Scheme 7) of *para*- and *meta*-methoxystyrenes (**P42**). Herein, the well-known chain-growth polymerization, addition at the double bond, was operative concomitant with the step-growth polymerization, addition of an aromatic C–H moiety to the C–C double bond (Scheme 7). Thus, new polymer architectures could be obtained. While using *ortho*-methoxystyrene the step-growth polymerization could not be observed, affording only syndiotactic poly(*ortho*-methoxystyrene) (*rrrr* >99%).<sup>[107]</sup>



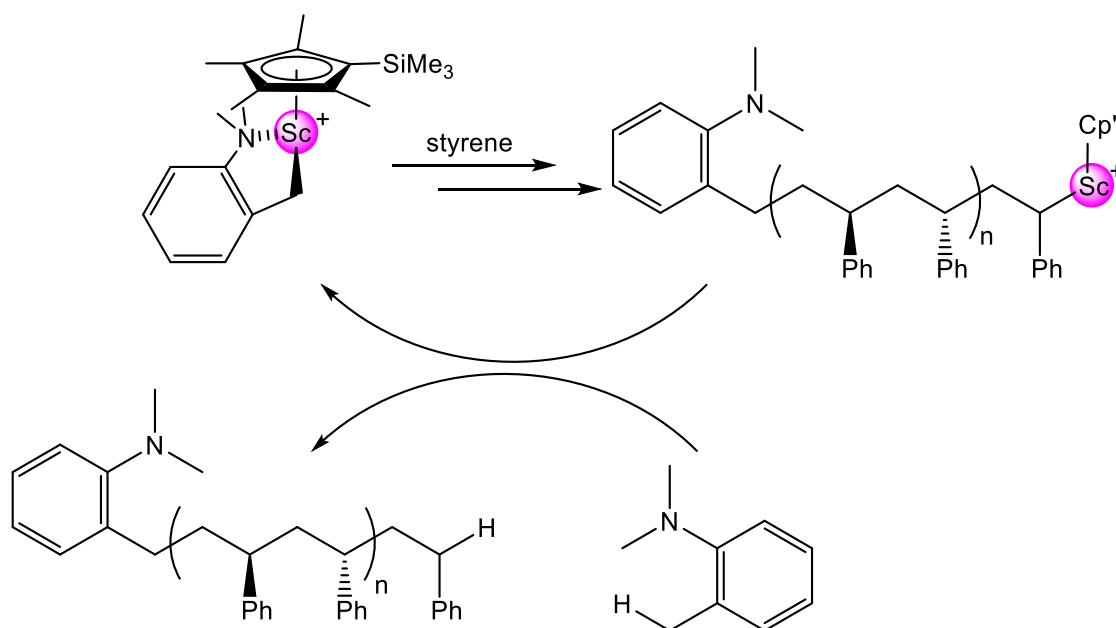
**Scheme 7.** (Synchronous) chain- and step-growth polymerization.

In another study 1,4-dimethoxybenzene was copolymerized for the first time with unconjugated dienes like norbornadiene (**P44**) or 1,4-divinylbenzene (**P45**) using **a8** and **a9** in combination with cocatalyst **A**. Herein, a perfect alternation of dimethoxybenzene and diene was observed. Moreover, a step-growth polymerization mechanism was indicated, wherein a dimerization of 1,4-dimethoxybenzene (DMB) and norbornadiene (NBA) occurs firstly. Replacing the dimer with an already formed dimer at the active center by a C–H bond activation of an aromatic C–H bond, a species is formed into which another DMB-NBA dimer can insert to continue the copolymerization reaction (Scheme 8). Thereby, an alternating DMB-NBA copolymer was obtained. Beside **a7** and **a9** also **a11** and **a12** were successfully tested for this copolymerization.<sup>[108]</sup>



**Scheme 8.** Mechanism of 1,4-dimethoxybenzene and norbornadiene copolymerization.

Recently, complex **a11** was used in many polymerization reactions. Herein, the main focus was on the polymerization of styrene and styrene derivatives with various substitution pattern. For the homopolymerization of styrene (**P33**) with **a11** and cocatalyst **A**, the influence of different anisoles or *N,N*-dimethyl-*o*-toluidine as a syndiospecific chain transfer agent was assessed. Due to *ortho* C–H bond activation of anisole or dimethyltoluidine, end-functionalized polystyrene was obtained. The molecular weight of the resulting polymer was tuned by adjusting the styrene/anisole ratio (Scheme 9).<sup>[109,110]</sup>



**Scheme 9.** Chain-transfer mechanism of *N,N*-dimethyl-*o*-toluidine.

For the polymerization of 4-vinylphenyldimethylsilane (**P34**), **a11** in combination with cocatalyst **A** was used. Hereby, the syndiotactic polystyrene derivative **P34** was isolated. Due to the reactive Si–H moiety a further functionalization of the polymer could be achieved. By hydrosilylation with a perylene derivative, a novel polymer with liquid crystal behavior, as well electron transport, and fluorescence properties was obtained.<sup>[111]</sup>

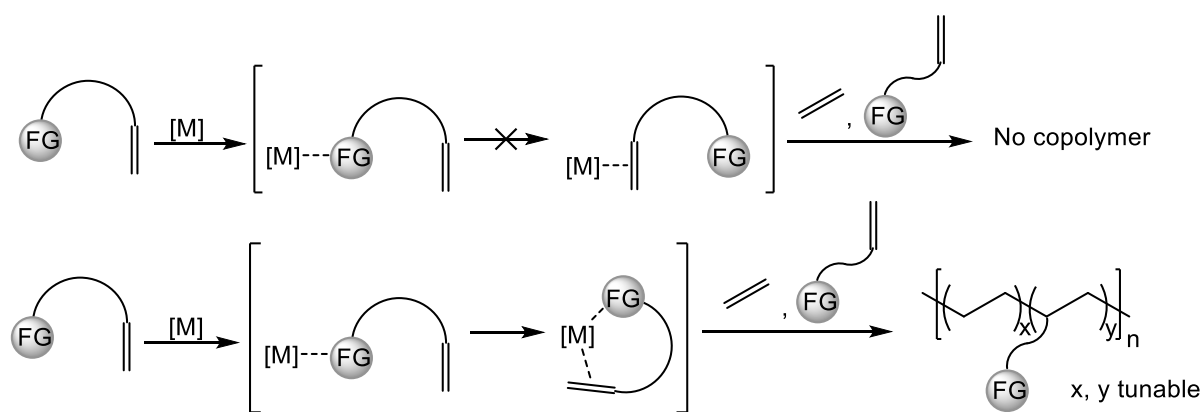
The same binary system (**a11/A**) was employed for the polymerization of (*N,N*-dimethylamino)styrene (**P35**), (*N,N*-diethylamino)styrene (**P36**), and (*N,N*-diphenylamino)styrene (**P37**). The isolated polystyrenes (**P35** – **P37**) were semicrystalline highly syndiotactic polymers (*rrrr* > 99%) with high melting temperatures (up to 289 °C). The polymer was used as an anchoring matrix for Pd-nanoparticles. Noteworthy, FTIR spectroscopy revealed that the particles are coordinated by the nitrogen atoms of the polymer.<sup>[112]</sup>

The polymerization of halogenated styrene (**P38** – **P41**) and the copolymerization with styrene (**P43**) were successfully conducted with **a11** activated with cocatalyst **A**. In accord with other studies on styrene polymerization, there was a significant syndiotactic selectivity (>99%). Precatalyst **a15** activated with cocatalyst **A**, which was also tested in the polymerization reaction of styrene, showed only minor stereoselectivity. The authors attribute



this to the fact that the catalyst contains thf as an additional LEWIS acid which lead to a decrease in the stereoselectivity.<sup>[113]</sup>

Catalysts **a6** – **a8**, **a11** – **a15** combined with cocatalyst **A** afforded not only functionalized polystyrenes but also functionalized  $\alpha$ -olefins were successfully applied in the polymerization reaction. The group of HOU investigated the polymerization by varying the functional group (FG = O, N, S, P, Se) or the chain length between the functional group and the double bond (**P11** – **P28**). The copolymerization of these functional  $\alpha$ -olefins with ethylene (**P29**) was also successful (Scheme 10). Usually, the incorporation of ethylene is favored over the functional  $\alpha$ -olefin, but HOU was able to vary the content of functional monomer up to 73%. The amount of incorporated functional monomer was controlled via different monomer loadings.<sup>[114]</sup>



**Scheme 10.** Copolymerization of ethylene and functional  $\alpha$ -olefins.

The polymerization of isobutylene (**P30**) using  $\text{Cp}^*\text{Sc}(\text{CH}_2\text{SiMe}_3)_2(\text{thf})$  (**a15**) with cocatalyst **A** as a cationic initiator proceeded even at low temperatures ( $-35\text{ }^\circ\text{C}$ ). The resulting polymers feature high molecular weights (up to  $48 \cdot 10^5$  g/mol) and a high content of *exo*-olefin end groups (90%).<sup>[115]</sup>

Activating **a15** or **a17** with cocatalyst **A** the terpolymerization of ethylene, propylene, and isoprene (**P7**) was successfully conducted. It was possible to control the ethylene content (38 – 84%) as well as the isoprene content (4 – 43%). The vinylic 3,4-isoprene content in these terpolymers were up to 54%. The postfunctionalization by epoxidation of the 1,4-isoprene units was achieved with *meta*-chloroperoxybenzoic acid, while 3,4-isoprene units remain unaltered for further vulcanization. Chloride and hydroxyl groups were introduced into the backbone of the polymer by a subsequent reaction at the epoxy groups.<sup>[116]</sup>

The monomeric **a15** and dimeric complex **a16** have been used in the isoprene polymerization (**P1**) upon activation with cocatalyst **A** or a dianionic version of **A** (Figure 6). The study revealed that the *trans*-content increases significantly while using the dianionic cocatalyst instead of **A**. The *cis*-selectivity correlated with the Sc...Sc distances in precatalyst **a16**. Compound **a15** gave **P1** with 24% *cis*-1,4-content while **a16** (with  $n = 2$ ) and **a16** (with  $n = 0$ ) afforded 32% and 48% respectively. Using **a16** in the isoprene/ethylene copolymerization (**P9**) the incorporation of isoprene was reduced by roughly 50% and the molecular weight was higher compared to polymerizations with the monomeric complex **a15**. This work showed the significant influence of the catalyst/cocatalyst nuclearity in the polymerization.<sup>[117]</sup>

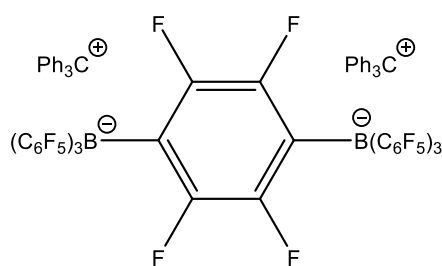


**Figure 6.** Dianionic version of cocatalyst **A**.

The chiral cyclopentadienyl half-sandwich complexes **a18** – **a21** were used for the first polymerization of ocimene (**P8**), a noncyclic monoterpene. Herein **a18** produced *cis*-1,4-polyocimene in up to 100%. For comparison, compounds **a19** – **a21** gave rather *trans*-1,2-polyocimene (up to 100%).<sup>[118]</sup>

The *cis*-1,4-selective copolymerization of butadiene and ethylene (**P10**) revealed to be challenging. By adjusting the steric and electronic properties of the ligand CUI and coworkers were able to obtain *cis*-1,4-selective butadiene/ethylene copolymer using **a22** as a precatalyst. The activation with cocatalyst **A** and TIBA led to **P10** with up to 90% *cis*-1,4-content and varying amount of ethylene, while for **a23** the 1,2-content increased up to 20%.<sup>[119]</sup>

A similar copolymerization of isoprene with ethylene (**P9**) and homopolymerization of isoprene (**P1**) was achieved using fluorenyl half-sandwich complexes **a24**, **a25**, **a28**, and **a31** activated with cocatalyst **A** and TIBA. It was shown that an addition of TIBA increased the activity and *cis*-selectivity in the isoprene polymerization. The fluorenyl ligand has a significant influence on the microstructure of the copolymer. The *cis*-content was tuned

between 79% and 1%, while the total isoprene content was between 32% and 97%. High performance polymers were accessed via further epoxidation of the 1,4 double bond.<sup>[120]</sup>

Precatalysts **a24** – **a31** have been used for the cyclohexadiene (CHD) homo- (**P31**) and CHD/styrene copolymerization (**P32**). For the homopolymerization, scandium complexes displayed the highest activity compared to yttrium and the lutetium (Sc>Y>Lu). The CHD content of the copolymer ranges from 22% to 74%. LI and coworkers indicated that ligand, metal, cocatalyst, temperature, and the CHD/styrene ratio significantly affected the CHD content. A subsequent epoxidation of the double bonds was accomplished by meta-chloroperoxobenzoic acid.<sup>[121]</sup>

### 3.2 Sandwich Complex Promoted Polymerization Reactions

Especially when it comes to reactions with unsaturated substrates, bis(cyclopentadienyl) rare-earth-metal alkyl complexes give access to different catalytic transformations. There are numerous examples in the literature for hydrogenation,<sup>[57,122]</sup> hydroamination,<sup>[123,124]</sup> hydrophosphination,<sup>[125–127]</sup> hydrosilylation,<sup>[128,129]</sup> and hydroboration<sup>[130,131]</sup> using sandwich complexes. Although the focus is clearly on half-sandwich complexes, bis(cyclopentadienyl) rare-earth-metal alkyl complexes can be used in polymerization reactions as well.<sup>[96,100,101,104]</sup> Crucially, the activation reactions are less feasible for metallocene derivatives. Nevertheless, this chapter covers publications of rare-earth metallocene alkyl complexes applied in polymerization reactions, published between 2015 and 2018. Ansa metallocene complexes have not been included in this chapter. Complexes discussed in this chapter are summarized in Figure 7. Polymers discussed in this chapter are compiled in Figure 8.

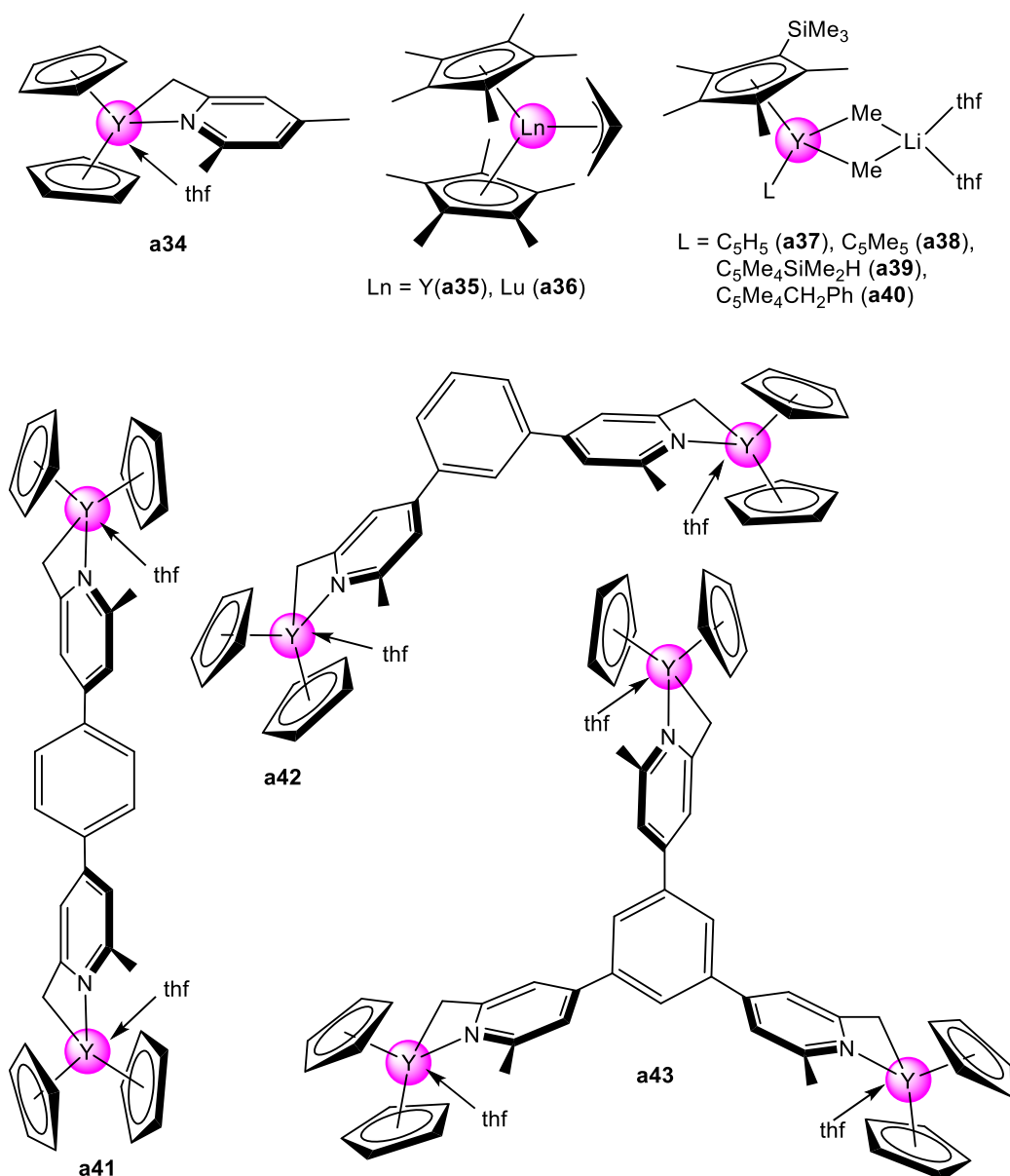


**Figure 7.** Lanthanidocene complexes employed in polymerization reactions.

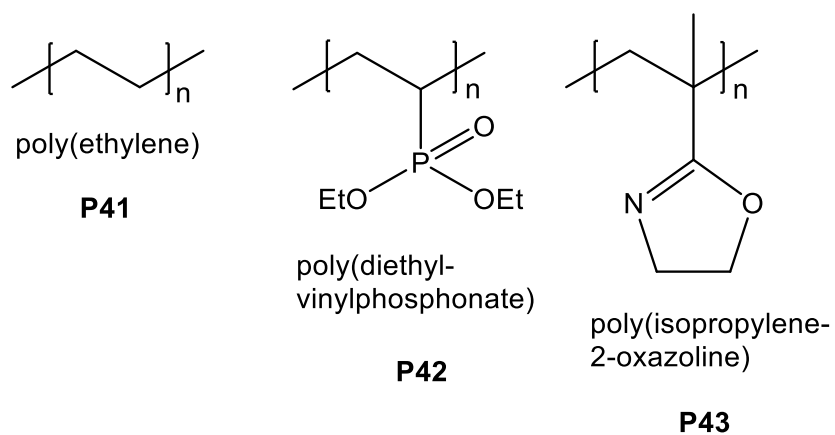
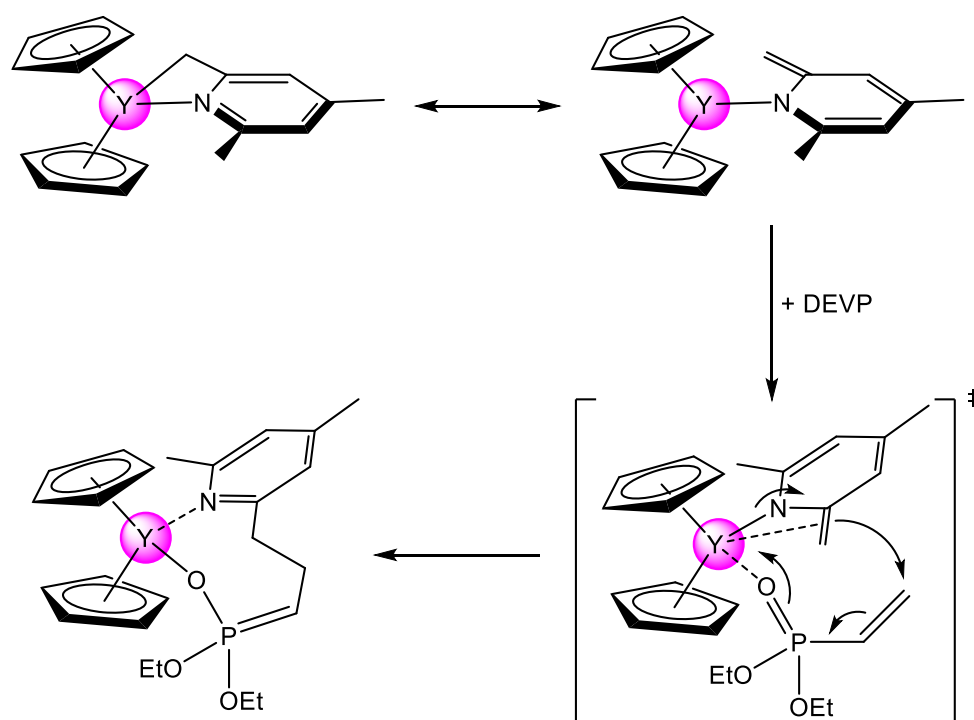


**Figure 8.** Polymers obtained by lanthanidocene complexes.

The sandwich complex bis(cyclopentadienyl)(4,6-dimethylpyridine-2-yl)methyl yttrium (**a34**) was synthesized by C–H bond activation of 2,4,6-trimethylpyridine and successfully tested in the polymerization of diethyl vinylphosphonate (DEVP, **P42**) and 2-isopropylene-2-oxazoline (IPOx, **P43**).<sup>[132]</sup> Similar systems **a41** – **a43** produced di- and three-armed star-shaped polymers of DEVP and IPOx.<sup>[133]</sup> The initiation proceeded via a transient eight-membered ring as shown in Scheme 11.



**Scheme 11.** Initiation of DEVP polymerization.

Interestingly, the study revealed that **a35** and **a36** polymerize isoprene (**P1**) by irradiation with light. The microstructure of the resulting polymer showed a high 3,4-content which is in good agreement with a radical polymerization mechanism as no specific rare-earth metal dependent microstructure was observed.<sup>[134]</sup>

The group of HORÁČEK showed that complexes **a37** – **a40** can serve as single-component catalysts for the fabrication of high-density polyethylene (**P41**), with a narrow molecular weight distribution.

## 4 Pincer Complexes

In the area of post-metallocene polymerization catalysis, pincer complexes received increasing attention due to the versatile properties of the latter. For instance, the avoidance of ate-complex formation, dimerization or solvent coordination is combined with the great variability in steric and electronic properties.<sup>[135]</sup>

Associated with the continuous progress in the synthesis of new rare-earth-metal catalysts, pincer complexes are also primarily accessed via salt metathesis and protonolysis reactions. For comparison, the synthesis strategies of (half-)sandwich complexes are shown in Scheme 6. Generally, there are five important approaches, which have already been successfully applied for the synthesis of different rare-earth-metal pincer complexes (Scheme 12). These strategies are applied considering actor and spectator ligands.

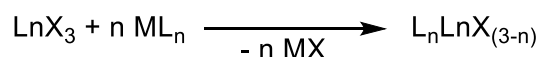
The salt metathesis protocol (Scheme 12) was used in 1988 for an early example of a rare-earth-metal pincer complex.<sup>[136]</sup> Herein, yttrium(III) chloride was treated with two equivalents of  $\text{LiN}(\text{SiMe}_2\text{CH}_2\text{PMe}_2)_2$ . This route is not restricted to rare-earth-metal chlorides, but can also be used for the heavier halides<sup>[137]</sup> or pseudohalides.<sup>[138]</sup> The popularity of this route originates in the simple starting material and the versatility of the resulting halogenide complexes.

The amine- or alcohol elimination route is a protonolysis reaction of a rare-earth-metal amido or alkoxy complex respectively (Scheme 12). MASHIMA, for example, applied successfully the amine elimination route for the synthesis of yttrium pincer complexes.<sup>[139]</sup> The advantage is the volatile side product  $\text{HN}(\text{SiMe}_3)_2$  that can be easily removed under reduced pressure. For the alcohol elimination, as for example ARNOLD showed, more acidic ligands were required.<sup>[140]</sup> However, a major drawback might be that the resulting alcohol cannot be removed under reduced pressure. For both elimination routes the conversion of the ligand into an alkali metal salt, as it is necessary for the salt metathesis reaction, is not required.

The alkane elimination is another elegant protonolysis reaction for the synthesis of pincer complexes (Scheme 12). Herein, usually rare-earth-metal alkyl complexes are protonated by a protic pincer ligand. ANWANDER for example, used  $\text{Ln}(\text{CH}_2\text{SiMe}_3)_3$  in combination with an amine functionalized pincer ligand to liberate neosilyl and the desired pincer complex.<sup>[141]</sup> Thus synthesis route requires a highly reactive rare-earth-metal alkyl complex but on the

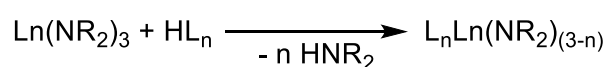
other hand the BRØNSTED acidity of the pincer proligand can be low and the coproduct, the inert alkane, can easily be removed under reduced pressure.

### **Salt metathesis**

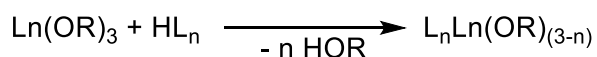


### **Protonolysis reaction**

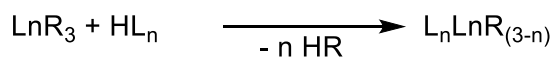
#### amine elimination



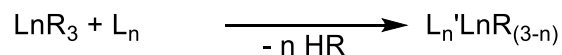
#### alcohol elimination



#### alkane elimination



### **C–H bond activation**



Ln = rare earth metal; X = halogenido; M = alkali metal;  
L<sub>n</sub> = tridentate ligand; R = alkyl or aryl group

**Scheme 12.** Synthesis routes to pincer complexes.

The synthesis of pincer complexes by C–H bond activation is rather adventitious (Scheme 12), since a rational approach is hard to predict. Bidentate ligands can easily be transformed into pincer complexes using C–H bond activation. However, using this method, pincer complexes can be obtained which otherwise would be difficult to afford via other synthetic routes. Usually, this occurs at ligands with bulky substituents, as depicted in Figure 9.<sup>[142–145]</sup>

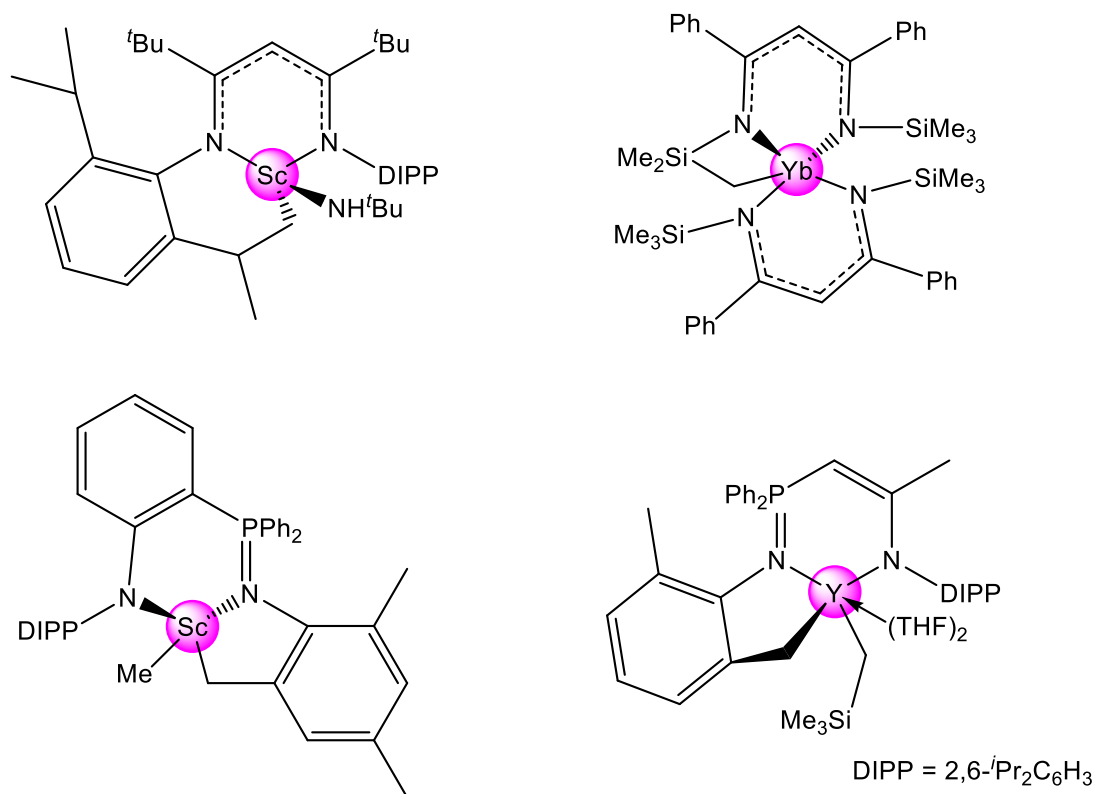


**Figure 9.** Rare-earth-metal pincer complexes obtained by C–H bond activation.

The chemistry of rare-earth-metal pincer complexes has been comprehensively reviewed by HÄNNINEN *et al.* in 2015.<sup>[135]</sup> This chapter covers publications of rare-earth-metal pincer complexes coordinated by alkyl ligands covering the years 2015 to 2018.

Complexes discussed in this chapter are compiled in Figure 10. Figure 11 comprises the polymers, obtained by rare-earth-metal pincer complexes.



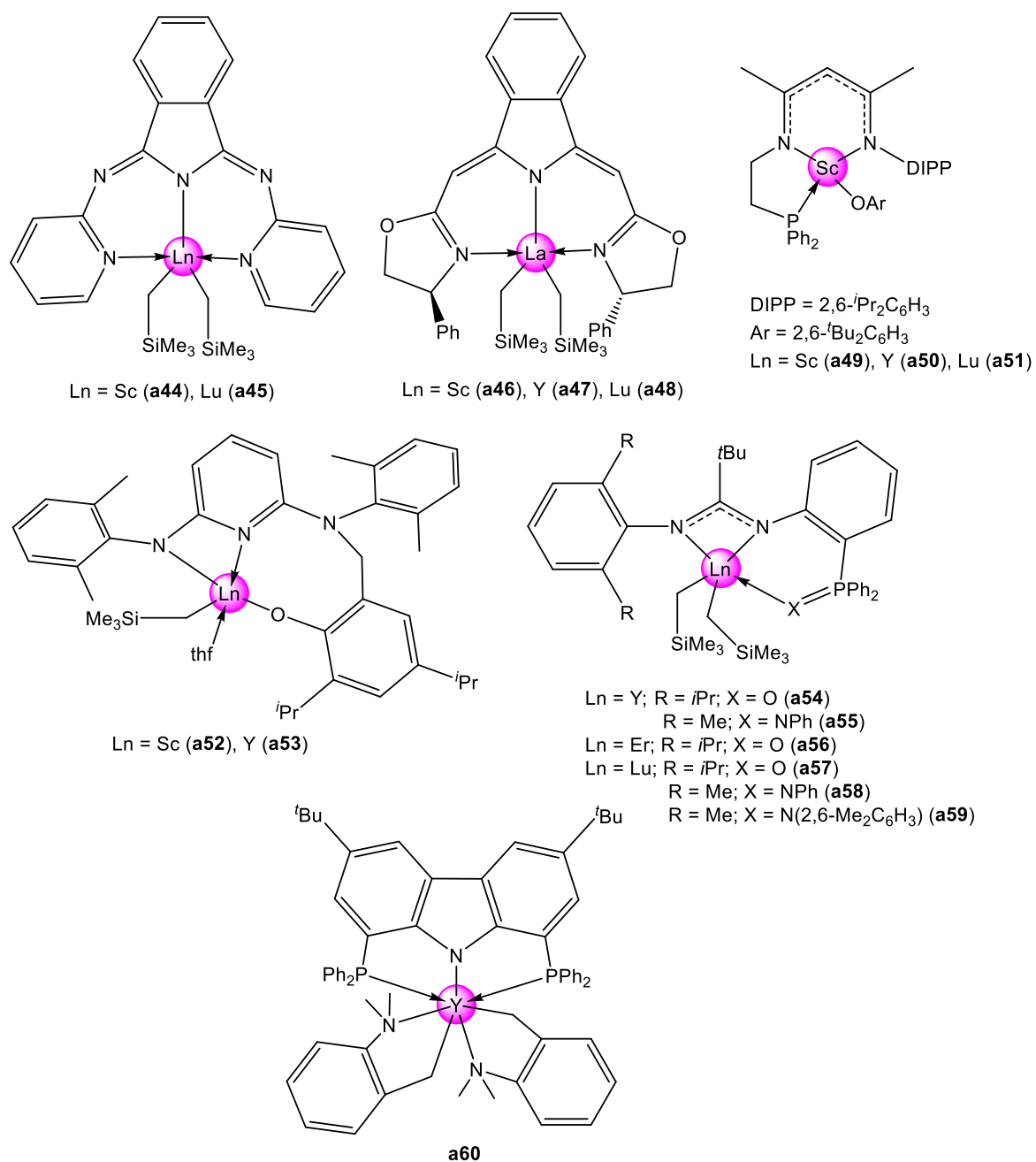


**Figure 10.** Rare-earth-metal pincer complexes studied in polymerization reactions.

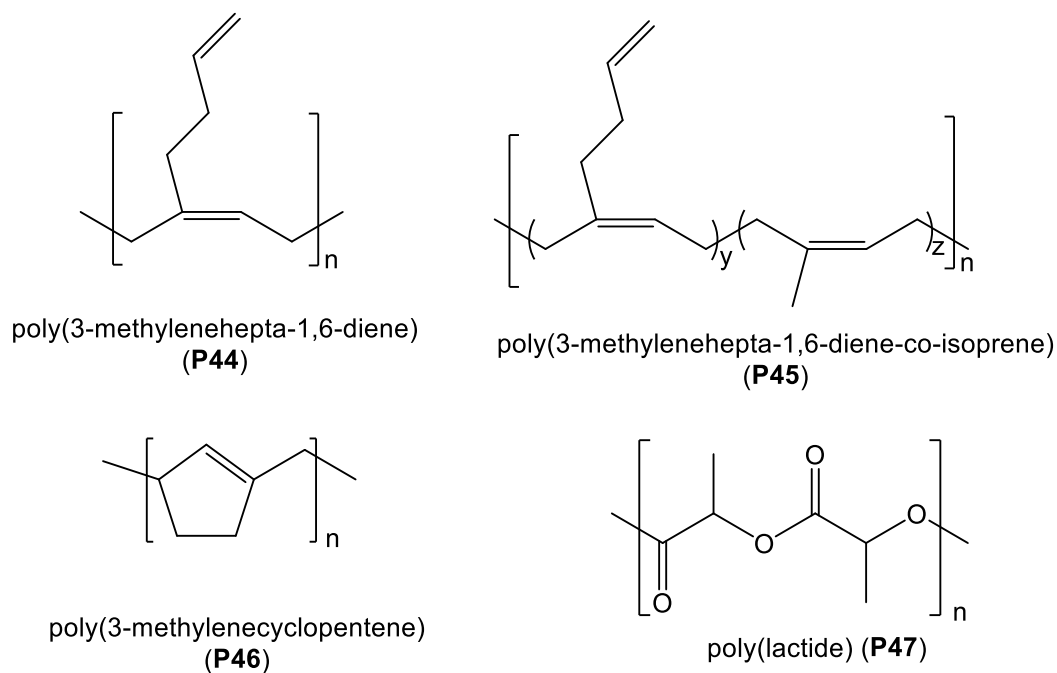


**Figure 11.** (Co-)polymers obtained by rare-earth-metal pincer complexes.

LI and coworkers have been particularly interested in the selective isoprene polymerization with pincer-based rare-earth-metal complexes. For the *cis*-selective polymerization of isoprene (**P1**) complexes **a44** and **a45** were used.<sup>[146]</sup> These complexes achieved upon activation with cocatalyst **A** and trialkylaluminum up to 99% *cis*-1,4-selectivity with high molecular weights ( $M_n$  up to 610000 g/mol) and narrow PDIs (1.26 – 2.08). For complexes **a46** – **a48** the same high *cis*-selectivities like for the aforementioned complexes were observed.<sup>[147]</sup> In previous studies LI revealed that similar pincer complexes produce *trans*-1,4 polyisoprene.<sup>[148]</sup>

A change of selectivity from *cis*- to *trans*-1,4-polyisoprene (**P1**) was indicated with precatalysts **a54** – **a59**. All complexes showed good catalytic activity upon activation with cocatalyst **A** or **B** in combination with TIBA. Catalysts with coordinated  $\text{Ph}_2\text{P}=\text{O}$  (**a54**, **a56**, **a57**) had a higher catalytic activity than the catalysts with  $\text{Ph}_2\text{P}=\text{NPh}$  coordination (**a55**, **a58**). By changing the coordinating group, the selectivity was reversed as well. Complexes **a54**, **a56**, and **a57** showed a *cis*-1,4-selectivity with up to 98%, while complexes **a55** and **58** showed *trans* enriched polyisoprene with contents up to 85%. Not only is the coordinating group of importance but also the steric effect of this donor group. The lutetium amidinate complex **a59** produced *cis*-enriched polyisoprene.<sup>[149]</sup>

The diversity of pincer ligands is reflected in the diversity of monomers they can polymerize. As already shown pincer complexes are suitable for olefin and 1,3-diene polymerization, but also suitable for the polymerization of functionalized monomers. The polymerization of *rac*-lactide (**P47**) was successful with complexes **a52** and **a53** under mild conditions. These complexes were able to polymerize *rac*-lactide without any addition of an alcohol, yet reactivity increases upon addition of isopropanol.<sup>[150]</sup>

Complex **a60** activated by cocatalyst **A** and TIBA was used for the polymerization of 3-methylenecyclopentene (MCP) (**P46**). The polymerization yielded pure 1,4-poly(3-methylenecyclopentene). However, due to the steric influence of the pincer ligand, the reaction rates lag behind in comparison to half-sandwich complexes.<sup>[151]</sup>

The metalated yttrium catalyst **a60** was also successfully applied for the polymerization of 3-methylenehepta-1,6-diene (MHD) (**P44**) and the copolymerization of MHD and isoprene (**P45**). It was possible to polymerize MHD in a living way, accomplishing high *cis*-content (99%). Due to the living character it was also possible to obtain copolymers with isoprene as block- or random-copolymer. By variations of the monomer feeding ratio, the isoprene content could be varied over a wide range.<sup>[152]</sup>



---

# B

## **Summary of the Main Results**

# 1 Synthesis of Rare-Earth-Metal Indenyl and Fluorenyl Complexes

Rare-earth-metal complexes bearing cyclopentadienyl ligands are well established and thoroughly investigated.<sup>[95–105]</sup> Herein, especially the half-sandwich bis-alkyl species were extensively studied in polymerization reactions.<sup>[95–98]</sup> EVANS *et al.* reported on the synthesis of tris(tetramethylaluminate) complexes  $\text{Ln}(\text{AlMe}_4)_3$ . In our group these bimetallic complexes were assessed in 1,3-diene polymerization and a new class of rare-earth-metal alkyl precatalyst was established.<sup>[153–156]</sup> Especially the rare-earth-metal  $\text{Cp}^{\text{R}}$  bis(aluminate) complexes are versatile precursors for inorganic synthesis and catalysis.<sup>[88,89,157,158]</sup> While these systems are well investigated, the corresponding indenyl and fluorenyl derivatives attracted less attention. In a few studies, indenyl and fluorenyl half-sandwich complexes of the small and medium-sized rare-earth metals were isolated.<sup>[81,82,116,121,159]</sup> Due to this apparent dearth of data, we aimed at the synthesis of fluorenyl and indenyl rare-earth-metal complexes.

The  $\text{Cp}^{\text{R}}$ -based bis(tetramethylaluminate) rare-earth-metal complexes were obtained by an established protonolysis reaction of  $\text{Cp}^{\text{R}}\text{H}$  with  $\text{Ln}(\text{AlMe}_4)_3$ , resulting in the selective formation of  $\text{Cp}^{\text{R}}\text{Ln}(\text{AlMe}_4)_2$ .<sup>[89]</sup> Unfortunately, this reaction protocol could not be adopted for indenyl and fluorenyl ligands. The reaction rate of lanthanum-based systems with indene and fluorene was much slower compared to the reaction rates of  $\text{HCp}^{\text{R}}$  congeners. The hypothesis that indene ( $\text{p}K_{\text{a}} = 20.1$ ) and fluorene ( $\text{p}K_{\text{a}} = 22.6$ ) should react smoothly considering the BRØNSTED acidities, being more acidic than  $\text{Cp}^*$  ( $\text{p}K_{\text{a}} = 26.1$ ), has not been confirmed.<sup>[160]</sup> The question why there is this mismatch of  $\text{p}K_{\text{a}}$  value and expected reaction rate, could not completely be clarified. Changing the rare-earth metal to the smaller lutetium, the attempted protonolysis reaction did not occur, indicating that steric effects might hinder the reaction.

Due to the lack of accessibility by protonolysis reaction, salt metathesis protocols were established. Here, the potassium salts  $\text{KFlu}$  (potassium fluorenyl) and  $\text{KFlu}^{\text{tBu}}$  (potassium di(tertbutyl) fluorenyl) have been obtained by the reaction of  $\text{HFlu}^{\text{R}}$  with  $\text{KH}$  in toluene, or via deprotonation of  $\text{HFlu}^{\text{Si}}$  (trimethylsilyl fluorene) with  $\text{K}(\text{N}(\text{SiMe}_3)_2)$ . X-ray analysis revealed a polymeric structure for  $\text{KFlu}^{\text{Si}}$  (potassium trimethylsilyl fluorene) in the solid state. Herein, potassium centers bridge the fluorenyl moieties while being centered at the six-

membered ring of the fluorenyl moiety (Figure S1). The synthesis of  $\text{LiInd}^{\text{R}}$  complexes was accomplished by lithiation of  $\text{HInd}^{\text{R}}$  with  $n\text{-BuLi}$ .

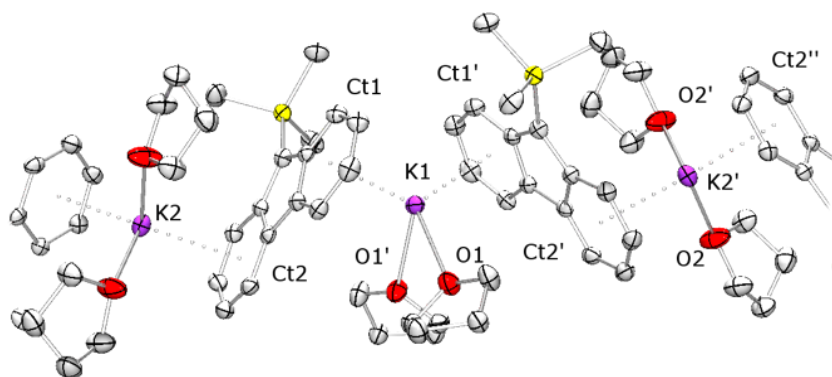
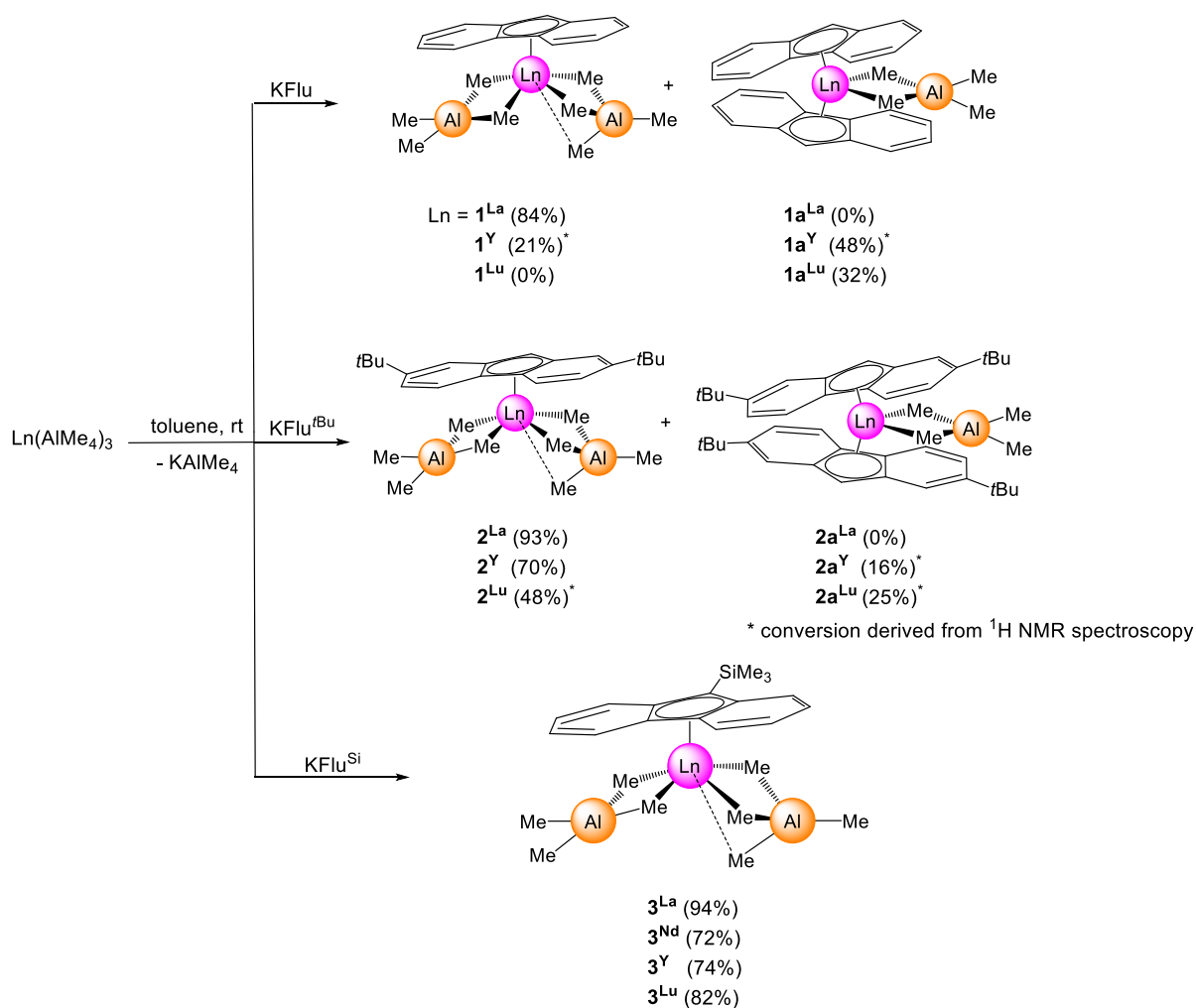


**Figure S1:** Solid-state structure of  $\text{KFlu}^{\text{Si}}$ .

The synthesis of half-sandwich complexes  $\text{Flu}^{\text{R}}\text{Ln}(\text{AlMe}_4)_2/\text{Ind}^{\text{R}}\text{Ln}(\text{AlMe}_4)_2$  and sandwich complexes  $(\text{Flu}^{\text{R}})_2\text{Ln}(\text{AlMe}_4)/(\text{Ind}^{\text{R}})_2\text{Ln}(\text{AlMe}_4)$  was accomplished by the reaction of  $\text{Ln}(\text{AlMe}_4)_3$  with  $\text{KFlu}^{\text{R}}$  or  $\text{LiInd}^{\text{R}}$ , obtaining  $\text{K/Li}(\text{AlMe}_4)$  as a coproduct. Depending on the steric influence of the ligand and more importantly on the size of the rare-earth metal center, either the half-sandwich or the sandwich complex was formed.

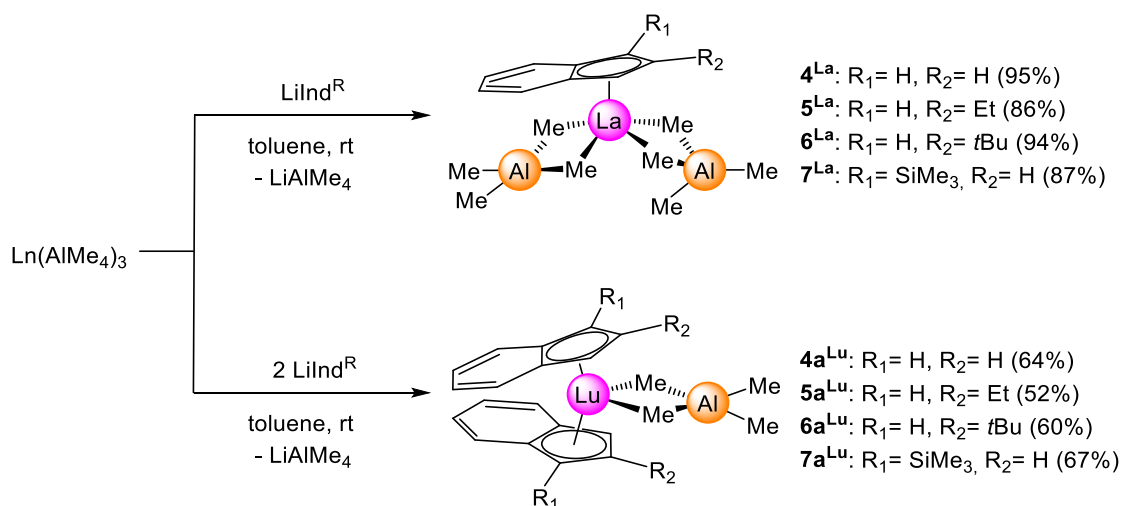
In Scheme S1 the fluorenyl (half-)sandwich complexes are compiled, obtained as major or minor product with respect to the ionic radii of the rare-earth metal center and the steric demand of the fluorenyl ligand. Lanthanum as the largest rare-earth metal formed selectively the respective half-sandwich complex with the envisaged fluorenyls. The steric demand of the fluorenyl had no impact on the reactivity of the La-alkylaluminates. For comparison, the medium-sized yttrium congener afforded the half-sandwich complex only by coordination of a sterically demanding fluorenyl. Therefore, two *tert*-butyl groups at the fluorenyl ligand were introduced, to afford  $\text{Flu}^{\text{tBu}}\text{Y}(\text{AlMe}_4)_2$  (Scheme S1). The introduction of a trimethylsilyl group at the fluorenyl ligand resulted in such a strong steric shielding that beside yttrium, also lutetium with the smallest ionic radius in the lanthanide series could be isolated as a half-sandwich complex. Therefore, the combination of rare-earth metal and fluorenyl ligand had to be complementary to result in half-sandwich complexes, otherwise reaction mixtures of half-sandwich and sandwich complexes were formed.



**Scheme S1:** Synthesis of fluorenyl (half-)sandwich complexes and the corresponding yields.

The coordination chemistry of rare-earth-metal indenyls was examined in another study. Noteworthy, the substitution pattern of the indenyl ligands with regard to the steric demand enabled only the isolation of sandwich complexes for lutetium, while the selective formation of the half-sandwich complexes was observed for lanthanum (Scheme S2). In accord with this finding, the middle-sized yttrium formed mixtures of sandwich and half-sandwich complexes.





**Scheme S2:** Synthesis of indenyl (half-)sandwich complexes and the corresponding yields.

Nevertheless, the substituent at the indenyl ligand had a significant influence on the solid-state structure. For half-sandwich complexes three different structural motifs were obtained. While the mononuclear structure (**6<sup>La</sup>**) and a dimeric structure (**4<sup>La</sup>**) have been already established for the  $\text{Cp}^{\text{R}}$  half-sandwich complexes,<sup>[88,155]</sup> **7<sup>La</sup>** shows a new dimeric structural motif (Figure S2). Herein, the bridging methyl groups is positioned *trans* to the indenyl ligand, while in **4<sup>La</sup>** the bridging methyl group is in a *cis* like position to the ligand.

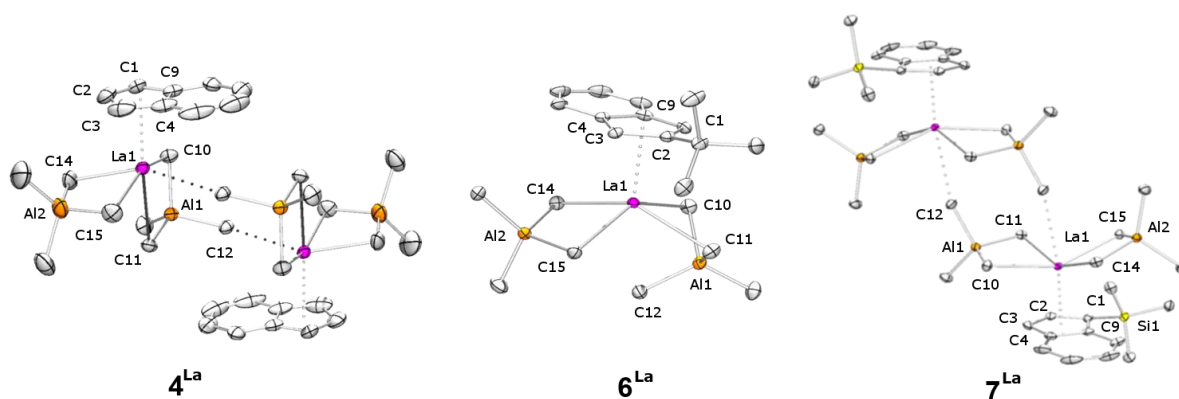
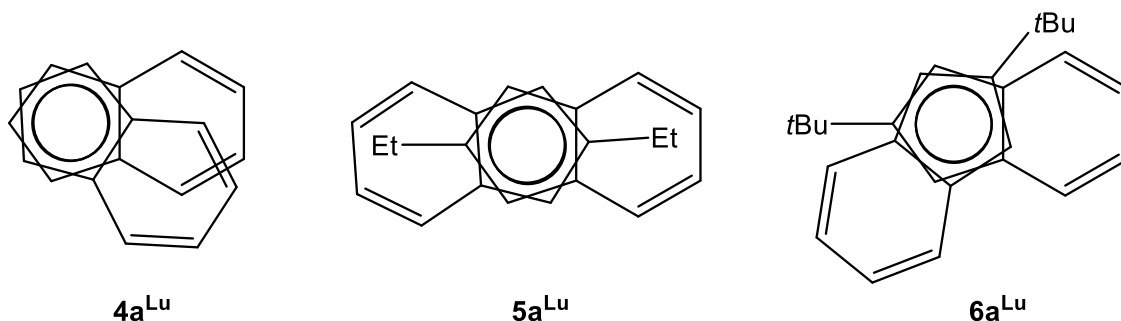


**Figure S2:** Solid-state structures of  $\text{IndLa}(\text{AlMe}_4)_2$  (left),  $\text{Ind}^{t\text{Bu}}\text{La}(\text{AlMe}_4)_2$  (middle), and  $\text{Ind}^{\text{Si}}\text{La}(\text{AlMe}_4)_2$  (right).

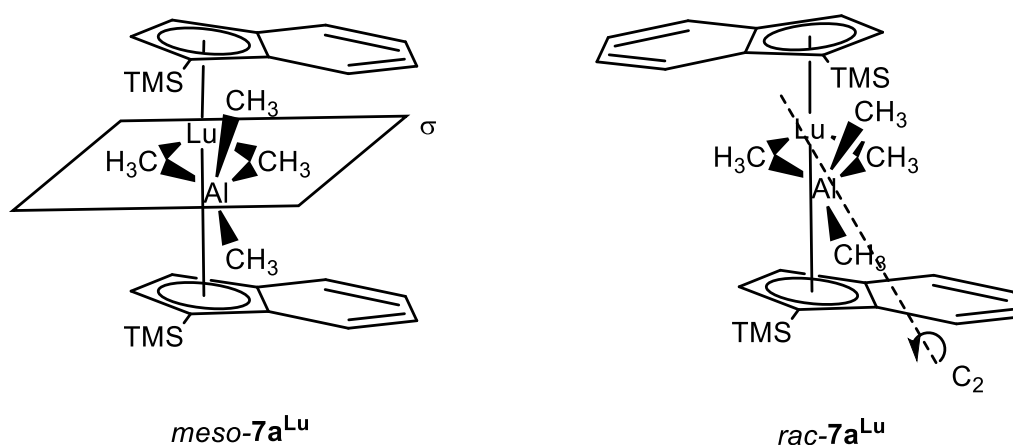
The influence of the substituent at the indenyl ligand also affects the conformation of the indenyl sandwich complexes (Scheme S3). The two indenyls without further substituents adopt an almost eclipsed conformation. The introduction of an ethyl group increases the steric congestion, which causes the indenyls to adopt a “staggered” conformation with a torsion

angle of  $178^\circ$ . The introduction of a *tert*-butyl group instead of an ethyl moiety increased the steric strain between the substituent and the aromatic six-membered ring, resulting in a torsion angle of  $130^\circ$ .



**Scheme S3:** Different conformations of indenyl sandwich complexes **4a<sup>Lu</sup>**, **5a<sup>Lu</sup>**, and **6a<sup>Lu</sup>**. Lutetium center and AlMe<sub>4</sub> moiety are omitted for clarity.

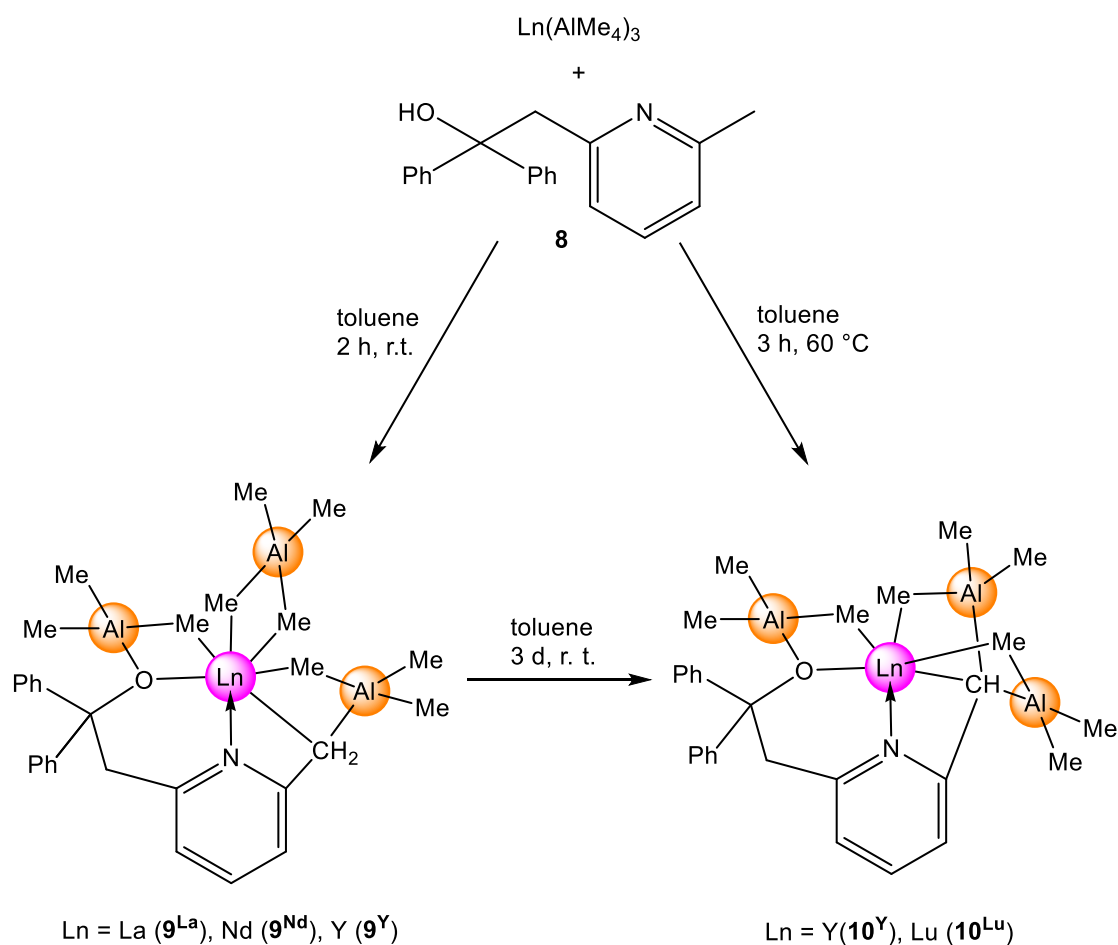
The sandwich complex **7a<sup>Lu</sup>** showed special behavior. Due to the trimethylsilyl substituent at C1, the ligand is prochiral. Therefore, two isomers could be detected by <sup>1</sup>H NMR spectroscopy. Depending on which of the enantiotopic sites (*re*- or *si*-site) the indenyl ligand reacts, either the racemic complex (*re/re* or *si/si*-coordination) or the *meso* isomer (*re/si*-coordination) were formed (Scheme S4). The *meso*:*rac* ratio was 9:1 while only the crystal structure of the *meso*-isomer could be isolated.



**Scheme S4:** Symmetry of *meso*- and *rac*-**7a<sup>Lu</sup>**.

## 2 Synthesis of Pincer-Like Rare-Earth-Metal Complexes

Several advantages of pincer complexes have already been discussed in Part A. Over the course of our own studies the synthesis of pyridyl-alkoxide complexes  $(\text{ONCH}_2)\text{Ln}(\text{AlMe}_4)(\text{AlMe}_3)_2$  ( $\text{Ln} = \text{La}$  (**9<sup>La</sup>**),  $\text{Nd}$  (**9<sup>Nd</sup>**),  $\text{Y}$  (**9<sup>Y</sup>**)) and  $(\text{ONCH})\text{Ln}(\text{AlMe}_3)_3$  ( $\text{Ln} = \text{Y}$  (**10<sup>Y</sup>**),  $\text{Lu}$  (**10<sup>Lu</sup>**)) was accomplished by deprotonation and C–H bond activation of 2-(6-methyl-2-pyridyl)-1,1-diphenyl-ethanol ( $\text{HONCH}_3$ , **8**) with  $\text{Ln}(\text{AlMe}_4)_3$  (Scheme S5).



**Scheme S5:** Synthesis of  $(\text{ONCH}_2)\text{Ln}(\text{AlMe}_4)(\text{AlMe}_3)_2$  (**9<sup>Ln</sup>**) and  $(\text{ONCH})\text{Ln}(\text{AlMe}_3)_3$  (**10<sup>Ln</sup>**) complexes.

The isolation of compound **9<sup>Ln</sup>** and **10<sup>Ln</sup>** revealed that the conversion of  $\text{Ln}(\text{AlMe}_4)_3$  with pyridyl-ethanol derivative **8** proceeds via (a) protonolysis to coordinate the rare-earth metal center in a bidentate fashion, (b) C–H bond activation to afford compounds **9<sup>Ln</sup>** for the middle- and large-sized metals, and (c) an additional C–H bond activation with another alkylaluminum moiety giving complexes **10<sup>Ln</sup>** for the middle- and small-sized metals. These

findings indicate that the formation of the final product was driven by steric constraints. Noteworthy, the only coproduct of the reaction cascade was methane.

In accord with the methane elimination protocol a tridentate ONCH<sub>x</sub> (x = 1, 2) pincer-like system was obtained. The reaction with Ln(AlMe<sub>4</sub>)<sub>3</sub> (Ln = La, Nd) gave selectively the mono C–H bond activated **9**<sup>Ln</sup>, while conducting the experiment with Lu(AlMe<sub>4</sub>)<sub>3</sub> it was only possible to isolate **10**<sup>Lu</sup> wherein a second C–H activation at the same carbon occurred. The ionic radius of yttrium is in between the radii of lanthanum and lutetium. Therefore, it was possible to isolate **9**<sup>Y</sup> and **10**<sup>Y</sup>. Unfortunately, **9**<sup>Y</sup> was labile in solution and reacts to **10**<sup>Y</sup>. It is not obvious, but both complexes are chiral around the metal center. In Figure S3 both enantiomers of **9**<sup>Nd</sup> and **10**<sup>Lu</sup> are displayed.

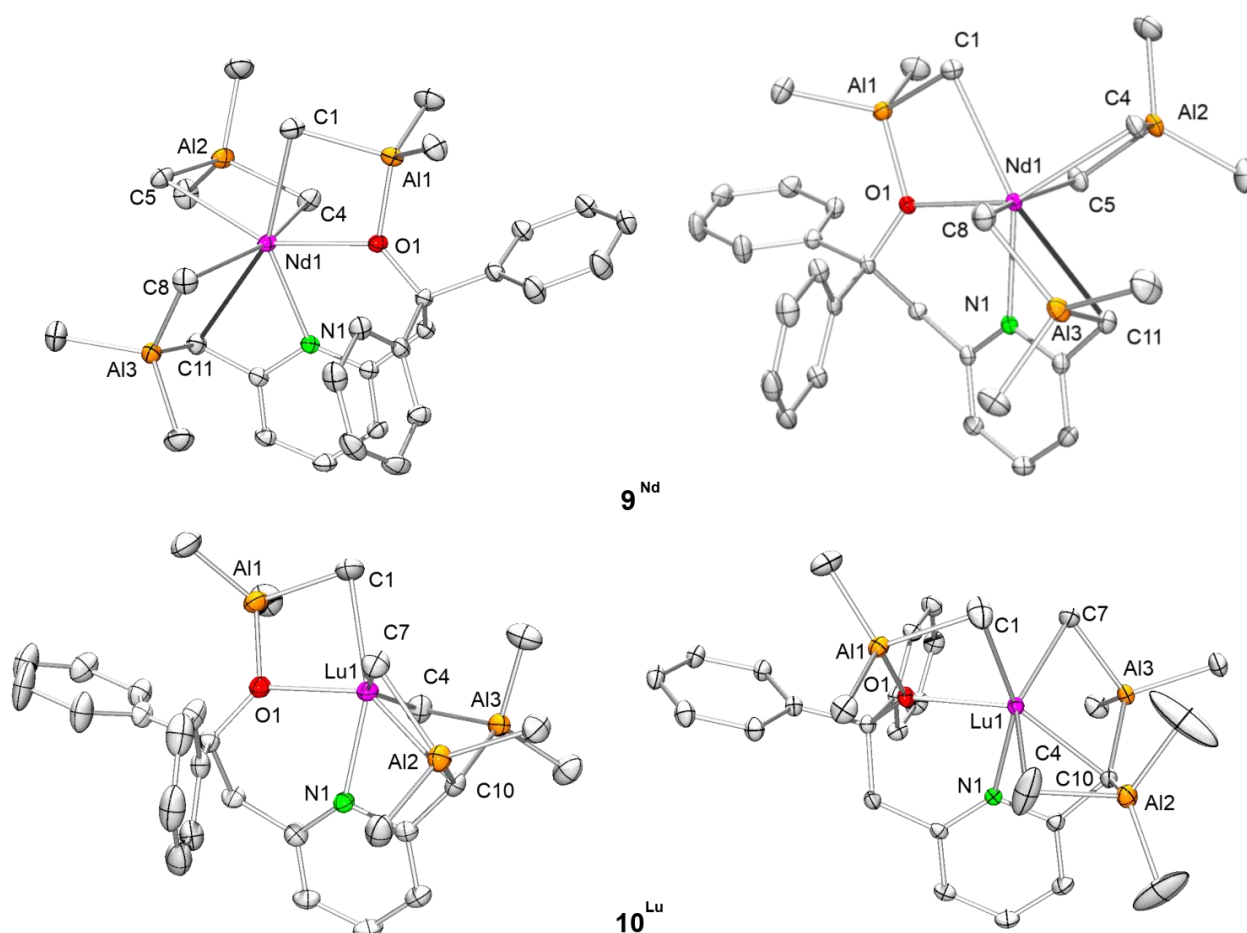


**Figure S3:** Solid-state structures of enantiomers of **9**<sup>Nd</sup> and **10**<sup>Lu</sup>.

Besides the solid-state structures, the chirality can also be detected by <sup>1</sup>H NMR spectroscopy. Herein, both –CH<sub>2</sub>– groups (signals 4 and 5, Figure S4) split into two doublets due to chemical inequality of the protons. At lower temperatures, the <sup>1</sup>H NMR spectrum of complex

**9<sup>La</sup>** shows also separate proton signals for every proton of the phenyl groups, resulting in 10 different signals (Figure S5).

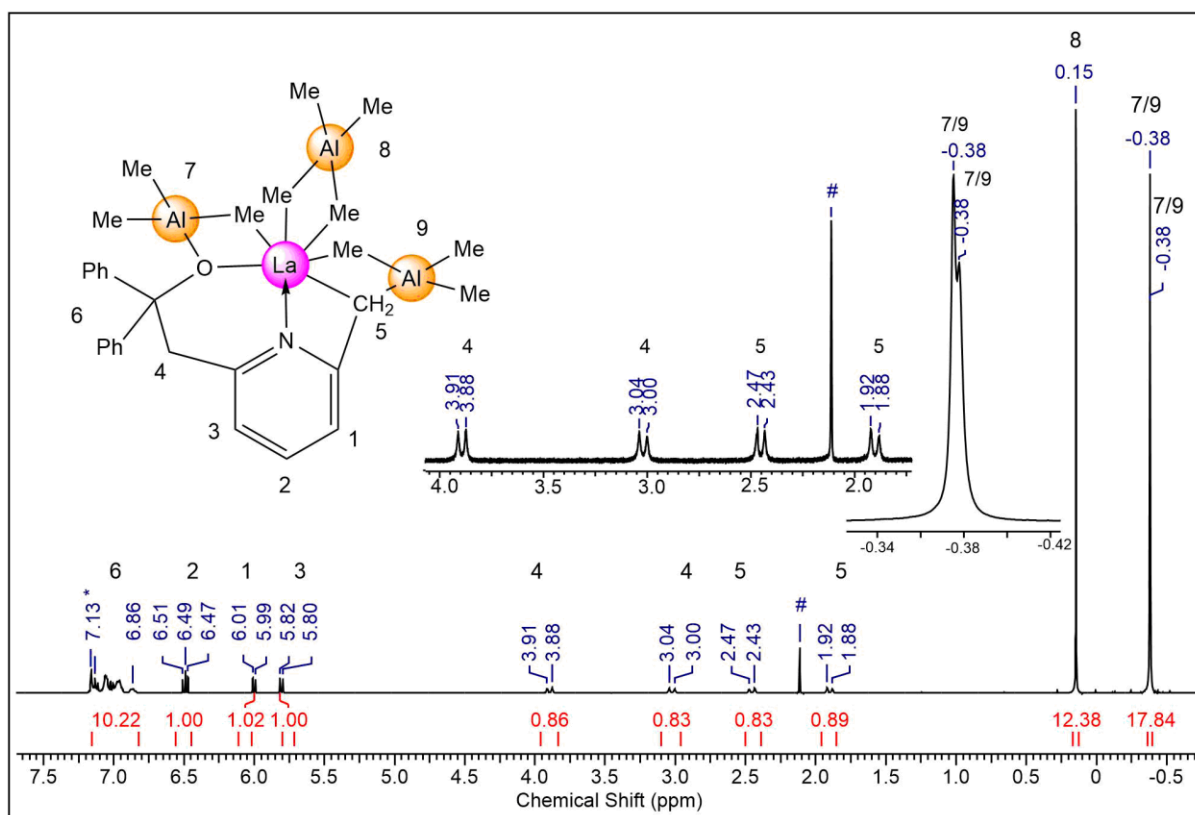


**Figure S4:** <sup>1</sup>H NMR spectrum of **9<sup>La</sup>** in C<sub>6</sub>D<sub>6</sub> (26 °C).

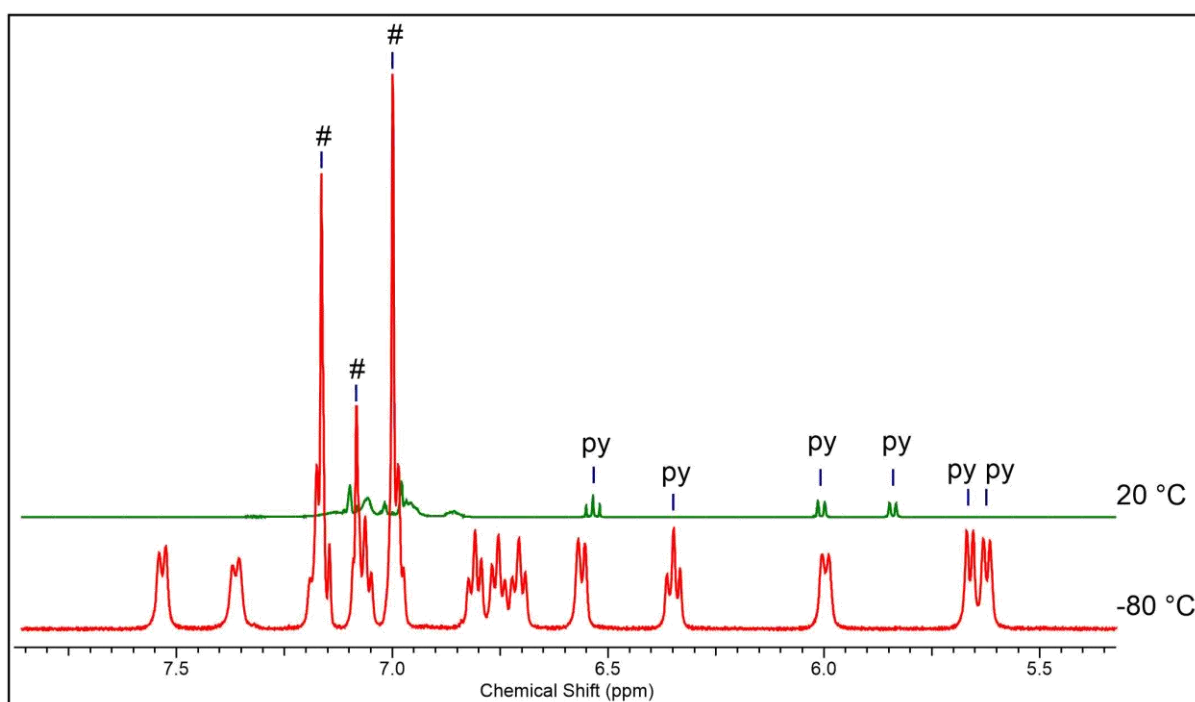


**Figure S5:** <sup>1</sup>H NMR spectrum of **9<sup>La</sup>** at -80 °C and 20 °C in tol-*d*<sub>8</sub>.

For complexes  $10^{Ln}$  the chirality indicated in the solid-state structure, could not be detected in the  $^1H$  NMR at ambient temperature. Decreasing the temperature, the mobility of the  $-CH_2-$   $CPh_2-$  linker decreased as well, indicated by the splitting of the signal of the remaining methylene group (Figure S6). This results in a rigid chiral system in accord with the solid-state structure, and the atropisomerism of complexes  $10^{Ln}$  is due to the axial chirality.

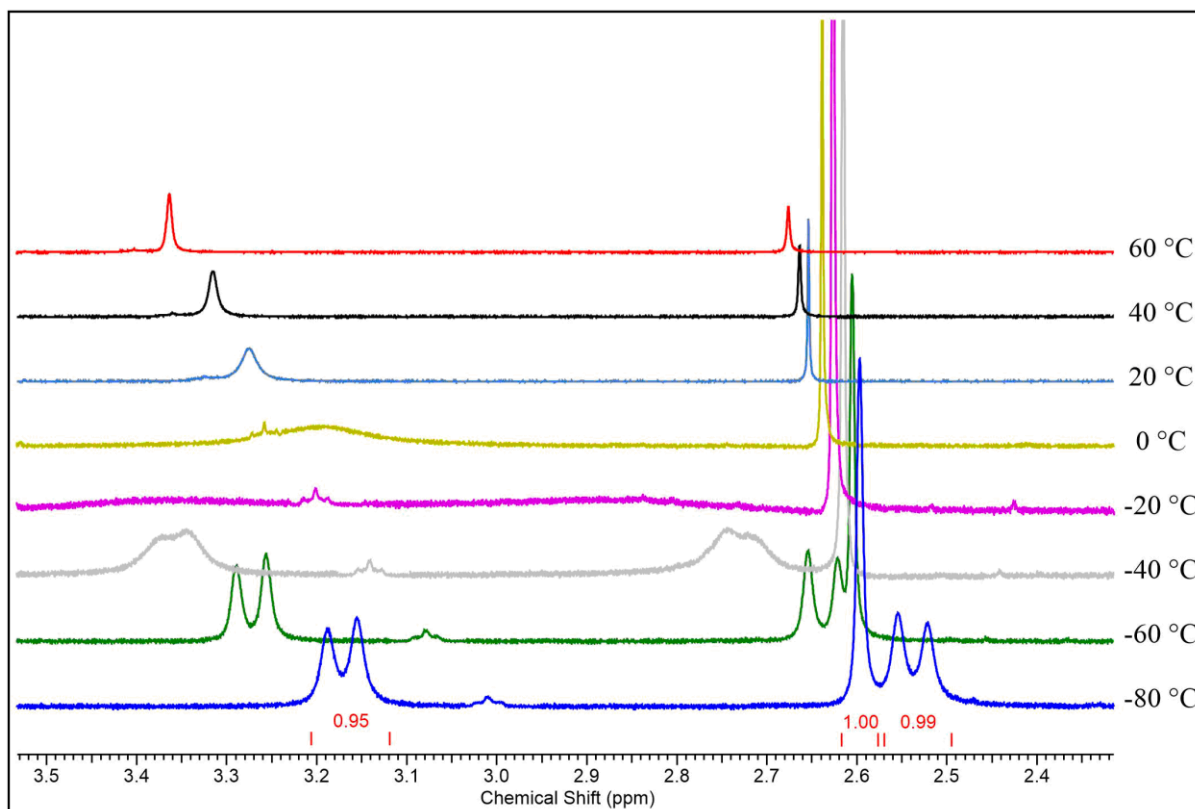
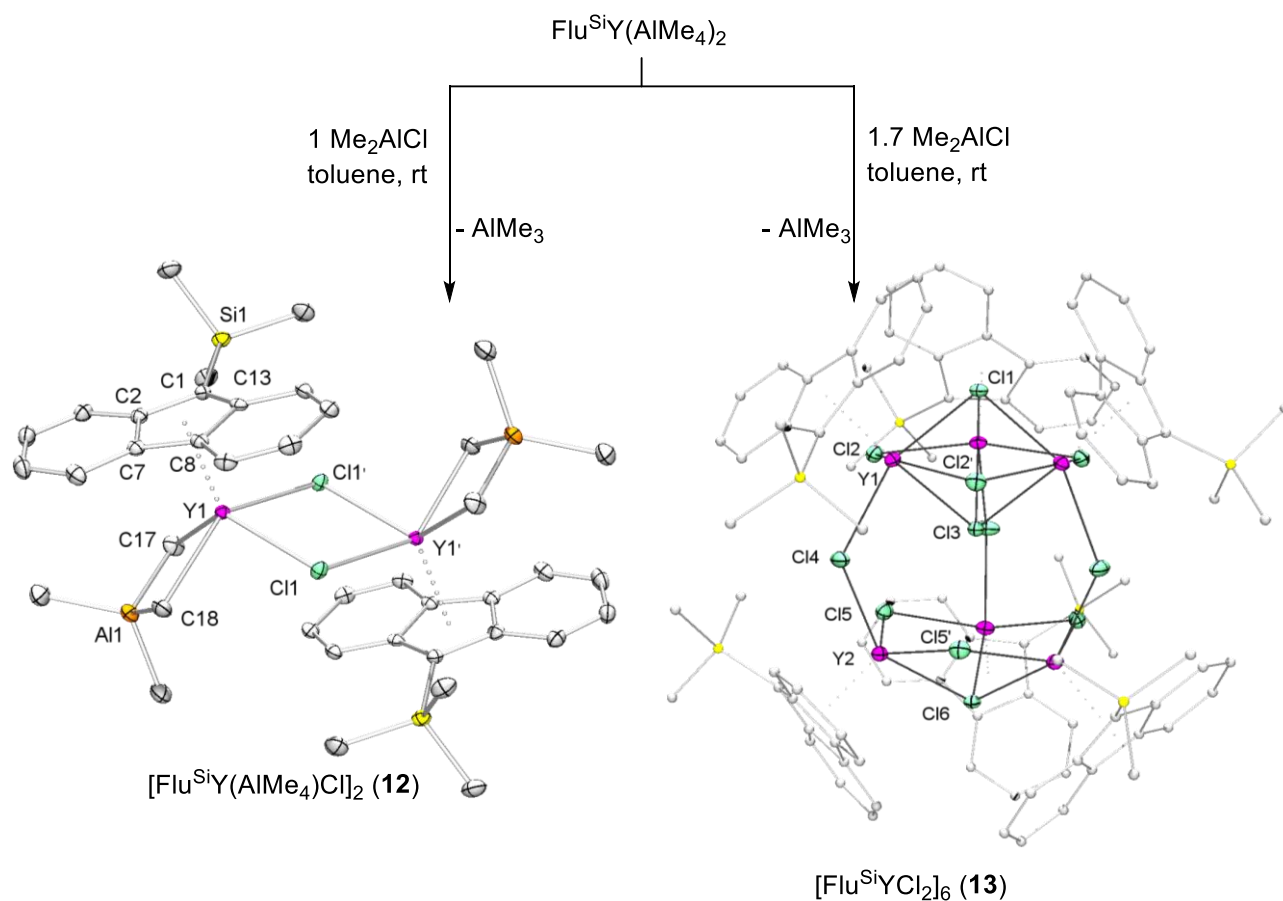


**Figure S6:** VT  $^1H$  NMR spectra of  $10^{Lu}$  at  $-80$  to  $60$  °C in toluene- $d_8$ .

### 3 Isoprene Polymerization with Rare-Earth-Metal Alkyl Complexes

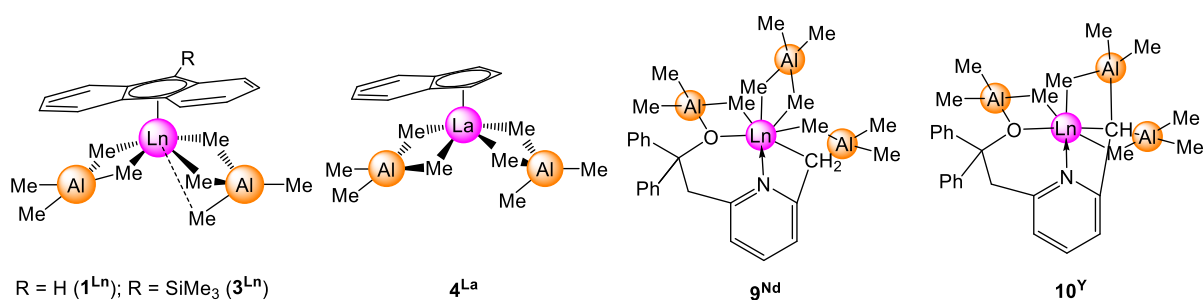
For the 1,3-diene polymerization homoleptic complexes  $Ln(AlMe_4)_3$  can be activated by  $Me_2AlCl$  (**D**) and  $Et_2AlCl$  (**E**). Employing these cocatalysts for the activation of indenyl- and fluorenyl half-sandwich complexes in the isoprene polymerization, no activity could be

detected. Reaction of  $\text{Flu}^{\text{SiY}}(\text{AlMe}_4)_2$  with **D** led to the formation of dimeric or higher aggregated clusters (Scheme S6).



**Scheme S6:** Synthesis of yttrium chloride dimers and clusters using  $\text{Flu}^{\text{SiY}}(\text{AlMe}_4)_2$  and  $\text{Me}_2\text{AlCl}$ .

In our studies the pincer-type complexes and moreover, the indenyl- and fluorenyl half-sandwich complexes show excellent activities in the isoprene polymerization upon activation with borate or borane activators ( $[\text{Ph}_3\text{C}][\text{B}(\text{C}_6\text{F}_5)_4]$  (**A**),  $[\text{PhNMe}_2\text{H}][\text{B}(\text{C}_6\text{F}_5)_4]$  (**B**), and  $\text{B}(\text{C}_6\text{F}_5)_3$  (**C**)). Selected polymerization results are compiled in Table S1.

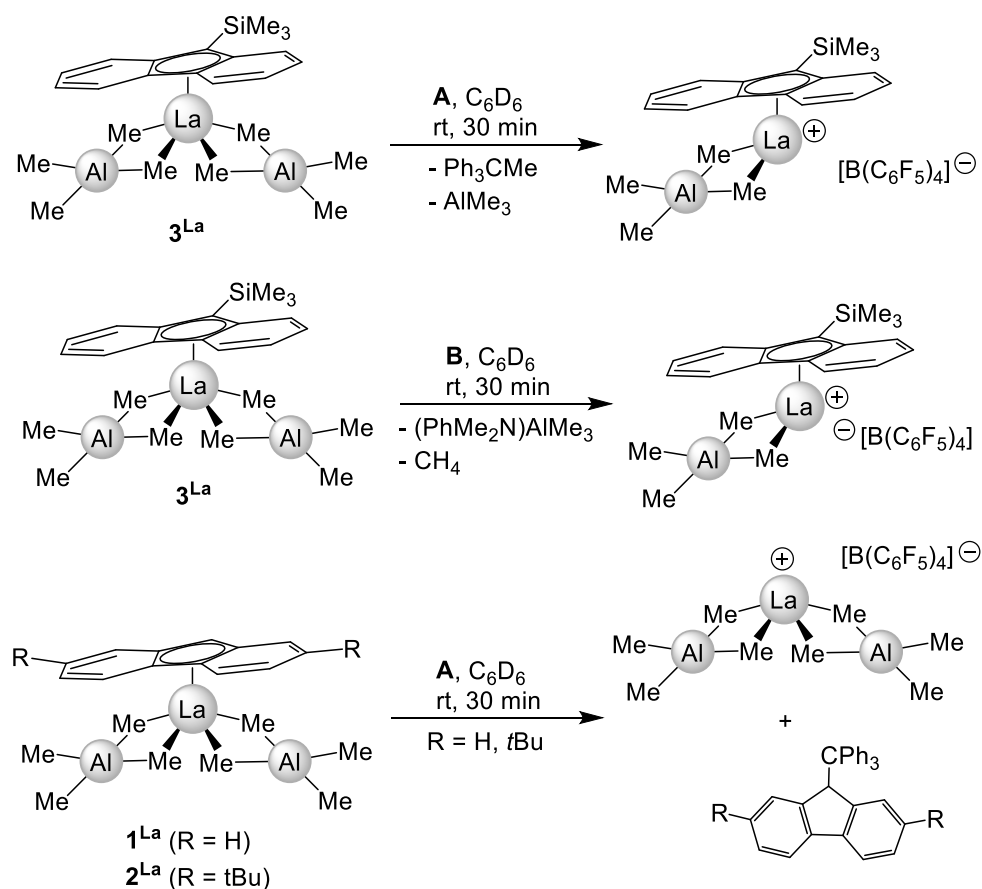
**Table S1:** Isoprene polymerization with rare-earth-metal tetramethylaluminates under study.

entry <sup>[a]</sup>	pre-catalyst	cocatalyst <sup>[b]</sup>	time [h]	yield [%]	<i>trans</i> -1,4- <sup>[c]</sup>	<i>cis</i> -1,4- <sup>[c]</sup>	3,4- <sup>[c]</sup>	$M_n^{[d]}$ (x10 <sup>4</sup> )	$M_w/M_n^{[d]}$	$T_g^{[e]}$ [°C]
1	$1^{La}$	<b>1A</b>	1	93	49.4	46.6	4.1	4.3	1.21	-61.3
2 <sup>[154]</sup>	La(AlMe <sub>4</sub> ) <sub>3</sub>	<b>1A</b>	1	>99	51.4	46.3	2.3	5.0	1.29	-
3	$3^{La}$	<b>1B</b>	1	98	80.0	9.6	10.4	4.9	1.17	-64
4	$3^{Nd}$	<b>1B</b>	1	96	54.1	25.9	20.0	5.4	1.13	-55
5	$3^Y$	<b>1B</b>	1	94	18.3	48.7	33.0	9.0	1.41	-43
6	$3^{Lu}$	<b>1B</b>	1	89	11.5	72.9	15.6	8.0	1.47	-55
7 <sup>f</sup>	$4^{La}$	<b>1A</b>	1	95	82.6	14.9	2.6	3.2	1.04	-65
8	$4^{La}$	<b>1A</b>	1	98	76.6	19.9	3.5	6.1	1.08	-63
9 <sup>g</sup>	$4^{La}$	<b>1A</b>	3	>99	77.7	18.4	3.9	9.1	1.07	-63
10 <sup>h</sup>	$4^{La}$	<b>1A</b>	2	99	84.8	12.8	2.5	6.2	1.05	-64
11	$9^{Nd}$	<b>1A</b>	1	82	47.6	47.7	4.8	9.7	1.29	-62
12	$9^{Nd}$	<b>2A</b>	1	93	12.8	74.4	12.8	9.9 <sup>i</sup>	6.50 <sup>i</sup>	-45
13	$10^Y$	<b>1B</b>	1	26	3.7	73.0	23.3	35.5 <sup>i</sup>	2.19 <sup>i</sup>	-47
14	$10^Y$	<b>2B</b>	0.25	92	0.0	83.5	16.5	35.9	2.83	-51

<sup>[a]</sup> General polymerization procedure: 0.02 mmol of pre-catalyst, 8 mL of toluene, 20 mmol of isoprene, 1 h, 40 °C. <sup>[b]</sup> **A** = [Ph<sub>3</sub>C][B(C<sub>6</sub>F<sub>5</sub>)<sub>4</sub>]; **B** = [PhNMe<sub>2</sub>H][B(C<sub>6</sub>F<sub>5</sub>)<sub>4</sub>]; C = B(C<sub>6</sub>F<sub>5</sub>)<sub>3</sub>; Catalyst pre-formation: 30 min. <sup>[c]</sup> Determined by <sup>1</sup>H-, and <sup>13</sup>C NMR spectroscopy in CDCl<sub>3</sub>. <sup>[d]</sup> Determined by GPC against polystyrene standards. <sup>[e]</sup> Determined by DSC at 20 K/min. <sup>f</sup> 10 mmol of isoprene, polymerization for 1 h. <sup>g</sup> 30 mmol of isoprene, polymerization for 3 h. <sup>h</sup> 2 × 10 mmol isoprene, addition of the second portion after 1 h, polymerization for 2 h in total. <sup>[i]</sup> generation of a bimodal species, listed entry only for the higher molecular peak, second peak was not possible to analyze.

The stoichiometric reactions of half-sandwich complex Flu<sup>Si</sup>La(AlMe<sub>4</sub>)<sub>2</sub> in combination with cocatalyst **A** or **B** were examined, see Scheme S7. In fact, for the reaction with complexes FluLa(AlMe<sub>4</sub>)<sub>2</sub> and Flu<sup>tBu</sup>La(AlMe<sub>4</sub>)<sub>2</sub> a different activation mechanism was found. In the cationization with cocatalyst **A** an abstraction of the fluorenyl group instead of the tetramethylaluminato moiety was observed, as displayed in Scheme S7. Thereby, the active complex is the same as the active catalyst resulting from the combination of La(AlMe<sub>4</sub>)<sub>3</sub> and **A**. Since there is the same active species, the polymer microstructure was similar, as depicted in Table S1, entry 1 and 2. The coupling reaction of the trityl moiety with the fluorenyl was exclusively observed for  $1^{La}$  and  $2^{Ln}$  (Ln = La, Y) in combination with cocatalyst **A**, while cocatalyst **B** showed the expected reaction pathway.





**Scheme S7:** Activation mechanism for fluorenyl rare-earth-metal half-sandwich complexes.

Since the  $\text{Flu}^{\text{Si}}$  ligand was inert toward this unusual ligand abstraction and the entire Ln metal size range could be obtained as half-sandwich complexes, the impact of the ionic radii of the rare-earth metal on the microstructure of the polymer has been examined. Herein, the central metal has a significant influence on the *cis*-1,4- and *trans*-1,4-content of the polymer. The isoprene polymerization with the binary system  $\text{Flu}^{\text{Si}}\text{La}(\text{AlMe}_4)_2/\mathbf{B}$ , gave polyisoprene with a high *trans*-1,4-content of 80.0% and 9.6% *cis*-1,4-content (Table S1, entry 3). By decreasing the ionic radius of the rare earth metal, also the *trans*-1,4-content decreased while the *cis*-1,4-content increased (Table S1, entry 3-6).

For indenyl half-sandwich complexes this trend could not be determined since it was not possible to obtain half-sandwich complexes with different rare-earth metals. But it has been tested if the system fulfills the requirements of a living polymerization. Therefore, different amounts of isoprene have been polymerized with  $\text{IndLa}(\text{AlMe}_4)_2$  activated by cocatalyst **A**

(Table S1, entry 7-9). Herein, the molecular weight of the polymer increases linearly with the added amount of isoprene, while the polydispersity index remained constant (Figure S7). Furthermore, it was possible to polymerize a certain amount of polymer and add subsequently a second portion of isoprene, while the resulting polymer was the same as if the total amount of isoprene was added at once (Table S1, entry 10).

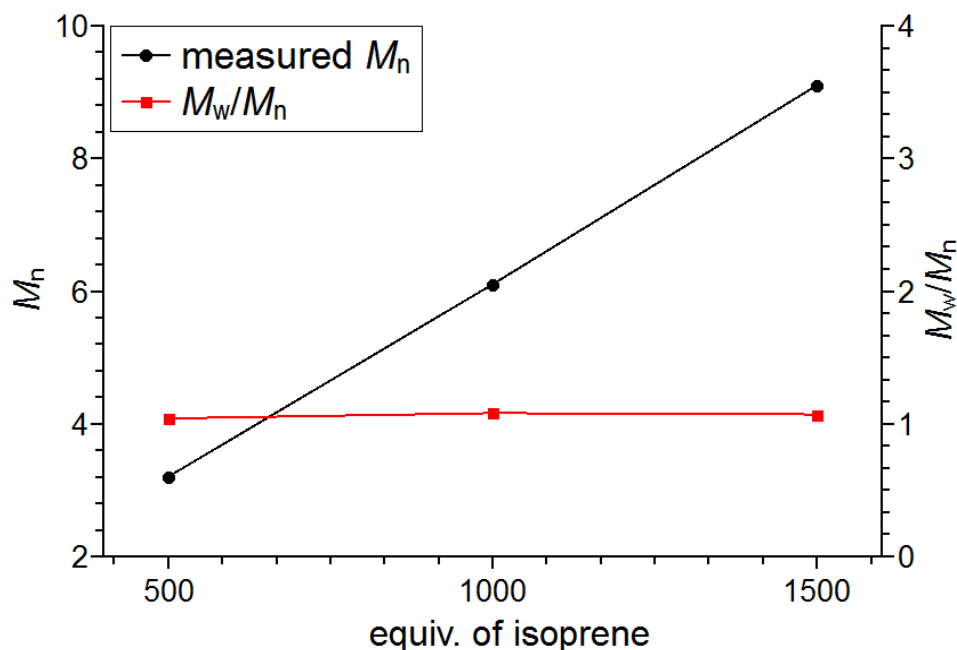


**Figure S7:** Molecular weight vs. isoprene equivalents (■) and  $M_w/M_n$  vs. isoprene equivalents (●).

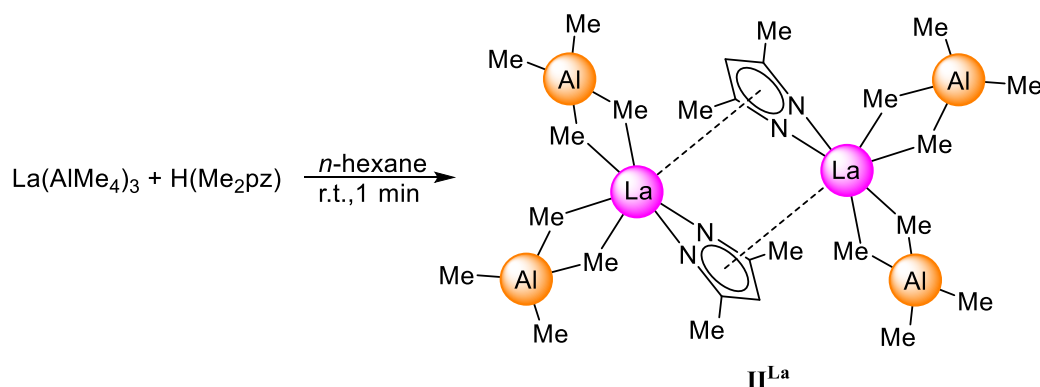
The experiments with the pincer complexes **9<sup>La</sup>** and **10<sup>La</sup>** revealed that the amount of cocatalyst effects the polymerization reaction as well. The addition of a second equivalent of cocatalyst led to an increase of the reaction rate (Table S1, entry 11-14). Remarkable is that the second equivalent of cocatalyst also led to an increase of the *cis*-1,4-content in the polymer.

C

**Unpublished Results**

Please note that the studies on the coordination polymerization obtained in collaboration with the Bridgestone company, Japan, are not part of this thesis. Therefore, only investigations concerning pyrazolate complexes and their polymerization performance are discussed in this section.

The protonolysis of  $\text{La}(\text{AlMe}_4)_3$  with  $\text{HMe}_2\text{pz}$  afforded dimeric complexes  $[(\text{Me}_2\text{pz})\text{La}(\text{AlMe}_4)_2]_2$  (**II<sup>La</sup>**, Scheme C1).



**Scheme C1:** Synthesis of  $[(\text{Me}_2\text{pz})\text{La}(\text{AlMe}_4)_2]_2$  (**II<sup>La</sup>**).

The solid-state structure of the lanthanum congener (Figure C1) is isostructural to the neodymium complex obtained previously by coworker DANIEL WERNER. Herein, the lanthanum center is coordinated by two tetramethylaluminato moieties in the usual  $\eta^2$  mode. The La1–C distances of C1/2/4/5 2.720(2) - 2.77(2) Å are similar to the bond lengths in  $\text{Cp}^{\text{R}}$  half-sandwich complexes (2.694(1) - 2.790(2) Å).<sup>[89]</sup> The pyrazolato ligands are in the bridging position and coordinate to the lanthanum center with both nitrogens in a  $\eta^2$  fashion and the aromatic  $\pi$ -system in the  $\eta^5$  bonding mode. The La1–N1/2 distances of 2.61(1) and 2.52(1) Å are similar to La–N(pz) distances in  $[\text{La}(\text{Me}_2\text{pz})_3]_n$  (2.475(3) - 2.617(3) Å).<sup>[161]</sup> The lanthanum pyrazolyl centroid distance of 2.725 Å is significantly shorter than in the lanthanum pyrazolate complex  $[\text{La}(\text{Me}_2\text{pz})_3]_n$  (2.821(2) – 2.872(2) Å) indicating a stronger interaction between lanthanum and the aromatic  $\pi$ -system.<sup>[161]</sup>

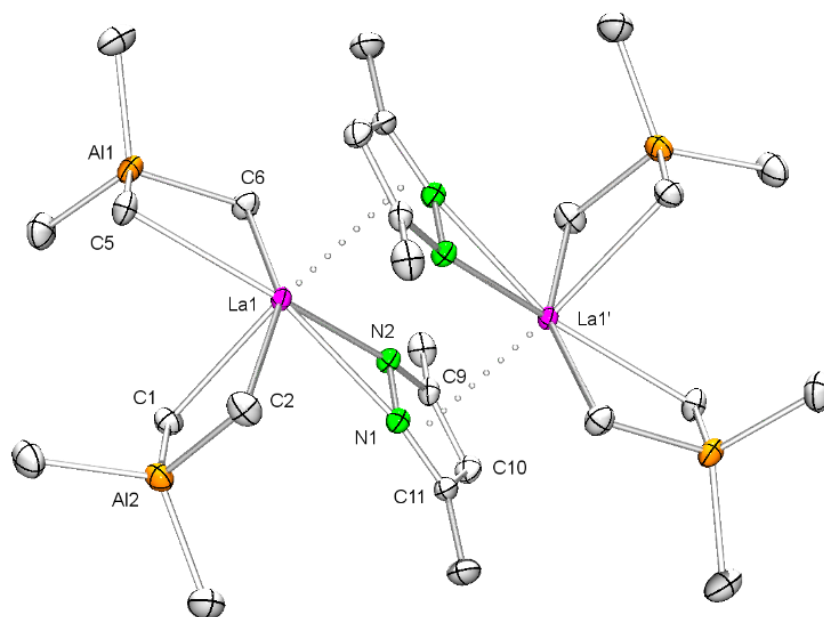
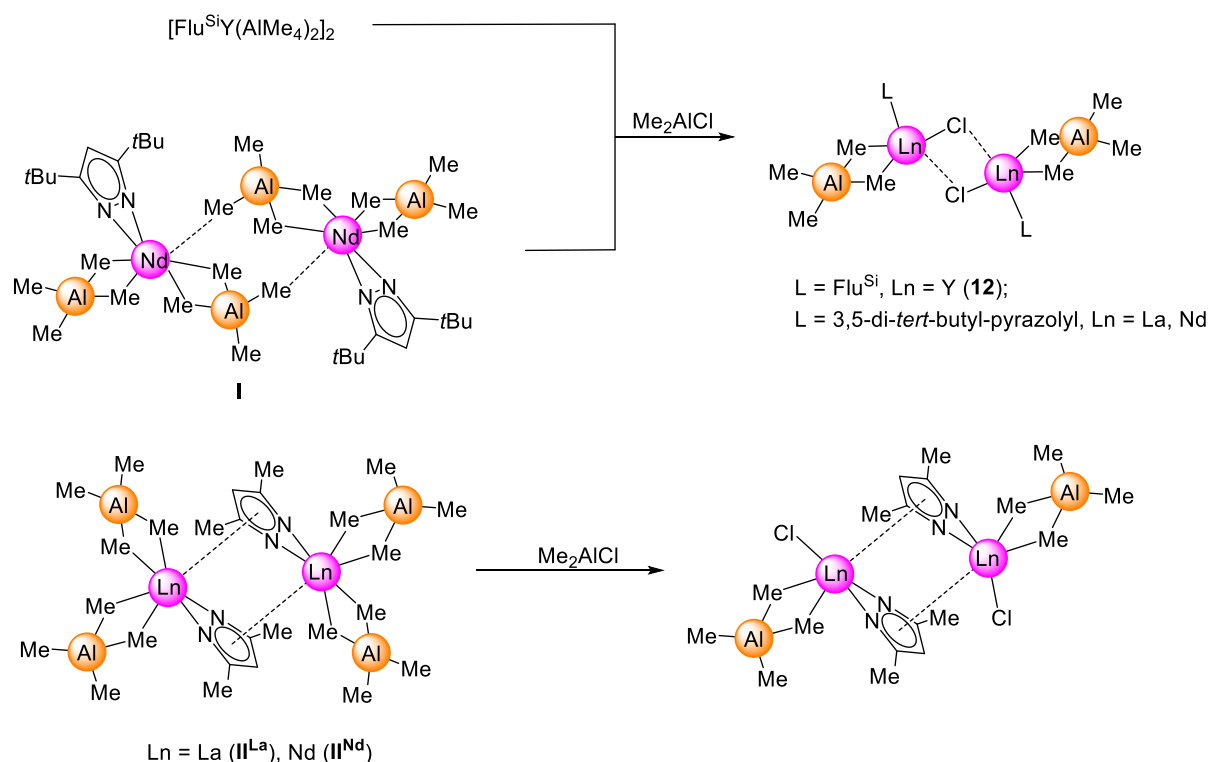


**Figure C1:** Solid-state structure of  $(\text{Me}_2\text{pz})\text{La}(\text{AlMe}_4)_2$  ( $\text{II}^{\text{La}}$ ). Hydrogen atoms are omitted for clarity. Atomic displacement parameters are set at the 50% probability level. Selected bond lengths [ $\text{\AA}$ ] and angles [deg]: La1–C1 2.720(2), La1–C2 2.73(2), La1–C5 2.74(2), La1–C6 2.78(2), La1 $\cdots$ Al1 3.306(8), La1 $\cdots$ Al2 3.288(8), La1–N1 2.61(1), La1–N2 2.52(1), La1 $\cdots$ Ct 2.725.

In this study the polymerization performances of precatalysts  $[\text{R}_2\text{pzLn}(\text{AlMe}_4)_2]_2$  ( $\text{R} = \text{Me}$ ,  $t\text{Bu}$ ;  $\text{Ln} = \text{La}$ ,  $\text{Nd}$ ) upon activation with cocatalysts **A**, **B**, **C**, **D**, and **E** have been assessed. The structural analysis of complex  $[(t\text{Bu}_2\text{pz})\text{Nd}(\text{AlMe}_4)_2]$  (**I**) by means of single crystal XRD revealed a similar solid-state structure as of dimeric half-sandwich complexes (Scheme C2). Noteworthy, upon activation of  $[\text{AlMe}_4]$  bridged dimeric precatalysts with chlorinating agents **D** or **E** chloride bridged dimers form, which show no activity in isoprene polymerization (Scheme C2). For comparison, the pyrazolato bridged complexes  $[(\text{Me}_2\text{pz})\text{Ln}(\text{AlMe}_4)_2]_2$  ( $\text{II}^{\text{La}}$ ,  $\text{II}^{\text{Nd}}$ ) are active in polymerization reactions upon activation with cocatalyst **D** and **E**. Herein, the structural motif differs from established half-sandwich complexes and **I**. The significant difference in activity might be due to the coordination chemistry of heteroleptic complexes  $\text{II}^{\text{La}}$  and  $\text{II}^{\text{Nd}}$ . Complex **I** displayed the same reactivity in the polymerization as fluorenyl and indenyl half-sandwich complexes and also has the same structural motif in the solid state, indicating similar coordination of the chlorido and  $\text{AlMe}_4$  ligand. Since fluorenyl half-sandwich complexes form a dimeric complex with one equivalent of cocatalyst **D**, a similar finding for **I** is possible (Scheme C2). For complexes  $\text{II}^{\text{La}}$  and  $\text{II}^{\text{Nd}}$  the pyrazolato ligand is already in a bridging position, therefore the chlorido ligands coordinates terminally. Thereby two different structural motifs are obtained upon addition with **D** (Scheme C2). The structural differences and more precisely the coordination of the pyrazolato, chloride and alkylaluminum

ligands indicate the impact on the polymerization performance: complexes  $\text{II}^{\text{La}}$  and  $\text{II}^{\text{Nd}}$  were active, while **I** was inactive for isoprene polymerization upon activation with **D** or **E**.



**Scheme C2:** Reaction of **I**,  $\text{II}^{\text{Ln}}$  with  $\text{Me}_2\text{AlCl}$ .

The microstructure of the polyisoprene obtained by  $\text{II}^{\text{Ln}}$  bears similarity to polymers received from precatalysts  $\text{Ln}(\text{AlMe}_4)_3$ . Therefore, another activation mechanism for  $\text{II}^{\text{Ln}}$  is also possible. A ligand abstraction as observed for fluorenyl half-sandwich complexes (Chapter B 3) offers also an explanation for the observed activity in the isoprene polymerization.

**Table C1:** Isoprene polymerization with **I**, **II<sup>Ln</sup>**.

entry <sup>[a]</sup>	precatalyst	cocatalyst <sup>[b]</sup>	Nd:cocatalyst ratio	yield [%]	<i>cis</i> -1,4- <sup>[c]</sup>	<i>trans</i> -1,4- <sup>[c]</sup>	3,4- <sup>[c]</sup>	$M_n$ <sup>[d]</sup> ( $\times 10^4$ )	$M_w/M_n$ <sup>[d]</sup>	$T_g$ <sup>[e]</sup> [°C]
1	<b>I</b>	<b>A</b>	1:1	98	37.3	50.6	12.1	10.8	1.39	-57.5
2	<b>I</b>	<b>B</b>	1:1	95	46.2	41.4	12.4	11.5	1.41	-57.3
3	<b>I</b>	<b>C</b>	1:1	79	73.5	22.0	4.5	35.8	1.27	-59.0
4	<b>I</b>	<b>D</b>	1:1	0	-	-	-	-	-	-
5	<b>I</b>	<b>E</b>	1:1	tr	-	-	-	-	-	-
6	<b>II<sup>La</sup></b>	<b>A</b>	1:1	64	45.5	49.4	4.1	5.4	1.21	-
7	<b>II<sup>La</sup></b>	<b>B</b>	1:1	59	50.1	45.3	4.6	6.2	1.20	-
8	<b>II<sup>La</sup></b>	<b>C</b>	1:1	23	65.7	31.2	3.1	1.8	1.22	-
9	<b>II<sup>La</sup></b>	<b>D</b>	1:1	11	84.2	12.3	3.5	1.2	19.52	-63.6
10	<b>II<sup>La</sup></b>	<b>E</b>	1:1	19	89.4	7.2	3.4	1.3	19.52	-62.4
11	<b>II<sup>Nd</sup></b>	<b>A</b>	2:1	92	55.3	39.7	5.0	3.2	1.33	-64.7
12	<b>II<sup>Nd</sup></b>	<b>B</b>	2:1	91	61.4	33.3	5.3	3.3	1.34	-63.3
13	<b>II<sup>Nd</sup></b>	<b>C</b>	2:1	60	47.7	48.6	3.7	3.9	1.77	-64.4
14	<b>II<sup>Nd</sup></b>	<b>D</b>	2:1	20	98.2	0.0	1.8	6.7	9.67	-62.3
15	<b>II<sup>Nd</sup></b>	<b>E</b>	2:1	14	97.1	1.3	1.6	2.0	8.2	-64.2
16	<b>II<sup>Nd</sup></b>	<b>A</b>	1:1	99	60.0	34.4	5.6	2.9	1.71	-63.7
17	<b>II<sup>Nd</sup></b>	<b>B</b>	1:1	86	67.2	27.0	5.8	3.2	1.51	-64.7
18	<b>II<sup>Nd</sup></b>	<b>C</b>	1:1	79	73.7	22.3	4.0	8.5	1.59	-64.5
19	<b>II<sup>Nd</sup></b>	<b>D</b>	1:1	97	97.9	0.0	2.1	4.6	4.27	-64.4
20	<b>II<sup>Nd</sup></b>	<b>E</b>	1:1	97	96.1	1.9	2.0	4.9	3.34	-64.1

<sup>[a]</sup> General polymerization procedure: 0.02 mmol of precatalyst, 8 mL of toluene, 20 mmol of isoprene, 1 h, 40 °C. <sup>[b]</sup> **A** = [Ph<sub>3</sub>C][B(C<sub>6</sub>F<sub>5</sub>)<sub>4</sub>]; **B** = [PhNMe<sub>2</sub>H][B(C<sub>6</sub>F<sub>5</sub>)<sub>4</sub>]; **C** = B(C<sub>6</sub>F<sub>5</sub>)<sub>3</sub>; Catalyst pre-formation: 30 min. <sup>[c]</sup> Determined by <sup>1</sup>H, and <sup>13</sup>C NMR spectroscopy in CDCl<sub>3</sub>. <sup>[d]</sup> Determined by GPC against polystyrene standards. <sup>[e]</sup> Determined by DSC at 20 K/min.

Polymerization reactions using binary system **I/A** and **I/B** revealed no significant selectivity regarding the microstructure (Table C1, entry 1,2), while cocatalyst **C** shifted the selectivity towards *cis*-1,4-polyisoprene (73.5% Table C1, entry 3). The molecular weights of the polyisoprenes obtained by precatalyst **I** were all rather high ( $M_n = 10.8 - 35.8 \times 10^4$ ), while the molecular weight distribution was narrow (1.27 – 1.41). The selectivity, and hence, the microstructure of the polymer in binary systems **II<sup>La</sup>** and **II<sup>Nd</sup>** in combination with cocatalyst **A**, **B** or **C** was random. Fortunately, enhancement of the selectivity is achieved upon increasing the cocatalyst:neodymium ratio (Table C1, entry 13 and 18). A significant increase in selectivity was observed using **II<sup>La</sup>** and **II<sup>Nd</sup>** upon addition of cocatalyst **D** or **E**. The *cis*-1,4-content was up to 98.2% without any further *trans*-1,4-content Table C1, entry 14). The activity increased significantly upon increasing the cocatalyst:neodymium ratio (Table C1, entry 14 and 19), while the microstructure remains similar. The *cis*-1,4-selectivity and activity of **II<sup>Nd</sup>** was significantly higher than for **II<sup>La</sup>** (“Neodymium effect”,<sup>[162]</sup> Table C1, entry 9 and 19). The use of **D** or **E** as cocatalyst with **II<sup>Nd</sup>** afforded polyisoprene with high PDI’s (3.34 – 9.67) compared to cocatalysts **A**, **B** or **C** (1.33 – 1.77).

## Experimental

**General procedures.** All manipulations were performed with rigorous exclusion of air and water, using standard Schlenk, high-vacuum, and glovebox techniques (MBraun UNIlab-pro-dp; < 0.5 ppm O<sub>2</sub>, < 0.5 ppm H<sub>2</sub>O). Toluene and *n*-hexane were purified by using Grubbs-type columns (MBraun SPS, solvent purification system) and stored inside a glovebox. [D<sub>8</sub>] thf and [D<sub>6</sub>]benzene were purchased from Aldrich, degassed and dried over NaK for 24 h, filtered, and stored inside a glovebox. [Ph<sub>3</sub>C][B(C<sub>6</sub>F<sub>5</sub>)<sub>4</sub>] (**A**), [PhNM<sub>2</sub>H][B(C<sub>6</sub>F<sub>5</sub>)<sub>4</sub>] (**B**), and B(C<sub>6</sub>F<sub>5</sub>)<sub>3</sub> (**C**) were obtained from Boulder Scientific Company and used without further purification. 3,5-dimethylpyrazole and 3,5-di-*tert*-butylpyrazole, trioctylaluminum, and isoprene were obtained from Sigma Aldrich. Isoprene was dried over trioctylaluminum and distilled prior to use. Homoleptic Ln(AIME<sub>4</sub>)<sub>3</sub> (Ln = La, Nd) were prepared according to literature procedures.<sup>[155]</sup> NMR spectra were recorded on a Bruker AVBII+400 (<sup>1</sup>H: 400.11 MHz; <sup>13</sup>C: 100.61 MHz) spectrometer. <sup>1</sup>H and <sup>13</sup>C NMR resonances are referenced to internal solvent resonances and reported in parts per million relative to tetramethylsilane (TMS). Coupling constants are given in Hz. Elemental analyses were performed on an Elementar Vario Micro Cube. IR spectra were recorded on a NICOLET 6700 FTIR spectrometer with a DRIFT cell (KBr window). Size exclusion chromatography (SEC) was performed on a Viscotek GPCmax apparatus and a model TDA 302 triple detector array. Sample solutions (1.0 mg polymer per mL thf) were filtered through a 0.45 μm syringe filter prior to injection. The flow rate was mL/min. dn/dc and dA/dc data were determined by means of the integrated OmniSec™ software. The microstructure of the polyisoprenes was determined on a Bruker AVBII+400 and Bruker DRX250 spectrometer in [D]chloroform at ambient temperature. Glass transition temperature (*T*<sub>g</sub>) of the polyisoprenes were determined on a Perkin-Elmer DSC 8000 with heating rates of 20 K/min and cooling rates of 60 K/min.

### Synthesis of [(Me<sub>2</sub>pz)La(AIME<sub>4</sub>)<sub>2</sub>]<sub>2</sub> (II<sup>La</sup>)

A toluene solution (1.2 mL) of Me<sub>2</sub>pzH (60.0 mg, 0.625 mmol) was added to a solution (1.2 mL) of La(AIME<sub>4</sub>)<sub>3</sub> (250 mg, 0.625 mmol) in *n*-hexane. The mixture was stirred for one minute. Afterwards the precipitated product was centrifuged off to afford [(Me<sub>2</sub>pz)La(AIME<sub>4</sub>)<sub>2</sub>]<sub>2</sub> as a white powder (174 mg, 57%). Colorless single crystals suitable for X-ray crystallography were grown from a saturated toluene solution at -35 °C. <sup>1</sup>H NMR (C<sub>6</sub>D<sub>6</sub> 400 MHz, 300 K): δ = -0.22 (s, 24 H, Al(Me)<sub>4</sub>), 2.02 (s, 6 H, Me<sub>2</sub>pz), 5.53 (s, 1 H, Me<sub>2</sub>pz) ppm. <sup>13</sup>C NMR spectra were not obtained due to the low solubility of **I**. IR (DRIFT): ν = 3107 (w), 2925 (s), 2891 (s), 2818 (w), 2791 (w), 1506 (s), 1418 (w), 1400 (m), 1384 (w), 1373 (w), 1203 (s), 1182 (vs), 1035 (w), 1004 (w), 855 (w), 734 (m), 727 (vs), 721 (vs), 715 (vs), 707 (s), 698 (vs), 691 (vs), 679 (vs), 663 (m), 655 (w), 645 (w), 638 (w), 628 (w), 603 (s), 594 (m), 586 (s), 571 (s), 563 (vs), 547 (s) cm<sup>-1</sup>. Elemental analysis calcd. (%) for C<sub>26</sub>H<sub>62</sub>Al<sub>4</sub>N<sub>4</sub>La<sub>2</sub> (816.55 g mol<sup>-1</sup>): C 38.24, H 7.65, N 6.86; found: C 38.38, H 7.55, N 6.86.

### Synthesis of [(Me<sub>2</sub>pz)Nd(AIME<sub>4</sub>)<sub>2</sub>]<sub>2</sub> (II<sup>Nd</sup>)

A toluene solution of Me<sub>2</sub>pzH (1.2 mL) (150 mg, 0.156 mmol) was added to a solution (1.2 mL) of Nd(AIME<sub>4</sub>)<sub>3</sub> (63.4 mg, 0.156 mmol) in *n*-hexane. The mixture was shaken, and a colorless precipitate formed. The mixture was filtered and stored at -35 °C to afford blue single crystals of [(Me<sub>2</sub>pz)Nd(AIME<sub>4</sub>)<sub>2</sub>]<sub>2</sub> suitable for X-ray crystallography (47.5 mg, 70%). The crystals were washed with *n*-hexane and dried *in vacuo*. <sup>1</sup>H NMR (C<sub>6</sub>D<sub>6</sub>, 400 MHz, 300 K): δ = -1.92 (s, 1 H, Me<sub>2</sub>pz), 1.90 (s, 6 H, Me<sub>2</sub>pz), 10.31 (s, 1 H), 14.0 (br s, 24 H, Al(Me)<sub>4</sub>) ppm. IR (DRIFT): ν = 3114 (vw), 2927 (m), 2889 (m), 2822 (w), 1518 (s), 1507 (s), 1267 (w), 1204 (m), 1186 (s), 1148 (vw), 1037 (vw), 1000 (w), 945 (w), 829 (w), 714 (vs), 696 (vs), 569 (s), 545 (m) cm<sup>-1</sup>. Elemental analysis calcd. (%) for C<sub>26</sub>H<sub>62</sub>Al<sub>4</sub>N<sub>4</sub>Nd<sub>2</sub> (827.21 g mol<sup>-1</sup>): C 37.75, H 7.56, N 6.77; found: C 37.74, H 7.52, N 6.59.

### Synthesis of [(*t*Bu<sub>2</sub>pz)Nd(AIME<sub>4</sub>)<sub>2</sub>]<sub>2</sub> (I)

Nd(AIME<sub>4</sub>)<sub>3</sub> (80.5 mg, 0.199 mmol) was dissolved in toluene (1.2 mL), and a toluene solution (1.2 mL) of *t*Bu<sub>2</sub>pzH (36.0 mg, 0.199 mmol) was added dropwise under vigorous stirring. After one hour the sample was evaporated to dryness *in vacuo* to afford a pale blue powder. The solid was dissolved in *n*-hexane, and crystallization under reduced pressure, gave large pale blue needles of [(*t*Bu<sub>2</sub>pz)Nd(AIME<sub>4</sub>)<sub>2</sub>]<sub>2</sub>, the supernatant was then discarded. The crystals were further dried *in vacuo* to afford a microcrystalline powder (80.6 g, 81%). <sup>1</sup>H NMR (C<sub>6</sub>D<sub>6</sub>, 400 MHz, 300 K): δ = -0.21 (s), 0.67 (s), 1.26 (s), 3.30 (br s), 4.63 (br s), 10.27 (br s), 24.76 ppm (br s) ppm. IR (DRIFT): ν = 2964 (s), 2917 (s), 2882 (s), 2784 (m), 1537 (vw), 1515 (m), 1484 (vw), 1460 (m), 1442 (m), 1417 (w), 1392 (vw), 1362 (m), 1309 (vw), 1293 (vw), 1255 (m), 1204 (s), 1198 (s), 1094 (vw), 1070 (vw), 1031 (m), 978 (w), 816 (w), 810 (w), 775 (w), 767 (vw), 723 (s), 715 (s), 708 (vs), 704 (vs), 698 (vs), 685 (vs), 685 (s), 677 (m), 661 (m), 638 (w), 624 (m) cm<sup>-1</sup>. Elemental analysis calcd. (%) for C<sub>19</sub>H<sub>43</sub>Al<sub>2</sub>N<sub>2</sub>Nd (497.76 g mol<sup>-1</sup>): C 45.84, H 8.71, N 5.63; found: C 46.27, H 9.02, N 4.80.



**D**

**Bibliography**

- [1] H. J. Paul, R. L. Banks, *Polymers and Production Thereof*, **1958**, US2825721A.
- [2] F. Eric, O. Reginald, P. John, W. Edmond, *Improvements in or Relating to the Polymerisation of Ethylene*, **1937**, GB471590A.
- [3] K. Ziegler, H. Breil, E. Holzkamp, H. Martin, *Verfahren zur Herstellung von hochmolekularen Polyäthylenen*, **1960**, DE973626C.
- [4] K. Ziegler, E. Holzkamp, H. Breil, H. Martin, *Angew. Chem.* **1955**, 67, 426–426.
- [5] K. Ziegler, E. Holzkamp, H. Breil, H. Martin, *Angew. Chem.* **1955**, 67, 541–547.
- [6] M. P. McDaniel, in *Adv. Catal.* (Eds.: B.C. Gates, H. Knözinger), Academic Press, **2010**, pp. 123–606.
- [7] K. Ziegler, *Angew. Chem.* **1964**, 76, 545–553.
- [8] G. Natta, P. Corradini, G. Allegra, *J. Polym. Sci.* **1961**, 51, 399–410.
- [9] H. Uelzmann, *J. Polym. Sci.* **1958**, 32, 457–476.
- [10] G. Natta, I. Pasquon, A. Zambelli, G. Gatti, *J. Polym. Sci.* **1961**, 51, 387–398.
- [11] M. L. Huggins, *J. Polym. Sci.* **1960**, 48, 473–475.
- [12] G. Natta, G. Mazzanti, *Tetrahedron* **1960**, 8, 86–100.
- [13] G. Natta, I. Pasquon, in *Adv. Catal.* Academic Press, **1959**, pp. 1–66.
- [14] F. Patat, H. Sinn, *Angew. Chem.* **1958**, 70, 496–500.
- [15] P. Cossee, *J. Catal.* **1964**, 3, 80–88.
- [16] E. J. Arlman, *J. Catal.* **1964**, 3, 89–98.
- [17] E. J. Arlman, P. Cossee, *J. Catal.* **1964**, 3, 99–104.
- [18] G. Natta, P. Pino, P. Corradini, F. Danusso, E. Mantica, G. Mazzanti, G. Moraglio, *J. Am. Chem. Soc.* **1955**, 77, 1708–1710.
- [19] L. L. Böhm, *J. Appl. Polym. Sci.* **1984**, 29, 279–289.
- [20] Yu. V. Kissin, in *Fortschritte Hochpolym.-Forsch.*, Springer Berlin Heidelberg, **1974**, pp. 91–155.
- [21] A. S. Hoffman, B. A. Fries, P. C. Condit, *J. Polym. Sci. Part C Polym. Symp.* **1963**, 4, 109–126.
- [22] L. L. Böhm, *Polymer* **1978**, 19, 545–552.
- [23] L. L. Böhm, *Polymer* **1978**, 19, 562–566.

- 
- [24] P. C. Barbé, G. Cecchin, L. Noristi, in *Catal. Radic. Polym.*, Springer Berlin Heidelberg, Berlin, Heidelberg, **1986**, pp. 1–81.
- [25] P. Galli, L. Luciani, G. Cecchin, *Angew. Makromol. Chem.* **1981**, *94*, 63–89.
- [26] L. L. Böhm, *Macromol. Symp.* **2001**, *173*, 53–64.
- [27] L. L. Böhm, *Polymer* **1978**, *19*, 553–561.
- [28] G. Natta, *Angew. Chem.* **1956**, *68*, 393–403.
- [29] G. Natta, *J. Polym. Sci.* **1955**, *16*, 143–154.
- [30] G. Natta, F. Danusso, *Stereoregular Polymers and Stereospecific Polymerizations: The Contributions of Giulio Natta and His School to Polymer Chemistry*, Elsevier, **2013**.
- [31] G. Natta, P. Pino, G. Mazzanti, U. Giannini, *J. Am. Chem. Soc.* **1957**, *79*, 2975–2976.
- [32] G. Natta, P. Pino, G. Mazzanti, R. Lanzo, *Chim Ind* **1957**, *39*, 1032–1033.
- [33] D. S. Breslow, N. R. Newburg, *J. Am. Chem. Soc.* **1957**, *79*, 5072–5073.
- [34] D. S. Breslow, N. R. Newburg, *J. Am. Chem. Soc.* **1959**, *81*, 81–86.
- [35] W. Spaleck, F. Kueber, A. Winter, J. Rohrmann, B. Bachmann, M. Antberg, V. Dolle, E. F. Paulus, *Organometallics* **1994**, *13*, 954–963.
- [36] J. A. Ewen, R. L. Jones, A. Razavi, J. D. Ferrara, *J. Am. Chem. Soc.* **1988**, *110*, 6255–6256.
- [37] C. Janiak, H.-J. Meyer, D. Gudat, R. Alsfasser, H.-J. Meyer, *Riedel Moderne Anorganische Chemie*, De Gruyter, **2012**.
- [38] J. A. Tully, *The Devil's Milk: A Social History of Rubber*, Monthly Review Press, New York, **2011**.
- [39] D. Hosler, S. L. Burkett, M. J. Tarkanian, *Science* **1999**, *284*, 1988–1991.
- [40] G. Charles, **1844**, US3633A.
- [41] C. Harries, *Justus Liebigs Ann. Chem.* **1911**, *383*, 157–227.
- [42] C. G. Williams, *Proc. R. Soc. Lond.* **1859**, *10*, 516–519.
- [43] H. F., *Manufacture and Production of a Caoutchouc Substance.*, **1909**, DE250690 (C).
- [44] F. Hofmann, *Angew. Chem.* **1912**, *25*, 1462–1467.
- [45] D. W. Bock, E. Tschunkur, *Verfahren zur Darstellung von kuenstlichem Kautschuk*, **1930**, DE511145C.

- 
- [46] E. Tschunkur, D. W. Bock, *Verfahren zur Herstellung von kautschukartigen Mischpolymerisaten*, **1933**, DE570980C.
- [47] S. E. Horne, J. P. Kiehl, J. J. Shipman, V. L. Folt, C. F. Gibbs, E. A. Willson, E. B. Newton, M. A. Reinhart, *Ind. Eng. Chem.* **1956**, *48*, 784–791.
- [48] J. S. E. Horne, *Method of Preparing Synthetic Rubber*, **1963**, US3114743A.
- [49] C. Carlson, S. Horne, *Polymerization of Conjugated Polyolefins*, **1973**, US3728325A.
- [50] D. W. C. Von, T. P. Wilson, E. G. Caflisch, *Production of Cis-1,4-Polydienes by Polymerization of 1, 3-Dienes*, **1967**, US3297667A.
- [51] G. D. C. D. Sylvester, J. D. C. D. Witte, G. D. C. D. Marwede, *Polymerisation of Conjugated Dienes in Solution.*, **1980**, DE2830080 (A1).
- [52] A. Carbonaro, D. Ferraro, *Isoprene Polymerization Process*, **1987**, US4696984A.
- [53] H. Van der Heijden, C. J. Schaverien, A. Guy. Orpen, *Organometallics* **1989**, *8*, 255–258.
- [54] A. Mandel, J. Magull, *Z. Anorg. Allg. Chem.* **1996**, *622*, 1913–1919.
- [55] J. Hitzbleck, K. Beckerle, J. Okuda, *J. Organomet. Chem.* **2007**, *692*, 4702–4707.
- [56] Y. Luo, H.-L. Teng, C. Xue, M. Nishiura, Z. Hou, *ACS Catal.* **2018**, *8*, 8027–8032.
- [57] G. Jeske, H. Lauke, H. Mauermann, P. N. Swepston, H. Schumann, T. J. Marks, *J. Am. Chem. Soc.* **1985**, *107*, 8091–8103.
- [58] H. Mauermann, P. N. Swepston, T. J. Marks, *Organometallics* **1985**, *4*, 200–202.
- [59] H. Schumann, W. Genthe, N. Bruncks, *Angew. Chem. Int. Ed. Engl.* **1981**, *20*, 119–120.
- [60] K. H. Den Haan, J. L. De Boer, J. H. Teuben, A. L. Spek, B. Kojic-Prodic, G. R. Hays, R. Huis, *Organometallics* **1986**, *5*, 1726–1733.
- [61] N. S. Radu, T. Don Tilley, A. L. Rheingold, *J. Organomet. Chem.* **1996**, *516*, 41–49.
- [62] H. J. Heeres, J. Renkema, M. Booiij, A. Meetsma, J. H. Teuben, *Organometallics* **1988**, *7*, 2495–2502.
- [63] H. Schumann, E. C. E. Rosenthal, G. Kociok-Köhn, G. A. Molander, J. Winterfeld, *J. Organomet. Chem.* **1995**, *496*, 233–240.
- [64] W. J. Evans, R. Dominguez, T. P. Hanusa, *Organometallics* **1986**, *5*, 263–270.
- [65] J. Holton, M. F. Lappert, D. G. H. Ballard, R. Pearce, J. L. Atwood, W. E. Hunter, *J. Chem. Soc. Dalton Trans.* **1979**, *0*, 45–53.
- [66] S. Arndt, P. Voth, T. P. Spaniol, J. Okuda, *Organometallics* **2000**, *19*, 4690–4700.

- [67] H. Schumann, D. M. M. Freckmann, S. Dechert, *Z. Anorg. Allg. Chem.* **2002**, 628, 2422–2426.
- [69] M. F. Lappert, R. Pearce, *J. Chem. Soc. Chem. Commun.* **1973**, 126–126.
- [69] S. Harder, *Organometallics* **2005**, 24, 373–379.
- [70] D. Barisic, D. Schneider, C. Maichle-Mössmer, R. Anwander, *Angew. Chem. Int. Ed.* **2019**, 58, 1515–1518.
- [71] D. Diether, K. Tyulyunov, C. Maichle-Mössmer, R. Anwander, *Organometallics* **2017**, 36, 4649–4659.
- [72] D. Barisic, D. A. Buschmann, D. Schneider, C. Maichle-Mössmer, R. Anwander, *Chem. – Eur. J.* **2019**, 25, 4821–4832.
- [73] D. Diether, C. Maichle-Mössmer, R. Anwander, *Organometallics* **2019**, DOI 10.1021/acs.organomet.9b00344.
- [74] X. Li, M. Nishiura, L. Hu, K. Mori, Z. Hou, *J. Am. Chem. Soc.* **2009**, 131, 13870–13882.
- [75] M. Nishiura, J. Baldamus, T. Shima, K. Mori, Z. Hou, *Chem. – Eur. J.* **2011**, 17, 5033–5044.
- [76] J. Hitzbleck, K. Beckerle, J. Okuda, T. Halbach, R. Mülhaupt, *Macromol. Symp.* **2006**, 236, 23–29.
- [77] J. Hitzbleck, J. Okuda, *Z. Anorg. Allg. Chem.* **2006**, 632, 1947–1949.
- [78] X. Li, J. Baldamus, Z. Hou, *Angew. Chem. Int. Ed.* **2005**, 44, 962–965.
- [79] K. C. Hultsch, T. P. Spaniol, J. Okuda, *Angew. Chem. Int. Ed.* **1999**, 38, 227–230.
- [80] O. Tardif, M. Nishiura, Z. Hou, *Organometallics* **2003**, 22, 1171–1173.
- [81] X. Xu, Y. Chen, J. Sun, *Chem. – Eur. J.* **2009**, 15, 846–850.
- [83] X. Li, X. Wang, X. Tong, H. Zhang, Y. Chen, Y. Liu, H. Liu, X. Wang, M. Nishiura, H. He, *Organometallics* **2013**, 32, 1445–1458.
- [83] W.-X. Zhang, Z. Wang, M. Nishiura, Z. Xi, Z. Hou, *J. Am. Chem. Soc.* **2011**, 133, 5712–5715.
- [84] T. Shima, M. Nishiura, Z. Hou, *Organometallics* **2011**, 30, 2513–2524.
- [85] X. Li, M. Nishiura, K. Mori, T. Mashiko, Z. Hou, *Chem. Commun.* **2007**, 0, 4137–4139.
- [87] S. Harder, D. Naglav, C. Ruspic, C. Wickleder, M. Adlung, W. Hermes, M. Eul, R. Pöttgen, D. B. Rego, F. Poineau, *Chem. – Eur. J.* **2013**, 19, 12272–12280.

- 
- [87] H. M. Dietrich, C. Zapilko, E. Herdtweck, R. Anwander, *Organometallics* **2005**, *24*, 5767–5771.
- [88] M. Zimmermann, J. Volbeda, K. W. Törnroos, R. Anwander, *Comptes Rendus Chim.* **2010**, *13*, 651–660.
- [89] M. Zimmermann, K. W. Törnroos, H. Sitzmann, R. Anwander, *Chem. – Eur. J.* **2008**, *14*, 7266–7277.
- [90] G. Song, B. Wang, M. Nishiura, Z. Hou, *Chem. – Eur. J.* **2015**, *21*, 8394–8398.
- [91] H. Tsurugi, K. Yamamoto, H. Nagae, H. Kaneko, K. Mashima, *Dalton Trans.* **2014**, *43*, 2331–2343.
- [92] K. R. D. Johnson, P. G. Hayes, *Chem. Soc. Rev.* **2013**, *42*, 1947–1960.
- [93] M. Nishiura, Z. Hou, Y. Wakatsuki, T. Yamaki, T. Miyamoto, *J. Am. Chem. Soc.* **2003**, *125*, 1184–1185.
- [94] Y. Luo, H.-L. Teng, M. Nishiura, Z. Hou, *Angew. Chem. Int. Ed.* **2017**, *56*, 9207–9210.
- [95] A. A. Trifonov, D. M. Lyubov, *Coord. Chem. Rev.* **2017**, *340*, 10–61.
- [96] X. Li, Z. Hou, *Coord. Chem. Rev.* **2008**, *252*, 1842–1869.
- [97] F. Yang, X. Li, *J. Polym. Sci. Part Polym. Chem.* **2017**, *55*, 2271–2280.
- [98] J. Huang, Z. Liu, D. Cui, X. Liu, *ChemCatChem* **2018**, *10*, 42–61.
- [99] S. A. Cotton, *Coord. Chem. Rev.* **1997**, *160*, 93–127.
- [100] Y. Nakayama, H. Yasuda, *J. Organomet. Chem.* **2004**, *689*, 4489–4498.
- [101] J. Gromada, J.-F. Carpentier, A. Mortreux, *Coord. Chem. Rev.* **2004**, *248*, 397–410.
- [102] S. Arndt, J. Okuda, *Chem. Rev.* **2002**, *102*, 1953–1976.
- [103] M. Nishiura, Z. Hou, *Nat. Chem.* **2010**, *2*, 257–268.
- [104] Z. Hou, Y. Wakatsuki, *Coord. Chem. Rev.* **2002**, *231*, 1–22.
- [105] H. Schumann, J. A. Meese-Marktscheffel, L. Esser, *Chem. Rev.* **1995**, *95*, 865–986.
- [106] F. Guo, R. Meng, Y. Li, Z. Hou, *Polymer* **2015**, *76*, 159–167.
- [107] X. Shi, M. Nishiura, Z. Hou, *Angew. Chem. Int. Ed.* **2016**, *55*, 14812–14817.
- [108] X. Shi, M. Nishiura, Z. Hou, *J. Am. Chem. Soc.* **2016**, *138*, 6147–6150.
- [109] A. Yamamoto, M. Nishiura, J. Oyamada, H. Koshino, Z. Hou, *Macromolecules* **2016**, *49*, 2458–2466.

- [110] A. Yamamoto, M. Nishiura, Y. Yang, Z. Hou, *Organometallics* **2017**, *36*, 4635–4642.
- [111] F. Guo, B. Wang, H. Ma, T. Li, Y. Li, *J. Polym. Sci. Part Polym. Chem.* **2016**, *54*, 735–739.
- [112] Z. Shi, F. Guo, Y. Li, Z. Hou, *J. Polym. Sci. Part Polym. Chem.* **2015**, *53*, 5–9.
- [113] F. Guo, N. Jiao, L. Jiang, Y. Li, Z. Hou, *Macromolecules* **2017**, *50*, 8398–8405.
- [114] C. Wang, G. Luo, M. Nishiura, G. Song, A. Yamamoto, Y. Luo, Z. Hou, *Sci. Adv.* **2017**, *3*, e1701011.
- [115] K. Yang, T. Li, R. Tan, K. Shen, Y. Li, *J. Polym. Sci. Part Polym. Chem.* **2018**, *56*, 467–470.
- [116] R. Tan, Z. Shi, F. Guo, L. He, L. Han, Y. Li, *Polym. Chem.* **2017**, *8*, 4651–4658.
- [117] J. Chen, Y. Gao, S. Xiong, M. Delferro, T. L. Lohr, T. J. Marks, *ACS Catal.* **2017**, *7*, 5214–5219.
- [118] D. Peng, G. Du, P. Zhang, B. Yao, X. Li, S. Zhang, *Macromol. Rapid Commun.* **2016**, *37*, 987–992.
- [119] C. Wu, B. Liu, F. Lin, M. Wang, D. Cui, *Angew. Chem.* **2017**, *129*, 7079–7083.
- [120] G. Du, J. Xue, D. Peng, C. Yu, H. Wang, Y. Zhou, J. Bi, S. Zhang, Y. Dong, X. Li, *J. Polym. Sci. Part Polym. Chem.* **2015**, *53*, 2898–2907.
- [121] G. Du, Y. Long, J. Xue, S. Zhang, Y. Dong, X. Li, *Macromolecules* **2015**, *48*, 1627–1635.
- [122] G. Jeske, L. E. Schock, P. N. Swepston, H. Schumann, T. J. Marks, *J. Am. Chem. Soc.* **1985**, *107*, 8103–8110.
- [123] T. E. Müller, K. C. Hultsch, M. Yus, F. Foubelo, M. Tada, *Chem. Rev.* **2008**, *108*, 3795–3892.
- [124] S. Hong, T. J. Marks, *Acc. Chem. Res.* **2004**, *37*, 673–686.
- [125] M. R. Douglass, T. J. Marks, *J. Am. Chem. Soc.* **2000**, *122*, 1824–1825.
- [126] M. R. Douglass, C. L. Stern, T. J. Marks, *J. Am. Chem. Soc.* **2001**, *123*, 10221–10238.
- [127] A. Motta, I. L. Fragalà, T. J. Marks, *Organometallics* **2005**, *24*, 4995–5003.
- [128] P. W. Roesky, U. Denninger, C. L. Stern, T. J. Marks, *Organometallics* **1997**, *16*, 4486–4492.
- [129] G. A. Molander, J. A. C. Romero, *Chem. Rev.* **2002**, *102*, 2161–2186.
- [130] K. N. Harrison, T. J. Marks, *J. Am. Chem. Soc.* **1992**, *114*, 9220–9221.

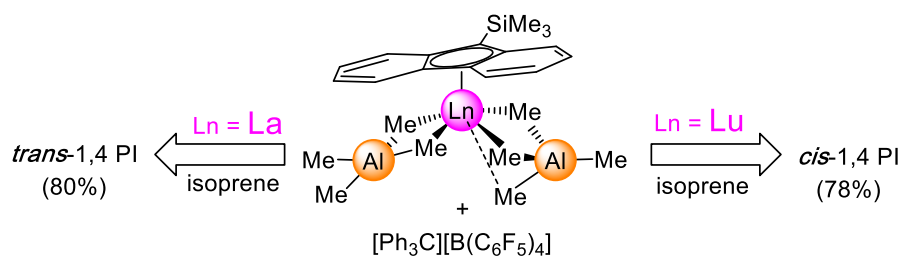
- 
- [131] E. A. Bijpost, R. Duchateau, J. H. Teuben, *J. Mol. Catal. Chem.* **1995**, *95*, 121–128.
- [132] B. S. Soller, S. Salzinger, C. Jandl, A. Pöthig, B. Rieger, *Organometallics* **2015**, *34*, 2703–2706.
- [133] P. Pahl, C. Schwarzenböck, F. A. D. Herz, B. S. Soller, C. Jandl, B. Rieger, *Macromolecules* **2017**, *50*, 6569–6576.
- [134] M. E. Fieser, C. W. Johnson, J. E. Bates, J. W. Ziller, F. Furche, W. J. Evans, *Organometallics* **2015**, *34*, 4387–4393.
- [136] M. M. Hänninen, M. T. Zamora, P. G. Hayes, in *Privileged Pincer-Met. Platf. Coord. Chem. Appl.* Springer International Publishing, Cham, **2016**, pp. 93–177.
- [136] M. D. Fryzuk, T. S. Haddad, *J. Am. Chem. Soc.* **1988**, *110*, 8263–8265.
- [137] D. A. Evans, S. G. Nelson, M. R. Gagne, A. R. Muci, *J. Am. Chem. Soc.* **1993**, *115*, 9800–9801.
- [138] N. Meyer, J. Jenter, P. W. Roesky, G. Eickerling, W. Scherer, *Chem. Commun.* **2009**, *0*, 4693–4695.
- [139] Y. Matsuo, K. Mashima, K. Tani, *Organometallics* **2001**, *20*, 3510–3518.
- [140] P. L. Arnold, L. S. Natrajan, J. J. Hall, S. J. Bird, C. Wilson, *J. Organomet. Chem.* **2002**, *647*, 205–215.
- [141] F. Estler, G. Eickerling, E. Herdtweck, R. Anwender, *Organometallics* **2003**, *22*, 1212–1222.
- [142] K. D. Conroy, W. E. Piers, M. Parvez, *J. Organomet. Chem.* **2008**, *693*, 834–846.
- [143] D. Li, S. Li, D. Cui, X. Zhang, *J. Organomet. Chem.* **2010**, *695*, 2781–2788.
- [144] P. B. Hitchcock, M. F. Lappert, A. V. Protchenko, *Chem. Commun.* **2005**, *0*, 951–953.
- [145] L. K. Knight, W. E. Piers, R. McDonald, *Organometallics* **2006**, *25*, 3289–3292.
- [146] P. Zhang, H. Liao, H. Wang, X. Li, F. Yang, S. Zhang, *Organometallics* **2017**, *36*, 2446–2451.
- [147] C. Yu, D. Zhou, X. Yan, F. Gao, L. Zhang, S. Zhang, X. Li, *Polymers* **2017**, *9*, 531.
- [148] H. Liu, J. He, Z. Liu, Z. Lin, G. Du, S. Zhang, X. Li, *Macromolecules* **2013**, *46*, 3257–3265.
- [149] N. Y. Rad'kova, A. O. Tolpygin, V. Y. Rad'kov, N. M. Khamaletdinova, A. V. Cherkasov, G. K. Fukin, A. A. Trifonov, *Dalton Trans.* **2016**, *45*, 18572–18584.
- [150] J. El Haj Hassan, V. Radkov, V. Dorcet, J.-F. Carpentier, E. Kirillov, *J. Organomet. Chem.* **2016**, *823*, 34–39.



- [151] B. Liu, S. Li, M. Wang, D. Cui, *Angew. Chem. Int. Ed.* **2017**, *56*, 4560–4564.
- [152] L. Li, S. Li, D. Cui, *Macromolecules* **2016**, *49*, 1242–1251.
- [153] S. Arndt, K. Beckerle, P. M. Zeimentz, T. P. Spaniol, J. Okuda, *Angew. Chem. Int. Ed.* **2005**, *44*, 7473–7477.
- [154] R. Litlabo, H. S. Lee, M. Niemeyer, K. W. Tornroos, R. Anwander, *Dalton Trans.* **2010**, *39*, 6815–6825.
- [155] M. Zimmermann, N. Å. Frøystein, A. Fischbach, P. Sirsch, H. M. Dietrich, K. W. Törnroos, E. Herdtweck, R. Anwander, *Chem. – Eur. J.* **2007**, *13*, 8784–8800.
- [156] C. O. Hollfelder, L. N. Jende, D. Diether, T. Zelger, R. Stauder, C. Maichle-Mössmer, R. Anwander, *Catalysts* **2018**, *8*, 61.
- [157] L. N. Jende, C. Maichle-Mössmer, R. Anwander, *Chem. – Eur. J.* **2013**, *19*, 16321–16333.
- [158] M. Zimmermann, K. W. Törnroos, R. Anwander, *Angew. Chem. Int. Ed.* **2008**, *47*, 775–778.
- [159] W. Miao, S. Li, H. Zhang, D. Cui, Y. Wang, B. Huang, *J. Organomet. Chem.* **2007**, *692*, 4828–4834.
- [160] F. G. Bordwell, M. J. Bausch, *J. Am. Chem. Soc.* **1983**, *105*, 6188–6189.
- [161] D. Werner, U. Bayer, N. E. Rad, P. C. Junk, G. B. Deacon, R. Anwander, *Dalton Trans.* **2018**, *47*, 5952–5955.
- [162] L. Friebe, O. Nuyken, W. Obrecht, in *Neodymium Based Ziegler Catal. – Fundam. Chem.* (Ed.: O. Nuyken), **2006**, pp. 1–154.



**Fluorenyl Half-Sandwich  
Bis(tetramethylaluminate)  
Complexes of the Rare-Earth  
Metals: Synthesis, Structure,  
and Isoprene Polymerization**



<https://doi.org/10.1021/acs.organomet.7b00543>

Reprinted (adapted) with permission from the authors of this paper.  
Copyright 2019 American Chemical Society.



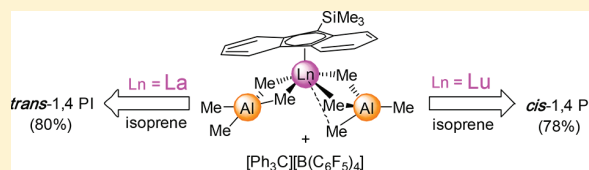
# Fluorenyl Half-Sandwich Bis(tetramethylaluminate) Complexes of the Rare-Earth Metals: Synthesis, Structure, and Isoprene Polymerization

Dominic Diether, Konstantin Tyulyunov, Cécilia Maichle-Mössmer, and Reiner Anwander\*

Institut für Anorganische Chemie, Eberhard Karls Universität Tübingen, Auf der Morgenstelle 18, 72076 Tübingen, Germany

## Supporting Information

**ABSTRACT:** Aiming at half-sandwich complexes of the type  $(\text{Flu}^R)\text{Ln}(\text{AlMe}_4)_2$ , homoleptic tetramethylaluminates  $\text{Ln}(\text{AlMe}_4)_3$  ( $\text{Ln} = \text{Y}, \text{La}, \text{Nd}, \text{and Lu}$ ) were treated with equimolar amounts of R-substituted potassium fluorenyls. The salt metathesis reaction of  $\text{La}(\text{AlMe}_4)_3$  with  $\text{K}(\text{Flu})$  ( $\text{Flu} = \text{fluorenyl} = \text{C}_{13}\text{H}_9$ ) and  $\text{K}(\text{Flu}^{\text{tBu}})$  ( $\text{Flu}^{\text{tBu}} = \text{di}(\text{tert-butyl}) \text{ fluorenyl}$ ) selectively gave the desired half-sandwich complexes  $(\text{Flu}^R)\text{La}(\text{AlMe}_4)_2$ . The corresponding reactions of  $\text{Y}(\text{AlMe}_4)_3$  with  $\text{K}(\text{Flu})/\text{K}(\text{Flu}^{\text{tBu}})$  and  $\text{Lu}(\text{AlMe}_4)_3$  with  $\text{K}(\text{Flu}^{\text{tBu}})$  gave mixtures of half-sandwich and sandwich complexes, while treatment of  $\text{Lu}(\text{AlMe}_4)_3$  with  $\text{K}(\text{Flu})$  produced only the lutetocene complex  $(\text{Flu})_2\text{Lu}(\text{AlMe}_4)$ . Sterically more demanding 1-trimethylsilyl fluorenyl ( $\text{Flu}^{\text{Si}}$ ) allowed for the isolation of half-sandwich complexes for the entire Ln(III) size range ( $\text{Ln} = \text{La}, \text{Nd}, \text{Y}, \text{and Lu}$ ), in crystalline yields up to 94%. Upon activation with routinely employed borate or borane activators  $[\text{Ph}_3\text{C}][\text{B}(\text{C}_6\text{F}_5)_4]$ ,  $[\text{PhNMe}_2\text{H}][\text{B}(\text{C}_6\text{F}_5)_4]$ , and  $\text{B}(\text{C}_6\text{F}_5)_3$ , highly active initiators for isoprene polymerization were obtained. The catalyst activity as well as molecular weight (distribution) and stereoregularity of the obtained polyisoprenes are governed by the rare-earth metal size, fluorenyl ligand, and cocatalyst: highest activity for  $\text{La}/\text{Flu}^{\text{Si}}/[\text{Ph}_3\text{C}][\text{B}(\text{C}_6\text{F}_5)_4]$ , lowest  $M_w/M_n = 1.11$  for  $\text{La}/\text{Flu}/[\text{PhNMe}_2\text{H}][\text{B}(\text{C}_6\text{F}_5)_4]$ , maximum *trans*-1,4 selectivity = 85% for  $\text{La}/\text{Flu}^{\text{tBu}}/[\text{PhNMe}_2\text{H}][\text{B}(\text{C}_6\text{F}_5)_4]$ , maximum *cis*-1,4 selectivity = 78% for  $\text{Lu}/\text{Flu}^{\text{Si}}/[\text{Ph}_3\text{C}][\text{B}(\text{C}_6\text{F}_5)_4]$ . The formations of the active species were investigated by NMR spectroscopy revealing not only established cationization pathways but also fluorenyl abstraction in lanthanum complexes  $(\text{Flu})\text{La}(\text{AlMe}_4)_2$  and  $(\text{Flu}^{\text{tBu}})\text{La}(\text{AlMe}_4)_2$  by trityl borate  $[\text{Ph}_3\text{C}][\text{B}(\text{C}_6\text{F}_5)_4]$ . The reaction of half-sandwich complexes  $(\text{Flu}^R)\text{Ln}(\text{AlMe}_4)_2$  with equimolar amounts of  $\text{Me}_2\text{AlCl}$  did not give access to catalytically active species. Crystallization of binary mixtures  $(\text{Flu}^{\text{Si}})\text{Y}(\text{AlMe}_4)_2/\text{Me}_2\text{AlCl}$  in distinct molar ratios of 1:1 and 1:1.7 yielded complexes  $[(\text{Flu}^{\text{Si}})\text{Y}(\text{AlMe}_4)(\mu\text{-Cl})_2]$  and  $(\text{Flu}^{\text{Si}})_6\text{Y}_6\text{Cl}_{12}$ , respectively.



## INTRODUCTION

Man-made stereoregular polyisoprene (“synthetic rubber”) is of ever increasing importance, and its sustainable fabrication poses a challenging task for industrial and academic research alike.<sup>1–6</sup>

Depending on their microstructure, polyisoprenes show different physical, mechanical, and chemical properties.<sup>7–9</sup>

This is reflected most compellingly in their range of applications, since *cis*-1,4 polyisoprene is used as tire raw material, whereas the *trans*-1,4 stereoisomer is applied in orthopedic medicine.<sup>10</sup> Natural 1,4-*cis*-polyisoprene can be obtained from the sap of *Hevea brasiliensis* (*cis*-1,4-content >99%;  $M_n \approx 2 \times 10^6 \text{ g mol}^{-1}$ ),<sup>11</sup> whereas the *Palaquium gutta* tree produces all-*trans* polyisoprene (*trans*-1,4-content >99%;  $M_n = 1.4\text{--}1.72 \times 10^5 \text{ g mol}^{-1}$ ).<sup>11,12</sup> In contrast, natural 3,4- and 1,2-polyisoprenes seem nonexistent, but their artificial synthesis is as challenging.<sup>13</sup> Their potential application in more sophisticated copolymer materials has been emphasized.<sup>14,15</sup>

As the increasing demand for polyisoprene cannot be satisfied by natural resources alone (the most promising alternative to rubber trees is dandelion caoutchouc),<sup>16,17</sup> it is essential to develop catalytic systems for the production of high performance isoprene homo- and copolymers. Today, some catalytic systems produce polymers with microstructures almost as

selective as nature does.<sup>18–22</sup> Additionally, few catalyst systems are known which allow for a switch of the microstructure, depending on the metal center, ancillary ligand, and cocatalyst(s) applied.<sup>23–25</sup>

Coordinative 1,3-diene polymerization has developed into a lucrative market for rare-earth metal (Ln)-based catalysts, which are arguably the most efficient initiators concerning joint activity and selectivity issues.<sup>1,2,5,26</sup> Regarding this, the ubiquitous cyclopentadienyl (Cp) ligand has played a pivotal role in synthesizing the first single-component catalysts.<sup>26–28</sup> The polymerization performance has been assessed for various subsets of Cp derivatives, including half-sandwich,<sup>19,22,29–31</sup> (*ansa*-)metallocene,<sup>32–34</sup> or constrained geometry complexes.<sup>35</sup> Far less attention has been paid to fluorenyl derivatives, possibly because of the favorable occurrence of haptotropic rearrangements ( $\eta^5$ -to- $\eta^6$ ) or ( $\eta^5$ -to- $\eta^3$ -to- $\eta^1$ ).<sup>36,37</sup> However, such haptotropic shifts might considerably affect the appearance of the initiating species and hence the stereoregularity of

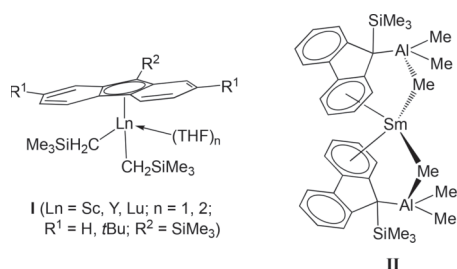
**Special Issue:** Organometallic Actinide and Lanthanide Chemistry

**Received:** July 19, 2017

**Published:** October 11, 2017

the polymer. Successfully employed Ln-fluorenyl polymerization precatalysts comprise mainly *ansa*-metallocene (monomers: ethylene, styrene, ethylene/styrene, methyl methacrylate, and lactones)<sup>38–44</sup> and constrained geometry complexes (monomers: isoprene, ethylene, ethylene/1-hexene, ethylene/1-octene, and methyl methacrylate).<sup>45–51</sup> Li and co-workers have described the synthesis of archetypal fluorenyl half-sandwich complexes (Flu<sup>R</sup>)Ln(CH<sub>2</sub>SiMe<sub>3</sub>)<sub>2</sub>(THF)<sub>x</sub> (**I**, Chart 1) for the smaller-sized rare-earth metal centers scandium,

Chart 1. Selected Ln Fluorenyl Complexes



yttrium, and lutetium<sup>52,53</sup> and employed as polymerization precatalyst (homopolymerization: isoprene, ethylene, styrene, and 1,3-cyclohexadiene; copolymerization: isoprene/ethylene, isoprene/1,3-cyclohexadiene, styrene/1,3-cyclohexadiene, and ethylene/styrene).<sup>52–55</sup> Highly relevant for the present study, Kai and co-workers reported on the reactivity of divalent (Flu<sup>Si</sup>)<sub>2</sub>Sm(THF)<sub>2</sub><sup>56,57</sup> toward trimethylaluminum TMA and triethylaluminum TEA, affording heteroaluminato ligands and the fluorenyl ligand experiencing a  $\eta^5$ -to- $\eta^6$  haptotropic shift (**II**, Chart 1).<sup>56</sup>

Herein we report on the synthesis and comprehensive characterization of a series of rare-earth metal fluorenyl half-sandwich complexes, and assess their performance in the polymerization of isoprene. This study is an extension of our previously introduced bis(tetramethylaluminum) library.<sup>22,29–31,35,58,59</sup>

## RESULTS AND DISCUSSION

**Synthesis of Ln(III) Fluorenyl Half-Sandwich Complexes.** Although the protonolysis protocol applying Ln(AlMe<sub>4</sub>)<sub>3</sub> and C<sub>5</sub>Me<sub>5</sub>H (Cp\*H) afforded the corresponding half-sandwich complexes Cp\*Ln(AlMe<sub>4</sub>)<sub>2</sub> in high yield,<sup>29</sup> such treatment was not as straightforward for the synthesis of the fluorenyl half-sandwich complexes under study. The reactions of La(AlMe<sub>4</sub>)<sub>3</sub> with fluorene (Flu), di(*tert*-butyl) fluorene

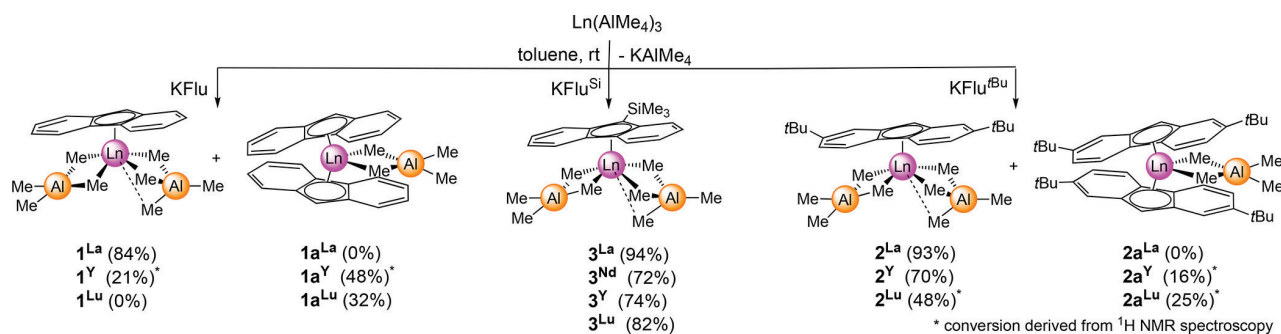
(Flu<sup>*t*Bu</sup>), and trimethylsilyl fluorene (Flu<sup>Si</sup>) indicated only slow formation of the desired monofluorenyl derivatives, and no reaction at all occurred with Lu(AlMe<sub>4</sub>)<sub>3</sub>. In contrast, the salt metathesis protocol<sup>60</sup> employing equimolar amounts of La(AlMe<sub>4</sub>)<sub>3</sub> and K(Flu) or K(Flu<sup>*t*Bu</sup>) at ambient temperature resulted in the efficient formation of the corresponding half-sandwich complexes (Flu)La(AlMe<sub>4</sub>)<sub>2</sub> (**1<sup>La</sup>**) and (Flu<sup>*t*Bu</sup>)La(AlMe<sub>4</sub>)<sub>2</sub> (**2<sup>La</sup>**), respectively (Scheme 1). Rather unexpectedly, the reaction of Lu(AlMe<sub>4</sub>)<sub>3</sub>, featuring the considerably smaller lutetium center, with 1 equiv of K(Flu) selectively gave the sandwich complex (Flu)<sub>2</sub>Lu(AlMe<sub>4</sub>) (**1<sup>Lu</sup>**), independent of the molar ratio of the reagents. The salt metathesis reaction of Lu(AlMe<sub>4</sub>)<sub>3</sub> with the sterically more demanding K(Flu<sup>*t*Bu</sup>) resulted in a mixture of half-sandwich (Flu<sup>*t*Bu</sup>)Lu(AlMe<sub>4</sub>)<sub>2</sub> (**2<sup>Lu</sup>**) and sandwich complexes (Flu<sup>*t*Bu</sup>)<sub>2</sub>Lu(AlMe<sub>4</sub>) (**2<sup>Lu</sup>**). A similar behavior was observed for the mid-sized yttrium center giving mixtures of (Flu)Y(AlMe<sub>4</sub>)<sub>2</sub> (**1<sup>Y</sup>**, 21% conversion) and (Flu)<sub>2</sub>Y(AlMe<sub>4</sub>) (**1<sup>Y</sup>**, 48%), as well as (Flu<sup>*t*Bu</sup>)Y(AlMe<sub>4</sub>)<sub>2</sub> (**2<sup>Y</sup>**, 70%) and (Flu<sup>*t*Bu</sup>)<sub>2</sub>Y(AlMe<sub>4</sub>) (**2<sup>Y</sup>**, 16%).

While the yield of half-sandwich complex **2<sup>Y</sup>** was substantial enough to allow for its isolation and full characterization, the individual components of the half-sandwich/metallocene mixtures **1<sup>Y</sup>/1<sup>Y</sup>** and **2<sup>Lu</sup>/2<sup>Lu</sup>** could not be obtained in pure form. The overall reaction behavior clearly indicates that larger rare-earth metal cations like La(III) favor the formation of half-sandwich complexes (at least for ligands Flu and Flu<sup>*t*Bu</sup>). In contrast, the smaller rare-earth metal cations like Lu(III) give preferably the respective bis(fluorenyl) derivatives. In case of the sterically more demanding ligand Flu<sup>Si</sup>, selective formation of the half-sandwich complexes becomes feasible for the entire Ln<sup>3+</sup> size range (Scheme 1). All half-sandwich complexes are stable toward ligand scrambling with decomposition taking place only at elevated temperatures.

**NMR Spectroscopy of Ln(III) Fluorenyl Half-Sandwich Complexes.** The <sup>1</sup>H NMR spectra of the half-sandwich complexes revealed all similar features. The [AlMe<sub>4</sub>] ligands show one singlet in the range of –0.40 to –0.60 ppm, indicative of highly fluxional methyl groups.

Compared to the Cp\* congeners, these signals are shifted upfield (e.g., (C<sub>5</sub>Me<sub>4</sub>SiMe<sub>3</sub>)Lu(AlMe<sub>4</sub>)<sub>2</sub>,  $\delta$  = –0.14 ppm), indicating electron-rich [AlMe<sub>4</sub>] groups.<sup>29</sup> The aromatic protons of the fluorenyl ligands could be assigned by <sup>1</sup>H–<sup>13</sup>C HSQC and <sup>1</sup>H–<sup>1</sup>H COSY NMR experiments (Figures S3 and S4: fluorenyl protons at positions C3–C12, 7.95–6.97 ppm; C1 position: 6.20–6.34 ppm). Due to the NMR active yttrium nucleus, the [AlMe<sub>4</sub>] peak appeared as a doublet with coupling constants of 2.2 Hz (**2<sup>Y</sup>**) and 2.3 Hz (**3<sup>Y</sup>**). This is a well-known

Scheme 1. Synthesis of Donor-Free Rare-Earth Metal Mixed Fluorenyl/Hydrocarbyl Complexes according to a Salt Metathesis Protocol



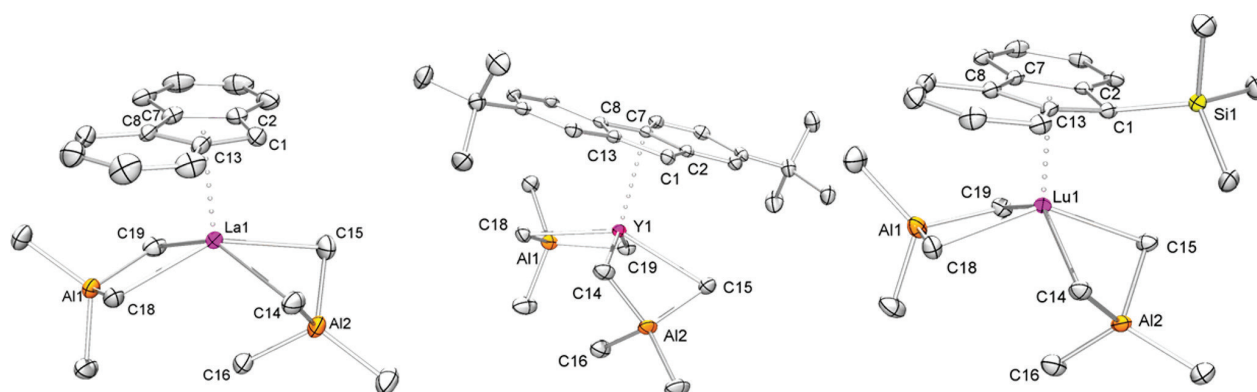


**Figure 1.** Molecular structures of (Flu)La(AlMe<sub>4</sub>)<sub>2</sub> (**1<sup>La</sup>**, left), (Flu<sup>tBu</sup>)Y(AlMe<sub>4</sub>)<sub>2</sub> (**2<sup>Y</sup>**, middle), and (Flu<sup>Si</sup>)Lu(AlMe<sub>4</sub>)<sub>2</sub> (**3<sup>Lu</sup>**, right); complexes **2<sup>La</sup>**, **3<sup>Y</sup>**, and **3<sup>Nd</sup>** are isostructural (Figures S17, S18, and S19). Hydrogen atoms are omitted for clarity. Atomic displacement parameters are set at the 50% probability level. Selected bond lengths are given in Table 1.

feature of yttrium tris(tetramethylaluminate) or cyclopentadienyl half-sandwich complexes.<sup>29,61</sup> Such high mobility of the [AlMe<sub>4</sub>] ligands is not observed in sandwich complex **1a<sup>Lu</sup>**, revealing separate signals for the terminal and bridging methyl protons at  $-0.52$  and  $-1.70$  ppm. It is noteworthy that an additional coupling could be observed between yttrium and the proton at position C1 of the Flu<sup>tBu</sup> ligand ( $^2J_{\text{HY}} = 2.4$  Hz; **2<sup>Y</sup>**). Moreover, a rare  $^1J_{\text{CY}}$  coupling of 2.7 and 4.8 Hz was detected involving C1 in **2<sup>Y</sup>** and **3<sup>Y</sup>**, respectively. The significant difference in coupling constants between **2<sup>Y</sup>** and **3<sup>Y</sup>** indicates distinct electronic environments, mainly caused by the trimethylsilyl substituent of the Flu<sup>Si</sup> ligand.

**X-ray Structure Analyses of Ln(III) Fluorenyl Half-Sandwich Complexes.** All isolated half-sandwich complexes were examined by X-ray crystallography. Single crystals were obtained from saturated *n*-hexane solutions at  $-40$  °C. The molecular structures of (Flu)La(AlMe<sub>4</sub>)<sub>2</sub> (**1<sup>La</sup>**), (Flu<sup>tBu</sup>)Y(AlMe<sub>4</sub>)<sub>2</sub> (**2<sup>Y</sup>**), and (Flu<sup>Si</sup>)Lu(AlMe<sub>4</sub>)<sub>2</sub> (**3<sup>Lu</sup>**) are shown representatively in Figure 1; those of complexes **2<sup>La</sup>**, **3<sup>Y</sup>**, and **3<sup>Nd</sup>** are isostructural and depicted in the Supporting Information (Figures S17, S18, and S19). Selected bond lengths for all half-sandwich complexes are given in Table 1. All fluorenyl half-sandwich complexes display the structural motif, previously detected in cyclopentadienyl-supported bis-(tetramethylaluminate) complexes.<sup>29,62,63</sup>

The Ln(III) metal centers are coordinated by the fluorenyl ligands via the 5-membered ring in a distorted  $\eta^5$ -fashion. For example, tilting of the fluorenyl ligand in complex **3<sup>Lu</sup>** results in Lu–C bond lengths of 2.515(2) (C1) and 2.734(2) (C7) as well as 2.750(2) Å (C8). The Ln–C1 bond lengths (stated for complexes **3**) decrease in the order La (2.732(2)) > Nd (2.6562(15)) > Y (2.574(2)) > Lu (2.515(2) Å) in accordance with the decreasing ionic radii of the Ln(III) centers. Most typically, one [AlMe<sub>4</sub>] ligand adopts a nondistorted (planar)  $\eta^2$  coordination mode, while the second appears bent to an extent, depending on the size of the metal center and the stereoelectronic features of the fluorenyl ligand. As detected previously such bending of the tetramethylaluminate ligand is most pronounced for the lanthanum complexes, forming additional Ln–CH<sub>3</sub> contacts as close as 3.045(4) Å (C16, **1<sup>La</sup>**).<sup>13,43</sup> Characteristically, these additional interactions involve an elongation of the adjacent Ln–CH<sub>3</sub> bonds (**1<sup>La</sup>**: La–C14/C15 2.767(4)/2.816(4) Å; cf., undistorted: La–C18/C19 2.664(5)/2.678(4) Å).

Interestingly, the asymmetric unit of the silyl-substituted fluorenyl complex **3<sup>La</sup>** contains two distinct molecules: a monomeric unit similar to those discussed above (Figure 2, La1) and a dimeric arrangement (Figure 2, La2/La2'). The lanthanum centers of the latter dimeric molecule are connected asymmetrically by two aluminato ligands in a  $\mu\text{-}\eta^1, \eta^2$  fashion. Here, steric saturation of the lanthanum centers is achieved by an additional elongated La–CH<sub>3</sub>  $\eta^1$  contact (C38, 2.976(2) Å) involving the bridging [AlMe<sub>4</sub>] ligand. The planes spanned by C39–La2–C40 and C35–La2–C36 are twisted to each other confining an angle of 80.2°, likely due to the coordination of the additional methyl group (C38). The same structural motif has already been described for complex (C<sub>5</sub>Me<sub>4</sub>H)La(AlMe<sub>4</sub>)<sub>2</sub>.<sup>30</sup>

Comparing lanthanum fluorenyl half-sandwich complexes **1<sup>La</sup>**, **2<sup>La</sup>**, and **3<sup>La</sup>**, it is worth mentioning that the Flu ligand is located more distant from the lanthanum center (La1–Ct 2.581 Å) than the Flu<sup>tBu</sup> (La1–Ct 2.556 Å) or the Flu<sup>Si</sup> ligands (La1–Ct 2.552 Å). As stated above the La–fluorenyl bonding also affects the La1–C16 distance of the bent [AlMe<sub>4</sub>] unit, since it is significantly longer in **3<sup>La</sup>** (3.297(2) Å) compared to **1<sup>La</sup>** (3.045(4) Å) and **2<sup>La</sup>** (3.071(3) Å).

**X-ray Structure Analyses of Lutetocene Complex (Flu)<sub>2</sub>Lu(AlMe<sub>4</sub>) and the Bis(THF) Adduct of K(Flu<sup>Si</sup>).** In the solid state, sandwich complex **1a<sup>Lu</sup>** revealed a staggered conformation of the fluorenyl ligands (Figure 3), spanning an angle of 51.4°. This is in good agreement with the 49.2° reported for Cp<sub>2</sub>Yb(AlMe<sub>4</sub>).<sup>64</sup> The [AlMe<sub>4</sub>] ligand adopts an  $\eta^2$  coordination mode, routinely observed for lanthanidocene tetramethylaluminate complexes.<sup>64</sup> The lutetium methyl distances of Lu1–C28 2.489(5) Å and Lu1–C27 2.502(5) Å are in the expected range.<sup>65</sup>

On one occasion, we could harvest single crystals of K(Flu<sup>Si</sup>) from a saturated THF solution. Herein, the potassium centers are sandwiched by two trimethylsilyl fluorenyl moieties involving  $\eta^6$ -coordination of the six-membered arene rings (Figure 4). Each Flu<sup>Si</sup> ligand bridges two potassium centers, in this way building up a polymeric zig-zag chain. Two THF molecules complete the distorted tetrahedral coordination geometry of the potassium centers. Analogous structural motifs are known from *tert*-butyl- and hypersilyl-fluorenyl derivatives of potassium.<sup>66,67</sup>

**Polymerization of Isoprene and Active Species.** Previous studies revealed that half-sandwich complexes (Cp<sup>R</sup>)–

Table 1. Selected Bond Lengths [Å] of  $1^{Ln}$ ,  $2^{Ln}$ , and  $3^{Ln}$ 

	Ln–C1	Ln–C2	Ln–C7	Ln–C8	Ln–C13	Ln–C14	Ln–C15	Ln–C16	Ln–C18	Ln–C19	Ln–Al1	Ln–Al2
$1^{La}$	2.698(3)	2.822(4)	2.949(4)	2.963(4)	2.835(4)	2.767(4)	2.816(4)	3.045(4)	2.664(5)	2.678(4)	2.989(3)	3.222(2)
$2^{La}$	2.686(2)	2.800(2)	2.935(2)	2.942(2)	2.796(2)	2.808(3)	2.785(3)	3.071(3)	2.696(2)	2.675(2)	2.9878(8)	3.2325(8)
$3^{La}$	2.732(2)	2.8126(19)	2.913(2)	2.899(2)	2.799(2)	2.740(2)	2.739(2)	3.297(2)	2.694(2)	2.662(2)	3.0390(7)	3.2378(7)
$3^{Nd}$	2.6562(15)	2.7354(15)	2.8579(15)	2.8720(15)	2.7499(15)	2.7036(19)	2.6720(19)	3.2688(19)	2.6058(18)	2.6080(17)	2.9830(5)	3.1605(5)
$2^Y$	2.5306(18)	2.6788(18)	2.8218(18)	2.8145(18)	2.6696(18)	2.662(2)	2.668(2)	3.063(2)	2.510(2)	2.527(2)	2.8583(6)	3.0589(6)
$3^Y$	2.5741(16)	2.6570(15)	2.7780(15)	2.7898(15)	2.6730(16)	2.632(2)	2.6021(19)	3.429(2)	2.5244(19)	2.527(2)	2.9473(7)	3.0789(6)
$3^{Lu}$	2.515(2)	2.6094(19)	2.7339(19)	2.7501(19)	2.625(2)	2.580(2)	2.549(2)	3.523(2)	2.475(2)	2.475(2)	2.9210(6)	3.0234(6)

<sup>a</sup>Selected distances are taken of the monomeric unit of the crystal structure.

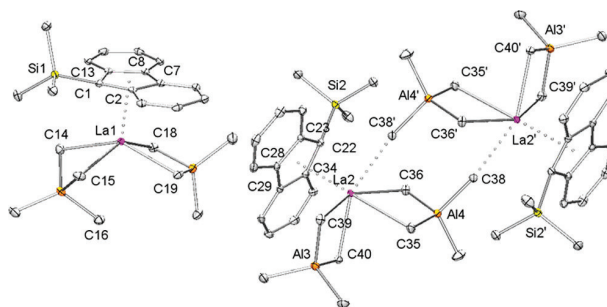


**Figure 2.** Molecular structure of  $(\text{Flu}^{\text{Si}})\text{Lu}(\text{AlMe}_4)_2$  ( $3^{\text{La}}$ ). Hydrogen atoms are omitted for clarity. Atomic displacement parameters are set at the 50% probability level. Selected bond lengths [Å] not listed in Table 1: La2–C22 2.7324(19), La2–C23 2.8235(19), La2–C28 2.957(2), La2–C29 2.969(2), La2–C34 2.845(2), La2–C35 2.870(2), La2–C36 2.812(2), La2'–C38 2.976(2), La2–C39 2.708(2), La2–C40 2.671(2).

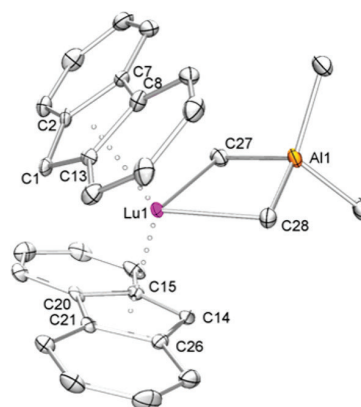


**Figure 3.** Molecular structure of  $(\text{Flu})_2\text{Lu}(\text{AlMe}_4)$  ( $1^{\text{Lu}}$ ). Hydrogen atoms are omitted for clarity. Atomic displacement parameters are set at the 50% probability level. Selected bond lengths [Å]: Lu1–C1 2.504(3), Lu1–C2 2.607(4), Lu1–C7 2.727(4), Lu1–C8 2.748(5), Lu1–C13 2.624(4), Lu1–C14 2.558(3), Lu1–C15 2.641(4), Lu1–C20 2.677(4), Lu1–C21 2.680(4), Lu1–C26 2.641(4), Lu1–C27 2.502(5), Lu1–C28 2.489(5), Lu1–Al1 3.0017(14).

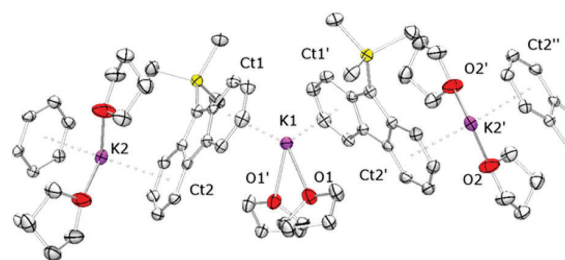


**Figure 4.** Section of the molecular structure of  $\text{K}(\text{Flu}^{\text{Si}})(\text{THF})_2$ . Hydrogen atoms are omitted for clarity. One out of two independent zig-zag chains is depicted. Atomic displacement parameters are set at the 50% probability level. Selected bond lengths [Å] and angles [deg]: K1–O1 2.654(2), K1–Ct1 2.867, O1–K1–O1' 73.36(10), Ct1–K1–Ct1' 129.41, K2–O2 2.611(2), K2–Ct2 2.851, O2–K2–O2' 81.41(11), Ct2–K2–Ct2' 129.86.

$\text{Ln}(\text{AlMe}_4)_2$  ( $\text{Ln} = \text{La}, \text{Nd}, \text{and Y}$ ) are efficient precatalysts for the polymerization of isoprene.<sup>22,29,30</sup> Thus, the fluorenyl half-sandwich complexes  $1^{\text{La}}$ ,  $2^{\text{La}}$ , and  $3^{\text{Ln}}$  were further examined in the polymerization of isoprene. As a standard procedure, each



Table 2. Polymerization of Isoprene by Fluorenyl Half-Sandwich Complexes

entry <sup>a</sup>	precatalyst	cocatalyst <sup>b</sup>	yield [%]	<i>trans</i> -1,4- <sup>c</sup>	<i>cis</i> -1,4- <sup>c</sup>	3,4- <sup>c</sup>	$M_n$ ( $\times 10^4$ ) <sup>d</sup>	$M_w/M_n$ <sup>d</sup>	$T_g$ [°C] <sup>e</sup>
1	(Flu)La(AlMe <sub>4</sub> ) <sub>2</sub> (1 <sup>La</sup> )	A	93	49.4	46.6	4.1	4.3	1.21	-61.3
2	(Flu)La(AlMe <sub>4</sub> ) <sub>2</sub> (1 <sup>La</sup> )	B	92	78.7	15.3	6.0	6.0	1.11	-64.0
3	(Flu)La(AlMe <sub>4</sub> ) <sub>2</sub> (1 <sup>La</sup> )	C	78	61.2	36.0	2.8	22.6	1.24	-65.7
4	(Flu <sup>tBu</sup> )La(AlMe <sub>4</sub> ) <sub>2</sub> (2 <sup>La</sup> )	A	94	52.1	44.0	3.9	5.3	1.20	-64.1
5	(Flu <sup>tBu</sup> )La(AlMe <sub>4</sub> ) <sub>2</sub> (2 <sup>La</sup> )	B	93	85.1	10.7	4.2	5.4	1.12	-63.1
6	(Flu <sup>tBu</sup> )La(AlMe <sub>4</sub> ) <sub>2</sub> (2 <sup>La</sup> )	C	91	32.0	62.0	6.0	17.1	1.29	-62.4
7 <sup>o</sup>	La(AlMe <sub>4</sub> ) <sub>3</sub>	A	>99	51.4	46.3	2.3	5.0	1.29	
8	(Flu <sup>Si</sup> )La(AlMe <sub>4</sub> ) <sub>2</sub> (3 <sup>La</sup> )	A	>99	74.3	16.3	9.4	4.8	1.27	-65.5
9	(Flu <sup>Si</sup> )La(AlMe <sub>4</sub> ) <sub>2</sub> (3 <sup>La</sup> )	B	98	80.0	9.6	10.4	4.9	1.17	-63.7
10	(Flu <sup>Si</sup> )La(AlMe <sub>4</sub> ) <sub>2</sub> (3 <sup>La</sup> )	C	84	56.7	26.7	16.6	14.2	1.42	-60.4
11	(Flu <sup>Si</sup> )Nd(AlMe <sub>4</sub> ) <sub>2</sub> (3 <sup>Nd</sup> )	A	93	44.8	38.1	17.1	5.1	1.28	-56.8
12	(Flu <sup>Si</sup> )Nd(AlMe <sub>4</sub> ) <sub>2</sub> (3 <sup>Nd</sup> )	B	96	54.1	25.9	20.0	5.4	1.13	-55.3
13	(Flu <sup>Si</sup> )Nd(AlMe <sub>4</sub> ) <sub>2</sub> (3 <sup>Nd</sup> )	C	94	37.4	38.3	24.3	8.1	1.42	-55.7
14	(Flu <sup>Si</sup> )Y(AlMe <sub>4</sub> ) <sub>2</sub> (3 <sup>Y</sup> )	A	88	23.5	56.5	20.0	9.8	1.57	-53.0
15	(Flu <sup>Si</sup> )Y(AlMe <sub>4</sub> ) <sub>2</sub> (3 <sup>Y</sup> )	B	94	18.3	48.7	33.0	9.0	1.41	-42.5
16	(Flu <sup>Si</sup> )Y(AlMe <sub>4</sub> ) <sub>2</sub> (3 <sup>Y</sup> )	C	23	26.7	62.2	11.1	1.8	1.95	-58.9
17	(Flu <sup>Si</sup> )Lu(AlMe <sub>4</sub> ) <sub>2</sub> (3 <sup>Lu</sup> )	A	88	17.7	78.2	4.1	9.4	1.67	-62.0
18	(Flu <sup>Si</sup> )Lu(AlMe <sub>4</sub> ) <sub>2</sub> (3 <sup>Lu</sup> )	B	89	11.5	72.9	15.6	8.0	1.47	-55.0
19	(Flu <sup>Si</sup> )Lu(AlMe <sub>4</sub> ) <sub>2</sub> (3 <sup>Lu</sup> )	C	91	18.0	75.4	6.6	5.4	1.95	-64.4

<sup>a</sup>General polymerization procedure: 0.02 mmol of precatalyst, 8 mL of toluene, 20 mmol of isoprene, 1 h, 40 °C. <sup>b</sup>A = [Ph<sub>3</sub>C][B(C<sub>6</sub>F<sub>5</sub>)<sub>4</sub>]; B = [C<sub>6</sub>H<sub>5</sub>NMe<sub>2</sub>H][B(C<sub>6</sub>F<sub>5</sub>)<sub>4</sub>]; C = B(C<sub>6</sub>F<sub>5</sub>)<sub>3</sub>; catalyst preformation: 30 min. <sup>c</sup>Determined by <sup>1</sup>H and <sup>13</sup>C NMR spectroscopy in CDCl<sub>3</sub>. <sup>d</sup>Determined by GPC against polystyrene standards. <sup>e</sup>Determined by DSC at 20 K/min.

fluorenyl half-sandwich complex was activated/cationized with fluorinated borate or borane cocatalysts (A = [Ph<sub>3</sub>C][B(C<sub>6</sub>F<sub>5</sub>)<sub>4</sub>]; B = [PhNMe<sub>2</sub>H][B(C<sub>6</sub>F<sub>5</sub>)<sub>4</sub>]; C = B(C<sub>6</sub>F<sub>5</sub>)<sub>3</sub>) prior to testing for the homopolymerization of isoprene. The polymerization results are summarized in Table 2. To probe whether the active species correspond to those observed for cyclopentadienyl-supported catalysts,<sup>22</sup> we examined the most efficient equimolar precatalyst/cocatalyst mixtures by NMR spectroscopy. The most enlightening spectra were obtained for the reactions of lanthanum complexes 1<sup>La</sup>, 2<sup>La</sup>, and 3<sup>La</sup> with cocatalysts A and B (Scheme 2, Figures S31–S34).

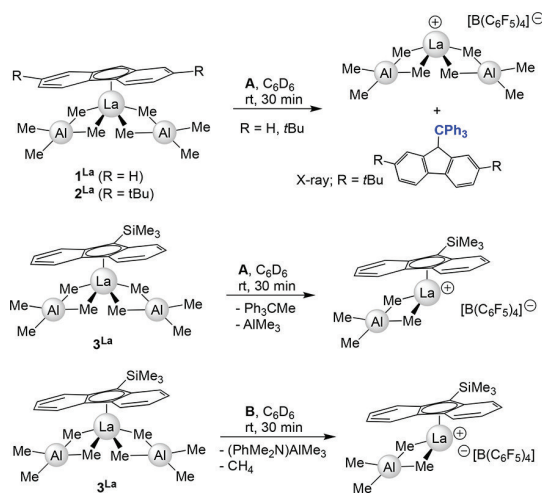
Treatment of 3<sup>La</sup> featuring the sterically most demanding fluorenyl ligand (SiMe<sub>3</sub>-shielded C1 atom) with A and B proceeded as expected via methyl group abstraction and

protonolysis, respectively, involving one tetramethylaluminato ligand. Particularly, the reaction of 3<sup>La</sup> with B gave a clean activation product, whereas A produced two additional minor side products, according to the <sup>1</sup>H and <sup>19</sup>F NMR spectra. In contrast, the reaction of complexes (Flu)La(AlMe<sub>4</sub>)<sub>2</sub> (1<sup>La</sup>) and (Flu<sup>tBu</sup>)La(AlMe<sub>4</sub>)<sub>2</sub> (2<sup>La</sup>), exhibiting the shortest La–C1 distances, with A resulted in fluorenyl abstraction and formation of trityl-substituted fluorene. The solid-state structure of CPh<sub>3</sub>Flu<sup>tBu</sup> is shown in Figure S21. Concomitantly, the formation of a cationic bis(tetramethylaluminato) species is suggested, similar to the active species obtained when homoleptic La(AlMe<sub>4</sub>)<sub>3</sub> is treated with A. Similar “ancillary” ligand abstractions via cocatalyst A were described previously for the indenyl sandwich complex (2-Me-Ind)<sub>2</sub>Sc[N(SiMe<sub>3</sub>)<sub>2</sub>] and Ln(III) indenyl half-sandwich complexes (1-SiMe<sub>3</sub>-Ind)-Ln(CH<sub>2</sub>SiMe<sub>3</sub>)<sub>2</sub>(THF) (Ln = Sc and Lu).<sup>68,69</sup> The distinct (and envisaged) reactivity of complex 3<sup>La</sup> compared to 1<sup>La</sup> and 2<sup>La</sup> can be explained by the steric shielding of the fluorenyl C1-position by the SiMe<sub>3</sub>-group.

The protonolysis reaction of 1<sup>La</sup> and 2<sup>La</sup> with B (not shown in Scheme 2) mainly follows the reaction pathway depicted for 3<sup>La</sup> (involving formation of methane and dimethyl aniline adduct AlMe<sub>3</sub>(NPhMe<sub>2</sub>)), but the generation of fluorene (as a result of fluorenyl protonolysis) was detected as a minor side product as well. This means that binary systems 1<sup>La</sup>/B and 2<sup>La</sup>/B should contain at least two different catalytic species.

**Effect of the Fluorenyl Substitution Pattern in Lanthanum Initiators.** As proposed by the above NMR spectroscopic study abstraction of the fluorenyl (Flu) and di(*tert*-butyl)-fluorenyl (Flu<sup>tBu</sup>) ligands by cocatalyst A gave initiators showing similar performance as the binary system La(AlMe<sub>4</sub>)<sub>3</sub>/A (Table 2, entries 1, 4, and 7). In general, all catalytic species gave molecular weight distributions  $M_w/M_n$  narrower than 2.0, reaching minimum values for the sterically least hindered fluorenyl ligands (e.g., entry 2:  $M_w/M_n$  = 1.11). The highest *trans*-1,4-contents were obtained for the sterically most demanding Flu<sup>Si</sup> ligand.

Scheme 2. Active Species Obtained from Lanthanum Complexes 1<sup>La</sup>, 2<sup>La</sup>, and 3<sup>La</sup> with Cocatalysts A and B, as Proposed by NMR Spectroscopy



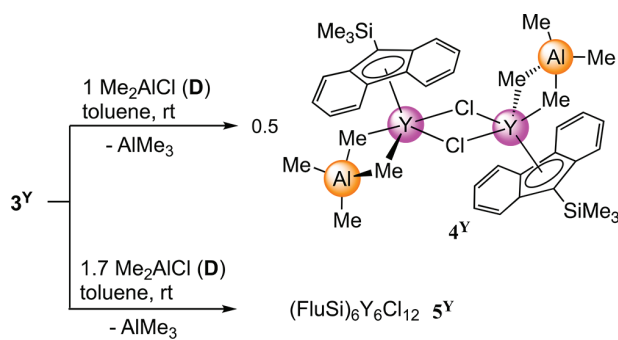
**Effect of the Rare-Earth Metal Center in Complexes (Flu<sup>Si</sup>)Ln(AlMe<sub>4</sub>)<sub>2</sub> (3).** First, the lanthanum-derived catalytic species displayed the highest activity (yield >99% after 1 h, entry 8), in accordance with a maximum steric unsaturation of the La(III) center. Second, decreasing metal size resulted in higher values  $M_w/M_n$  for all tested cocatalysts (e.g., A: entries 8, 11, 14, and 17). This behavior might originate from (a) competing chain transfer reactions (due to the decreasing activity of the catalyst system), (b) proneness of complexes derived from smaller rare-earth metal centers to engage in ligand redistribution under these conditions, and/or (c) fundamental changes in the relative rates of termination versus propagation. Next, changing the metal from lanthanum over neodymium and yttrium to lutetium increased the *cis*-1,4 content from 9.6% (entry 9) over 25.9% (entry 12) and 48.7% (entry 15) to 72.9% (entry 18). Correspondingly, the highest *trans*-1,4-content of 80.0% was observed for lanthanum complex 3<sup>La</sup> (c.f., cocatalyst B: entries 18, 15, 12, and 9). Generally, this behavior was observed for all tested cocatalysts, with the larger rare-earth metals producing mainly *trans*-1,4-polyisoprene (maximum 80%), and the smaller ones giving access to higher *cis*-1,4 content (maximum 78.2%, entry 17). These findings are in good agreement with the polymerization performance of the cyclopentadienyl-supported half-sandwich complexes (C<sub>5</sub>Me<sub>4</sub>H)Ln(AlMe<sub>4</sub>)<sub>2</sub>, (C<sub>5</sub>Me<sub>5</sub>)Ln(AlMe<sub>4</sub>)<sub>2</sub>, (C<sub>5</sub>Me<sub>4</sub>SiMe<sub>3</sub>)Ln(AlMe<sub>4</sub>)<sub>2</sub>, [1,3-(Me<sub>3</sub>Si)<sub>2</sub>C<sub>5</sub>H<sub>3</sub>]Ln(AlMe<sub>4</sub>)<sub>2</sub>, and [1,2,4-(Me<sub>3</sub>C)<sub>3</sub>C<sub>5</sub>H<sub>2</sub>]Ln(AlMe<sub>4</sub>)<sub>2</sub>, revealing the best performance for (C<sub>5</sub>Me<sub>5</sub>)La(AlMe<sub>4</sub>)<sub>2</sub>/C (*trans*-1,4 content: 99.5%,  $M_w/M_n = 1.18$ ).<sup>29</sup>

**Effect of the Cocatalyst.** For lanthanum complexes 1<sup>La</sup>, 2<sup>La</sup>, and 3<sup>La</sup>, cocatalyst A afforded the highest polymer yields while C provided comparatively lower yields. Generally, cocatalyst B produced polymers with lower *cis*-1,4 content, but the smallest  $M_w/M_n$  values (entries 2, 5, 9, 12, 15, 18). Furthermore, the catalysts obtained in the presence of C displayed low efficiency (molecular weights as high as  $M_n = 22.6 \times 10^4$ ; entry 3; catalyst efficiency = 30.1%) and gave polymers with comparatively broader  $M_w/M_n$  (entries 3, 6, 10, 13, 16, and 19). Comparatively higher molecular weights were also observed for the binary systems composed of yttrium and lutetium half-sandwich complexes when combined with cocatalyst A (entries 14 and 17) and B (entries 15 and 18). Activation of complex 3<sup>La</sup> with cocatalyst B led to a higher *trans*-1,4-content (entry 9) compared to those obtained with the use of A (entry 8) and C (entry 10). In contrast, activation of complexes 3<sup>Y</sup> or 3<sup>Lu</sup> with B produced polymers with lower *trans*-1,4 contents (entries 15 and 18) compared to that of the activation with A (entries 14 and 17) or C (entries 16 and 19). For further comparison, the catalytic system (Flu)Sc-(CH<sub>2</sub>SiMe<sub>3</sub>)<sub>2</sub>(THF)/C/Al*i*Bu<sub>3</sub> reported by Li et al. produced polyisoprenes with high *cis*-1,4 (up to 93%) but no *trans*-1,4 content.<sup>55</sup>

**Reactivity of Ln(III) Fluorenyl Half-Sandwich Complexes toward Dimethylaluminum Chloride.** It has been shown that activation of homoleptic Ln(AlMe<sub>4</sub>)<sub>3</sub> with chlorinating reagents such as Me<sub>2</sub>AlCl (D) gives highly *cis*-selective catalyst systems,<sup>18</sup> while the same reaction with cyclopentadienyl-supported bis(tetramethylaluminate) complexes produces discrete chloro-bridged half-sandwich complexes, which are inactive.<sup>29</sup> Given the fluorenyl abstraction observed when treating complexes (Flu)La(AlMe<sub>4</sub>)<sub>2</sub> (1<sup>La</sup>) or (Flu<sup>bu</sup>)La(AlMe<sub>4</sub>)<sub>2</sub> (2<sup>La</sup>) with cocatalyst A, we wondered whether an active catalyst would form by treating the fluorenyl-supported

bis(tetramethylaluminate) complexes with D, via fluorenyl/Cl interchange. However, like the cyclopentadienyl derivatives, equimolar mixtures of complexes 1<sup>La</sup> (or 2<sup>La</sup>) and D did not initiate the polymerization of isoprene. Particularly, binary system 3<sup>Y</sup>/D gave access to partly and fully AlMe<sub>4</sub>/Cl-exchanged crystalline products 4<sup>Y</sup> and 5<sup>Y</sup> (Scheme 3), the

**Scheme 3.** Reactivity of Complex (Flu<sup>Si</sup>)Y(AlMe<sub>4</sub>)<sub>2</sub> toward Dimethylaluminum Chloride (D)



structural features of which are discussed briefly in the following. Small amounts of colorless single crystals of complexes [(Flu<sup>Si</sup>)Y(AlMe<sub>4</sub>)(μ-Cl)]<sub>2</sub> (4<sup>Y</sup>) and (Flu<sup>Si</sup>)<sub>6</sub>Y<sub>6</sub>Cl<sub>12</sub> (5<sup>Y</sup>) could be harvested from the reactions mixtures upon storing for several days at ambient temperature (Figures 5 and 6). The very low yields of crystalline 4<sup>Y</sup> and 5<sup>Y</sup> did not allow for further characterization.

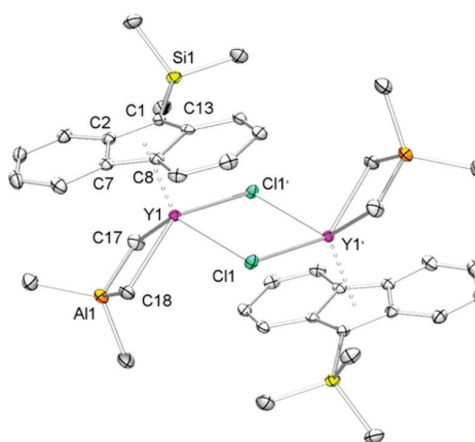


**Figure 5.** Molecular structure of [(Flu<sup>Si</sup>)Y(AlMe<sub>4</sub>)(μ-Cl)]<sub>2</sub> (4<sup>Y</sup>). Hydrogen atoms are omitted for clarity. Atomic displacement parameters are set at the 50% probability level. Selected bond lengths [Å]: Y1–C1 2.5768(3), Y1–C2 2.6961(3), Y1–C7 2.7211(3), Y1–C8 2.6588(3), Y1–C13 2.6012(3), Y1–C17 2.4751(3), Y1–C18 2.5833(3), Y1–Cl1 2.6554(3), Y1–Cl1' 2.6878(3).

The dimeric arrangement of complex 4<sup>Y</sup> with formally 7-coordinate yttrium centers is similar to that of previously reported [((Me<sub>3</sub>Si)<sub>2</sub>C<sub>5</sub>H<sub>3</sub>)Y(AlMe<sub>4</sub>)Cl]<sub>2</sub>.<sup>29</sup> Compared to precursor 3<sup>Y</sup>, the tilting of the fluorenyl ligand toward the yttrium center is even more pronounced, as reflected by shorter Y1–C1/C13 bond lengths of 2.5768(3) and 2.6012(3) Å, respectively, along with an elongation of the Y1–C7 bond to 2.7211(3) Å. The bridging Y–Cl bond lengths appear slightly asymmetric (Y1–Cl1 2.6554(3) Å and Y1–Cl1' 2.6878(3) Å),

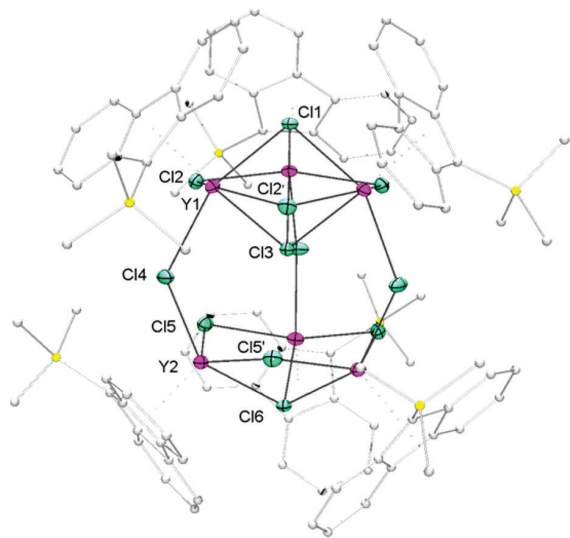


**Figure 6.** Molecular structure of  $(\text{Flu}^{\text{Si}})_6\text{Y}_6\text{Cl}_{12}$  ( $S^{\text{Y}}$ ). Hydrogen atoms are omitted for clarity. Carbon and silicon atoms are shown with reduced radii in ball and stick representation. All other atoms are shown with atomic displacement parameters set at the 50% probability level. Selected bond lengths [Å] and angles [deg]: Y1–Cl1 2.7678(9), Y1–Cl2 2.6710(10), Y1–Cl3 2.9115(10), Y1–Cl4 2.6642(10), Y2–Cl4 2.6239(10), Y2–Cl5 2.6472(10), Y2–Cl6 2.7741(8), Cl2–Y1–Cl2' 142.51(3), Y1–Cl4–Y2 127.65(4), Cl5–Y2–Cl5' 128.14(4), Cl1–Cl3–Cl6 179.98(7).

matching those of previously reported  $[((\text{Me}_3\text{Si})_2\text{C}_5\text{H}_3)\text{Y}(\text{AlMe}_4)\text{Cl}]_2$ .<sup>29</sup> Remarkably, the tetramethylaluminato bonding is highly asymmetric, as evidenced by Y1–Cl17/18 bond lengths of 2.4751(3) and 2.5833(3) Å, differing by more than 0.1 Å. It is noteworthy that the shorter Y1–Cl17 bond is located trans to the bridging chloro ligand. Such an asymmetry was neither detected in precursor  $3^{\text{Y}}$  nor in the corresponding cyclopentadienyl half-sandwich  $[((\text{Me}_3\text{Si})_2\text{C}_5\text{H}_3)\text{Y}(\text{AlMe}_4)\text{Cl}]_2$ .<sup>29</sup>

The hexametallic cluster  $(\text{Flu}^{\text{Si}})_6\text{Y}_6\text{Cl}_{12}$  ( $S^{\text{Y}}$ ) obtained from the 1.7 equiv reaction (Figure 6), crystallized in the trigonal space group R3c. The molecular structure features two six-membered rings of alternating yttrium and chlorine atoms which are interconnected by additional three Y–Cl–Y linkages (Y1–Cl4 2.6642(10) and Y2–Cl4 2.6239(10) Å, Y1–Cl4–Y2 127.65(4)°).

The upper ring spanned by Y1, Cl2, and their symmetry-related positions (Y1–Cl2 2.6710(10) Å) is almost planar (Cl2–Y1–Cl2' 142.51(3)°). This is caused by two  $\mu_3$ -bridging chloro caps (Y1–Cl1 2.7678(9) Å and Y1–Cl3 2.9115(10) Å), accomplishing a hexagonal bipyramidal unit. In contrast, the lower ring spanned by Y2 and Cl5 shows a chairlike structure (Y2–Cl5 2.6472(10) Å, Cl5–Y2–Cl5' 128.14(4)°), which is implied by only one  $\mu_3$ -bridging chloro cap (Y2–Cl6 2.7741(8) Å). Due to the high symmetry of the cluster the angle Cl1–Cl3–Cl6 is 179.98(7)°. The coordination sphere of each yttrium is completed by a  $\text{Flu}^{\text{Si}}$  ligand, resulting in 7- and 8-coordinate metal centers. The structural motif of  $S^{\text{Y}}$  is new, but comparable structures with two hexagonal bipyramidal units bridged by two chloro ligands are known:  $[((\text{Me}_2\text{C}_5\text{H}_3)_3\text{Nd}_3(\mu_2\text{-Cl})_3(\mu_3\text{-Cl})_2)\{\mu_2\text{-Cl}\}]_2$  and  $[((\text{C}_3\text{Me}_4\text{CH}_2\text{CH}_2\text{NMe}_2\text{AlEt}_3)_2\text{-}(\text{C}_5\text{Me}_4\text{CH}_2\text{CH}_2\text{NMe}_2)\text{-Ln}_3(\mu_2\text{-Cl})_3(\mu_3\text{-Cl})_2)\{\mu_2\text{-Cl}\}]_2$ .<sup>35,71</sup>

## CONCLUSION

The selective formation of half-sandwich complexes of the type  $(\text{Flu}^{\text{R}})\text{Ln}(\text{AlMe}_4)_2$  via salt metathesis protocols, applying  $\text{Ln}(\text{AlMe}_4)_3$  and  $\text{K}(\text{Flu}^{\text{R}})$ , is governed by the rare-earth metal size and sterics of the fluorenyl ligand. Rather unexpectedly, the largest rare-earth metal center lanthanum favors half-sandwich complexes for both unsubstituted (Flu), 6-ring-substituted ( $\text{Flu}^{\text{tBu}}$ ) and 5-ring-substituted fluorenyl ligands ( $\text{Flu}^{\text{Si}}$ ). For the sterically less demanding Flu and  $\text{Flu}^{\text{tBu}}$  ligands, the smaller-sized rare-earth metal centers yttrium and lutetium give either mixtures of half-sandwich/sandwich complexes or in case of  $\text{Lu}(\text{AlMe}_4)_3/\text{K}(\text{Flu})$  only the lutetocene complex  $(\text{Flu})_2\text{Lu}(\text{AlMe}_4)$ . Crucially, the 5-ring-substituted fluorenyl ligand  $\text{Flu}^{\text{Si}}$  (“Cl-protected”) provides the highest immediate shielding of the Ln(III) center, allowing for the high-yield synthesis of  $(\text{Flu}^{\text{Si}})\text{Ln}(\text{AlMe}_4)_2$  for the entire Ln(III) size range (Ln = La, Nd, Y, and Lu). Important structural features of such monomeric half-sandwich complexes comprise tilted fluorenyl ligands (asymmetric  $\eta^5$ -coordination) and distinct tetramethylaluminato coordination.

Like the cyclopentadienyl congeners, the fluorenyl half-sandwich complexes display efficient catalysts for isoprene polymerization when pretreated with perfluorinated borates or borane activators. Cl1-unprotected fluorenyl ligands can be easily abstracted by trityl borate  $[\text{Ph}_3\text{C}][\text{B}(\text{C}_6\text{F}_5)_4]$ , as evidenced for complexes  $(\text{Flu})\text{La}(\text{AlMe}_4)_2$  and  $(\text{Flu}^{\text{tBu}})\text{La}(\text{AlMe}_4)_2$  by NMR spectroscopy. This cationization pathway is distinct from that observed for cyclopentadienyl derivatives and has direct implications for the polymerization reaction. Choice of the rare-earth metal (size), fluorenyl ligand, and cocatalyst affects decisively the catalytic activity and microstructure of the polyisoprenes. Generally, the larger rare-earth metals are more efficient and produce mainly *trans*-1,4-polyisoprene (maximum 85%), while the smaller ones give access to higher *cis*-1,4-contents (maximum 78%). Finally, like in the case of the cyclopentadienyl congeners, equimolar reactions of  $(\text{Flu}^{\text{R}})\text{Ln}(\text{AlMe}_4)_2$  with  $\text{Me}_2\text{AlCl}$  did not produce catalytically active species but afforded the crystalline  $\text{AlMe}_4/\text{Cl}$  interchange products  $[(\text{Flu}^{\text{Si}})\text{Y}(\text{AlMe}_4)(\mu\text{-Cl})]_2$  and  $(\text{Flu}^{\text{Si}})_6\text{Y}_6\text{Cl}_{12}$ .

## EXPERIMENTAL SECTION

**General Procedures.** All manipulations were performed with rigorous exclusion of air and water, using standard Schlenk, high-vacuum, and glovebox techniques (MBraun UNILab-pro-dp; < 0.5 ppm of  $\text{O}_2$ , < 0.5 ppm of  $\text{H}_2\text{O}$ ). Toluene and *n*-hexane were purified by using Grubbs columns (MBraun SPS, solvent purification system) and stored inside a glovebox.  $[\text{D}_8]\text{thf}$  and  $[\text{D}_6]\text{benzene}$  were purchased from Aldrich, degassed and dried over NaK for 24 h, filtered, and stored inside a glovebox. Fluorene was purchased from Merck and used as received. 2,7-Di-*tert*-butylfluorene and KH were obtained from abcr. KH was washed several times with *n*-hexane prior to use.  $[\text{Ph}_3\text{C}][\text{B}(\text{C}_6\text{F}_5)_4]$ ,  $[\text{PhNMe}_2\text{H}][\text{B}(\text{C}_6\text{F}_5)_4]$ , and  $\text{B}(\text{C}_6\text{F}_5)_3$  were obtained from Boulder Scientific Company and used without further purification. Dimethylaluminum chloride, triethylaluminum, and isoprene were obtained from Sigma-Aldrich. Isoprene was dried over triethylaluminum and distilled prior to use. Homoleptic  $\text{Ln}(\text{AlMe}_4)_3$  (Ln = Y, La, Nd, and Lu) were prepared according to literature procedures.<sup>72</sup>  $\text{K}(\text{Flu})$ ,  $\text{K}(\text{Flu}^{\text{tBu}})$ ,<sup>73</sup> and  $\text{K}(\text{Flu}^{\text{Si}})$ <sup>74</sup> were prepared according to slightly modified literature procedures. NMR spectra were recorded on a Bruker AVBII+400 ( $^1\text{H}$ : 400.11 MHz;  $^{13}\text{C}$ : 100.61 MHz) spectrometer.  $^1\text{H}$  and  $^{13}\text{C}$  shifts are referenced to internal solvent resonances and reported in parts per million relative to tetramethylsilane (TMS). Coupling constants are given in Hz. Elemental analyses were performed on an ElementarVario Micro Cube. IR spectra were recorded on a NICOLET 6700 FTIR

spectrometer with a DRIFT cell (KBr window). Size exclusion chromatography (SEC) was performed on a Viscotek GPCmax consists of a GPCmax apparatus and a model TDA 302 triple detector array. Sample solutions (1.0 mg polymer per mL thf) were filtered through a 0.45  $\mu\text{m}$  syringe filter prior injection. The flow rate was 1 mL/min  $dn/dc$  and  $dA/dc$  data were determined by means of the integrated OmniSec software. The microstructure of the polyisoprenes was determined on a Bruker AVBII+400 spectrometer in [D]-chloroform at ambient temperatures. Glass transition temperatures of the polyisoprenes ( $T_g$ ) were recorded on a Perkin–Elmer DSC 8000, calibrated with cyclohexane and indium standards, and scanning from  $-100$  °C up to  $+100$  °C with heating rates of 20 K/min and cooling rates of 60 K/min in  $N_2$  atmosphere.

**Synthesis of (Flu)La(AlMe<sub>4</sub>)<sub>2</sub> (1<sup>La</sup>).** La(AlMe<sub>4</sub>)<sub>3</sub> (50 mg, 0.13 mmol) was dissolved in toluene (5 mL), and K(Flu) (26 mg, 0.13 mmol) was slowly added under vigorous stirring. After stirring the reaction mixture for 5 h at 40 °C, the suspension was filtered, and the solvent was removed in vacuo to give 1<sup>La</sup> as a solid. Crystalline 1<sup>La</sup> was obtained from a saturated *n*-hexane solution at  $-35$  °C (50 mg, 0.11 mmol, 84%). <sup>1</sup>H NMR (400 MHz, [D<sub>6</sub>]benzene, 26 °C):  $\delta$  = 7.90 (dq, <sup>3</sup>J<sub>HH</sub> = 8.2 Hz, <sup>4</sup>J<sub>HH</sub> = 0.9 Hz, 2 H, 6/9FluH), 7.37 (dt, <sup>3</sup>J<sub>HH</sub> = 8.4 Hz, <sup>4</sup>J<sub>HH</sub> = 1.0 Hz, 2 H, 3/12FluH), 7.10 (ddd, <sup>3</sup>J<sub>HH</sub> = 8.3 Hz, <sup>3</sup>J<sub>HH</sub> = 6.9 Hz, <sup>4</sup>J<sub>HH</sub> = 1.2 Hz, 2 H, 4/11FluH), 7.00 (ddd, <sup>3</sup>J<sub>HH</sub> = 8.1 Hz, <sup>3</sup>J<sub>HH</sub> = 6.9 Hz, <sup>4</sup>J<sub>HH</sub> = 1.1 Hz, 2 H, 5/10FluH), 6.28 (t, <sup>4</sup>J<sub>HH</sub> = 0.8 Hz, 1 H, 1FluH),  $-0.53$  (s, 24 H, AlMe<sub>4</sub>) ppm. <sup>13</sup>C{<sup>1</sup>H} NMR (101 MHz, [D<sub>6</sub>]benzene, 26 °C):  $\delta$  = 135.0 (s, 2/13Flu), 127.8 (s, 4/11Flu), 124.2 (s, 6/9Flu), 123.27 (s, 7/8Flu), 122.1 (s, 3/12Flu), 121.1 (s, 5/10Flu), 91.3 (s, 1Flu), 3.4 (br s, AlMe<sub>4</sub>) ppm. IR (DRIFT):  $\tilde{\nu}$  = 3059 (vw), 3041 (vw), 2923 (w), 2888 (w), 2829 (vw), 2783 (vw), 1939 (vw), 1910 (vw), 1887 (vw), 1819 (vw), 1791 (vw), 1702 (vw), 1592 (vw), 1504 (vw), 1473 (w), 1445 (w), 1430 (w), 1329 (w), 1282 (vw), 1220 (w), 1200 (w), 1185 (m), 1147 (vw), 1116 (vw), 1006 (vw), 986 (vw), 943 (vw), 823 (vw), 754 (s), 725 (vs), 716 (vs), 703 (vs), 692 (vs), 586 (m), 570 (s), 535 (m), 516 (m), 484 (w), 475 (w), 433 (m), 424 (w) cm<sup>-1</sup>. Elemental analysis of crystalline 1<sup>La</sup>, calcd for C<sub>29</sub>H<sub>49</sub>Al<sub>2</sub>La (478.63): C 52.73, H 6.95; found: C 52.55, H 6.97.

**Synthesis of (Flu<sup>Si</sup>)La(AlMe<sub>4</sub>)<sub>2</sub> (2<sup>La</sup>).** La(AlMe<sub>4</sub>)<sub>3</sub> (50 mg, 0.13 mmol) was dissolved in toluene (5 mL), and K(Flu<sup>Si</sup>) (40 mg, 0.13 mmol) was slowly added under vigorous stirring. After stirring the reaction mixture for 5 h at 40 °C, the suspension was filtered, and the solvent was removed in vacuo to give 2<sup>La</sup> as a solid. Crystalline 2<sup>La</sup> was obtained from a saturated *n*-hexane solution at  $-35$  °C (69 mg, 0.12 mmol, 93%). <sup>1</sup>H NMR (400 MHz, [D<sub>6</sub>]benzene, 26 °C):  $\delta$  = 7.95 (d, <sup>3</sup>J<sub>HH</sub> = 8.7 Hz, 2 H, 6/9FluH), 7.50–7.56 (m, 2 H, 3/12FluH), 7.20 (dd, <sup>3</sup>J<sub>HH</sub> = 8.7 Hz, <sup>4</sup>J<sub>HH</sub> = 1.7 Hz, 2 H, 5/10FluH), 6.34 (s, 1 H, 1FluH), 1.31 (s, 18 H, Flu-CMe<sub>3</sub>),  $-0.52$  (s, 24 H, AlMe<sub>4</sub>) ppm. <sup>13</sup>C{<sup>1</sup>H} NMR (101 MHz, [D<sub>6</sub>]benzene, 26 °C):  $\delta$  = 150.8 (s, 4/11Flu), 135.4 (s, 7/8Flu), 123.9 (s, 6/9Flu), 121.2 (s, 2/13Flu), 120.3 (s, 5/10Flu), 117.4 (s, 3/12Flu), 91.6 (s, 1Flu), 35.6 (s, Flu-CMe<sub>3</sub>), 31.7 (s, Flu-CMe<sub>3</sub>), 3.2 (brs, AlMe<sub>4</sub>) ppm. IR (DRIFT):  $\tilde{\nu}$  = 3074 (vw), 2963 (m), 2903 (w), 2883 (w), 2785 (vw), 1904 (vw), 1758 (vw), 1594 (w), 1522 (vw), 1481 (w), 1460 (vw), 1440 (w), 1423 (w), 1394 (vw), 1363 (w), 1340 (vw), 1309 (vw), 1262 (w), 1202 (w), 1183 (m), 1137 (vw), 1086 (vw), 1023 (vw), 987 (vw), 954 (vw), 924 (vw), 908 (vw), 880 (w), 812 (m), 719 (vs), 689 (vs), 656 (s), 569 (s), 538 (m), 476 (m), 445 (vw), 411 (w) cm<sup>-1</sup>. Elemental analysis of crystalline 2<sup>La</sup>, calcd for C<sub>29</sub>H<sub>49</sub>Al<sub>2</sub>La (590.58): C 58.98, H 8.36; found: C 58.53, H 8.39. Although these results are outside the range viewed as establishing analytical purity (C:  $-0.45\%$ ), they are provided to illustrate the best values obtained to date.

**Synthesis of (Flu<sup>Si</sup>)Y(AlMe<sub>4</sub>)<sub>2</sub> (2<sup>Y</sup>).** Y(AlMe<sub>4</sub>)<sub>3</sub> (50 mg, 0.14 mmol) was dissolved in toluene (5 mL), and K(Flu<sup>Si</sup>) (45 mg, 0.14 mmol) was slowly added under vigorous stirring. After stirring the reaction mixture for 8 h at 40 °C, the suspension was filtered and the solvent was removed in vacuo to give 2<sup>Y</sup> as a solid. Crystalline 2<sup>Y</sup> was obtained from a saturated *n*-hexane solution at  $-35$  °C (54 mg, 0.10 mmol, 70%). <sup>1</sup>H NMR (400 MHz, [D<sub>6</sub>]benzene, 26 °C):  $\delta$  = 7.89 (dt, <sup>3</sup>J<sub>HH</sub> = 8.8 Hz, <sup>4</sup>J<sub>HH</sub> = 0.9 Hz, 2 H, 6/10FluH), 7.54 (dd, <sup>4</sup>J<sub>HH</sub> = 1.8 Hz, <sup>4</sup>J<sub>HH</sub> = 0.9 Hz, 2 H, 3/12FluH), 7.20 (dd, <sup>3</sup>J<sub>HH</sub> = 8.9 Hz, <sup>4</sup>J<sub>HH</sub> = 1.8 Hz,

2 H, 5/10FluH), 6.20 (q, <sup>4</sup>J<sub>HH</sub> = 0.8 Hz, 1 H, 1FluH), 1.30 (s, 18 H, Flu-CMe<sub>3</sub>),  $-0.60$  (d, <sup>3</sup>J<sub>YH</sub> = 2.2 Hz, 24 H, AlMe<sub>4</sub>) ppm. <sup>13</sup>C{<sup>1</sup>H} NMR (101 MHz, [D<sub>6</sub>]benzene, 26 °C):  $\delta$  = 150.0 (s, 4/11Flu), 132.8 (s, 7/8Flu), 124.2 (s, 6/9Flu), 120.8 (s, 5/10Flu), 119.4 (s, 2/13Flu), 118.7 (s, 3/12Flu), 88.3 (d, <sup>1</sup>J<sub>CY</sub> = 2.7 Hz, 1Flu), 35.5 (s, Flu-CMe<sub>3</sub>), 31.6 (s, Flu-CMe<sub>3</sub>),  $-0.5$  (br s, AlMe<sub>4</sub>) ppm. IR (DRIFT):  $\tilde{\nu}$  = 3078 (vw), 2964 (s), 2899 (w), 2879 (w), 2824 (vw), 1906 (vw), 1764 (vw), 1596 (w), 1522 (vw), 1481 (w), 1461 (w), 1439 (w), 1424 (w), 1393 (vw), 1363 (w), 1344 (w), 1309 (vw), 1262 (w), 1235 (vw), 1212 (w), 1185 (m), 1138 (vw), 1087 (vw), 1023 (vw), 986 (vw), 955 (vw), 924 (vw), 908 (vw), 882 (w), 812 (s), 731 (vs), 721 (vs), 712 (vs), 702 (vs), 691 (vs), 654 (s), 600 (m), 593 (m), 580 (vs), 574 (vs), 562 (s), 555 (m), 546 (s), 521 (w), 475 (m), 450 (vw), 415 (vs), 405 (vw) cm<sup>-1</sup>. Elemental analysis of crystalline 2<sup>Y</sup>, calcd for C<sub>29</sub>H<sub>49</sub>Al<sub>2</sub>Y (540.58): C 64.43, H 9.14; found: C 64.04, H 9.04.

**Synthesis of (Flu)<sub>2</sub>Lu(AlMe<sub>4</sub>) (1<sup>Lu</sup>).** Lu(AlMe<sub>4</sub>)<sub>3</sub> (50 mg, 0.12 mmol) was dissolved in toluene (5 mL), and K(Flu) (46 mg, 0.24 mmol) was slowly added under vigorous stirring. After stirring the reaction mixture for 8 h at 40 °C, the suspension was filtered, and the solvent was removed in vacuo to give 1<sup>Lu</sup> as a solid. Crystalline 1<sup>Lu</sup> was obtained from a saturated *n*-hexane solution at  $-35$  °C (41 mg, 0.07 mmol, 60%). <sup>1</sup>H NMR (400 MHz, [D<sub>6</sub>]benzene, 26 °C):  $\delta$  = 7.81–7.87 (m, 4 H, 3/12FluH), 7.17–7.20 (m, 4 H, 6/9FluH), 6.90–6.97 (m, 8 H, 4/5/10/11FluH), 6.13 (s, 2 H, 1FluH),  $-0.52$  (s, 6 H, AlMe<sub>2</sub>),  $-1.71$  (s, 6 H, LuMe<sub>2</sub>AlMe<sub>2</sub>) ppm. <sup>13</sup>C{<sup>1</sup>H} NMR (101 MHz, [D<sub>6</sub>]benzene, 26 °C):  $\delta$  = 130.6 (s, 2/13Flu), 126.7 (s, 4/11Flu), 124.4 (s, 3/12Flu), 122.0 (s, 6/9Flu), 120.6 (s, 5/10Flu), 119.5 (s, 7/8Flu), 84.1 (s, 1Flu), 14.9 (br s, AlMe<sub>4</sub>) ppm. IR (DRIFT):  $\tilde{\nu}$  = 3088 (vw), 3076 (vw), 3054 (vw), 2938 (w), 2889 (vw), 2818 (vw), 1946 (vw), 1890 (vw), 1819 (vw), 1792 (vw), 1695 (vw), 1594 (w), 1508 (vw), 1473 (w), 1440 (w), 1331 (m), 1284 (vw), 1238 (w), 1223 (w), 1200 (m), 1188 (w), 1153 (vw), 1119 (vw), 999 (vw), 985 (vw), 943 (w), 875 (vw), 848 (w), 823 (w), 757 (vs), 743 (vs), 732 (vs), 726 (vs), 705 (vs), 624 (w), 590 (s), 563 (m), 497 (w), 480 (w), 439 (s), 422 (w) cm<sup>-1</sup>. Elemental analysis of crystalline 1<sup>Lu</sup>, calcd for C<sub>30</sub>H<sub>30</sub>AlLu (592.52): C 60.81, H 5.10; found: C 60.75, H 5.03.

**General Procedure for the Preparation of (Flu<sup>Si</sup>)Ln(AlMe<sub>4</sub>)<sub>2</sub> (3<sup>La</sup>, 3<sup>Nd</sup>, 3<sup>Y</sup>, and 3<sup>Lu</sup>).** Ln(AlMe<sub>4</sub>)<sub>3</sub> was dissolved in toluene (5 mL), and an equimolar amount of K(Flu<sup>Si</sup>) was slowly added under vigorous stirring. After stirring the reaction mixture for 2 h at 40 °C, the suspension was filtered and the solvent was removed in vacuo to give 3<sup>Ln</sup> as solids. Crystallization was accomplished from saturated *n*-hexane solutions at  $-35$  °C to yield single crystals suitable for X-ray diffraction analysis.

**Synthesis of (Flu<sup>Si</sup>)La(AlMe<sub>4</sub>)<sub>2</sub> (3<sup>La</sup>).** Following the procedure described above, La(AlMe<sub>4</sub>)<sub>3</sub> (200 mg, 0.50 mmol) and K(Flu<sup>Si</sup>) (138 mg, 0.50 mmol) yielded 259 mg of 3<sup>La</sup> (0.47 mmol, 94%) as yellow crystals. <sup>1</sup>H NMR (400 MHz, [D<sub>6</sub>]benzene, 26 °C):  $\delta$  = 7.92 (d, <sup>3</sup>J<sub>HH</sub> = 8.2 Hz, 2 H, 6/9FluH), 7.75 (d, <sup>3</sup>J<sub>HH</sub> = 8.4 Hz, 2 H, 3/12FluH), 7.16–7.22 (m, 2 H, 4/11FluH), 7.03–7.09 (m, 2 H, 5/10FluH), 0.41 (s, 9 H, SiMe<sub>3</sub>),  $-0.52$  (s, 24 H, AlMe<sub>4</sub>) ppm. <sup>13</sup>C{<sup>1</sup>H} NMR (101 MHz, [D<sub>6</sub>]benzene, 26 °C):  $\delta$  = 141.6 (s, 2/13Flu), 128.5 (s, 4/11Flu), 128.3 (s, 7/8Flu), 124.5 (s, 6/9Flu), 123.7 (s, 3/12Flu), 122.2 (s, 5/10Flu), 97.55 (s, 1Flu), 3.6 (br s, AlMe<sub>4</sub>), 2.4 (s, SiMe<sub>3</sub>) ppm. IR (DRIFT):  $\tilde{\nu}$  = 3079 (w), 3054 (w), 3040 (w), 2949 (m), 2934 (m), 2892 (m), 2833 (w), 2783 (w), 1941 (w), 1911 (vw), 1880 (vw), 1821 (vw), 1790 (vw), 1699 (vw), 1591 (w), 1531 (vw), 1506 (vw), 1497 (vw), 1470 (w), 1456 (m), 1433 (m), 1405 (m), 1328 (m), 1289 (w), 1277 (m), 1260 (w), 1248 (s), 1208 (s), 1186 (m), 1154 (m), 1122 (w), 1020 (m), 992 (w), 960 (s), 943 (w), 866 (s), 836 (vs), 801 (w), 763 (s), 754 (m), 740 (m), 732 (s), 713 (vs), 708 (vs), 699 (vs), 691 (vs), 639 (m), 625 (m), 615 (m), 584 (s), 576 (s), 557 (m), 550 (s), 537 (w), 519 (m), 509 (w), 493 (w), 480 (w), 472 (w), 444 (s), 434 (s), 429 (s), 412 (m), 405 (w) cm<sup>-1</sup>. Elemental analysis of crystalline 3<sup>La</sup>, calcd for C<sub>24</sub>H<sub>41</sub>Al<sub>2</sub>SiLa (550.55): C 52.36, H 7.51; found: C 51.89, H 7.46. Although these results are outside the range viewed as establishing analytical purity (C:  $-0.47\%$ ), they are provided to illustrate the best values obtained to date.

**Synthesis of (Flu<sup>Si</sup>)Nd(AlMe<sub>4</sub>)<sub>2</sub> (3<sup>Nd</sup>).** Following the procedure described above, Nd(AlMe<sub>4</sub>)<sub>3</sub> (203 mg, 0.50 mmol) and K(Flu<sup>Si</sup>) (138

mg, 0.50 mmol) yielded 200 mg of  $3^{\text{Nd}}$  (0.36 mmol, 72%) as green crystals.  $^1\text{H}$  NMR (400 MHz,  $[\text{D}_6]$ benzene, 26 °C):  $\delta$  = 10.23 (brs, 24 H,  $\text{AlMe}_4$ ), 8.13 (brs, 9 H,  $\text{SiMe}_3$ ), 7.46 (brs, 2 H, FluH), 1.79 (brs, 2 H, FluH), 1.56 (brs, 2 H, FluH), -2.19 (brs, 2 H, FluH) ppm. IR (DRIFT):  $\bar{\nu}$  = 3080 (vw), 3041 (vw), 2948 (w), 2934 (vw), 2891 (vw), 2826 (vw), 2788 (vw), 1943 (vw), 1913 (vw), 1883 (vw), 1823 (vw), 1791 (vw), 1591 (vw), 1531 (vw), 1505 (vw), 1470 (vw), 1456 (w), 1433 (m), 1406 (w), 1328 (w), 1304 (vw), 1290 (w), 1278 (m), 1260 (w), 1249 (s), 1207 (m), 1189 (m), 1155 (w), 1122 (vw), 1016 (vw), 993 (vw), 960 (m), 943 (vw), 866 (m), 852 (m), 835 (vs), 763 (s), 752 (m), 733 (s), 715 (vs), 702 (vs), 693 (vs), 625 (m), 613 (w), 582 (m), 568 (m), 552 (m), 519 (w), 499 (w), 471 (w), 440 (s), 431 (m), 414 (w)  $\text{cm}^{-1}$ . Elemental analysis of crystalline  $3^{\text{Nd}}$ , calcd for  $\text{C}_{24}\text{H}_{41}\text{Al}_2\text{SiNd}$  (555.88): C 51.86, H 7.43; found: C 51.49, H 7.17.

**Synthesis of  $(\text{Flu}^{\text{Si}})\text{Y}(\text{AlMe}_4)_2$  ( $3^{\text{Y}}$ ).** Following the procedure described above,  $\text{Y}(\text{AlMe}_4)_3$  (175 mg, 0.50 mmol) and  $\text{K}(\text{Flu}^{\text{Si}})$  (138 mg, 0.50 mmol) yielded 185 mg of  $3^{\text{Y}}$  (0.37 mmol, 74%) as yellow crystals.  $^1\text{H}$  NMR (400 MHz,  $[\text{D}_6]$ benzene, 26 °C):  $\delta$  = 7.95 (dq,  $^3J_{\text{HH}} = 8.2$  Hz,  $^4J_{\text{HH}} = 0.8$  Hz, 2 H, 6/9FluH), 7.74 (dt,  $^3J_{\text{HH}} = 8.3$  Hz,  $^4J_{\text{HH}} = 1.0$  Hz, 2 H, 3/12FluH), 7.09–7.14 (m, 2 H, 4/11FluH), 7.03–7.08 (m, 2 H, 5/10FluH), 0.38 (s, 9 H,  $\text{SiMe}_3$ ), -0.56 ppm (d,  $^2J_{\text{YH}} = 2.3$  Hz, 24 H,  $\text{AlMe}_4$ ).  $^{13}\text{C}\{^1\text{H}\}$  NMR (101 MHz,  $[\text{D}_6]$ benzene, 26 °C):  $\delta$  = 138.5 (s, 2/13Flu), 128.0 (s, 4/11Flu), 126.9 (s, 7/8Flu), 125.2 (s, 6/9Flu), 124.9 (s, 3/12Flu), 122.5 (s, 5/10Flu), 93.3 (d,  $J_{\text{CY}} = 4.8$ , 1Flu), 2.3 (s,  $\text{SiMe}_3$ ), 1.4 (br s,  $\text{AlMe}_4$ ). IR (DRIFT):  $\bar{\nu}$  = 3077 (vw), 2949 (w), 2888 (w), 2822 (vw), 1945 (w), 1915 (vw), 1885 (vw), 1822 (vw), 1792 (vw), 1699 (vw), 1593 (vw), 1506 (vw), 1471 (vw), 1456 (w), 1435 (m), 1405 (w), 1329 (w), 1277 (m), 1249 (s), 1228 (w), 1208 (m), 1191 (m), 1156 (m), 1124 (vw), 1011 (vw), 991 (vw), 961 (m), 864 (m), 835 (vs), 763 (s), 714 (vs), 706 (vs), 697 (vs), 626 (m), 581 (s), 571 (s), 519 (w), 493 (m), 463 (m), 441 (vs), 415 (w)  $\text{cm}^{-1}$ . Elemental analysis of crystalline  $3^{\text{Y}}$ , calcd for  $\text{C}_{24}\text{H}_{41}\text{Al}_2\text{SiY}$  (500.55): C 57.59, H 8.26; found: C 57.41, H 8.58.

**Synthesis of  $(\text{Flu}^{\text{Si}})\text{Lu}(\text{AlMe}_4)_2$  ( $3^{\text{Lu}}$ ).** Following the procedure described above,  $\text{Lu}(\text{AlMe}_4)_3$  (218 mg, 0.50 mmol) and  $\text{K}(\text{Flu}^{\text{Si}})$  (138 mg, 0.50 mmol) yielded 241 mg of  $3^{\text{Lu}}$  (0.41 mmol, 82%) as yellow crystals.  $^1\text{H}$  NMR (400 MHz,  $[\text{D}_6]$ benzene, 26 °C):  $\delta$  = 7.91–7.95 (m, 2 H, 6/9FluH), 7.75–7.78 (m, 2 H, 3/12FluH), 7.04–7.12 (m, 4 H, 4/5/10/11FluH), 0.38 (s, 9 H,  $\text{SiMe}_3$ ), -0.40 (s, 24 H,  $\text{AlMe}_4$ ) ppm.  $^{13}\text{C}\{^1\text{H}\}$  NMR (101 MHz,  $[\text{D}_6]$ benzene, 26 °C):  $\delta$  = 138.1 (s, 2/13Flu), 127.9 (s, 4/11Flu), 126.5 (s, 7/8Flu), 125.1 (s, 6/9Flu), 125.0 (s, 3/12Flu), 122.5 (s, 5/10Flu), 91.3 (s, 1Flu), 2.9 (br s,  $\text{AlMe}_4$ ), 2.3 (s,  $\text{SiMe}_3$ ). IR (DRIFT):  $\bar{\nu}$  = 3081 (w), 3041 (w), 2948 (m), 2884 (m), 2820 (w), 1945 (w), 1915 (w), 1885 (w), 1822 (w), 1791 (w), 1699 (w), 1593 (w), 1539 (vw), 1531 (w), 1506 (w), 1470 (w), 1456 (m), 1434 (s), 1405 (m), 1361 (w), 1329 (m), 1305 (w), 1288 (m), 1276 (s), 1260 (m), 1248 (vs), 1233 (s), 1208 (s), 1192 (s), 1155 (m), 1124 (w), 1014 (w), 990 (w), 961 (s), 945 (w), 863 (s), 834 (vs), 763 (vs), 752 (s), 739 (s), 715 (vs), 709 (vs), 696 (vs), 649 (m), 625 (s), 601 (m), 594 (m), 581 (s), 571 (s), 558 (s), 531 (m), 519 (m), 482 (s), 468 (m), 460 (m), 454 (m), 441 (vs), 418 (m), 403 (w)  $\text{cm}^{-1}$ . Elemental analysis of crystalline  $3^{\text{Lu}}$ , calcd for  $\text{C}_{24}\text{H}_{41}\text{Al}_2\text{SiLu}$  (586.61): C 49.14, H 7.05; found: C 49.16, H 7.13.

**Synthesis of  $(\text{Flu}^{\text{Si}})\text{Y}(\text{AlMe}_4)\text{Cl}_2$  ( $4^{\text{Y}}$ ).** To a *n*-hexane solution of  $(\text{Flu}^{\text{Si}})\text{Y}(\text{AlMe}_4)_2$  (25 mg, 0.05 mmol) was added a solution of  $\text{Me}_2\text{AlCl}$  (4.5  $\mu\text{L}$ , 6 mg, 0.05 mmol) in *n*-hexane at -35 °C without stirring. After 2 days, a small amount of yellow crystals had formed which were subjected to an X-ray diffraction experiment.

**Synthesis of  $(\text{Flu}^{\text{Si}})_6\text{Y}_6\text{Cl}_{12}$  ( $5^{\text{Y}}$ ).** To a *n*-hexane solution of  $(\text{Flu}^{\text{Si}})\text{Y}(\text{AlMe}_4)_2$  (25 mg, 0.05 mmol) was added a solution of  $\text{Me}_2\text{AlCl}$  (8  $\mu\text{L}$ , 10 mg, 0.09 mmol) in *n*-hexane at -35 °C without stirring. After 1 week, a small amount of colorless crystals had formed which were subjected to an X-ray diffraction experiment.

**Polymerization of Isoprene.** Exemplarily, the polymerization procedure is described for entry 1 of Table 2.  $[\text{Ph}_3\text{C}][\text{B}(\text{C}_6\text{F}_5)_4]$  (cocatalyst **A**) (18.22 mg, 0.02 mmol) was added to a solution of  $1^{\text{La}}$  (9.56 mg, 0.02 mmol) in toluene (8 mL). The mixture was aged at ambient temperature for 30 min. Then, isoprene (1.36 g, 20 mmol) was added and the polymerization carried out at 40 °C for 1 h. The reaction was terminated by pouring the polymerization mixture into 25

mL of methanol containing 0.1% (w/w) 2,6-di-*tert*-butyl-4-methylphenol as a stabilizer. The polymer was washed with methanol and dried under vacuum at ambient temperature to constant weight.

**Crystallography.** Crystals from all half-sandwich complexes suitable for X-ray crystallography were grown by standard techniques from saturated *n*-hexane solutions at -40 °C. Crystalline  $1^{\text{La}}$  was obtained from a saturated *n*-hexane solution at -35 °C.  $[\text{K}(\text{Flu}^{\text{Si}})(\text{THF})_2]_n$  was crystallized from THF and 1-CPh<sub>3</sub>-Flu<sup>tbu</sup> from difluorobenzene at -40 °C. Single crystals were selected inside a glovebox, coated with Parabar 10312 (previously known as Paratone N, Hampton Research) or perfluorinated ether and fixed on a microloop. Data were collected on a Bruker APEX DUO instrument equipped with an  $I\mu\text{S}$  microfocus sealed tube and QUAZAR optics for Mo  $K_\alpha$  radiation ( $\lambda = 0.71073$  Å). The data collection strategy was determined using COSMO<sup>75</sup> employing  $\omega$  and  $\phi$  scans. Raw data were processed using APEX<sup>76</sup> and SAINT<sup>77</sup> corrections for absorption effects were applied using SADABS.<sup>78</sup> Data for  $[\text{K}(\text{Flu}^{\text{Si}})(\text{THF})_2]_n$  and 1-CPh<sub>3</sub>-Flu<sup>tbu</sup> were processed using APEX3<sup>76</sup> software package.  $1^{\text{La}}$  and  $1^{\text{Lu}}$  were refined as twins, and TWINABS<sup>79</sup> was used for absorption correction. The structures were solved by direct methods and refined against all data by full-matrix least-squares methods on  $F^2$  using SHELXTL<sup>80</sup> and Shelxle.<sup>81</sup> All graphics were produced employing ORTEP-3<sup>82</sup> and POV-Ray.<sup>83</sup>

## ■ ASSOCIATED CONTENT

### ● Supporting Information

The Supporting Information is available free of charge on the ACS Publications website at DOI: 10.1021/acs.organomet.7b00543.

$^1\text{H}/^{13}\text{C}/^{19}\text{F}$  NMR spectra, DSC and GPC curves, and X-ray crystallographic data for 1-5,  $[\text{K}(\text{Flu}^{\text{Si}})(\text{THF})_2]_n$ , and 1-CPh<sub>3</sub>-Flu<sup>tbu</sup> (PDF)

### Accession Codes

CCDC 1562938–1562949 contain the supplementary crystallographic data for this paper. These data can be obtained free of charge via [www.ccdc.cam.ac.uk/data\\_request/cif](http://www.ccdc.cam.ac.uk/data_request/cif), or by emailing [data\\_request@ccdc.cam.ac.uk](mailto:data_request@ccdc.cam.ac.uk), or by contacting The Cambridge Crystallographic Data Centre, 12 Union Road, Cambridge CB2 1EZ, UK; fax: +44 1223 336033.

## ■ AUTHOR INFORMATION

### Corresponding Author

\*E-mail: [reiner.anwander@uni-tuebingen.de](mailto:reiner.anwander@uni-tuebingen.de).

### ORCID

Reiner Anwander: 0000-0002-1543-3787

### Notes

The authors declare no competing financial interest.

## ■ ACKNOWLEDGMENTS

We are grateful to the German Science Foundation (Grant: An238/14-2) and BRIDGESTONE Japan for generous support.

## ■ REFERENCES

- (1) Nishiura, M.; Hou, Z. *Nat. Chem.* **2010**, *2*, 257–268.
- (2) Nishiura, M.; Guo, F.; Hou, Z. *Acc. Chem. Res.* **2015**, *48*, 2209–2220.
- (3) Kelly, R. P.; Roesky, P. W. *Struct. Bonding (Berlin, Ger.)* **2015**, *172*, 85–117.
- (4) Trifonov, A. A.; Lyubov, D. M. *Coord. Chem. Rev.* **2017**, *340*, 10–61.
- (5) Yang, F.; Li, X. *J. Polym. Sci., Part A: Polym. Chem.* **2017**, *55*, 2271–2280.

- (6) Thiele, D. S. K.-H.; Wilson, D. D. R. *J. Macromol. Sci., Polym. Rev.* **2003**, *43*, 581–628.
- (7) Friebe, L.; Nuyken, O.; Obrecht, W. *Adv. Polym. Sci.* **2006**, *204*, 1–154.
- (8) Fischbach, A.; Anwander, R. *Adv. Polym. Sci.* **2006**, *204*, 155–281.
- (9) Zhiquan, S.; Ouyang, J. *Handb. Phys. Chem. Rare Earths* **1987**, *9*, 395–428.
- (10) Jones, R. H.; Wei, Y. K. *J. Biomed. Mater. Res.* **1971**, *5*, 19–30.
- (11) Kang, H.; Kang, M. Y.; Han, K.-H. *Plant Physiol.* **2000**, *123*, 1133–1142.
- (12) Koyoma, E.; Steinbüchel, A. *Polyisoprenoids*; Biopolymers series, Vol. 2; Wiley-VCH: Weinheim, 2001; p 435.
- (13) Liu, B.; Li, L.; Sun, G.; Liu, J.; Wang, M.; Li, S.; Cui, D. *Macromolecules* **2014**, *47*, 4971–4978.
- (14) Golub, M. A. *Macromolecules* **1969**, *2*, 550–552.
- (15) Ashitaka, H.; Kusuki, Y.; Asano, Y.; Yamamoto, S.; Ueno, H.; Nagasaka, A. *J. Polym. Sci., Polym. Chem. Ed.* **1983**, *21*, 1111–1124.
- (16) Natural rubber from dandelions. <http://www.fraunhofer.de/en/press/research-news/2015/June/natural-rubber-from-dandelions.html> (accessed July 13, 2017).
- (17) Makshina, E. V.; Dusselier, M.; Janssens, W.; Degève, J.; Jacobs, P. A.; Sels, B. F. *Chem. Soc. Rev.* **2014**, *43*, 7917–7953.
- (18) Fischbach, A.; Klimpel, M. G.; Widenmeyer, M.; Herdtweck, E.; Scherer, W.; Anwander, R. *Angew. Chem., Int. Ed.* **2004**, *43*, 2234–2239.
- (19) Bonnet, F.; Visseaux, M.; Pereira, A.; Barbier-Baudry, D. *Macromolecules* **2005**, *38*, 3162–3169.
- (20) Zhang, L.; Suzuki, T.; Luo, Y.; Nishiura, M.; Hou, Z. *Angew. Chem., Int. Ed.* **2007**, *46*, 1909–1913.
- (21) Gao, W.; Cui, D. *J. Am. Chem. Soc.* **2008**, *130*, 4984–4991.
- (22) Zimmermann, M.; Törnroos, K. W.; Anwander, R. *Angew. Chem., Int. Ed.* **2008**, *47*, 775–778.
- (23) Yang, Y.; Lv, K.; Wang, L.; Wang, Y.; Cui, D. *Chem. Commun.* **2010**, *46*, 6150–6152.
- (24) Zhang, L.; Nishiura, M.; Yuki, M.; Luo, Y.; Hou, Z. *Angew. Chem., Int. Ed.* **2008**, *47*, 2642–2645.
- (25) Rad'kova, N. Y.; Tolpygin, A. O.; Rad'kov, V. Y.; Khamaletdinova, N. M.; Cherkasov, A. V.; Fukin, G. K.; Trifonov, A. A. *Dalton Trans.* **2016**, *45*, 18572–18584.
- (26) Zhang, Z.; Cui, D.; Wang, B.; Liu, B.; Yang, Y. *Struct. Bonding* **2010**, *137*, 49–108.
- (27) Hou, Z.; Luo, Y.; Li, X. *J. Organomet. Chem.* **2006**, *691*, 3114–3121.
- (28) Nishiura, M.; Hou, Z. *Bull. Chem. Soc. Jpn.* **2010**, *83*, 595–608.
- (29) Zimmermann, M.; Törnroos, K. W.; Sitzmann, H.; Anwander, R. *Chem. - Eur. J.* **2008**, *14*, 7266–7277.
- (30) Zimmermann, M.; Volbeda, J.; Törnroos, K. W.; Anwander, R. *C. R. Chim.* **2010**, *13*, 651–660.
- (31) Robert, D.; Spaniol, T. P.; Okuda, J. *Eur. J. Inorg. Chem.* **2008**, *2008*, 2801–2809.
- (32) Kaita, S.; Hou, Z.; Wakatsuki, Y. *Macromolecules* **1999**, *32*, 9078–9079.
- (33) Kaita, S.; Hou, Z.; Nishiura, M.; Doi, Y.; Kurazumi, J.; Horiuchi, A. C.; Wakatsuki, Y. *Macromol. Rapid Commun.* **2003**, *24*, 179–184.
- (34) Kaita, S.; Doi, Y.; Kaneko, K.; Horiuchi, A. C.; Wakatsuki, Y. *Macromolecules* **2004**, *37*, 5860–5862.
- (35) Jende, L. N.; Hollfelder, C. O.; Maichle-Mössmer, C.; Anwander, R. *Organometallics* **2015**, *34*, 32–41.
- (36) Kirillov, E.; Saillard, J.-Y.; Carpentier, J.-F. *Coord. Chem. Rev.* **2005**, *249*, 1221–1248.
- (37) Kirillov, E.; Kahlal, S.; Roisnel, T.; Georgelin, T.; Saillard, J.-Y.; Carpentier, J.-F. *Organometallics* **2008**, *27*, 387–393.
- (38) Rodrigues, A.-S.; Kirillov, E.; Lehmann, C. W.; Roisnel, T.; Vuillemin, B.; Razavi, A.; Carpentier, J.-F. *Chem. - Eur. J.* **2007**, *13*, 5548–5565.
- (39) Wang, C.; Xiang, L.; Leng, X.; Chen, Y. *Organometallics* **2016**, *35*, 1995–2002.
- (40) Kirillov, E.; Lehmann, C. W.; Razavi, A.; Carpentier, J.-F. *Organometallics* **2004**, *23*, 2768–2777.
- (41) Qian, C.; Nie, W.; Chen, Y.; Sun, J. *J. Organomet. Chem.* **2002**, *645*, 82–86.
- (42) Lee, M. H.; Hwang, J.-W.; Kim, Y.; Kim, J.; Han, Y.; Do, Y. *Organometallics* **1999**, *18*, 5124–5129.
- (43) Qian, C.; Nie, W.; Sun, J. *Organometallics* **2000**, *19*, 4134–4140.
- (44) Kirillov, E.; Toupet, L.; Lehmann, C. W.; Razavi, A.; Kahlal, S.; Saillard, J.-Y.; Carpentier, J.-F. *Organometallics* **2003**, *22*, 4038–4046.
- (45) Kirillov, E.; Toupet, L.; Lehmann, C. W.; Razavi, A.; Carpentier, J.-F. *Organometallics* **2003**, *22*, 4467–4479.
- (46) Lin, F.; Wang, X.; Pan, Y.; Wang, M.; Liu, B.; Luo, Y.; Cui, D. *ACS Catal.* **2016**, *6*, 176–185.
- (47) Kirillov, E.; Lehmann, C. W.; Razavi, A.; Carpentier, J.-F. *J. Am. Chem. Soc.* **2004**, *126*, 12240–12241.
- (48) Rodrigues, A.-S.; Kirillov, E.; Lehmann, C. W.; Roisnel, T.; Vuillemin, B.; Razavi, A.; Carpentier, J.-F. *Chem. - Eur. J.* **2007**, *13*, 5548–5565.
- (49) Yao, C.; Wu, C.; Wang, B.; Cui, D. *Organometallics* **2013**, *32*, 2204–2209.
- (50) Downing, S. P.; Guadaño, S. C.; Pugh, D.; Danopoulos, A. A.; Bellabarba, R. M.; Hanton, M.; Smith, D.; Toozee, R. P. *Organometallics* **2007**, *26*, 3762–3770.
- (51) Wang, B.; Cui, D.; Lv, K. *Macromolecules* **2008**, *41*, 1983–1988.
- (52) Li, X.; Wang, X.; Tong, X.; Zhang, H.; Chen, Y.; Liu, Y.; Liu, H.; Wang, X.; Nishiura, M.; He, H.; Lin, Z.; Zhang, S.; Hou, Z. *Organometallics* **2013**, *32*, 1445–1458.
- (53) Du, G.; Long, Y.; Xue, J.; Zhang, S.; Dong, Y.; Li, X. *Macromolecules* **2015**, *48*, 1627–1635.
- (54) Du, G.; Yan, X.; Zhang, P.; Wang, H.; Dong, Y.; Li, X. *Polym. Chem.* **2017**, *8*, 698–707.
- (55) Du, G.; Xue, J.; Peng, D.; Yu, C.; Wang, H.; Zhou, Y.; Bi, J.; Zhang, S.; Dong, Y.; Li, X. *J. Polym. Sci., Part A: Polym. Chem.* **2015**, *53*, 2898–2907.
- (56) Nakamura, H.; Nakayama, Y.; Yasuda, H.; Maruo, T.; Kanehisa, N.; Kai, Y. *Organometallics* **2000**, *19*, 5392–5399.
- (57) Evans, W. J.; Gummshheimer, T. S.; Boyle, T. J.; Ziller, J. W. *Organometallics* **1994**, *13*, 1281–1284.
- (58) Dettenrieder, N.; Hollfelder, C. O.; Jende, L. N.; Maichle-Mössmer, C.; Anwander, R. *Organometallics* **2014**, *33*, 1528–1531.
- (59) Litlabø, R.; Enders, M.; Törnroos, K. W.; Anwander, R. *Organometallics* **2010**, *29*, 2588–2595.
- (60) Le Roux, E.; Nief, F.; Jaroschik, F.; Törnroos, K. W.; Anwander, R. *Dalton Trans.* **2007**, *42*, 4866–4870.
- (61) Evans, W. J.; Anwander, R.; Ziller, J. W. *Organometallics* **1995**, *14*, 1107–1109.
- (62) Anwander, R.; Klimpel, M. G.; Dietrich, H. M.; Shorokhov, D. J.; Scherer, W. *Chem. Commun.* **2003**, *8*, 1008–1009.
- (63) Dietrich, H. M.; Zapilko, C.; Herdtweck, E.; Anwander, R. *Organometallics* **2005**, *24*, 5767–5771.
- (64) Holton, J.; Lappert, M. F.; Ballard, D. G. H.; Pearce, R.; Atwood, J. L.; Hunter, W. E. *J. Chem. Soc., Dalton Trans.* **1979**, *1*, 45–53.
- (65) Dietrich, H. M.; Törnroos, K. W.; Herdtweck, E.; Anwander, R. *Organometallics* **2009**, *28*, 6739–6749.
- (66) Janiak, C. *Chem. Ber.* **1993**, *126*, 1603–1607.
- (67) Feil, F.; Harder, S. *Eur. J. Inorg. Chem.* **2003**, *2003*, 3401–3408.
- (68) Tardif, O.; Kaita, S. *Dalton Trans.* **2008**, 2531–2533.
- (69) Xu, X.; Chen, Y.; Sun, J. *Chem. - Eur. J.* **2009**, *15*, 846–850.
- (70) Litlabø, R.; Lee, H. S.; Niemeyer, M.; Törnroos, K. W.; Anwander, R. *Dalton Trans.* **2010**, *39*, 6815–6825.
- (71) Sieler, J.; Simon, A.; Peters, K.; Taube, R.; Geitner, M. *J. Organomet. Chem.* **1989**, *362*, 297–303.
- (72) Zimmermann, M.; Frøystein, N. Å.; Fischbach, A.; Sirsch, P.; Dietrich, H. M.; Törnroos, K. W.; Herdtweck, E.; Anwander, R. *Chem. - Eur. J.* **2007**, *13*, 8784–8800.
- (73) Zaeni, A.; Behrens, U.; Liebing, P.; Olbrich, F.; Edelman, F. T. *J. Organomet. Chem.* **2017**, *830*, 141–145.
- (74) Harder, S.; Feil, F.; Repo, T. *Chem. - Eur. J.* **2002**, *8*, 1991–1999.
- (75) COSMO, v. 1.61; Bruker AXS Inc.: Madison, WI, 2012.
- (76) (a) APEX2, v. 2012.10.0; Bruker AXS Inc.: Madison, WI, 2012. (b) APEX3, V. 2016.5–0; Bruker AXS Inc.: Madison, WI, 2016.

- (77) SAINT, v. 8.34A; Bruker AXS Inc.: Madison, WI, 2013.
- (78) SADABS: Krause, L.; Herbst-Imer, R.; Sheldrick, G. M.; Stalke, D. *J. Appl. Crystallogr.* **2015**, *48*, 3.
- (79) Sheldrick, G. M. *TWINABS Bruker AXS scaling for twinned crystals*, version 2007/3; Bruker AXS Inc.: Madison, WI, 2007.
- (b) SADABS; Bruker AXS Inc.: Göttingen, Germany, 2007.
- (80) (a) SHELXTL: Sheldrick, G. M. *Acta Crystallogr., Sect. A: Found. Adv.* **2015**, *71*, 3–8. (b) SHELXL: Sheldrick, G. M. *Acta Crystallogr., Sect. C: Struct. Chem.* **2015**, *71*, 3–8.
- (81) SHELXLE: Hubschle, C. B.; Sheldrick, G. M.; Dittrich, B. *J. Appl. Crystallogr.* **2011**, *44*, 1281–1284.
- (82) Farrugia, L. J. *J. Appl. Crystallogr.* **1997**, *30*, 565.
- (83) POV-Ray v. 3.6; Persistence of Vision Pty. Ltd.: Williamstown, Victoria, Australia, 2004. <http://www.povray.org/>.

# Supporting Information

## **Fluorenyl Half-Sandwich Bis(tetramethylaluminate) Complexes of the Rare-Earth Metals: Synthesis, Structure, and Isoprene Polymerization**

Dominic Diether, Konstantin Tyulyunov, Cécilia Maichle-Mössmer, and Reiner Anwander\*

Institut für Anorganische Chemie, Eberhard Karls Universität Tübingen, Auf der Morgenstelle 18, 72076 Tübingen, Germany.

### **Corresponding Author**

\* [reiner.anwander@uni-tuebingen.de](mailto:reiner.anwander@uni-tuebingen.de)



# Table of Contents

Figure S1: $^1\text{H}$ NMR spectrum of $(\text{Flu})\text{La}(\text{AlMe}_4)_2$ ( $\mathbf{1}^{\text{La}}$ )	S3
Figure S2: $^{13}\text{C}\{^1\text{H}\}$ NMR spectrum of $(\text{Flu})\text{La}(\text{AlMe}_4)_2$ ( $\mathbf{1}^{\text{La}}$ )	S3
Figure S3: $^1\text{H}^{13}\text{C}$ -HSQC NMR spectrum of $(\text{Flu})\text{La}(\text{AlMe}_4)_2$ ( $\mathbf{1}^{\text{La}}$ )	S4
Figure S4: $^1\text{H}^1\text{H}$ -COSY NMR spectrum of $(\text{Flu})\text{La}(\text{AlMe}_4)_2$ ( $\mathbf{1}^{\text{La}}$ )	S4
Figure S5: $^1\text{H}$ NMR spectrum of $(\text{Flu}^{\text{tBu}})\text{La}(\text{AlMe}_4)_2$ ( $\mathbf{2}^{\text{La}}$ )	S5
Figure S6: $^{13}\text{C}\{^1\text{H}\}$ NMR spectrum of $(\text{Flu}^{\text{tBu}})\text{La}(\text{AlMe}_4)_2$ ( $\mathbf{2}^{\text{La}}$ )	S5
Figure S7: $^1\text{H}$ NMR spectrum of $(\text{Flu}^{\text{Si}})\text{La}(\text{AlMe}_4)_2$ ( $\mathbf{3}^{\text{La}}$ )	S6
Figure S8: $^{13}\text{C}\{^1\text{H}\}$ NMR spectrum of $(\text{Flu}^{\text{Si}})\text{La}(\text{AlMe}_4)_2$ ( $\mathbf{3}^{\text{La}}$ )	S6
Figure S9: $^1\text{H}$ NMR spectrum of $(\text{Flu}^{\text{Si}})\text{Y}(\text{AlMe}_4)_2$ ( $\mathbf{3}^{\text{Y}}$ )	S7
Figure S10: $^{13}\text{C}\{^1\text{H}\}$ NMR spectrum of $(\text{Flu}^{\text{Si}})\text{Y}(\text{AlMe}_4)_2$ ( $\mathbf{3}^{\text{Y}}$ )	S7
Figure S11: $^1\text{H}$ NMR spectrum of $(\text{Flu}^{\text{tBu}})\text{Y}(\text{AlMe}_4)_2$ ( $\mathbf{2}^{\text{Y}}$ )	S8
Figure S12: $^{13}\text{C}\{^1\text{H}\}$ NMR spectrum of $(\text{Flu}^{\text{tBu}})\text{Y}(\text{AlMe}_4)_2$ ( $\mathbf{2}^{\text{Y}}$ )	S8
Figure S13: $^1\text{H}$ NMR spectrum of $(\text{Flu}^{\text{Si}})\text{Lu}(\text{AlMe}_4)_2$ ( $\mathbf{3}^{\text{Lu}}$ )	S9
Figure S14: $^{13}\text{C}\{^1\text{H}\}$ NMR spectrum of $(\text{Flu}^{\text{Si}})\text{Lu}(\text{AlMe}_4)_2$ ( $\mathbf{3}^{\text{Lu}}$ )	S9
Figure S15: $^1\text{H}$ NMR spectrum of $(\text{Flu})_2\text{Lu}(\text{AlMe}_4)$ ( $\mathbf{1a}^{\text{Lu}}$ )	S10
Figure S16: $^{13}\text{C}\{^1\text{H}\}$ NMR spectra of $(\text{Flu})_2\text{Lu}(\text{AlMe}_4)$ ( $\mathbf{1a}^{\text{Lu}}$ )	S10
Figure S17: Molecular structure of $(\text{Flu}^{\text{tBu}})\text{La}(\text{AlMe}_4)_2$ ( $\mathbf{2}^{\text{La}}$ )	S11
Figure S18: Molecular structure of $(\text{Flu}^{\text{Si}})\text{Y}(\text{AlMe}_4)_2$ ( $\mathbf{3}^{\text{Y}}$ )	S11
Figure S19: Molecular structure of $(\text{Flu}^{\text{Si}})\text{Nd}(\text{AlMe}_4)_2$ ( $\mathbf{3}^{\text{Nd}}$ )	S12
Figure S20: Section of the molecular structure of $[\text{K}(\text{Flu}^{\text{Si}})(\text{THF})_2]_n$	S12
Figure S21: Molecular structure of $\text{CPh}_3\text{Flu}^{\text{tBu}}$	S13
Table S1: Crystallographic data for $\mathbf{1}^{\text{La}}$ , $\mathbf{2}^{\text{La}}$ , $\mathbf{3}^{\text{La}}$ , and $\mathbf{3}^{\text{Lu}}$	S14
Table S2: Crystallographic data for $\mathbf{2}^{\text{Y}}$ , $\mathbf{3}^{\text{Y}}$ , $\mathbf{3}^{\text{Nd}}$ , and $\mathbf{1a}^{\text{Lu}}$	S15
Table S2: Crystallographic data for $\mathbf{4}^{\text{Y}}$ , $\mathbf{5}^{\text{Y}}$ , $[\text{K}(\text{Flu}^{\text{Si}})(\text{THF})_2]_n$ , and 1- $\text{CPh}_3$ - $\text{Flu}^{\text{tBu}}$	S16
Figure S22: $^1\text{H}$ NMR spectra of polyisoprene (entry 5)	S17
Figure S23: $^{13}\text{C}\{^1\text{H}\}$ NMR spectra of polyisoprene (entry 5)	S17
Figure S24: GPC curve of polyisoprene (entry 5)	S18
Figure S25: DSC curve of polyisoprene (entry 5)	S18
Figure S26: $^1\text{H}$ NMR spectra of polyisoprene (entry 19)	S19
Figure S27: $^{13}\text{C}\{^1\text{H}\}$ NMR spectra of polyisoprene (entry 19)	S19
Figure S28: GPC curve of polyisoprene (entry 19)	S20
Figure S29: DSC curve of polyisoprene (entry 19)	S20
Figure S30: $^1\text{H}$ NMR spectrum of $(\text{Flu}^{\text{tBu}})\text{La}(\text{AlMe}_4)_2$ ( $\mathbf{2}^{\text{La}}$ ) activated with cocatalyst <b>A</b>	S21
Figure S31: $^1\text{H}$ NMR spectrum of $(\text{Flu}^{\text{Si}})\text{La}(\text{AlMe}_4)_2$ ( $\mathbf{3}^{\text{La}}$ ) activated with cocatalyst <b>A</b>	S21
Figure S32: $^{19}\text{F}$ NMR spectrum of $(\text{Flu}^{\text{Si}})\text{La}(\text{AlMe}_4)_2$ ( $\mathbf{3}^{\text{La}}$ ) activated with cocatalyst <b>A</b>	S22
Figure S33: $^1\text{H}$ NMR spectrum of $(\text{Flu}^{\text{tBu}})\text{La}(\text{AlMe}_4)_2$ ( $\mathbf{2}^{\text{La}}$ ) activated with cocatalyst <b>B</b>	S22
Figure S34: $^1\text{H}$ NMR spectrum of $(\text{Flu}^{\text{Si}})\text{La}(\text{AlMe}_4)_2$ ( $\mathbf{3}^{\text{La}}$ ) activated with cocatalyst <b>B</b>	S23

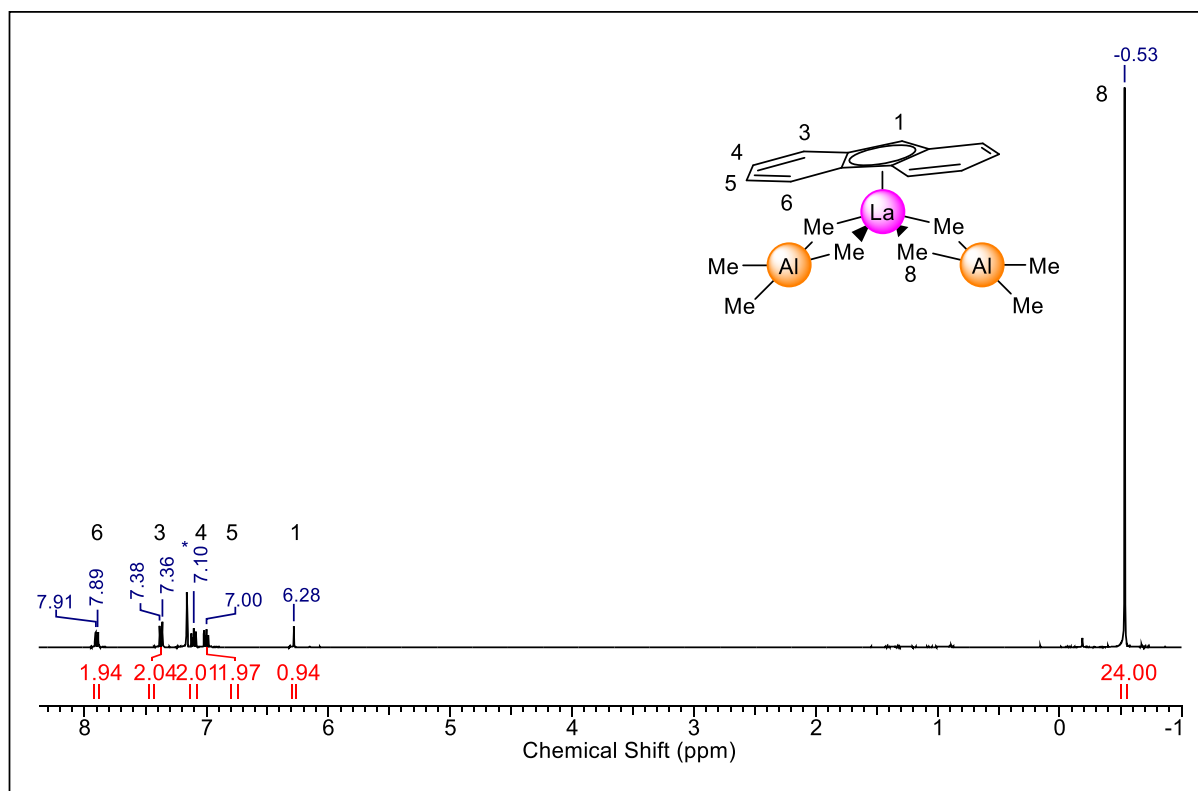


**Figure S1.**  $^1\text{H}$  NMR spectrum (400 MHz) of  $(\text{Flu})\text{La}(\text{AlMe}_4)_2$  ( $\mathbf{1}^{\text{La}}$ ) in  $\text{C}_6\text{D}_6$  at  $26^\circ\text{C}$ .

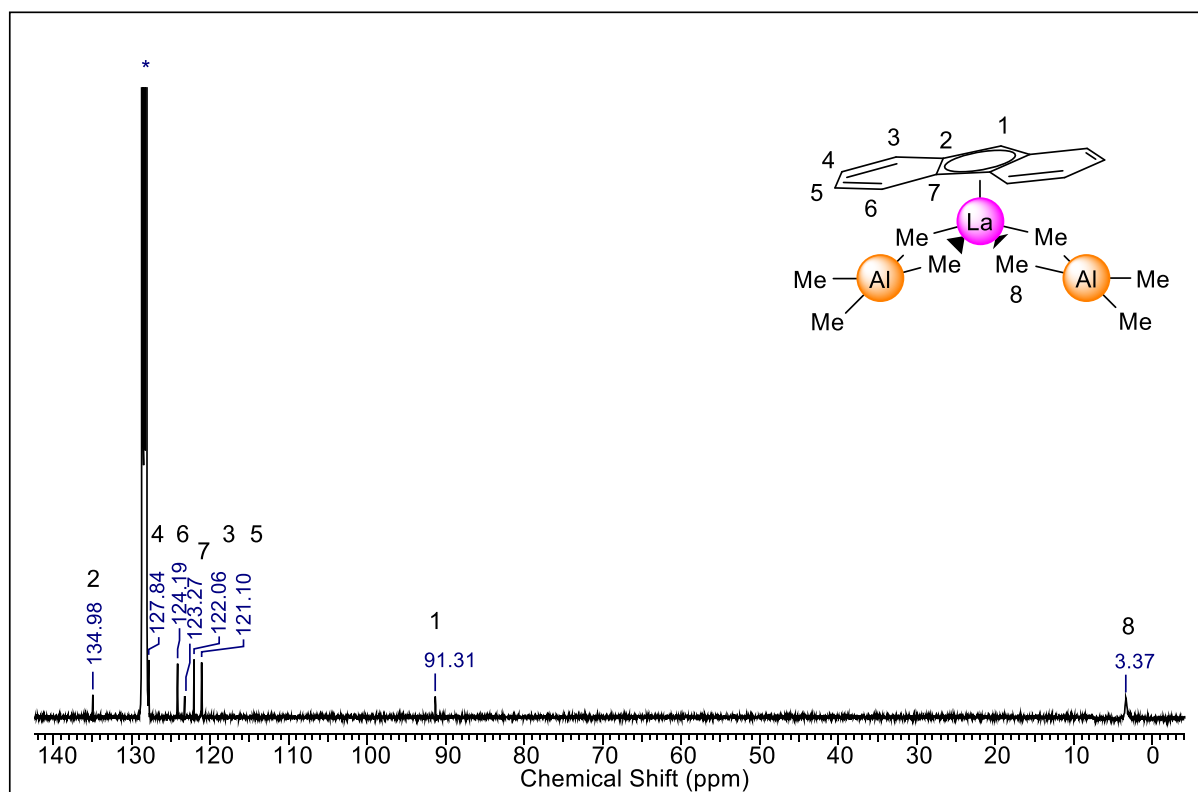


**Figure S2.**  $^{13}\text{C}\{^1\text{H}\}$  NMR spectrum (101 MHz) of  $(\text{Flu})\text{La}(\text{AlMe}_4)_2$  ( $\mathbf{1}^{\text{La}}$ ) in  $\text{C}_6\text{D}_6$  at  $26^\circ\text{C}$ .

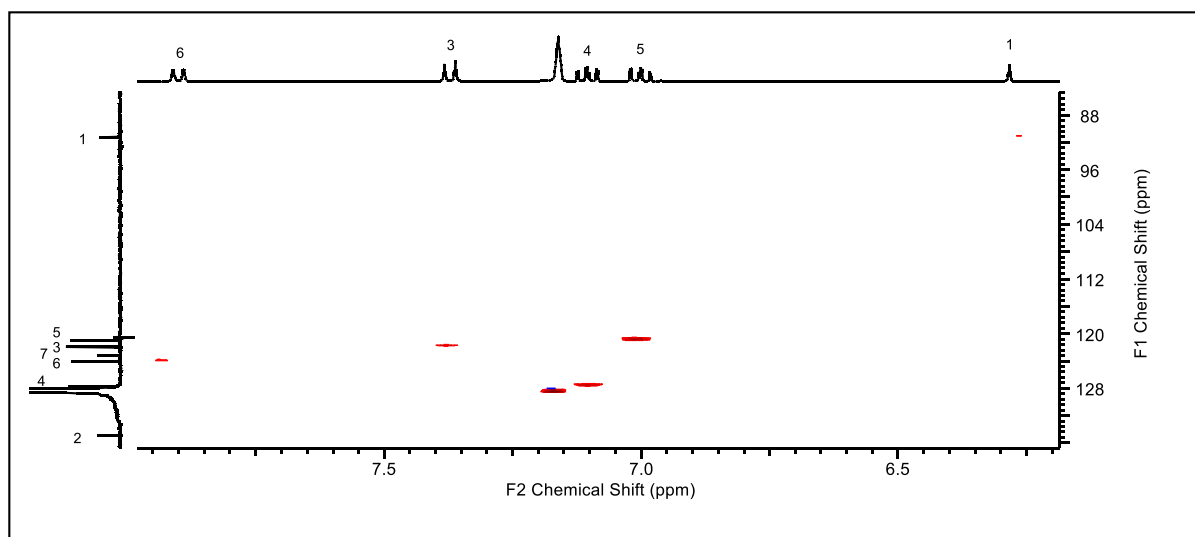


**Figure S3.**  $^{13}\text{C}$ -HSQC NMR spectrum (400/101 MHz) of (Flu)La(AlMe<sub>4</sub>)<sub>2</sub> (**1<sup>La</sup>**) in C<sub>6</sub>D<sub>6</sub> at 26 °C.

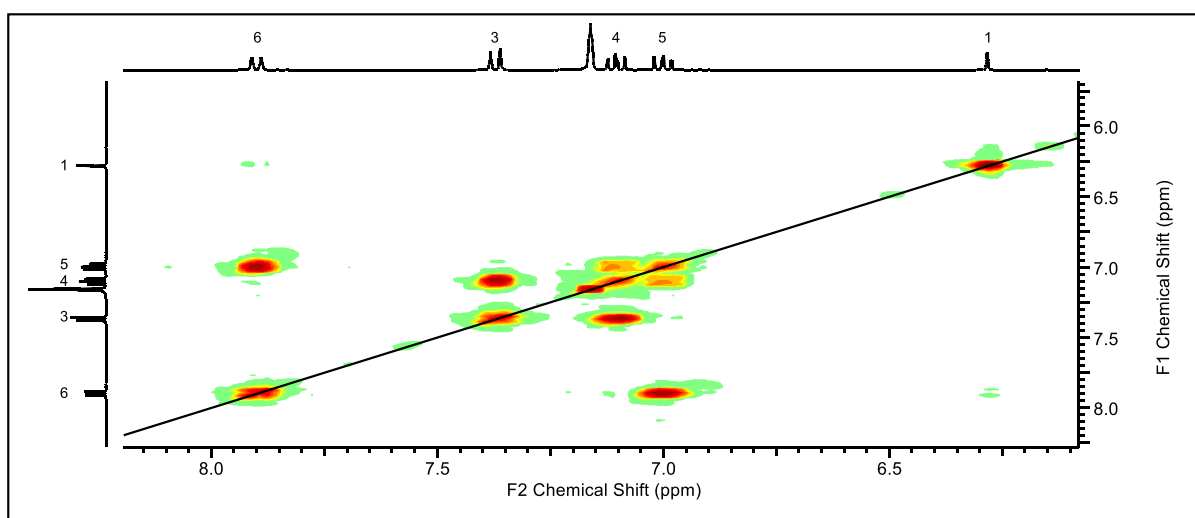


**Figure S4.**  $^1\text{H}$ -H-COSY NMR spectrum (400/400 MHz) of (Flu)La(AlMe<sub>4</sub>)<sub>2</sub> (**1<sup>La</sup>**) in C<sub>6</sub>D<sub>6</sub> at 26 °C.

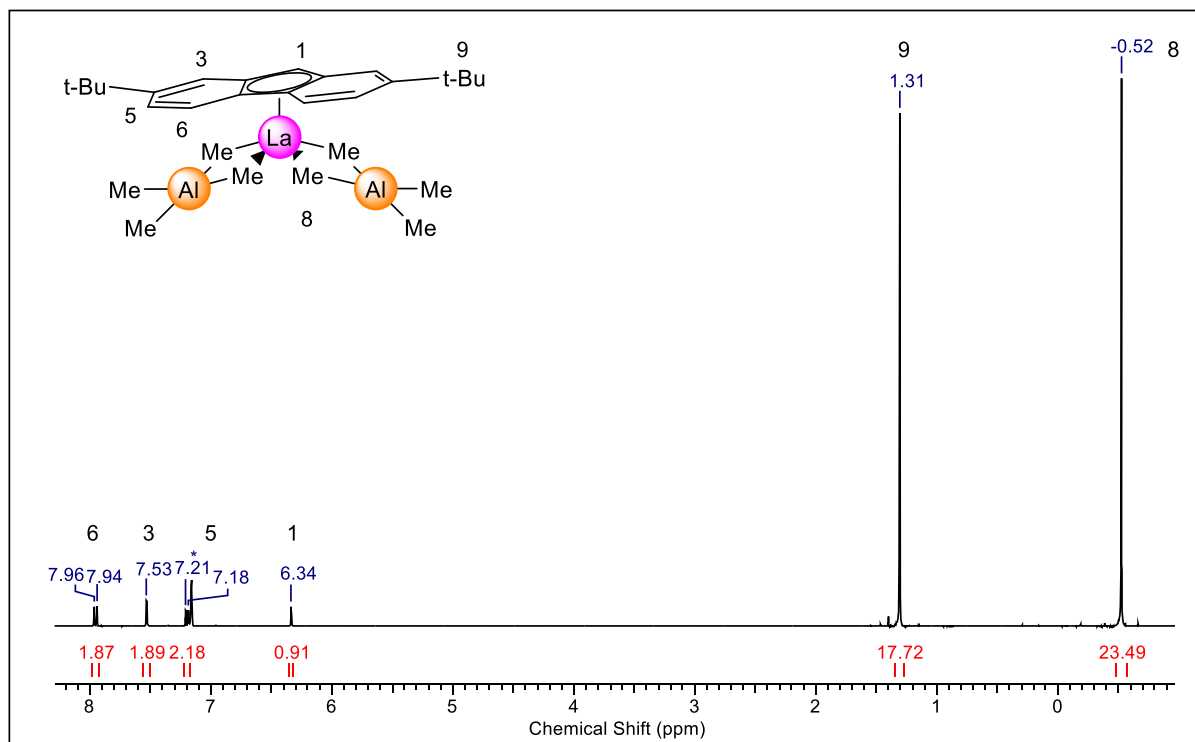


**Figure S5.**  $^1\text{H}$  NMR spectrum (400 MHz) of  $(\text{Flu}^{\text{tBu}})\text{La}(\text{AlMe}_4)_2$  ( $2^{\text{La}}$ ) in  $\text{C}_6\text{D}_6$  at  $26^\circ\text{C}$ .

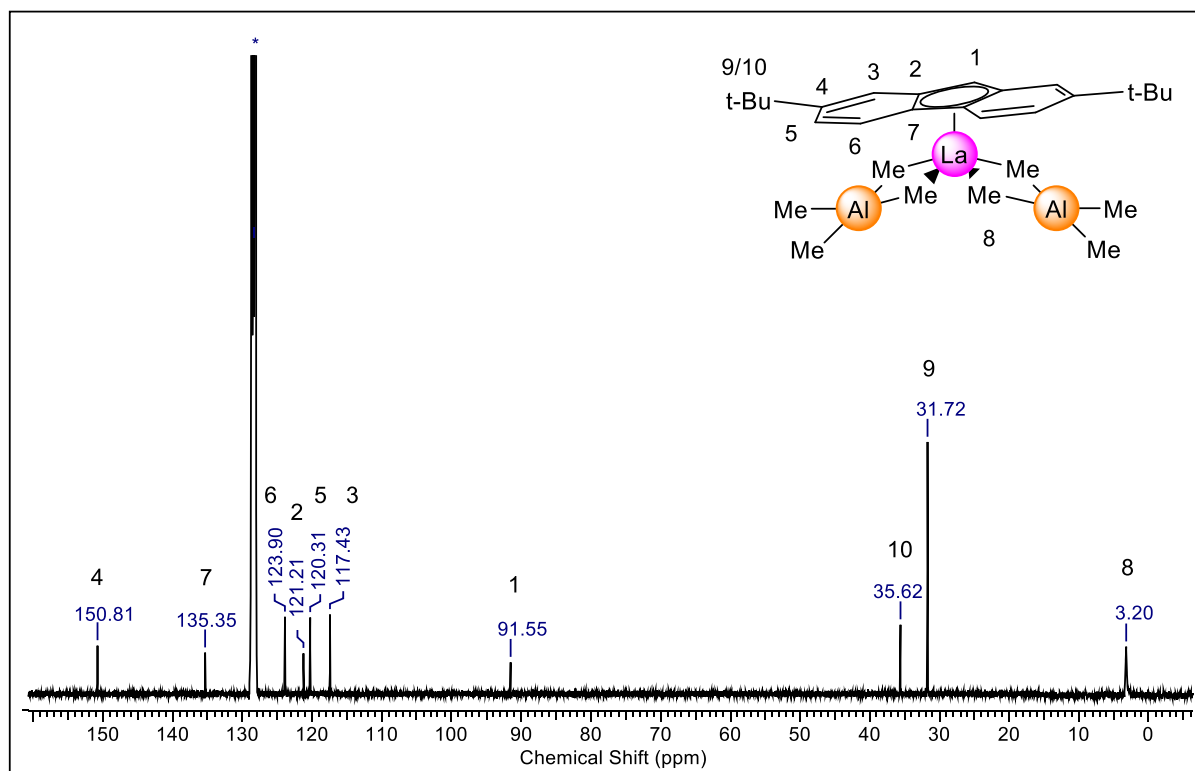


**Figure S6.**  $^{13}\text{C}\{^1\text{H}\}$  NMR spectrum (101 MHz) of  $(\text{Flu}^{\text{tBu}})\text{La}(\text{AlMe}_4)_2$  ( $2^{\text{La}}$ ) in  $\text{C}_6\text{D}_6$  at  $26^\circ\text{C}$ .

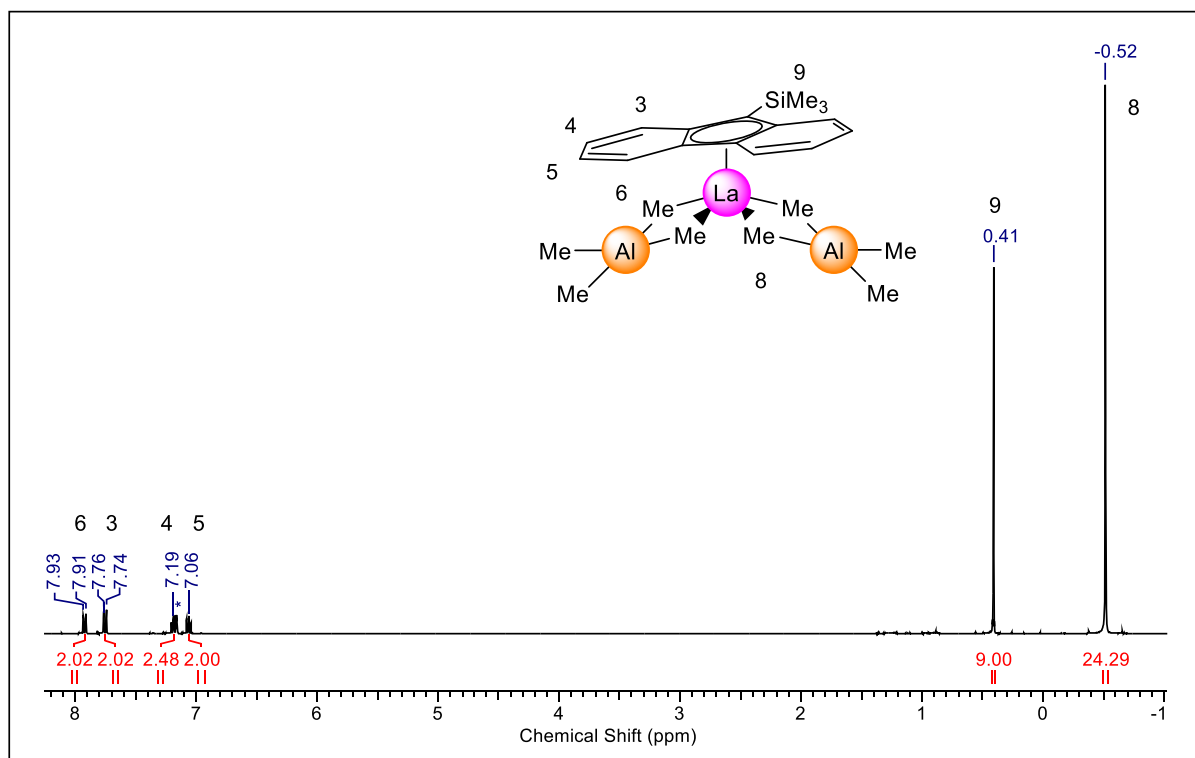


**Figure S7.**  $^1\text{H}$  NMR spectrum (400 MHz) of  $(\text{Flu}^{\text{Si}})\text{La}(\text{AlMe}_4)_2$  ( $3^{\text{La}}$ ) in  $\text{C}_6\text{D}_6$  at  $26^\circ\text{C}$ .

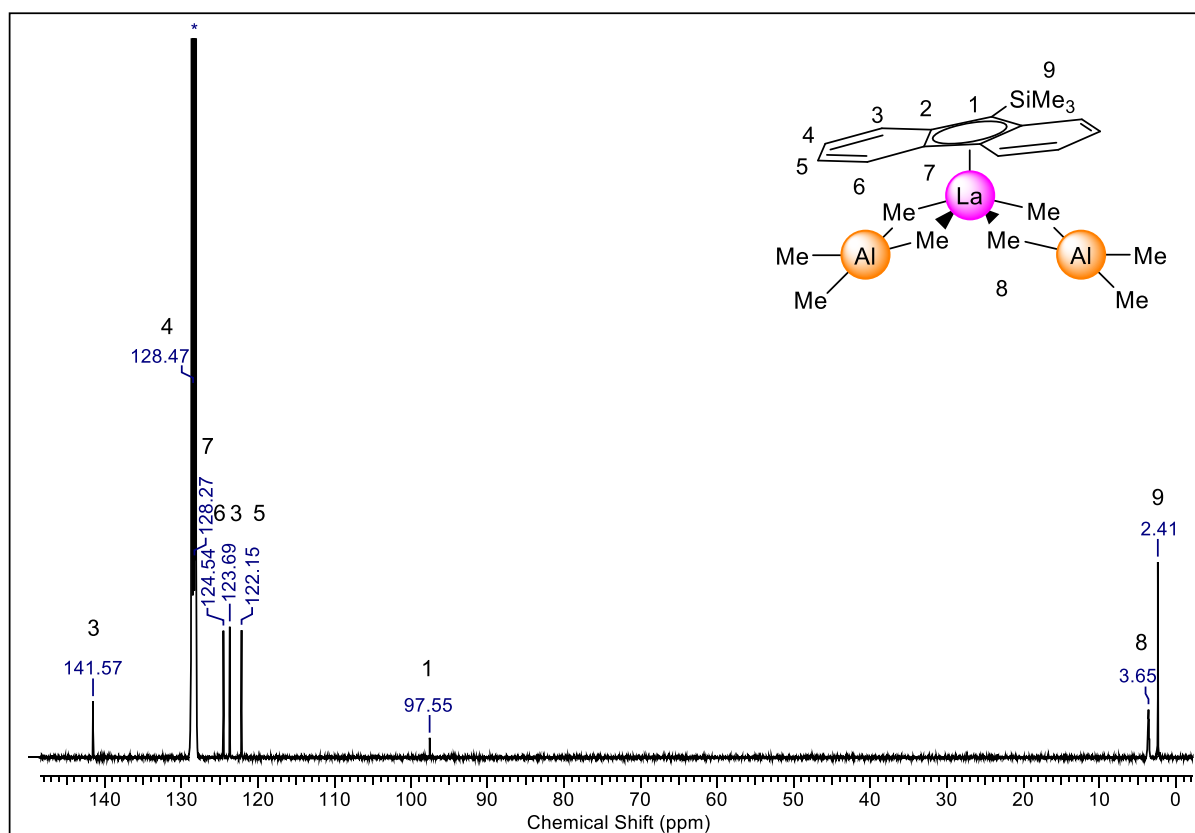


**Figure S8.**  $^{13}\text{C}\{^1\text{H}\}$  spectrum (101 MHz) of  $(\text{Flu}^{\text{Si}})\text{La}(\text{AlMe}_4)_2$  ( $3^{\text{La}}$ ) in  $\text{C}_6\text{D}_6$  at  $26^\circ\text{C}$ .

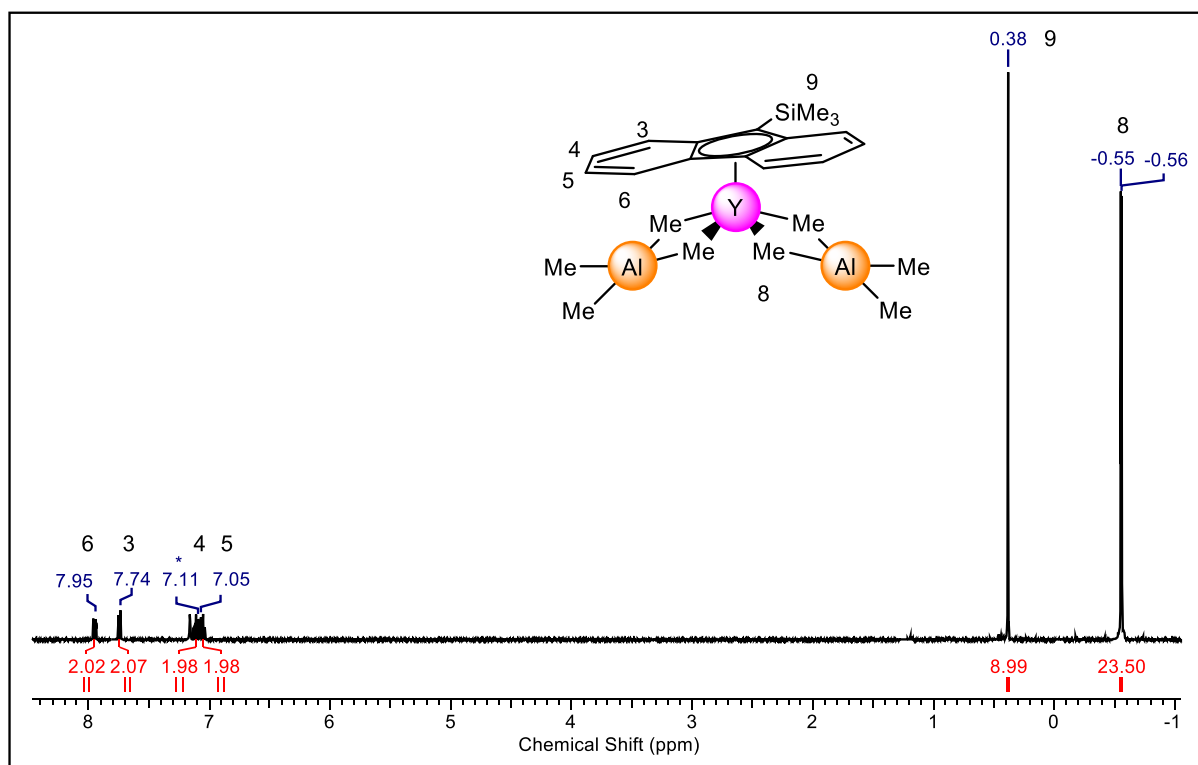


**Figure S9.**  $^1\text{H}$  NMR spectrum (400 MHz) of  $(\text{Flu}^{\text{Si}})\text{Y}(\text{AlMe}_4)_2$  ( $3^{\text{Y}}$ ) in  $\text{C}_6\text{D}_6$  at  $26^\circ\text{C}$ .

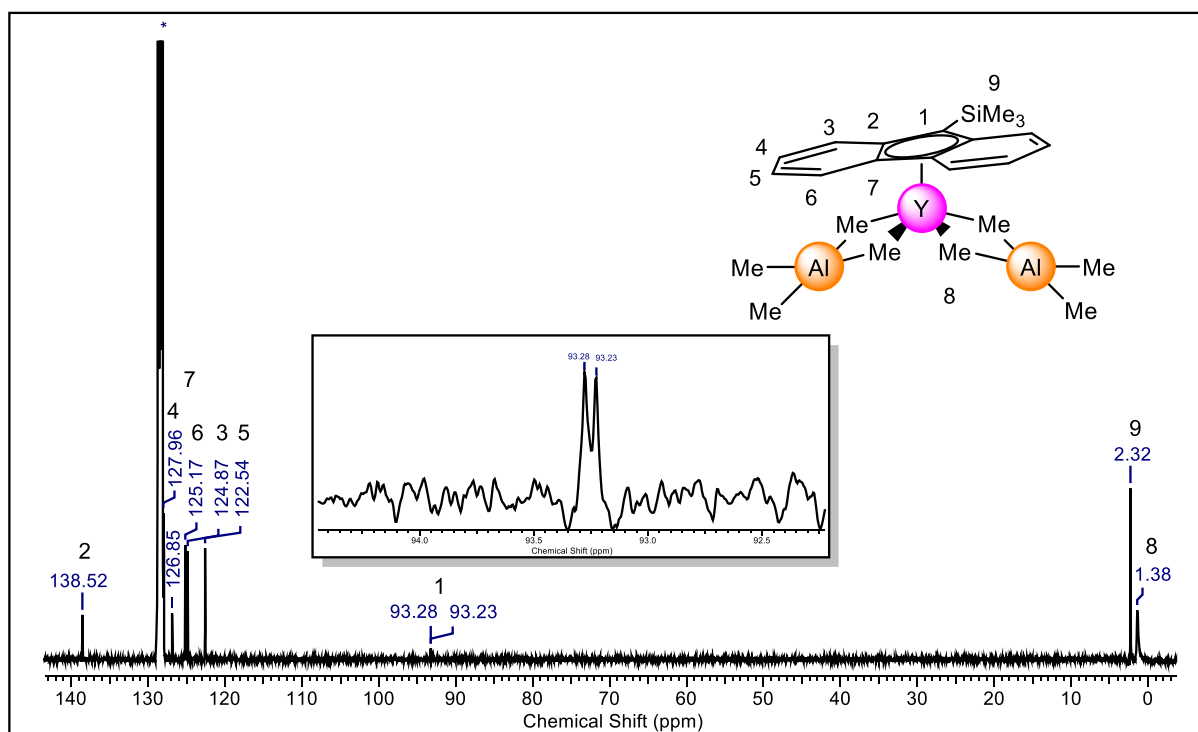


**Figure S10.**  $^{13}\text{C}\{^1\text{H}\}$  NMR spectrum (101 MHz) of  $(\text{Flu}^{\text{Si}})\text{Y}(\text{AlMe}_4)_2$  ( $3^{\text{Y}}$ ) in  $\text{C}_6\text{D}_6$  at  $26^\circ\text{C}$ .

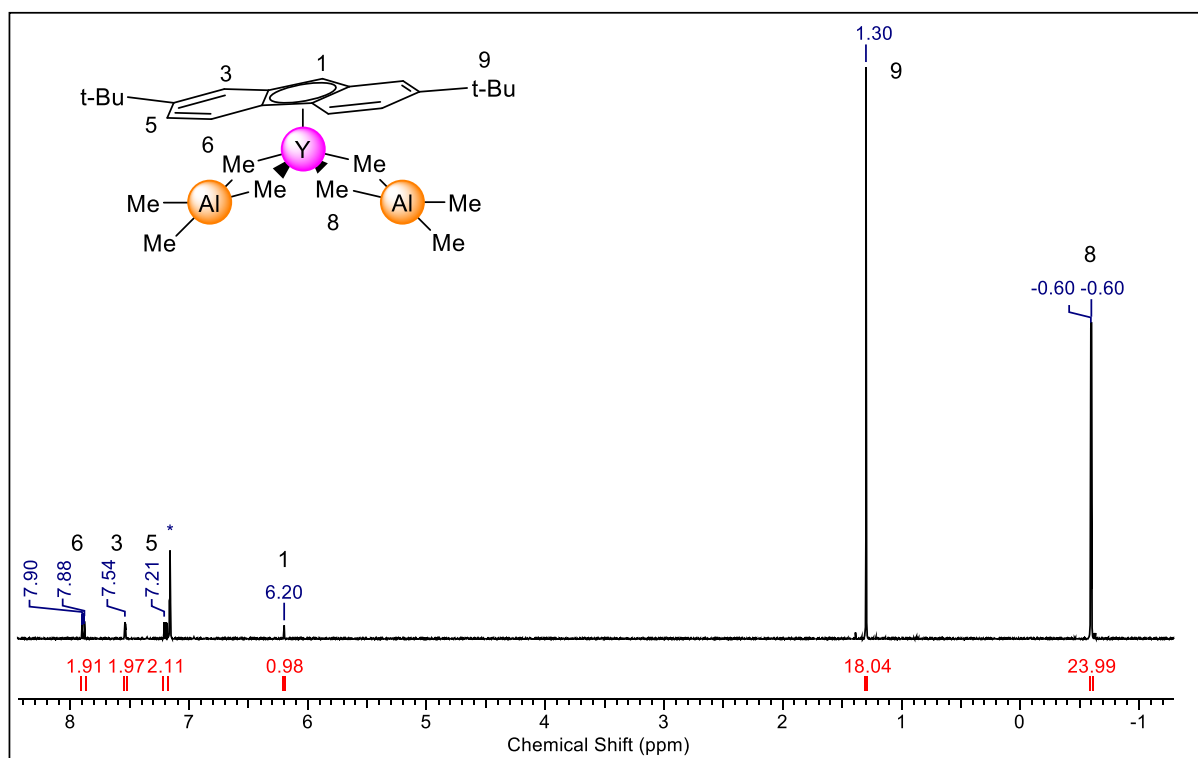


**Figure S11.**  $^1\text{H}$  NMR spectrum (400 MHz) of  $(\text{Flu}^{\text{t-Bu}})\text{Y}(\text{AlMe}_4)_2$  ( $2^{\text{Y}}$ ) in  $\text{C}_6\text{D}_6$  at  $26^\circ\text{C}$ .

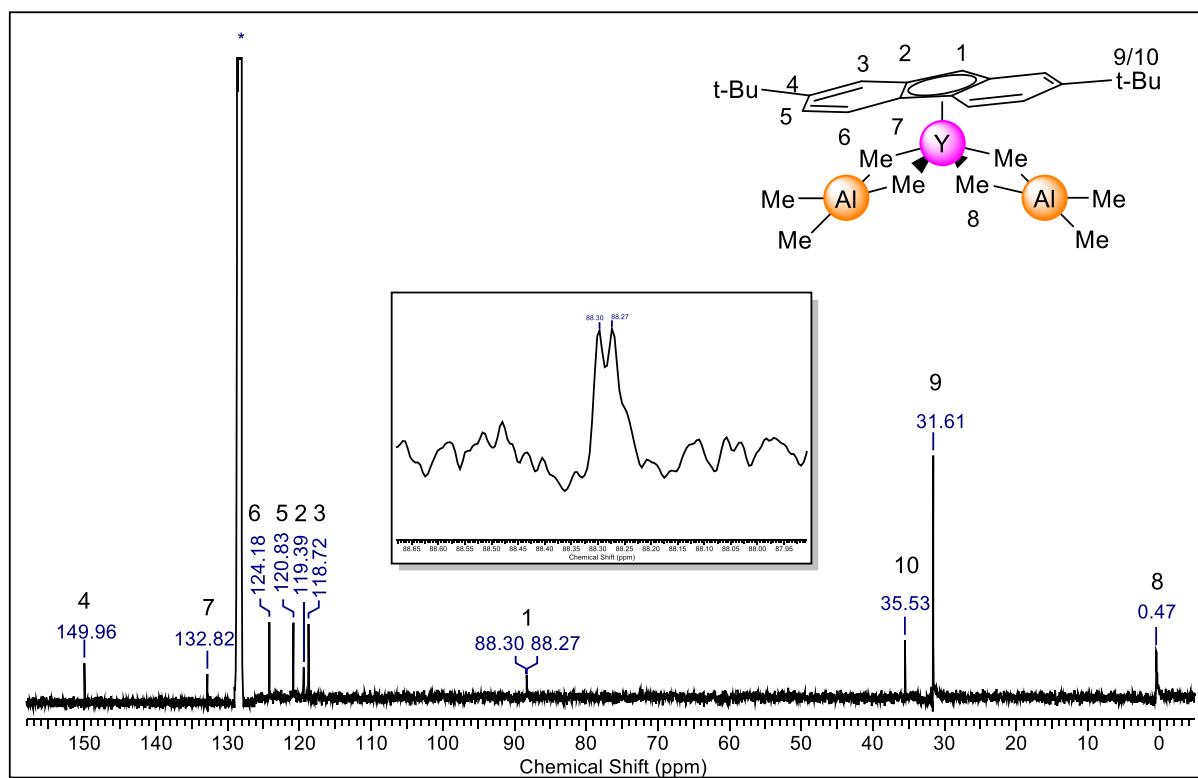


**Figure S12.**  $^{13}\text{C}\{^1\text{H}\}$  NMR spectrum (101 MHz) of  $(\text{Flu}^{\text{t-Bu}})\text{Y}(\text{AlMe}_4)_2$  ( $2^{\text{Y}}$ ) in  $\text{C}_6\text{D}_6$  at  $26^\circ\text{C}$ .

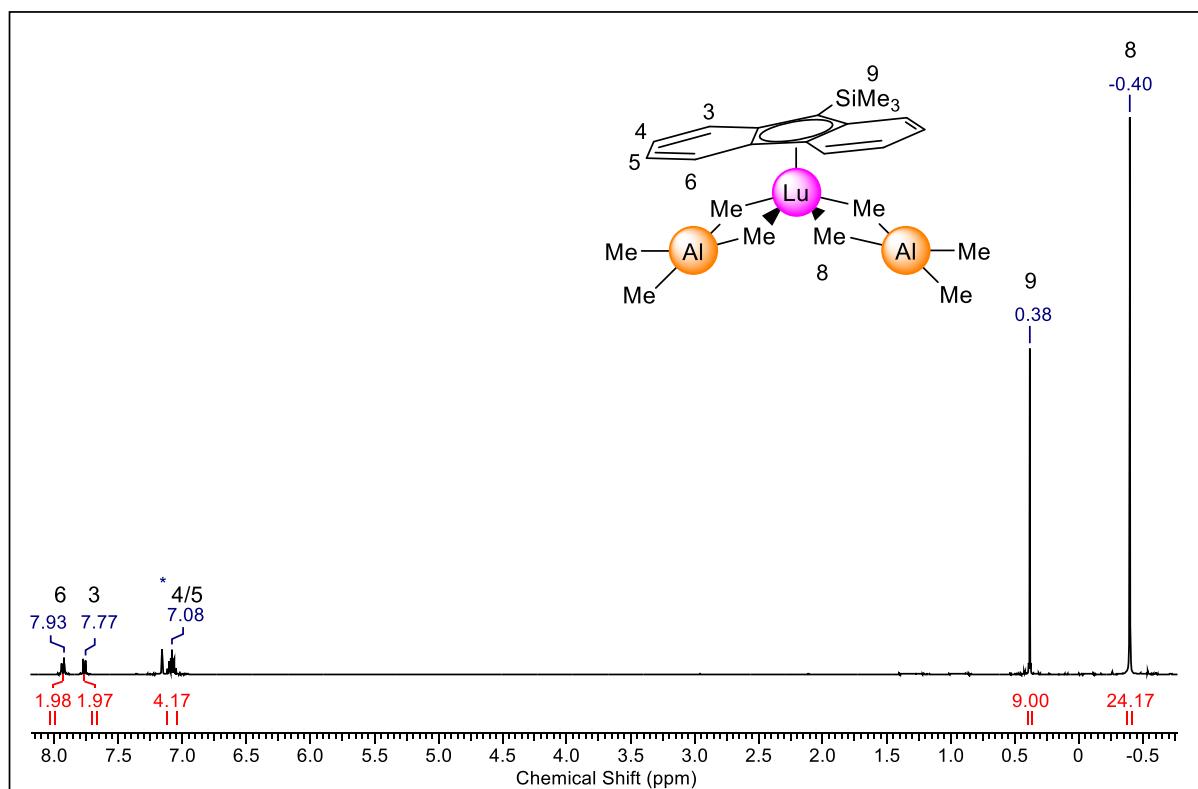


**Figure S13.**  $^1\text{H}$  NMR spectrum (400 MHz) of  $(\text{Flu}^{\text{Si}})\text{Lu}(\text{AlMe}_4)_2$  ( $\mathbf{3}^{\text{Lu}}$ ) in  $\text{C}_6\text{D}_6$  at  $26^\circ\text{C}$ .

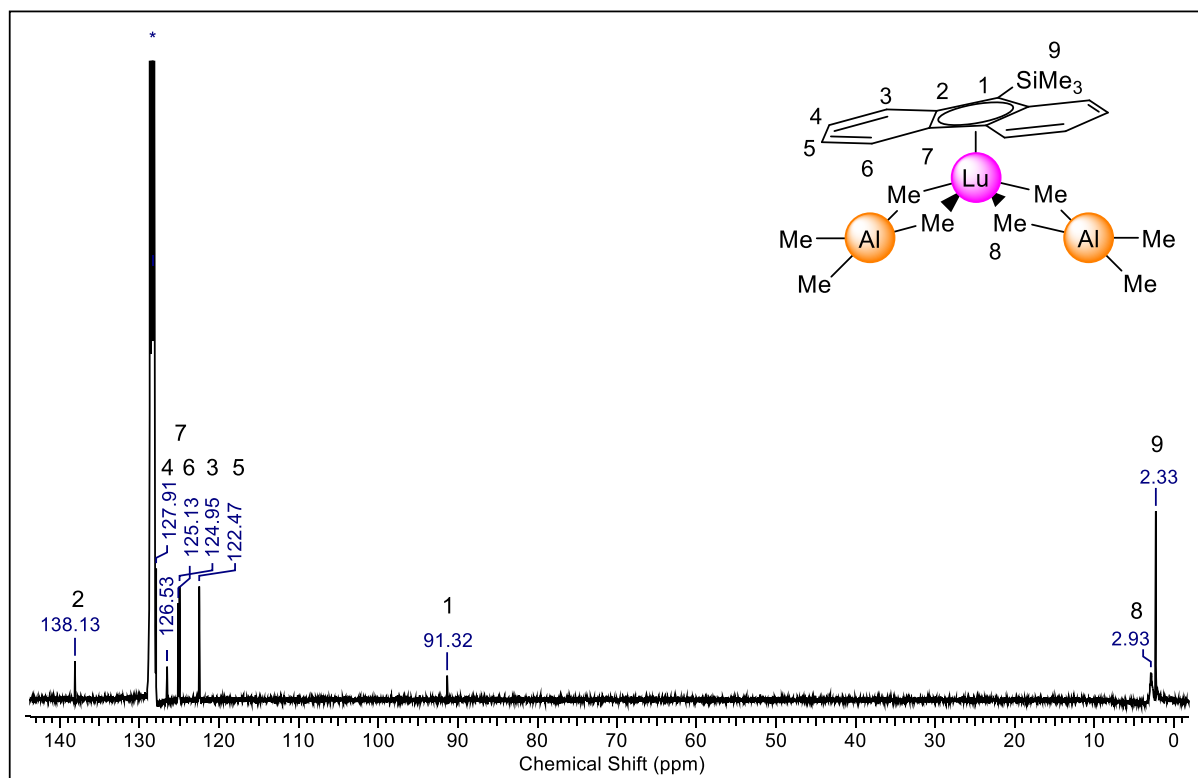


**Figure S14.**  $^{13}\text{C}\{^1\text{H}\}$  NMR spectrum (101 MHz) of  $(\text{Flu}^{\text{Si}})\text{Lu}(\text{AlMe}_4)_2$  ( $\mathbf{3}^{\text{Lu}}$ ) in  $\text{C}_6\text{D}_6$  at  $26^\circ\text{C}$ .



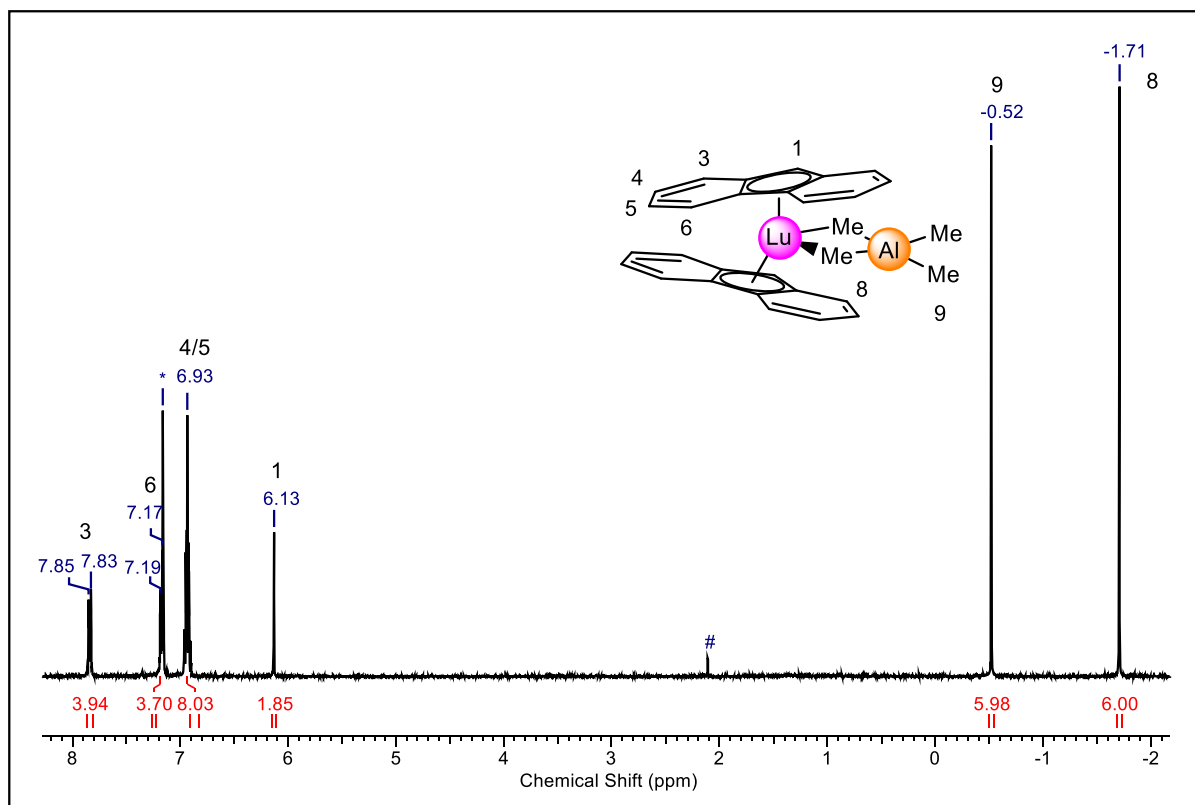


**Figure S15.**  $^1\text{H}$  NMR spectrum (400 MHz) of  $(\text{Flu})_2\text{Lu}(\text{AlMe}_4)$  ( $1\text{a}^{\text{Lu}}$ ) in  $\text{C}_6\text{D}_6$  at  $26^\circ\text{C}$ . Residual toluene marked with #.

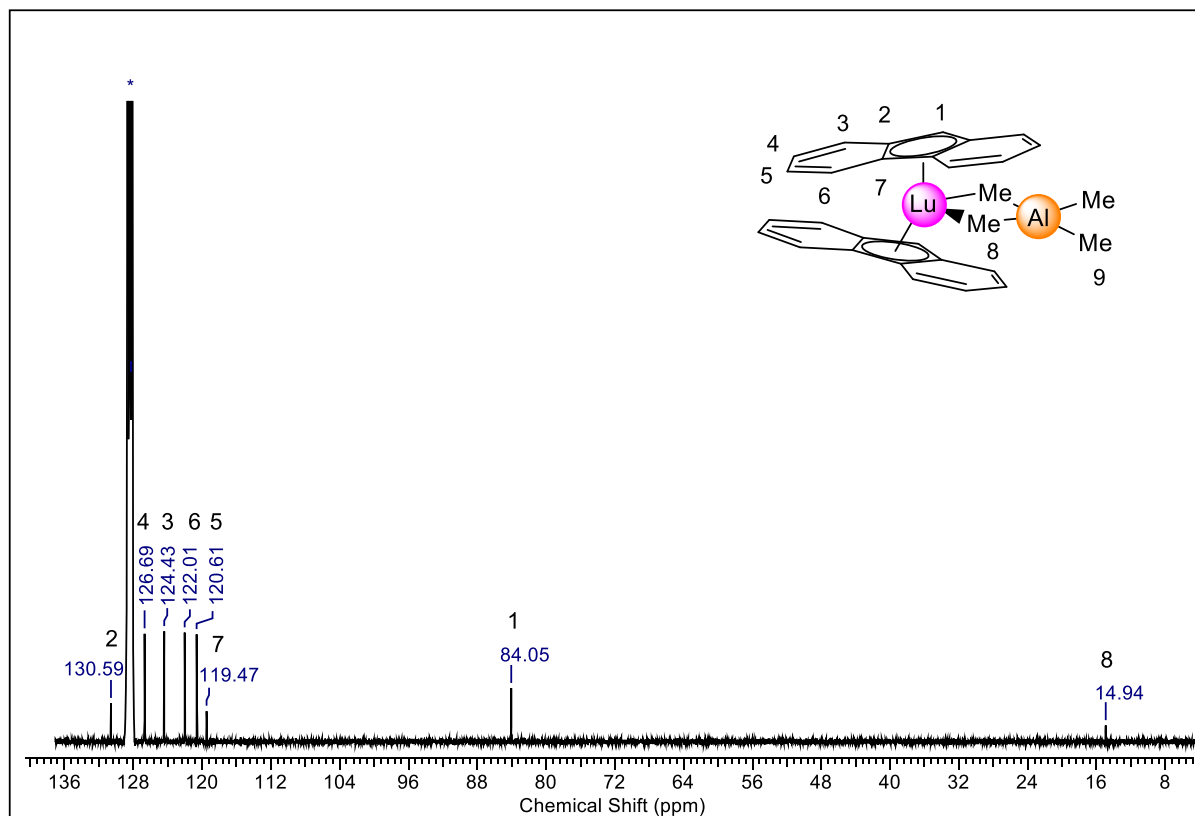


**Figure S16.**  $^{13}\text{C}\{^1\text{H}\}$  spectrum (101 MHz) of  $(\text{Flu})_2\text{Lu}(\text{AlMe}_4)$  ( $1\text{a}^{\text{Lu}}$ ) in  $\text{C}_6\text{D}_6$  at  $26^\circ\text{C}$ .

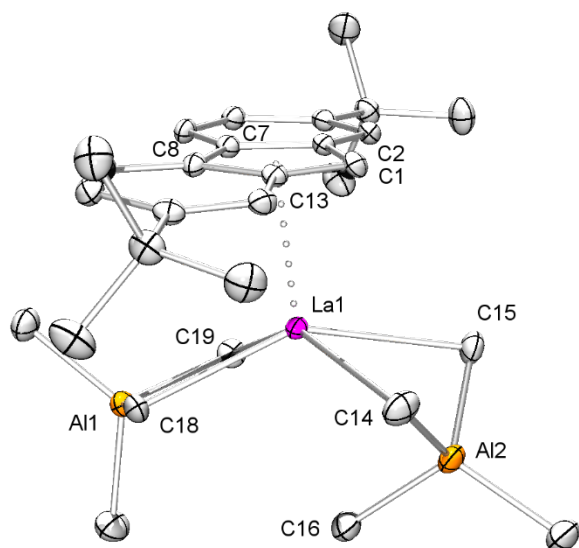


**Figure S17.** Molecular structure of (Flu<sup>Bu</sup>)La(AlMe<sub>4</sub>)<sub>2</sub> (**2<sup>La</sup>**). Hydrogen atoms are omitted for clarity. The asymmetric unit contains two independent molecules. The second molecule is omitted for clarity. Atomic displacement parameters set at the 50% probability level. Selected bond lengths [Å] and angles [°]: La1–C1 2.686(2), La1–C2 2.800(2), La1–C7 2.935(2), La1–C8 2.942(2), La1–C13 2.796(2), La1–C14 2.808(3), La1–C15 2.785(3), C14–La1–C15 71.76(8), La1···C16 3.071(3), La1–C18 2.696(2), La1–C19 2.675(2), C18–La1–C19 79.82(7), La···Al1 2.9878(8), La1···Al2 3.2325(8).

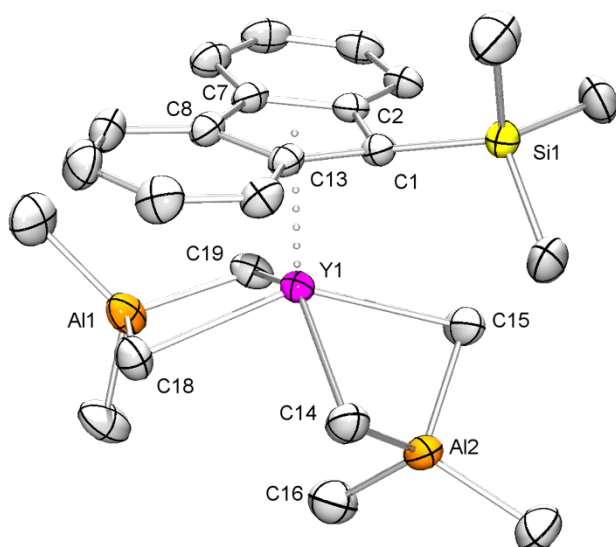


**Figure S18.** Molecular structure of (Flu<sup>Si</sup>)Y(AlMe<sub>4</sub>)<sub>2</sub> (**3<sup>Y</sup>**). Hydrogen atoms are omitted for clarity. Atomic displacement parameters set at the 50% probability level. Selected bond lengths [Å] and angles [°]: Y1–C1 2.5741(16), Y1–C2 2.6570(15), Y1–C7 2.7780(15), Y1–C8 2.7898(15), Y1–C13 2.6730(16), Y1–C14 2.632(2), Y1–C15 2.6021(19), C14–Y1–C15 79.00(7), Y1···C16 3.429(2), Y1–C18 2.5244(19), Y1–C19 2.527(2), C18–Y1–C19 83.87(6), Y1···Al1 2.9473(7), Y···Al2 3.0789(6).

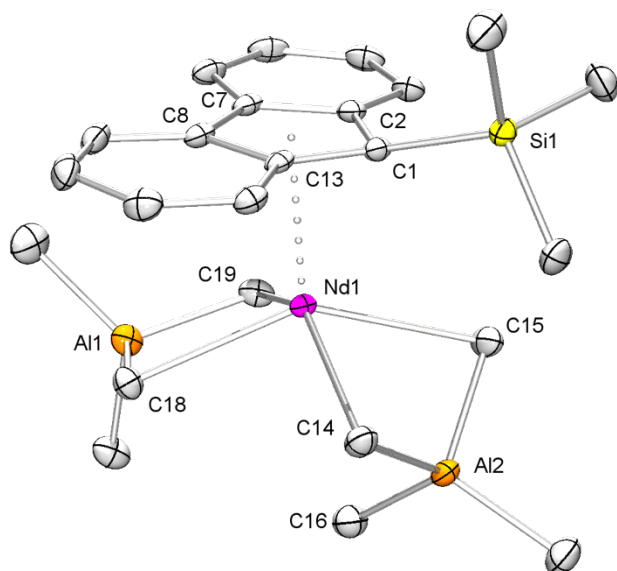


**Figure S19.** Molecular structure of  $(\text{Flu}^{\text{Si}})\text{Nd}(\text{AlMe}_4)_2$  ( $3^{\text{Nd}}$ ). Hydrogen atoms are omitted for clarity. Atomic displacement parameters set at 50% probability level. Selected bond lengths [Å] and angles [°]: Nd1–C1 2.6562(15), Nd1–C2 2.7354(15), Nd1–C7 2.8579(15), Nd1–C8 2.8720(15), Nd1–C13 2.7499(15), Nd1–C14 2.7036(19), Nd1–C15 2.6720(19), C14–Nd1–C15 76.93(6), Nd1···C16 3.2688(19), Nd1–C18 2.6058(18), Nd1–C19 2.6080(17), C18–Nd1–C19 81.41(6), Nd1···Al1 3.1605(5), Nd··Al2 2.9830(5).

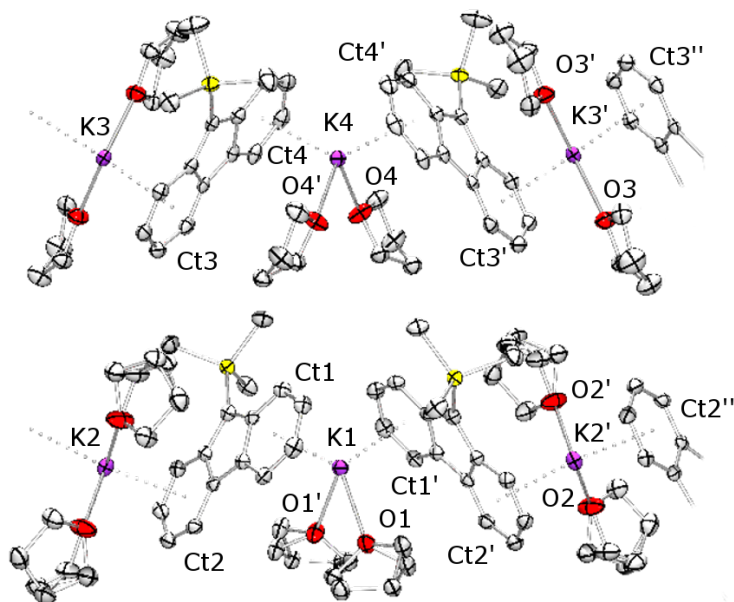


**Figure S20.** Section of the molecular structure of  $[\text{K}(\text{Flu}^{\text{Si}})(\text{THF})_2]_n$ . Hydrogen atoms are omitted for clarity. Atomic displacement parameters set at 50% probability level. Selected bond lengths [Å] and angles [°]: K1–O1 2.654(2), K1–Ct1 2.867, O1–K1–O1' 73.36(10), Ct1–K1–Ct1' 129.41, K2–O2 2.611(2), K2–Ct2 2.851, O2–K2–O2' 81.41(11), Ct2–K2–Ct2' 129.86, K3–O3 2.643(2), K3–Ct3 2.847, O3–K3–O3' 102.40(9), Ct3–K3–Ct3' 131.54, K4–O4 2.624(2), K4–Ct4 2.813, O4–K4–O4' 96.00(10), Ct4–K4–Ct4' 129.46.

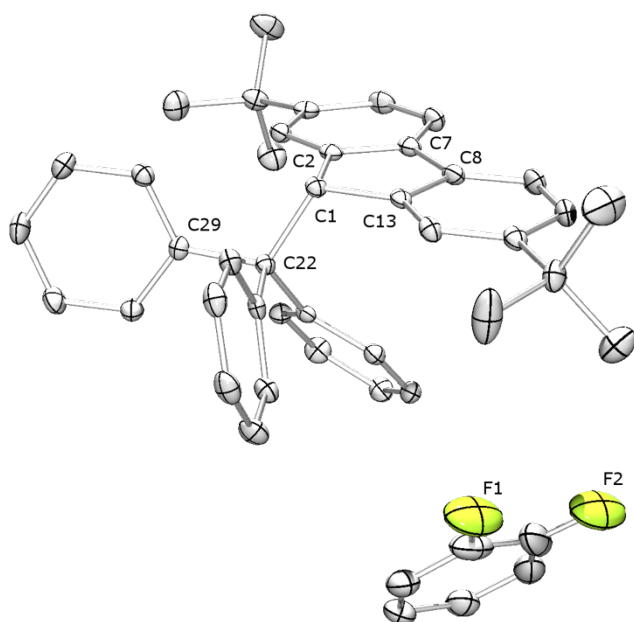


**Figure S21.** Molecular structure of 1-CPh<sub>3</sub>-Flu<sup>tBu</sup>. Hydrogen atoms are omitted for clarity. Atomic displacement parameters set at the 50% probability level. Selected bond lengths [Å] and angles [°]: C1–C2 1.532(2), C1–C13 1.534(2), C1–C22 1.588(2), C2–C7 1.402(2), C7–C8 1.468(2), C8–C13 1.399(2), C22–C29 1.555(2), C13–C1–C22 114.37(12).

**Table S1.** Crystallographic data for compounds **1<sup>La</sup>**, **2<sup>La</sup>**, **3<sup>La</sup>**, and **3<sup>Lu</sup>**

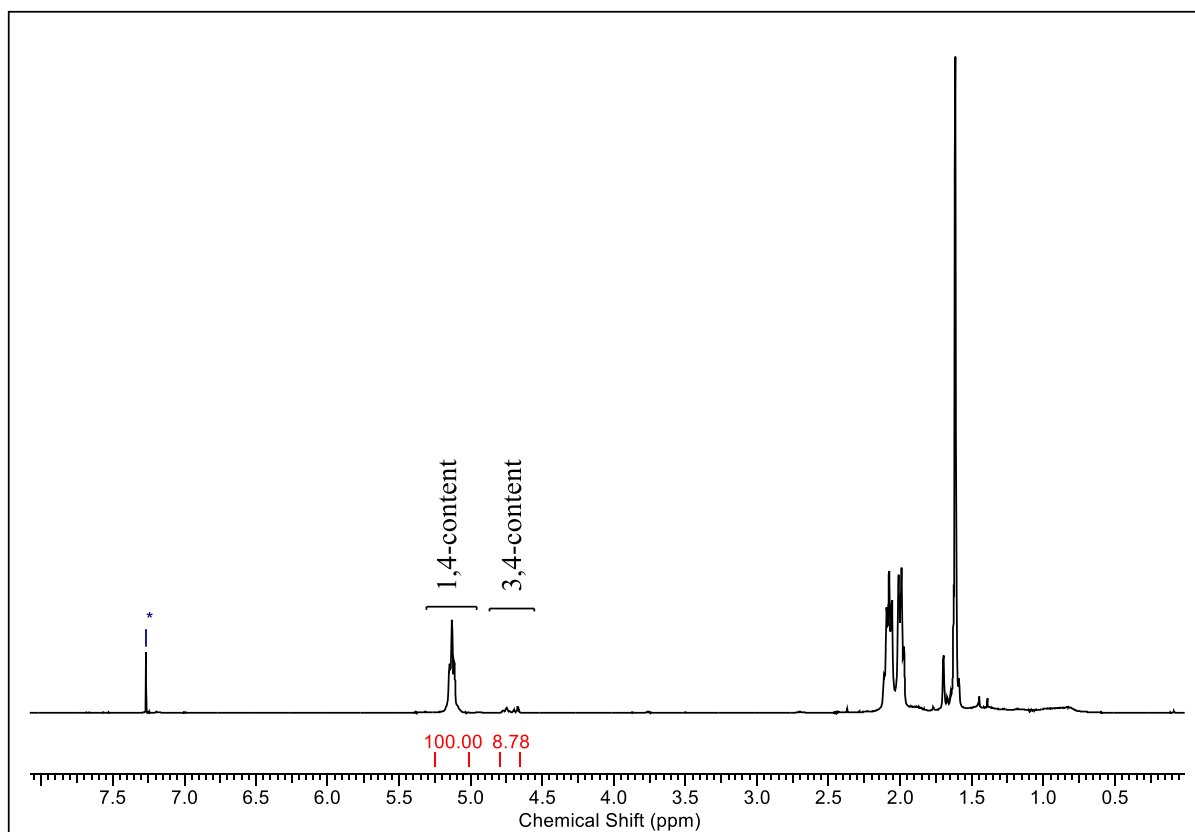
	<b>1<sup>La</sup></b>	<b>2<sup>La</sup></b>	<b>3<sup>La</sup></b>	<b>3<sup>Lu</sup></b>
CCDC number	1562938	1562942	1562943	1562939
formula	C <sub>21</sub> H <sub>33</sub> Al <sub>2</sub> La	C <sub>29</sub> H <sub>49</sub> Al <sub>2</sub> La	C <sub>24</sub> H <sub>41</sub> Al <sub>2</sub> LaSi	C <sub>24</sub> H <sub>41</sub> Al <sub>2</sub> LuSi
M [g·mol <sup>-1</sup> ]	478.34	590.55	550.53	586.59
Color	yellow	yellow	yellow	yellow
Crystal dimensions [mm]	0.427 x 0.168 x 0.118	0.538 x 0.145 x 0.117	0.230 x 0.194 x 0.172	0.348 x 0.180 x 0.074
Crystal system	monoclinic	triclinic	monoclinic	monoclinic
space group	P21/n	P $\bar{1}$	P21/c	P21/n
a [Å]	11.470(9)	11.1616(13)	26.4046(15)	15.7037(6)
b [Å]	11.946(9)	11.7580(14)	10.8729(7)	10.6911(4)
c [Å]	17.154(13)	24.411(3)	19.5779(11)	16.3490(7)
$\alpha$ [°]	90	86.709(4)	90	90
$\beta$ [°]	104.953(16)	77.961(5)	106.750(2)	104.3100(10)
$\gamma$ [°]	90	88.963(3)	90	90
V [Å <sup>3</sup> ]	2271(3)	3127.9(7)	5382.2(6)	2659.67(18)
Z	4	4	8	4
T [K]	150(2)	173(2)	100(2)	100(2)
$\rho_{\text{calcd}}$ [g·cm <sup>-3</sup> ]	1.399	1.254	1.359	1.465
$\mu$ [mm <sup>-1</sup> ]	1.959	1.435	1.705	3.830
F(000)	968	1224	2256	1184
Unique reflns	6955	16771	13351	6618
Observed reflns (I>2 $\sigma$ )	6955	62574	117556	53073
R1/wR2 (I>2 $\sigma$ )	0.0374/0.0746	0.0298/0.0649	0.0248/0.0531	0.0185/0.0413
R1/wR2 (all data)	0.0476/0.0799	0.0408/0.0696	0.0349/0.0574	0.0251/0.0443
Goodness of fit	1.086	1.025	1.034	1.035

Table S2. Crystallographic data for compounds **2<sup>Y</sup>**, **3<sup>Y</sup>**, **3<sup>Nd</sup>**, and **1a<sup>Lu</sup>**

	<b>2<sup>Y</sup></b>	<b>3<sup>Y</sup></b>	<b>3<sup>Nd</sup></b>	<b>1a<sup>Lu</sup></b>
CCDC number	1562940	1562948	1562941	1562945
formula	C <sub>29</sub> H <sub>49</sub> Al <sub>2</sub> Y	C <sub>24</sub> H <sub>41</sub> Al <sub>2</sub> YSi	C <sub>24</sub> H <sub>41</sub> Al <sub>2</sub> NdSi	C <sub>30</sub> H <sub>30</sub> AlLu
M [g·mol <sup>-1</sup> ]	540.55	500.53	555.86	592.49
Color	yellow	yellow	green	yellow
Crystal dimensions [mm]	0.289 x 0.238 x 0.148	0.335 x 0.333 x 0.249	0.243 x 0.169 x 0.158	0.254 x 0.057 x 0.046
cell	monoclinic	monoclinic	monoclinic	monoclinic
space group	P21/n	P21/n	P21/n	P21/n
a [Å]	11.0158(5)	15.832(3)	15.8567(4)	16.505(5)
b [Å]	11.5807(6)	10.8273(18)	10.8519(2)	8.171(2)
c [Å]	24.2766(12)	16.446(3)	16.1728(4)	18.751(6)
α [°]	90	90	90	90
β [°]	100.552(2)	104.301(4)	103.0250(10)	107.435(5)
γ [°]	90	90	90	90
V [Å <sup>3</sup> ]	100.552(2)	2731.7(8)	2711.34(11)	2412.6(12)
Z	4	4	4	4
T [K]	100(2)	180(2)	100(2)	100(2)
ρ <sub>calcd</sub> [g·cm <sup>-3</sup> ]	1.179	1.217	1.362	1.631
μ [mm <sup>-1</sup> ]	1.987	2.251	2.031	4.144
F(000)	1152	1056	2.031	1176
Unique reflns	7596	6518	6731	6694
Observed reflns (I>2σ)	60571	41037	36141	6694
R1/wR2 (I>2σ)	0.0338/0.0757	0.0270/0.0628	0.0184/0.0417	0.0321/0.0739
R1/wR2 (all data)	0.0492/0.0805	0.0423/0.0676	0.0216/0.0430	0.0382/0.0770
Goodness of fit	1.036	1.053	1.062	1.020

**Table S3.** Crystallographic data for compounds **4<sup>Y</sup>**, **5<sup>Y</sup>**, [K(Flu<sup>Si</sup>)(THF)<sub>2</sub>]<sub>n</sub>, and 1-CPh<sub>3</sub>-Flu<sup>tBu</sup>

	<b>4<sup>Y</sup></b>	<b>5<sup>Y</sup></b>	[K(Flu <sup>Si</sup> )(THF) <sub>2</sub> ] <sub>n</sub>	1-CPh <sub>3</sub> -Flu <sup>tBu</sup>
CCDC number	1562946	1562947	1562949	1562944
formula	C <sub>40</sub> H <sub>58</sub> Al <sub>2</sub> Cl <sub>2</sub> Si <sub>2</sub> Y <sub>2</sub>	C <sub>96</sub> H <sub>102</sub> Si <sub>6</sub> Y <sub>6</sub>	C <sub>24</sub> H <sub>33</sub> KO <sub>2</sub> Si	C <sub>46</sub> H <sub>44</sub> F <sub>2</sub>
M [g·mol <sup>-1</sup> ]	897.72	2383.17	420.69	634.81
Color	yellow	colorless	yellow	colorless
Crystal dimensions [mm]	0.325 x 0.192 x 0.188	0.264 x 0.225 x 0.152	0.481 x 0.091 x 0.083	0.527 x 0.072 x 0.056
cell	orthorhombic	trigonal	orthorhombic	triclinic
space group	Pccn	R3c:H	Pcca	P-1
a [Å]	15.8941(17)	16.5690(9)	27.9926(13)	11.204(4)
b [Å]	22.110(2)	16.5690(9)	18.4572(8)	12.226(4)
c [Å]	12.3246(13)	72.969(6)	18.4455(7)	14.342(5)
α [°]	90	90	90	65.850(5)
β [°]	90	90	90	85.282(5)
γ [°]	90	120	90	79.516(5)
V [Å <sup>3</sup> ]	4331.2(8)	17348(2)	9530.1(7)	1762.7(10)
Z	4	6	16	2
T [K]	100(2)	100(2)	100(2)	100(2)
ρ <sub>calcd</sub> [g·cm <sup>-3</sup> ]	1.377	1.396	1.173	1.196
μ [mm <sup>-1</sup> ]	2.912	3.354	0.289	0.075
F(000)	1856	7200	3616	676
Unique reflns	5374	9535	11437	7797
Observed reflns (I>2σ)	35735	140892	123776	25927
R1/wR2 (I>2σ)	0.0265/0.0551	0.0280/0.0631	0.0513/0.1112	0.0508/0.1137
R1/wR2 (all data)	0.0400/0.0592	0.0335/0.0648	0.0898/0.1269	0.0803/0.1297
Goodness of fit	1.009	1.039	1.039	1.025



**Figure S22.**  $^1\text{H}$  NMR spectrum (400 MHz) of polyisoprene (entry 5) in  $\text{CDCl}_3$  at 26 °C.

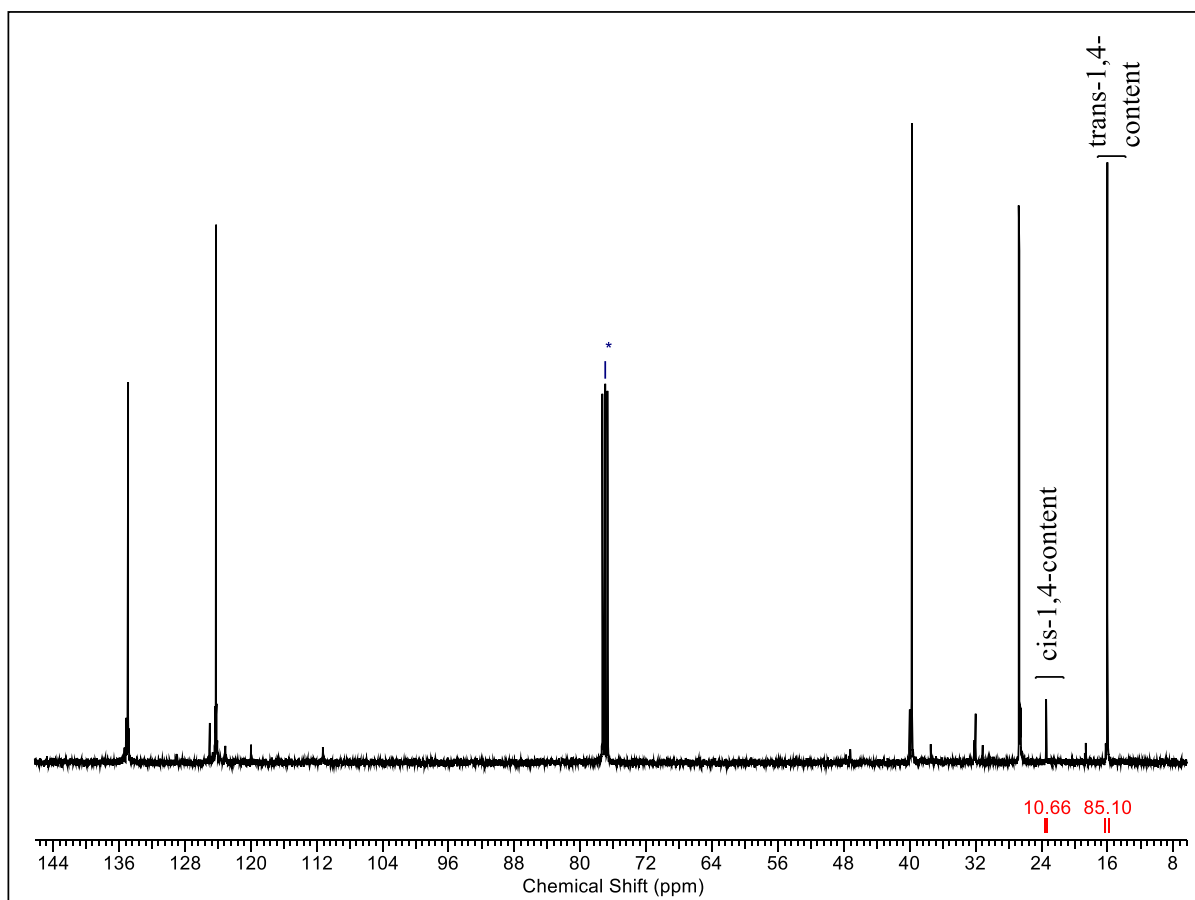


**Figure S23.**  $^{13}\text{C}\{^1\text{H}\}$  NMR spectrum (101 MHz) of polyisoprene (entry 5) in  $\text{CDCl}_3$  at 26 °C.



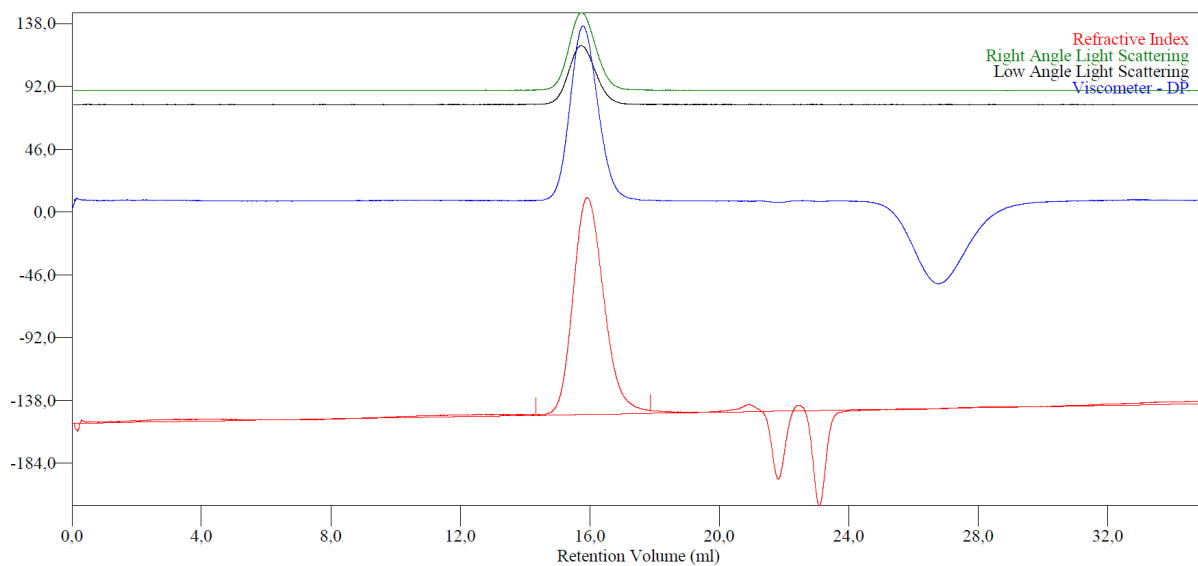


**Figure S24.** GPC curve of polyisoprene (entry5).

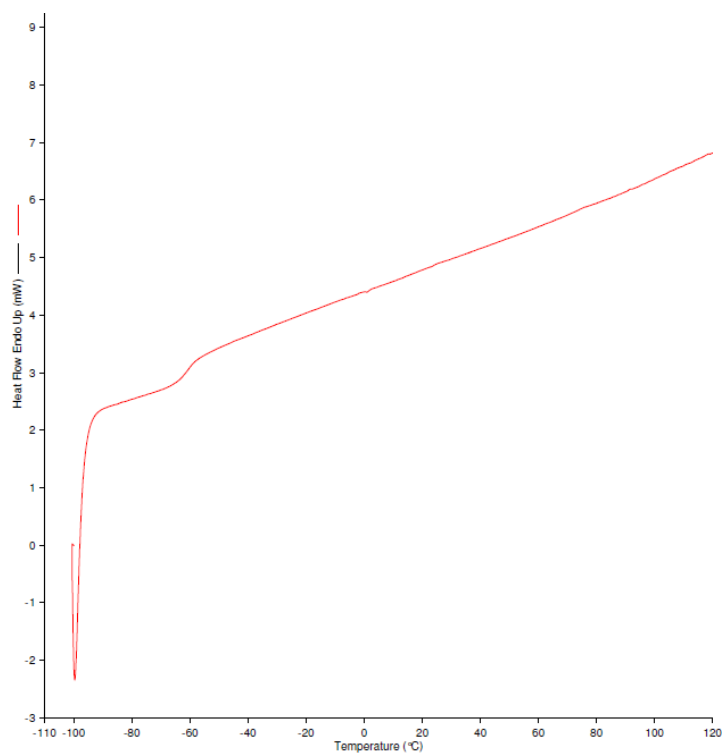


**Figure S25.** DSC curve of polyisoprene (entry 5).

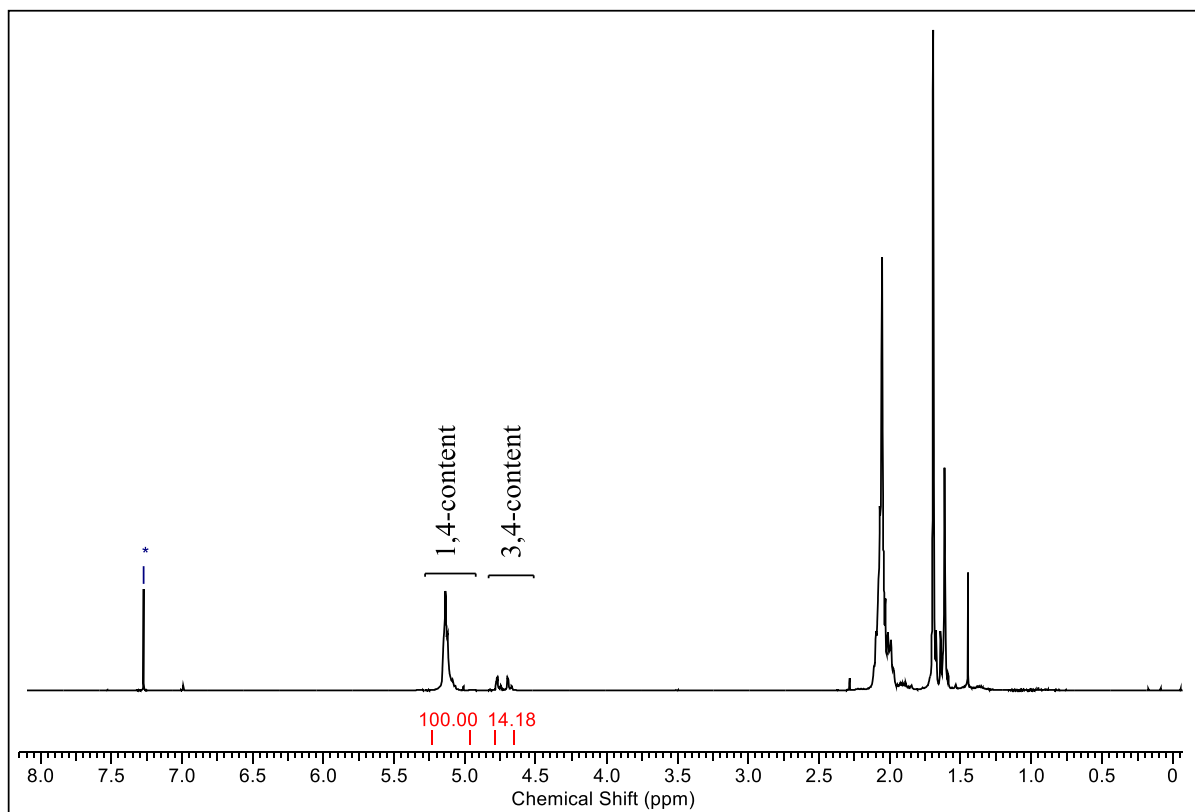


**Figure S26.**  $^1\text{H}$  NMR spectrum (400 MHz) of polyisoprene (entry 19) in  $\text{CDCl}_3$  at 26  $^\circ\text{C}$ .

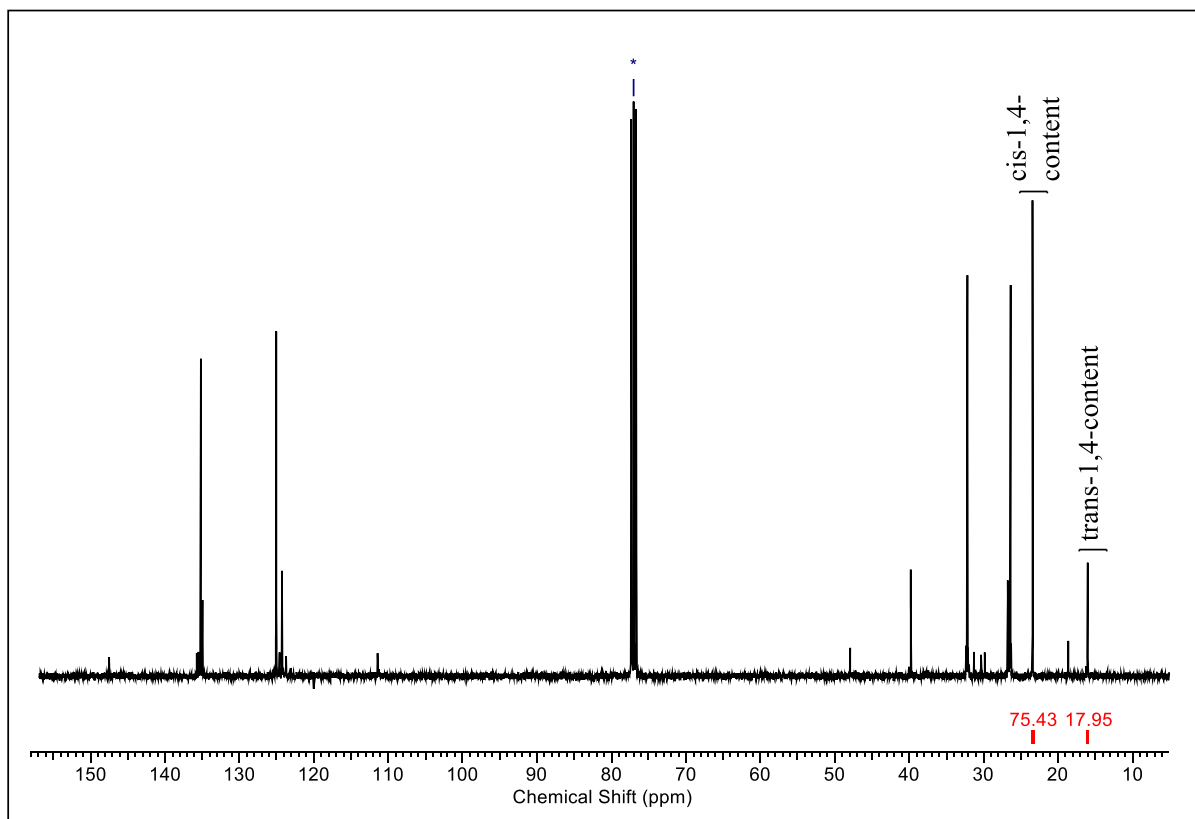


**Figure S27.**  $^{13}\text{C}\{^1\text{H}\}$  NMR spectrum (101 MHz) of polyisoprene (entry 19) in  $\text{CDCl}_3$  at 26  $^\circ\text{C}$ .

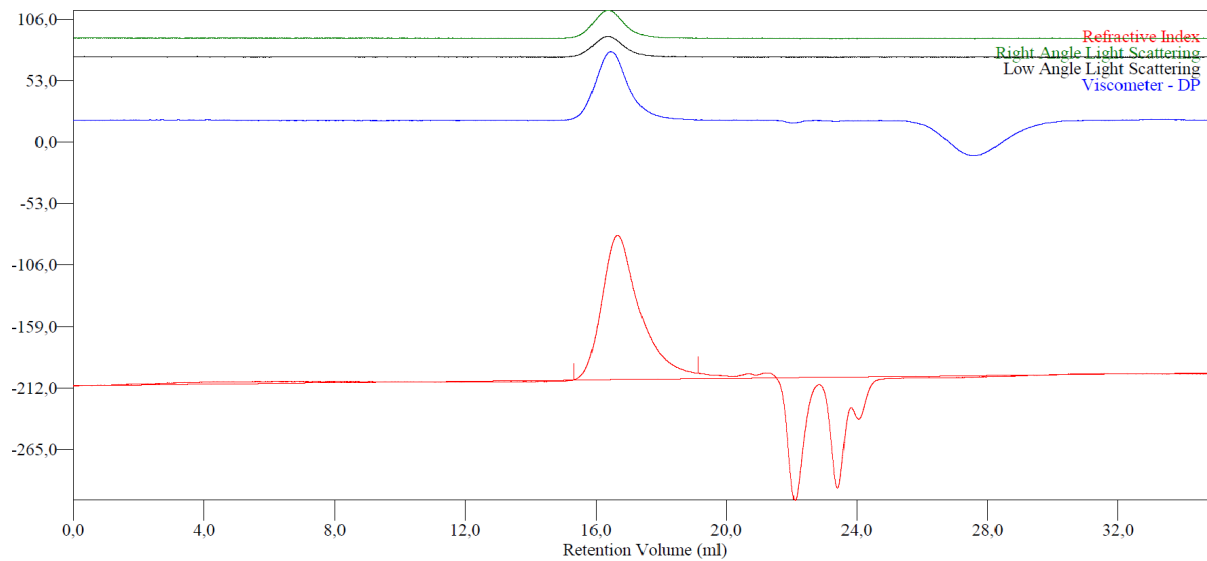


**Figure S28.** GPC curve of polyisoprene (entry 19).

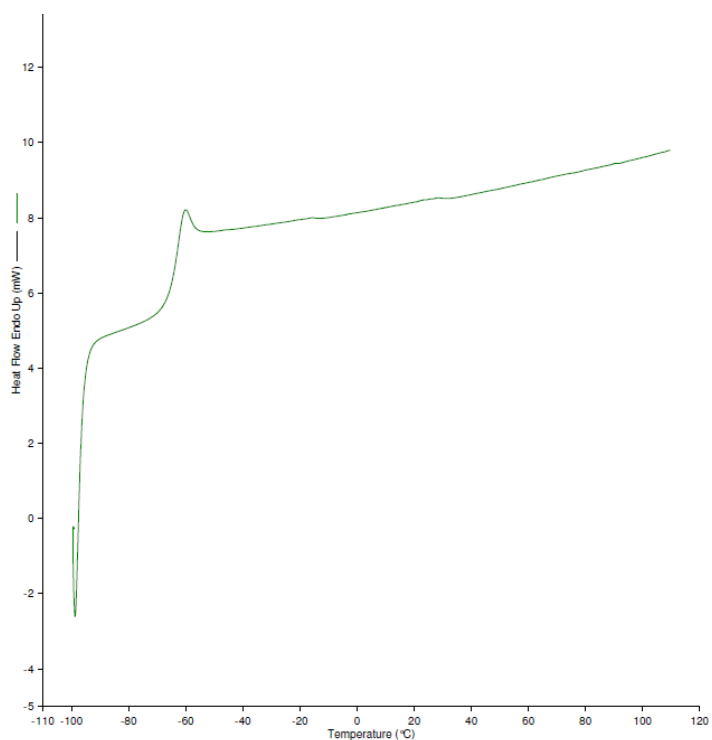


**Figure S29.** DSC curve of polyisoprene (entry 19).

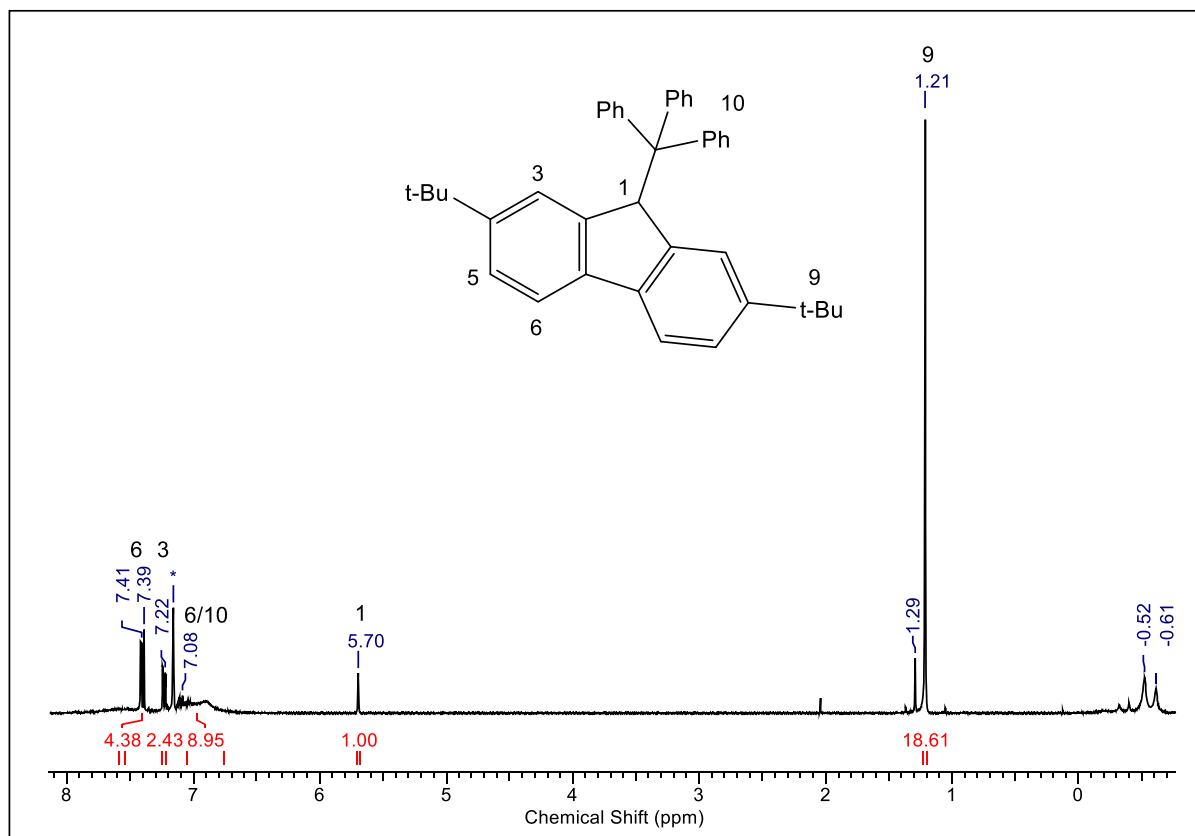


**Figure S30.**  $^1H$  NMR spectrum (400 MHz) in  $C_6D_6$  of  $(Flu^{tBu})La(AlMe_4)_2$  ( $2^{La}$ ) activated with cocatalyst A yielding  $1-CPh_3-Flu^{tBu}$  as main product.

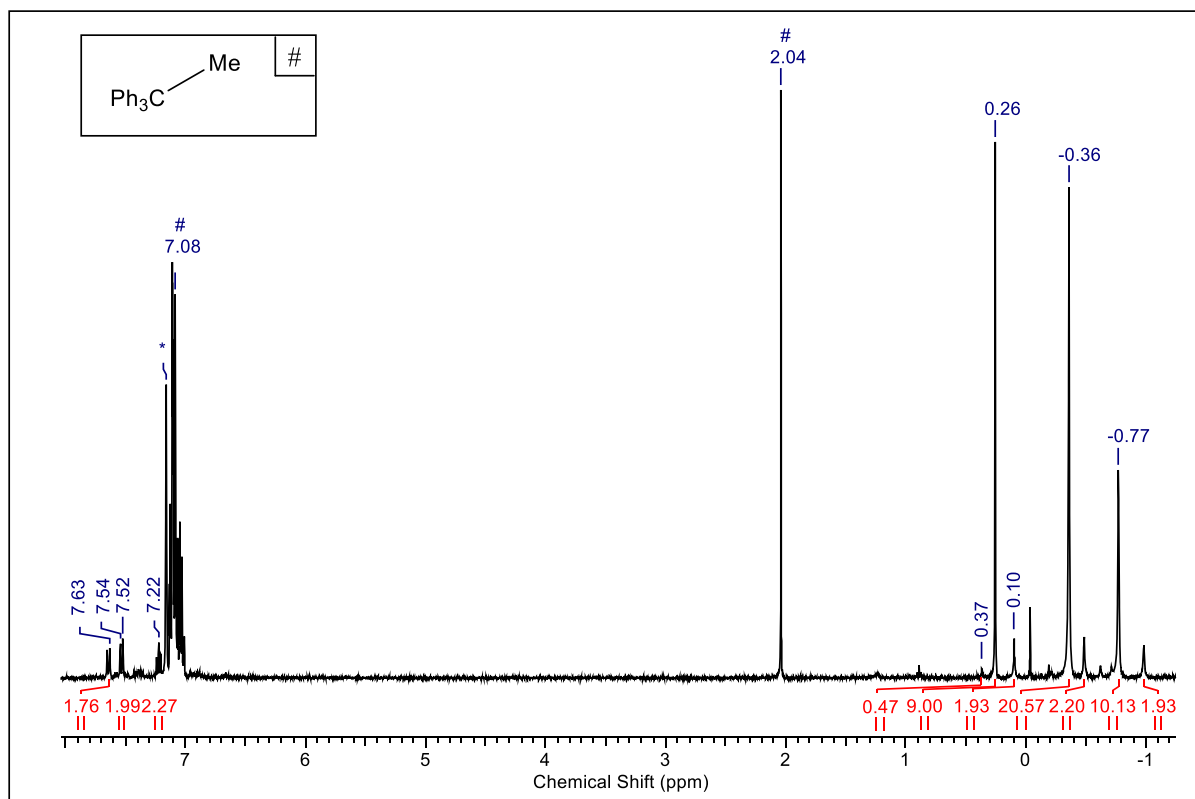


**Figure S31.**  $^1H$  NMR spectrum (400 MHz) in  $C_6D_6$  of  $(Flu^{Si})La(AlMe_4)_2$  ( $3^{La}$ ) activated with cocatalyst A. Three different  $Me_3Si$  signals ( $0.37$ ;  $0.26$ ;  $0.10$ ) indicating three different activation products (cf.,  $^{19}F$  NMR spectrum, Figure 32).

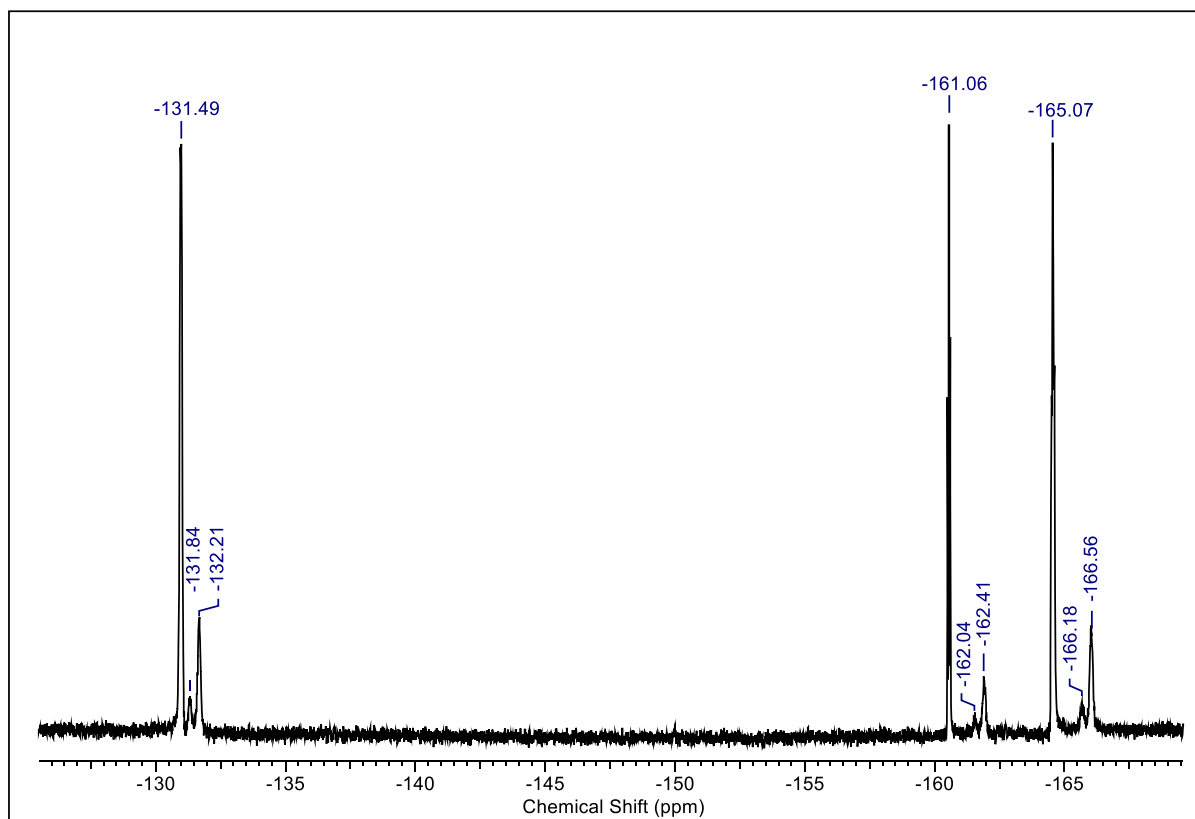


**Figure S32.**  $^{19}\text{F}$  NMR spectrum (400 MHz) in  $\text{C}_6\text{D}_6$  of  $(\text{Flu}^{\text{Si}})\text{La}(\text{AlMe}_4)_2$  ( $\mathbf{3}^{\text{La}}$ ) activated with cocatalyst A.

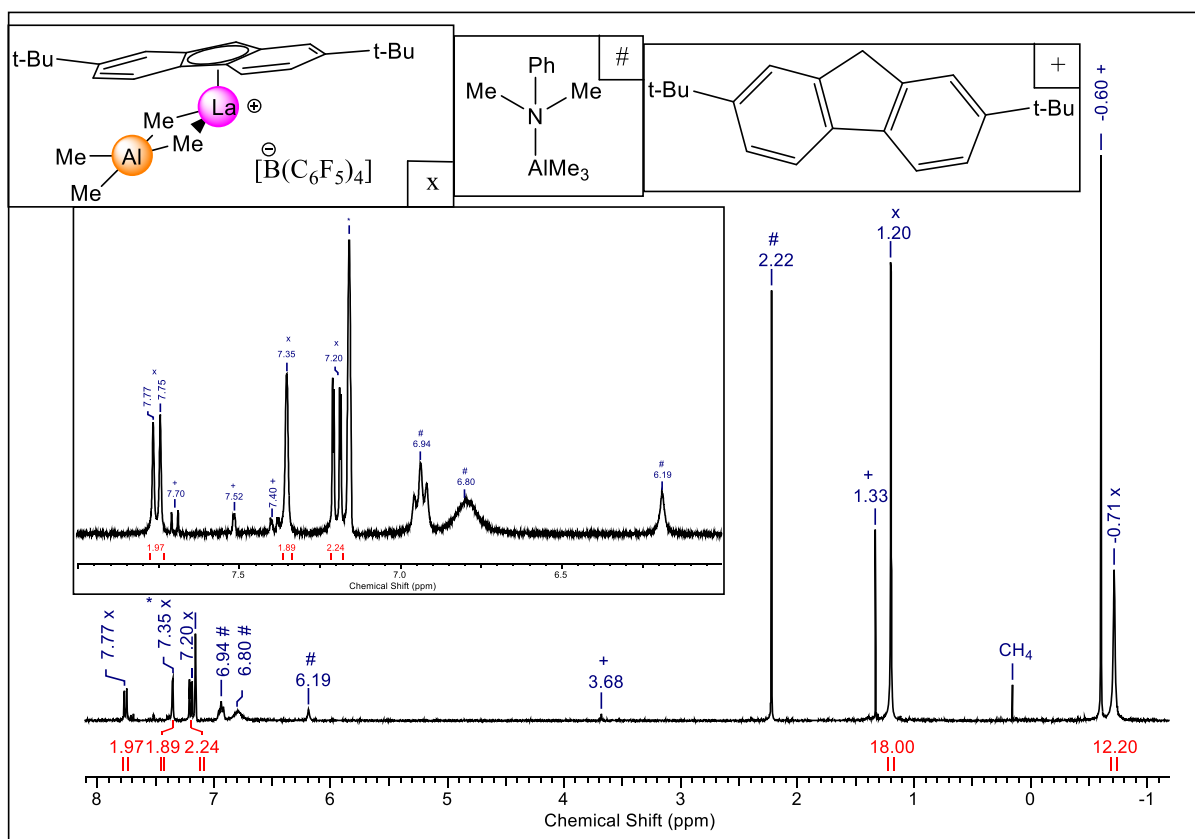


**Figure S33.**  $^1\text{H}$  NMR spectrum (400 MHz) in  $\text{C}_6\text{D}_6$  of  $(\text{Flu}^{\text{tBu}})\text{La}(\text{AlMe}_4)_2$  ( $\mathbf{2}^{\text{La}}$ ) activated with cocatalyst B. Signals labeled with "+" are assigned to  $\text{HFlu}^{\text{tBu}}$ , signals labeled with "#" are assigned to the dimethyl aniline adduct of trimethylaluminum. Signals X correspond to the active species.

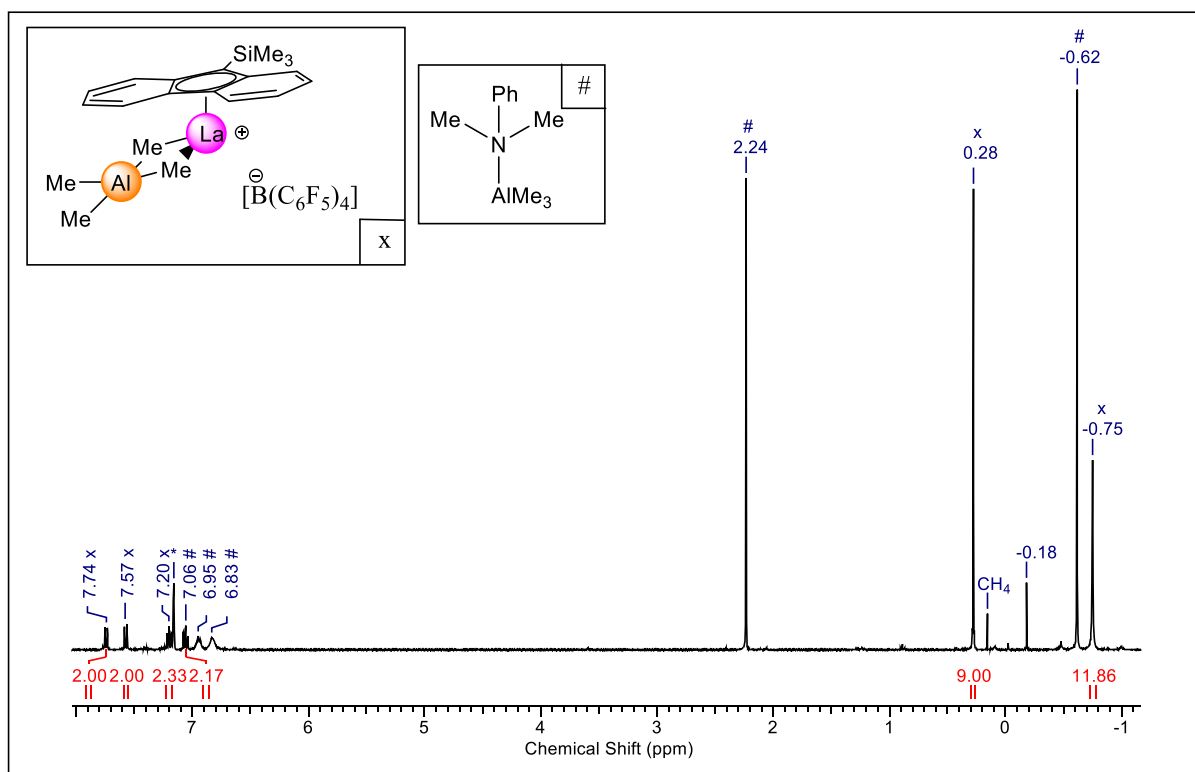
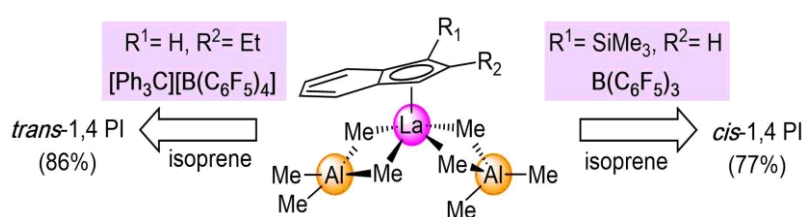


**Figure S34.**  $^1\text{H}$  NMR spectrum (400 MHz) in  $\text{C}_6\text{D}_6$  of  $(\text{Flu}^{\text{Si}})\text{La}(\text{AlMe}_4)_2$  ( $3^{\text{La}}$ ) activated with cocatalyst **B**. Signals labeled with "#" are assigned to the dimethyl aniline adduct of trimethylaluminum. Signals X correspond to the active species.

# Implications of Indenyl Substitution for the Structural Chemistry of Rare-Earth-Metal (Half-)Sandwich Complexes and Performance in Living Isoprene Polymerization



<https://doi.org/10.1021/acs.organomet.9b00344>

Reprinted (adapted) with permission from the authors of this paper.  
Copyright 2019 American Chemical Society.





# Implications of Indenyl Substitution for the Structural Chemistry of Rare-Earth Metal (Half-)Sandwich Complexes and Performance in Living Isoprene Polymerization

Dominic Diether, Cécilia Maichle-Mössmer, and Reiner Anwander\*<sup>1B</sup>

Institut für Anorganische Chemie, Eberhard Karls Universität Tübingen, Auf der Morgenstelle 18, 72076 Tübingen, Germany

## Supporting Information

**ABSTRACT:** Lanthanum indenyl half-sandwich complexes of the composition  $(\text{Ind}^R)\text{La}(\text{AlMe}_4)_2$  were synthesized in high crystalline yields by a salt-metathesis protocol applying  $\text{La}(\text{AlMe}_4)_3$  and  $\text{Li}(\text{Ind}^R)$ . In the solid state, the parent indenyl (Ind) and 2-ethylindenyl ( $\text{Ind}^{\text{Et}}$ ) complexes exhibit a dimeric structural motif with the methyl groups of the linearly aligned  $\text{La}(\mu\text{-CH}_3)\text{Al}$  moieties being *cis*-positioned to the indenyl ligand. In contrast, 1-trimethylsilyl indenyl ( $\text{Ind}^{\text{Si}}$ ) directs the  $\eta^1$ -coordinated methyl group of the bridging aluminato ligand into a *trans*-position, while 2-*tert*-butyl indenyl afforded the monomeric half-sandwich complex  $(\text{Ind}^{\text{tBu}})\text{La}(\text{AlMe}_4)_2$ . The reactions of  $\text{Lu}(\text{AlMe}_4)_3$  with 1 or 2 equiv of  $\text{Li}(\text{Ind}^R)$  gave predominantly bis(indenyl) sandwich complexes  $(\text{Ind}^R)_2\text{Lu}(\text{AlMe}_4)$ . All (half-)sandwich complexes were characterized by X-ray structure analysis,  $^1\text{H}/^{13}\text{C}\{^1\text{H}\}$  NMR and FTIR spectroscopy, and microanalysis. The performance of all half-sandwich complexes in isoprene polymerization was assessed upon activation with  $[\text{Ph}_3\text{C}][\text{B}(\text{C}_6\text{F}_5)_4]$ ,  $[\text{PhNMe}_2\text{H}][\text{B}(\text{C}_6\text{F}_5)_4]$ , or  $\text{B}(\text{C}_6\text{F}_5)_3$ . The choice of indenyl ligand and cocatalyst had a major impact on the polymerization efficiency and stereospecificity. The highest selectivities could be achieved with the binary catalyst systems  $(\text{Ind}^{\text{Et}})\text{La}(\text{AlMe}_4)_2/[\text{Ph}_3\text{C}][\text{B}(\text{C}_6\text{F}_5)_4]$  (*cis/trans* content 10.4/85.9) and  $(\text{Ind}^{\text{Si}})\text{La}(\text{AlMe}_4)_2/\text{B}(\text{C}_6\text{F}_5)_3$  (*cis/trans* content 77.0/13.0).



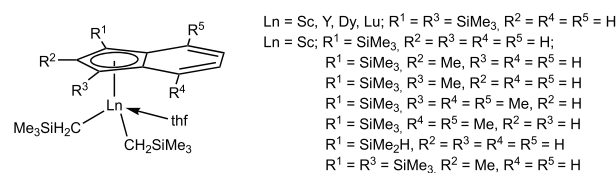
## INTRODUCTION

Rubber synthesis was pioneered by the chemical industry more than 100 years ago<sup>1</sup> with considerable impact on our everyday life. Still, efficient stereospecific 1,3-diene polymerization is an important task for industry and academia alike, while rare-earth metal-based catalysts having emerged as the most efficient.<sup>2–4</sup> Over the past decades, a plethora of ancillary ligands have been examined with the aim of generating more selective catalysts.<sup>5–7</sup> Unsurprisingly, cyclopentadienyl (Cp) ligands played a pivotal role in accessing thermally robust rare-earth metal environments in polymerization (pre)catalysts.<sup>8–10</sup> Except for the prominent half-sandwich complexes, also (*ansa*-)metallocene<sup>11–13</sup> or constrained geometry catalysts were thoroughly investigated.<sup>9,14,15</sup> Contrary to Cp ligands, indenyl (Ind) congeners have been far less examined despite their ability to promote superior performance.<sup>16</sup> The first rare-earth metal indenyl complexes,  $\text{SmInd}_3(\text{thf})$ , were studied by Tsutsui in 1968.<sup>17</sup> Since then, efforts have been undertaken to utilize indenyl ancillary ligands for polymerization catalysis. For example, indenyl-supported ytterbocene(II) complexes initiate the polymerization of  $\epsilon$ -caprolactone ( $\epsilon$ -CL)<sup>18</sup> and methyl methacrylate (MMA).<sup>19,20</sup> *ansa*-Metallocene complexes of the type  $[(\text{IndCMe}_2\text{Ind})\text{Ln}(\text{allyl})(\text{thf})_x]$  ( $\text{Ln} = \text{Y}, \text{Nd}$ ) were described by Carpentier and co-workers as versatile precatalysts mediating the polymerization of styrene and isoprene (IP) as well as the formation of styrene/IP copolymers.<sup>21–23</sup> The fabrication of poly-MMA was achieved in the presence of *ansa*-metallocene amide and metallocene hydrocarbyl complexes ( $\text{Ln} = \text{Y}, \text{Nd}, \text{Sm}, \text{Dy}, \text{Yb}, \text{Lu}$ ).<sup>24,25</sup>

Especially Wang and co-workers but also others developed donor-functionalized indenyl ligands for  $\text{Ln}(\text{II})$  complexation ( $\text{Ln} = \text{Eu}, \text{Yb}$ ) and the polymerization of MMA and  $\epsilon$ -CL.<sup>26,27</sup> Moreover, indenyl-supported constrained geometry catalysts with trivalent rare-earth metals were shown to polymerize lactides, ethylene, IP, and styrene.<sup>28,29</sup>

Bis(alkyl) complexes of the general formula  $\text{LLnR}_2$  ( $\text{L} =$  anionic ligand;  $\text{Ln} =$  rare-earth metal;  $\text{R} =$  alkyl, allyl, benzyl group) display the most active systems for the polymerization of dienes<sup>4</sup> and are the most pertinent to the present work. The group of Chen used indenyl half-sandwich complexes of small- to middle-sized rare-earth metals ( $\text{Ln} = \text{Sc}, \text{Dy}, \text{Y}, \text{Lu}$ ) to polymerize styrene, MMA, and  $\beta$ -methyl- $\alpha$ -methylene- $\gamma$ -butyrolactone (Chart 1).<sup>32,33</sup> Furthermore, the terpolymerization of ethylene/propylene/isoprene was accomplished with the scandium complex  $[\text{Ind}(\text{SiMe}_3)_2]\text{Sc}(\text{CH}_2\text{SiMe}_3)_2(\text{thf})$ .<sup>32</sup>

**Chart 1. Indenyl-Supported Ln(III) Half-Sandwich Dialkyl Complexes Employed in Polymerization Reactions**



Received: May 22, 2019

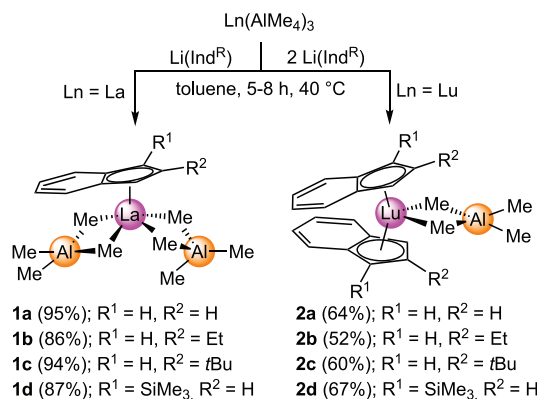
Published: July 18, 2019

The yttrium indenyl half-sandwich complex (Ind)Y-(CH<sub>2</sub>SiMe<sub>3</sub>)[(4,6-(CMe<sub>3</sub>)<sub>2</sub>-2-(MeOCH<sub>2</sub>CH<sub>2</sub>)<sub>2</sub>-NCH<sub>2</sub>-C<sub>6</sub>H<sub>2</sub>-O)] also revealed activity in the polymerization of lactide.<sup>33</sup> Tardif et al. showed that activation of the indenyl sandwich complexes (MeInd)<sub>2</sub>Ln[N(SiMe<sub>3</sub>)<sub>2</sub>] (Ln = Sc, Gd) by [Ph<sub>3</sub>C][B(C<sub>6</sub>F<sub>5</sub>)<sub>4</sub>] or [PhNM<sub>2</sub>H][B(C<sub>6</sub>F<sub>5</sub>)<sub>4</sub>] results in the abstraction of an indenyl ligand<sup>34</sup> and, consequently, generates half-sandwich species capable of polymerizing butadiene. It is interesting to note that, in the realm of indenyl-supported half-sandwich complexes for polymerization reactions, mainly those of rare-earth metals with smaller ionic radii (Yb, Lu, Sc) have been studied. This is in contrast to Cp<sup>-</sup> and fluorenyl-supported<sup>35</sup> half-sandwich complexes, which were also examined for the larger-sized Ln<sup>3+</sup> ions. Herein, we report on the successful synthesis of new lutetocene and indenyl-supported lanthanum half-sandwich complexes and their performance in the polymerization of isoprene.

## RESULTS AND DISCUSSION

**Synthesis of Ln(III) Indenyl Half-Sandwich and Sandwich Complexes.** The protonolysis reaction based on homoleptic tetramethylaluminates as precursors, which was feasible for the synthesis of cyclopentadienyl-supported half-sandwich complexes,<sup>8</sup> indicated only low conversion rates for La(AlMe<sub>4</sub>)<sub>3</sub> and indene. Therefore, a salt-metathesis protocol, similar to that successfully applied for the synthesis of fluorenyl-supported half-sandwich complexes,<sup>35</sup> was employed to access the indenyl congeners (Scheme 1). Accordingly,

**Scheme 1. Synthesis of Rare-Earth Metal Indenyl (Half-) Sandwich Complexes According to Salt-Metathesis Protocols**



treatment of La(AlMe<sub>4</sub>)<sub>3</sub> with 1 equiv of lithium indenide led to the isolation of the envisaged half-sandwich complexes in high yields (86–95%). Complexes **1a–1d** are inert toward ligand scrambling (and formation of the respective metallocene derivatives) at ambient temperature. However, at elevated temperatures (110 °C), such ligand rearrangements were found to be quantitative.

When performing the salt-metathesis reaction with Lu(AlMe<sub>4</sub>)<sub>3</sub>, only a small amount of the corresponding half-sandwich complex could be detected by <sup>1</sup>H NMR spectroscopy, whereas the formation of the corresponding sandwich complex prevailed. As expected, the yield of the lutetium bis(indenyl) complex could be improved when employing 2 equiv of lithium indenide. Increasing the steric demand of the indenyl ligand by varying the substitution pattern at C1 and C2

did not favor the formation of the putative lutetium half-sandwich complex. The bis(indenyl) complex was even formed as the main product when a bulky *tert*-butyl group is attached to the C2 position.

In a previous study, we were able to isolate the corresponding fluorenyl half-sandwich complexes for the entire Ln(III) size range by using a trimethylsilyl-substituted fluorenyl ligand.<sup>35</sup> For comparison, the equimolar reactions of La(AlMe<sub>4</sub>)<sub>3</sub> with lithium (1-trimethylsilyl) indenide gave exclusively the half-sandwich complex (Ind<sup>Si</sup>)La(AlMe<sub>4</sub>)<sub>2</sub> (**1d**), while the Lu(AlMe<sub>4</sub>)<sub>3</sub> reaction yielded the bis(indenyl) complex **2d**.

**NMR Spectroscopy of Ln(III) Indenyl Half-Sandwich and Sandwich Complexes.** The <sup>1</sup>H NMR spectra of half-sandwich complexes **1a–d** revealed a high fluxionality of the [AlMe<sub>4</sub>] moieties in solution, as indicated by the singlet signals in the high-field region between –0.33 and –0.41 ppm. For comparison, the [AlMe<sub>4</sub>] signals of **1a–d** lie well within the expected range of the Cp<sup>R</sup> congeners (Cp<sup>R</sup>)Ln(AlMe<sub>4</sub>)<sub>2</sub> (–0.12 to –0.33 ppm)<sup>8</sup> and fluorenyl complexes (Flu<sup>R</sup>)Ln(AlMe<sub>4</sub>)<sub>2</sub> (–0.40 to –0.60 ppm; R = H, <sup>*t*</sup>Bu, SiMe<sub>3</sub>).<sup>35</sup> Like in **1a**, the signal sets for the indenyl hydrogen atoms in **1b** and **1c** indicate a highly symmetric environment at the lanthanum metal center caused by the substituents at position C2. Due to the trimethylsilyl substitution at C1, the aromatic protons of the indenyl ligand Ind<sup>Si</sup> display distinct chemical shifts. Ind<sup>Si</sup> is prochiral which impacts the formation of sandwich complex **2d**, since Ind<sup>Si</sup> can coordinate with either side (*re*- or *si*-site) of the enantiotopic faces.<sup>36–40</sup> Accordingly, the reaction of Lu(AlMe<sub>4</sub>)<sub>3</sub> with Li(Ind<sup>Si</sup>) afforded **2d** with an approximately 9:1 mixture of *meso* (*re*, *si* attachment) and *rac* isomer (*re*, *re* or *si*, *si* attachment), as assigned by <sup>1</sup>H NMR spectroscopy at ambient temperature (Figure 1). The isomeric mixture could not be separated by fractional crystallization, but we could obtain single crystals of *meso*-**2d** suitable for X-ray structure analysis (vide infra). In *meso*-**2d**, the terminal methyl groups of the AlMe<sub>4</sub> moiety are related by a mirror plane, while the bridging ones have a different environment, resulting in a 3:6:3 (0.06/–0.49/–1.02 ppm) signal pattern. Because of the C<sub>2</sub> symmetry of *rac*-**2d**, one signal each for the terminal and bridging methyl protons (–0.48/–0.49 ppm) was observed, respectively. The existence of two isomers is also evidenced by <sup>29</sup>Si–<sup>1</sup>H DEPT-45 NMR spectroscopy. The strong signal at –8.40 ppm can be assigned to *meso*-**2d**, while the minor product *rac*-**2d** resonates at –8.27 ppm (Figure S33). Any silyl group migration can be ruled out, since the <sup>1</sup>H NMR spectrum shows only signal sets of an asymmetrically substituted indenyl ligand.<sup>41</sup> A variable-temperature <sup>1</sup>H NMR experiment revealed that an interconversion of the isomers does not occur. However, at 100 °C, broadening of the Lu/Al–CH<sub>3</sub> signals was observed, indicative of emerging [AlMe<sub>4</sub>] methyl ligand exchange (Figure S35). Cooling a solution of **2d** to –85 °C resulted in a splitting of the indenyl (6.10 ppm) and Al–CH<sub>3</sub> signals (–0.29 ppm) of the *meso* isomer (Figure S36). The <sup>1</sup>H and <sup>13</sup>C{<sup>1</sup>H} NMR spectra of the symmetric lutetocene indenyl complexes **2a–c** show one set of signals for the indenyl hydrogen atoms, in agreement with the observations made for symmetric cyclopentadienyl or fluorenyl sandwich complexes. The splitting of the [AlMe<sub>4</sub>] resonance into two singlets (1:1 ratio at ambient temperature) is indicative of bridging and terminal positions of the methyl groups.

**X-ray Structure Analysis of Ln(III) Indenyl Complexes.** The (half-)sandwich complexes **1** and **2** were examined by X-

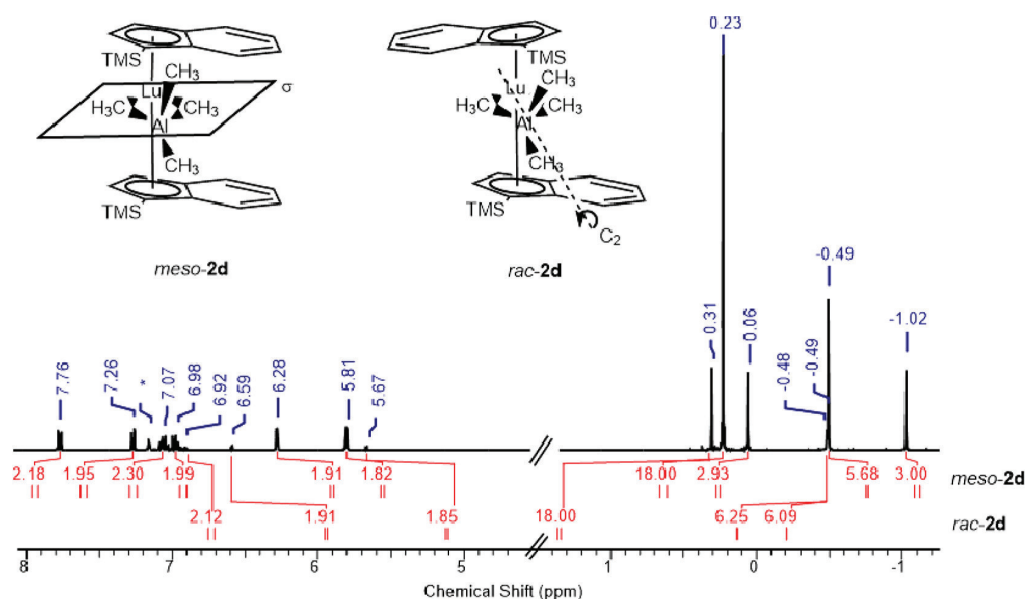


**Figure 1.**  $^1\text{H}$  NMR spectrum of  $(\text{Ind}^{\text{Si}})_2\text{Lu}(\text{AlMe}_4)$  (**2d**) in  $\text{C}_6\text{D}_6$  at  $26^\circ\text{C}$  (*meso-2d*: major product; *rac-2d*: minor product).

ray crystallography. Suitable single crystals were obtained from toluene/*n*-hexane mixtures. Compound **1c** crystallized as a monomer reminiscent of the solid-state structures of cyclopentadienyl<sup>8</sup> and fluorenyl complexes<sup>35</sup> (Figure 2, second from bottom). The molecular structure of **1c** features a planar and a bent  $[\text{AlMe}_4]$  unit, as evidenced by the elongation of the  $\text{La}-\text{C}(\mu\text{-CH}_3)$  in the bent unit (av.  $2.762(3)$  Å, cf. Table 1) in comparison to the planar one (av.  $2.693(3)$  Å). This is also reflected by distinct  $\text{La}1\cdots\text{Al}1$  ( $3.0329(8)$  Å, “bent”) and  $\text{La}1\cdots\text{Al}2$  distances ( $3.2352(8)$  Å, “planar”). The terminal methyl group C12 of the bent  $[\text{AlMe}_4]$  ligand is located close to the lanthanum center. The  $\text{La}1\cdots\text{C}12$  distance of  $3.234(3)$  Å is in accord with the metrical parameters in  $(\text{Me}_3\text{C}_5\text{H}_2)\text{La}(\text{AlMe}_4)_2$  ( $3.293(2)$  Å) and  $(\text{Flu}^{\text{Si}})\text{La}(\text{AlMe}_4)_2$  ( $3.297(2)$  Å), but longer than that in  $(\text{Flu})\text{La}(\text{AlMe}_4)_2$  and  $(\text{Flu}^{\text{tBu}})\text{La}(\text{AlMe}_4)_2$  ( $3.045(4)/3.071(3)$  Å).<sup>35</sup> The  $\text{La}\cdots\text{C}t$  distance of  $2.539$  Å is comparable to the corresponding metrics in  $(\text{tBu}_3\text{C}_5\text{H}_2)\text{La}(\text{AlMe}_4)_2$  ( $2.53$  Å).<sup>8</sup>

The single crystal X-ray diffraction studies of  $(\text{Ind})\text{La}(\text{AlMe}_4)_2$  (**1a**) and  $(\text{Ind}^{\text{Et}})\text{La}(\text{AlMe}_4)_2$  (**1b**) revealed a dilanthanum structure with bridging  $\text{La}(\mu\text{-CH}_3)\text{Al}$  moieties (Figure 2, two upper depictions, and Figure S41). The dimerization of such half-sandwich complexes is per se uncommon but has been observed before in the solid-state structures of  $(\text{Me}_4\text{C}_5\text{H})\text{La}(\text{AlMe}_4)_2$  and  $(\text{Flu}^{\text{Si}})\text{La}(\text{AlMe}_4)_2$ .<sup>35,42</sup> Considering a  $\mu_2\text{-}\eta^1\text{-}\eta^2$   $[\text{AlMe}_4]$  bridging mode, the lanthanum centers in **1a** and **1b** adopt a distorted octahedral coordination geometry. The  $\text{Al}(\mu\text{-CH}_3)\text{La}$  moieties are almost linear and positioned “*cis*” to the indenyl ligands. The  $\text{La}1-\text{C}(\mu\text{-CH}_3)$  distances of the  $\eta^2$ -coordinated  $[\text{AlMe}_4]$  ligands (**1a**:  $\text{La}1-\text{C}14$   $2.672(3)$  Å,  $\text{La}1-\text{C}15$   $2.725(3)$  Å) are comparable to those of the planar unit in monomeric complex **1c**. In contrast, the  $\mu_2\text{-}\eta^1\text{-}\eta^2$ -bridging  $[\text{AlMe}_4]$  ligands exhibit elongated  $\text{La}-\text{C}(\mu\text{-CH}_3)$  distances ( $\text{La}1-\text{C}10$   $2.763(3)$  Å,  $\text{La}1-\text{C}11$   $2.940(3)$  Å). Noteworthy, the  $\text{La}1-\text{C}11$  distance is even longer than the  $\text{La}1\cdots\text{C}12'$  one of the linear  $\text{Al}(\mu\text{-CH}_3)\text{La}$  unit ( $2.896(3)$  Å), which is also reflected in a longer  $\text{La}1\cdots\text{Al}1$  distance of  $3.370(1)$  Å compared to the  $\text{La}1\cdots\text{Al}2$  distance of

$3.212(1)$  Å. The lanthanum–centroid distance of  $2.535$  Å is comparable to that in monomeric complex **1c**.

The X-ray diffraction study of complex **1d** (Figure 2, bottom) also revealed a dimeric structural motif, but distinct from that of **1a** and **1b**. In **1d**, namely, the  $\mu_2\text{-}\eta^1\text{-}\eta^2$   $[\text{AlMe}_4]$  ligands are now positioned “*trans*” to the indenyl ligands. Each lanthanum center in **1d** is formally seven-coordinate by the indenyl ligand and four methyl groups reminiscent of a four-legged piano-stool geometry with one additional contact to the terminal methyl group of the second subunit. The  $\text{La}-\text{C}(\mu\text{-CH}_3)$  bond lengths range from  $2.712(1)$  to  $2.753(1)$  Å and the  $\text{La}1\cdots\text{Al}$  distances of  $3.2600(3)$  and  $3.2779(3)$  Å are very similar, indicating a symmetric coordination of virtually identical  $[\text{AlMe}_4]$  units. The distance of the bridging methyl group C12' to the lanthanum center is  $3.277(1)$  Å and thus longer than that in dimeric **1a** and **1b**, but in accord with the  $\text{La}1\cdots\text{C}12'$  distance of  $3.234(3)$  Å in **1c**. The  $\text{La}1\cdots\text{C}t1$  distance of  $2.531$  Å is in the same range as that for complexes **1a–c**, although the indenyl ligands have a strong impact on the overall structure in the solid state.

In contrast to the diversity of the solid-state structures found for half-sandwich complexes **1**, the bis(indenyl) compounds **2** show, irrespective of the substitution pattern at the indenyl ligand, the same structural motif (Figure 3, Table 2). For example, in **2c**, the  $\text{Lu}\cdots\text{C}t$  distances of  $2.335/2.334$  Å are comparable to the corresponding distances in bis(Cp) lutetium complexes<sup>43</sup> and the  $\text{Lu}-\text{C}(\text{CH}_3)$  bond lengths of  $2.505(2)$  and  $2.511(2)$  Å are in accord with those observed for  $(\text{Flu})_2\text{Lu}(\text{AlMe}_4)$  ( $\text{Lu}-\text{C}$ ,  $2.489(5)$  Å,  $2.502(5)$  Å).<sup>35</sup>

Because of steric constraints of the indenyl ligands in complexes **2a–c**, the orientations in the solid state vary with respect to the substituent in the 2-position and the arene moiety (Figure 3), which is indicated by the torsion angle  $\text{C}2-\text{C}t1-\text{C}t2-\text{C}11$ .<sup>36,44</sup> Compound **2a**, exhibiting the sterically least hindered complex, adopts an almost eclipsed conformation of the indenyls (torsion angle  $\text{C}2-\text{C}t1-\text{C}t2-\text{C}11$   $33.9^\circ$ , Figure 3, top). In **2b**, the sterics of the ethyl groups prevent this eclipsed conformation and force the ligands into a staggered conformation (torsion angle  $\text{C}2-\text{C}t1-\text{C}t2-\text{C}11$

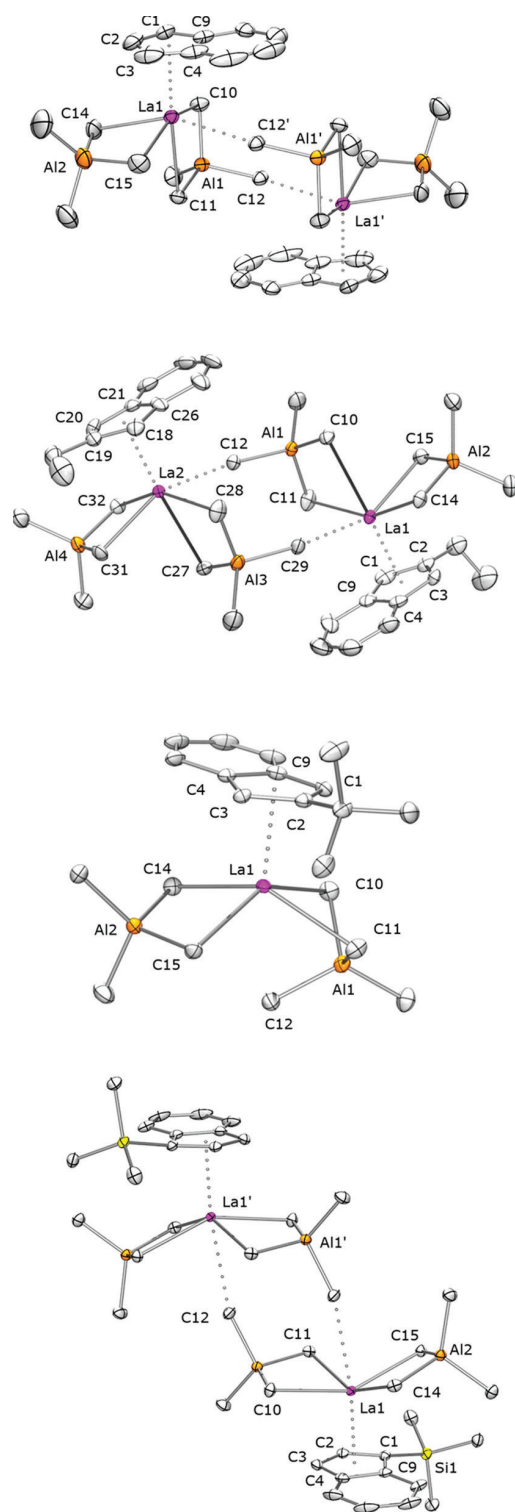


**Figure 2.** Molecular structures of **1a**, **1b**, **1c**, and **1d** (from top down). Hydrogen atoms are omitted for clarity. The asymmetric unit for **1a** contains two independent molecules. The second molecule and lattice solvent (toluene) are omitted for clarity. The second molecule of **1b** is symmetrically nonequivalent due to distortion of the ethyl moiety. Bond lengths and angles of **1b** are listed in Figure S41. Atomic displacement parameters are set at the 50% probability level. Selected bond lengths [Å] and angles [deg] are displayed in Table 1.

178.0°, Figure 3, top). In complex **2c**, a staggered conformation seems disfavored because of secondary interactions of the sterically more demanding *tert*-butyl substituent with the six-membered ring of the second indenyl ligand. Because of this, the torsion angle of **2c** is smaller than that detected for complex **2b** (torsion angle C2–Ct1–Ct2–C11 129.4°, Figure 3, top). Due to the 1-positioned substituent in **2d**, a torsion angle of 172.1° can be observed, which is similar to that in complex **2b**.

**Polymerization of Isoprene.** Previous studies from our group investigating the rare-earth metal bis(tetramethylaluminate) library revealed that half-sandwich complexes (L)Ln(AlMe<sub>4</sub>)<sub>2</sub> (L = Cp<sup>R</sup>, Flu<sup>R</sup>, pentadienyl)<sup>8,35,45</sup> display the most efficient precatalysts for the polymerization of isoprene, in terms of activity and stereospecificity of the polymer. In order to assess the performance of indenyl complexes **1a–d**, the respective binary catalyst systems were examined in IP polymerization (Table 3). For better comparability, the polymerization data of previously investigated related half-sandwich complexes are included in Table 3. Accordingly, the precatalysts **1a–d** were activated with 1 equiv of cocatalyst [Ph<sub>3</sub>C][B(C<sub>6</sub>F<sub>5</sub>)<sub>4</sub>] (**A**), [PhNHMe<sub>2</sub>][B(C<sub>6</sub>F<sub>5</sub>)<sub>4</sub>] (**B**), or B(C<sub>6</sub>F<sub>5</sub>)<sub>3</sub> (**C**). As previously shown, fluorenyl and pentadienyl half-sandwich complexes can undergo “ancillary” ligand abstraction when activated with cocatalyst **A** or **B**.<sup>35,45</sup> Therefore, it was crucial to examine whether indenyl half-sandwich complexes would behave like the fluorenyl congeners or display the desirable coordination stability of Cp\* complexes. The <sup>1</sup>H NMR spectra of **1** with cocatalyst **A** in C<sub>6</sub>D<sub>6</sub> at ambient temperature indicated that the activation proceeds via methyl group abstraction and formation of 1,1,1-triphenylethane and noncoordinated trimethylaluminum (Scheme 2, Figure S37). The protonolysis reaction of **1** with cocatalyst **B** led to the exclusive formation of methane and dimethyl aniline adduct AlMe<sub>3</sub>(NMe<sub>2</sub>Ph) (Scheme 2; no indene detectable, Figure S38).

Consequently, it can be assumed that the activation of the indenyl half-sandwich complexes proceeds as in the case of Cp\* half-sandwich complexes and not via indenyl abstraction like for the fluorenyl congeners<sup>35</sup> or indenyl abstractions in (Ind<sup>R</sup>)Sc(CH<sub>2</sub>SiMe<sub>3</sub>)<sub>2</sub>(thf) (Chart 1) and (Ind<sup>Me</sup>)<sub>2</sub>Sc[N(SiMe<sub>3</sub>)<sub>2</sub>], respectively.<sup>31,34</sup> Such distinct reactivities of Cp\*, fluorenyl, and indenyl complexes were already observed for the oxidation of Yb(II) metallocenes.<sup>46</sup> For the activation with cocatalyst **C**, <sup>1</sup>H NMR spectroscopy suggests a similar scenario as observed for Cp\* or pentadienyl half-sandwich complexes (Scheme 2, formation of BMe<sub>3</sub>, Figures S39 and S40).<sup>8,45</sup>

Precatalysts **1a** gave polyisoprenes of narrow molecular weight distributions  $M_w/M_n$ , in particular, when activated with cocatalyst **A** (Table 3, entry 2,  $M_w/M_n = 1.08$ ). A systematic investigation of the effect of the amount of isoprene (500–1500 equiv) using binary system **1a/A** revealed not only the presence of highly active, *trans*-1,4-selective catalysts but also the occurrence of living polymerization (entries 1–3). As shown in Figure 4, the molecular weight of the polymers increased linearly with the addition of isoprene, whereas  $M_w/M_n$  remained constant. It is noteworthy that living polymerization was also observed when the monomer was added in two portions (run 4), with the molecular weight matching that of run 2.

**Influence of the Indenyl Ligand.** The binary system (Ind<sup>Et</sup>)La(AlMe<sub>4</sub>)<sub>2</sub> (**1b**)/**A** produced polymers with the highest *trans/cis* selectivity (85.9%/10.4%), while the un-

Table 1. Selected Bond Lengths [Å] and Angles [deg] of 1a–1d

	1a	1b	1c	1d
La1...Ct <sup>a</sup>	2.535	2.533	2.539	2.531
La1–C1-4/9	2.762(3)–2.853(3)	2.781(5)–2.836(4)	2.772(2)–2.868(2)	2.763(1)–2.8484(9)
La1–C10	2.763(3)	2.967(5)	2.794(3)	2.753(1)
La1–C11	2.940(3)	2.757(5)	2.729(3)	2.734(1)
La1–C14	2.672(3)	2.694(5)	2.711(3)	2.719(1)
La1–C15	2.725(3)	2.714(5)	2.674(3)	2.712(1)
La1'...C12/La1...C12	2.896(3)	2.973(5)	3.234(3)	3.277(1)
La1...Al1	3.370(1)	3.382(2)	3.0329(8)	3.2600(3)
La1...Al2	3.212(1)	3.221(2)	3.2352(8)	3.2779(3)
C10–La1–C11	74.34(8)	73.7(1)	72.98(9)	77.85(3)
C14–La1–C15	79.29(9)	79.2(2)	78.97(8)	78.26(3)

<sup>a</sup>Ct = centroid of the five-membered ring involving C1, C2, C3, C4, C9.

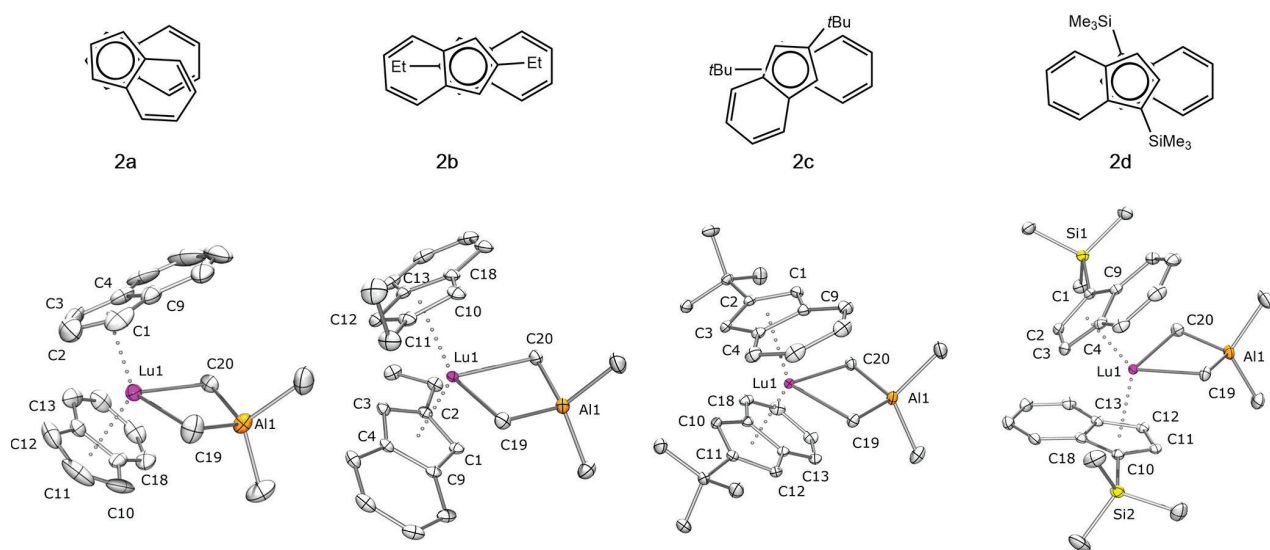


Figure 3. Top: Illustrations of the indenyl arrangements in sandwich complexes **2a**, **2b**, **2c**, and **2d**. The lutetium center and [AlMe<sub>4</sub>] unit are omitted for clarity. Bottom: Molecular structures of **2a**, **2b**, **2c**, and **2d** (left to right). Hydrogen atoms are omitted for clarity. Atomic displacement parameters are set at the 50% probability level. Selected bond lengths [Å] and angles [deg] are displayed in Table 2.

Table 2. Selected Bond Lengths [Å] and Angles [deg] of 2a–2d

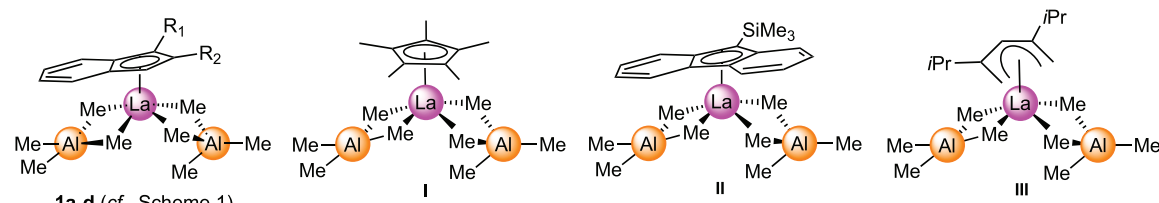
	1a	1b	1c	1d
Lu1...Ct1 <sup>a</sup>	2.305	2.292	2.335	2.315
Lu1...Ct2	2.293	2.304	2.334	2.300
Lu1–C1-4/9	2.544(7)–2.674(6)	2.526(1)–2.648(1)	2.583(2)–2.674(2)	2.548(2)–2.681(2)
Lu1–C10-13/18	2.542(7)–2.655(6)	2.549(1)–2.646(2)	2.583(2)–2.672(2)	2.562(2)–2.658(2)
Lu1–C19	2.510(7)	2.497(2)	2.511(2)	2.490(2)
Lu1–C20	2.484(6)	2.491(2)	2.505(2)	2.514(2)
Lu1...Al1	2.9770(5)	2.9796(1)	2.998(1)	2.9947(4)
C2–Ct1–Ct2–C11	33.9	178.0	129.4	172.1

<sup>a</sup>Ct1 = centroid of the five-membered ring involving C1, C2, C3, C4, C9; Ct2 = centroid of the five-membered ring involving C10, C11, C12, C13, C18.

substituted indenyl derivative, meaning the mixture (Ind)Ln-(AlMe<sub>4</sub>)<sub>2</sub> (**1a**)/A, gave the lowest one (76.6%/19.9%) (Table 3, entries 2, 5). However, further increasing the steric demand of the indenyl ligand in **1c** did not result in a more selective catalytic performance. This is shown by the *trans/cis* content of polymers produced by **1b** activated with cocatalyst B (84.5%/11.4%) compared to polymers obtained from the binary systems **1c**/B (80.4%/13.6%) (entries 9, 10) and **1a**/B (74.4%/21.4%) (entry 8). The minor influence of ancillary

ligand substitution was already observed for Cp<sup>R</sup>La(AlMe<sub>4</sub>)<sub>2</sub>.<sup>8</sup> Moreover, comparison of **1c** and **1d** reflects the effect of the substitution position C1 or C2 at the indenyl ligand on the catalytic performance. Unsurprisingly, and in accord with the similar steric bulk of Ind<sup>tBu</sup> and Ind<sup>Si</sup>, the *trans/cis* selectivities obtained with the binary systems **1c**/A (82.5%/12.1%) and **1d**/A (83.2%/12.0%) are similar (Table 3, entries 6, 7). The (NMR-confirmed) stability of the La–Ind<sup>R</sup> moiety toward cationization was corroborated by the polymerization results,

Table 3. Polymerization of Isoprene with Half-Sandwich Ln(III) Precatalysts



entry <sup>a</sup>	precatalyst	cocatalyst <sup>b</sup>	yield [%]	<i>cis</i> -1,4- <sup>c</sup>	<i>trans</i> -1,4- <sup>c</sup>	3,4- <sup>c</sup>	$M_n^d$ ( $\times 10^4$ )	$M_w/M_n^d$	$T_g$ [ $^{\circ}\text{C}$ ] <sup>e</sup>	ref
1 <sup>g</sup>	1a	A	95	14.9	82.6	2.6	3.2	1.04	-65	f
2	1a	A	98	19.9	76.6	3.5	6.1	1.08	-63	f
3 <sup>h</sup>	1a	A	>99	18.4	77.7	3.9	9.1	1.07	-63	f
4 <sup>i</sup>	1a	A	99	12.8	84.8	2.5	6.2	1.05	-64	f
5	1b	A	>99	10.4	85.9	3.7	6.6	1.11	-61	f
6	1c	A	96	12.1	82.5	5.4	6.0	1.08	-64	f
7	1d	A	>99	12.0	83.2	4.8	5.7	1.10	-64	f
8	1a	B	98	21.4	74.4	4.2	8.4	1.10	-62	f
9	1b	B	>99	11.4	84.5	4.1	5.9	1.11	-62	f
10	1c	B	94	13.6	80.4	6.0	6.7	1.06	-63	f
11	1d	B	97	13.9	81.0	5.1	6.1	1.12	-63	f
12	1a	C	57	57.6	37.1	5.3	25.3	1.30	-62	f
13	1b	C	58	56.7	39.6	3.7	26.3	1.32	-62	f
14	1c	C	82	51.3	46.0	2.7	25.4	1.29	-63	f
15	1d	C	34.5	77.0	13.0	10.0	26.1	1.34	-58	f
16 <sup>j</sup>	I	A	>99	1.2	89.4	9.4	7.0	1.28		10
17 <sup>j</sup>	I	B	>99	2.9	87.5	9.6	7.0	1.23		10
18 <sup>k</sup>	I	C	>99		99.5	0.5	24.0	1.18		10
19	II	A	>99	16.3	74.3	9.4	4.8	1.27	-65.7	35
20	II	B	98	9.6	80.0	10.4	4.9	1.17	-63.7	35
21	II	C	84	26.7	56.7	16.6	14.2	1.42	-60.4	35
22 <sup>l</sup>	III	A	>99	44.1	52.0	3.9	4.7	1.12	-61.9	45
23 <sup>l</sup>	III	B	>99	43.6	51.7	4.7	4.4	1.10	-61.8	45
24 <sup>l</sup>	III	C	>99	55.4	41.7	2.9	6.7	1.15	-61.4	45

<sup>a</sup>General polymerization procedure: 0.02 mmol of precatalyst, 8 mL of toluene, 20 mmol of isoprene, 1 h, 40  $^{\circ}\text{C}$ . <sup>b</sup>A =  $[\text{Ph}_3\text{C}][\text{B}(\text{C}_6\text{F}_5)_4]$ ; B =  $[\text{PhNMe}_2\text{H}][\text{B}(\text{C}_6\text{F}_5)_4]$ ; C =  $\text{B}(\text{C}_6\text{F}_5)_3$ ; catalyst preformation: 30 min. <sup>c</sup>Determined by  $^1\text{H}$  and  $^{13}\text{C}$   $\{^1\text{H}\}$  NMR spectroscopy in  $\text{CDCl}_3$ .

<sup>d</sup>Determined by GPC against polystyrene standards. <sup>e</sup>Determined by DSC at 20 K/min. <sup>f</sup>This work. <sup>g</sup>10 mmol of isoprene, polymerization for 1 h. <sup>h</sup>30 mmol of isoprene, polymerization for 3 h. <sup>i</sup> $2 \times 10$  mmol of isoprene, addition of the second portion after 1 h, polymerization for 2 h in total.

<sup>j</sup>General polymerization procedure: 0.02 mmol of precatalyst, 8 mL of toluene, 20 mmol of isoprene, 1 h, 40  $^{\circ}\text{C}$ , preformation 20 min. <sup>k</sup>General polymerization procedure: 0.02 mmol of precatalyst, 8 mL of toluene, 20 mmol of isoprene, 18 h, 40  $^{\circ}\text{C}$ , preformation 20 min. <sup>l</sup>General polymerization procedure: 0.02 mmol of precatalyst, 8 mL of toluene, 20 mmol of isoprene, 2 h, 40  $^{\circ}\text{C}$ , preformation 30 min.

Scheme 2. Active Species Obtained from Lanthanum Complexes 1 with Cocatalysts A, B, and C as Proposed by NMR Spectroscopy

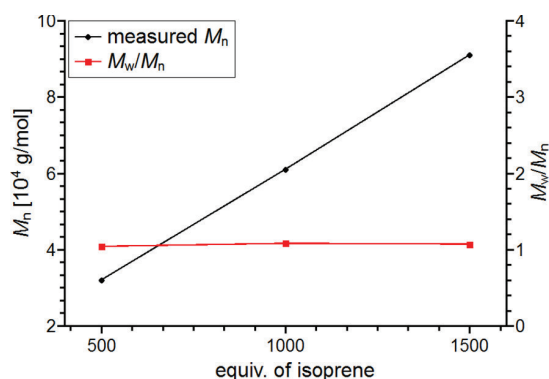
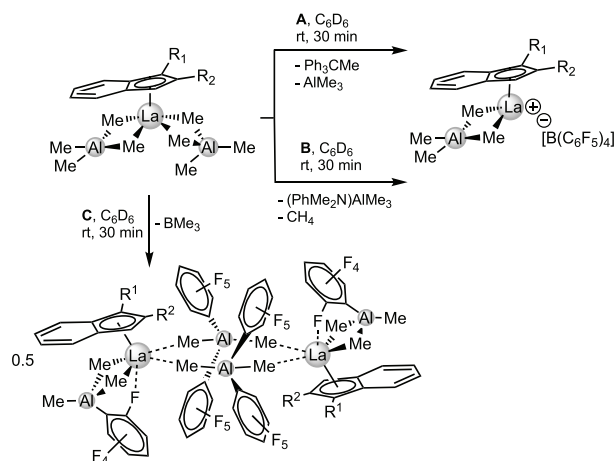


Figure 4. Isoprene polymerization with 1a/A. Molecular weight vs equiv of isoprene (●) and  $M_w/M_n$  vs equiv of isoprene (■).

documenting that, with respect to *trans*-1,4 selectivity, the binary systems 1/A and 1/B outperform the catalyst based on fluorenyl (II, entries 19 and 20) and pentadienyl (III, entries 22 and 23) ligands, coming closest to the striking performance

of the pentamethylcyclopentadienyl derivative (**I**, entries 16 and 17). Surely, unrivalled remains the performance of  $(C_5Me_5)La(AlMe_4)_2/C$  (*trans*-1,4 content: 99.5%,  $M_w/M_n = 1.18$ , entry 18).<sup>10,35,45</sup>

**Influence of the Cocatalyst.** In general, cationic species generated in situ by treatment of  $(Ind^R)La(AlMe_4)_2$  (**1**) with  $[Ph_3C][B(C_6F_5)_4]$  (**A**) or  $[PhNMe_2H][B(C_6F_5)_4]$  (**B**) showed high activation efficiencies and gave  $M_w/M_n$  narrower than 1.4, reaching minimum values for cocatalyst **A** (e.g., Table 3, entries 2 and 6). The observed catalyst activities are comparable to the ones reported for other lanthanum-based catalysts.<sup>8,35</sup> In accordance with literature data is also the finding that the overall polymer yields are higher in the presence of cocatalysts **A** and **B**, than for the activation with **C**, reflecting a different activation mechanism. Polymers produced by catalysts **1/A** have slightly lower *cis*-1,4 contents (12.0%, entry 7), compared to **1/B** (13.9%, entry 11). Correspondingly, the *trans*-1,4 contents are vice versa, with systems **1d/A** and **1d/B** giving *trans*-1,4 contents of 83.2% (entry 7) and 81.0% (entry 11), respectively. Cocatalysts **A** and **B** also significantly affect the molecular weights  $M_n$  of the polyisoprenes (e.g.,  $6.1 \times 10^4$ , entry 2 versus  $8.4 \times 10^4$ , entry 8). Striking is that the indenyl complexes **1** activated by neutral borane **C** give preferentially *cis*-1,4 polyisoprenes (maximum 77.0% for **1d**, entry 15). This behavior is similar to that of the open half-sandwich complex **III** (55.4% *cis*-1,4, entry 15) but in stark contrast to the benchmark system  $(C_5Me_5)La(AlMe_4)_2$  (<1% *cis*-1,4, entry 18). In general, activation of half-sandwich complexes with **C** is considerably less efficient, as revealed by larger molecular weights, ranging from  $26.3 \times 10^4$  (**1b**, entry 13) to  $14.2 \times 10^4$  g·mol<sup>-1</sup> (**II**, entry 21). This can be explained by the presence of a smaller number of catalytically active rare-earth metal centers. An exception here is open half-sandwich complex **III** (55.4% *cis*-1,4; entry 15), revealing close-to-ideal efficiency ( $M_n = 6.7 \times 10^4$  g·mol<sup>-1</sup>, entry 24).

## CONCLUSION

Salt-metathesis protocols applying  $Ln(AlMe_4)_3$  and  $Li(Ind^R)$  give efficient access to lanthanum half-sandwich complexes  $(Ind^R)La(AlMe_4)_2$  and lutetium sandwich complexes  $(Ind^R)_2Lu(AlMe_4)$ . The substitution pattern of the indenyl ligand, featured by the steric demand of the substituent ( $R = H, Et, tBu, SiMe_3$ ) and its ring position (1 versus 2), markedly impacts the solid-state structural chemistry of the half-sandwich derivatives. Distinct dimeric motifs prevail for indenyl, 2-ethylindenyl, and 1-trimethylsilylindenyl, while 2-*tert*-butylindenyl displays a monomeric structure, reminiscent of the cyclopentadienyl congeners. The indenyl substitution bears also on the metallocene structure as revealed by varying indenyl orientations in the solid state and the formation of invertible *racemic* and *meso* isomers for  $(Ind^{Si})_2Lu(AlMe_4)$ .

The polymerization experiments complement nicely the previous studies on the fluorenyl and cyclopentadienyl congeners to reveal efficient catalysts for isoprene polymerization. Upon activation with perfluorinated borates  $[Ph_3C][B(C_6F_5)_4]$  and  $[PhNMe_2H][B(C_6F_5)_4]$ , the cationized indenyl half-sandwich tetramethylaluminate complexes show excellent activities (yield > 99%). Like with cyclopentadienyl and unlike with fluorenyl and pentadienyl half-sandwich complexes, any “ancillary” ligand abstraction was not observed. Thus, the combination of indenyl with tetramethylaluminate ligands provides the desired coordination site stability of the

active species. Although the indenyl-based catalysts do not achieve the high *trans*-1,4 contents accessible with the pentamethylcyclopentadienyl congener (maximum 85.9% for  $(Ind^{Et})La(AlMe_4)_2$ ), the living manner of the isoprene polymerization is clearly evidenced. Interestingly, using borane  $B(C_6F_5)_3$  as an activator switches the regioselectivity to *cis*-1,4 (maximum 77.0% for  $(Ind^{Si})La(AlMe_4)_2$ ).

## EXPERIMENTAL SECTION

**General Procedures.** All manipulations were performed with rigorous exclusion of air and water, using standard Schlenk, high-vacuum, and glovebox techniques (MBraun UNILab-pro-dp; <0.5 ppm of O<sub>2</sub>, <0.5 ppm of H<sub>2</sub>O). Toluene and *n*-hexane were purified by using Grubbs-type columns (MBraun SPS, solvent purification system) and stored inside a glovebox.  $[D_6]thf$  and  $[D_6]benzene$  were purchased from Aldrich, degassed and dried over NaK for 24 h, filtered, and stored inside a glovebox. Ethylindene was obtained from abcr.  $[Ph_3C][B(C_6F_5)_4]$ ,  $[PhNMe_2H][B(C_6F_5)_4]$ , and  $B(C_6F_5)_3$  were obtained from Boulder Scientific Company and used without further purification. Indene, trioctylaluminum, and isoprene were purchased from Sigma-Aldrich. Isoprene was dried over trioctylaluminum and distilled prior to use. Homoleptic  $Ln(AlMe_4)_3$  ( $Ln = La, Lu$ ),<sup>47</sup>  $HInd^{Si}$ , and  $HInd^{tBu}$ ,<sup>48,49</sup> as well as  $Li(Ind)$ ,  $Li(Ind^{Et})$ ,  $Li(Ind^{Si})$ , and  $Li(Ind^{tBu})$ , were prepared according to literature procedures.<sup>50</sup> NMR spectra were recorded on a Bruker AVBII+400 (<sup>1</sup>H: 400.11 MHz; <sup>13</sup>C: 100.61 MHz) spectrometer. Variable-temperature NMR experiments were recorded on a Bruker AVII+500 spectrometer (<sup>1</sup>H: 500.13 MHz; <sup>13</sup>C: 125.76 MHz). <sup>1</sup>H and <sup>13</sup>C shifts are referenced to internal solvent resonances and reported in parts per million relative to tetramethylsilane (TMS). Coupling constants are given in Hz. Elemental analyses were performed on an Elementar Vario Micro Cube. IR spectra were recorded on a NICOLET 6700 FTIR spectrometer with a DRIFT cell (KBr window). Size exclusion chromatography (SEC) was performed on a Viscotek GPCmax apparatus and a model TDA 302 triple detector array. Sample solutions (1.0 mg polymer per mL thf) were filtered through a 0.45 μm syringe filter prior to injection. The flow rate was 1 mL/min.  $dn/dc$  and  $dA/dc$  data were determined by means of the integrated OmniSec software. The microstructure of the polyisoprenes was determined on Bruker AVBII+400 and Bruker DRX250 spectrometers in  $[D]chloroform$  at ambient temperature. The glass transition temperature ( $T_g$ ) of the polyisoprenes was determined on an PerkinElmer DSC 8000 with heating rates of 20 K/min and cooling rates of 60 K/min.

**Synthesis of  $(Ind)La(AlMe_4)_2$  (**1a**).**  $La(AlMe_4)_3$  (50 mg, 0.13 mmol) was dissolved in toluene (5 mL), and  $Li(Ind)$  (15 mg, 0.13 mmol) was slowly added under vigorous stirring. After stirring the reaction mixture for 5 h at 40 °C, the solid residue ( $LiAlMe_4$ ) was filtered off and the solvent was removed in vacuo to give **1a** as a colorless solid. Crystalline **1a** was obtained from a saturated *n*-hexane/toluene solution at -35 °C (51 mg, 0.12 mmol, 95%). <sup>1</sup>H NMR (400 MHz,  $[D_6]benzene$ , 26 °C):  $\delta = 7.25$ – $7.30$  (m, 2 H, 5/8IndH), 6.85– $6.90$  (m, 2 H, 6/7IndH), 6.44 (t, <sup>3</sup>J<sub>HH</sub> = 3.4 Hz, 1 H, 2IndH), 6.19– $6.21$  (m, 2 H, 1/3IndH), -0.41 (s, 24 H,  $AlMe_4$ ) ppm. <sup>13</sup>C{<sup>1</sup>H} NMR (101 MHz,  $[D_6]benzene$ , 26 °C):  $\delta = 131.4$  (4/9Ind), 125.2 (2Ind), 124.3 (6/7Ind), 123.4 (5/8Ind), 105.2 (1/3Ind), 2.80 (br. s,  $AlMe_4$ ) ppm. IR (DRIFT):  $\tilde{\nu} = 3075$  (vw), 3049 (vw), 3033 (vw), 2922 (w), 2883 (w), 2791 (vw), 1940 (vw), 1916 (vw), 1792 (vw), 1695 (vw), 1559 (vw), 1477 (vw), 1446 (vw), 1418 (vw), 1401 (vw), 1384 (vw), 1332 (w), 1256 (vw), 1208 (m), 1182 (m), 1119 (vw), 1039 (w), 1000 (m), 946 (vw), 865 (vw), 790 (vs), 750 (s), 705 (vs), 699 (vs), 692 (vs), 621 (m), 600 (m), 583 (s), 568 (vs), 508 (w), 485 (w), 444 (s) cm<sup>-1</sup>. Elemental analysis of crystalline **1a**, calcd for C<sub>17</sub>H<sub>31</sub>Al<sub>2</sub>La (428.30 g·mol<sup>-1</sup>): C 47.67, H 7.30; found: C 47.55, H 7.29.

**Synthesis of  $(Ind^{Et})La(AlMe_4)_2$  (**1b**).**  $La(AlMe_4)_3$  (50 mg, 0.13 mmol) was dissolved in toluene (5 mL), and  $Li(Ind^{Et})$  (19 mg, 0.13 mmol) was slowly added under vigorous stirring. After stirring the reaction mixture for 5 h at 40 °C, the solid residue ( $LiAlMe_4$ ) was

filtered off and the solvent was removed in vacuo to give **1b** as a colorless solid. Crystalline **1b** was obtained from a saturated *n*-hexane/toluene solution at  $-35\text{ }^{\circ}\text{C}$  (51 mg, 0.11 mmol, 86%).  $^1\text{H}$  NMR (400 MHz,  $[\text{D}_6]$ benzene,  $26\text{ }^{\circ}\text{C}$ ):  $\delta = 7.23\text{--}7.28$  (m, 2 H, 5/8IndH), 6.82–6.91 (m, 2 H, 6/7IndH), 6.05 (s, 2 H, 1/3IndH), 2.46 (q,  $^3J_{\text{HH}} = 7.50$  Hz, 2 H, IndCH<sub>2</sub>Me), 1.03 (t,  $^3J_{\text{HH}} = 7.54$  Hz, 3 H, IndCH<sub>2</sub>Me),  $-0.37$  (s, 24 H, AlMe<sub>4</sub>) ppm.  $^{13}\text{C}\{^1\text{H}\}$  NMR (101 MHz,  $[\text{D}_6]$ benzene,  $26\text{ }^{\circ}\text{C}$ ):  $\delta = 145.5$  (2Ind), 132.1 (4/9Ind), 123.8 (6/7Ind), 123.0 (5/8Ind), 104.2 (1/3Ind), 24.7 (IndCH<sub>2</sub>Me), 16.6 (IndCH<sub>2</sub>Me), 2.9 (br. s, AlMe<sub>4</sub>) ppm. IR (DRIFT):  $\tilde{\nu} = 3074$  (vw), 3060 (vw), 2964 (w), 2930 (m), 2887 (m), 2822 (w), 2773 (w), 1937 (vw), 1909 (vw), 1883 (vw), 1815 (vw), 1788 (vw), 1694 (vw), 1595 (vw), 1558 (vw), 1530 (vw), 1473 (w), 1455 (w), 1438 (w), 1418 (w), 1389 (vw), 1375 (vw), 1348 (w), 1331 (w), 1315 (vw), 1297 (w), 1280 (w), 1211 (s), 1202 (s), 1189 (s), 1169 (w), 1153 (vw), 1125 (w), 1060 (vw), 1047 (vw), 1010 (m), 943 (vw), 930 (vw), 885 (vw), 814 (vs), 783 (m), 748 (vs), 710 (vs), 698 (vs), 687 (vs), 677 (vs), 658 (m), 645 (m), 619 (s), 613 (s), 598 (s), 592 (s), 586 (vs), 574 (vs), 565 (vs), 548 (vs), 537 (s), 526 (m), 509 (m), 493 (m), 482 (s), 471 (w), 458 (m), 444 (w), 425 (vw), 418 (vw), 407 (w)  $\text{cm}^{-1}$ . Elemental analysis of crystalline **1b**, calcd for C<sub>19</sub>H<sub>35</sub>Al<sub>2</sub>La (456.36 g·mol<sup>-1</sup>): C 50.01, H 7.73; found: C 49.89, H 7.93.

**Synthesis of (Ind<sup>bu</sup>)La(AlMe<sub>4</sub>)<sub>2</sub> (1c).** La(AlMe<sub>4</sub>)<sub>3</sub> (50 mg, 0.13 mmol) was dissolved in toluene (5 mL), and Li(Ind<sup>bu</sup>) (22 mg, 0.13 mmol) was slowly added under vigorous stirring. After stirring the reaction mixture for 5 h at  $40\text{ }^{\circ}\text{C}$ , the solid residue (LiAlMe<sub>4</sub>) was filtered off and the solvent was removed in vacuo to give **1c** as a colorless solid. Crystalline **1c** was obtained from a saturated *n*-hexane/toluene solution at  $-35\text{ }^{\circ}\text{C}$  (58 mg, 0.12 mmol, 94%).  $^1\text{H}$  NMR (400 MHz,  $[\text{D}_6]$ benzene,  $26\text{ }^{\circ}\text{C}$ ):  $\delta = 7.26\text{--}7.31$  (m, 2 H, 5/8IndH), 6.81–6.86 (m, 2 H, 6/7IndH), 6.16 (s, 2 H, 1/3IndH), 1.17 (s, 9 H, IndCMe<sub>3</sub>),  $-0.33$  (s, 24 H, AlMe<sub>4</sub>) ppm.  $^{13}\text{C}\{^1\text{H}\}$  NMR (101 MHz,  $[\text{D}_6]$ benzene,  $26\text{ }^{\circ}\text{C}$ ):  $\delta = 154.8$  (2Ind), 132.0 (4/9Ind), 123.5 (5/8Ind), 123.3 (6/7Ind), 102.3 (1/3Ind), 33.7 (CMe<sub>3</sub>), 32.2 (CMe<sub>3</sub>), 3.4 (AlMe<sub>4</sub>) ppm. IR (DRIFT):  $\tilde{\nu} = 3058$  (vw), 2964 (m), 2953 (m), 2927 (m), 2883 (m), 2780 (w), 1937 (vw), 1909 (vw), 1884 (vw), 1813 (vw), 1786 (vw), 1693 (vw), 1595 (vw), 1573 (vw), 1558 (vw), 1539 (vw), 1505 (vw), 1478 (w), 1463 (w), 1455 (w), 1440 (w), 1429 (w), 1393 (vw), 1367 (w), 1360 (w), 1347 (w), 1286 (m), 1223 (m), 1203 (s), 1181 (s), 1087 (vw), 1022 (vw), 999 (vw), 940 (vw), 918 (vw), 846 (vw), 825 (w), 803 (s), 772 (w), 766 (w), 750 (s), 706 (vs), 697 (vs), 688 (vs), 681 (vs), 639 (w), 593 (m), 585 (s), 577 (s), 567 (s), 561 (s), 546 (s), 526 (m), 517 (m), 511 (m), 498 (w), 483 (m), 456 (vw), 449 (w), 438 (w), 418 (m), 403 (vw)  $\text{cm}^{-1}$ . Elemental analysis of crystalline **1c**, calcd for C<sub>21</sub>H<sub>39</sub>Al<sub>2</sub>La (484.41 g·mol<sup>-1</sup>): C 52.07, H 8.12; found: C 52.30, H 8.25.

**Synthesis of (Ind<sup>si</sup>)La(AlMe<sub>4</sub>)<sub>2</sub> (1d).** La(AlMe<sub>4</sub>)<sub>3</sub> (50 mg, 0.13 mmol) was dissolved in toluene (5 mL), and Li(Ind<sup>si</sup>) (24 mg, 0.13 mmol) was slowly added under vigorous stirring. After stirring the reaction mixture for 5 h at  $40\text{ }^{\circ}\text{C}$ , the solid residue (LiAlMe<sub>4</sub>) was filtered off and the solvent was removed in vacuo to give **1d** as a colorless solid. Crystalline **1d** was obtained from a saturated *n*-hexane/toluene solution at  $-35\text{ }^{\circ}\text{C}$  (57 mg, 0.11 mmol, 87%).  $^1\text{H}$  NMR (400 MHz,  $[\text{D}_6]$ benzene,  $26\text{ }^{\circ}\text{C}$ ):  $\delta = 7.60\text{--}7.65$  (m, 1 H, 5IndH), 7.26–7.31 (m, 1 H, 8IndH), 6.91–6.97 (m, 2 H, 6/7IndH), 6.87 (d,  $^3J_{\text{HH}} = 3.42$  Hz, 1H, 2IndH), 6.62 (dd,  $^3J_{\text{HH}} = 3.42$  Hz,  $^4J_{\text{HH}} = 0.89$  Hz, 1H, 3IndH), 0.27 (s, 9H, IndSiMe<sub>3</sub>),  $-0.38$  (s, 24H, AlMe<sub>4</sub>) ppm.  $^{13}\text{C}\{^1\text{H}\}$  NMR (101 MHz,  $[\text{D}_6]$ benzene,  $26\text{ }^{\circ}\text{C}$ ):  $\delta = 137.7$  (9Ind), 135.1 (4Ind), 133.0 (2Ind), 124.9 (5Ind), 124.7 (6Ind), 124.6 (7Ind), 123.9 (8Ind), 114.0 (1Ind), 110.7 (3Ind), 3.1 (AlMe<sub>4</sub>), 1.2 (IndSiMe<sub>3</sub>) ppm. IR (DRIFT):  $\tilde{\nu} = 3078$  (vw), 2950 (w), 2887 (m), 2787 (vw), 1936 (vw), 1907 (vw), 1812 (vw), 1787 (vw), 1684 (vw), 1583 (vw), 1525 (vw), 1469 (vw), 1442 (w), 1416 (w), 1366 (vw), 1329 (w), 1291 (vw), 1251 (m), 1209 (m), 1186 (m), 1156 (w), 1145 (w), 1077 (w), 1055 (vw), 1005 (vw), 963 (w), 940 (vw), 896 (vw), 835 (vs), 792 (m), 750 (vs), 734 (s), 709 (vs), 698 (vs), 646 (w), 608 (m), 580 (s), 552 (w), 497 (w), 449 (m), 436 (w), 401 (w)  $\text{cm}^{-1}$ . Elemental analysis of crystalline **1d**, calcd for C<sub>20</sub>H<sub>39</sub>Al<sub>2</sub>SiLa (500.49 g·mol<sup>-1</sup>): C 48.00, H 7.85; found: C 48.20, H 8.02.

**Synthesis of (Ind)<sub>2</sub>Lu(AlMe<sub>4</sub>) (2a).** Lu(AlMe<sub>4</sub>)<sub>3</sub> (50 mg, 0.12 mmol) was dissolved in toluene (5 mL), and Li(Ind) (28 mg, 0.23 mmol) was slowly added under vigorous stirring. After stirring the reaction mixture for 8 h at  $40\text{ }^{\circ}\text{C}$ , the solid residue (LiAlMe<sub>4</sub>) was filtered off and the solvent was removed in vacuo to give **2a** as a colorless solid. Crystalline **2a** was obtained from a saturated *n*-hexane/toluene solution at  $-35\text{ }^{\circ}\text{C}$  (38 mg, 0.08 mmol, 64%).  $^1\text{H}$  NMR (400 MHz,  $[\text{D}_6]$ benzene,  $26\text{ }^{\circ}\text{C}$ ):  $\delta = 7.24\text{--}7.32$  (m, 4 H, 5/8IndH), 6.85–6.91 (m, 4 H, 6/7IndH), 5.83–5.87 (m, 2 H, 2IndH), 5.77–5.81 (m, 4 H, 1/3IndH),  $-0.45$  (s, 6 H, LuMe<sub>2</sub>AlMe<sub>2</sub>),  $-0.64$  (s, 6 H, LuMe<sub>2</sub>AlMe<sub>2</sub>) ppm.  $^{13}\text{C}\{^1\text{H}\}$  NMR (101 MHz,  $[\text{D}_6]$ benzene,  $26\text{ }^{\circ}\text{C}$ ):  $\delta = 126.7$  (4/8Ind), 124.1 (5/8Ind), 123.3 (6/7Ind), 119.9 (2Ind), 99.6 (1/3Ind), 15.2 (LuMe<sub>2</sub>AlMe<sub>2</sub>),  $-6.7$  (br. s, LuMe<sub>2</sub>AlMe<sub>2</sub>) ppm. IR (DRIFT):  $\tilde{\nu} = 3065$  (w), 3050 (w), 3032 (w), 3008 (vw), 2929 (m), 2883 (w), 2814 (w), 1932 (vw), 1906 (vw), 1783 (vw), 1684 (vw), 1604 (vw), 1588 (vw), 1524 (vw), 1478 (vw), 1447 (w), 1400 (vw), 1332 (vs), 1238 (m), 1214 (s), 1188 (s), 1120 (vw), 1041 (m), 997 (vw), 940 (vw), 893 (vw), 867 (w), 844 (vw), 787 (vs), 747 (vs), 706 (vs), 698 (vs), 621 (m), 593 (m), 575 (m), 549 (w), 484 (m), 447 (vs)  $\text{cm}^{-1}$ . Elemental analysis of crystalline **2a**, calcd for C<sub>22</sub>H<sub>26</sub>AlLu (492.40 g·mol<sup>-1</sup>): C 53.66, H 5.32; found: C 53.36, H 5.41.

**Synthesis of (Ind<sup>Et</sup>)<sub>2</sub>Lu(AlMe<sub>4</sub>) (2b).** Lu(AlMe<sub>4</sub>)<sub>3</sub> (50 mg, 0.12 mmol) was dissolved in toluene (5 mL), and Li(Ind<sup>Et</sup>) (35 mg, 0.23 mmol) was slowly added under vigorous stirring. After stirring the reaction mixture for 8 h at  $40\text{ }^{\circ}\text{C}$ , the solid residue (LiAlMe<sub>4</sub>) was filtered off and the solvent was removed in vacuo to give **2b** as a colorless solid. Crystalline **2b** was obtained from a saturated *n*-hexane/toluene solution at  $-35\text{ }^{\circ}\text{C}$  (34 mg, 0.06 mmol, 52%).  $^1\text{H}$  NMR (400 MHz,  $[\text{D}_6]$ benzene,  $26\text{ }^{\circ}\text{C}$ ):  $\delta = 7.28\text{--}7.33$  (m, 4 H, 5/8IndH), 6.80–6.86 (m, 4 H, 6/7IndH), 5.89 (s, 4 H, 1/3IndH), 2.13 (q,  $^3J_{\text{HH}} = 7.48$  Hz, 4 H, IndCH<sub>2</sub>Me) 0.96 (t,  $^3J_{\text{HH}} = 7.48$  Hz, 6 H, IndCH<sub>2</sub>Me),  $-0.34$  (s, 6 H, LuMe<sub>2</sub>AlMe<sub>2</sub>),  $-0.64$  (s, 6 H, LuMe<sub>2</sub>AlMe<sub>2</sub>) ppm.  $^{13}\text{C}\{^1\text{H}\}$  NMR (101 MHz,  $[\text{D}_6]$ benzene,  $26\text{ }^{\circ}\text{C}$ ):  $\delta = 138.4$  (2Ind), 126.6 (4/9Ind), 123.6 (5/8Ind), 122.2 (6/7Ind), 99.1 (1/3Ind), 24.1 (IndCH<sub>2</sub>Me), 16.9 (AlMe<sub>4</sub>), 16.6 (IndCH<sub>2</sub>Me) ppm. IR (DRIFT):  $\tilde{\nu} = 3102$  (vw), 2928 (m), 2917 (m), 2904 (m), 2887 (m), 2829 (m), 2821 (m), 2793 (w), 1809 (vw), 1765 (vw), 1688 (vw), 1528 (vw), 1435 (w), 1374 (vw), 1352 (vw), 1332 (vw), 1313 (vw), 1281 (w), 1227 (s), 1194 (s), 1121 (vw), 1053 (vw), 999 (vw), 943 (vw), 930 (vw), 888 (vw), 846 (vw), 807 (w), 762 (m), 746 (m), 725 (vs), 720 (vs), 707 (vs), 700 (vs), 693 (vs), 686 (vs), 671 (s), 661 (s), 646 (m), 630 (m), 615 (m), 607 (m), 601 (m), 590 (m), 571 (vs), 564 (s), 554 (s), 550 (vs), 542 (vs), 535 (vs), 524 (s), 514 (s), 502 (s), 486 (m), 472 (s), 467 (m), 455 (vs), 451 (vs), 446 (vs), 436 (w), 426 (vs), 409 (m), 403 (w)  $\text{cm}^{-1}$ . Elemental analysis of crystalline **2b**, calcd for C<sub>26</sub>H<sub>34</sub>AlLu (548.51 g·mol<sup>-1</sup>): C 56.93, H 6.25; found: C 56.75, H 6.24.

**Synthesis of (Ind<sup>bu</sup>)<sub>2</sub>Lu(AlMe<sub>4</sub>) (2c).** Lu(AlMe<sub>4</sub>)<sub>3</sub> (50 mg, 0.12 mmol) was dissolved in toluene (5 mL), and Li(Ind<sup>bu</sup>) (41 mg, 0.23 mmol) was slowly added under vigorous stirring. After stirring the reaction mixture for 8 h at  $40\text{ }^{\circ}\text{C}$ , the solid residue (LiAlMe<sub>4</sub>) was filtered off and the solvent was removed in vacuo to give **2c** as a colorless solid. Crystalline **2c** was obtained from a saturated *n*-hexane/toluene solution at  $-35\text{ }^{\circ}\text{C}$  (41 mg, 0.07 mmol, 60%).  $^1\text{H}$  NMR (400 MHz,  $[\text{D}_6]$ benzene,  $26\text{ }^{\circ}\text{C}$ ):  $\delta = 7.29\text{--}7.34$  (m, 4 H, 5/8IndH), 6.78–6.83 (m, 4 H, 6/7IndH), 6.06 (s, 4 H, 1/3IndH), 1.12 (s, 18 H, Me<sub>3</sub>C-Ind),  $-0.33$  (s, 6 H, LuMe<sub>2</sub>AlMe<sub>2</sub>),  $-0.56$  (s, 6 H, LuMe<sub>2</sub>AlMe<sub>2</sub>) ppm.  $^{13}\text{C}\{^1\text{H}\}$  NMR (101 MHz,  $[\text{D}_6]$ benzene,  $26\text{ }^{\circ}\text{C}$ ):  $\delta = 149.3$  (2Ind), 126.5 (4/9Ind), 124.2 (5/8Ind), 122.2 (6/7Ind), 97.3 (1/3Ind), 33.8 (CMe<sub>3</sub>), 32.2 (CMe<sub>3</sub>), 16.1 (LuMe<sub>2</sub>AlMe<sub>2</sub>)  $-5.30$  (s, LuMe<sub>2</sub>AlMe<sub>2</sub>) ppm. IR (DRIFT):  $\tilde{\nu} = 3081$  (w), 3054 (w), 3034 (w), 2964 (vs), 2935 (m), 2886 (m), 2818 (w), 1949 (vw), 1928 (vw), 1903 (vw), 1881 (vw), 1866 (vw), 1808 (vw), 1783 (vw), 1686 (vw), 1602 (vw), 1582 (vw), 1531 (vw), 1493 (w), 1478 (m), 1460 (m), 1444 (m), 1392 (w), 1367 (m), 1351 (s), 1330 (vw), 1289 (m), 1236 (m), 1223 (m), 1207 (m), 1193 (m), 1151 (vw), 1089 (w), 1023 (vw), 999 (w), 968 (vw), 943 (w), 918 (vw), 888 (vw), 843 (vw), 827 (w), 810 (s), 803 (vs), 777 (w), 761 (m), 747 (vs), 733 (vs), 698 (vs), 675 (vs), 614 (m), 602 (m), 582 (m),



571 (m), 518 (vw), 481 (s), 466 (w), 449 (vw), 425 (m)  $\text{cm}^{-1}$ . Elemental analysis of crystalline **2c**, calcd for  $\text{C}_{30}\text{H}_{42}\text{AlLu}\cdot 0.5\text{C}_7\text{H}_8$  (650.69  $\text{g}\cdot\text{mol}^{-1}$ ): C 63.78, H 7.23; found: C 62.99, H 7.21. Although these results are outside the range viewed as establishing analytical purity (C: -0.79%), they are provided to illustrate the best values obtained to date.

**Synthesis of  $(\text{Ind}^{\text{Si}})_2\text{Lu}(\text{AlMe}_4)$  (**2d**).**  $\text{Lu}(\text{AlMe}_4)_3$  (50 mg, 0.12 mmol) was dissolved in toluene (5 mL), and  $\text{Li}(\text{Ind}^{\text{Si}})$  (45 mg, 0.23 mmol) was slowly added under vigorous stirring. After stirring the reaction mixture for 8 h at 40 °C, the solid residue ( $\text{LiAlMe}_4$ ) was filtered off and the solvent was removed in vacuo to give **2d** as a colorless solid. Crystalline **2d** was obtained from a saturated *n*-hexane/toluene solution at -35 °C (51 mg, 0.08 mmol, 67%).  $^1\text{H}$  NMR (400 MHz,  $[\text{D}_6]$  benzene, 26 °C): Major isomer (90%)  $\delta = 7.75\text{--}7.79$  (m, 2 H, 8IndH), 7.25–7.29 (m, 2 H, 5IndH), 7.04–7.09 (m, 2 H, 6IndH), 6.95–7.00 (m, 2 H, 7IndH), 6.28 (dd,  $^3J_{\text{HH}} = 3.30$  Hz,  $^4J_{\text{HH}} = 0.89$  Hz, 2 H, 3IndH), 5.80 (d,  $^3J_{\text{HH}} = 3.29$  Hz, 2 H, 2IndH), 0.23 (s, 18 H,  $\text{SiMe}_3$ ), 0.06 (s, 3 H,  $\text{AlMe}$ ), -0.49 (s, 6 H,  $\text{AlMe}_2$ ), -1.02 (s, 3 H,  $\text{AlMe}$ ) ppm. Minor isomer (10%):  $\delta = 6.89\text{--}6.94$  (m, 2 H, IndH), 6.59 (d,  $^3J_{\text{HH}} = 3.30$  Hz, 2 H, Ind H), 5.67 (dd,  $^3J_{\text{HH}} = 3.29$  Hz,  $^4J_{\text{HH}} = 0.76$  Hz, 2 H, IndH), 0.31 (s, 18 H,  $\text{SiMe}_3$ ), -0.48 (br. s, 6 H,  $\text{AlMe}_2$ ), -0.49 (s, 6 H,  $\text{AlMe}_2$ ) ppm. Further minor isomer signals overlapping with peaks of major isomer.  $^{13}\text{C}\{^1\text{H}\}$  NMR (101 MHz,  $[\text{D}_6]$  benzene, 26 °C): Major isomer (90%)  $\delta = 134.2$  (4Ind), 129.8 (9Ind), 129.6 (2Ind), 126.3 (8Ind), 124.3 (5Ind), 124.0 (6Ind), 124.0 (7Ind), 107.9 (1Ind), 105.7 (3Ind) 16.1 ( $\text{AlMe}$ ), 13.2 ( $\text{AlMe}$ ), 1.4 ( $\text{SiMe}_3$ ), -7.35 (br. s,  $\text{AlMe}_2$ ) ppm. Minor isomer signals were not assigned.  $^{29}\text{Si}\text{--}^1\text{H}$  DEPT 45 (50 MHz,  $[\text{D}_6]$  benzene, 26 °C)  $\delta = -8.27$  (minor, *rac*-**2d**), -8.40 (major, *meso*-**2d**) ppm. IR (DRIFT):  $\tilde{\nu} = 3081$  (vw), 3053 (vw), 3023 (vw), 2999 (vw), 2957 (w), 2926 (w), 2885 (w), 2817 (vw), 1940 (vw), 1809 (vw), 1789 (vw), 1765 (vw), 1688 (vw), 1590 (vw), 1523 (vw), 1495 (vw), 1470 (w), 1444 (w), 1407 (w), 1366 (vw), 1330 (w), 1293 (w), 1249 (vs), 1191 (w), 1157 (m), 1144 (m), 1123 (vw), 1054 (vw), 1005 (vw), 963 (m), 943 (vw), 896 (vw), 881 (w), 843 (vs), 835 (vs), 796 (m), 780 (s), 760 (vs), 743 (s), 713 (s), 707 (s), 699 (vs), 645 (m), 621 (m), 590 (w), 571 (w), 553 (vw), 484 (m), 450 (m), 436 (m), 405 (vs)  $\text{cm}^{-1}$ . Elemental analysis of crystalline **2b**, calcd for  $\text{C}_{28}\text{H}_{42}\text{Si}_2\text{AlLu}$  (636.76  $\text{g}\cdot\text{mol}^{-1}$ ): C 52.82, H 6.65; found: C 53.03, H 6.81.

**Polymerization of Isoprene.** Exemplarily, the polymerization procedure is described for entry 2 of Table 3.  $[\text{Ph}_3\text{C}][\text{B}(\text{C}_6\text{F}_5)_4]$  (cocatalyst A) (18.22 mg, 0.02 mmol) was added to a solution of **1a** (8.57 mg, 0.02 mmol) in toluene (8 mL). The mixture was aged at ambient temperature for 30 min. Then isoprene (1.36 g, 20 mmol) was added and the polymerization was carried out at 40 °C for 1 h. The reaction was terminated by pouring the polymerization mixture into 25 mL of methanol containing 0.1% (w/w) 2,6-di-*tert*-butyl-4-methylphenol as a stabilizer. The polymer was washed with methanol and dried under vacuum at ambient temperature to constant weight.

**Crystallography.** Crystals from all (half-)sandwich complexes suitable for X-ray crystallography were grown by standard techniques from saturated *n*-hexane or *n*-hexane/toluene solutions at -40 °C. Single crystals were selected inside a glovebox, coated with Parabar 10312 (previously known as Paratone N, Hampton Research) or perflourinated ether and fixed on a microloop. Data were collected on a Bruker APEX DUO instrument equipped with an  $I\mu\text{S}$  microfocus sealed tube and QUAZAR optics for Mo  $K\alpha$  radiation ( $\lambda = 0.71073$  Å) except **1b**. There, data were collected on a Bruker SMART APEX II instrument equipped with a fine focus sealed tube and TRIUMPH monochromator using Mo  $K\alpha$  radiation ( $\lambda = 0.71073$  Å). The data collection strategy was determined using COSMO<sup>51</sup> employing  $\omega$  and  $\phi$  scans. Raw data were processed using APEX<sup>52</sup> and SAINT<sup>53</sup> corrections for absorption effects were applied using SADABS.<sup>54</sup> All data were processed using the APEX3<sup>52</sup> software package. The structures were solved by direct methods and refined against all data by full-matrix least-squares methods on  $F^2$  using SHELXTL<sup>54</sup> and Shelxle.<sup>55</sup> All graphics were produced employing ORTEP-3<sup>56</sup> and POV-Ray.<sup>57</sup>

## ■ ASSOCIATED CONTENT

### 📄 Supporting Information

The Supporting Information is available free of charge on the ACS Publications website at DOI: 10.1021/acs.organo-  
met.9b00344.

$^1\text{H}/^{13}\text{C}/^{11}\text{B}$  NMR spectra, DSC and GPC curves, and X-ray crystallographic data for **1a–d** and **2a–d** (PDF)

### Accession Codes

CCDC 1915976–1915983 contain the supplementary crystallographic data for this paper. These data can be obtained free of charge via [www.ccdc.cam.ac.uk/data\\_request/cif](http://www.ccdc.cam.ac.uk/data_request/cif), or by emailing [data\\_request@ccdc.cam.ac.uk](mailto:data_request@ccdc.cam.ac.uk), or by contacting The Cambridge Crystallographic Data Centre, 12 Union Road, Cambridge CB2 1EZ, UK; fax: +44 1223 336033.

## ■ AUTHOR INFORMATION

### Corresponding Author

\*E-mail: [reiner.anwander@uni-tuebingen.de](mailto:reiner.anwander@uni-tuebingen.de).

### ORCID

Reiner Anwander: 0000-0002-1543-3787

### Notes

The authors declare no competing financial interest.

## ■ ACKNOWLEDGMENTS

The authors are grateful to the German Science Foundation (Grant: An238/14-2) and BRIDGESTONE Japan for generous support.

## ■ REFERENCES

- Hofmann, F. Der Synthetische Kautschuk. Vom Standpunkt Der Technik. *Angew. Chem.* **1912**, *25*, 1462–1467.
- Yang, F.; Li, X. Novel Cationic Rare Earth Metal Alkyl Catalysts for Precise Olefin Polymerization. *J. Polym. Sci., Part A: Polym. Chem.* **2017**, *55*, 2271–2280.
- Nishiura, M.; Hou, Z. Novel Polymerization Catalysts and Hydride Clusters from Rare-Earth Metal Dialkyls. *Nat. Chem.* **2010**, *2*, 257–268.
- Nishiura, M.; Guo, F.; Hou, Z. Half-Sandwich Rare-Earth-Catalyzed Olefin Polymerization, Carbometalation, and Hydroarylation. *Acc. Chem. Res.* **2015**, *48*, 2209–2220.
- Du, G.; Wei, Y.; Ai, L.; Chen, Y.; Xu, Q.; Liu, X.; Zhang, S.; Hou, Z.; Li, X. Living 3,4-Polymerization of Isoprene by Cationic Rare Earth Metal Alkyl Complexes Bearing Iminoamido Ligands. *Organometallics* **2011**, *30*, 160–170.
- Liu, S.; Du, G.; He, J.; Long, Y.; Zhang, S.; Li, X. Cationic Tropicidyl Scandium Catalyst: A Perfectly Acceptable Substitute for Cationic Half-Sandwich Scandium Catalysts in Cis-1,4-Polymerization of Isoprene and Copolymerization with Norbornene. *Macromolecules* **2014**, *47*, 3567–3573.
- Liu, H.; He, J.; Liu, Z.; Lin, Z.; Du, G.; Zhang, S.; Li, X. Quasi-Living Trans-1,4-Polymerization of Isoprene by Cationic Rare Earth Metal Alkyl Species Bearing a Chiral (S,S)-Bis(Oxazolinyphenyl)-Amido Ligand. *Macromolecules* **2013**, *46*, 3257–3265.
- Zimmermann, M.; Törnroos, K. W.; Sitzmann, H.; Anwander, R. Half-Sandwich Bis(Tetramethylaluminate) Complexes of the Rare-Earth Metals: Synthesis, Structural Chemistry, and Performance in Isoprene Polymerization. *Chem. - Eur. J.* **2008**, *14*, 7266–7277.
- Li, X.; Nishiura, M.; Hu, L.; Mori, K.; Hou, Z. Alternating and Random Copolymerization of Isoprene and Ethylene Catalyzed by Cationic Half-Sandwich Scandium Alkyls. *J. Am. Chem. Soc.* **2009**, *131*, 13870–13882.
- Zimmermann, M.; Törnroos, K. W.; Anwander, R. Cationic Rare-Earth-Metal Half-Sandwich Complexes for the Living Trans-1,4-Isoprene Polymerization. *Angew. Chem., Int. Ed.* **2008**, *47*, 775–778.

- (11) Kaita, S.; Hou, Z.; Wakatsuki, Y. Stereospecific Polymerization of 1,3-Butadiene with Samarocene-Based Catalysts. *Macromolecules* **1999**, *32*, 9078–9079.
- (12) Kaita, S.; Doi, Y.; Kaneko, K.; Horiuchi, A. C.; Wakatsuki, Y. An Efficient Gadolinium Metallocene-Based Catalyst for the Synthesis of Isoprene Rubber with Perfect 1,4-Cis Microstructure and Marked Reactivity Difference between Lanthanide Metallocenes toward Dienes As Probed by Butadiene-Isoprene Copolymerization Catalysis. *Macromolecules* **2004**, *37*, 5860–5862.
- (13) Ihara, E.; Yoshioka, S.; Furo, M.; Katsura, K.; Yasuda, H.; Mohri, S.; Kanehisa, N.; Kai, Y. Synthesis and Olefin Polymerization Catalysis of New Trivalent Samarium and Yttrium Complexes with Bridging Bis(Cyclopentadienyl) Ligands. *Organometallics* **2001**, *20*, 1752–1761.
- (14) Jende, L. N.; Hollfelder, C. O.; Maichle-Mössmer, C.; Anwender, R. Rare-Earth-Metal Allyl Complexes Supported by the [2-(N,N-Dimethylamino)Ethyl]Tetramethylcyclopentadienyl Ligand: Structural Characterization, Reactivity, and Isoprene Polymerization. *Organometallics* **2015**, *34*, 32–41.
- (15) Jian, Z.; Cui, D.; Hou, Z.; Li, X. Living Catalyzed-Chain-Growth Polymerization and Block Copolymerization of Isoprene by Rare-Earth Metal Allyl Precursors Bearing a Constrained-Geometry-Conformation Ligand. *Chem. Commun.* **2010**, *46*, 3022–3024.
- (16) Trost, B. M.; Ryan, M. C. Indenylmetal Catalysis in Organic Synthesis. *Angew. Chem., Int. Ed.* **2017**, *56*, 2862–2879.
- (17) Tsutsui, M.; Gysling, H. J. Evidence for a Covalent Organolanthanide: Tris(Indenyl)Samarium-Tetrahydrofuran. *J. Am. Chem. Soc.* **1968**, *90*, 6880–6881.
- (18) Cui, D.; Tang, T.; Cheng, J.; Hu, N.; Chen, W.; Huang, B. Synthesis and Characterization of  $(C_5H_9C_9H_6)_2Yb(THF)_2(II)$  (1) and  $[(C_5H_9C_9H_6)_2Yb(THF)_2]_2O_2$  (2), and Ring-Opening Polymerization of Lactones with 1. *J. Organomet. Chem.* **2002**, *650*, 84–90.
- (19) Knjazhanski, S. Y.; Elizalde, L.; Cadenas, G.; Bulychov, B. M. Polymerization of Methyl Methacrylate with Alane Complexes of Bivalent Lanthanidocenes. *J. Organomet. Chem.* **1998**, *S68*, 33–40.
- (20) The synthesis of  $(Ind)_2Y(\mu-Et)_2AlEt_2$  and  $(Ind)_2Ln(NiPr_2)$  ( $Ln=Y, Yb$ ) was claimed and the compounds successfully employed as precatalysts for the polymerization of MMA and acrylonitrile: (a) Ying, L.; Ba, X.; Zhao, Y.; Li, G.; Tang, T.; Jin, Y. Polymerization of Methyl Methacrylate with Organolanthanides as Single-Component Catalysts. *Chin. J. Polym. Sci.* **2001**, *19*, 85–87. (b) Ying, L.; Ba, X.; Zhao, Y.; Li, G.; Tang, T.; Jin, Y. Polymerization of Acrylonitrile with Organolanthanides as Single-Component Catalysts. *Chin. J. Polym. Sci.* **2001**, *19*, 89–91.
- (21) Rodrigues, A.-S.; Kirillov, E.; Roisnel, T.; Razavi, A.; Vuillemin, B.; Carpentier, J.-F. Highly Isospecific Styrene Polymerization Catalyzed by Single-Component Bridged Bis(Indenyl) Allyl Yttrium and Neodymium Complexes. *Angew. Chem., Int. Ed.* **2007**, *46*, 7240–7243.
- (22) Annunziata, L.; Duc, M.; Carpentier, J.-F. Chain Growth Polymerization of Isoprene and Stereoselective Isoprene–Styrene Copolymerization Promoted by an Ansa-Bis(Indenyl)Allyl–Yttrium Complex. *Macromolecules* **2011**, *44*, 7158–7166.
- (23) Annunziata, L.; Rodrigues, A.-S.; Kirillov, E.; Sarazin, Y.; Okuda, J.; Perrin, L.; Maron, L.; Carpentier, J.-F. Isoselective Styrene Polymerization Catalyzed by Ansa-Bis(Indenyl) Allyl Rare Earth Complexes. Stereochemical and Mechanistic Aspects. *Macromolecules* **2011**, *44*, 3312–3322.
- (24) For O-donor-functionalized *ansa*-metallocenes, see: (a) Qian, C.; Zou, G.; Jiang, W.; Chen, Y.; Sun, J.; Li, N. Selective Synthesis, Structure, and Catalytic Behavior of Meso-Divalent 1,1'-(3-Oxapentamethylene)-Bridged Bis(Indenyl)Lanthanidocenes. *Organometallics* **2004**, *23*, 4980–4986. (b) Qian, C.; Zou, G.; Chen, Y.; Sun, J. Synthesis, Structure, and Catalytic Behavior of Rac-1,1'-(3-Oxapentamethylene)-Bridged Bis(Indenyl) Ansa-Lanthanidocenes. *Organometallics* **2001**, *20*, 3106–3112.
- (25) For silyl-substituted *ansa*-metallocenes, see: Lin, D.; Chen, J.; Luo, C.; Zhang, Y.; Yao, Y.; Luo, Y. Rare Earth Metal Benzyl Complexes Bearing Bridged-Indenyl Ligand for Highly Active Polymerization of Methyl Methacrylate. *J. Organomet. Chem.* **2009**, *694*, 2976–2980.
- (26) For N-donor-functionalized metallocenes, see: (a) Wang, S.; Zhou, S.; Sheng, E.; Xie, M.; Zhang, K.; Cheng, L.; Feng, Y.; Mao, L.; Huang, Z. Homolysis of the Eu–N Bond. Synthesis, Structural Characterization, and Catalytic Activity of Novel Europium(II) Complexes. *Organometallics* **2003**, *22* (17), 3546–3552. (b) Sheng, E.; Zhou, S.; Wang, S.; Yang, G.; Wu, Y.; Feng, Y.; Mao, L.; Huang, Z. Homolysis of the Ln–N ( $Ln=Yb, Eu$ ) Bond - Synthesis, Structure, and Catalytic Activity of Ytterbium(II) and Europium(II) Complexes Having (Dimethylamino)Propyl- and (Dimethylamino)Ethyl-Functionalized Indenyl Ligands. *Eur. J. Inorg. Chem.* **2004**, *2004*, 2923–2932. (c) Zhou, S.; Wang, S.; Sheng, E.; Zhang, L.; Yu, Z.; Xi, X.; Chen, G.; Luo, W.; Li, Y. Synthesis, Characterization, and Catalytic Activity of Some Neodymium(III), Ytterbium(II), and Europium(II) Complexes with Pyrrolidinyl- and Piperidinyl-Functionalized Indenyl Ligands. *Eur. J. Inorg. Chem.* **2007**, *2007*, 1519–1528. (d) Cheng, J.; Cui, D.; Chen, W.; Hu, N.; Tang, T.; Huang, B. Organolanthanides with 3-(2-Pyridylmethyl) Indenyl Ligands: Synthesis, Crystal Structures and Catalytic Activities of Divalent Complexes for  $\epsilon$ -Caprolactone Polymerization. *J. Organomet. Chem.* **2004**, *689*, 2646–2653.
- (27) For O-donor-functionalized metallocenes, see: (a) Zhang, K.; Zhang, W.; Wang, S.; Sheng, E.; Yang, G.; Xie, M.; Zhou, S.; Feng, Y.; Mao, L.; Huang, Z. Homolysis of the Ln–N ( $Ln=Yb, Eu$ ) Bond. Synthesis, Structural Characterization and Catalytic Activity of Ytterbium(II) and Europium(II) Complexes with Methoxyethyl Functionalized Indenyl Ligands. *Dalton Trans.* **2004**, *7*, 1029–1037. (b) Wang, S.; Wang, S.; Zhou, S.; Yang, G.; Luo, W.; Hu, N.; Zhou, Z.; Song, H.-B. Synthesis, Characterization, and Catalytic Activity of Divalent Organolanthanide Complexes with New Tetrahydro-2H-Pyranlyl-Functionlized Indenyl Ligands. *J. Organomet. Chem.* **2007**, *692*, 2099–2106.
- (28) For complexes with an N-donor sidearm, see: (a) Lei, Y.; Wang, Y.; Luo, Y. Synthesis, Characterization, and Styrene Polymerization Catalysis of Pyridyl-Functionalized Indenyl Rare Earth Metal Bis(Silylamide) Complexes. *J. Organomet. Chem.* **2013**, *738*, 24–28. (b) Jian, Z.; Petrov, A. R.; Hangaly, N. K.; Li, S.; Rong, W.; Mou, Z.; Rufanov, K. A.; Harms, K.; Sundermeyer, J.; Cui, D. Phosphazene-Functionalized Cyclopentadienyl and Its Derivatives Ligated Rare-Earth Metal Alkyl Complexes: Synthesis, Structures, and Catalysis on Ethylene Polymerization. *Organometallics* **2012**, *31*, 4267–4282. (c) Wang, Y.; Lei, Y.; Chi, S.; Luo, Y. Rare Earth Metal Bis(Silylamide) Complexes Bearing Pyridyl-Functionalized Indenyl Ligand: Synthesis, Structure and Performance in the Living Polymerization of L-Lactide and Rac-Lactide. *Dalton Trans.* **2013**, *42*, 1862–1871.
- (29) For complexes with an NHC-donor sidearm, see: Wang, B.; Cui, D.; Lv, K. Highly 3,4-Selective Living Polymerization of Isoprene with Rare Earth Metal Fluorenyl N-Heterocyclic Carbene Precursors. *Macromolecules* **2008**, *41*, 1983–1988.
- (30) Hu, Y.; Xu, X.; Zhang, Y.; Chen, Y.; Chen, E. Y.-X. Polymerization of Naturally Renewable Methylene Butyrolactones by Half-Sandwich Indenyl Rare Earth Metal Dialkyls with Exceptional Activity. *Macromolecules* **2010**, *43*, 9328–9336.
- (31) Xu, X.; Chen, Y.; Sun, J. Indenyl Abstraction versus Alkyl Abstraction of  $[(Indenyl)ScR_2(Thf)]$  by  $[Ph_3C][B(C_6F_5)_4]$ : Aspecific and Syndiospecific Styrene Polymerization. *Chem. - Eur. J.* **2009**, *15*, 846–850.
- (32) Tan, R.; Shi, Z.; Guo, F.; He, L.; Han, L.; Li, Y. The Terpolymerization of Ethylene and Propylene with Isoprene via THF-Containing Half-Sandwich Scandium Catalysts: A New Kind of Ethylene-Propylene-Diene Rubber and Its Functionalization. *Polym. Chem.* **2017**, *8*, 4651–4658.
- (33) Miao, W.; Li, S.; Zhang, H.; Cui, D.; Wang, Y.; Huang, B. Mixed Ligands Supported Yttrium Alkyl Complexes: Synthesis, Characterization and Catalysis toward Lactide Polymerization. *J. Organomet. Chem.* **2007**, *692*, 4828–4834.

- (34) Tardif, O.; Kaita, S. Generation of Cationic Indenyl Silylamide Gadolinium and Scandium Complexes  $[(\text{Ind})\text{Ln}\{\text{N}(\text{SiMe}_3)_2\}]^+[\text{B}(\text{C}_6\text{F}_5)_4]^-$  and Their Reactivity for 1,3-Butadiene Polymerization. *Dalton Trans.* **2008**, *19*, 2531–2533.
- (35) Diether, D.; Tyulyunov, K.; Maichle-Mössmer, C.; Anwender, R. Fluorenyl Half-Sandwich Bis(Tetramethylaluminate) Complexes of the Rare-Earth Metals: Synthesis, Structure, and Isoprene Polymerization. *Organometallics* **2017**, *36*, 4649–4659.
- (36) Grimmer, N. E.; Coville, N. J.; de Koning, C. B.; Smith, J. M.; Cook, L. M. Zirconium Bis-Indenyl Compounds. Synthesis and X-Ray Crystallography Study of 1- and 2-Substituted Bis(R-Indenyl) Zirconium Dichloride Metallocenes. *J. Organomet. Chem.* **2000**, *616*, 112–127.
- (37) Krüger, C.; Lutz, F.; Nolte, M.; Erker, G.; Aulbach, M. Torsional Isomerism of Bent Metallocene Complexes. The Structures of Meso- and Rac-Bis(1-Cyclohexyltetrahydroindenyl)Zirconium Dichloride in the Solid State. *J. Organomet. Chem.* **1993**, *452*, 79–86.
- (38) Erker, G.; Aulbach, M.; Knickmeier, M.; Wingbermuehle, D.; Krueger, C.; Nolte, M.; Werner, S. The Role of Torsional Isomers of Planarly Chiral Nonbridged Bis(Indenyl)Metal Type Complexes in Stereoselective Propene Polymerization. *J. Am. Chem. Soc.* **1993**, *115*, 4590–4601.
- (39) Knickmeier, M.; Erker, G.; Fox, T. Conformational Analysis of Nonbridged Bent Metallocene Ziegler-Catalyst Precursors Detection of the Third Torsional Isomer. *J. Am. Chem. Soc.* **1996**, *118*, 9623–9630.
- (40) Herrmann, W. A.; Eppinger, J.; Spiegler, M.; Runte, O.; Anwender, R.  $\beta$ -Si-H Agostic Rigidity in a Solvent-Free Indenyl-Derived Ansa-Ytrocene Silylamide. *Organometallics* **1997**, *16*, 1813–1815.
- (41) Lorenz, V.; Liebing, P.; Bathelier, A.; Engelhardt, F.; Maron, L.; Hilfert, L.; Busse, S.; Edelmann, F. T. The “Wanderlust” of Me<sub>3</sub>Si Groups in Rare-Earth Triple-Decker Complexes: A Combined Experimental and Computational Study. *Chem. Commun.* **2018**, *54*, 10280–10283.
- (42) Zimmermann, M.; Volbeda, J.; Törnroos, K. W.; Anwender, R. Tetramethylcyclopentadienyl-Supported Rare-Earth Metal Bis-(Tetramethyl)Aluminate Complexes: Synthesis, Structural Chemistry, Cation Formation, and Isoprene Polymerization. *C. R. Chim.* **2010**, *13*, 651–660.
- (43) Evans, W. J.; Wayda, A. L.; Hunter, W. E.; Atwood, J. L. Heteroleptic T-Butyl Lanthanoid Complexes: Synthesis and X-Ray Crystal Structure of Monomeric Bis(Cyclopentadienyl)(t-Butyl) Lutetium Tetrahydrofuranate. *J. Chem. Soc., Chem. Commun.* **1981**, *6*, 292–293.
- (44) Ma, H.; Huang, J.; Qian, Y. Synthesis and Characterization of Planarly Chiral Nonbridged Bis(1-R-Indenyl) Zirconium Dichloride Complexes and X-Ray Structure of Rac- $[(\eta^5\text{-C}_9\text{H}_6\text{-1-C}(\text{CH}_3)_2\text{-o-C}_6\text{H}_4\text{-OCH}_3)_2\text{ZrCl}_2]\cdot\text{THF}$ . *J. Organomet. Chem.* **2002**, *650*, 114–122.
- (45) Barisic, D.; Buschmann, D. A.; Schneider, D.; Maichle-Mössmer, C.; Anwender, R. Rare-Earth-Metal Pentadienyl Half-Sandwich and Sandwich Tetramethylaluminates—Synthesis, Structure, Reactivity, and Performance in Isoprene Polymerization. *Chem. - Eur. J.* **2019**, *25*, 4821–4832.
- (46) Trifonov, A. A.; Fedorova, E. A.; Borovkov, I. A.; Fukin, G. K.; Baranov, E. V.; Larionova, J.; Druzhkov, N. O. Steric Manipulation of the Reductive Reactivity of Ytterbocenes toward 2-(((2,6-Diisopropylphenyl)Imino)Methyl)Pyridine: Insertion of the N=C Bond into the Yb-Indenyl Bond or Oxidative Cleavage of the  $\eta^5$  Yb-Cp (Cp=C<sub>13</sub>H<sub>9</sub>, Cp\*) Bond. *Organometallics* **2007**, *26*, 2488–2491.
- (47) Zimmermann, M.; Frøystein, N. Å.; Fischbach, A.; Sirsch, P.; Dietrich, H. M.; Törnroos, K. W.; Herdtweck, E.; Anwender, R. Homoleptic Rare-Earth Metal(III) Tetramethylaluminates: Structural Chemistry, Reactivity, and Performance in Isoprene Polymerization. *Chem. - Eur. J.* **2007**, *13*, 8784–8800.
- (48) Ready, T. E.; Chien, J. C. W.; Rausch, M. D. Alkyl-Substituted Indenyl Titanium Precursors for Syndiospecific Ziegler-Natta Polymerization of Styrene. *J. Organomet. Chem.* **1996**, *519*, 21–28.
- (49) Möller, A. C.; Blom, R.; Heyn, R. H.; Swang, O.; Kopf, J.; Seraidar, T. A General One-Pot Synthesis for Elusive 2-Substituted Indenes: Does Bis[2-(Tert-Butyl)Indenyl]Zirconium(IV) Dichloride/MAO Polymerise Ethene? *Dalton Trans.* **2006**, *17*, 2098–2105.
- (50) Merola, J. S.; Kacmarcik, R. T. Synthesis and Reaction Chemistry of ( $\eta^5$ -Indenyl)(Cyclooctadiene)Iridium: Migration of Indenyl from Iridium to Cyclooctadiene. *Organometallics* **1989**, *8*, 778–784.
- (51) COSMO v. 1.61; Bruker AXS Inc.: Madison, WI, 2012.
- (52) (a) APEX2 v. 2012.10\_0; Bruker AXS Inc.: Madison, WI, 2012. (b) APEX 3V. 2016.5-0; Bruker AXS Inc.: Madison, WI, 2016.
- (53) SAINT v. 8.34A; Bruker AXS, Inc.: Madison, WI, 2013.
- (54) SHELXTL: (a) Sheldrick, G. M. SHELXTL: Integrated Space-Group and Crystal-Structure Determination. *Acta Cryst.* **2015**, *A71*, 3–8. SHELXL: (b) Sheldrick, G. M. Crystal Structure Refinement with SHELXL. *Acta Cryst.* **2015**, *C71*, 3–8.
- (55) Hubschle, C. B.; Sheldrick, G. M.; Dittrich, B. ShelXle: A Qt graphical user interface for SHELXL. *J. Appl. Crystallogr.* **2011**, *44*, 1281–1284.
- (56) Farrugia, L. J. ORTEP-3 for Windows – a version of ORTEP-III with a Graphical User Interface (GUI). *J. Appl. Crystallogr.* **1997**, *30*, S65.
- (57) POV-Ray v. 3.6; Persistence of Vision Raytracer Pty. Ltd.: Williamstown, Victoria, Australia, 2004. <http://www.povray.org/>.

Supporting Information

# **Implications of Indenyl Substitution for the Structural Chemistry of Rare-Earth-Metal (Half-) Sandwich Complexes and Performance in Living Isoprene Polymerization**

Dominic Diether, Cäcilia Maichle-Mössmer, and Reiner Anwander\*

Institut für Anorganische Chemie, Eberhard Karls Universität Tübingen, Auf der Morgenstelle 18, 72076 Tübingen, Germany.

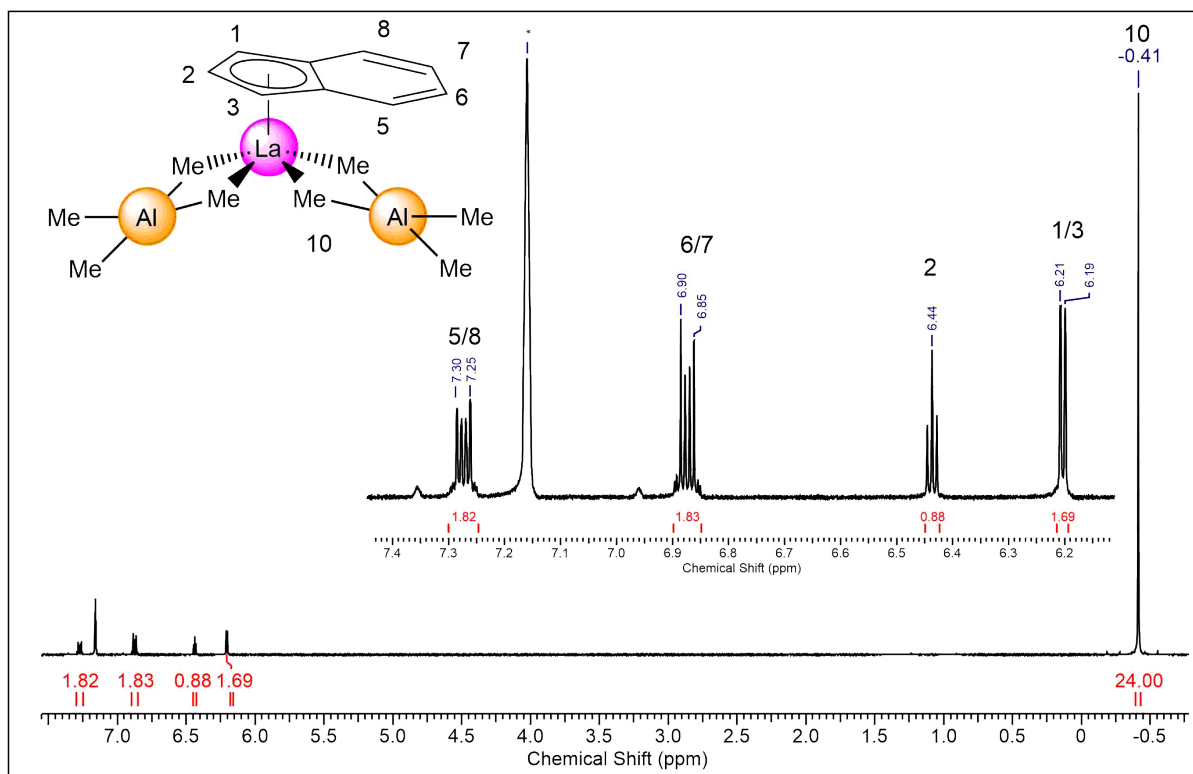
**Corresponding Author**

\* reiner.anwander@uni-tuebingen.de

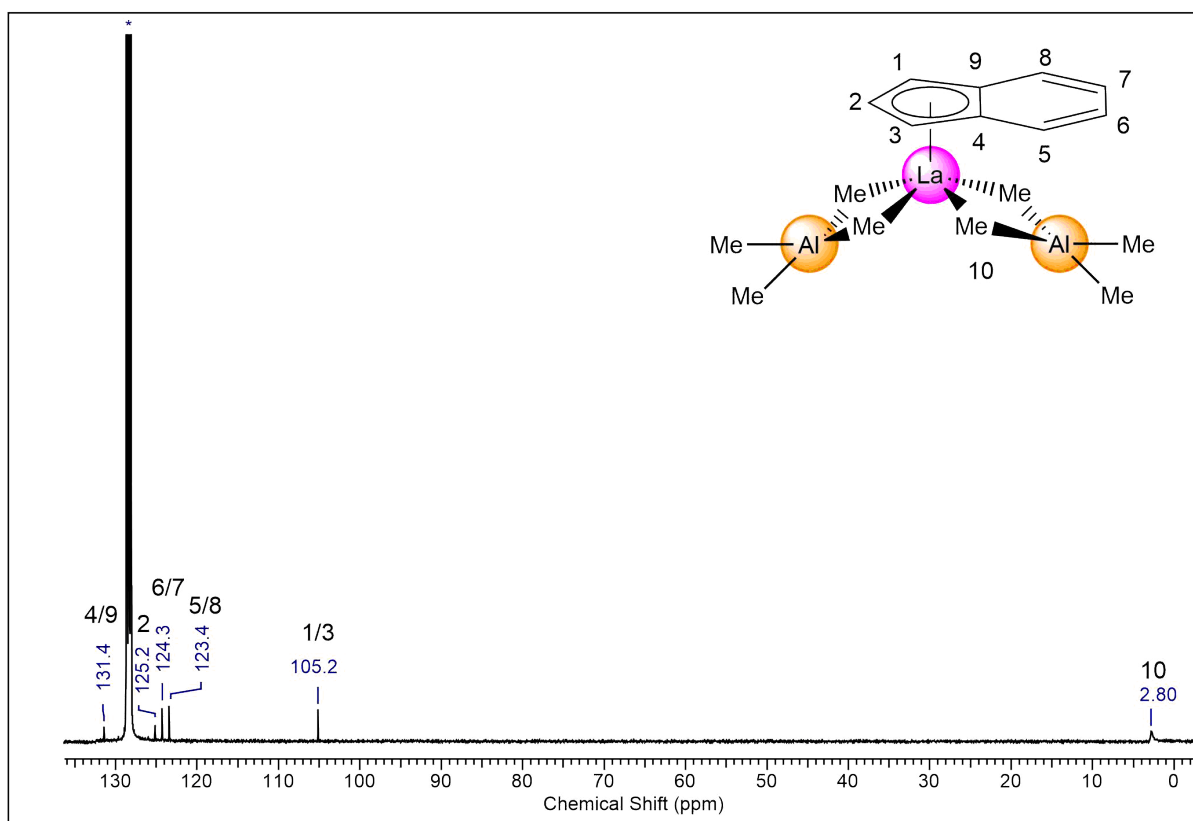
## Table of Contents

Figure S1. $^1\text{H}$ NMR spectrum of $(\text{Ind})\text{La}(\text{AlMe}_4)_2$ ( <b>1a</b> )	S4
Figure S2. $^{13}\text{C}\{^1\text{H}\}$ NMR spectrum of $(\text{Ind})\text{La}(\text{AlMe}_4)_2$ ( <b>1a</b> )	S4
Figure S3. $^1\text{H}^{13}\text{C}$ -HSQC NMR spectrum of $(\text{Ind})\text{La}(\text{AlMe}_4)_2$ ( <b>1a</b> )	S5
Figure S4. $^1\text{H}^1\text{H}$ -COSY NMR spectrum of $(\text{Ind})\text{La}(\text{AlMe}_4)_2$ ( <b>1a</b> )	S5
Figure S5. $^1\text{H}$ NMR spectrum of $(\text{Ind}^{\text{Et}})\text{La}(\text{AlMe}_4)_2$ ( <b>1b</b> )	S6
Figure S6. $^{13}\text{C}\{^1\text{H}\}$ NMR spectrum of $(\text{Ind}^{\text{Et}})\text{La}(\text{AlMe}_4)_2$ ( <b>1b</b> )	S6
Figure S7. $^1\text{H}^{13}\text{C}$ -HSQC NMR spectrum of $(\text{Ind}^{\text{Et}})\text{La}(\text{AlMe}_4)_2$ ( <b>1b</b> )	S7
Figure S8. $^1\text{H}^1\text{H}$ -COSY NMR spectrum of $(\text{Ind}^{\text{Et}})\text{La}(\text{AlMe}_4)_2$ ( <b>1b</b> )	S8
Figure S9. $^1\text{H}$ NMR spectrum of $(\text{Ind}^{\text{tBu}})\text{La}(\text{AlMe}_4)_2$ ( <b>1c</b> )	S9
Figure S10. $^{13}\text{C}\{^1\text{H}\}$ NMR spectrum of $(\text{Ind}^{\text{tBu}})\text{La}(\text{AlMe}_4)_2$ ( <b>1c</b> )	S9
Figure S11. $^1\text{H}^{13}\text{C}$ -HSQC NMR spectrum of $(\text{Ind}^{\text{tBu}})\text{La}(\text{AlMe}_4)_2$ ( <b>1c</b> )	S10
Figure S12. $^1\text{H}^1\text{H}$ -COSY NMR spectrum of $(\text{Ind}^{\text{tBu}})\text{La}(\text{AlMe}_4)_2$ ( <b>1c</b> )	S11
Figure S13. $^1\text{H}$ NMR spectrum of $(\text{Ind}^{\text{Si}})\text{La}(\text{AlMe}_4)_2$ ( <b>1d</b> )	S12
Figure S14. $^{13}\text{C}\{^1\text{H}\}$ NMR spectrum of $(\text{Ind}^{\text{Si}})\text{La}(\text{AlMe}_4)_2$ ( <b>1d</b> )	S12
Figure S15. $^1\text{H}^{13}\text{C}$ -HSQC NMR spectrum of $(\text{Ind}^{\text{Si}})\text{La}(\text{AlMe}_4)_2$ ( <b>1d</b> )	S13
Figure S16. $^1\text{H}^1\text{H}$ -COSY NMR spectrum of $(\text{Ind}^{\text{Si}})\text{La}(\text{AlMe}_4)_2$ ( <b>1d</b> )	S14
Figure S17. $^1\text{H}$ NMR spectrum of $(\text{Ind})_2\text{Lu}(\text{AlMe}_4)$ ( <b>2a</b> )	S15
Figure S18. $^{13}\text{C}\{^1\text{H}\}$ NMR spectrum of $(\text{Ind})_2\text{Lu}(\text{AlMe}_4)$ ( <b>2a</b> )	S15
Figure S19. $^1\text{H}^{13}\text{C}$ -HSQC NMR spectrum of $(\text{Ind})_2\text{Lu}(\text{AlMe}_4)$ ( <b>2a</b> )	S16
Figure S20. $^1\text{H}^1\text{H}$ -COSY NMR spectrum of $(\text{Ind})_2\text{Lu}(\text{AlMe}_4)$ ( <b>2a</b> )	S16
Figure S21. $^1\text{H}$ NMR spectrum of $(\text{Ind}^{\text{Et}})_2\text{Lu}(\text{AlMe}_4)$ ( <b>2b</b> )	S17
Figure S22. $^{13}\text{C}\{^1\text{H}\}$ NMR spectrum of $(\text{Ind}^{\text{Et}})_2\text{Lu}(\text{AlMe}_4)$ ( <b>2b</b> )	S17
Figure S23. $^1\text{H}^{13}\text{C}$ -HSQC NMR spectrum of $(\text{Ind}^{\text{Et}})_2\text{Lu}(\text{AlMe}_4)$ ( <b>2b</b> )	S18
Figure S24. $^1\text{H}^1\text{H}$ -COSY NMR spectrum of $(\text{Ind}^{\text{Et}})_2\text{Lu}(\text{AlMe}_4)$ ( <b>2b</b> )	S19
Figure S25. $^1\text{H}$ NMR spectrum of $(\text{Ind}^{\text{tBu}})_2\text{Lu}(\text{AlMe}_4)$ ( <b>2c</b> )	S20
Figure S26. $^{13}\text{C}\{^1\text{H}\}$ NMR spectrum of $(\text{Ind}^{\text{tBu}})_2\text{Lu}(\text{AlMe}_4)$ ( <b>2c</b> )	S20
Figure S27. $^1\text{H}^{13}\text{C}$ -HSQC NMR spectrum of $(\text{Ind}^{\text{tBu}})_2\text{Lu}(\text{AlMe}_4)$ ( <b>2c</b> )	S21
Figure S28. $^1\text{H}^1\text{H}$ -COSY NMR spectrum of $(\text{Ind}^{\text{tBu}})_2\text{Lu}(\text{AlMe}_4)$ ( <b>2c</b> )	S22
Figure S29. $^1\text{H}$ NMR spectrum of $(\text{Ind}^{\text{Si}})_2\text{Lu}(\text{AlMe}_4)$ ( <b>2d</b> )	S23
Figure S30. $^{13}\text{C}\{^1\text{H}\}$ NMR spectrum of $(\text{Ind}^{\text{Si}})_2\text{Lu}(\text{AlMe}_4)$ ( <b>2d</b> )	S23
Figure S31. $^1\text{H}^{13}\text{C}$ -HSQC NMR spectrum of $(\text{Ind}^{\text{Si}})_2\text{Lu}(\text{AlMe}_4)$ ( <b>2d</b> )	S24
Figure S32. $^1\text{H}^1\text{H}$ -COSY NMR spectrum of $(\text{Ind}^{\text{Si}})_2\text{Lu}(\text{AlMe}_4)$ ( <b>2d</b> )	S25
Figure S33. $^{29}\text{Si}$ - $^1\text{H}$ DEPT45 NMR spectrum of $(\text{Ind}^{\text{Si}})_2\text{Lu}(\text{AlMe}_4)$ ( <b>2d</b> )	S26
Figure S34. $^1\text{H}^{29}\text{Si}$ -HMBC NMR spectrum of $(\text{Ind}^{\text{Si}})_2\text{Lu}(\text{AlMe}_4)$ ( <b>2d</b> )	S26
Figure S35. VT $^1\text{H}$ NMR spectrum (25-100°C) of $(\text{Ind}^{\text{Si}})_2\text{Lu}(\text{AlMe}_4)$ ( <b>2d</b> )	S27
Figure S36. VT $^1\text{H}$ NMR spectrum (-90-25°C) of $(\text{Ind}^{\text{Si}})_2\text{Lu}(\text{AlMe}_4)$ ( <b>2d</b> )	S28
Figure S37. $^1\text{H}$ NMR spectrum of the reaction of $(\text{Ind})\text{La}(\text{AlMe}_4)_2$ with $[\text{Ph}_3\text{C}][\text{B}(\text{C}_6\text{F}_5)_4]$	S29
Figure S38. $^1\text{H}$ NMR spectrum of the reaction of $(\text{Ind})\text{La}(\text{AlMe}_4)_2$ with $[\text{PhNM}_2\text{H}][\text{B}(\text{C}_6\text{F}_5)_4]$	S29
Figure S39. $^1\text{H}$ NMR spectrum of the reaction of $(\text{Ind})\text{La}(\text{AlMe}_4)_2$ with $\text{B}(\text{C}_6\text{F}_5)_3$	S30
Figure S40. $^{11}\text{B}$ NMR spectrum of the reaction of $(\text{Ind})\text{La}(\text{AlMe}_4)_2$ with $\text{B}(\text{C}_6\text{F}_5)_3$	S30
Figure S41. Molecular structure of $(\text{Ind}^{\text{Et}})\text{La}(\text{AlMe}_4)_2$ ( <b>1b</b> )	S31
Table S1. Crystallographic data for <b>1a</b> , <b>1b</b> , <b>1c</b> , and <b>1d</b>	S32
Table S2. Crystallographic data for <b>2a</b> , <b>2b</b> , <b>2c</b> , and <b>2d</b>	S32

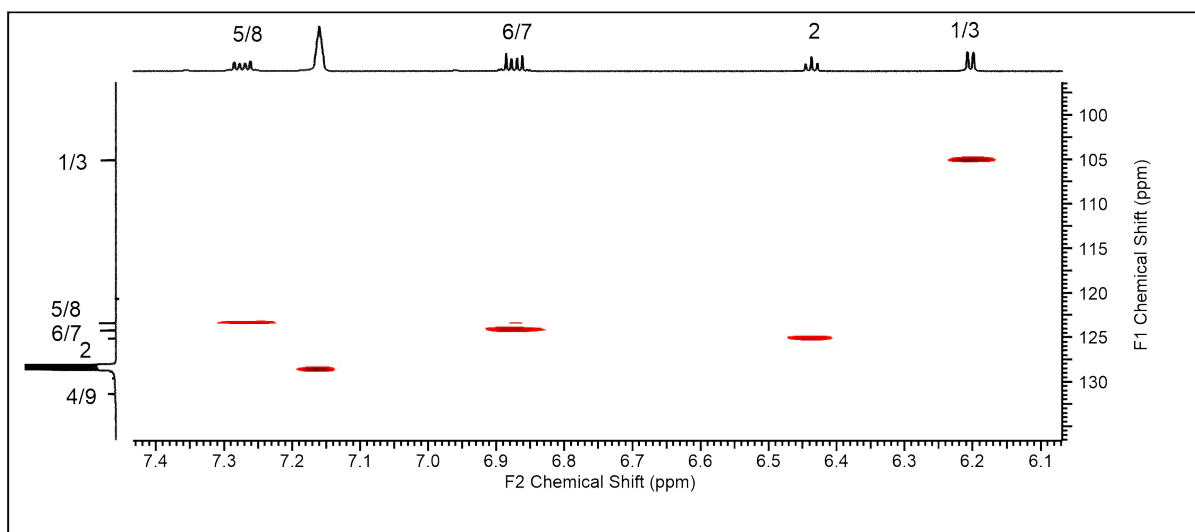
Figure S42. $^1\text{H}$ NMR spectrum of polyisoprene	S34
Figure S43. $^{13}\text{C}\{^1\text{H}\}$ NMR spectrum of polyisoprene	S34
Figure S44. GPC curve of polyisoprene	S35
Figure S45. DSC curve of polyisoprene	S35
Figure S46. $^1\text{H}$ NMR spectrum of polyisoprene	S36
Figure S47. $^{13}\text{C}\{^1\text{H}\}$ NMR spectrum of polyisoprene	S36
Figure S48. GPC curve of polyisoprene	S37
Figure S49. DSC curve of polyisoprene	S37



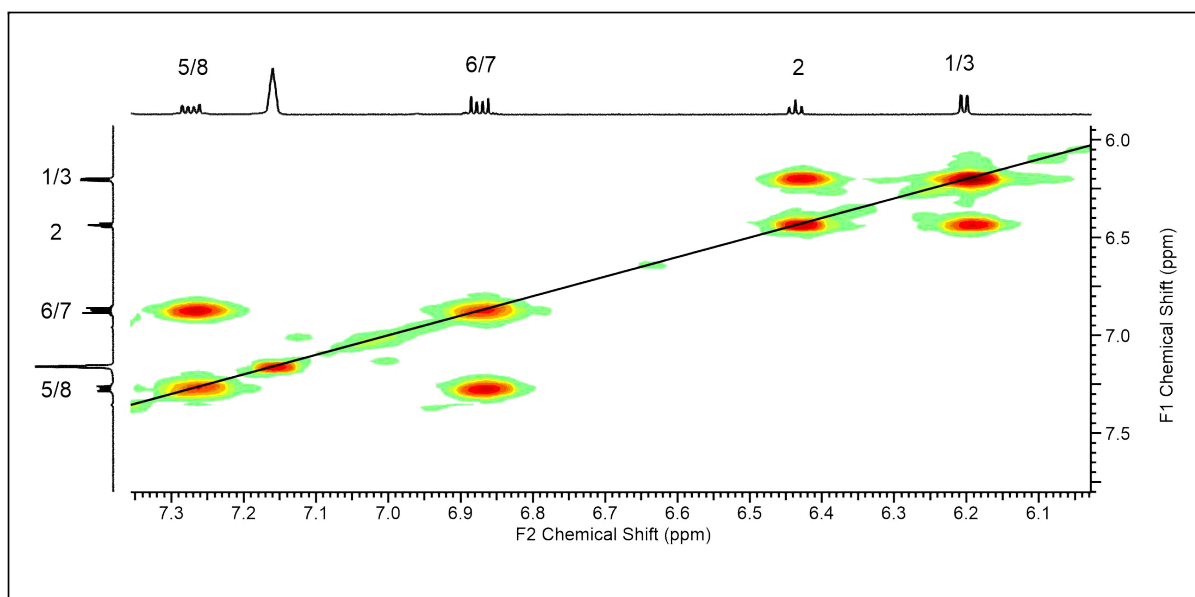
**Figure S1.**  $^1\text{H}$  NMR spectrum (400 MHz) of  $(\text{Ind})\text{La}(\text{AlMe}_4)_2$  (**1a**) in  $\text{C}_6\text{D}_6$  at  $26^\circ\text{C}$ .



**Figure S2.**  $^{13}\text{C}\{^1\text{H}\}$  NMR spectrum (101 MHz) of  $(\text{Ind})\text{La}(\text{AlMe}_4)_2$  (**1a**) in  $\text{C}_6\text{D}_6$  at  $26^\circ\text{C}$ .

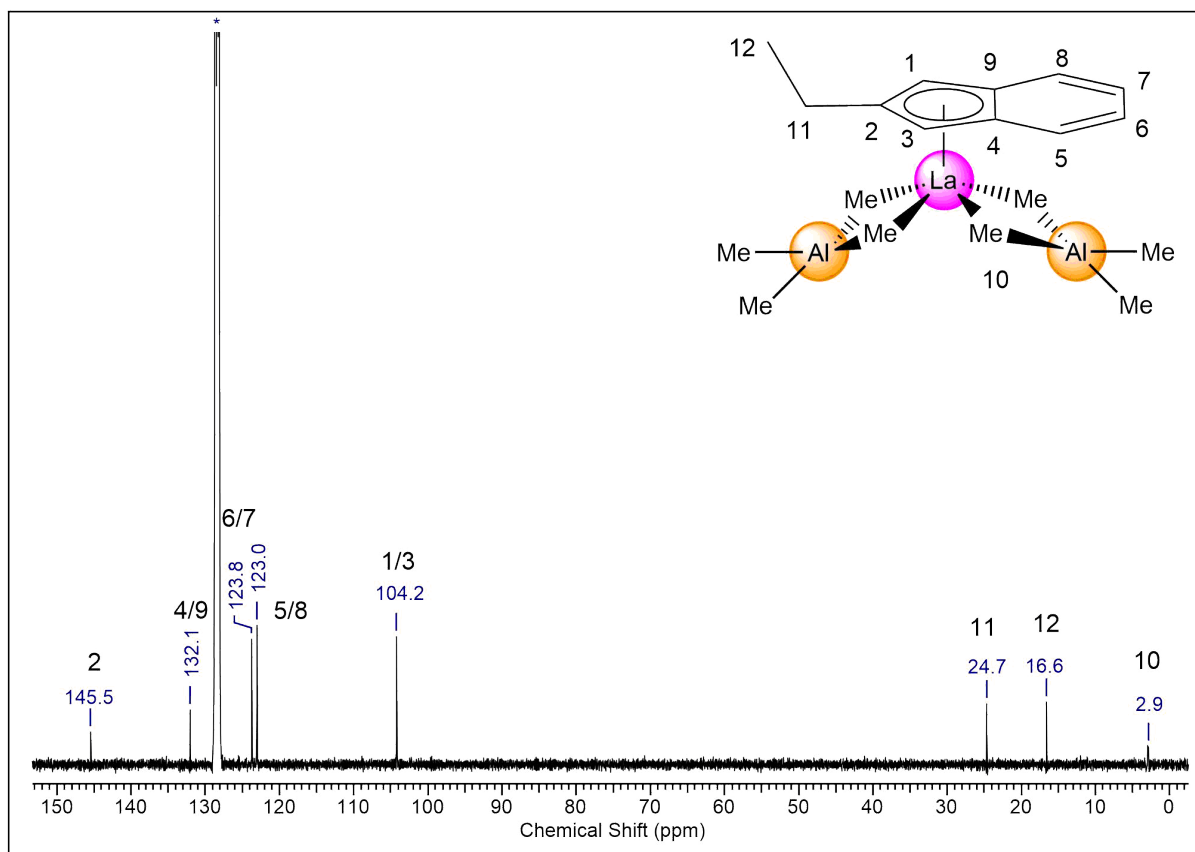
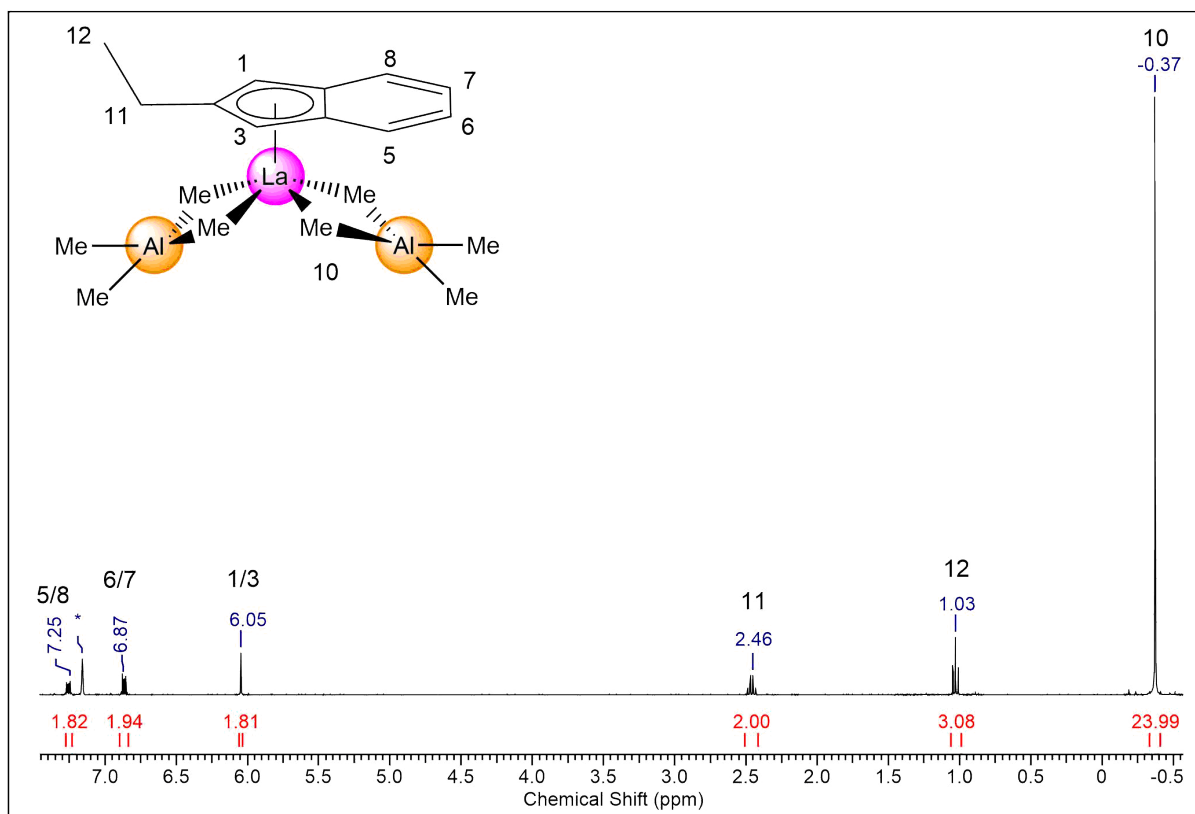


**Figure S3.**  $^1\text{H}/^{13}\text{C}$ -HSQC NMR spectrum (400/101 MHz) of  $(\text{Ind})\text{La}(\text{AlMe}_4)_2$  (**1a**) in  $\text{C}_6\text{D}_6$  at 26 °C.



**Figure S4.** Section of the  $^1\text{H}/^1\text{H}$ -COSY NMR spectrum (400/400 MHz) of  $(\text{Ind})\text{La}(\text{AlMe}_4)_2$  (**1a**) in  $\text{C}_6\text{D}_6$  at 26 °C.





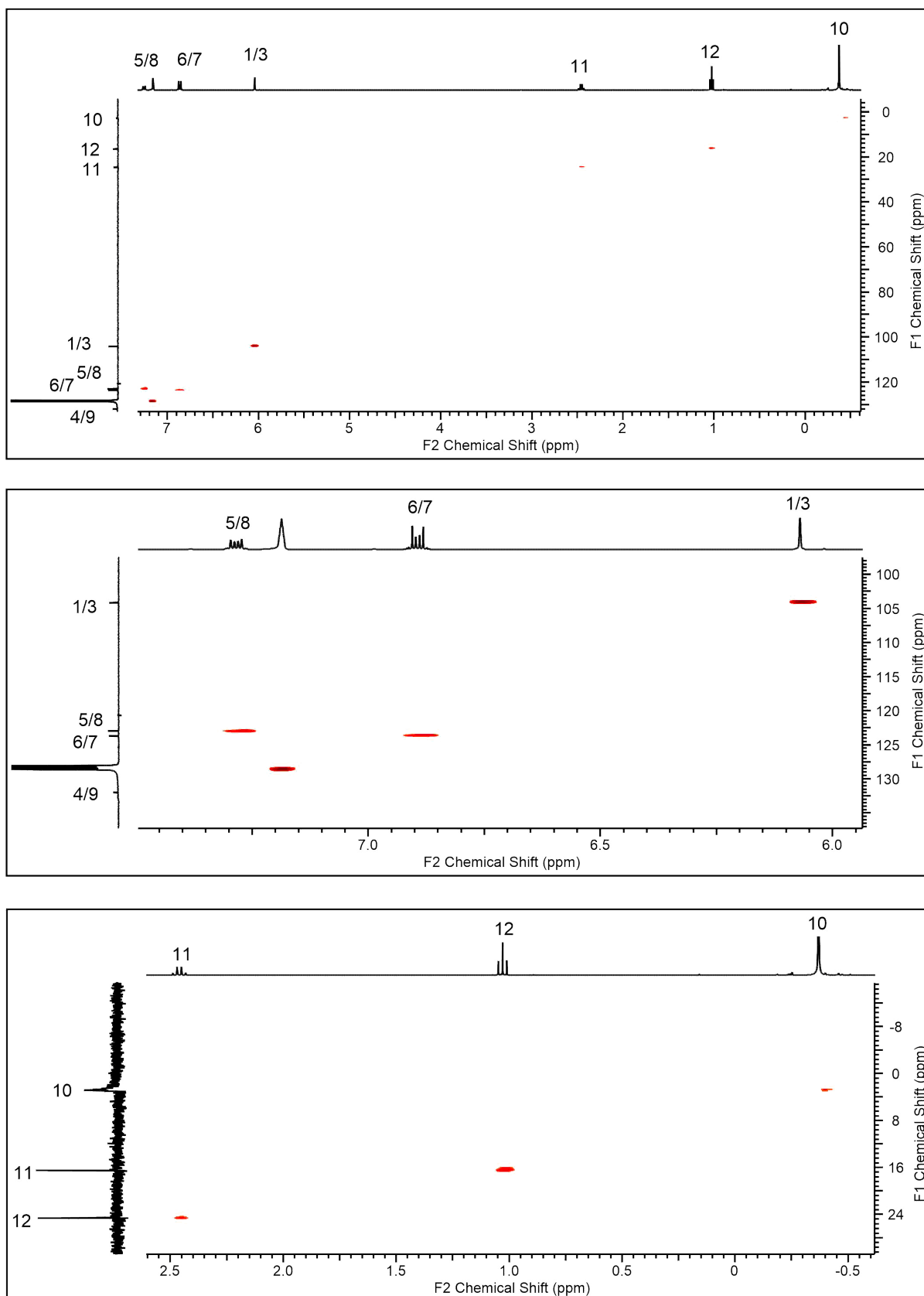


**Figure S7.**  $^1\text{H}/^{13}\text{C}$ -HSQC NMR spectrum (400/101 MHz) of  $(\text{Ind}^{\text{E}})\text{Lu}(\text{AlMe}_4)_2$  (**1b**) in  $\text{C}_6\text{D}_6$  at  $26^\circ\text{C}$ , including enlarged sections.

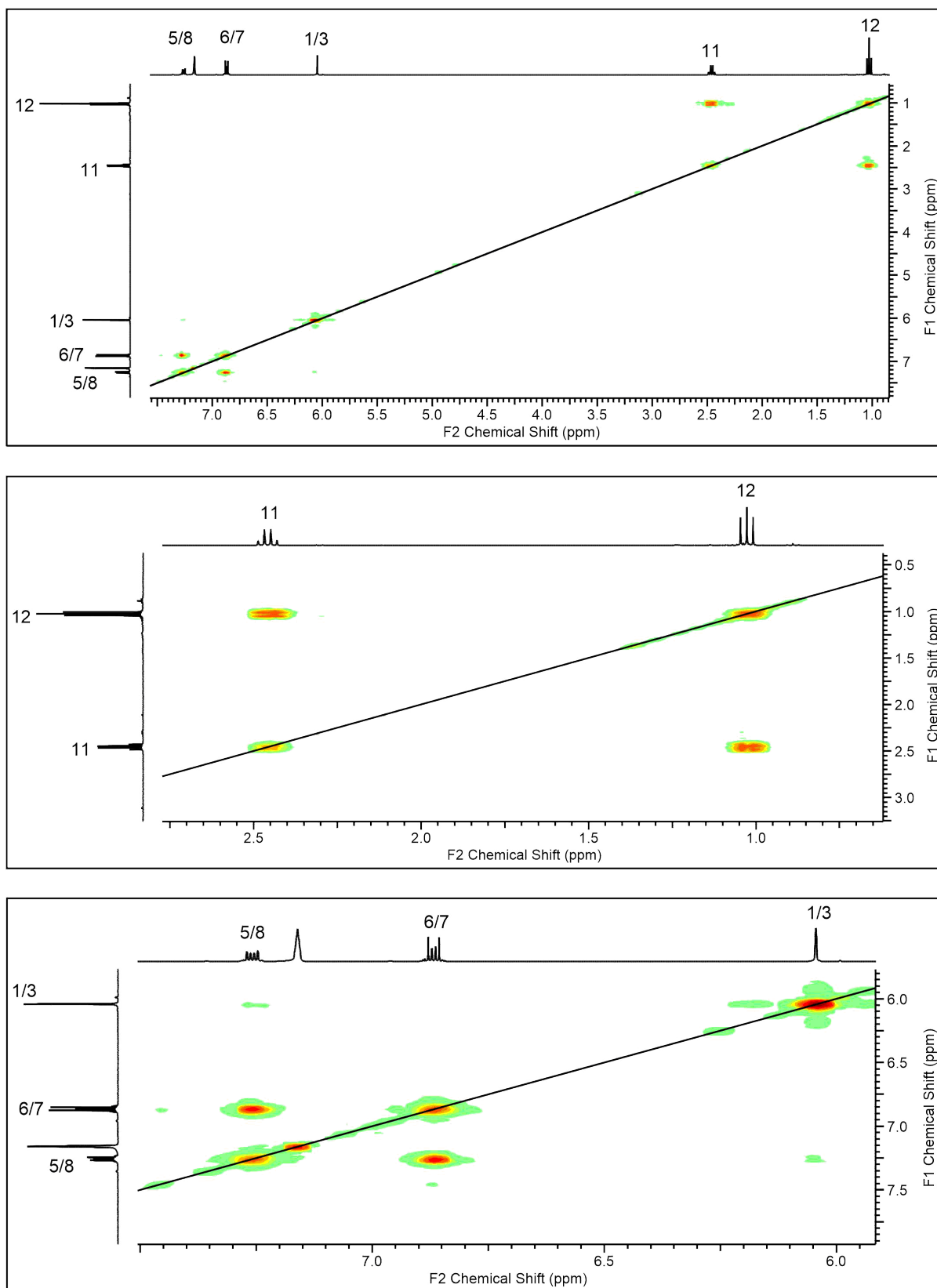


**Figure S8.**  $^1\text{H}$ - $^1\text{H}$ -COSY NMR spectrum (400/400 MHz) of  $(\text{Ind}^{\text{Et}})\text{La}(\text{AlMe}_4)_2$  (**1b**) in  $\text{C}_6\text{D}_6$  at  $26\text{ }^\circ\text{C}$ , including enlarged sections.

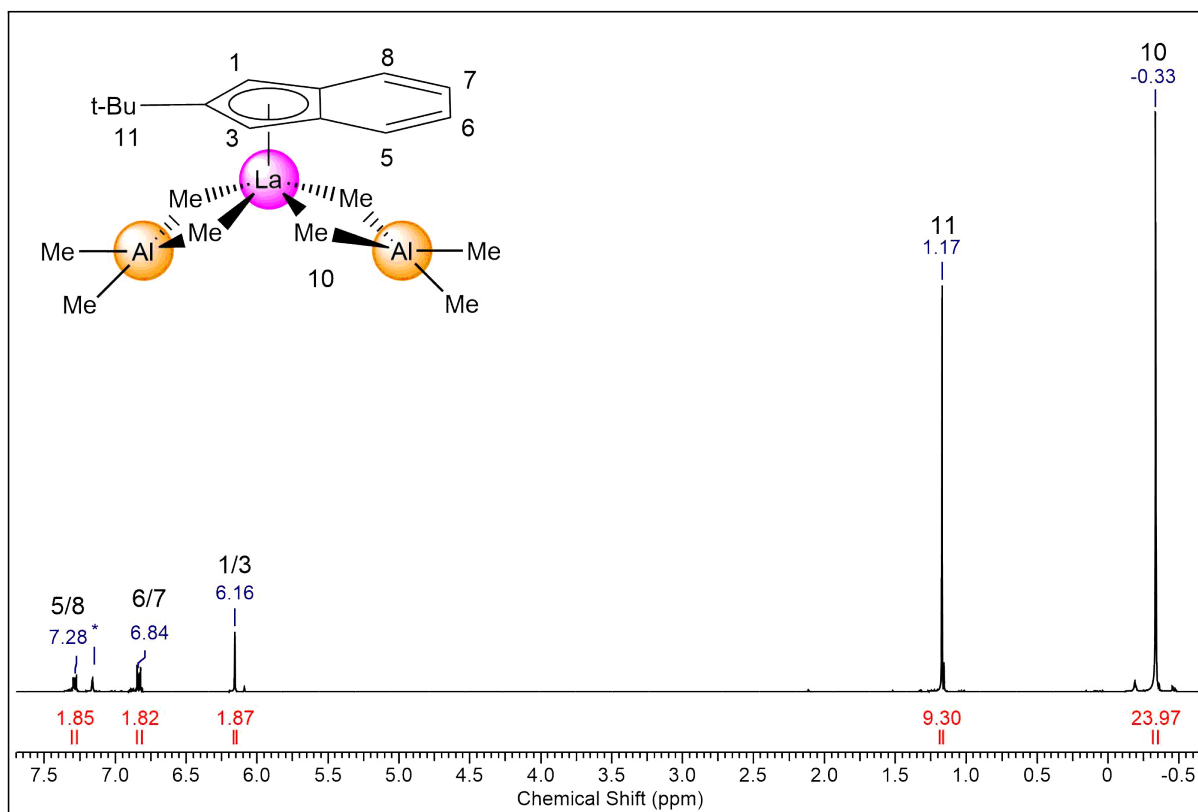


**Figure S9.**  $^1\text{H}$  NMR spectrum (400 MHz) of  $(\text{Ind}^{\text{tBu}})\text{La}(\text{AlMe}_4)_2$  (**1c**) in  $\text{C}_6\text{D}_6$  at  $26^\circ\text{C}$ .

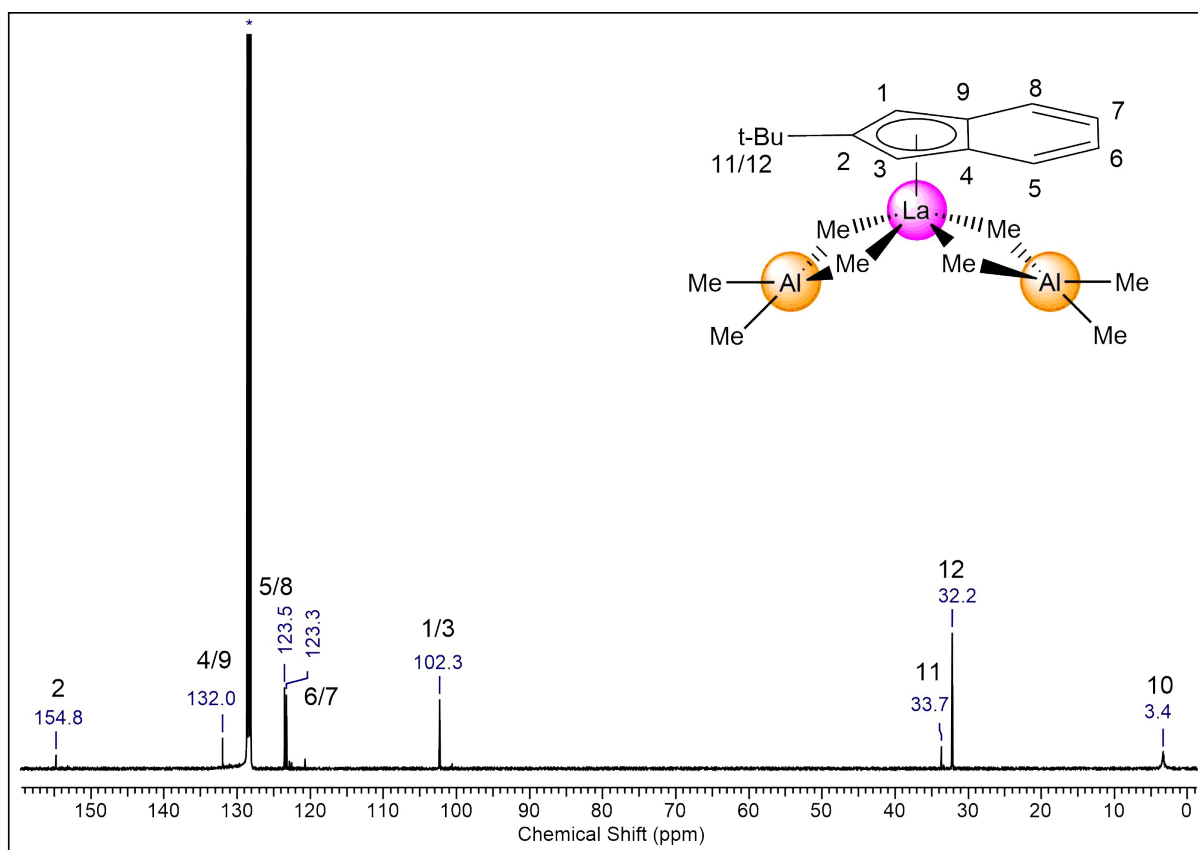


**Figure S10.**  $^{13}\text{C}\{^1\text{H}\}$  NMR spectrum (101 MHz) of  $(\text{Ind}^{\text{tBu}})\text{La}(\text{AlMe}_4)_2$  (**1c**) in  $\text{C}_6\text{D}_6$  at  $26^\circ\text{C}$ .

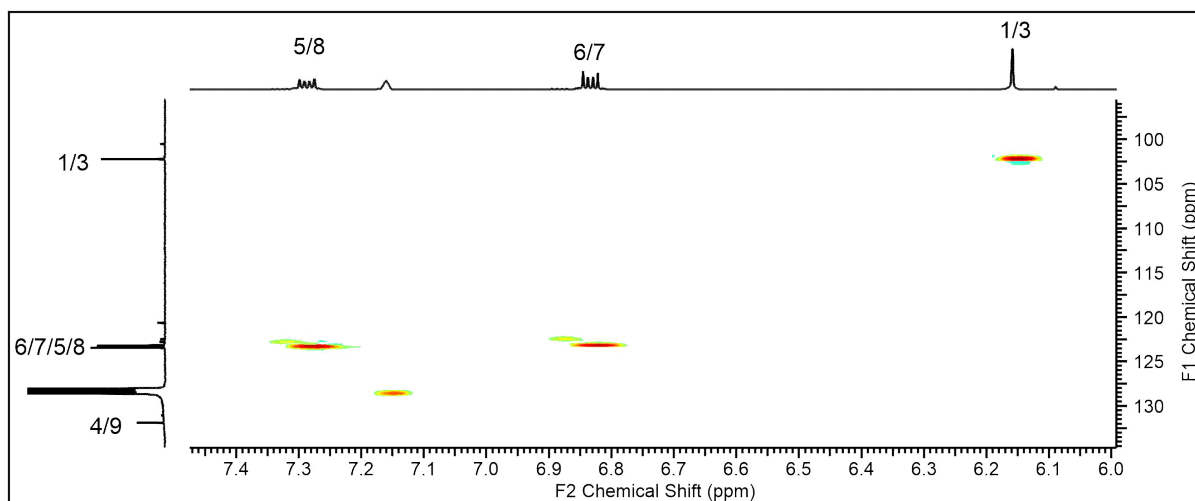
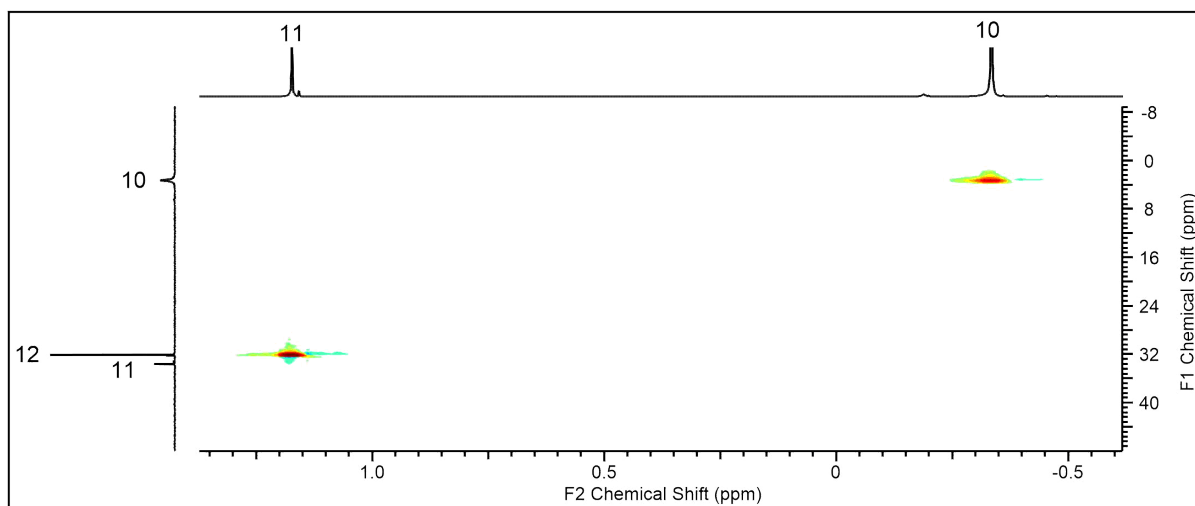
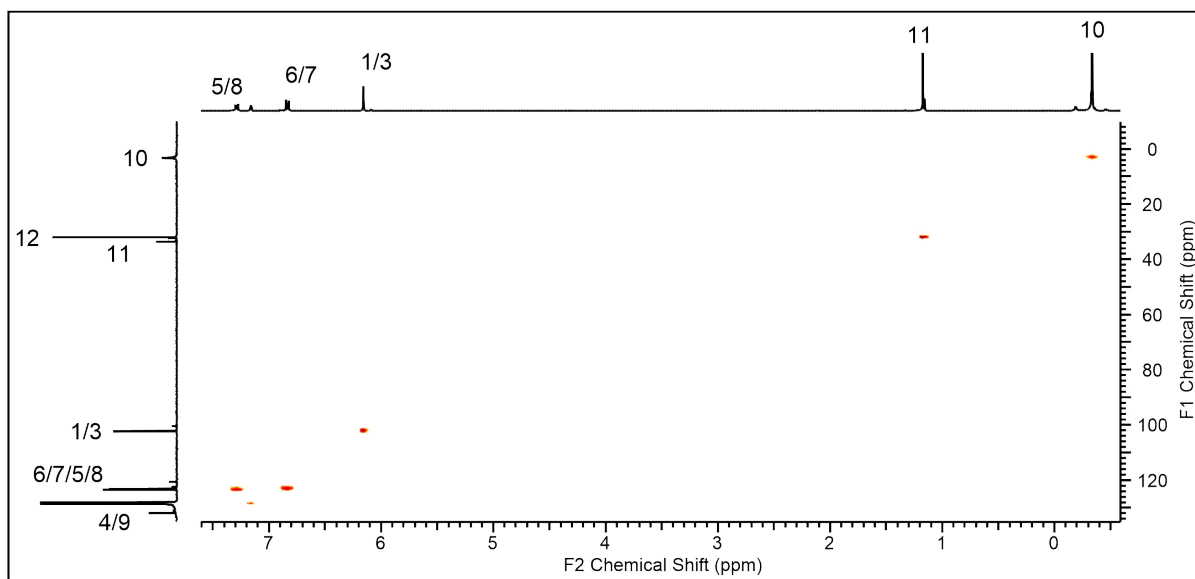


**Figure S11.**  $^1\text{H}^{13}\text{C}$ -HSQC NMR spectrum (400/101 MHz) of  $(\text{Ind}^{t\text{Bu}})\text{La}(\text{AlMe}_4)_2$  (**1c**) in  $\text{C}_6\text{D}_6$  at 26  $^\circ\text{C}$ , including enlarged sections.

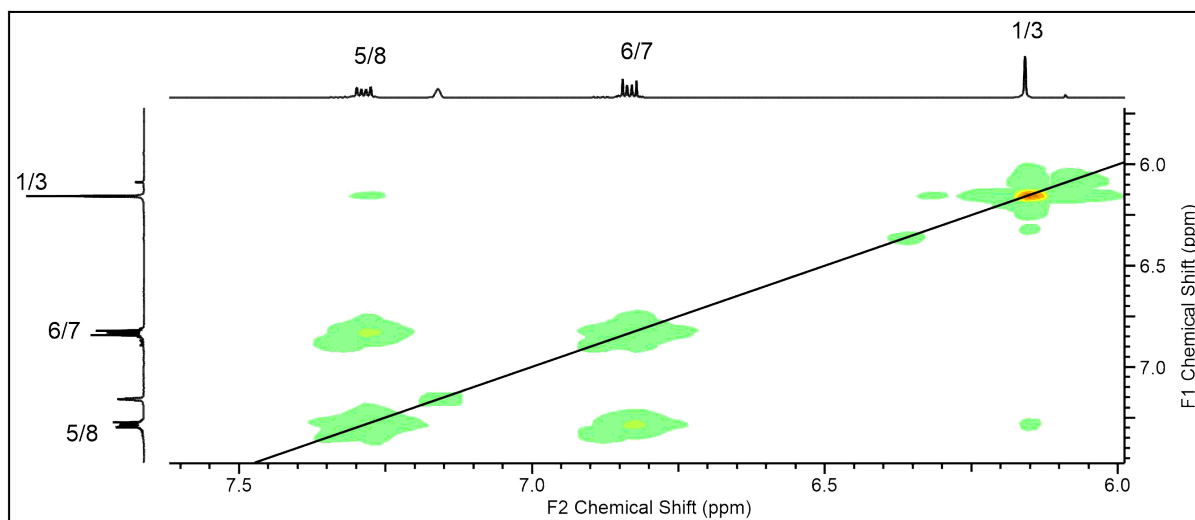
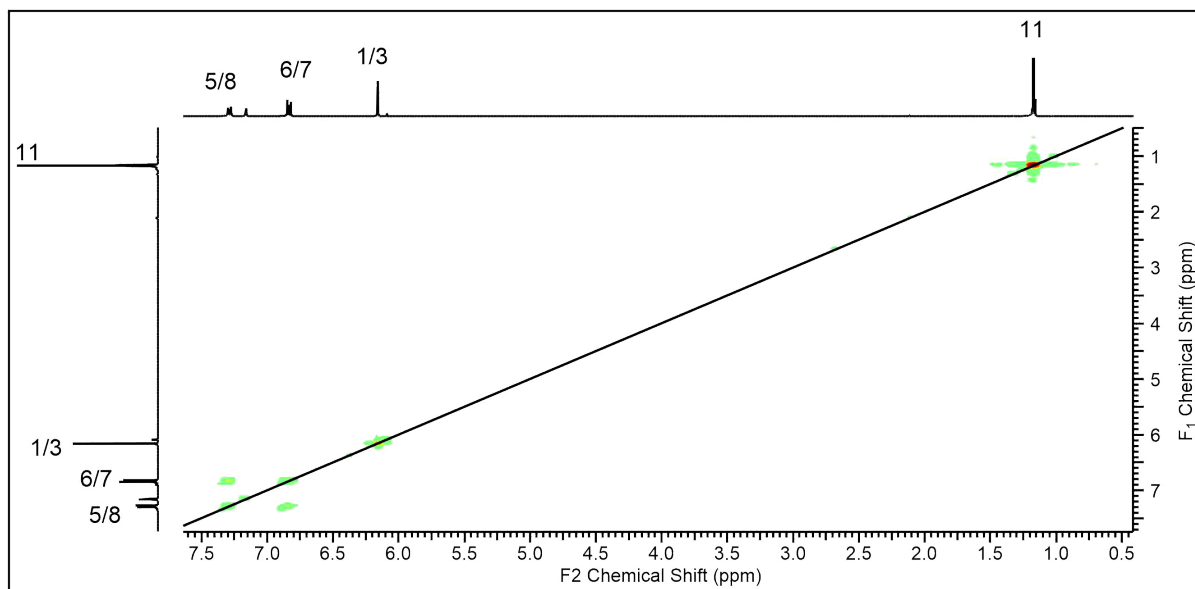


**Figure S12.**  $^1\text{H}$ - $^1\text{H}$ -COSY NMR spectrum (400/400 MHz) of  $(\text{Ind}^{t\text{Bu}})\text{La}(\text{AlMe}_4)_2$  (**1c**) in  $\text{C}_6\text{D}_6$  at 26 °C, including an enlarged section.

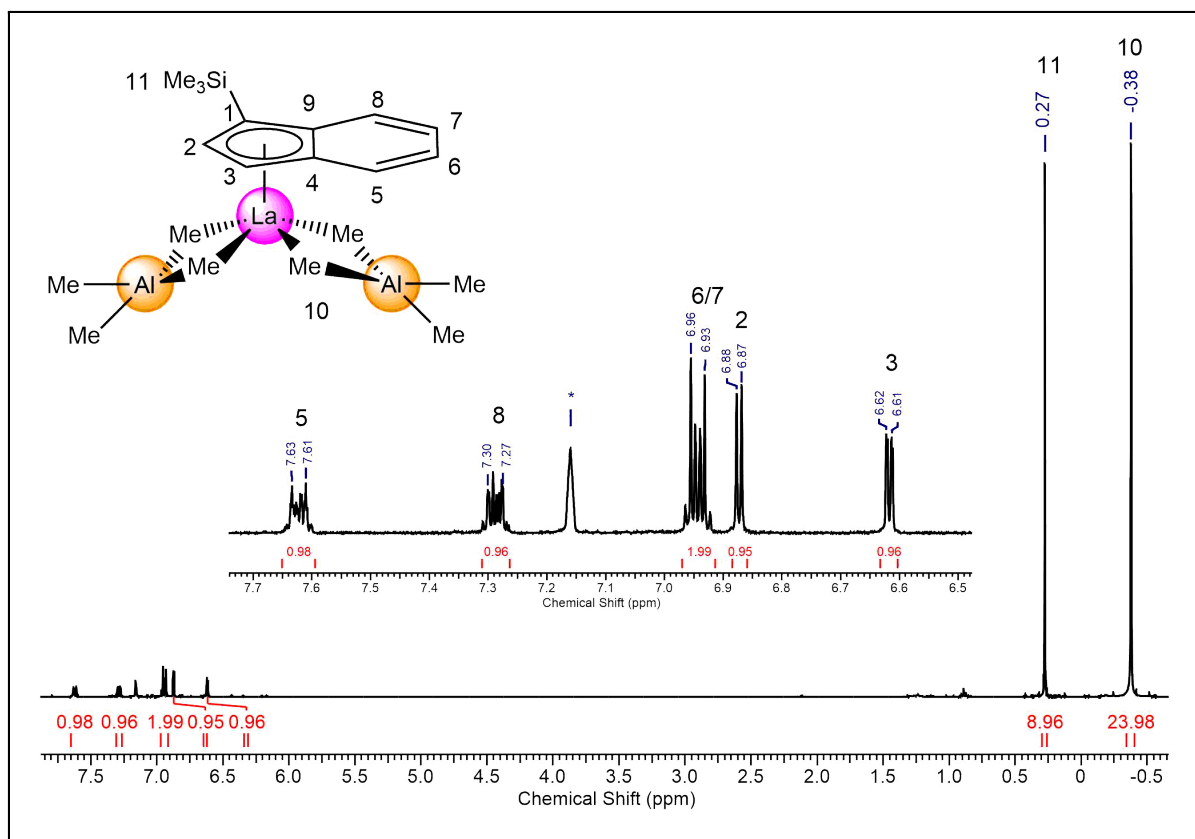


**Figure S13.**  $^1\text{H}$  NMR spectrum (400 MHz) of  $(\text{Ind}^{\text{Si}})\text{La}(\text{AlMe}_4)_2$  (**1d**) in  $\text{C}_6\text{D}_6$  at  $26^\circ\text{C}$ .

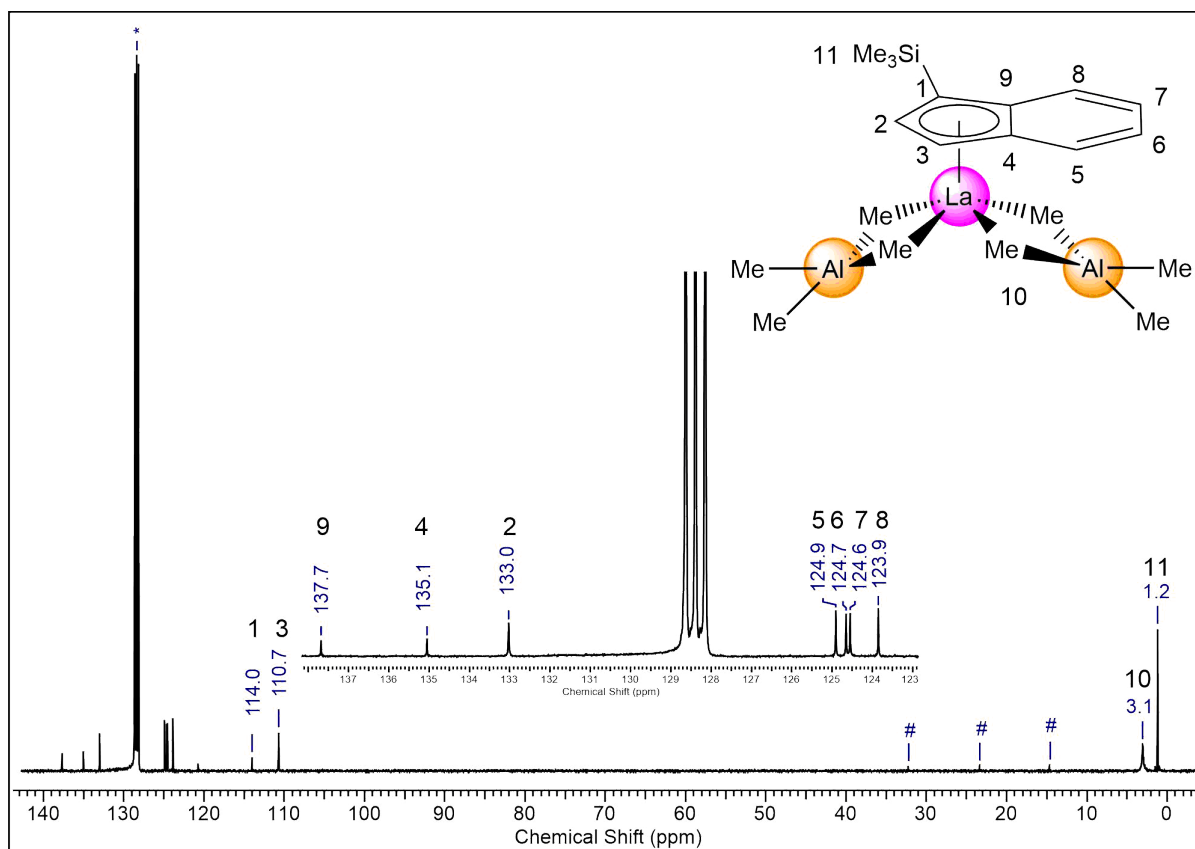


**Figure S14.**  $^{13}\text{C}\{^1\text{H}\}$  NMR spectrum (101 MHz) of  $(\text{Ind}^{\text{Si}})\text{La}(\text{AlMe}_4)_2$  (**1d**) in  $\text{C}_6\text{D}_6$  at  $26^\circ\text{C}$ . Residual *n*-hexane marked with #.

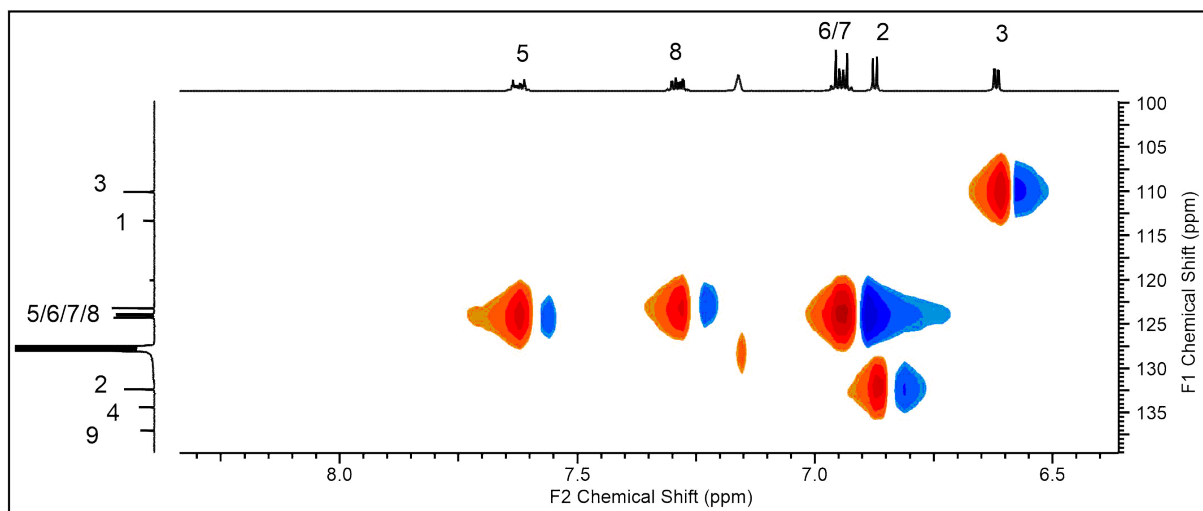
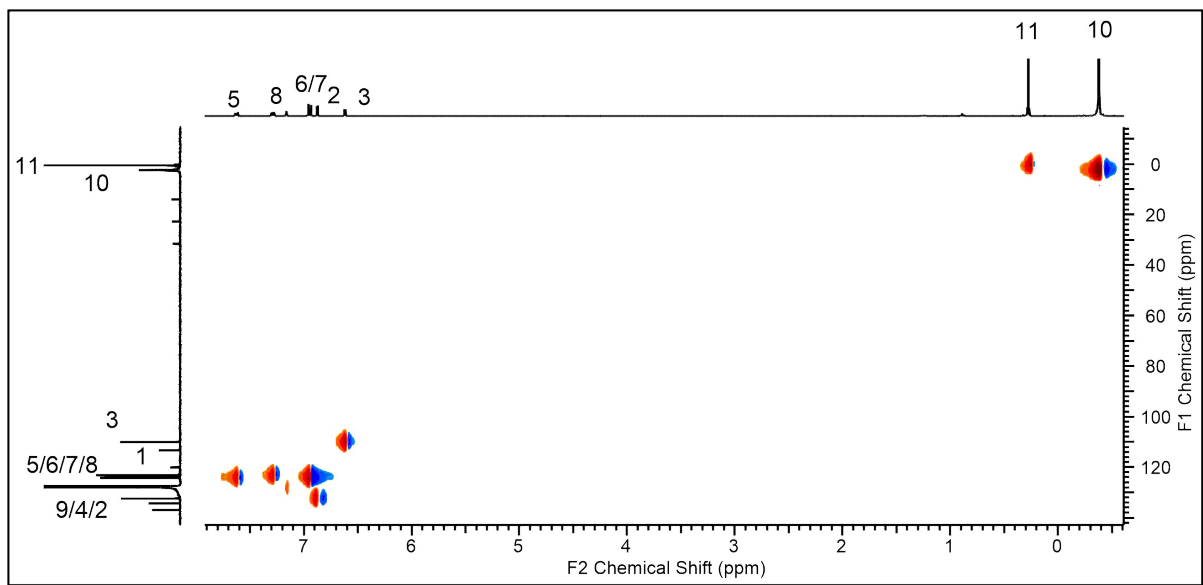


**Figure S15.**  $^1\text{H}/^{13}\text{C}$ -HSQC NMR spectrum (400/101 MHz) of  $(\text{Ind}^{\text{Si}})\text{La}(\text{AlMe}_4)_2$  (**1d**) in  $\text{C}_6\text{D}_6$  at  $26^\circ\text{C}$ , including an enlarged section.



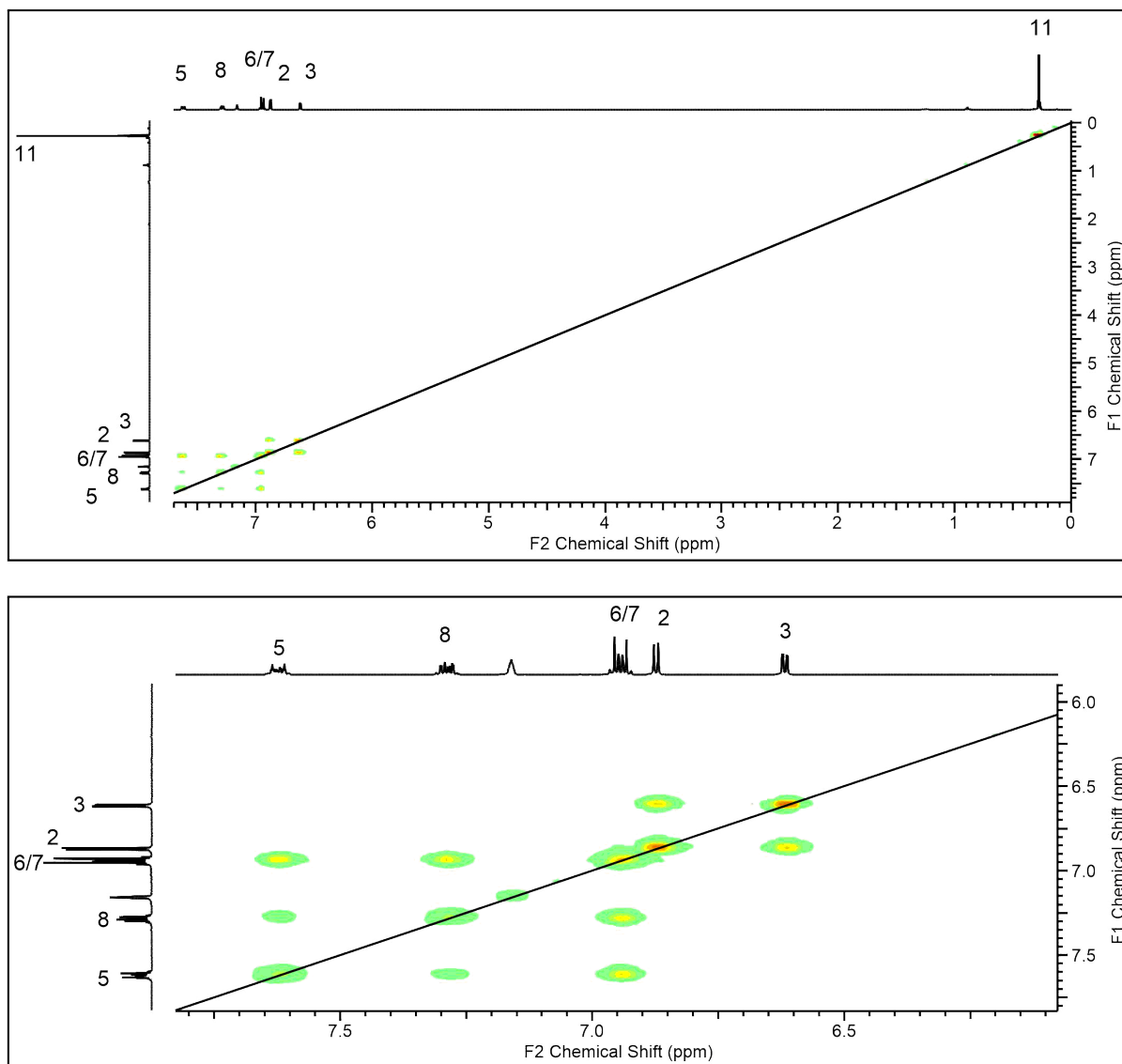


**Figure S16.**  $^1\text{H}$ - $^1\text{H}$ -COSY NMR spectrum (400/400 MHz) of  $(\text{Ind}^{\text{Si}})\text{La}(\text{AlMe}_4)_2$  (**1d**) in  $\text{C}_6\text{D}_6$  at  $26\text{ }^\circ\text{C}$ , including an enlarged section.

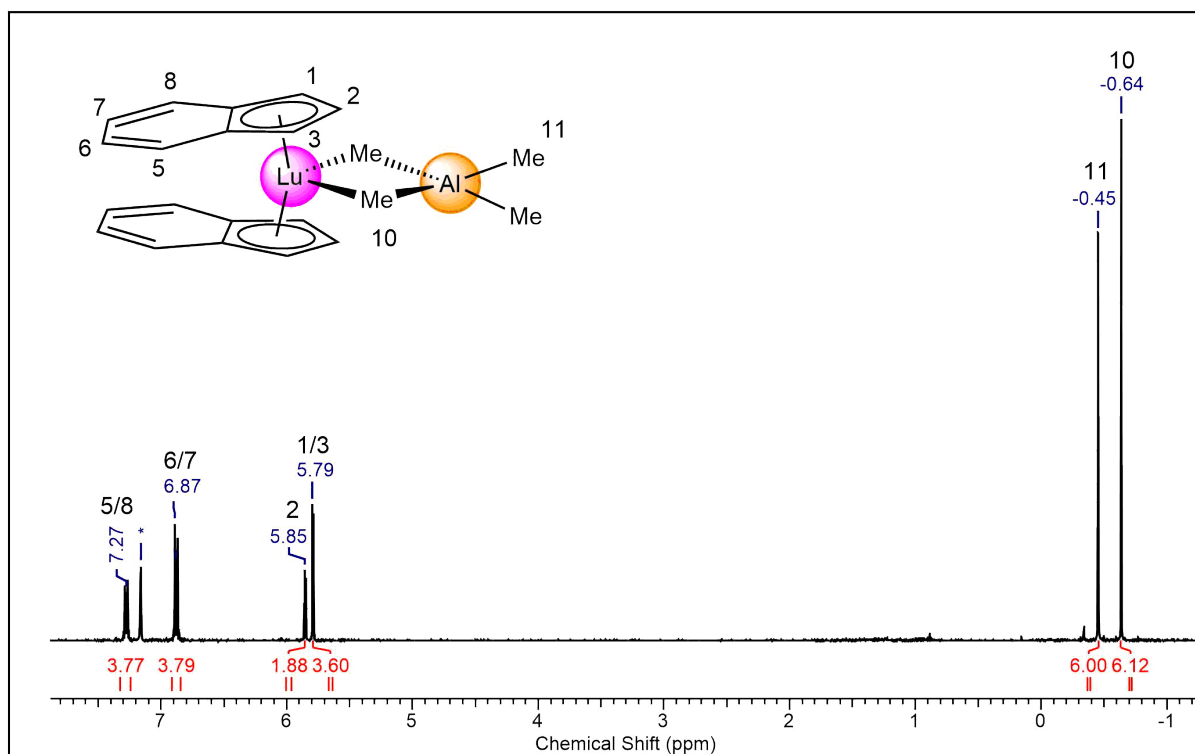


**Figure S17.**  $^1\text{H}$  NMR spectrum (400 MHz) of  $(\text{Ind})_2\text{Lu}(\text{AlMe}_4)$  (**2a**) in  $\text{C}_6\text{D}_6$  at  $26\text{ }^\circ\text{C}$ .

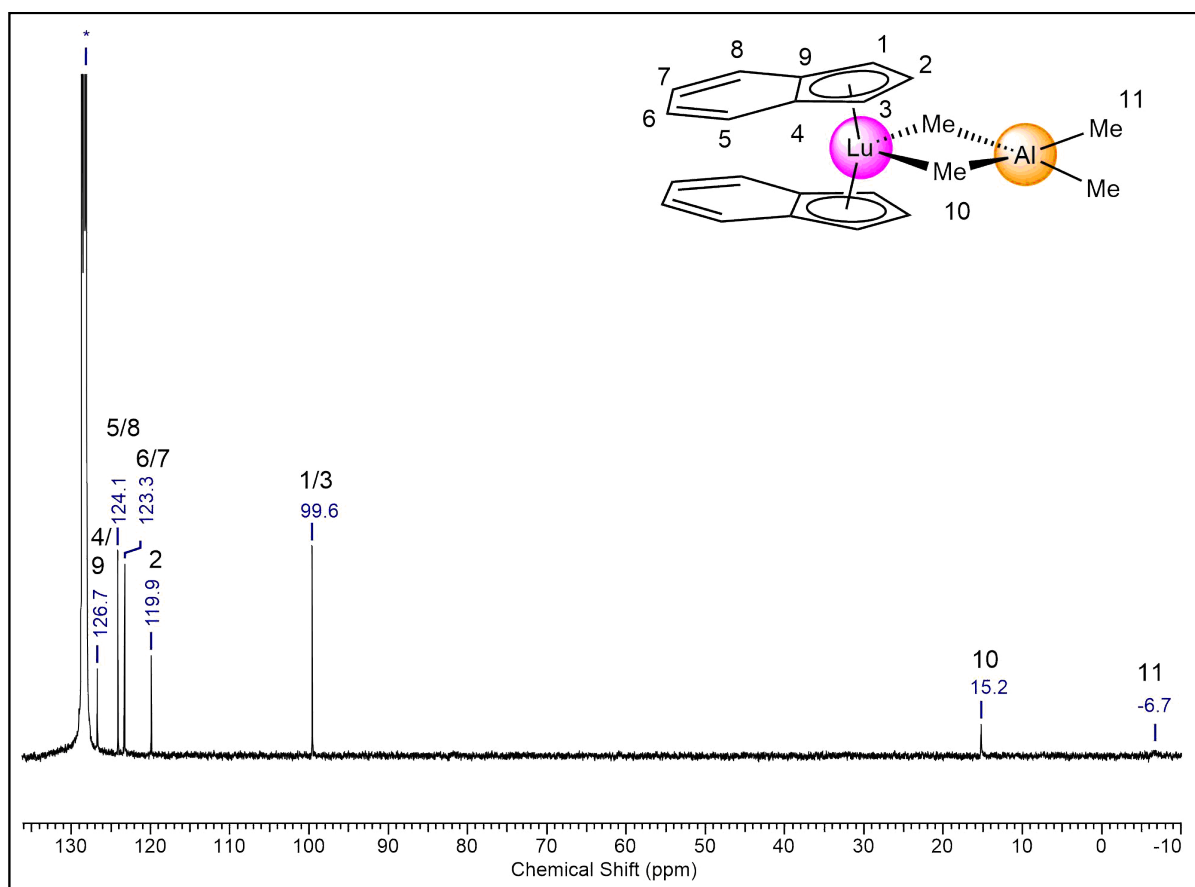


**Figure S18.**  $^{13}\text{C}\{^1\text{H}\}$  NMR spectrum (101 MHz) of  $(\text{Ind})_2\text{Lu}(\text{AlMe}_4)$  (**2a**) in  $\text{C}_6\text{D}_6$  at  $26\text{ }^\circ\text{C}$ .

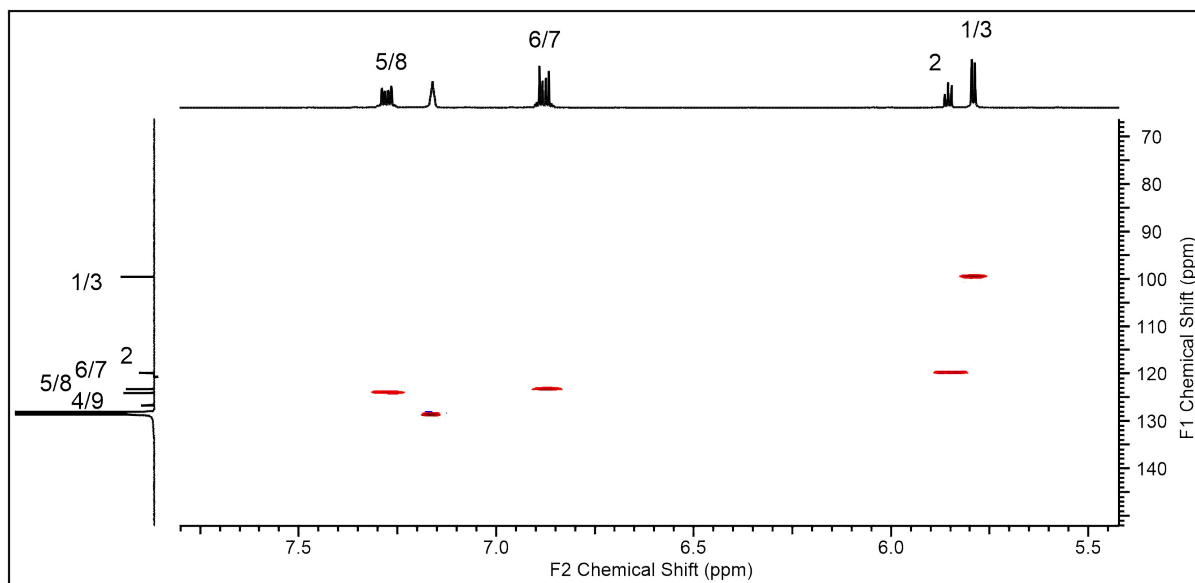


**Figure S19.** Section of the  $^1\text{H}^{13}\text{C}$ -HSQC NMR spectrum (400/101 MHz) of  $(\text{Ind})_2\text{Lu}(\text{AlMe}_4)$  (**2a**) in  $\text{C}_6\text{D}_6$  at 26 °C.

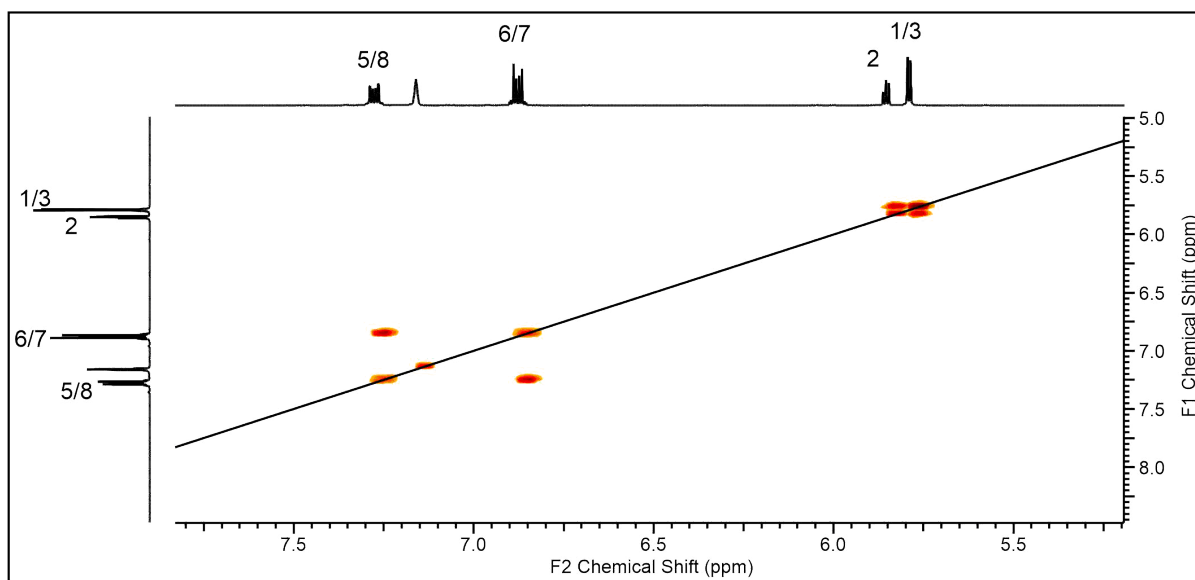


**Figure S20.** Section of the  $^1\text{H}^1\text{H}$ -COSY NMR spectrum (400/400 MHz) of  $(\text{Ind})_2\text{Lu}(\text{AlMe}_4)$  (**2a**) in  $\text{C}_6\text{D}_6$  at 26 °C.

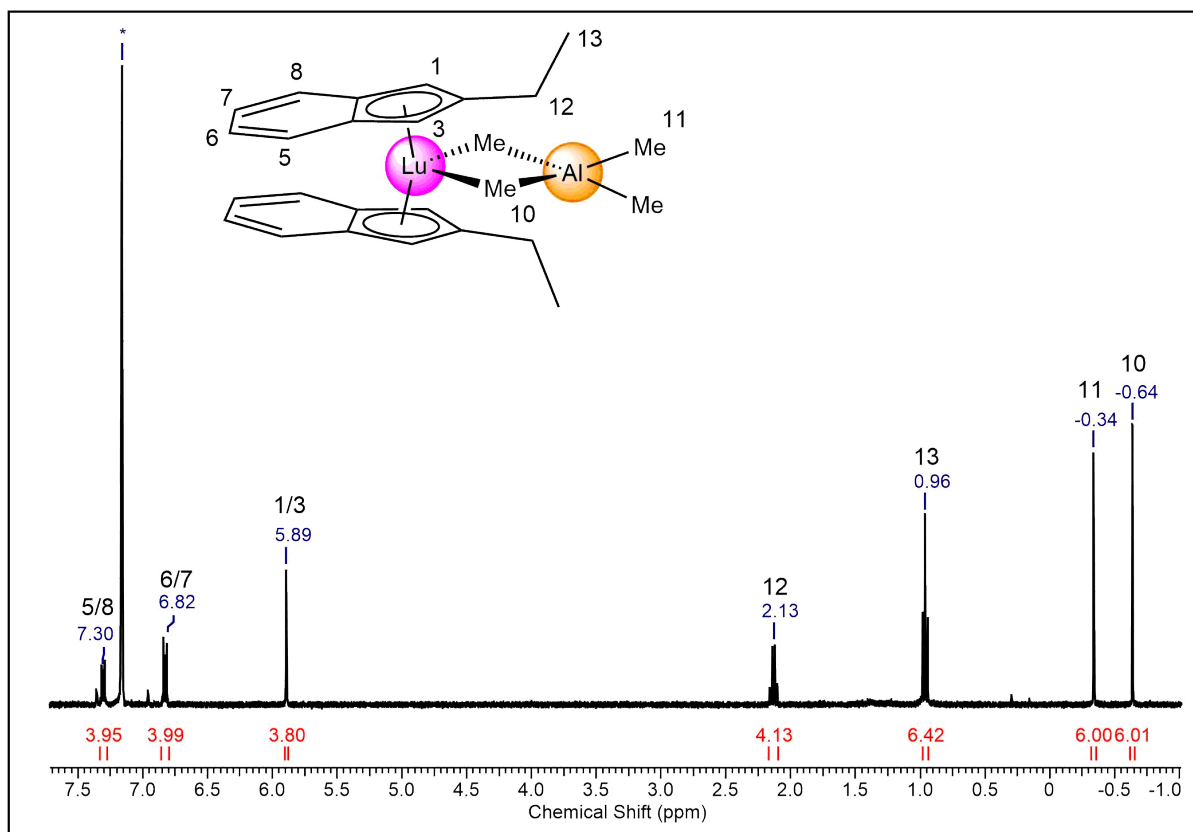


Figure S21.  $^1\text{H}$  NMR spectrum (400 MHz) of  $(\text{Ind}^{\text{Et}})_2\text{Lu}(\text{AlMe}_4)$  (**2b**) in  $\text{C}_6\text{D}_6$  at  $26^\circ\text{C}$ .

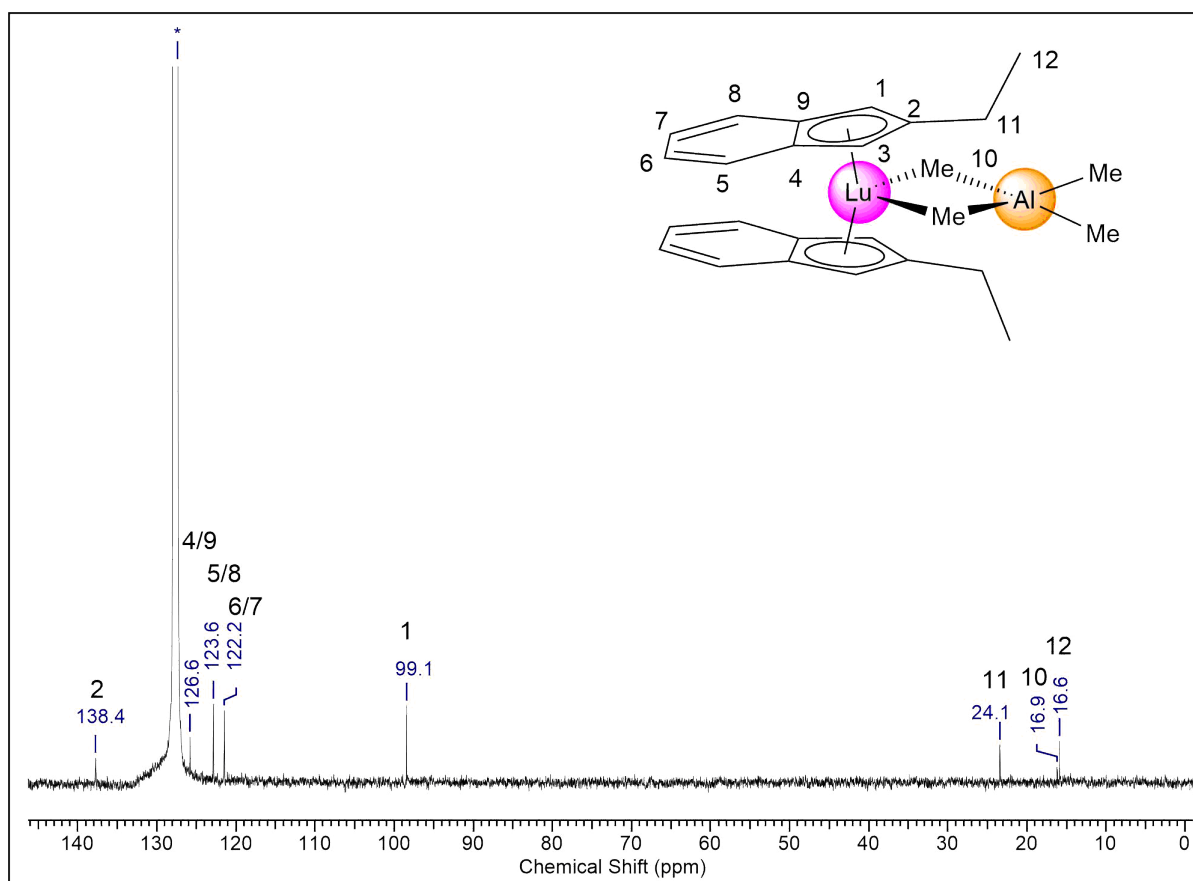
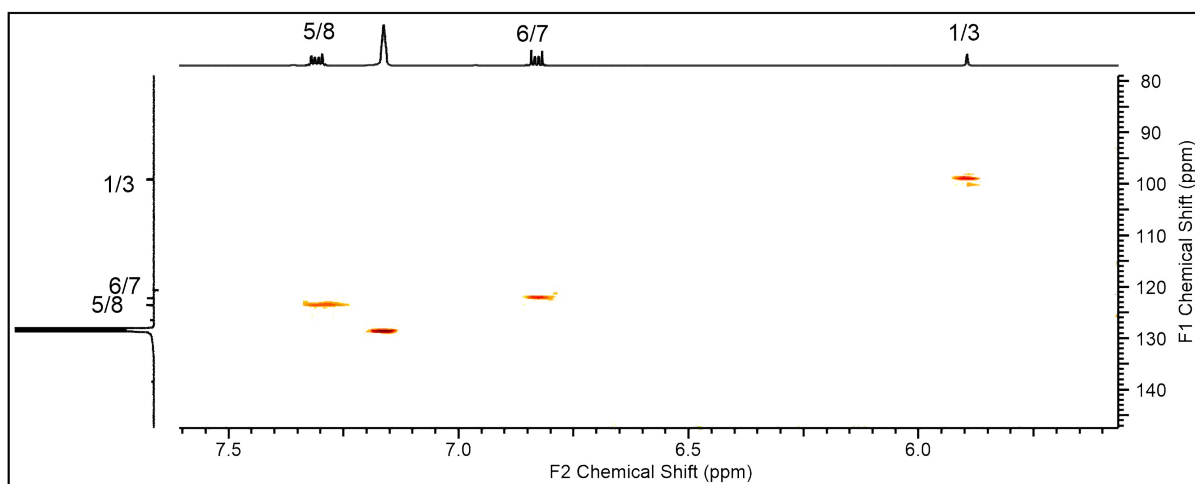
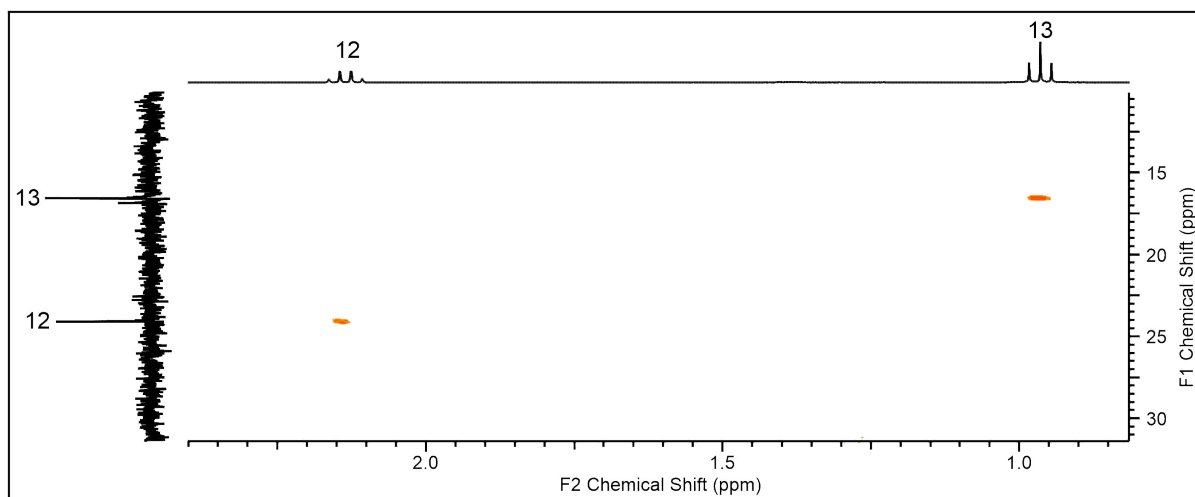
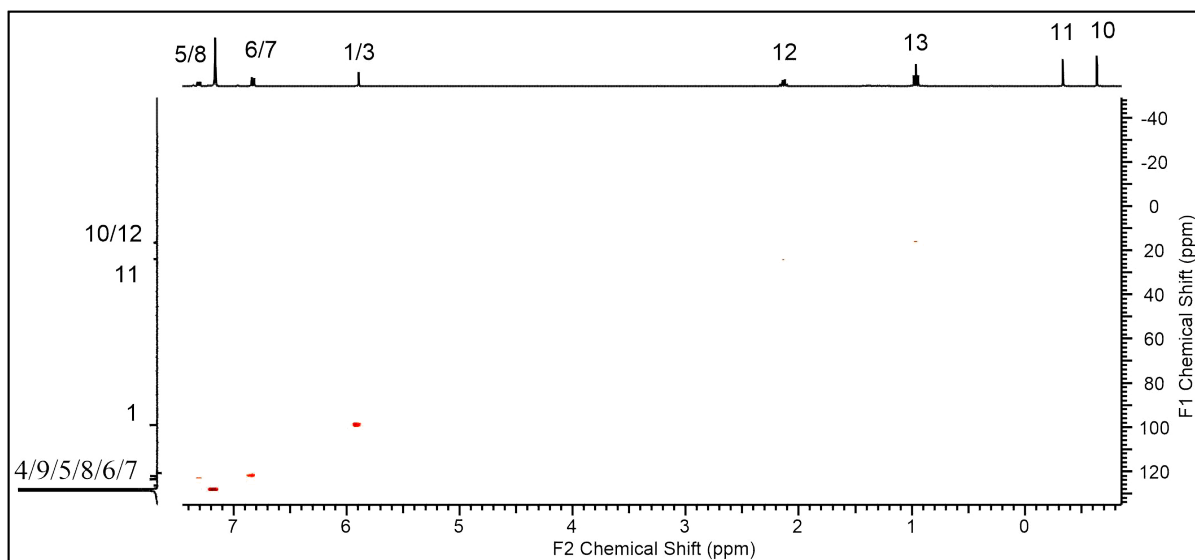
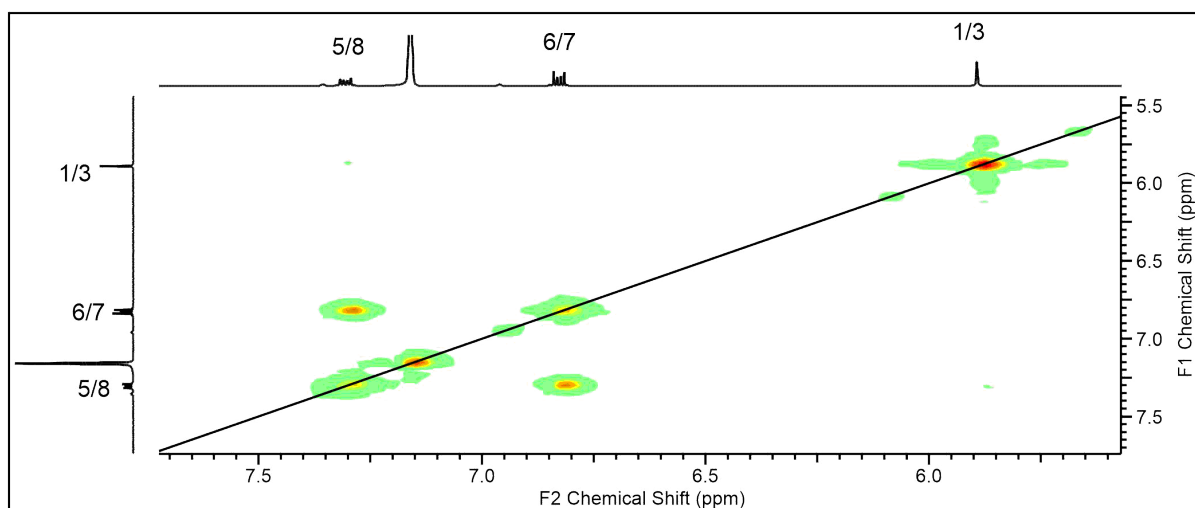
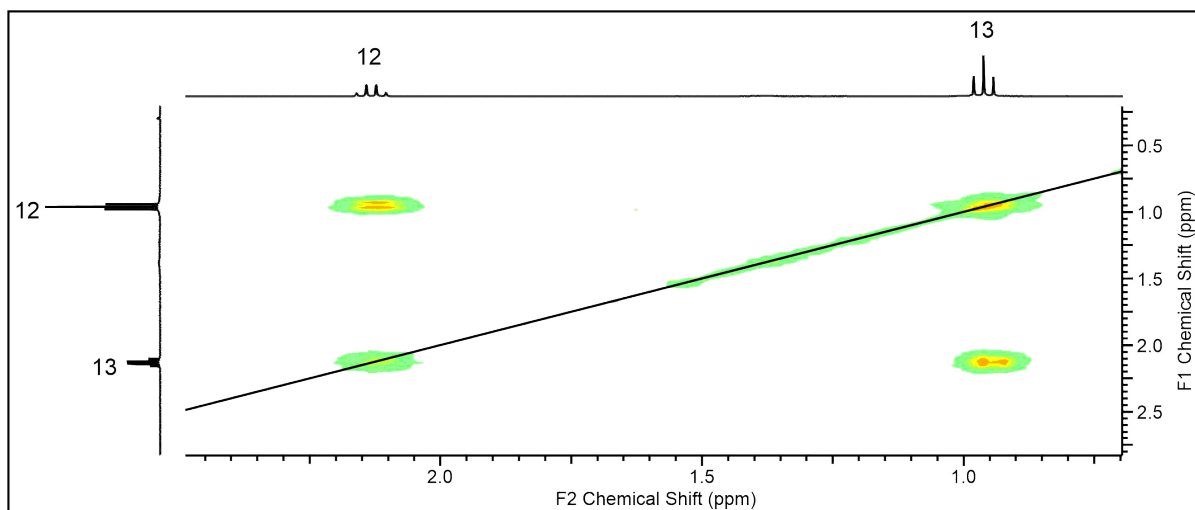
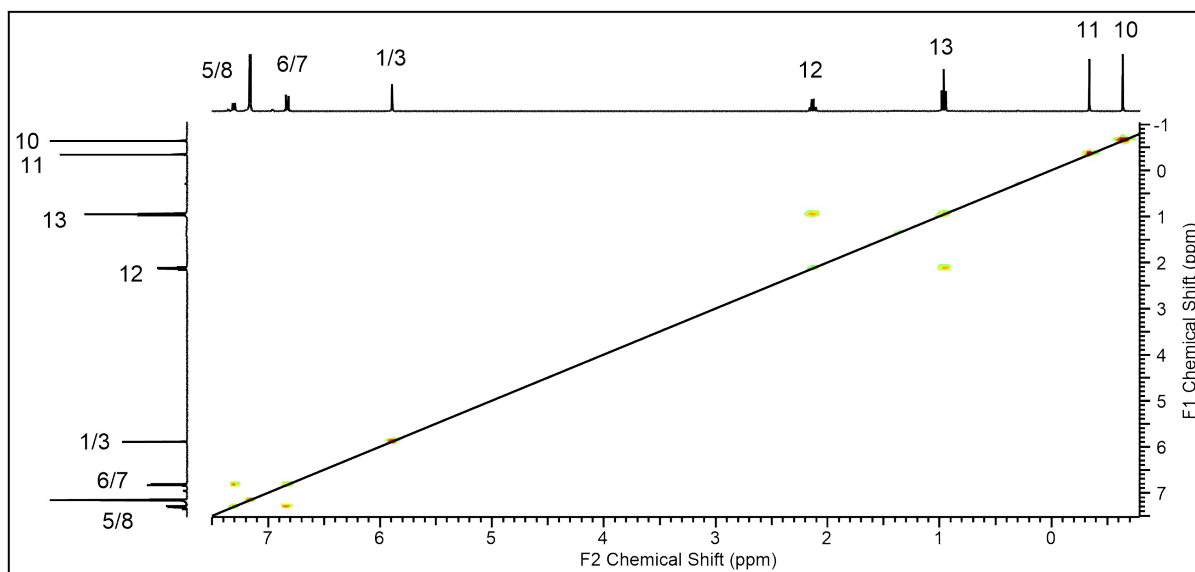


Figure S22.  $^{13}\text{C}\{^1\text{H}\}$  NMR spectrum (101 MHz) of  $(\text{Ind}^{\text{Et}})_2\text{Lu}(\text{AlMe}_4)$  (**2b**) in  $\text{C}_6\text{D}_6$  at  $26^\circ\text{C}$ .



**Figure S23.**  $^1\text{H}^{13}\text{C}$ -HSQC NMR spectrum (400/101 MHz) of  $(\text{Ind}^{\text{Et}})_2\text{La}(\text{AlMe}_4)$  (**2b**) in  $\text{C}_6\text{D}_6$  at  $26\text{ }^\circ\text{C}$ , including enlarged sections.



**Figure S24.**  $^1\text{H}$ - $^1\text{H}$ -COSY NMR spectrum (400/400 MHz) of  $(\text{Ind}^{\text{Et}})_2\text{Lu}(\text{AlMe}_4)$  (**2b**) in  $\text{C}_6\text{D}_6$  at  $26\text{ }^\circ\text{C}$ , including enlarged sections.

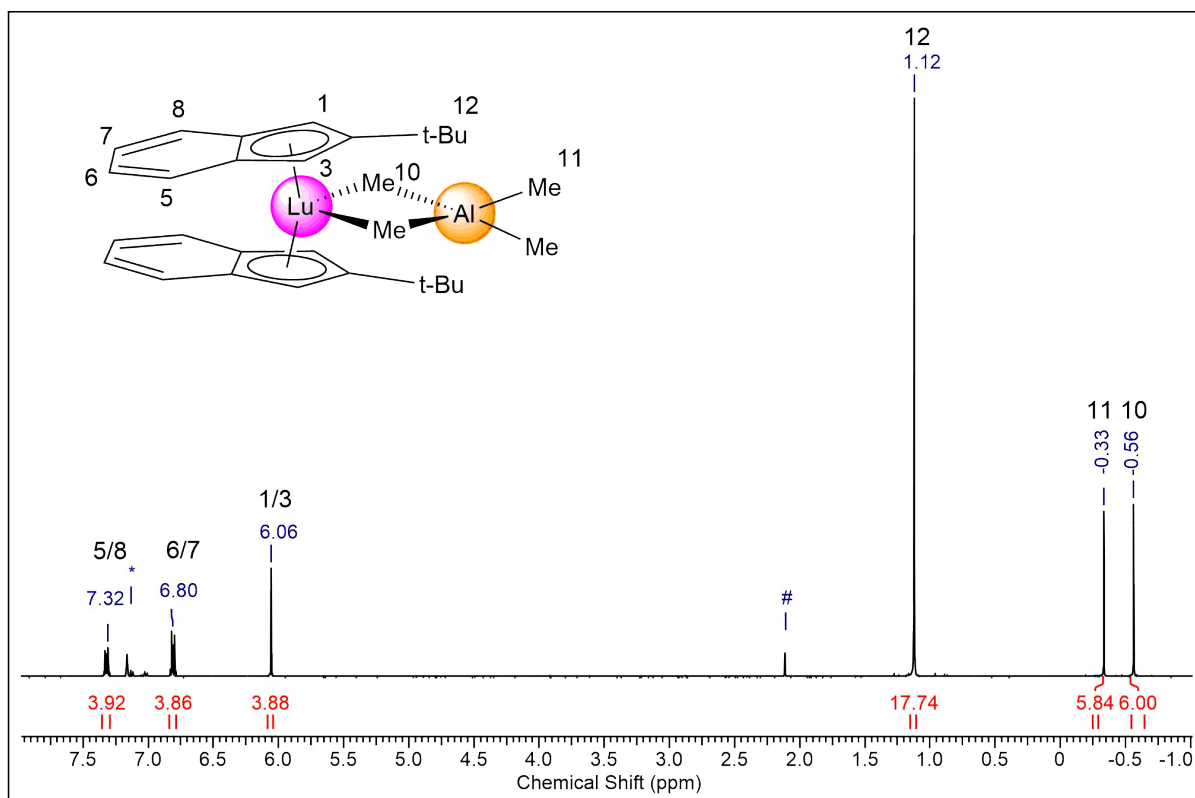


**Figure S25.**  $^1\text{H}$  NMR spectrum (400 MHz) of  $(\text{Ind}^{\text{tBu}})_2\text{Lu}(\text{AlMe}_4)$  (**2c**) in  $\text{C}_6\text{D}_6$  at  $26^\circ\text{C}$ . Residual toluene marked with #.

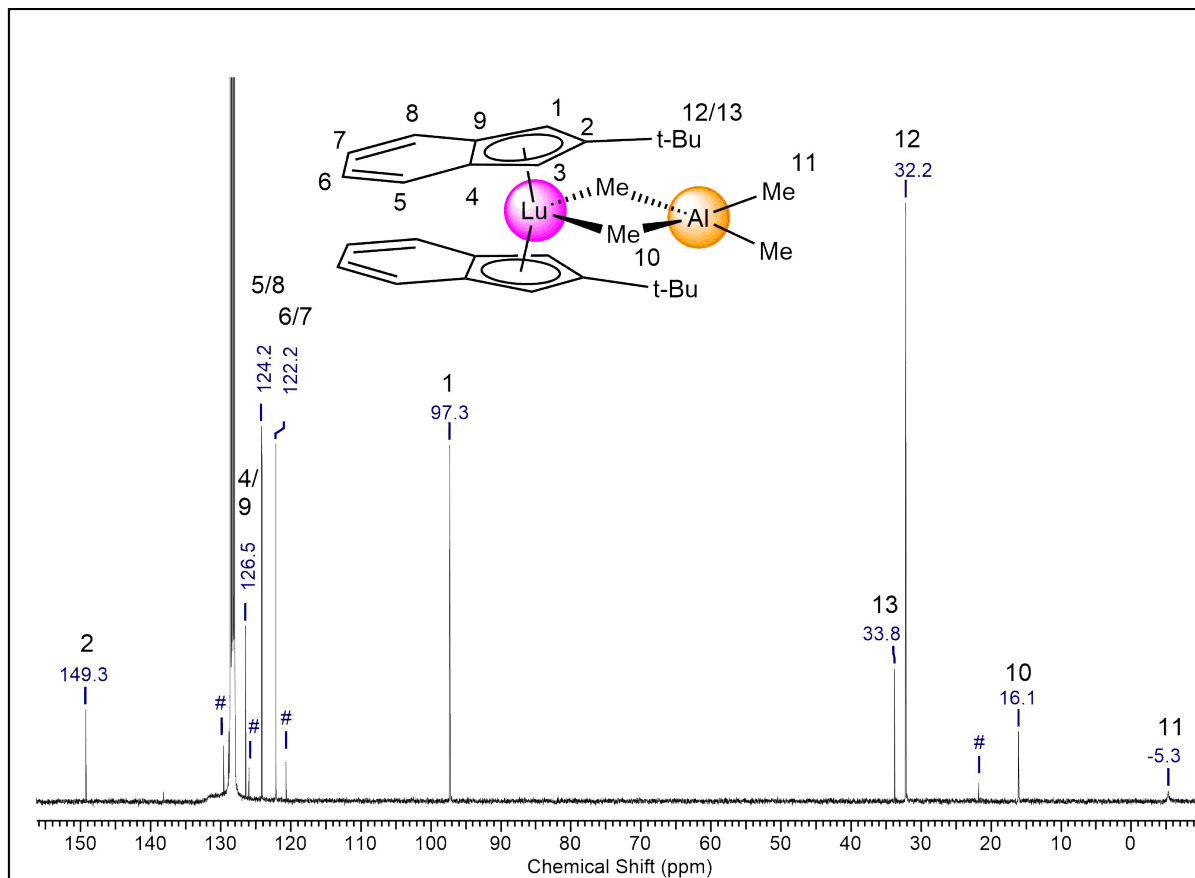


**Figure S26.**  $^{13}\text{C}\{^1\text{H}\}$  NMR spectrum (101 MHz) of  $(\text{Ind}^{\text{tBu}})_2\text{Lu}(\text{AlMe}_4)$  (**2c**) in  $\text{C}_6\text{D}_6$  at  $26^\circ\text{C}$ . Residual toluene marked with #.

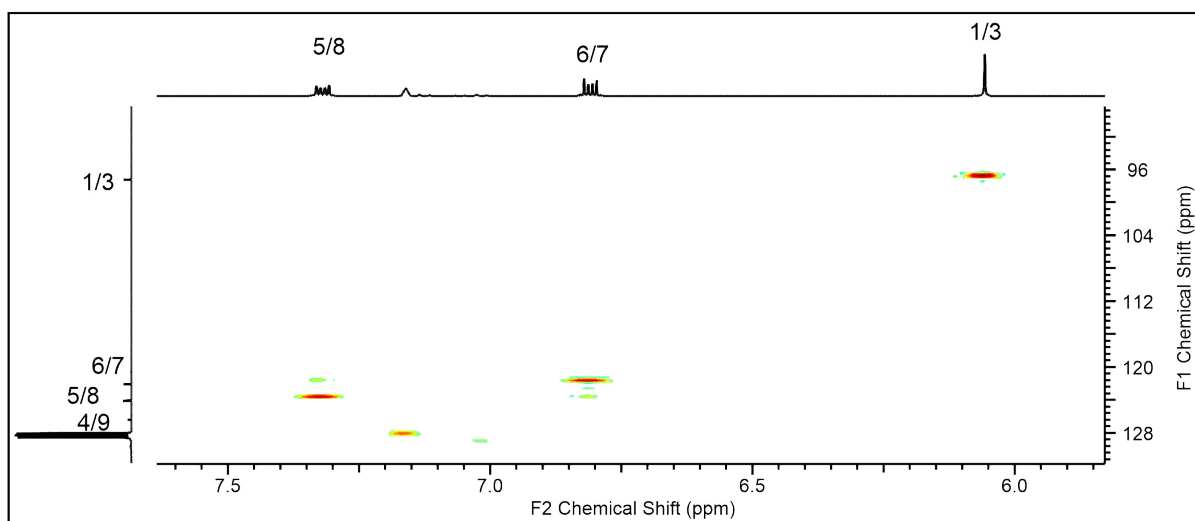
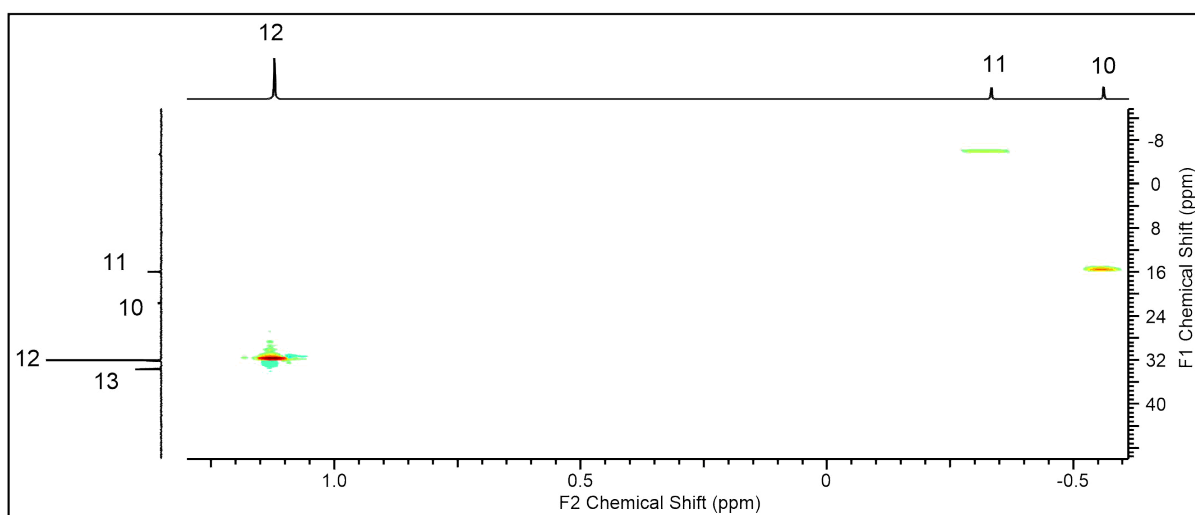
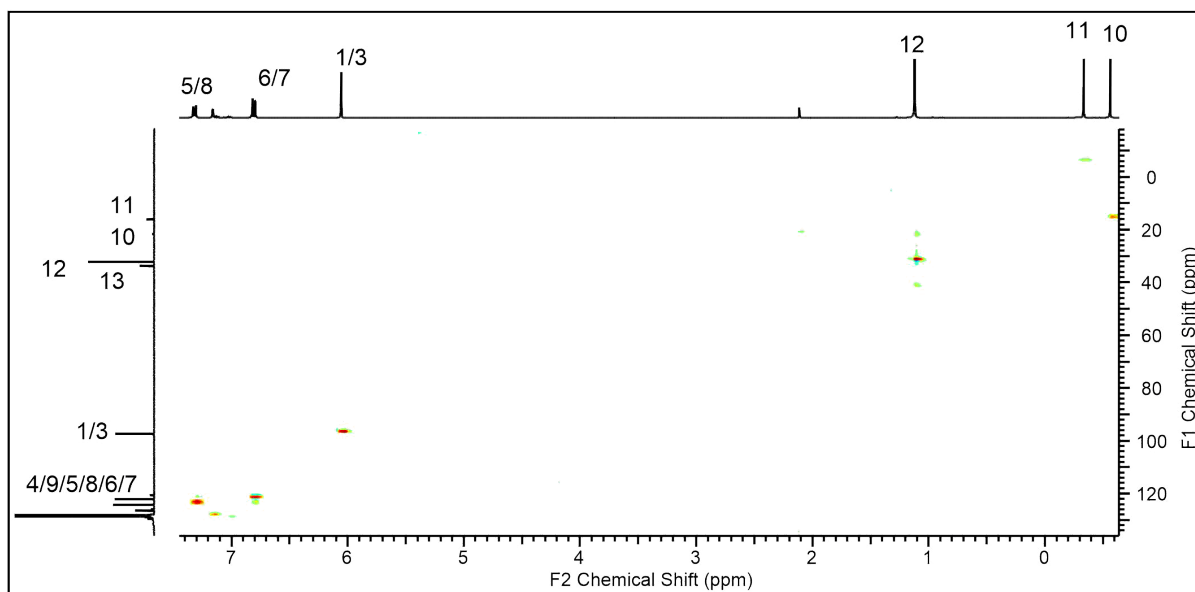


**Figure S27.** Section of  $^1\text{H}/^{13}\text{C}$ -HSQC NMR spectrum (400/101 MHz) of  $(\text{Ind}^{\text{Biu}})_2\text{Lu}(\text{AlMe}_4)$  (**2c**) in  $\text{C}_6\text{D}_6$  at 26 °C, including enlarged sections.



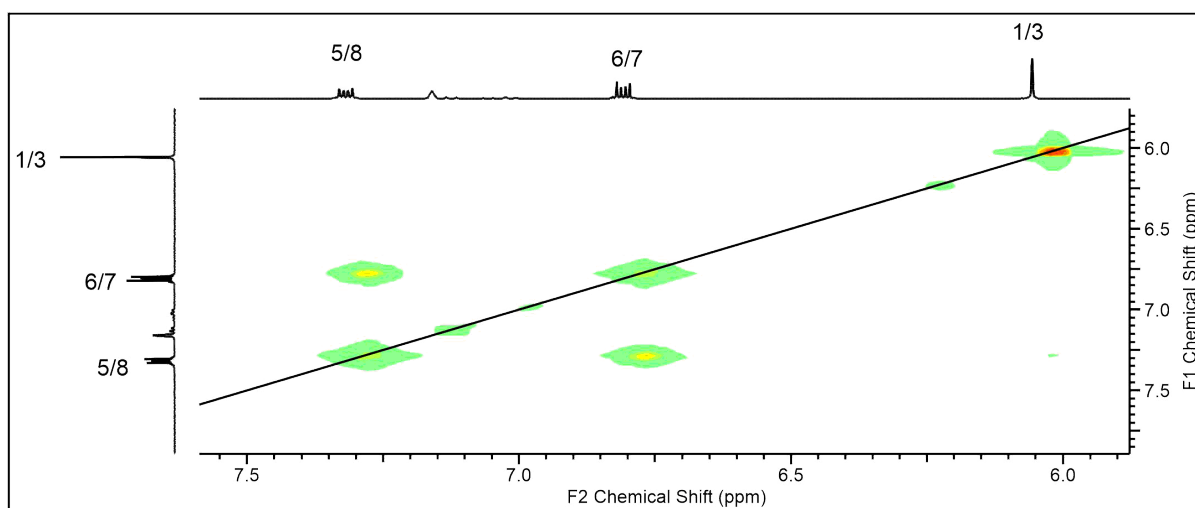
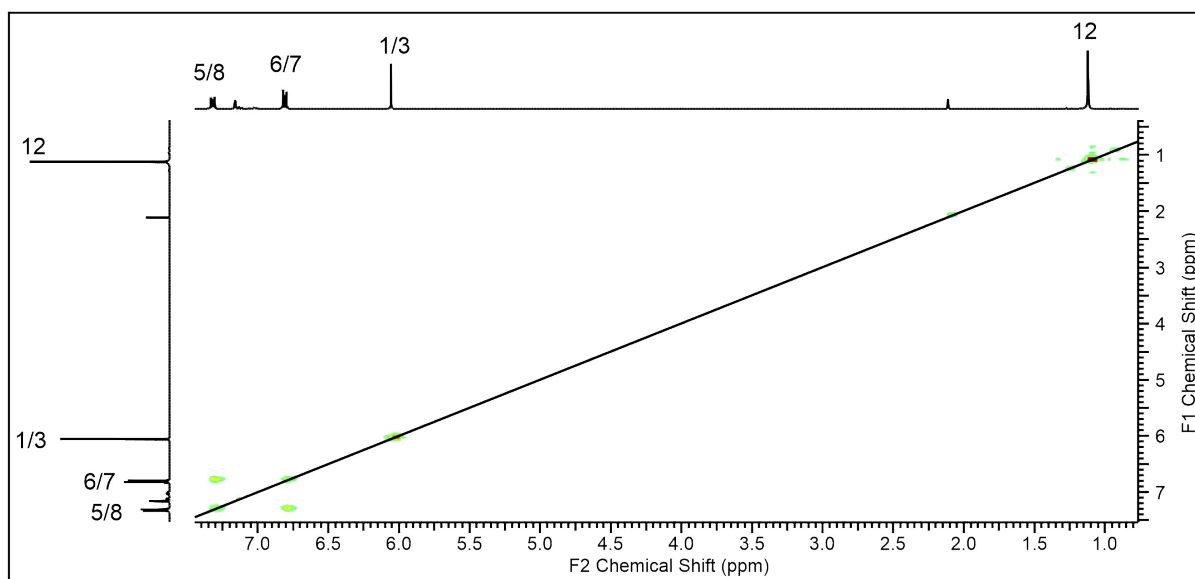


**Figure S28.**  $^1\text{H}$ -COSY NMR spectrum (400/400 MHz) of  $(\text{Ind}^{t\text{Bu}})_2\text{Lu}(\text{AlMe}_4)$  (**2c**) in  $\text{C}_6\text{D}_6$  at  $26^\circ\text{C}$ , including an enlarged section.

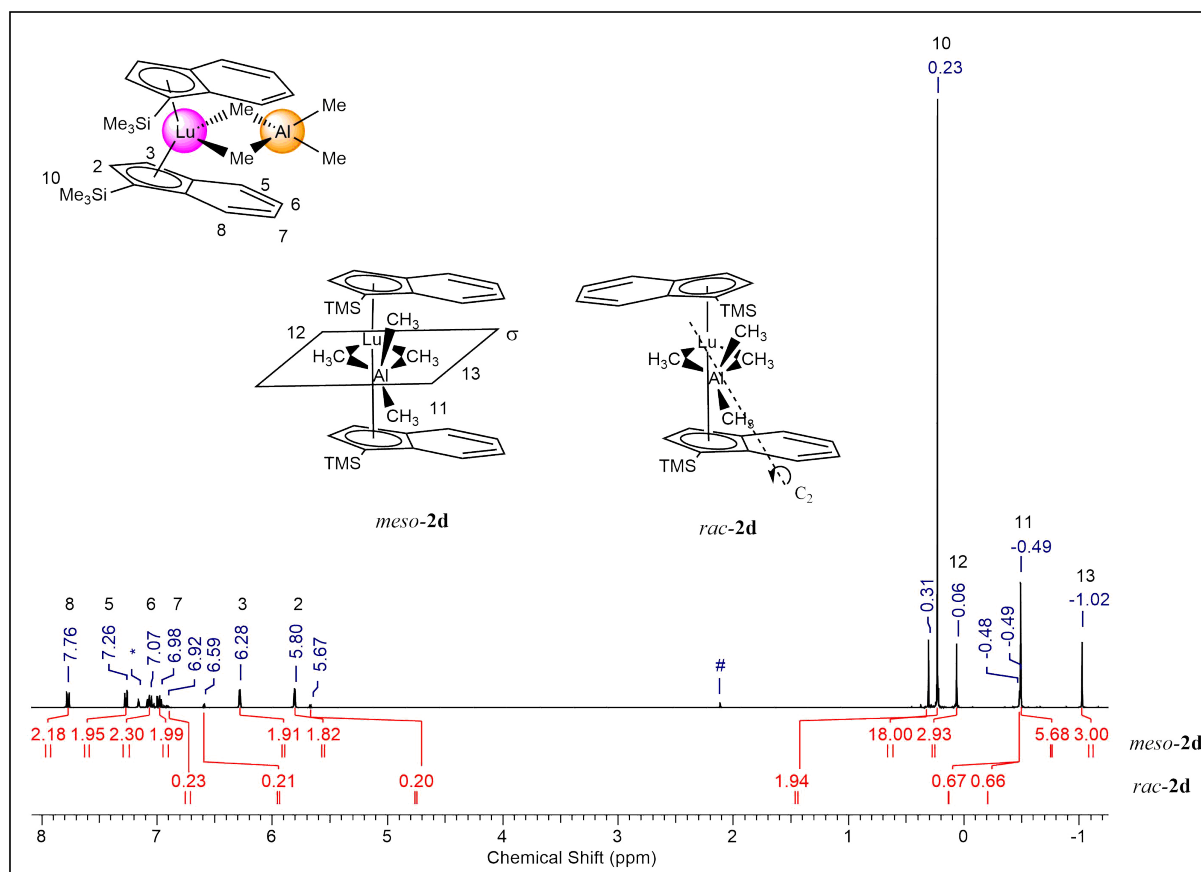


Figure S29.  $^1\text{H}$  NMR spectrum (400 MHz) of  $(\text{Ind}^{\text{Si}})_2\text{Lu}(\text{AlMe}_4)$  (**2d**) in  $\text{C}_6\text{D}_6$  at  $26^\circ\text{C}$ .

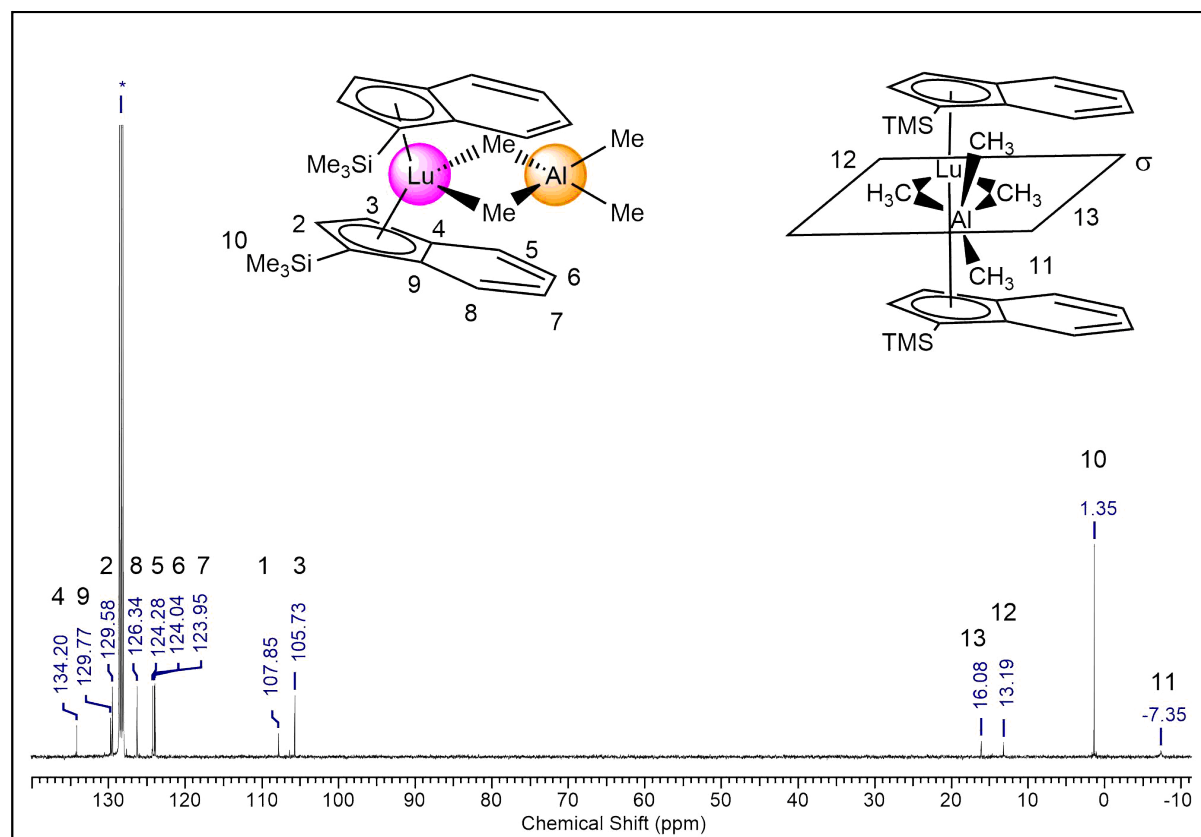
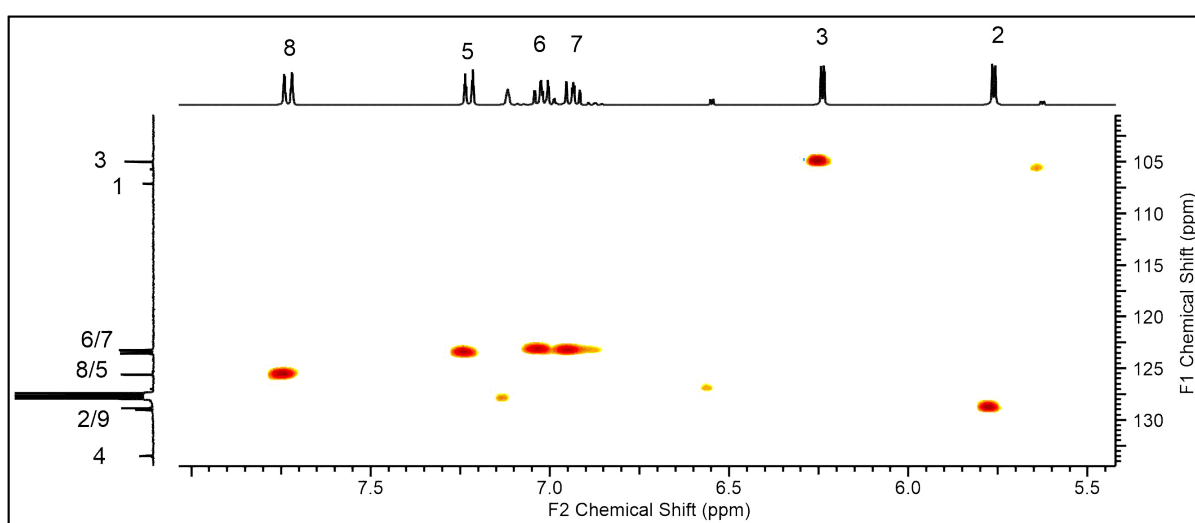
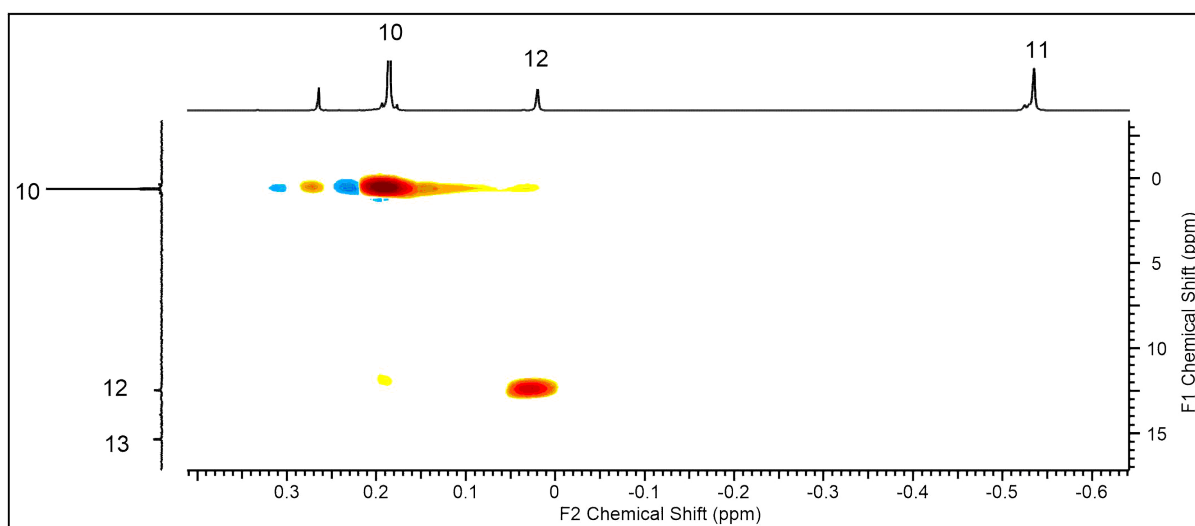
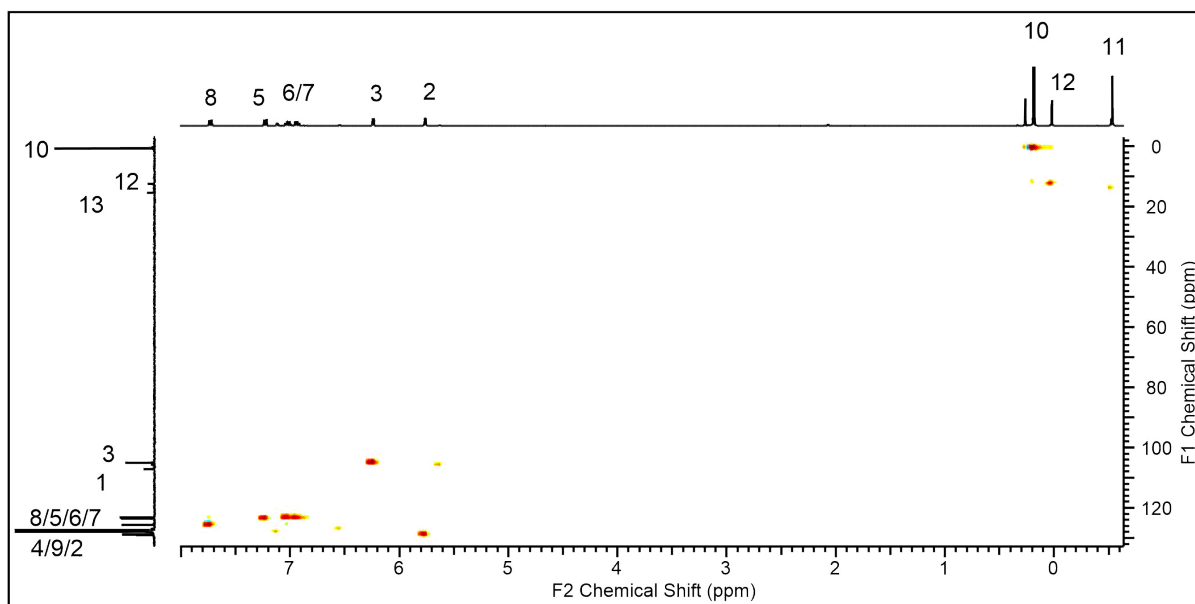
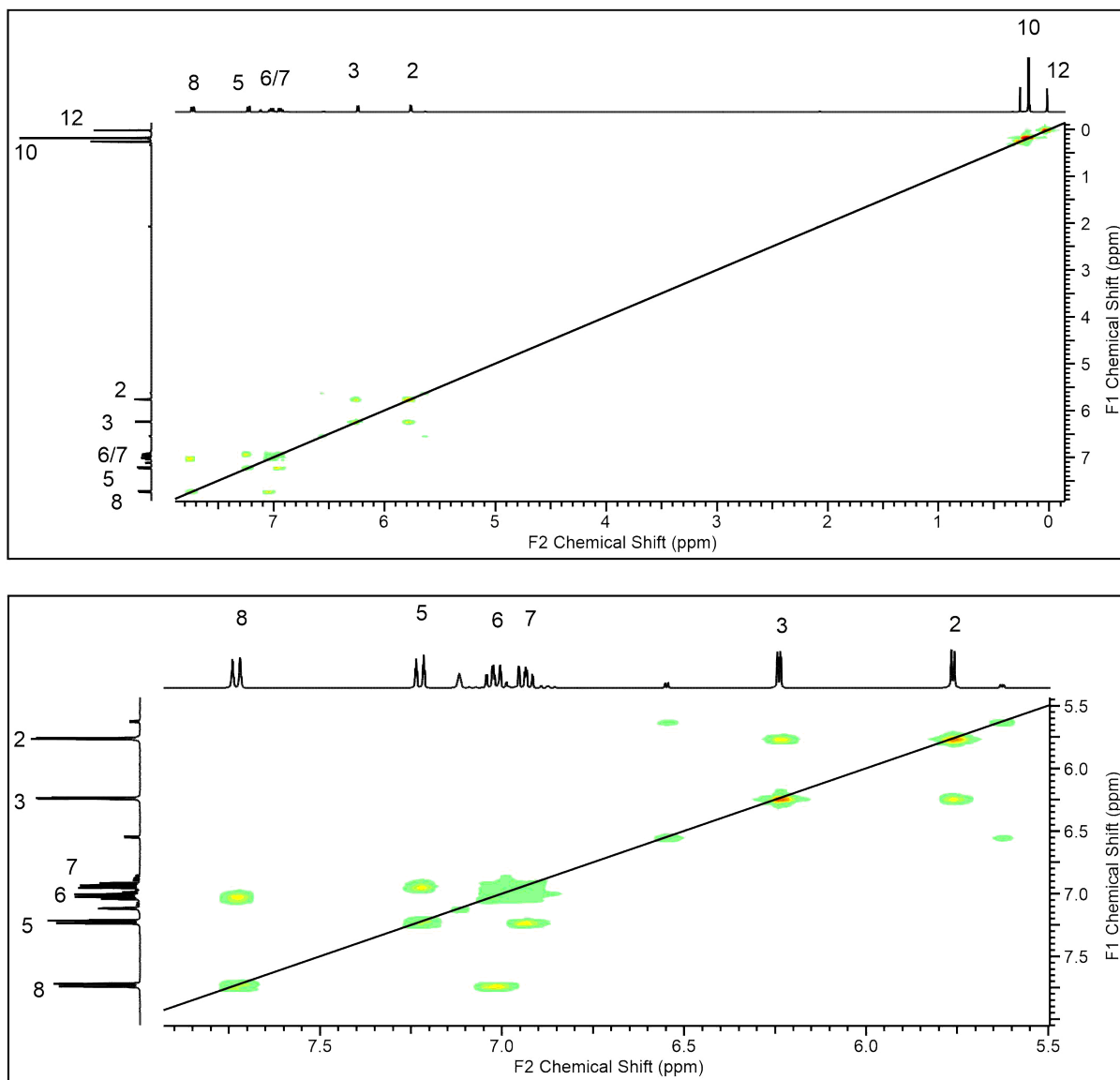


Figure S30.  $^{13}\text{C}\{^1\text{H}\}$  NMR spectrum (101 MHz) of  $(\text{Ind}^{\text{Si}})_2\text{Lu}(\text{AlMe}_4)$  (**2d**) in  $\text{C}_6\text{D}_6$  at  $26^\circ\text{C}$ .



**Figure S31.**  $^1\text{H}^{13}\text{C}$ -HSQC NMR spectrum (400/101 MHz) of  $(\text{Ind}^{\text{Si}})_2\text{Lu}(\text{AlMe}_4)$  (**2d**) in  $\text{C}_6\text{D}_6$  at 26 °C, including enlarged sections.



**Figure S32.**  $^1\text{H}$ - $^1\text{H}$ -COSY NMR spectrum (400/400 MHz) of  $(\text{Ind}^{\text{Si}})_2\text{Lu}(\text{AlMe}_4)$  (**2d**) in  $\text{C}_6\text{D}_6$  at  $26\text{ }^\circ\text{C}$ , including an enlarged section.

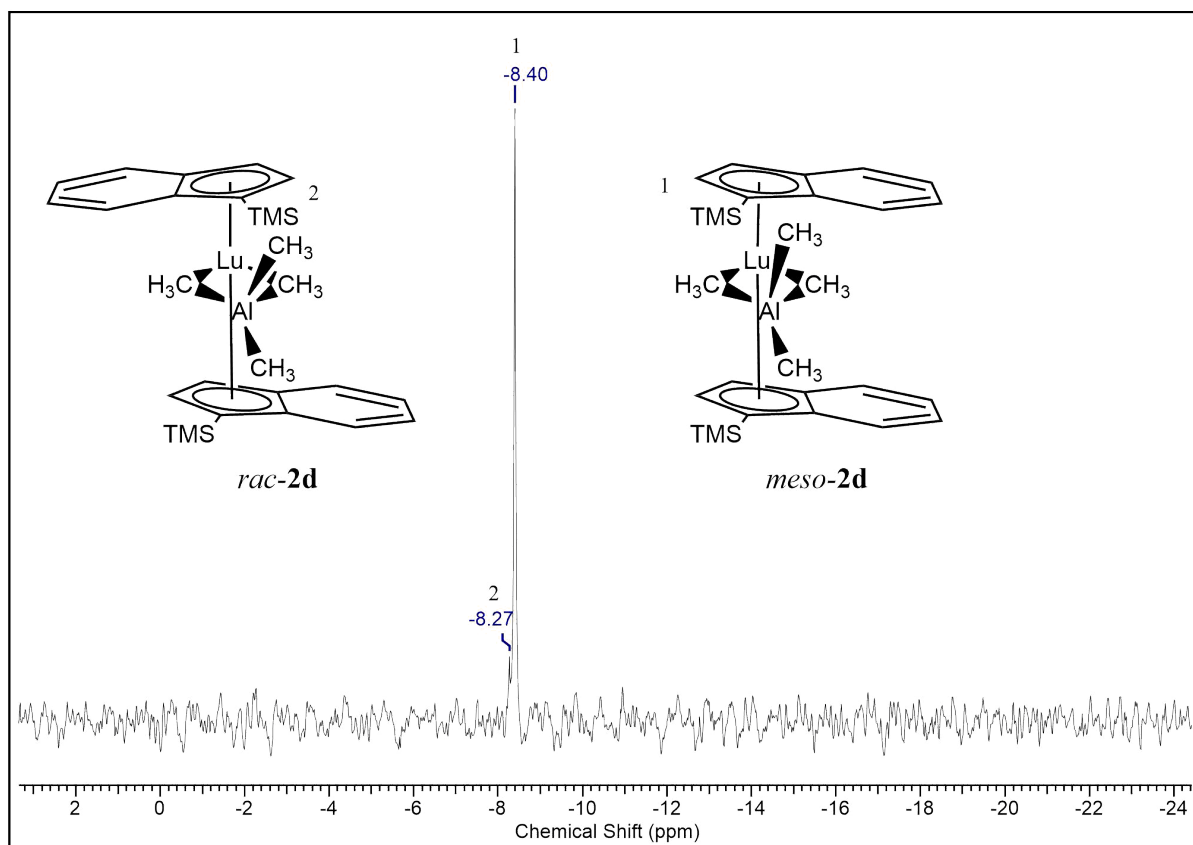


**Figure S33.**  $^{29}\text{Si}$ - $^1\text{H}$  DEPT45 NMR spectrum (50 MHz) of  $(\text{Ind}^{\text{Si}})_2\text{Lu}(\text{AlMe}_4)$  (**2d**) in  $\text{C}_6\text{D}_6$  at  $26\text{ }^\circ\text{C}$ .

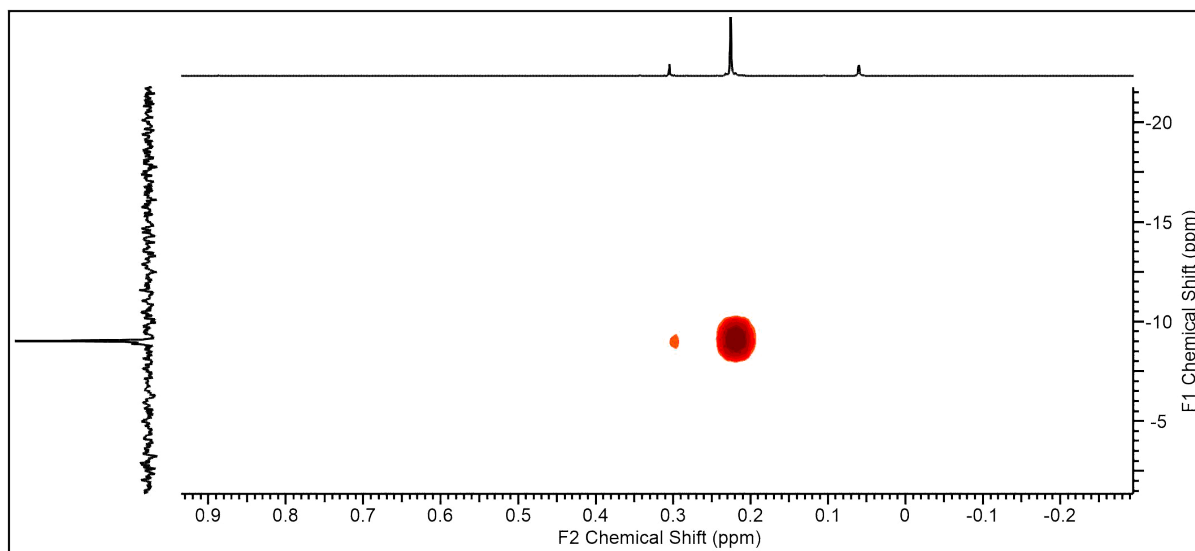


**Figure S34.**  $^1\text{H}$  $^{29}\text{Si}$ -HMBC NMR spectrum (500/99 MHz) of  $(\text{Ind}^{\text{Si}})_2\text{Lu}(\text{AlMe}_4)$  (**2d**) in  $\text{C}_6\text{D}_6$  at  $26\text{ }^\circ\text{C}$ .

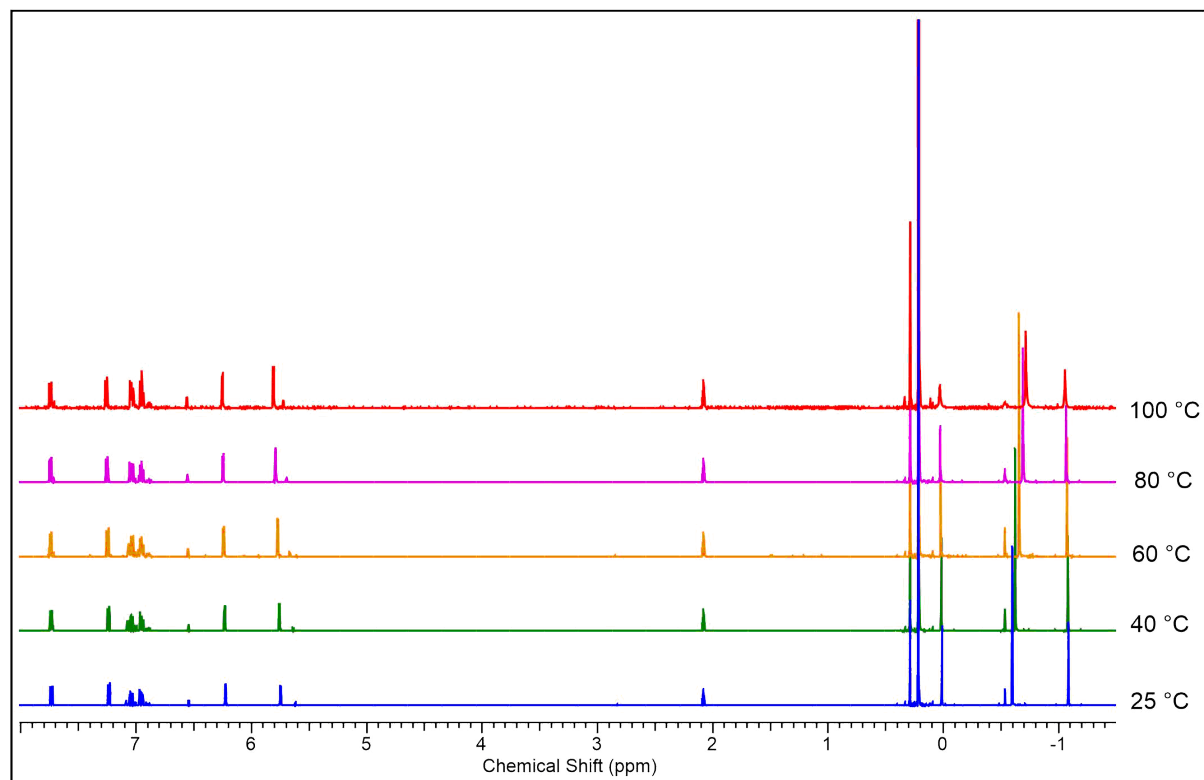


**Figure S35.** VT <sup>1</sup>H NMR spectrum (500 MHz) of (Ind<sup>Si</sup>)<sub>2</sub>Lu(AlMe<sub>4</sub>) (**2d**) in toluene-*d*<sub>8</sub>. From 25 °C to 100 °C.

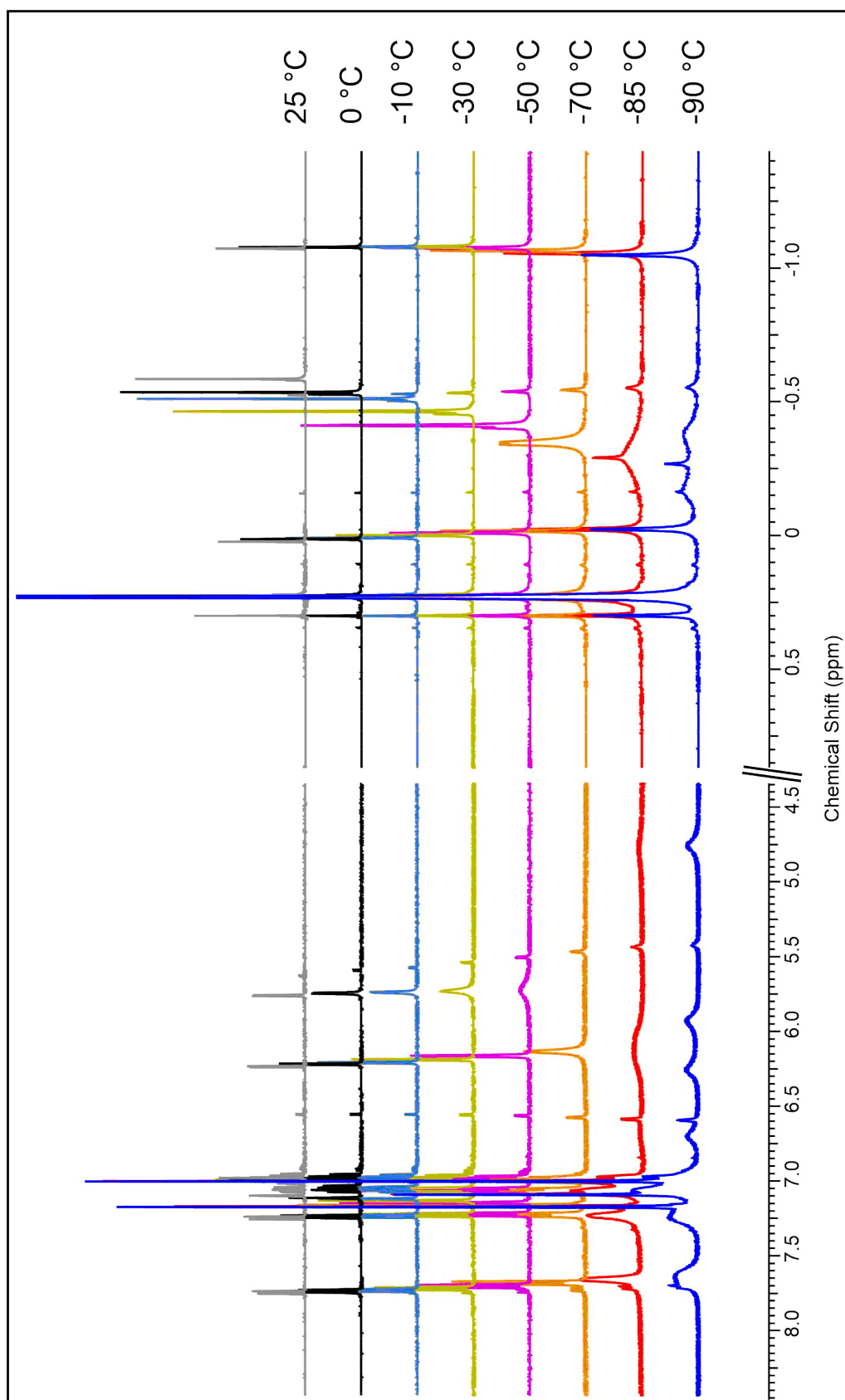


**Figure S36.** VT <sup>1</sup>H NMR spectrum (500 MHz) of (Ind<sup>Si</sup>)<sub>2</sub>Lu(AlMe<sub>4</sub>) (**2d**) in toluene-*d*<sub>8</sub>. From -90 °C to 25 °C.

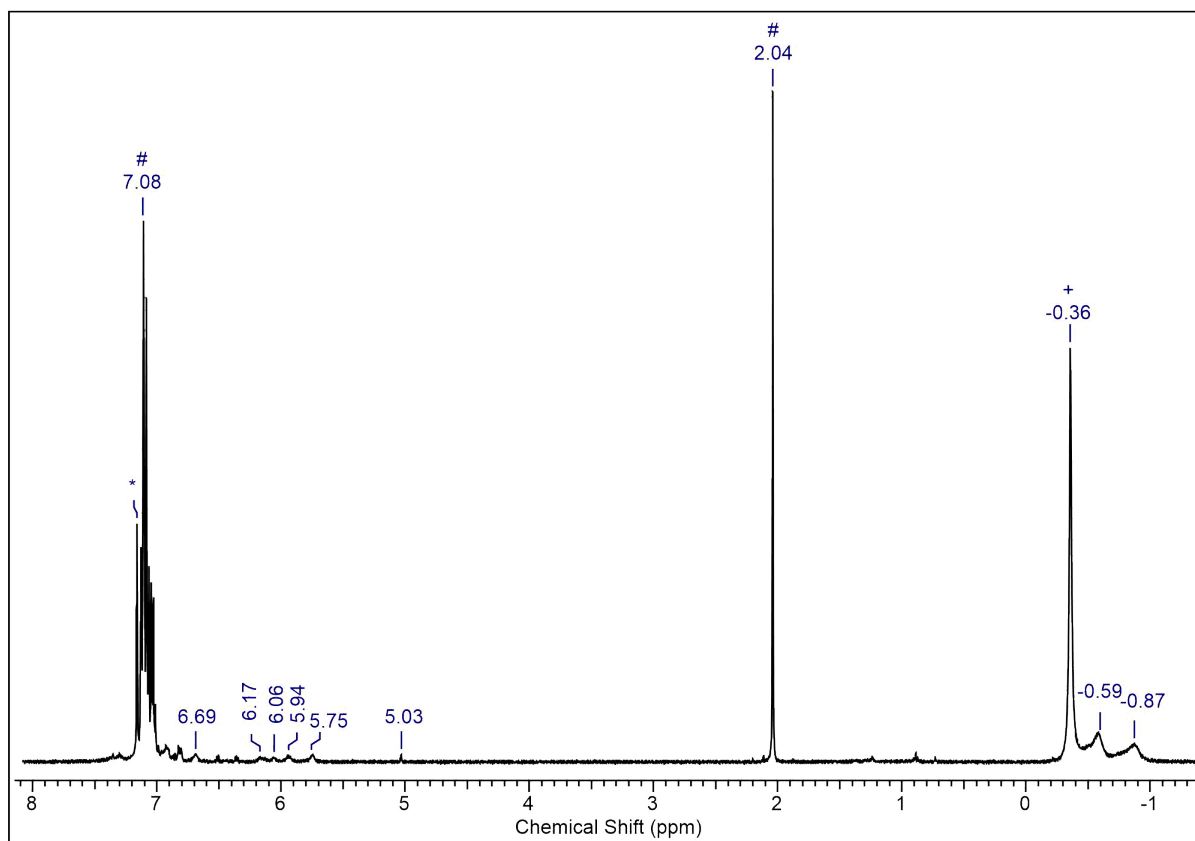


**Figure S37.** <sup>1</sup>H NMR spectrum (400 MHz) of the reaction of (Ind)La(AlMe<sub>4</sub>)<sub>2</sub> (**1a**) with [Ph<sub>3</sub>C][B(C<sub>6</sub>F<sub>5</sub>)<sub>4</sub>] in C<sub>6</sub>D<sub>6</sub> at 26 °C. Ph<sub>3</sub>CMe is marked with #; free trimethylaluminum is marked +.

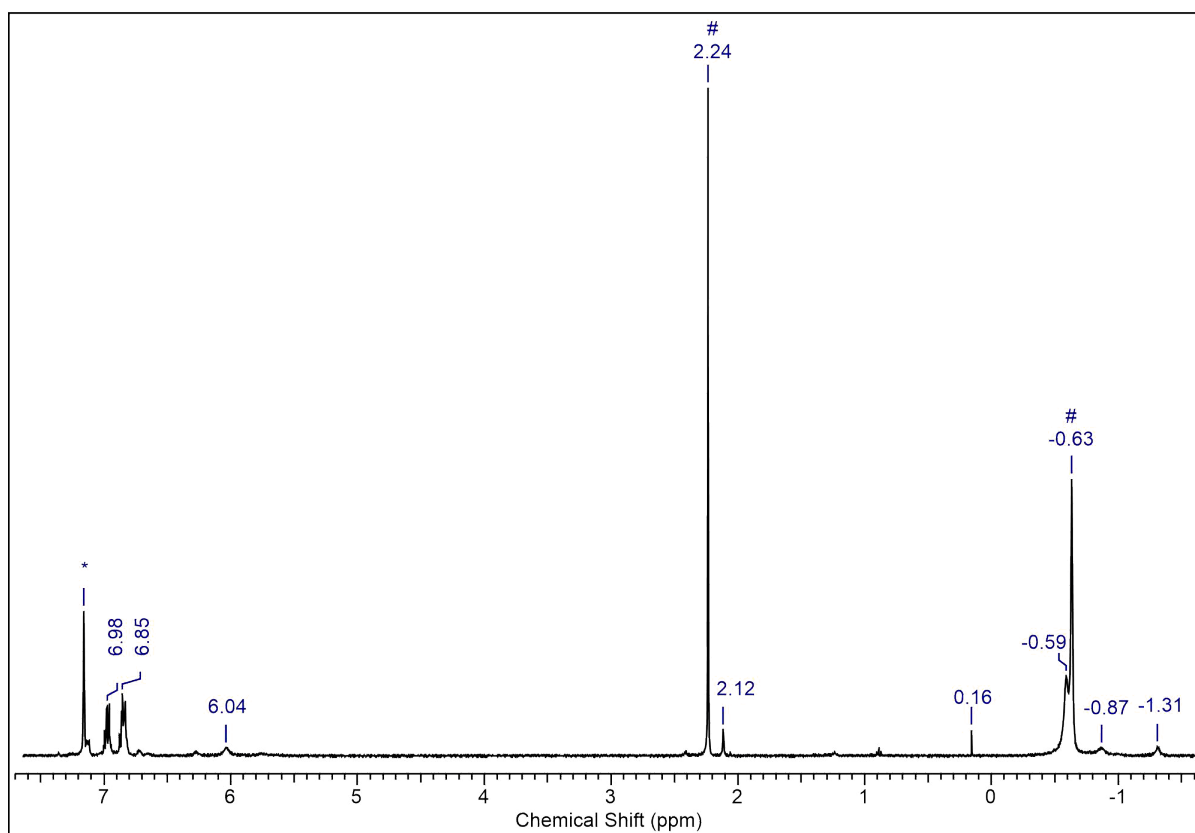


**Figure S38.** <sup>1</sup>H NMR spectrum (400 MHz) of the reaction of (Ind)La(AlMe<sub>4</sub>)<sub>2</sub> (**1a**) with [PhNMe<sub>2</sub>H][B(C<sub>6</sub>F<sub>5</sub>)<sub>4</sub>] in C<sub>6</sub>D<sub>6</sub> at 26 °C. PhNMe<sub>2</sub>(AlMe<sub>3</sub>) is marked with #.



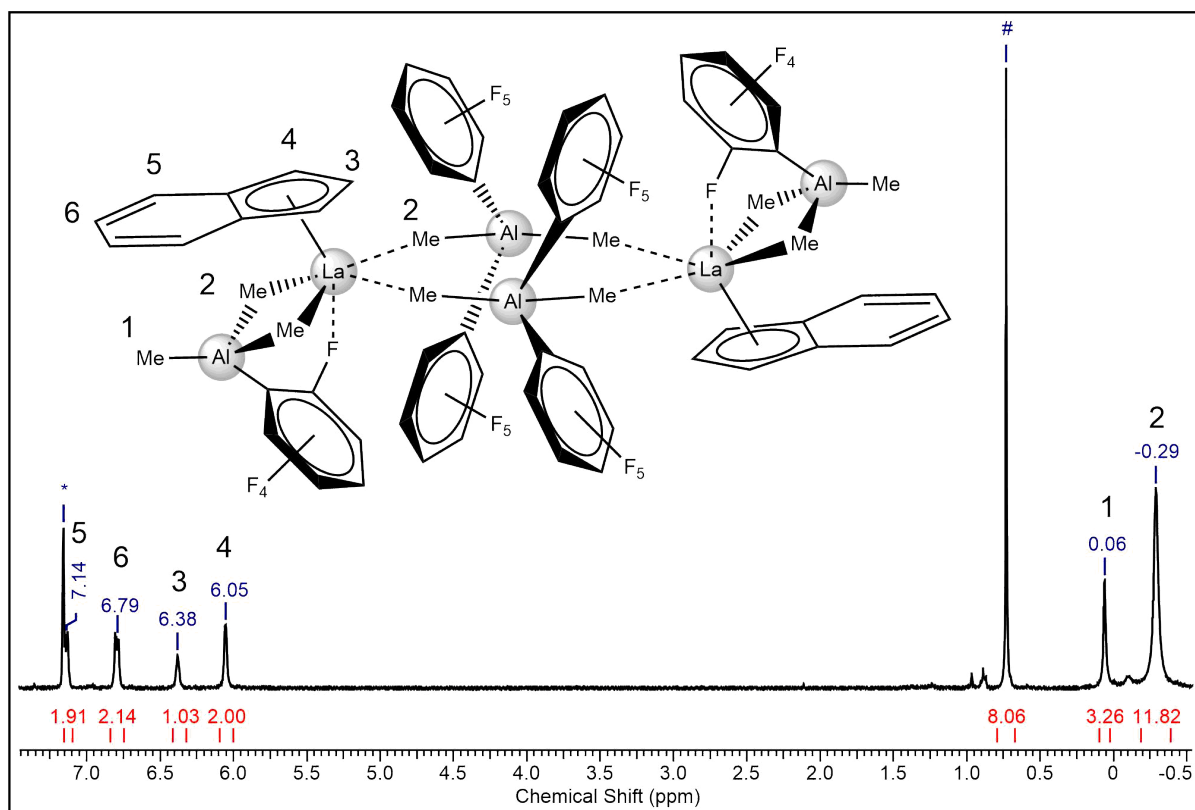


**Figure S39.**  $^1\text{H}$  NMR spectrum (400 MHz) of the reaction of  $(\text{Ind})\text{La}(\text{AlMe}_4)_2$  with  $\text{B}(\text{C}_6\text{F}_5)_3$  in  $\text{C}_6\text{D}_6$  at  $26^\circ\text{C}$ .  $\text{BMe}_3$  is marked with #.

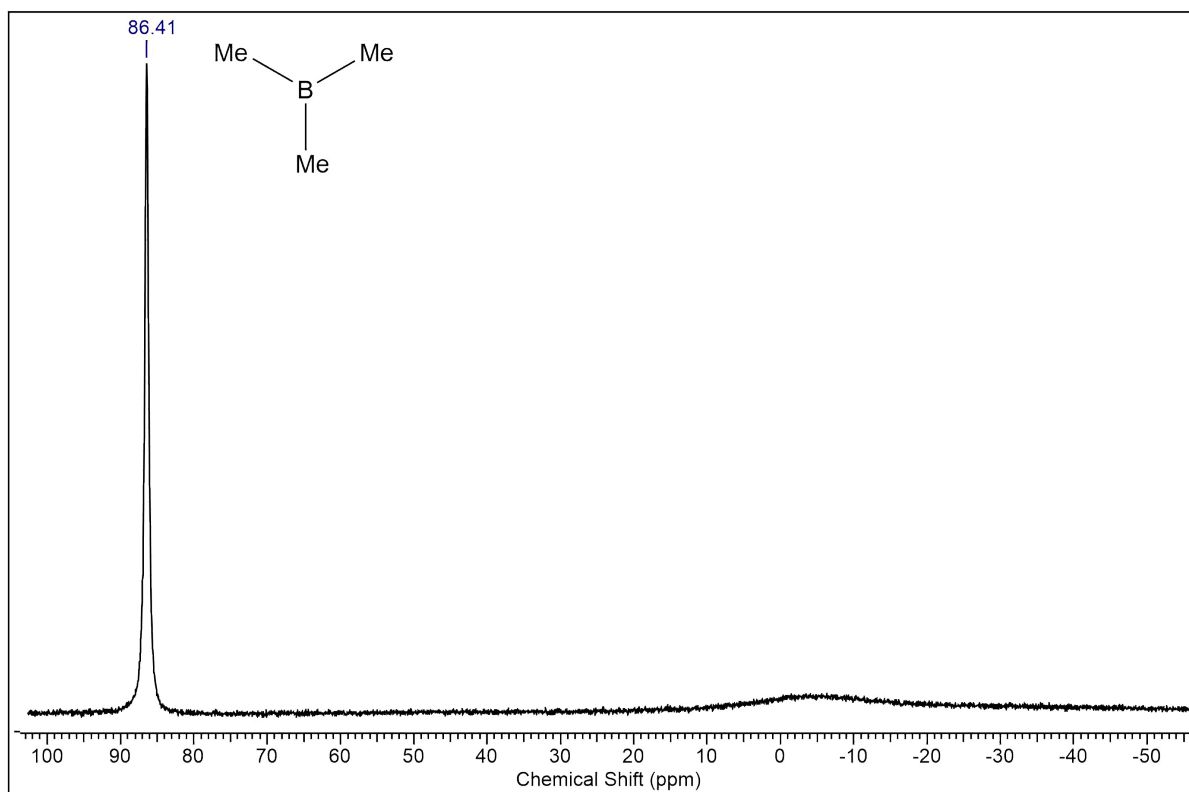


**Figure S40.**  $^{11}\text{B}$  NMR spectrum (400 MHz) of the reaction of  $(\text{Ind})\text{La}(\text{AlMe}_4)_2$  with  $\text{B}(\text{C}_6\text{F}_5)_3$  in  $\text{C}_6\text{D}_6$  at  $26^\circ\text{C}$  showing the formation of  $\text{BMe}_3$ .

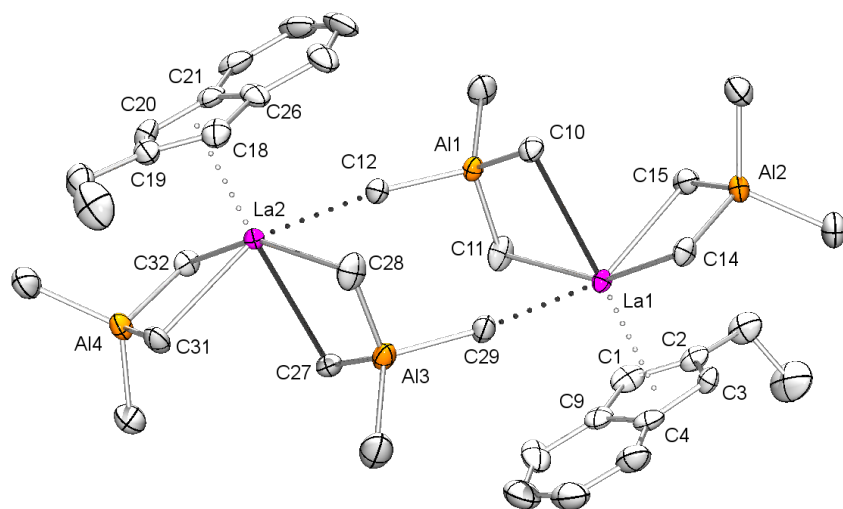


**Figure S41.** Molecular structure of  $(\text{Ind}^{\text{Et}})\text{La}(\text{AlMe}_4)_2$  (**1b**). Hydrogen atoms are omitted for clarity. Atomic displacement parameters set at the 50% probability level. Selected bond lengths [Å] and angles [°]: La1–C1 2.781(5), La1–C2 2.836(4), La1–C3 2.792(4), La1–C4 2.815(5), La1–C9 2.803(5), La1–C10 2.967(5), La1–C11 2.757(5), La1–C14 2.694(5), La1–C15 2.714(5), La1···C29 2.966(5), La1···Al1 3.3821(15), La1···Al2 3.2214(16), C10–La1–C11 73.69(14), C14–La1–C15 79.22(15), La2–C18 2.796(5), La2–C19 2.885(5), La2–C20 2.798(4), La2–C21 2.794(5), La2–C26 2.797(5), La2–C27 2.912(5), La2–C28 2.787(5), La2–C31 2.695(5), La2–C32 2.714(5), La2···C12 2.974(4), La2···Al3 3.3606(16), La2···Al4 3.2380(17), C27–La2–C28 74.55(15), C31–La2–C32 78.77(15).

**Table S1. Crystallographic Data for Compounds 1a, 1b, 1c, and 1d**

	<b>1a</b>	<b>1b</b>	<b>1c</b>	<b>1d</b>
CCDC number	1915979	1915982	1915976	1915977
formula	C <sub>20.5</sub> H <sub>35</sub> Al <sub>2</sub> La	C <sub>19</sub> H <sub>35</sub> Al <sub>2</sub> La	C <sub>21</sub> H <sub>39</sub> Al <sub>2</sub> La	C <sub>20</sub> H <sub>39</sub> Al <sub>2</sub> LaSi
M [g·mol <sup>-1</sup> ]	474.35	456.34	484.39	500.47
Color	colorless	colorless	colorless	colorless
Crystal dimensions [mm]	0.234 x 0.170 x 0.096	0.175 x 0.161 x 0.085	0.528 x 0.457 x 0.244	0.480 x 0.244 x 0.188
Crystal system	monoclinic	orthorhombic	trigonal	triclinic
space group	P2 <sub>1</sub> /c	Pca2 <sub>1</sub>	P3 <sub>1</sub>	P $\bar{1}$
a [Å]	19.459(5)	19.545(3)	9.7198(5)	9.4353(5)
b [Å]	11.634(3)	10.1865(17)	9.7198(5)	9.6041(5)
c [Å]	21.681(6)	22.334(4)	22.1290(10)	15.4562(8)
$\alpha$ [°]	90	90	90	93.888(2)
$\beta$ [°]	105.935(4)	90	90	103.960(2)
$\gamma$ [°]	90	90	120	116.010(2)
V [Å <sup>3</sup> ]	4720(2)	4446.7(13)	1810.5(2)	1197.13
Z	8	8	3	2
T [K]	155(2)	150(2)	103(2)	100(2)
$\rho_{\text{calcd}}$ [g·cm <sup>-3</sup> ]	1.335	1.363	1.333	1.388
$\mu$ [mm <sup>-1</sup> ]	1.884	1.997	1.843	1.908
F(000)	1928	1856	744	512
Unique reflns	13199	9267	7082	6161
Observed reflns	74853	90976	25431	35570
R1/wR2 (I>2 $\sigma$ )	0.0314/0.0604	0.0249/0.0450	0.0163/0.0407	0.0108/0.0288
R1/wR2 (all data)	0.0501/0.0683	0.0324/0.0472	0.0164/0.0407	0.0109/0.0289
Goodness of fit	1.022	1.038	1.077	1.080

**Table S2. Crystallographic Data for Compounds 2a, 2b, 2c, and 2d**

	<b>2a</b>	<b>2b</b>	<b>2c</b>	<b>2d</b>
CCDC number	1915980	1915981	1915978	1915983
formula	C <sub>22</sub> H <sub>26</sub> AlLu	C <sub>26</sub> H <sub>34</sub> AlLu	C <sub>33.5</sub> H <sub>46</sub> AlLu	C <sub>28</sub> H <sub>42</sub> AlLuSi <sub>2</sub>
M [g·mol <sup>-1</sup> ]	492.38	548.48	650.65	636.74
Color	colorless	colorless	colorless	Colorless
Crystal dimensions [mm]	0.269 x 0.159 x 0.136	0.331 x 0.158 x 0.153	0.247 x 0.126 x 0.115	0.495 x 0.223 x 0.220
Crystal system	monoclinic	monoclinic	triclinic	monoclinic
space group	Cc	P2 <sub>1</sub> /c	P $\bar{1}$	P2 <sub>1</sub> /c
a [Å]	14.297(2)	13.9877(6)	9.915(4)	9.4943(13)
b [Å]	14.304(2)	18.5367(8)	10.487(6)	16.796(2)
c [Å]	19.222(3)	9.3019(4)	15.091(5)	18.475(3)
$\alpha$ [°]	90	90	75.814(11)	90
$\beta$ [°]	97.286(2)	103.447(2)	81.200(6)	98.438(4)
$\gamma$ [°]	90	90	77.448(11)	90
V [Å <sup>3</sup> ]	3899.1(11)	2345.73(18)	1476.6(11)	2914.2(7)
Z	8	4	2	4
T [K]	150(2)	100(2)	100(2)	100(2)
$\rho_{\text{calcd}}$ [g·cm <sup>-3</sup> ]	1.678	1.553	1.463	1.451
$\mu$ [mm <sup>-1</sup> ]	5.108	4.254	3.392	3.513
F(000)	1936	1096	662	1288
Unique reflns	9619	6586	8656	7837
Observed reflns	29878	58663	63482	44485
R1/wR2 (I>2 $\sigma$ )	0.0221/0.0514	0.0144/0.0342	0.0204/0.0482	0.0172/0.0415
R1/wR2 (all data)	0.0227/0.0516	0.0163/0.0350	0.0228/0.0491	0.0185/0.0420
Goodness of fit	1.092	0.982	1.106	1.075

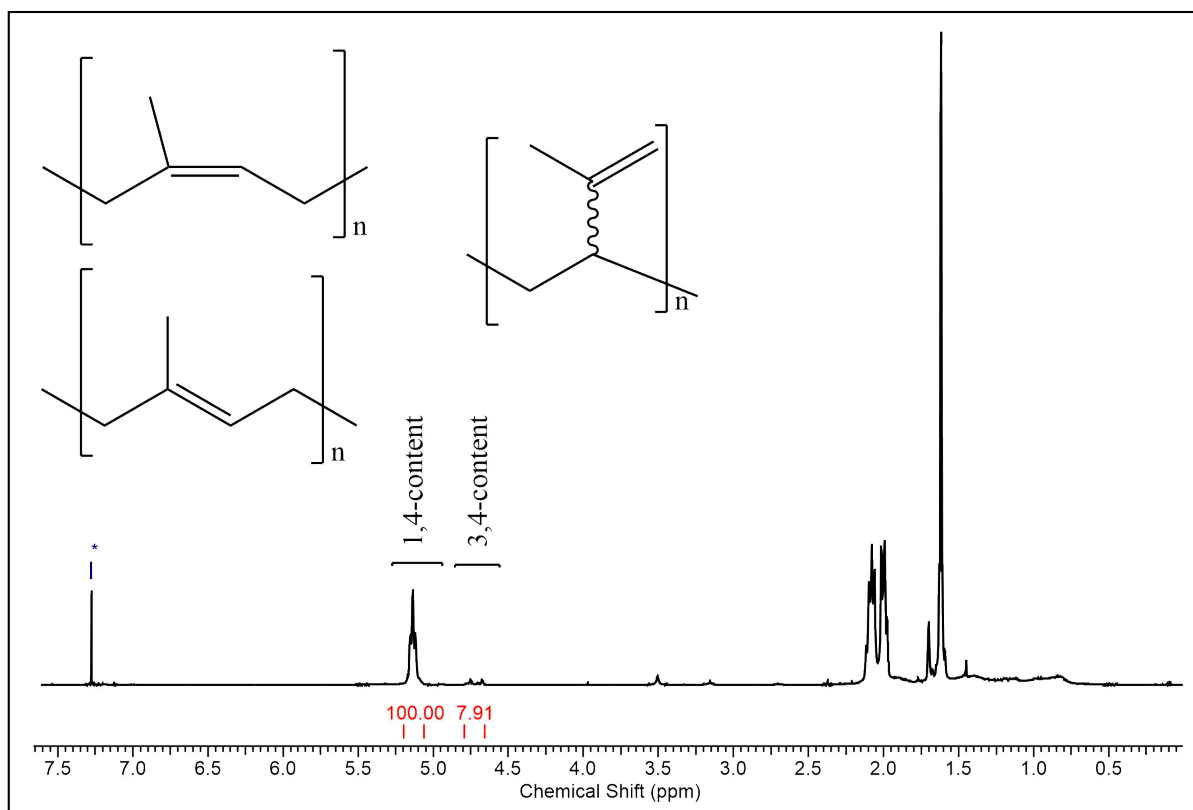


**Figure S42.**  $^1\text{H}$  NMR spectrum (400 MHz) of polyisoprene (entry 4) in  $\text{CDCl}_3$  at  $26^\circ\text{C}$ .

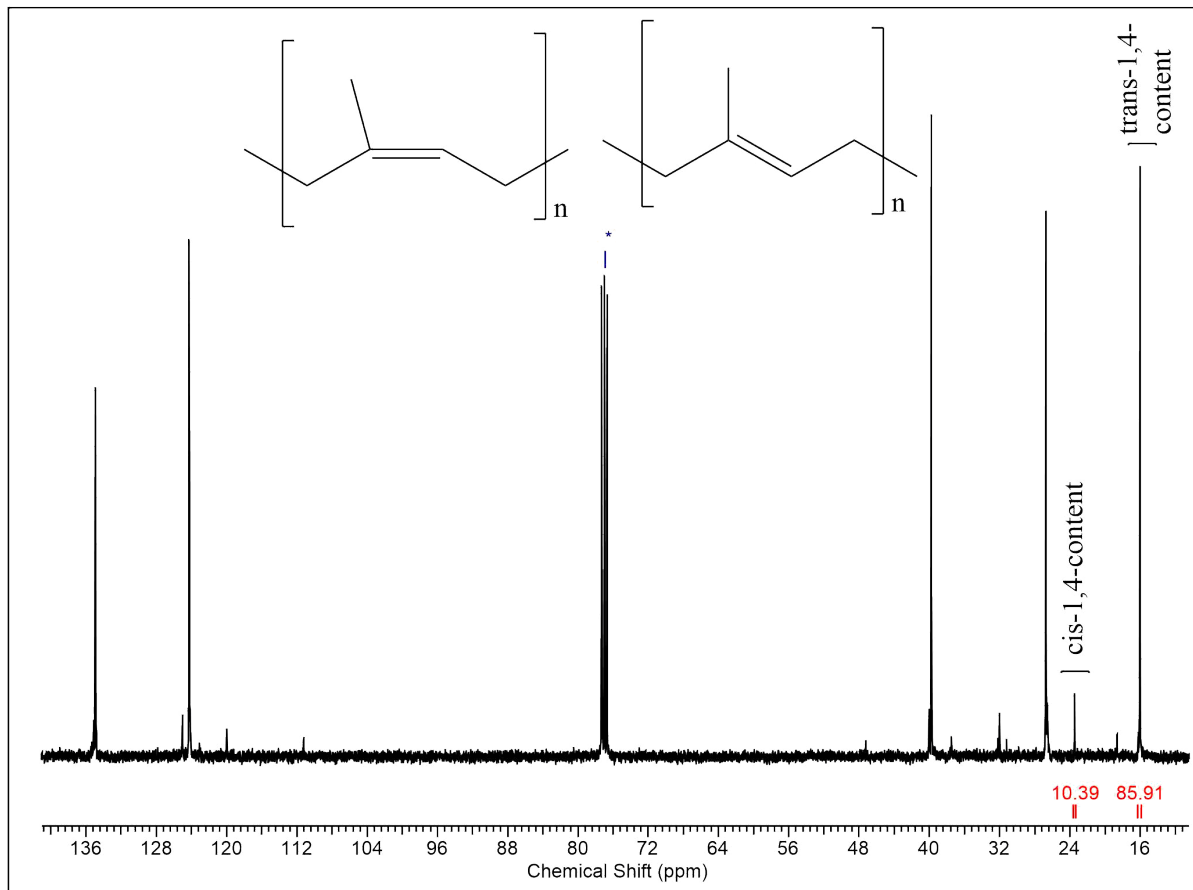


**Figure S43.**  $^{13}\text{C}\{^1\text{H}\}$  NMR spectrum (101 MHz) of polyisoprene (entry 4) in  $\text{CDCl}_3$  at  $26^\circ\text{C}$ .

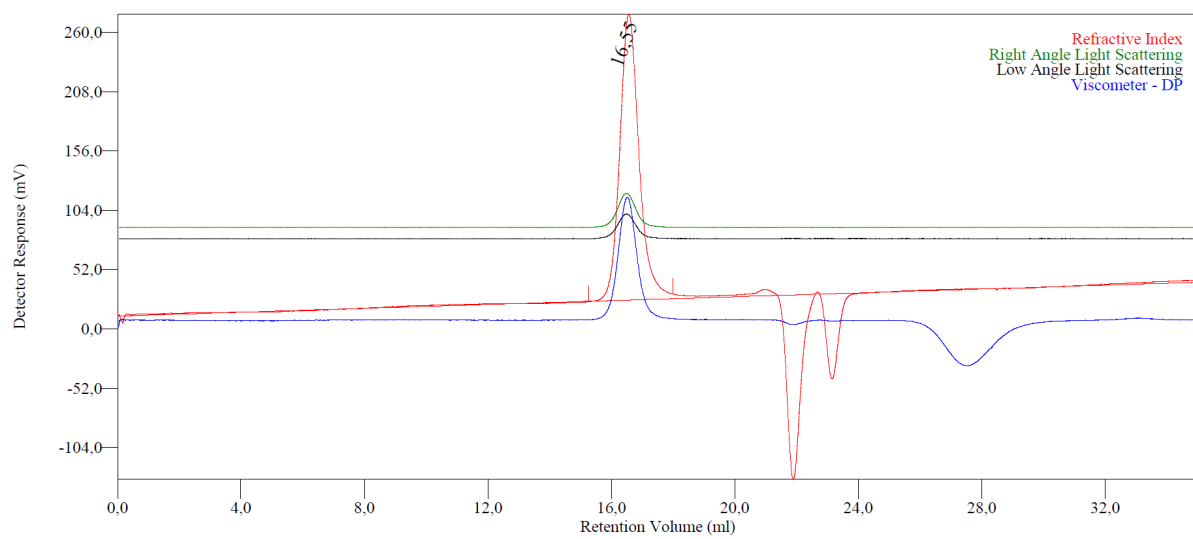


**Figure S44.** GPC curve of polyisoprene (entry 4).

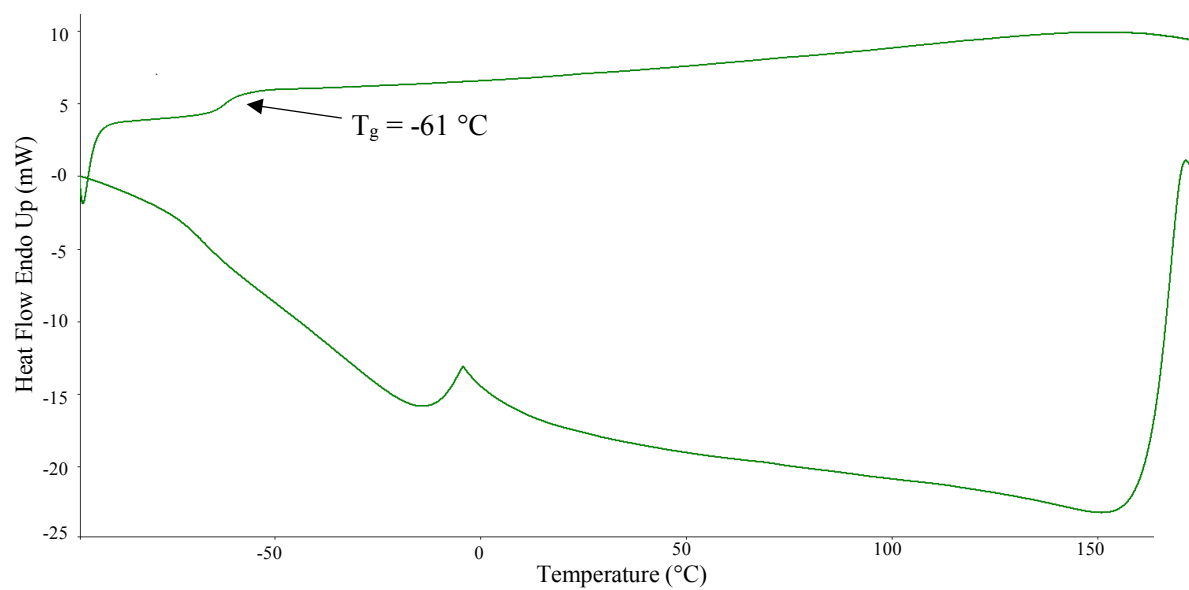


**Figure S45.** DSC curve of polyisoprene (entry 4).

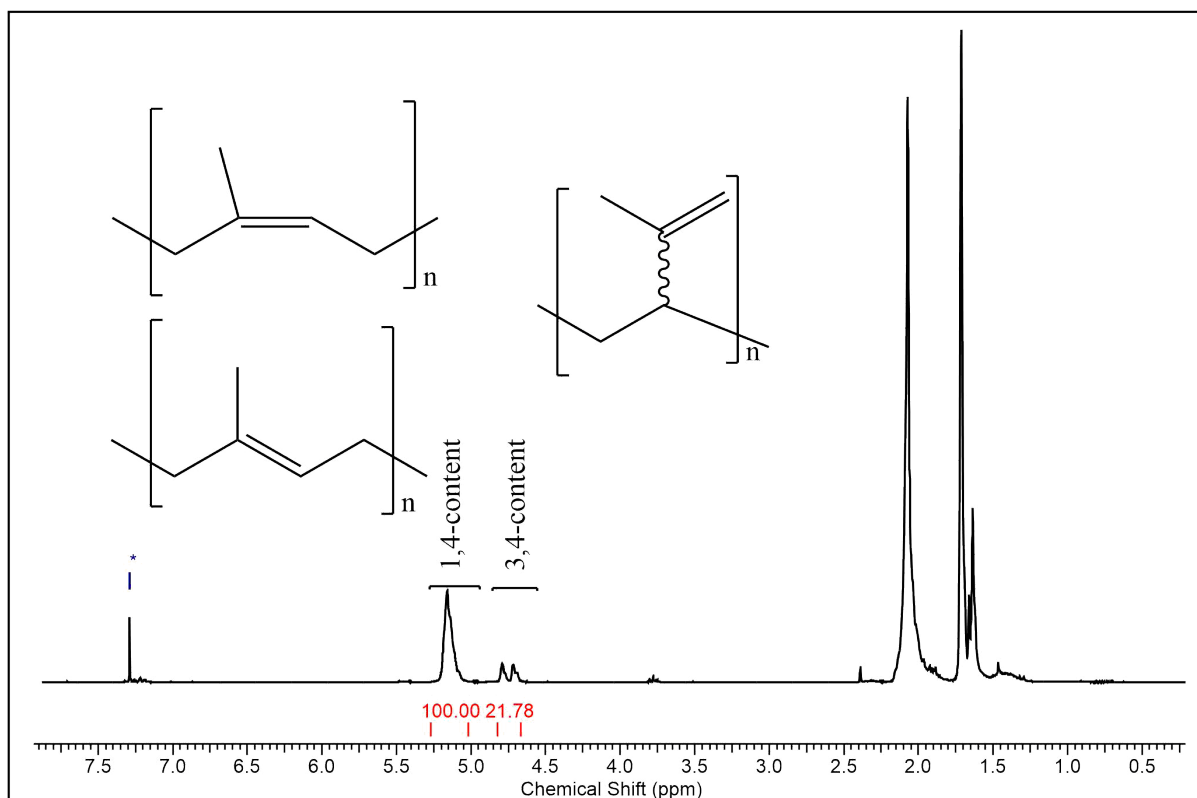


**Figure S46.**  $^1\text{H}$  NMR spectrum (400 MHz) of polyisoprene (entry 14) in  $\text{CDCl}_3$  at  $26^\circ\text{C}$ .

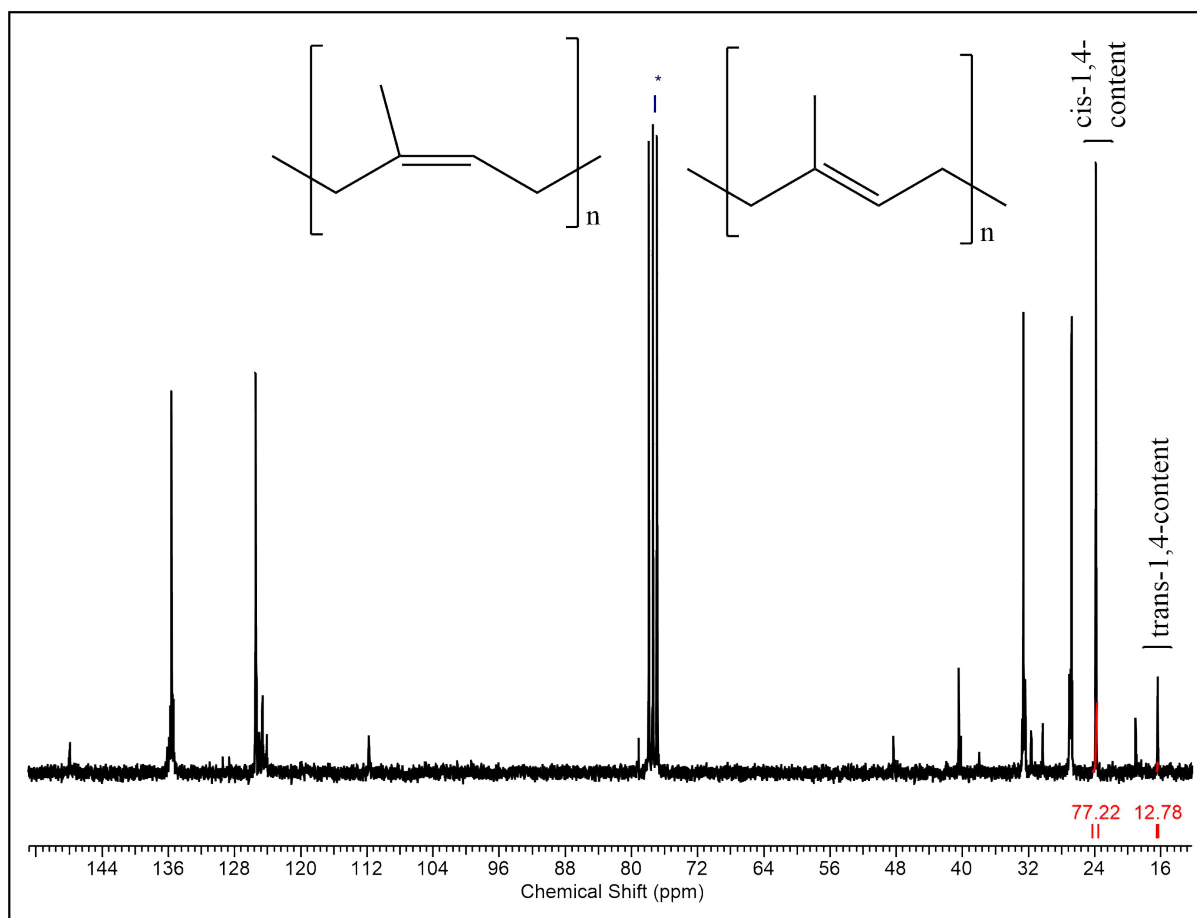


**Figure S47.**  $^{13}\text{C}\{^1\text{H}\}$  NMR spectrum (101 MHz) of polyisoprene (entry 14) in  $\text{CDCl}_3$  at  $26^\circ\text{C}$ .

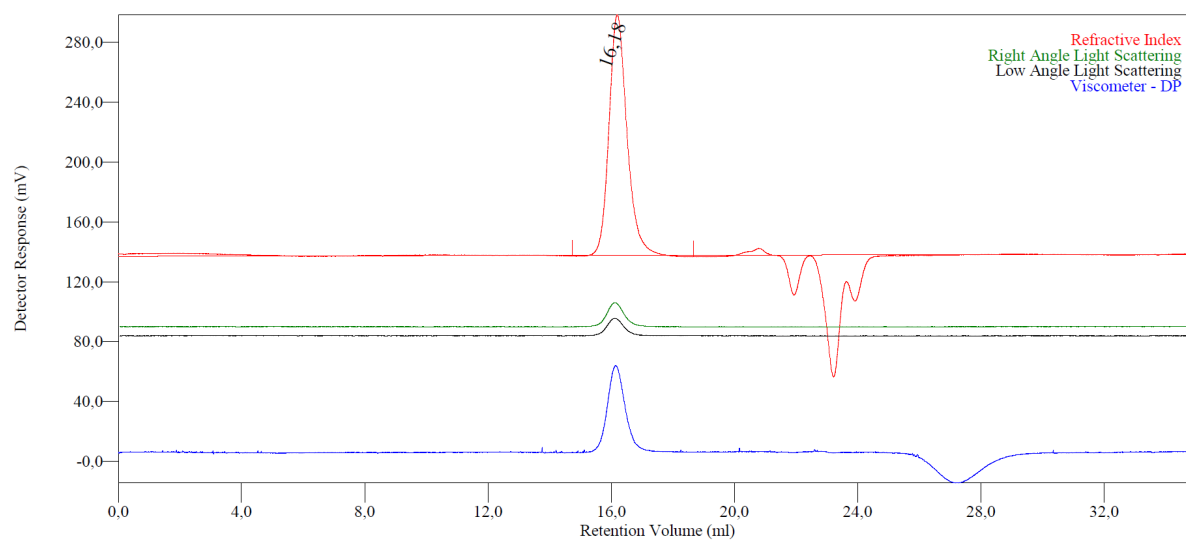


**Figure S48.** GPC curve of polyisoprene (entry 14).

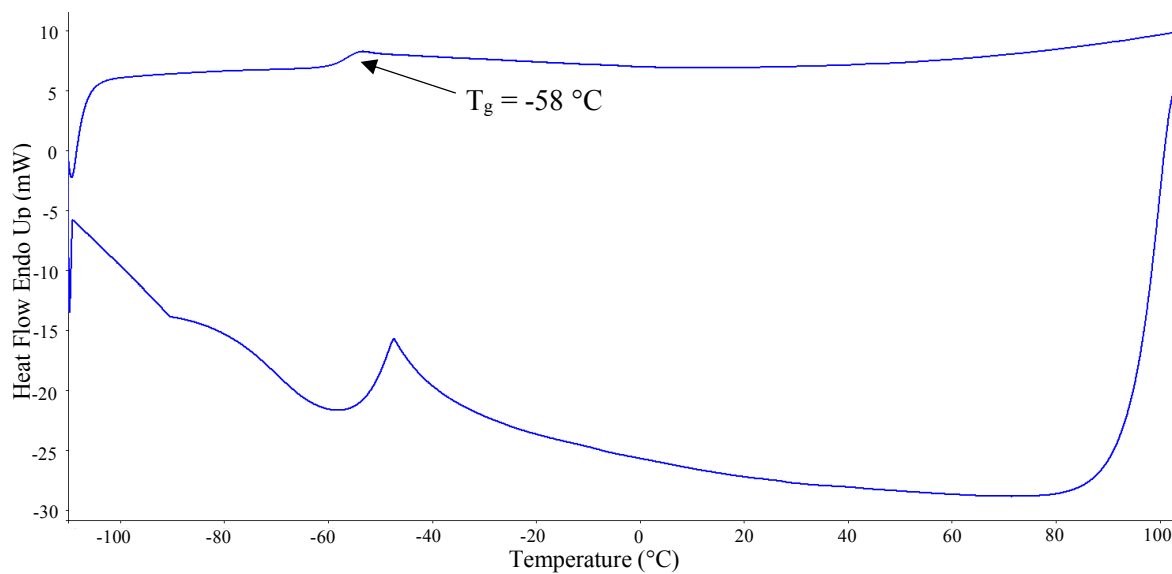
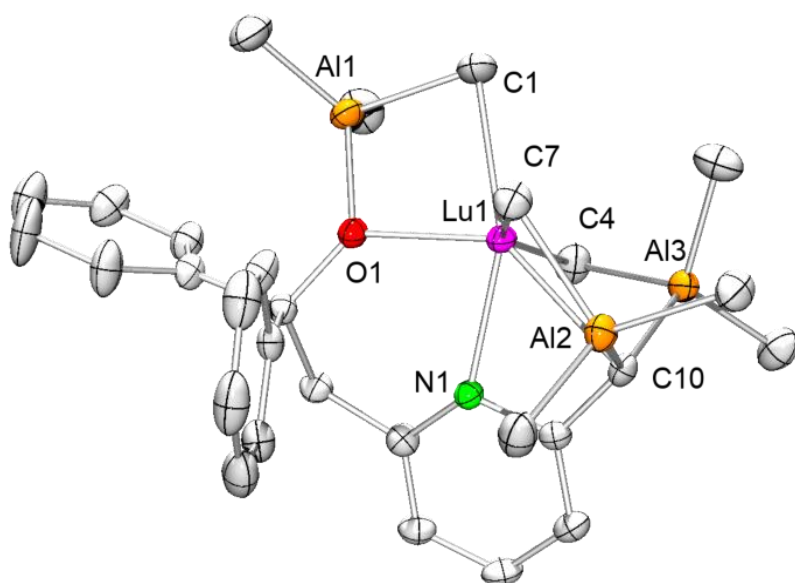


**Figure S49.** DSC curve of polyisoprene (entry 14).



**Rare-Earth Metal-Induced  
(Double) C–H Bond Activation of  
a Pyridyl-Functionalized Alkoxy  
Ligand: Formation of [ONC]<sup>(2-)</sup>  
Pincer-Type Ligands and  
Implications for Isoprene**





# Rare-Earth Metal-Induced (Double) C–H Bond Activation of a Pyridyl-Functionalized Alkoxy Ligand: Formation of [ONC]<sup>(2-)</sup> Pincer-Type Ligands and Implications for Isoprene Polymerization

Dominic Diether, Melanie Meermann-Zimmermann, Karl W. Törnroos, Cécilia Maichle-Mössmer, and Reiner Anwander\*

The reaction of 2-(6-methyl-2-pyridyl)-1,1-diphenyl-ethanol with Ln(AIME<sub>3</sub>)<sub>3</sub> (Ln = La, Nd, Y) via a deprotonation/C–H bond activation sequence gave complexes [ONCH<sub>2</sub>]Ln(AIME<sub>3</sub>)<sub>2</sub>(AIME<sub>4</sub>) (Ln = La, Nd, Y) bearing the dianionic tridentate ligand [ONCH<sub>2</sub>]. In contrast, the reactions involving the smaller rare-earth metals yttrium and lutetium resulted in a double C–H bond activation and formation of [ONCH]Ln(AIME<sub>3</sub>)<sub>3</sub> (Ln = Y, Lu) with the formally trianionic tridentate ligand [ONCH]. The solid-state structures of all complexes as obtained by X-ray structure analysis revealed an axial chirality which could be also verified by low-temperature <sup>1</sup>H NMR spectroscopy. All complexes displayed high activity in the polymerization of isoprene, upon activation with standard fluorinated borate/borane cocatalysts. The catalyst activity and *cis*-1,4-selectivity could be increased by addition of two equivalents of cocatalyst instead of one. For example, when activated with two equivalents of [PhNMe<sub>2</sub>H][B(C<sub>6</sub>F<sub>5</sub>)<sub>4</sub>] complex [ONCH]Y(AIME<sub>3</sub>)<sub>3</sub> gave almost complete conversion after 15 minutes fabricating a polyisoprene with a *cis*-1,4-content of 83.5% (no *trans*-1,4-content detected).

## Introduction

The ubiquitous cyclopentadienyl ligands have played a key role in the development of organorare-earth metal (Ln) catalysts for polymerization reactions.<sup>1,2</sup> This is attributed to robustness and structural variety of these ancillary ligands.<sup>3</sup> However, in recent years the use of pincer systems emerged as an attractive alternative. Their advantages are the ability to prevent dimerization, impede solvent coordination, and to counteract ate-complex formation and ligand scrambling.<sup>3</sup> In addition, pincer ligands are characterized by a great variability in steric and electronic properties. Unsurprisingly, these properties have been exploited for polymerization reactions as well.<sup>4,5</sup> For example, Li *et al.* showed that variation of the pincer ligands in neosilyl complexes (**I** and **II**, Fig. 1) affect the microstructure of polyisoprene generating either *cis*-1,4-polyisoprene (**I**)<sup>6,7</sup> or *trans*-1,4-polyisoprene (**II**).<sup>8</sup> Moreover, isoprene was successfully polymerized by Cui *et al.* using tridentate [NNN] pincer ligands (**III**, Fig. 1),<sup>9</sup> including other dienes,  $\alpha$ -olefins, functional monomers, as well as the copolymerization of the aforementioned monomers. Using bis(phosphino)carbazolide as a pincer ligand, the block copolymerization of isoprene with  $\epsilon$ -caprolactone was achieved.<sup>10</sup> With a [NPNPN] tridentate monoanionic ligand, the corresponding complexes (**IV**, Fig. 1) provide highly *trans*-1,4-selective polyisoprenes as well as polybutadienes could be accessed,<sup>11</sup> while using an [NCN] pincer system, butadiene could also be polymerized in a highly *cis*-1,4 selective manner.<sup>12</sup> Pincer complexes were also successfully used in  $\alpha$ -

olefin polymerization as shown by e.g., the polymerization of ethylene with complex **V** (Fig. 1).<sup>13</sup> Polymerizations of functional monomers like  $\epsilon$ -caprolactone,<sup>14</sup>  $\beta$ -butyrolactone<sup>15</sup> or lactide<sup>16,17</sup> were also investigated.

Examples of rare-earth metal pincer complexes featuring alkylaluminum moieties are rather rare.<sup>13,18–20</sup> This is probably due to the high reactivity of the alkylaluminum groups which might be prone to either pincer ligand backbone degradation or Lewis acid/base interactions with pincer heteroatoms.<sup>18–20</sup> Moreover, alkylaluminum or Ln-alkyl groups have a high tendency for C–H activation of ancillary ligands.<sup>20–24</sup>

The 2-(6-methyl-2-pyridyl)-1,1-diphenyl-ethanol proligand [HONCH<sub>3</sub>] under study has been studied in combination with palladium for the Suzuki<sup>25</sup> reaction or direct C–H arylation.<sup>26–28</sup> This pyridine-functionalized alkoxy ligand was shown to afford magnesium and zinc complexes (**VI**, Fig. 2), which showed high activities in the polymerization of L-lactides and  $\epsilon$ -caprolactone.<sup>29</sup> The corresponding benzylic alcohol with a lutidinyl substituents was also successfully applied for the syntheses of aluminium complexes used in L-lactide polymerization.<sup>30</sup> To date, the use of 2-(6-methyl-2-pyridyl)-1,1-diphenyl-ethanol was not reported as a ligand for rare-earth metal complexes.

Herein, we would like to introduce the 2-(6-methyl-2-pyridyl)-1,1-diphenyl-ethanol proligand into organorare-earth metal chemistry. It is revealed that the methyl group of the lutidinyl moiety undergoes mono and double C–H bond activation depending on the size of the Ln(III) centre.

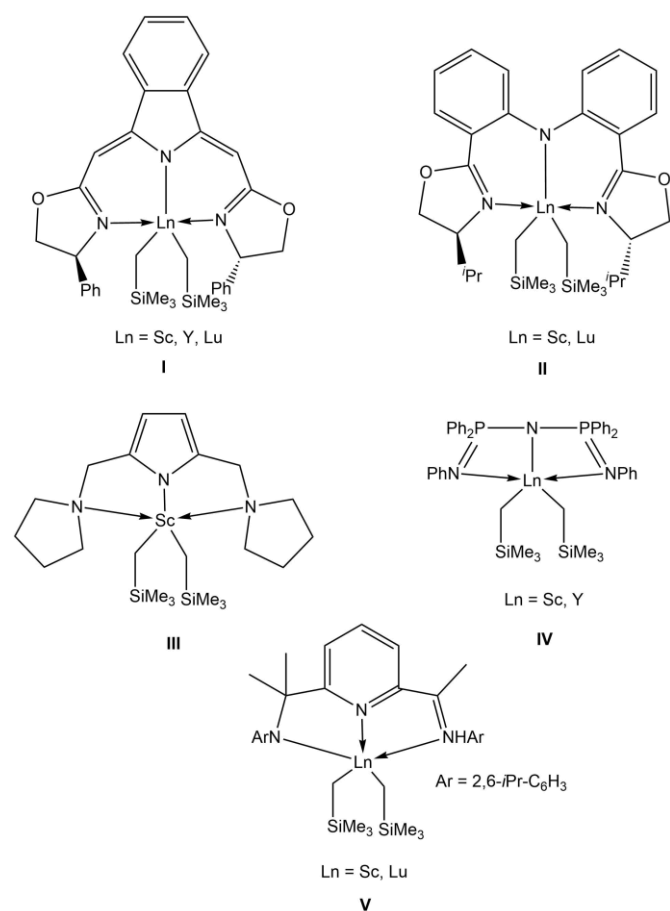
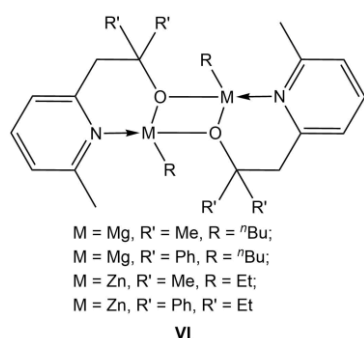


Fig. 1 Selection of pincer complexes from literature.

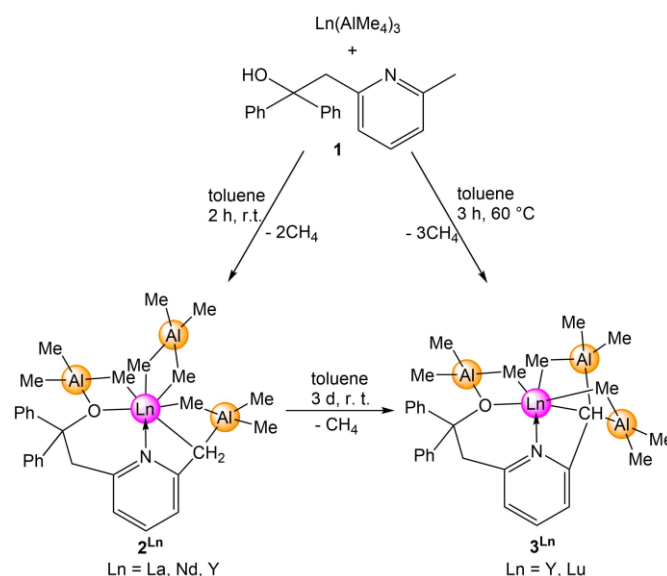
Fig. 2 Mg and Zn complexes for the L-lactide and  $\epsilon$ -caprolactone polymerization.

## Results and Discussion

### Synthesis of organolanthanide complexes

Addition of 2-(6-methyl-2-pyridyl)-1,1-diphenyl-ethanol (**1**) to a solution of homoleptic Ln(AlMe<sub>4</sub>)<sub>3</sub> (Ln = La, Nd) in toluene at ambient temperature caused an instant formation of methane,

while the solution slowly turned yellow (La) or green (Nd). As detectable by <sup>1</sup>H NMR spectroscopy, the reaction proceeds without formation of side products, and was found to be complete after two hours. Nevertheless, an additional recrystallisation step was implemented to obtain complexes



Scheme 1 Synthesis of complexes **2**<sup>Ln</sup> (Ln = La, Nd, Y) by protonolysis of Ln(AlMe<sub>4</sub>)<sub>3</sub> with **1** a subsequent reaction to **3**<sup>Ln</sup> (Ln = Y, Lu) via C–H bond activation. Alternative direct synthesis of complex **3**<sup>Ln</sup> (Ln = Y, Lu) by the direct reaction of Ln(AlMe<sub>4</sub>)<sub>3</sub> with **1** for 3 hours in toluene.

[ONCH<sub>2</sub>]Ln(AlMe<sub>3</sub>)<sub>2</sub>(AlMe<sub>4</sub>) (Ln = La, Nd) as pure products according to elemental analysis. It is reasonable to assume that the reaction is initiated by deprotonation of the alcoholic –OH moiety of **1** by a tetramethylaluminate group, but methane formation seems rapid. Due to the strongly chelating effect of the now monoanionic [ON] scaffold, the methyl group of the lutidynyl moiety comes in close proximity to another AlMe<sub>4</sub> moiety. This facilitates a C–H bond activation of the methyl group and concomitant cyclometallation (Scheme 1, complex **2**<sup>Ln</sup>). Performing the reaction of Y(AlMe<sub>4</sub>)<sub>3</sub> with **1** under the same conditions, gave not only the targeted complex **2**<sup>Y</sup> but also the doubly CH-bond activated complex [ONCH]Y(AlMe<sub>3</sub>)<sub>3</sub> (**3**<sup>Y</sup>) as a side product was observed. When carrying out the “yttrium” reaction at lower temperatures, formation of **3**<sup>Y</sup> gets suppressed but could not be prevented completely. Even after several recrystallisation steps it was not possible to obtain **2**<sup>Y</sup> without any contamination with **3**<sup>Y</sup> (minimum contamination: 5%). This is due to the fact that **2**<sup>Y</sup> is not stable at ambient temperature, which can be explained by the smaller ionic radii of Y(III) compared to La(III) and Nd(III). The smaller ionic radii brings the –CH<sub>2</sub>– group and a third AlMe<sub>4</sub> moiety in close proximity, enabling a second C–H activation at the same carbon atom, thus generating a third equivalent of methane.

Continued stirring of **2**<sup>Y</sup> at ambient temperature generated additional methane indicating the formation to **3**<sup>Y</sup>. Full conversion to **3**<sup>Y</sup> can be accomplished by stirring the reaction over three days at ambient temperature. Complexes **3**<sup>Ln</sup> (Ln = Y, Lu) are also accessible by the reaction of Ln(AlMe<sub>4</sub>)<sub>3</sub> with **1** at 60 °C. Stirring the reaction mixture for three hours and

subsequent recrystallisation from a saturated *n*-hexane solution gave **3<sup>Ln</sup>** as a pure products. The analysis of the reaction by <sup>1</sup>H NMR spectroscopy indicates that complex [ONCH]Lu(AlMe<sub>3</sub>)<sub>3</sub> (**3<sup>Lu</sup>**) is possibly formed via **2<sup>Lu</sup>**, but isolation of the latter was unsuccessful. Since the ionic radius of Lu(III) is even smaller than that of Y(III), putative intermediate **2<sup>Lu</sup>** is even more likely to undergo a second C–H activation. In order to force this second C–H bond activation in **2<sup>La</sup>**, a solution of **2<sup>La</sup>** was heated to 80 °C for two hours. However, the NMR-scale reaction did not indicate the formation of **3<sup>La</sup>** but a complicate product mixture. It is noteworthy that the cyclometallation steps to yield **3<sup>Ln</sup>** afford a rare example of a rare-earth metal alkylidene moiety. To the best of our knowledge this is the first example of an [ONC] pincer ligand complexing a rare-earth metal.

It is not obvious that **2<sup>Ln</sup>** as well as **3<sup>Ln</sup>** are also chiral complexes. The chirality of the complexes can be proven by the NMR spectra and the crystal structures.

### X-ray structure analyses

Crystals of **2<sup>Ln</sup>** suitable for X-ray structure analysis were obtained from a mixture of toluene/*n*-hexane. The racemic mixtures of **2<sup>Ln</sup>** crystallise in the space group P1 or P21/c, respectively. This centrosymmetric space groups confirm the absence of enantiomerically pure crystals. Complexes **3<sup>Ln</sup>** crystallize also in the centrosymmetric space group P1 or P21/n, but, fortunately, we also succeeded in obtaining **3<sup>Lu</sup>** as an enantiomerically pure crystal possessing the space group P 21 21 21.

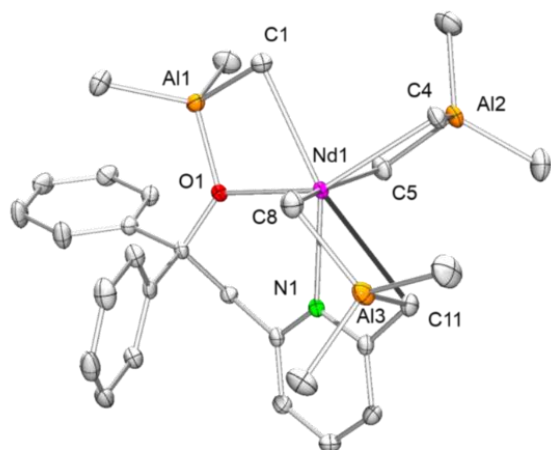


Fig. 3 Molecular structure of **2<sup>Nd</sup>**. All complexes **2<sup>Ln</sup>** are isostructural (see ESI Figure S14 (**2<sup>La</sup>**), S15 (**2<sup>Y</sup>**)). Hydrogen atoms are omitted for clarity. Atomic displacement parameters are set at 50% probability level. Selected bond lengths are given in Å and angles are given in °: **2<sup>Nd</sup>**: Nd1–C1 2.700(2), Nd1–C4 2.620(2), Nd1–C5 2.725(2), Nd1–C8 2.654(2), Nd1–C11 2.859(2), Nd1–Al1 3.3198(6), Nd1–Al2 3.2179(6), Nd1–Al3 3.3140(6), Nd1–N1 2.475(2), Nd1–O1 2.356(1), Al1–O1 1.859(1), Al3–C11 2.091(2), O1–Nd1–C11 128.40(5), O1–Nd1–N1 76.57(5), N1–Nd1–C11 52.80(5), N1–Nd1–Al2 109.18(4).

As complexes **2<sup>Ln</sup>** were found to be isostructural in the solid state, only the molecular structure of **2<sup>Nd</sup>** is depicted in Fig. 3 representatively (see ESI Figure S14, S15 for the structures of **2<sup>La</sup>** and **2<sup>Y</sup>**). The dianionic ligand [ONCH<sub>2</sub>] coordinates to the rare-earth metal centre in a meridional “pincer-type” manner. Additionally, both the alkoxy group (O1) and the C–H bond

activated methylene moiety (C11) of the [ONCH<sub>2</sub>] ligand show interactions with one AlMe<sub>3</sub>. The AlMe<sub>4</sub> moiety is coordinated in the usual η<sup>2</sup> mode.<sup>31–33</sup>

The Nd1–C<sub>Me</sub> (C1, C4, C5, C8) distances in 7-coordinate **2<sup>Nd</sup>** range between 2.654(2) and 2.700(2) Å being significantly longer than those in homoleptic Nd(AlMe<sub>4</sub>)<sub>3</sub> (2.563(14)–2.609(14) Å).<sup>34</sup> In line with this, the Nd1···Al2 distance of 3.2179(6) Å in **2<sup>Nd</sup>** is elongated compared to the Nd···Al distances in Nd(AlMe<sub>4</sub>)<sub>3</sub> (3.149(4)–3.155(5) Å).<sup>34</sup> The distances of Nd1···Al1 (3.3508(5) Å) and Nd1···Al3 (3.3140(6) Å) involving the alkoxy and methylene ligands, respectively are even longer. Thereby both the Nd1···Al1 and the Nd1–O1 distances in **2<sup>Nd</sup>** are comparable to trimethylaluminum-stabilized neodymium alkoxide complexes (Nd1···Al1 3.2756 – 3.300 Å; Nd1–O1 2.2940(7) – 2.324(3) Å).<sup>35–37</sup> The Nd1–N1 distance of 2.475(2) Å is in the range of the Nd–N<sub>Py</sub> distances of 6-coordinate complex ([2,6-{(iPr)<sub>2</sub>C<sub>6</sub>H<sub>5</sub>}N=C(CH<sub>3</sub>)<sub>2</sub>(C<sub>5</sub>H<sub>3</sub>N)]NdI<sub>2</sub>(THF) (Nd1–N1 2.376(7)) and 10-coordinate complex [2,6-di(pyrazolyl)pyridine]Nd(NO<sub>3</sub>)<sub>3</sub>(EtOH) (Nd1–N1 2.587(3)).<sup>38,39</sup> The Nd1–C11 bond length of 2.859(2) Å in **2<sup>Nd</sup>** is considerably longer than the Nd1–Me bonds, which is mainly caused by ring strain. In contrast the Al3–C11 bond length (2.091(2) Å) is comparable to the Al–Me distances, e.g. in Nd(AlMe<sub>4</sub>)<sub>3</sub> 2.067(14)–2.116(14) Å.<sup>34</sup> The difficulty of encompassing the rare-earth metal with the “pincer ligand” is also obvious from the O1–Ln1–C11 angle. While for **2<sup>La</sup>** the angle is 126.22(4)° it increases with decreasing radii of the rare-earth metal (**2<sup>Nd</sup>** 128.40(5)° **2<sup>Y</sup>** 130.21(7)°).

Complexes **3<sup>Ln</sup>** feature a similar ligand framework as **2<sup>Ln</sup>** (Fig. 4). Herein, O1, N1, and C10 are coordinating to the rare-earth

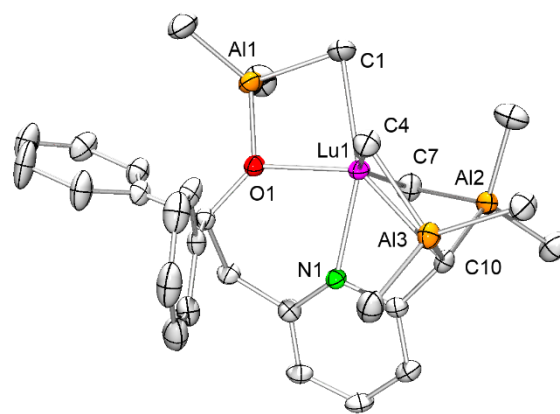


Fig. 4 Molecular structure of **3<sup>Lu</sup>**. **3<sup>Y</sup>** is isostructural (see ESI Figure S10 (**3<sup>Y</sup>**)). Hydrogen atoms are omitted for clarity. Atomic displacement parameters are set at 50% probability level. Selected bond lengths are given in Å and angles are given in °: **3<sup>Lu</sup>**: Lu1–C1 2.511(3), Lu1–C4 2.580(3), Lu1–C7 2.436(3), Lu1–C10 2.524(3), Lu1–Al1 3.1221(9), Lu1–Al2 2.8623(8), Lu1–Al3 3.0575(9), Lu1–N1 2.281(2), Lu1–O1 2.193(2), Al1–O1 1.848(2), Al2–C10 2.076(3), Al3–C10 2.073(3), O1–Lu1–C10 136.27(8), O1–Lu1–N1 78.38(7), N1–Lu1–C10 58.33(9).

metal centre in a meridional way. The Ln–O moiety is again stabilized by a AlMe<sub>3</sub> group and the Ln–C10 moiety, which is now involving a alkylidene functionality, is stabilized by two AlMe<sub>3</sub> molecules. In 6-coordinate **3<sup>Lu</sup>**, the Lu1–C<sub>Me</sub> (C1, C4, and C5) bond lengths (2.436(3)–2.580 Å) are in the same range as those detected for 6-coordinate Lu(AlMe<sub>4</sub>)<sub>3</sub> (2.466(2)–

2.471(2) Å).<sup>31</sup> The Lu1...Al1 distance (3.1221(9) Å) and Al1–O1 bond length (1.848(2) Å) are comparable to those in 7-coordinate Cp\*Lu(OCH<sub>2</sub>CMe<sub>3</sub>)<sub>3</sub>(AlMe<sub>3</sub>)<sub>3</sub> (3.119(1)–3.123(1) Å and 1.835(2)–1.844(3) Å).<sup>40</sup> The distinct distances of Lu1...Al2 (2.8623(8) Å) and Lu1...Al3 (3.0575(9) Å) originate from the position of the phenyl group. One of the phenyl group is on the same site as Al3, thereby causing the larger Lu1...Al3 distance. The bond length of Lu1–N1 (2.281(2) Å) is significantly shorter than the lutetium pyridine distances in comparable 6- and 9-coordinated pincer complexes ((NNN)LuCl<sub>3</sub> and (NNN)Lu(acac)(NO<sub>3</sub>)<sub>2</sub>: 2.419(4)–2.496(5) Å).<sup>41,42</sup> In spite of the higher charge on C10 compared to **2<sup>Ln</sup>**, the Al2–C10 (2.076(3) Å) and Al3–C10 (2.073(3) Å) bond lengths are

comparable to the other Al–C<sub>Me</sub> bond lengths (2.078(2)–2.089(2) Å). The Lu1–C10 bond length of 2.524(3) Å seems also not affected by the higher charge of the alkylidene moiety and is in the same range as the Lu–C<sub>Me</sub> distances in Lu(AlMe<sub>4</sub>)<sub>3</sub>.<sup>31</sup> While the aluminum moiety is not restricted by steric hindrance or extensive ring strain and the Al2/3–C10 bond lengths do not decrease, it is assumed that the bond order of Lu1–C10 increases but is not reflected in the bond length due to steric reasons. The angle of O1–Ln1–C10 exhibits significantly greater values of 134.96(5)° (**3<sup>Y</sup>**) and 136.27(8)° (**3<sup>Lu</sup>**) compared to those of **2<sup>Ln</sup>**.

Table 1. Selected bond lengths [Å] and angles [deg] of **2<sup>Ln</sup>** and **3<sup>Ln</sup>**.

	<b>2<sup>La</sup></b>	<b>2<sup>Nd</sup></b>	<b>2<sup>Y</sup></b>	<b>3<sup>Y</sup></b>	<b>3<sup>Lu</sup></b>
C1–C8	2.687(2) - 2.787(2)	2.620(2) - 2.725(2)	2.513(4) - 2.677(3)	2.483(2) - 2.640(2)	2.436(3) - 2.580(3)
Ln1–C11/C10	2.949(2)	2.859(2)	2.848(3)	2.611(2)	2.524(3)
Ln1–Al1	3.3508(5)	3.3198(6)	3.1934(8)	3.1899(6)	3.1221(9)
Ln1–Al2	3.2829(5)	3.2179(6)	3.1390(9)	2.8420(6)	2.8623(8)
Ln1–Al3	3.4012(5)	3.3140(6)	3.251(1)	3.1295(6)	3.0575(9)
Ln1–N1	2.516(1)	2.475(2)	2.386(2)	2.325(1)	2.281(2)
Ln1–O1	2.4114(9)	2.356(1)	2.270(2)	2.270(1)	2.193(2)
Al1–O1	1.862(1)	1.859(1)	1.851(2)	1.849(1)	1.848(2)
Al2–C10	-	-	-	2.052(2)	2.076(3)
Al3–C11/C10	2.091(2)	2.091(2)	2.070(3)	2.063(2)	2.073(3)
O1–Ln1–C11/C10	126.22(4)	128.40(5)	130.21(7)	134.96(5)	136.27(8)
O1–Ln1–N1	76.38(3)	76.57(5)	78.70(6)	75.10(5)	78.38(7)
C11/C10–Ln1–N1	51.40(4)	52.80(5)	53.16(8)	56.91(5)	58.33(9)
N1–Ln1–Al2	107.21(3)	109.18(4)	108.75(5)	-	-
N1–C12–C11	115.63	117.31	114.49	-	-
N1–C11–C10	-	-	-	113.67	112.67

### NMR spectroscopy

The chirality of complex **2<sup>Ln</sup>** could be proven by crystal structure analysis and be verified by NMR spectra. The <sup>1</sup>H NMR spectrum for **2<sup>La</sup>** shows a distinct signal pattern for both –CH<sub>2</sub>– groups. Two doublets at 3.89 ppm and 3.02 ppm can be assigned to the protons of the –CH<sub>2</sub>– group labelled as 4 (Fig. 6). Both signals split into a doublet with a coupling constant of 15.1 Hz, which is consistent with a geminal H–H coupling. The signals for the –CH<sub>2</sub>– group 5 at 2.45 ppm and 1.90 ppm, also split into doublets with coupling constants of 15.6 Hz. This geminal coupling shows the chiral character of complex **2<sup>La</sup>**. A chirality-implied splitting of other signals of **2<sup>La</sup>** could not be observed at ambient temperature. Hence, the Al–Me signals show a highly fluxional behaviour at ambient temperature, with one signal for the AlMe<sub>4</sub> group at 0.15 ppm and two overlapping signals of both AlMe<sub>3</sub> groups at –0.38 ppm. A broadening of the latter signal was revealed by a variable temperature (VT) <sup>1</sup>H NMR study at –80 ° (Figure S20).

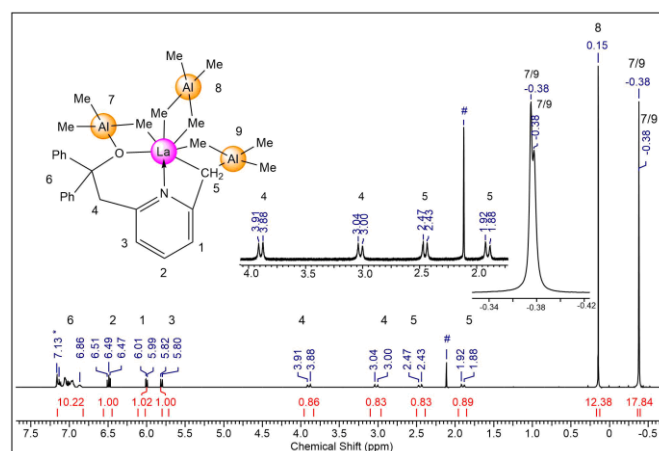


Fig. 5 <sup>1</sup>H-VT NMR spectra of **2<sup>La</sup>** in toluene from –80 to 40 °C.

When heating the sample to 40 °C, the two AlMe<sub>3</sub> groups showed two separated peaks (−0.46/−0.47 ppm). Moreover, at −80 °C the aromatic signals split into a total of 13 signals, in accordance with three signals for the pyridine moiety and 10 signals for each proton of the phenyl groups. Both phenyl groups exhibit distinct signals due to a different chemical environment caused by the chirality of complex **2<sup>La</sup>**. By heating the sample to 40 °C, the phenyl signals broadened and shifted into each other, which hampers an unequivocal assignment (Fig. 5).

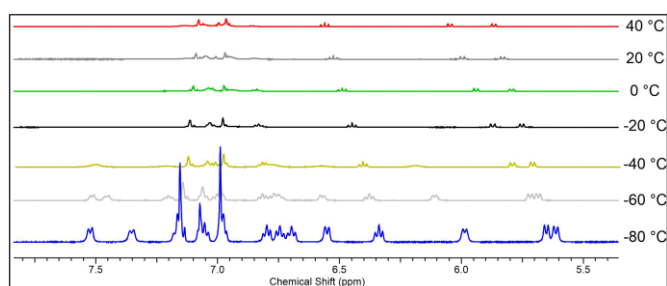


Fig. 6 <sup>1</sup>H NMR spectra of **2<sup>La</sup>** in C<sub>6</sub>D<sub>6</sub> at 26 °C.

An <sup>1</sup>H-VT NMR study of **2<sup>Y</sup>** gave a slightly different result. At low temperatures the aromatic region of the <sup>1</sup>H NMR spectra (5.5 – 8 ppm) shows also splitting of the phenyl signals but not as distinct as for **2<sup>La</sup>** (see ESI Figure S24). Heating the sample to 60 °C resulted in signal broadening and coalescence. As observed for **2<sup>La</sup>**, the signals of both –CH<sub>2</sub>– groups of **2<sup>Y</sup>** (4 and 5 in Fig. 6, Figure S22) remained rather unaffected by varying of the temperature. Enhanced dynamic behaviour at 60 °C of these groups was indicated by signal broadening. The high mobility of the Al–Me groups and the broadening of the –CH<sub>2</sub>– signals at higher temperatures might lead to a loss of axial chirality indicating atropisomerism. The major difference compared to **2<sup>La</sup>** is the change in signal pattern for the Al–Me groups). At −80 °C there are two sets of signals associated to the AlMe<sub>4</sub> and AlMe<sub>3</sub> groups. Four sharp signals at 0.47, 0.21, −0.14, and −1.26 ppm with an integral ratio of 6:3:3:3. The other set consists of rather broad signals at 0.22, 0.10, −0.18, −0.42, and −1.02 ppm with an integration ratio of 3:3:3:3:3 (Figure S23). Unfortunately, the signals could not be assigned to specific methyl groups. While heating the sample the originally sharp signals broadened while the signals which used to be broad at −80 °C merged to sharper signals above 0 °C.

The different fluxional behaviour of the Al–Me groups of **2<sup>Y</sup>** compared to **2<sup>La</sup>** is probably caused by the different ionic radii of Y(III) and La(III). Accordingly, the smaller Y(III) centre in **2<sup>Y</sup>** implies a rather restricted dynamic behaviour of the Al–Me groups at −80 °C as opposed to an increasingly sterically unsaturated **2<sup>La</sup>**. This leads to the assumption of an associative exchange mechanism for the Al–Me groups.<sup>31</sup> Unfortunately, a proper line shape analysis, to obtain thermodynamic data for the exchange process was not feasible. The formation of methane at 0.17 ppm (Fig. 5) shows the lability of **2<sup>Y</sup>** and formation of **3<sup>Y</sup>** which is much more predominant at elevated temperatures.

The chirality of **3<sup>Ln</sup>** which can be seen in the crystal structure could not be observed in the ambient temperature <sup>1</sup>H NMR spectrum. More specifically, the characteristic signal splitting of the –CH<sub>2</sub>– group was not observable at ambient temperature, whereas a VT <sup>1</sup>H NMR study revealed the chirality at lower temperatures (Fig. 7). At −80 °C, two doublets at 3.17 and 2.54 ppm with geminal coupling constants of 16.1 Hz were detected, with the coalescence temperature noted at −10 °C. Signal sharpening at elevated temperatures supports the presence of atropisomers at higher temperatures while at low temperatures, the chiral character prevails.

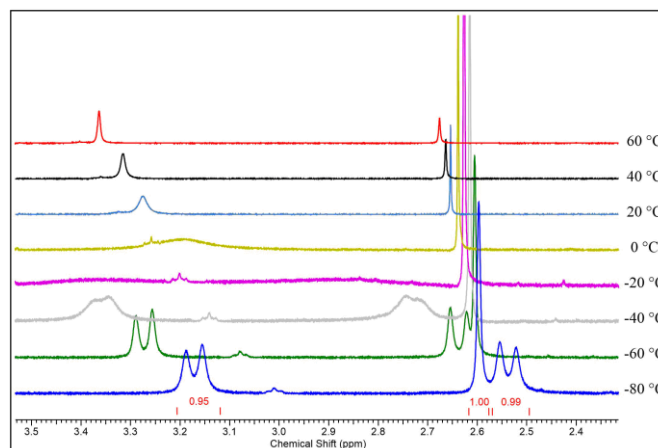


Fig. 7 <sup>1</sup>H-VT NMR spectra of **3<sup>Lu</sup>** in toluene from −80 to 60 °C.

### Isoprene Polymerization

Previously, it was shown that rare-earth metal alkyl pincer complexes can serve as good precatalysts for the diene polymerization.<sup>6–11</sup> Therefore, the polymerization of isoprene was investigated (Table 2). The established borate trityl tetrakis(pentafluorophenyl)borate (**A**) and dimethylanilinium tetrakis(pentafluorophenyl)borate (**B**) as well as tris(pentafluorophenyl)borane (**C**) were used successfully as cocatalysts. The use of chlorinating agents like dimethyl- or diethyl aluminiumchloride did not result in an active species, which is in agreement with [{Cp<sup>NMe</sup>(μ-CH<sub>2</sub>)AlMe<sub>3</sub>]<sub>2</sub>La(AlMe<sub>4</sub>)] a tridentate C–H bond activated complex.<sup>43</sup> However, other rare-earth-metal alkoxy aluminates (Ln(OR)<sub>3</sub>(AlMe<sub>3</sub>)<sub>3</sub>) are active in isoprene polymerization upon activation of diethyl aluminiumchloride.<sup>36</sup> The abstraction of the alkoxide of the rare-earth metal by chlorinating reagents to form an active catalyst is probably prohibited by the chelating ligand. Complex **2<sup>Y</sup>** was not probed as a precatalyst due to its lability at ambient temperature and formation of an unknown mixture of **2<sup>Y</sup>** and **3<sup>Y</sup>**. Crystals obtained from the reaction of **2<sup>La</sup>** and **3<sup>Y</sup>** with cocatalyst **A** revealed the formation of triphenylethane, indicating the desired reaction of cocatalyst **A** with a metal methyl group instead of the pincer-type ligands (ESI Figure S26). Also, the protonolysis of the rare-earth metal complexes under study with cocatalyst **B** proceeded as expected at a metal methyl moiety, as indicated by the formation of

methane and  $\text{PhNMe}_2/\text{AlMe}_3$  (ESI Figure S27). Unfortunately, the actual active species could not be further elucidated.

All polymerization reactions were conducted with either one or two equivalents of cocatalyst. It is revealed that  $2^{\text{Ln}}$  as well as  $3^{\text{Ln}}$  serve as a much better catalysts upon activation with two equivalents of cocatalyst **A**, **B**, or **C** (e.g. entry 4-6 and 10-12, Table 2). For the activation of  $2^{\text{La}}$  with two equivalents of **A** (entry 7, Table 2), an isoprene conversion of over 90% after one hour was observed, while the 1-equiv-activation (entry 1, Table 2) indicated only the formation of traces even after two hours. A similar behaviour could be observed for  $3^{\text{Y}}$  upon activation with cocatalyst **B**. With one equivalent of **B** (entry 14, Table 2) a conversion of only 26% after one hour was noted, while the activation with two equivalents of **B** (entry 18, Table 2) revealed almost full conversion after only 15

minutes, which is almost an eightfold increase in rate. The polymerization reactions promoted by  $2^{\text{Ln}}$  in the presence of two equivalents of cocatalyst also led to microstructures with higher *cis*-1,4-, and 3,4-content and lower *trans*-1,4-content compared to polymerizations with one equivalent of cocatalyst (e.g. entry 2/8, Table 2). Using two equivalents of cocatalyst **B** for the activation of  $2^{\text{La}}$ , a polyisoprene with 92% *cis*-1,4-content, no *trans*-1,4-content at all, and a narrow molecular weight distribution of 1.19 could be obtained (entry 8, Table 2). Polymerizations of  $2^{\text{Ln}}$  activated with cocatalyst **C** showed in general good activity albeit slightly lower than polymerizations conducted with cocatalyst **A** or **B**. The combinations  $3^{\text{Ln}}/\text{C}$  and  $3^{\text{Ln}}/2\text{C}$  did not any polymer.

**Table 2** Polymerization of isoprene with  $2^{\text{Ln}}$  and  $3^{\text{Ln}}$  under various conditions.

entry <sup>[a]</sup>	pre-catalyst	cocatalyst <sup>[b]</sup>	time [h]	yield [%]	<i>cis</i> -1,4- <sup>[c]</sup>	<i>trans</i> -1,4- <sup>[c]</sup>	3,4- <sup>[c]</sup>	$M_n$ ( $\times 10^4$ ) <sup>[d]</sup>	$M_w/M_n$ <sup>[d]</sup>	$T_g$ [°C] <sup>[e]</sup>
1	$2^{\text{La}}$	<b>1A</b>	2	tr	-	-	-	-	-	-
2	$2^{\text{La}}$	<b>1B</b>	2	42	55.4	40.3	4.3	7.6	1.24	-63
3	$2^{\text{La}}$	<b>1C</b>	2	tr	-	-	-	-	-	-
4	$2^{\text{Nd}}$	<b>1A</b>	1	82	47.7	47.6	4.8	9.7	1.29	-62
5	$2^{\text{Nd}}$	<b>1B</b>	1	78	62.2	31.4	6.4	13.5	1.51	-59
6	$2^{\text{Nd}}$	<b>1C</b>	2	73	84.3	12.1	3.6	11.5	1.66	-61
7	$2^{\text{La}}$	<b>2A</b>	1	92	75.1	12.4	12.5	7.3 <sup>f</sup>	1.56 <sup>f</sup>	-53
8	$2^{\text{La}}$	<b>2B</b>	1	70	92.0	0.0	8.1	6.9	1.19	-57
9	$2^{\text{La}}$	<b>2C</b>	2	78	91.4	3.0	5.6	9.6	1.25	-59
10	$2^{\text{Nd}}$	<b>2A</b>	1	93	74.4	12.8	12.8	9.9 <sup>f</sup>	6.50 <sup>f</sup>	-45
11	$2^{\text{Nd}}$	<b>2B</b>	1	85	82.1	9.7	8.3	7.4	1.74	-57
12	$2^{\text{Nd}}$	<b>2C</b>	1	83	91.0	2.6	6.4	14.3	1.46	-58
13	$3^{\text{Y}}$	<b>1A</b>	1	76	80.3	6.3	13.4	7.5 <sup>f</sup>	1.77 <sup>f</sup>	-51
14	$3^{\text{Y}}$	<b>1B</b>	1	26	73.0	3.7	23.3	35.5 <sup>f</sup>	2.19 <sup>f</sup>	-47
15	$3^{\text{Lu}}$	<b>1A</b>	2	51	77.0	11.0	12.1	3.8 <sup>f</sup>	2.10 <sup>f</sup>	-51
16	$3^{\text{Lu}}$	<b>1B</b>	2	15	85.1	0.0	17.2	22.5	1.69	-54
17	$3^{\text{Y}}$	<b>2A</b>	1	98	77.4	9.1	13.5	9.2 <sup>f</sup>	7.19 <sup>f</sup>	-38
18	$3^{\text{Y}}$	<b>2B</b>	0.25	92	83.5	0.0	16.5	35.9	2.83	-51
19	$3^{\text{Lu}}$	<b>2A</b>	1	tr	-	-	-	-	-	-
20	$3^{\text{Lu}}$	<b>2B</b>	0.25	41	82.2	7.9	9.9	16.2	3.30	-56

<sup>[a]</sup> General polymerization procedure: 0.02 mmol of pre-catalyst, 8 mL of toluene, 20 mmol of isoprene, r.t. <sup>[b]</sup> **A** =  $[\text{Ph}_3\text{C}][\text{B}(\text{C}_6\text{F}_5)_4]$ ; **B** =  $[\text{PhNMe}_2\text{H}][\text{B}(\text{C}_6\text{F}_5)_4]$ ; **C** =  $\text{B}(\text{C}_6\text{F}_5)_3$ ; Catalyst pre-formation: 30 min. <sup>[c]</sup> Determined by  $^1\text{H}$ ,  $^{13}\text{C}$  NMR spectroscopy in  $\text{CDCl}_3$ . <sup>[d]</sup> Determined by GPC against polystyrene standards. <sup>[e]</sup> Determined by DSC at 20 K/min. <sup>[f]</sup> generation of a bimodal species, listed entry only for the first peak, second peak was not possible to analyse.



For complex **2<sup>La</sup>** and **2<sup>Nd</sup>** (entries 9/12, Table 2), or **3<sup>Y</sup>** and **3<sup>Lu</sup>** (entries 18/20, Table 2) the influence of the metal on the microstructure is not significant. This is in striking contrast to polymerization performance of half-sandwich complexes.<sup>32,33</sup> It seems that the main influence of the metal lies on the activity. Complex **2<sup>Nd</sup>** (78% yield after 1 h (entry 5, Table 2)) is more active than the respective **2<sup>La</sup>** (42% yield after 2 h (entry 2, Table 2)), while **3<sup>Y</sup>** (92% yield after 15 minutes (entry 18, Table 2)) is more reactive than **3<sup>Lu</sup>** (41% yield after 15 minutes (entry 20, Table 2)). In general, it is assumed that cocatalysts **A** and **B** are forming the same active species. However, it was observed that the use of **A** or **B** lead to putatively different active species. The microstructures of polymers gained by **2<sup>Ln</sup>** activated with two equivalents of **A** or **B** seem to be comparable but the GPC measurements revealed a significant difference. Polymers obtained by using cocatalyst **B** show a monomodal polymer with a chain length of  $M_n = 7.4 \times 10^4$  Da (entry 11, Table 2) and a rather narrow molecular weight distribution (1.19; entry 8, Table 2). On the other hand using two equivalents of cocatalyst **A** results in a bimodal polymer (entries 7/10, Table 2). The polymer part with the lower molecular weight makes up to 45% (entry 10, Table 2) of the total polymer. The bimodal distribution using **2<sup>Ln</sup>** can only be observed while using two equivalents of **A** (entries 4/7, Table 2). The bimodal distribution of the polymer is observed for **3<sup>Ln</sup>** only in combination with one and two equivalents of cocatalyst **A** (entries 13, 15, 17, Table 2). The RI of the bimodal polyisoprene species are shown in the Supporting information (Figure S28).

## Conclusions

In this study the proligand 2-(6-Methyl-2-pyridyl)-1,1-diphenyl-ethanol [HONCH<sub>3</sub>] was shown to afford a pincer-type ligand upon multiple deprotonation with Ln(AlMe<sub>4</sub>)<sub>3</sub>. Crucially, the radii of the rare-earth metal center determines the degree of C–H bond activation on the lutidynyl methyl group. With lanthanum or neodymium a single C–H bond activation prevails, resulting in complexes [ONCH<sub>2</sub>]Ln(AlMe<sub>3</sub>)<sub>2</sub>(AlMe<sub>4</sub>). Employing Y(AlMe<sub>4</sub>)<sub>3</sub> the initially formed [ONCH<sub>2</sub>]Y(AlMe<sub>3</sub>)<sub>2</sub>(AlMe<sub>4</sub>) is unstable and undergoes a second C–H bond activation of the already deprotonated methyl group yielding alkylidene complex [ONCH]Y(AlMe<sub>3</sub>)<sub>2</sub>(AlMe<sub>4</sub>). The same complex is obtained directly for the smaller rare-earth metal lutetium. Complexes [ONCH<sub>2</sub>]Ln(AlMe<sub>3</sub>)<sub>2</sub>(AlMe<sub>4</sub>) display axial chirality according to their solid-state structure and <sup>1</sup>H NMR spectra. The triply de-protonated complexes [ONCH]Ln(AlMe<sub>3</sub>)<sub>2</sub>(AlMe<sub>4</sub>) revealed the chiral character only in the X-ray structure and at low temperatures in the <sup>1</sup>H NMR spectrum. At higher

temperatures the increased mobility of the ligands makes a case for atropisomerism.

Despite the di- and trianionic character of the pincer ligand, the complex showed excellent properties for isoprene polymerization upon activation with known borate/borane cocatalysts. In particular, the use of two equivalents of cocatalyst results in more active species and polymers with higher *cis*-1,4-contents. For example, the catalyst system **3<sup>Y</sup>/2B** achieved almost full conversion after 15 min, while the microstructure showed no *trans*-1,4-content and a *cis*-1,4-content of 83.5%. Activation of the pincer-type complexes with cocatalyst **A** resulted in bimodal polyisoprenes.

## Experimental

### General experimental procedures and instrumentation.

All manipulations were performed with rigorous exclusion of air and water, using standard Schlenk, high-vacuum, and glovebox techniques (MBraun UNILab-pro-dp; < 0.5 ppm O<sub>2</sub>, < 0.5 ppm H<sub>2</sub>O). Toluene and *n*-hexane were purified by using Grubbs-type columns (MBraun SPS, solvent purification system) and stored inside a glovebox. [D<sub>8</sub>]thf and [D<sub>6</sub>]benzene were purchased from Aldrich, degassed and dried over NaK for 24 h, filtered, and stored inside a glovebox. [Ph<sub>3</sub>C][B(C<sub>6</sub>F<sub>5</sub>)<sub>4</sub>] (**A**), [PhNMe<sub>2</sub>H][B(C<sub>6</sub>F<sub>5</sub>)<sub>4</sub>] (**B**), and B(C<sub>6</sub>F<sub>5</sub>)<sub>3</sub> (**C**) were obtained from Boulder Scientific Company and used without further purification. Trioctylaluminum and isoprene were obtained from Sigma Aldrich. Isoprene was dried over trioctylaluminum and distilled prior to use. Ligand **1** was synthesized according to literature procedures.<sup>44</sup> Homoleptic Ln(AlMe<sub>4</sub>)<sub>3</sub> (Ln = La, Nd, Lu) were prepared according to literature procedures.<sup>31</sup> NMR spectra were recorded on a Bruker AVBII+400 (<sup>1</sup>H: 400.11 MHz; <sup>13</sup>C: 100.61 MHz) spectrometer. Variable temperature NMR experiments were recorded on a Bruker AVII+500 (<sup>1</sup>H: 500.13 MHz; <sup>13</sup>C: 125.76 MHz). <sup>1</sup>H and <sup>13</sup>C shifts are referenced to internal solvent resonances and reported in parts per million relative to tetramethylsilane (TMS). Coupling constants are given in Hz. Elemental analyses were performed on an ElementarVario Micro Cube. IR spectra were recorded on a NICOLET 6700 FTIR spectrometer with a DRIFTS cell (KBr window). Size exclusion chromatography (SEC) was performed on a Viscotek GPCmax apparatus and a model TDA 305 triple detector array. Sample solutions (1.0 mg polymer per mL thf) were filtered through a 0.45 μm syringe filter prior injection. The flow rate was 1 mL/min. dn/dc and dA/dc data were determined by means of the integrated OmniSec™ software. The microstructure of the polyisoprenes was determined on a Bruker AVBII+400 and Bruker DRX250 spectrometer in [D]chloroform at ambient temperatures. Glass transition temperatures (*T*<sub>g</sub>) of the polyisoprenes were determined on a Perkin-

Elmer DSC 8000 with heating rates of 20 K/min and cooling rates of 60 K/min.

### Preparation and characterisation of compounds **2<sup>Ln</sup>** and **3<sup>Ln</sup>**

**[ONCH<sub>2</sub>]La(AlMe<sub>3</sub>)<sub>2</sub>(AlMe<sub>4</sub>) (2<sup>La</sup>).** La(AlMe<sub>4</sub>)<sub>3</sub> (250 mg, 0.620 mmol) was dissolved in toluene (5 mL), and a solution of [HONCH<sub>3</sub>] (**1**, 181 mg, 0.620 mmol) in toluene (5 mL) was added slowly under vigorous stirring. Immediately, CH<sub>4</sub> formation could be observed. After stirring the reaction for 2 h at ambient temperature, the solvent was removed *in vacuo* to give **2<sup>La</sup>** as a yellow solid. Crystalline **2<sup>La</sup>** was obtained from a saturated mixture of *n*-hexane and toluene solution at -35 °C as [ONCH<sub>2</sub>]La(AlMe<sub>3</sub>)<sub>2</sub>(AlMe<sub>4</sub>)·1/3(C<sub>7</sub>H<sub>8</sub>) (310 mg, 0.440 mmol, 71%). <sup>1</sup>H NMR (400 MHz, [D<sub>6</sub>]benzene, 26 °C): δ = 6.83 - 7.16 (m, 10 H, PhH and toluene), 6.49 (t, <sup>3</sup>J<sub>HH</sub>=7.8 Hz, 1 H, PyH), 6.00 (d, <sup>3</sup>J<sub>HH</sub>=8.0 Hz, 1 H, PyH), 5.81 (d, <sup>3</sup>J<sub>HH</sub>=7.4 Hz, 1 H, PyH), 3.89 (d, <sup>2</sup>J<sub>HH</sub>=15.1 Hz, 1 H, Py-CH<sub>2</sub>-CPh<sub>2</sub>), 3.02 (d, <sup>2</sup>J<sub>HH</sub>=15.1 Hz, 1 H, Py-CH<sub>2</sub>-CPh<sub>2</sub>), 2.45 (d, <sup>2</sup>J<sub>HH</sub>=15.6 Hz, 1 H, Py-CH<sub>2</sub>-Al), 2.11 (s, 1 H, toluene), 1.90 (d, <sup>2</sup>J<sub>HH</sub>=15.6 Hz, 1 H, Py-CH<sub>2</sub>-Al), 0.15 (s, 12 H, CH<sub>3</sub>), -0.38 (s, 18 H, CH<sub>3</sub>) ppm. <sup>13</sup>C {<sup>1</sup>H} NMR (101 MHz, [D<sub>6</sub>]benzene, 26 °C): δ = 165.9 (s, Py), 154.1 (s, Py), 144.8 (s, Ph), 143.2 (s, Ph), 140.3 (s, Py), 129.4 (br. s, Ph), 129.3 (s, Tol), 129.3 (br. s, Ph), 128.7 (br. s, Ph), 128.6 (s, Tol), 128.5 (br. s, Ph), 125.7 (s, Tol), 122.2 (s, Py), 120.9 (s, Py), 85.5 (s, Ph<sub>2</sub>C-CH<sub>2</sub>), 50.5 (s, Py-CH<sub>2</sub>-CPh<sub>2</sub>), 29.7 (s, Py-CH<sub>2</sub>-Al), 21.4 (s, Tol), 4.7 (s, AlMe<sub>4</sub>), 2.7 (s, AlMe<sub>3</sub>), 0.7 (s, AlMe<sub>3</sub>) ppm. IR (DRIFTS):  $\tilde{\nu}$  = 3084 (m), 3060 (m), 3026 (m), 2920 (vs), 2884 (vs), 2810 (s), 2786 (s), 1955 (w), 1874 (w), 1808 (w), 1776 (w), 1746 (w), 1692 (w), 1666 (w), 1603 (s), 1565 (s), 1493 (s), 1460 (vs), 1444 (vs), 1376 (w), 1334 (w), 1309 (m), 1268 (s), 1241 (m), 1205 (vs), 1187 (vs), 1157 (s), 1105 (m), 1088 (w), 1063 (m), 1036 (vs), 1000 (s), 968 (m), 931 (m), 919 (m), 904 (m), 889 (m), 874 (s), 801 (s), 775 (s), 764 (s), 750 (s), 721 (vs), 708 (vs), 700 (vs), 687 (vs), 614 (vs), 581 (vs), 551 (s), 525 (m), 488 (vs), 481 (vs), 465 (s), 458 (m), 452 (m), 444 (s), 425 (m), 410 (w), 404 (m) cm<sup>-1</sup>. Elemental analysis of crystalline **2<sup>La</sup>**, calcd. for C<sub>33.3</sub>H<sub>52.7</sub>Al<sub>3</sub>LaNO (703.31): C 56.93, H 7.55, N 1.99; found: C 56.80, H 7.12, N 2.14.

**[ONCH<sub>2</sub>]Nd(AlMe<sub>3</sub>)<sub>2</sub>(AlMe<sub>4</sub>) (2<sup>Nd</sup>).** Nd(AlMe<sub>4</sub>)<sub>3</sub> (250 mg, 0.620 mmol) was dissolved in toluene (5 mL), and a solution of [HONCH<sub>3</sub>] (**1**, 178 mg, 0.620 mmol) in toluene (5 mL) was added slowly under vigorous stirring. Immediately, CH<sub>4</sub> formation could be observed. After stirring the reaction for 2 h at ambient temperature, the solvent was removed *in vacuo* to give **2<sup>Nd</sup>** as a blue solid. Crystalline **2<sup>Nd</sup>** was obtained from a saturated mixture of *n*-hexane and toluene solution at -35 °C as [ONCH<sub>2</sub>]Nd(AlMe<sub>3</sub>)<sub>2</sub>(AlMe<sub>4</sub>)·1/3(C<sub>7</sub>H<sub>8</sub>) (369 mg, 0.520 mmol, 84%). <sup>1</sup>H NMR (400 MHz, [D<sub>6</sub>]benzene, 26 °C): δ = 25.29 (br. s., 1 H), 23.27 (br. s., 1 H), 19.04 (br. s., 1 H), 17.69 (br. s., 4 H), 17.53 (br. s., 2 H), 14.20 (br. s.,

2 H), 10.88 (br. s., 3 H), 9.76 (br. s., 2 H), 7.74 (br. s., 2 H), 5.68 (br. s., 2 H), 1.45 (br. s., 2 H) -6.17 (br. s., 24 H) ppm. IR (DRIFTS):  $\tilde{\nu}$  = 3086 (m), 3058 (s), 3024 (s), 2922 (vs), 2917 (vs), 2887 (vs), 2813 (s), 2792 (s), 1967 (m), 1873 (m), 1807 (m), 1604 (s), 1566 (s), 1493 (s), 1461 (vs), 1444 (vs), 1376 (m), 1336 (s), 1310 (m), 1271 (s), 1242 (s), 1208 (s), 1187 (vs), 1157 (s), 1105 (s), 1089 (m), 1061 (s), 1036 (s), 1007 (s), 999 (s), 969 (s), 932 (s), 919 (m), 905 (s), 887 (s), 875 (s), 801 (s), 775 (s), 764 (s), 750 (s), 733 (vs), 725 (vs), 718 (vs), 710 (vs), 706 (vs), 697 (vs), 690 (vs), 682 (vs), 675 (s), 645 (s), 618 (s), 611 (s), 592 (s), 581 (vs), 572 (s), 561 (s), 548 (s), 527 (s), 516 (s), 508 (s), 499 (s), 485 (vs), 472 (s), 462 (s), 457 (s), 445 (s), 437 (s), 427 (m), 417 (m), 407 (m), 401 (m) cm<sup>-1</sup>. Elemental analysis of crystalline **2<sup>Nd</sup>**, calcd. for C<sub>33.3</sub>H<sub>52.7</sub>Al<sub>3</sub>NdNO (708.64): C 56.50, H 7.49, N 1.98; found: C 56.39, H 7.49, N 1.98.

**[ONCH<sub>2</sub>]Y(AlMe<sub>3</sub>)<sub>2</sub>(AlMe<sub>4</sub>) (2<sup>Y</sup>).** Y(AlMe<sub>4</sub>)<sub>3</sub> (250 mg, 0.710 mmol) was dissolved in toluene (5 mL), and a solution of [HONCH<sub>3</sub>] (**1**, 207 mg, 0.710 mmol) in toluene (5 mL) was added slowly under vigorous stirring. Immediately, CH<sub>4</sub> formation could be observed. After stirring the reaction for 2 h at room temperature, the solvent was removed *in vacuo* to give **2<sup>Y</sup>** as a yellow solid. Crystalline **2<sup>Y</sup>** was obtained from a saturated mixture of *n*-hexane and toluene solution at -35 °C as [ONCH<sub>2</sub>]Y(AlMe<sub>3</sub>)<sub>2</sub>(AlMe<sub>4</sub>) (263 mg, 0.430 mmol, 61%). <sup>1</sup>H NMR (400 MHz, [D<sub>6</sub>]benzene, 26 °C): δ = 7.80 (br. s., 1 H, Ph), 6.84 - 7.11 (m, 6 H, Ph), 6.51 (t, <sup>3</sup>J<sub>HH</sub>=7.8 Hz, 1 H, Py), 6.03 (d, <sup>3</sup>J<sub>HH</sub>=8.1 Hz, 1 H, Py), 5.84 (d, <sup>3</sup>J<sub>HH</sub>=7.5 Hz, 1 H, Py), 3.92 (d, <sup>1</sup>J<sub>HH</sub>=15.1 Hz, 1 H, Py-CH<sub>2</sub>-CPh<sub>2</sub>), 3.07 (d, <sup>1</sup>J<sub>HH</sub>=15.2 Hz, 1 H, Py-CH<sub>2</sub>-CPh<sub>2</sub>), 2.28 (d, <sup>1</sup>J<sub>HH</sub>=16.1, 1 H, Py-CH<sub>2</sub>-Al) 2.13 (d, <sup>1</sup>J<sub>HH</sub>=16.1 Hz, 1 H, Py-CH<sub>2</sub>-Al), -0.02 (br. s., 14 H, AlMe), -0.41 (d, <sup>2</sup>J<sub>YH</sub>=1.0 Hz, 10 H, AlMe), -0.45 (d, <sup>2</sup>J<sub>YH</sub>=1.4 Hz, 1 H, AlMe), -1.28 (br. s., 4 H, AlMe) ppm. <sup>13</sup>C {<sup>1</sup>H} NMR (101 MHz, [D<sub>6</sub>]benzene, 26 °C): δ = 167.5 (s, Py), 154.3 (s, Py), 144.1 (s, Ph), 143.0 (s, Ph), 140.5 (s, Py), 129.6 (s, Ph), 129.5 (s, Ph), 128.8 (s, Ph), 121.4 (s, Py), 120.6 (s, Py), 85.2 (s, Ph<sub>2</sub>C-CH<sub>2</sub>), 48.3 (s, Py-CH<sub>2</sub>-CPh<sub>2</sub>), 27.0 (s, Py-CH<sub>2</sub>-Al), 0.2 (s, AlMe), -2.2 (s, AlMe) ppm. IR (DRIFTS):  $\tilde{\nu}$  = 3090 (m), 3059 (m), 3025 (m), 2921 (vs), 2886 (s), 2818 (m), 1988(w), 1967 (w), 1950 (w), 1901 (w), 1882 (w), 1802 (w), 1774 (w), 1755 (w), 1691 (w), 1666 (w), 1601 (vs), 1566 (s), 1494 (s), 1460 (vs), 1445 (s), 1340 (m), 1320 (m), 1272 (s), 1217 (s), 1191 (vs), 1160 (s), 1101 (m), 1042 (vs), 1012 (s), 992 (s), 973 (m), 933 (m), 918 (m), 904 (s), 889 (s), 867 (s), 800 (s), 773 (s), 764 (s), 753 (s), 712 (vs), 702 (vs), 690 (vs), 644 (s), 614 (s), 577 (vs), 548 (s), 538 (s), 493 (s), 486 (s), 478 (s), 450 (m), 428 (m), 415 (w), 407(m) cm<sup>-1</sup>. Elemental analysis of crystalline **2<sup>Y</sup>**, calcd. for C<sub>30</sub>H<sub>47</sub>Al<sub>3</sub>YNO (607.56): C 59.31, H 7.80, N 2.31; found: C 59.55, H 8.06, N 2.25.

**[ONCH]Y(AlMe<sub>3</sub>)<sub>3</sub> (3<sup>Y</sup>).** Y(AlMe<sub>4</sub>)<sub>3</sub> (250 mg, 0.710 mmol) was dissolved in toluene (5 mL), and a solution of

[HONCH<sub>3</sub>] (**1**, 207 mg, 0.710 mmol) in toluene (5 mL) was added slowly under vigorous stirring. Immediately, CH<sub>4</sub> formation could be observed. After stirring the reaction for 3 h at 60 °C, the solvent was removed *in vacuo* to give **3<sup>Y</sup>** as a yellow solid. Crystalline **3<sup>Y</sup>** was obtained from a saturated *n*-hexane solution at -35 °C as [ONCH]Y(AlMe<sub>3</sub>)<sub>3</sub> (292 mg, 0.480 mmol, 67%). <sup>1</sup>H NMR (400 MHz, [D<sub>6</sub>]benzene, 26 °C): δ = 7.00 – 7.20 (m, 10H, Ph), 6.66 (dd, <sup>3</sup>J<sub>HH</sub>=8.2, 7.4 Hz, 1 H, Py), 5.99 (d, <sup>3</sup>J<sub>HH</sub>=8.2 Hz, 1 H, Py), 5.85 (d, <sup>3</sup>J<sub>HH</sub>=7.4 Hz, 1 H, Py), 3.28 (s, 2 H, -CH<sub>2</sub>-), 2.36 (d, <sup>2</sup>J<sub>YH</sub>=5.1 Hz, 1-CH-), -0.42 (d, <sup>2</sup>J<sub>YH</sub>=1.5 Hz, 18 H, CH-AlMe<sub>3</sub>), -0.45 (d, <sup>2</sup>J<sub>YH</sub>=1.5 Hz, 9 H, O-AlMe<sub>3</sub>) ppm. <sup>13</sup>C {<sup>1</sup>H} NMR (101 MHz, [D<sub>6</sub>]benzene, 26 °C): δ = 176.8 (s, Py), 152.9 (s, Py), 144.1 (s, Ph), 140.0 (s, Py), 128.8 (s, Ph), 128.7 (s, Ph), 128.5 (s, Ph), 120.4 (s, Py), 114.2 (s, Py), 84.5 (s, Ph<sub>2</sub>C-CH<sub>2</sub>), 47.8 (s, Py-CH<sub>2</sub>-CPh<sub>2</sub>), 36.3 (s, Al-CH-Al), -0.5 (s, O-AlMe<sub>3</sub>), -2.2 (s, CH-AlMe<sub>3</sub>) ppm. IR (DRIFTS):  $\tilde{\nu}$  = 3053 (w), 2924 (m), 2884 (m), 2819 (w), 1597 (m), 1555 (s), 1495 (w), 1447 (vs), 1431 (m), 1335 (w), 1276 (s), 1222 (m), 1189 (s), 1157 (m), 1093 (w), 1074 (w), 1015 (s), 1005 (s), 982 (m), 938 (w), 921 (w), 907 (m), 881 (s), 871 (m), 814 (m), 801 (m), 780 (s), 767 (m), 745 (s), 734 (s), 693 (vs), 644 (s), 610 (s), 560 (s), 539 (s), 479 (s), 473 (s), 457 (s), 416 (w) cm<sup>-1</sup>. Elemental analysis of crystalline **3<sup>Y</sup>**, calcd. for C<sub>29</sub>H<sub>43</sub>Al<sub>3</sub>YNO (591.52): C 58.89, H 7.33, N 2.37; found: C 59.37, H 7.47, N 2.51.

[ONCH]Lu(AlMe<sub>3</sub>)<sub>3</sub> (**3<sup>Lu</sup>**). Lu(AlMe<sub>4</sub>)<sub>3</sub> (250 mg, 0.570 mmol) was dissolved in toluene (5 mL), and a solution of [HONCH<sub>3</sub>] (**1**, 166 mg, 0.570 mmol) in toluene (5 mL) was added slowly under vigorous stirring. Immediately, the formation of CH<sub>4</sub> took place. After stirring the reaction for 3 h at 60 °C, the solvent was removed *in vacuo* to give **3<sup>Lu</sup>** as a yellow solid. Crystalline **3<sup>Lu</sup>** was obtained from a saturated *n*-hexane solution at -35 °C as [ONCH]Lu(AlMe<sub>3</sub>)<sub>3</sub> (281 mg, 0.460 mmol, 81%). <sup>1</sup>H NMR (400 MHz, [D<sub>6</sub>]benzene, 26 °C): δ = 7.20 (br. s, 3 H, Ph), 6.95 – 7.13 (m, 6), 6.67 (dd, <sup>3</sup>J<sub>HH</sub>=7.8 Hz, 1 H, Py), 5.99 (d, <sup>3</sup>J<sub>HH</sub>=8.2 Hz, 1 H, Py), 5.89 (d, <sup>3</sup>J<sub>HH</sub>=7.4 Hz, 1 H, Py), 3.26 (s, 2 H, Py-CH<sub>2</sub>-CPh<sub>2</sub>), 2.72 (s, 1 H, Al-CH-Al), -0.29 (s, 18 H, CH-AlMe<sub>3</sub>), -0.30 (s, 9 H, O-AlMe<sub>3</sub>) ppm. <sup>13</sup>C {<sup>1</sup>H} NMR (101 MHz, [D<sub>6</sub>]benzene, 26 °C): δ = 175.8 (s, Py), 153.4 (s, Py), 144.0 (s, Ph), 140.6 (s, Py), 129.2 (s, Ph), 129.0 (s, Ph), 128.9 (s, Ph), 120.5 (s, Py), 114.6 (s, Py), 85.1 (s, Ph<sub>2</sub>C-CH<sub>2</sub>), 47.5 (s, Py-CH<sub>2</sub>-CPh<sub>2</sub>), 38.1 (s, Al-CH-Al), 0.5 (s, O-AlMe<sub>3</sub>), -1.3 (s, CH-AlMe<sub>3</sub>) ppm. IR (DRIFTS):  $\tilde{\nu}$  = 3062 (w), 2925 (s), 2886 (w), 2815 (w), 1955 (w), 1887 (w), 1811 (w), 1755 (w), 1593 (s), 1555 (vs), 1495 (m), 1448 (vs), 1430 (s), 1336 (w), 1278 (vs), 1256 (m), 1232 (m), 1198 (vs), 1191 (vs), 1159 (m), 1093 (w), 1069 (w), 1053 (w), 1017 (s), 1004 (s), 984 (m), 937 (w), 918 (w), 906 (m), 881 (m), 869 (m), 814 (s), 781 (s), 766 (m), 746 (m), 737 (s), 714 (s), 707 (vs), 680 (s), 669 (m), 659 (s), 639 (m), 608 (m), 602 (m), 588 (w), 580 (m), 570 (m), 560 (s), 542 (m), 525 (w), 514 (w), 499 (m),

468 (m) cm<sup>-1</sup>. Elemental analysis of crystalline **3<sup>Lu</sup>**, calcd. for C<sub>29</sub>H<sub>43</sub>Al<sub>3</sub>LuNO (677.58): C 51.41, H 6.40, N 2.07; found: C 51.81, H 6.38, N 2.17.

### Crystallography and crystal structure determination

Crystals from all complexes suitable for X-Ray crystallography were grown by standard techniques from saturated *n*-hexane/toluene solutions at -40 °C. Single crystals were selected inside a glovebox, coated with Parabar 10312 (previously known as Paratone N, Hampton Research) or perflourinated ether and fixed on a microloop. Data were collected on a Bruker APEX DUO instrument equipped with an I $\mu$ S microfocus sealed tube and QUAZAR optics for MoK $\alpha$  radiation ( $\lambda$  = 0.71073 Å). Therefore, data were collected on a Bruker SMART APEX II instrument equipped with a fine focus sealed tube and TRIUMPH monochromator using MoK $\alpha$  radiation ( $\lambda$  = 0.71073 Å). The data collection strategy was determined using COSMO<sup>45</sup> employing  $\omega$ - and  $\phi$  scans. Raw data were processed using APEX<sup>46</sup> and SAINT,<sup>47</sup> corrections for absorption effects were applied using SADABS.<sup>48</sup> All data were processed using APEX3<sup>46</sup> software package. The structures were solved by direct methods and refined against all data by full-matrix least-squares methods on F<sup>2</sup> using SHELXTL<sup>48</sup> and Shelxle<sup>49</sup>. All Graphics were produced employing ORTEP-3<sup>50</sup> and POV-Ray<sup>51</sup>.

### Conflicts of interest

There are no conflicts to declare.

### Acknowledgements

We are grateful to BRIDGESTONE Japan for generous support.

### Notes and references

- Z. Hou and Y. Wakatsuki, *Coordination Chemistry Reviews*, 2002, **231**, 1–22.
- Herbert. Schumann, J. A. Meese-Marktscheffel and Lothar. Esser, *Chem. Rev.*, 1995, **95**, 865–986.
- M. M. Hänninen, M. T. Zamora and P. G. Hayes, in *The Privileged Pincer-Metal Platform: Coordination Chemistry & Applications*, eds. G. van Koten and R. A. Gossage, Springer International Publishing, Cham, 2015, vol. 54, pp. 93–177.
- J. Huang, Z. Liu, D. Cui and X. Liu, *ChemCatChem*, 2018, **10**, 42–61.
- A. A. Trifonov and D. M. Lyubov, *Coordination Chemistry Reviews*, 2017, **340**, 10–61.
- P. Zhang, H. Liao, H. Wang, X. Li, F. Yang and S. Zhang, *Organometallics*, 2017, **36**, 2446–2451.
- C. Yu, D. Zhou, X. Yan, F. Gao, L. Zhang, S. Zhang and X. Li, *Polymers*, 2017, **9**, 531.
- H. Liu, J. He, Z. Liu, Z. Lin, G. Du, S. Zhang and X. Li, *Macromolecules*, 2013, **46**, 3257–3265.

- 9 L. Wang, D. Liu and D. Cui, *Organometallics*, 2012, **31**, 6014–6021.
- 10 L. Wang, D. Cui, Z. Hou, W. Li and Y. Li, *Organometallics*, 2011, **30**, 760–767.
- 11 W. Rong, D. Liu, H. Zuo, Y. Pan, Z. Jian, S. Li and D. Cui, *Organometallics*.
- 12 W. Gao and D. Cui, *Journal of the American Chemical Society*, 2008, **130**, 4984–4991.
- 13 M. Zimmermann, K. W. Törnroos, R. M. Waymouth and R. Anwander, *Organometallics*, 2008, **27**, 4310–4317.
- 14 W. Gao, D. Cui, X. Liu, Y. Zhang and Y. Mu, *Organometallics*, 2008, **27**, 5889–5893.
- 15 E. Grunova, E. Kirillov, T. Roisnel and J.-F. Carpentier, *Dalton Trans.*, 2010, **39**, 6739–6752.
- 16 X. Liu, X. Shang, T. Tang, N. Hu, F. Pei, D. Cui, X. Chen and X. Jing, *Organometallics*, 2007, **26**, 2747–2757.
- 17 X. Shang, X. Liu and D. Cui, *Journal of Polymer Science Part A: Polymer Chemistry*, 2007, **45**, 5662–5672.
- 18 M. Zimmermann, K. W. Törnroos and R. Anwander, *Organometallics*, 2006, **25**, 3593–3598.
- 19 M. Zimmermann, K. W. Törnroos and R. Anwander, *Angewandte Chemie International Edition*, 2007, **46**, 3126–3130.
- 20 M. Zimmermann, F. Estler, E. Herdtweck, K. W. Törnroos and R. Anwander, *Organometallics*, 2007, **26**, 6029–6041.
- 21 S. Hamidi, L. N. Jende, H. Martin Dietrich, C. Maichle-Mössmer, K. W. Törnroos, G. B. Deacon, P. C. Junk and R. Anwander, *Organometallics*, 2013, **32**, 1209–1223.
- 22 M. Bonath, C. O. Hollfelder, D. Schädle, C. Maichle-Mössmer, P. Sirsch and R. Anwander, *European Journal of Inorganic Chemistry*, 2017, 4683–4692.
- 23 P. G. Hayes, W. E. Piers, L. W. M. Lee, L. K. Knight, M. Parvez, M. R. J. Elsegood and W. Clegg, *Organometallics*, 2001, **20**, 2533–2544.
- 24 L. K. Knight, W. E. Piers, P. Fleurat-Lessard, M. Parvez and R. McDonald, *Organometallics*, 2004, **23**, 2087–2094.
- 25 Y. Li, X. Mi, M. Huang, R. Cai and Y. Wu, *Tetrahedron*, 2012, **68**, 8502–8508.
- 26 Y. Li, J. Wang, M. Huang, Z. Wang, Y. Wu and Y. Wu, *J. Org. Chem.*, 2014, **79**, 2890–2897.
- 27 Z. Wang, Y. Li, B. Yan, M. Huang and Y. Wu, *Synlett*, 2015, **26**, 531–536.
- 28 Y. Li, J. Wang, B. Yan, M. Huang, Y. Zhu, Y. Wu and Y. Wu, *Tetrahedron*, 2015, **71**, 2729–2735.
- 29 Y. Wang, W. Zhao, D. Liu, S. Li, X. Liu, D. Cui and X. Chen, *Organometallics*, 2012, **31**, 4182–4190.
- 30 M. M. Kireenko, E. A. Kuchuk, K. V. Zaitsev, V. A. Tafeenko, Y. F. Oprunenko, A. V. Churakov, E. Kh. Lermontova, G. S. Zaitseva and S. S. Karlov, *Dalton Trans.*, 2015, **44**, 11963–11976.
- 31 M. Zimmermann, N. Å. Frøystein, A. Fischbach, P. Sirsch, H. M. Dietrich, K. W. Törnroos, E. Herdtweck and R. Anwander, *Chem. Eur. J.*, 2007, **13**, 8784–8800.
- 32 M. Zimmermann, K. W. Törnroos, H. Sitzmann and R. Anwander, *Chem. Eur. J.*, 2008, **14**, 7266–7277.
- 33 D. Diether, K. Tyulyunov, C. Maichle-Mössmer and R. Anwander, *Organometallics*, 2017, **36**, 4649–4659.
- 34 W. J. Evans, R. Anwander and J. W. Ziller, *Organometallics*, 1995, **14**, 1107–1109.
- 35 P. Biagini, G. Lugli, L. Abis and R. Millini, *Journal of Organometallic Chemistry*, 1994, **474**, C16–C18.
- 36 A. Fischbach, C. Meermann, G. Eckerling, W. Scherer and R. Anwander, *Macromolecules*, 2006, **39**, 6811–6816.
- 37 G. Occhipinti, C. Meermann, H. M. Dietrich, R. Litlabø, F. Auras, K. W. Törnroos, C. Maichle-Mössmer, V. R. Jensen and R. Anwander, *J. Am. Chem. Soc.*, 2011, **133**, 6323–6337.
- 38 H. Sugiyama, I. Korobkov, S. Gambarotta, A. Möller and P. H. M. Budzelaar, *Inorg. Chem.*, 2004, **43**, 5771–5779.
- 39 N. Du, X. Gao, J. Song, Z.-N. Wang, Y.-H. Xing, F.-Y. Bai and Z. Shi, *RSC Adv.*, 2016, **6**, 71012–71024.
- 40 A. Fischbach, E. Herdtweck and R. Anwander, *Inorganica Chimica Acta*, 2006, **359**, 4855–4864.
- 41 T. K. Panda, D. Petrovic, T. Bannenberg, C. G. Hrib, P. G. Jones and M. Tamm, *Inorganica Chimica Acta*, 2008, **361**, 2236–2242.
- 42 Y. Fukuda, A. Nakao and K. Hayashi, *J. Chem. Soc., Dalton Trans.*, 2002, 527–533.
- 43 L. N. Jende, C. Maichle-Mössmer and R. Anwander, *Chem. Eur. J.*, 2013, **19**, 16321–16333.
- 44 B. Koning, J. Buter, R. Hulst, R. Stroetinga and R. M. Kellogg, *Eur. J. Org. Chem.*, 2000, 2735–2743.
- 50 *COSMO v. 1.61*, Bruker AXS Inc., Madison, WI, 2012.
- 51 a) *APEX2 v. 2012.10\_0*, Bruker AXS Inc., Madison, WI, 2012. b) *APEX 3 V. 2016.5-0*, Bruker AXS Inc., Madison, WI, 2016.
- 52 *SAINT v. 8.34A*, Bruker AXS Inc., Madison, WI, 2013.
- 53 *SHELXTL Acta Cryst.* 2015. **A71**, 3–8, *Shelx Acta Cryst.* 2015, **C71**, 3–8.
- 54 *SHELXL*, C. B. Hubschle, G. M. Sheldrick, B. Dittrich, *J. Appl. Crystallogr.* 2011, **44**, 1281–1284.
- 55 L. J. Farrugia, *J. Appl. Crystallogr.* 1997, **30**, 565.
- 56 *POV-Ray v. 3.6*, Persistence of Vision Pty. Ltd., Williamstown, Victoria, Australia, 2004. <http://www.povray.org/>.

## Supporting Information

### **Rare-Earth Metal-Induced (Double) C–H Bond Activation of a Pyridyl-Functionalized Alkoxy Ligand: Formation of [ONC]<sup>-(2-)</sup> Pincer-Type Ligands and Implications for Isoprene Polymerization**

Dominic Diether, Melanie Meermann-Zimmermann, Karl W. Törnroos, Cäcilia Maichle-Mössmer, and Reiner Anwander\*

Institut für Anorganische Chemie, Eberhard Karls Universität Tübingen, Auf der Morgenstelle 18, 72076 Tübingen, Germany.

#### **Corresponding Author**

\* reiner.anwander@uni-tuebingen.de

## Table of Contents

Figure S1. $^1\text{H}$ NMR spectrum of $[\text{ONCH}_2]\text{La}(\text{AlMe}_3)_2(\text{AlMe}_4)$ ( $2^{\text{La}}$ )	S3
Figure S2. $^{13}\text{C}\{^1\text{H}\}$ NMR spectrum of $[\text{ONCH}_2]\text{La}(\text{AlMe}_3)_2(\text{AlMe}_4)$ ( $2^{\text{La}}$ )	S3
Figure S3. $^1\text{H}^{13}\text{C}$ -HSQC NMR spectrum of $[\text{ONCH}_2]\text{La}(\text{AlMe}_3)_2(\text{AlMe}_4)$ ( $2^{\text{La}}$ )	S4
Figure S4. $^1\text{H}$ NMR spectrum of $[\text{ONCH}_2]\text{Nd}(\text{AlMe}_3)_2(\text{AlMe}_4)$ ( $2^{\text{Nd}}$ )	S4
Figure S5. $^1\text{H}$ NMR spectrum of $[\text{ONCH}_2]\text{Y}(\text{AlMe}_3)_2(\text{AlMe}_4)$ ( $2^{\text{Y}}$ )	S5
Figure S6. $^{13}\text{C}\{^1\text{H}\}$ NMR spectrum of $[\text{ONCH}_2]\text{Y}(\text{AlMe}_3)_2(\text{AlMe}_4)$ ( $2^{\text{Y}}$ )	S5
Figure S7. $^1\text{H}^{13}\text{C}$ -HSQC NMR spectrum of $[\text{ONCH}_2]\text{Y}(\text{AlMe}_3)_2(\text{AlMe}_4)$ ( $2^{\text{Y}}$ )	S6
Figure S8. $^1\text{H}$ NMR spectrum of $[\text{ONCH}]\text{Y}(\text{AlMe}_3)_3$ ( $3^{\text{Y}}$ )	S6
Figure S9. $^{13}\text{C}\{^1\text{H}\}$ NMR spectrum of $[\text{ONCH}]\text{Y}(\text{AlMe}_3)_3$ ( $3^{\text{Y}}$ )	S7
Figure S10. $^1\text{H}^{13}\text{C}$ -HSQC NMR spectrum of $[\text{ONCH}]\text{Y}(\text{AlMe}_3)_3$ ( $3^{\text{Y}}$ )	S7
Figure S11. $^1\text{H}$ NMR spectrum of $[\text{ONCH}]\text{Lu}(\text{AlMe}_3)_2(\text{AlMe}_4)$ ( $3^{\text{Lu}}$ )	S8
Figure S12. $^{13}\text{C}\{^1\text{H}\}$ NMR spectrum of $[\text{ONCH}]\text{Lu}(\text{AlMe}_3)_2(\text{AlMe}_4)$ ( $3^{\text{Lu}}$ )	S8
Figure S13. $^1\text{H}^{13}\text{C}$ -HSQC NMR spectrum of $[\text{ONCH}]\text{Lu}(\text{AlMe}_3)_3$ ( $3^{\text{Lu}}$ )	S9
Figure S14. Molecular structure of $[\text{ONCH}_2]\text{La}(\text{AlMe}_3)_2(\text{AlMe}_4)$ ( $2^{\text{LaA}}$ )	S9
Figure S15. Molecular structure of $[\text{ONCH}_2]\text{Y}(\text{AlMe}_3)_2(\text{AlMe}_4)$ ( $2^{\text{Y}}$ )	S10
Figure S16. Molecular structure of $[\text{ONCH}]\text{Y}(\text{AlMe}_3)_3$ ( $3^{\text{Y}}$ )	S10
Figure S17. Molecular structure of $[\text{ONCH}]\text{Lu}(\text{AlMe}_3)_3$ ( $3^{\text{Lu}}$ )	S11
Figure S18. Comparison of both enantiomers of $2^{\text{Nd}}$	S11
Table S1. Crystallographic data for $2^{\text{La}}$ , $2^{\text{Nd}}$ , and $2^{\text{Y}}$	S12
Table S2. Crystallographic data for $3^{\text{Y}}$ and $3^{\text{Lu}}$	S13
Figure S19. VT $^1\text{H}$ NMR spectrum of $[\text{ONCH}_2]\text{La}(\text{AlMe}_3)_2(\text{AlMe}_4)$ ( $2^{\text{La}}$ )	S14
Figure S20. Detailed view of VT $^1\text{H}$ NMR spectrum of $[\text{ONCH}_2]\text{La}(\text{AlMe}_3)_2(\text{AlMe}_4)$ ( $2^{\text{La}}$ )	S14
Figure S21. Detailed view of VT $^1\text{H}$ NMR spectrum of $[\text{ONCH}_2]\text{La}(\text{AlMe}_3)_2(\text{AlMe}_4)$ ( $2^{\text{La}}$ )	S15
Figure S22. VT $^1\text{H}$ NMR spectrum of $[\text{ONCH}_2]\text{Y}(\text{AlMe}_3)_2(\text{AlMe}_4)$ ( $2^{\text{Y}}$ )	S15
Figure S23. Detailed view of VT $^1\text{H}$ NMR spectrum of $[\text{ONCH}_2]\text{Y}(\text{AlMe}_3)_2(\text{AlMe}_4)$ ( $2^{\text{Y}}$ )	S16
Figure S24. Detailed view of VT $^1\text{H}$ NMR spectrum of $[\text{ONCH}_2]\text{Y}(\text{AlMe}_3)_2(\text{AlMe}_4)$ ( $2^{\text{Y}}$ )	S17
Figure S25. Detailed view of VT $^1\text{H}$ NMR spectrum of $[\text{ONCH}]\text{Y}(\text{AlMe}_3)_3$ ( $3^{\text{Y}}$ )	S17
Figure S26. $^1\text{H}$ NMR spectrum of the reaction of $2^{\text{La}}$ with $[\text{Ph}_3\text{C}][\text{B}(\text{C}_6\text{F}_5)_4]$	S18
Figure S27. $^1\text{H}$ NMR spectrum of the reaction of $2^{\text{La}}$ with $[\text{PhNMe}_2\text{H}][\text{B}(\text{C}_6\text{F}_5)_4]$	S18
Figure S28. Refractive index of bimodal polyisoprenes	S19

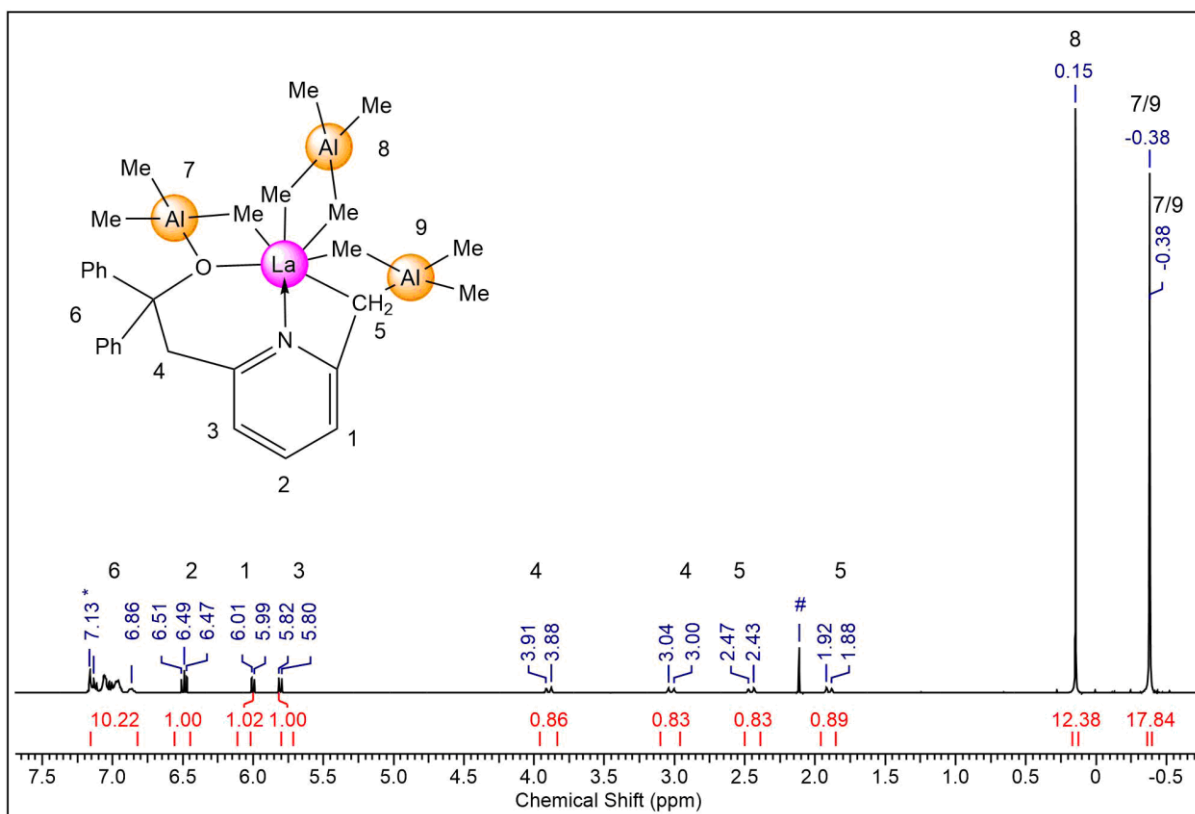


Figure S1.  $^1\text{H}$  NMR spectrum (400 MHz) of  $[\text{ONCH}_2]\text{La}(\text{AlMe}_3)_2(\text{AlMe}_4)$  ( $2^{\text{La}}$ ) in  $\text{C}_6\text{D}_6$  at  $26^\circ\text{C}$ .

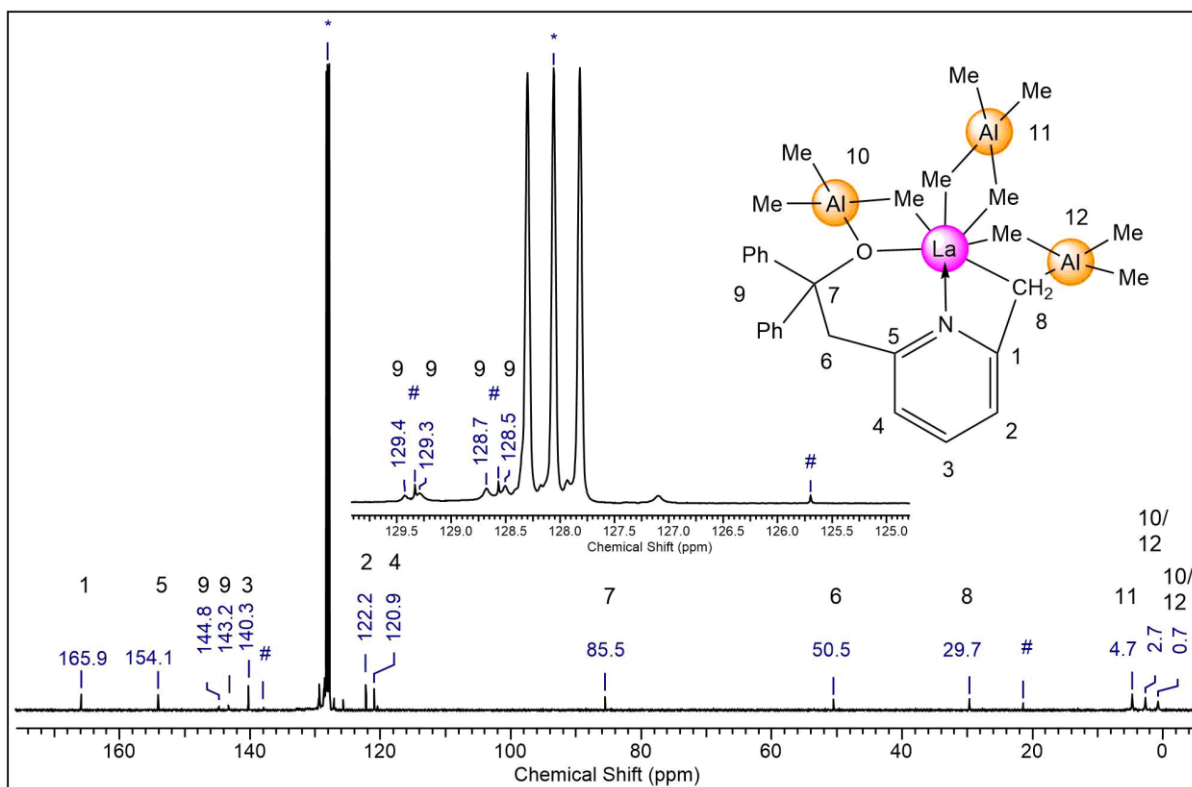
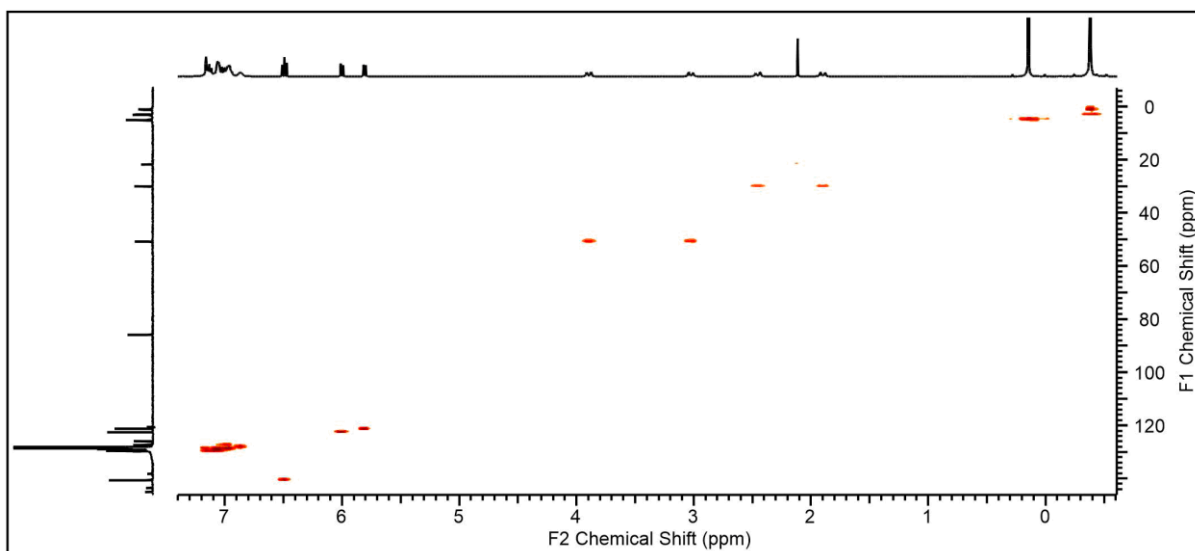
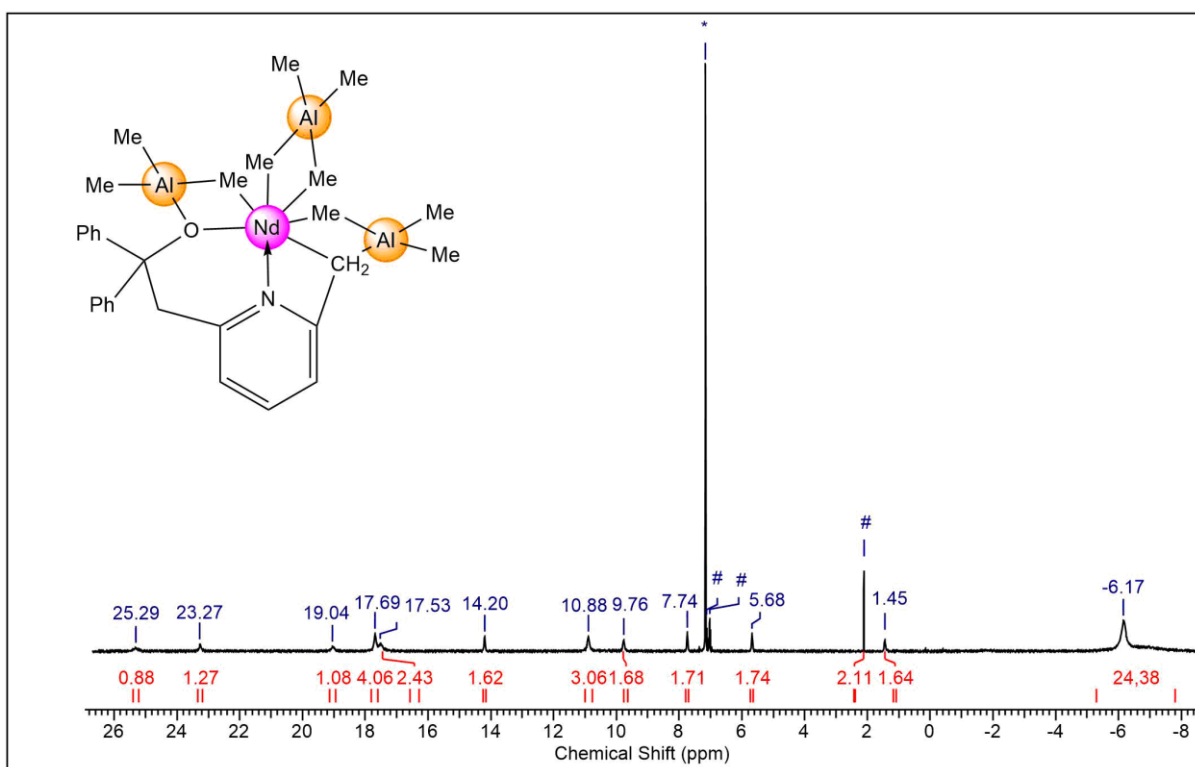


Figure S2.  $^{13}\text{C}\{^1\text{H}\}$  spectrum (101 MHz) of  $[\text{ONCH}_2]\text{La}(\text{AlMe}_3)_2(\text{AlMe}_4)$  ( $2^{\text{La}}$ ) in  $\text{C}_6\text{D}_6$  at  $26^\circ\text{C}$ . Toluene is marked with #.



**Figure S3.** <sup>1</sup>H/<sup>13</sup>C-HSQC NMR spectrum (400/101 MHz) of [ONCH<sub>2</sub>]La(AlMe<sub>3</sub>)<sub>2</sub>(AlMe<sub>4</sub>) (**2<sup>La</sup>**) in C<sub>6</sub>D<sub>6</sub> at 26 °C.



**Figure S4.** <sup>1</sup>H NMR spectrum (400 MHz) of [ONCH<sub>2</sub>]Nd(AlMe<sub>3</sub>)<sub>2</sub>(AlMe<sub>4</sub>) (**2<sup>Nd</sup>**) in C<sub>6</sub>D<sub>6</sub> at 26 °C. Toluene is marked with #.



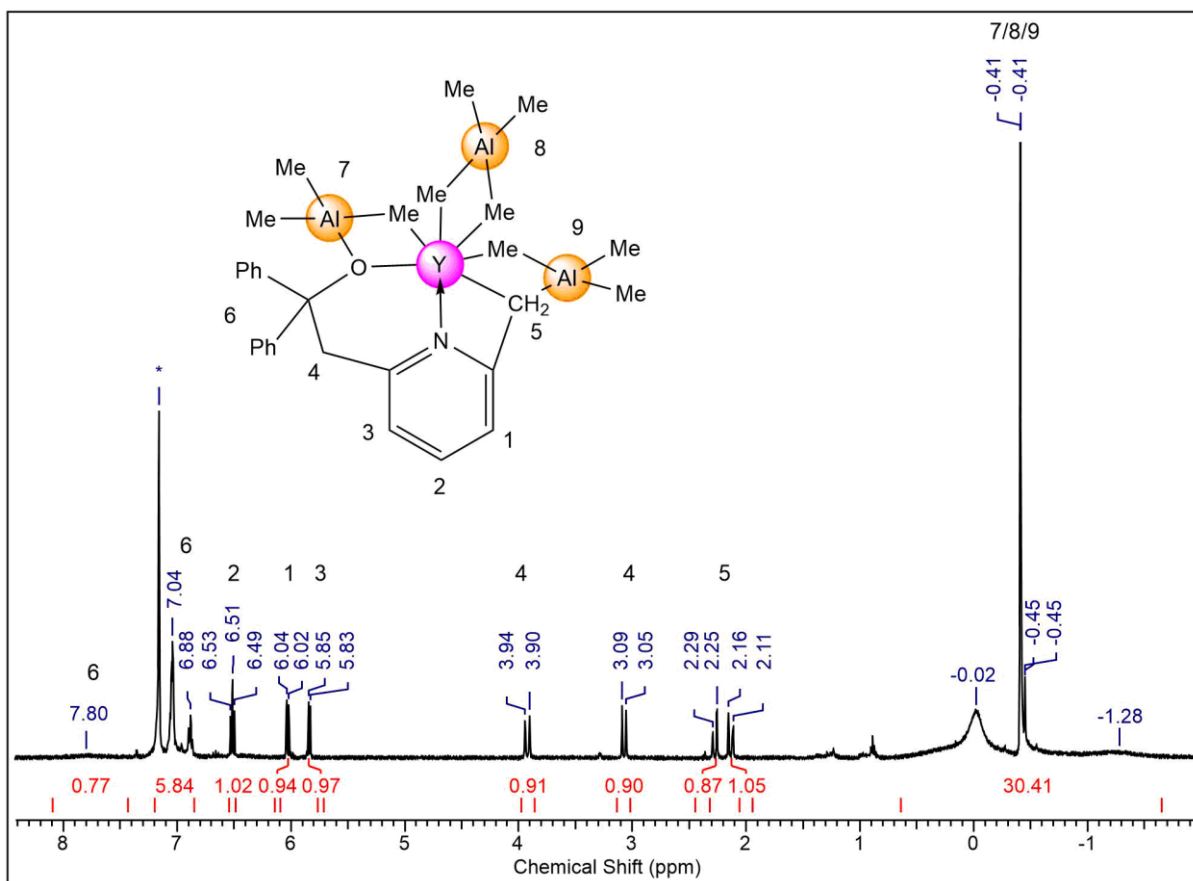


**Figure S5.**  $^1H$  NMR spectrum (400 MHz) of  $[ONCH_2]Y(AlMe_3)_2(AlMe_4)$  ( $2^Y$ ) in  $C_6D_6$  at 26 °C.

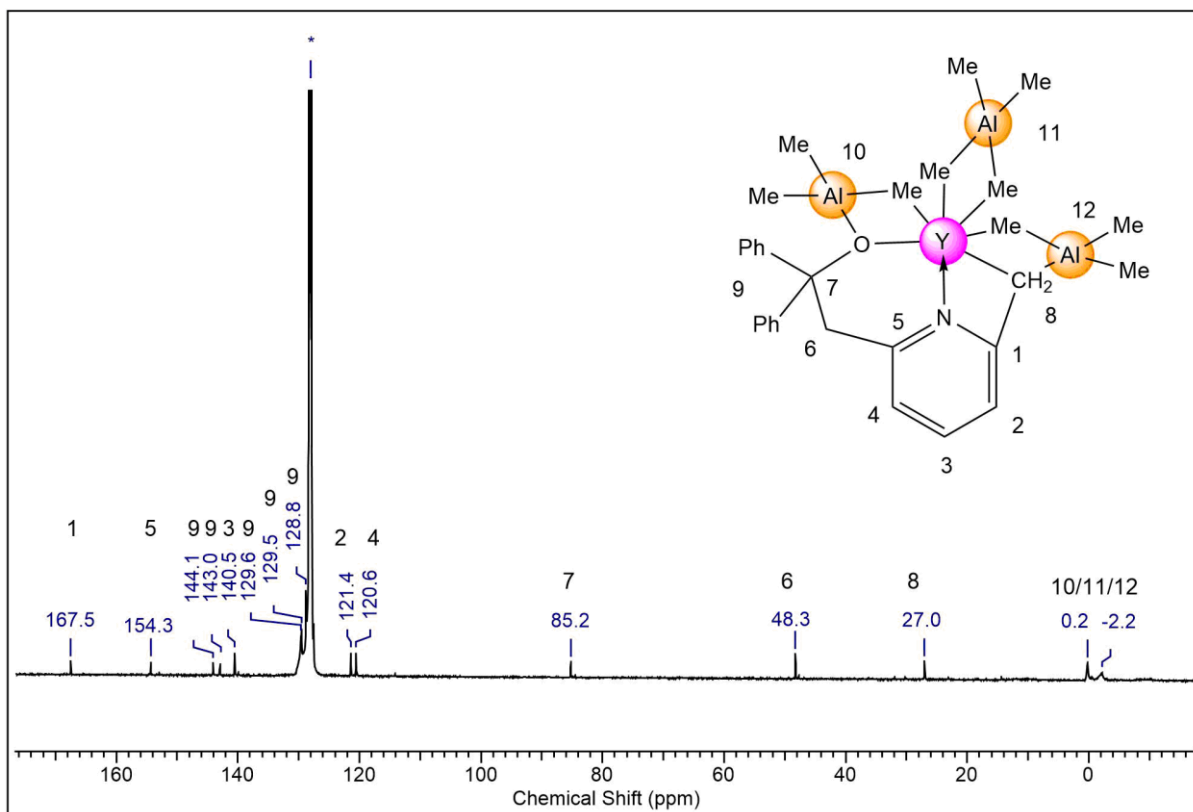


**Figure S6.**  $^{13}C\{^1H\}$  spectrum (101 MHz) of  $[ONCH_2]Y(AlMe_3)_2(AlMe_4)$  ( $2^Y$ ) in  $C_6D_6$  at 26 °C.

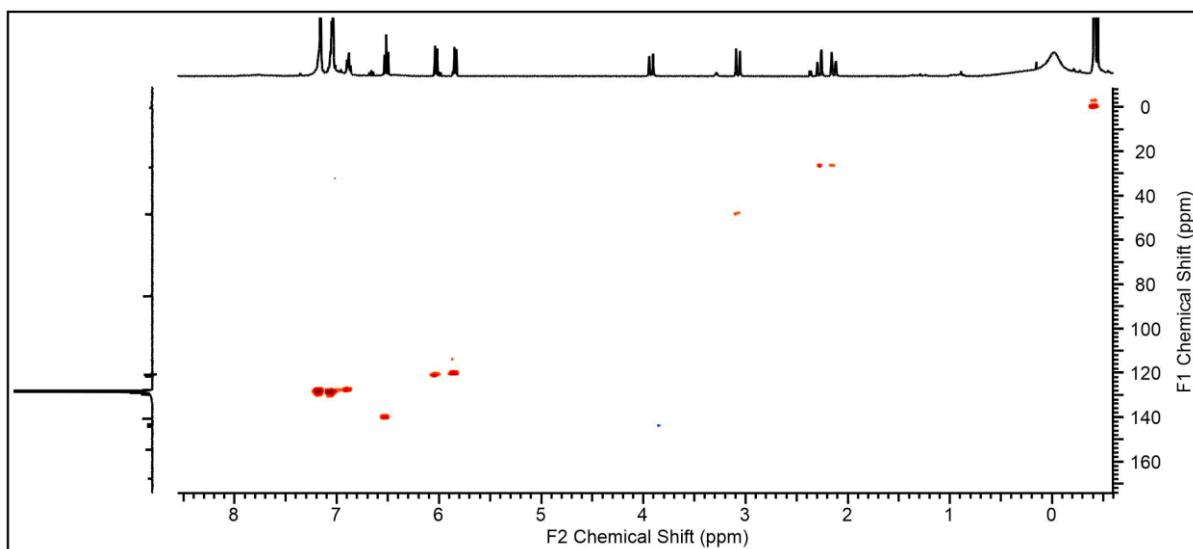


**Figure S7.**  $^1\text{H}^{13}\text{C}$ -HSQC NMR spectrum (400/101 MHz) of  $[\text{ONCH}_2]\text{Y}(\text{AlMe}_3)_2(\text{AlMe}_4)$  ( $2^{\text{Y}}$ ) in  $\text{C}_6\text{D}_6$  at  $26\text{ }^\circ\text{C}$ .

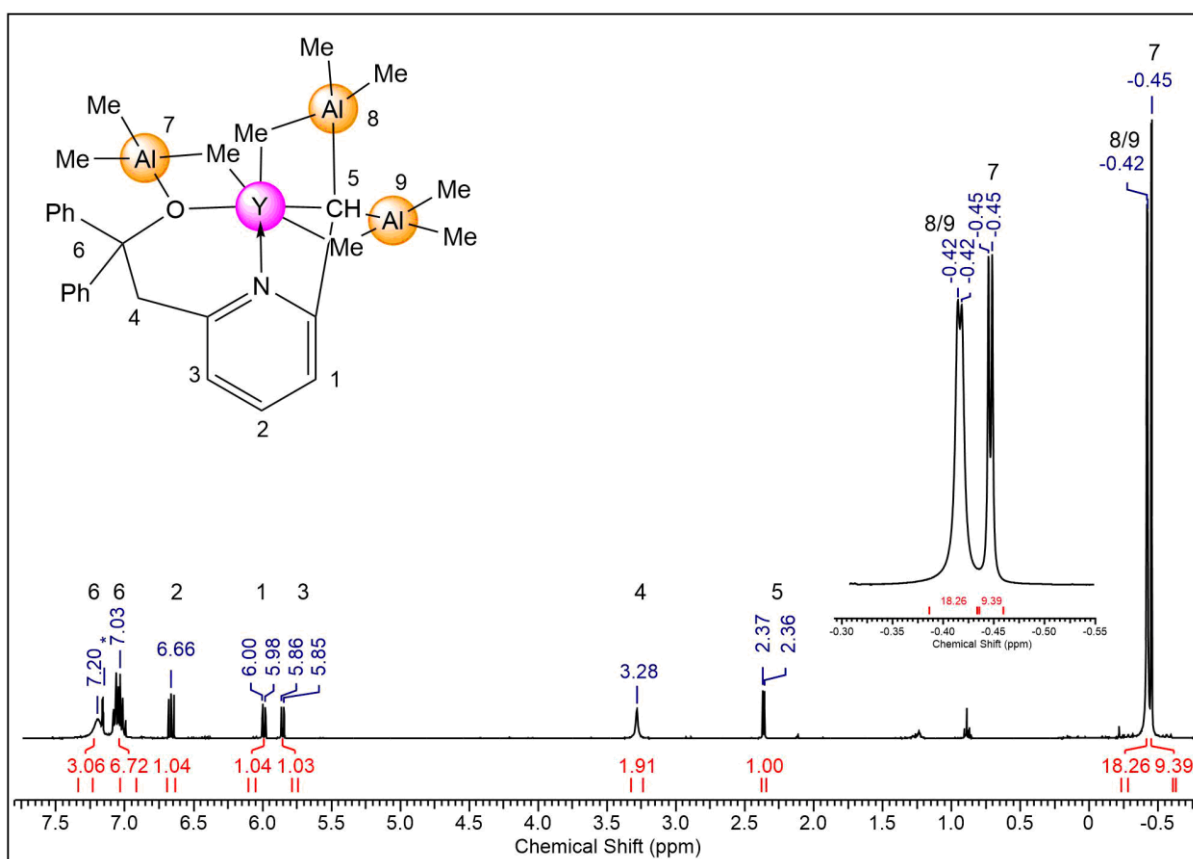


**Figure S8.**  $^1\text{H}$  NMR spectrum (400 MHz) of  $[\text{ONCH}]\text{Y}(\text{AlMe}_3)_3$  ( $3^{\text{Y}}$ ) in  $\text{C}_6\text{D}_6$  at  $26\text{ }^\circ\text{C}$ .

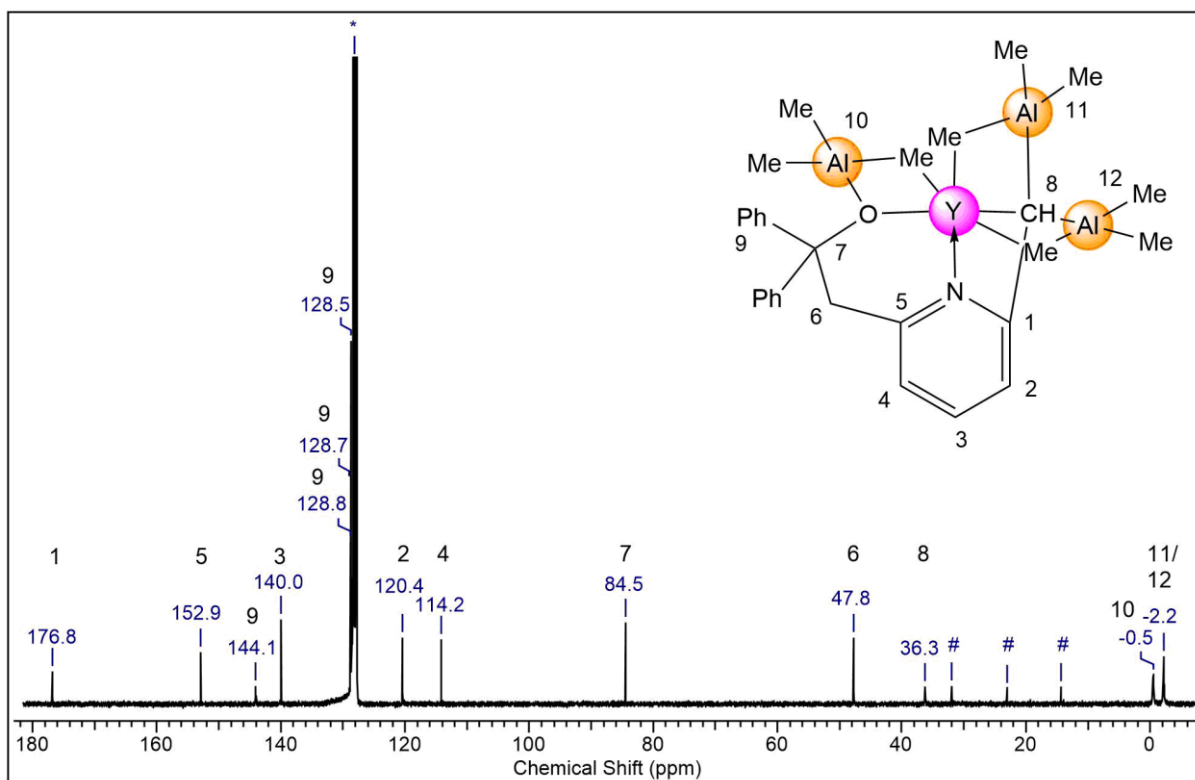


**Figure S9.**  $^{13}\text{C}\{^1\text{H}\}$  spectrum (101 MHz) of  $[\text{ONCH}]\text{Y}(\text{AlMe}_3)_3$  ( $3^{\text{Y}}$ ) in  $\text{C}_6\text{D}_6$  at  $26^\circ\text{C}$ . *n*-Hexane is marked with #.

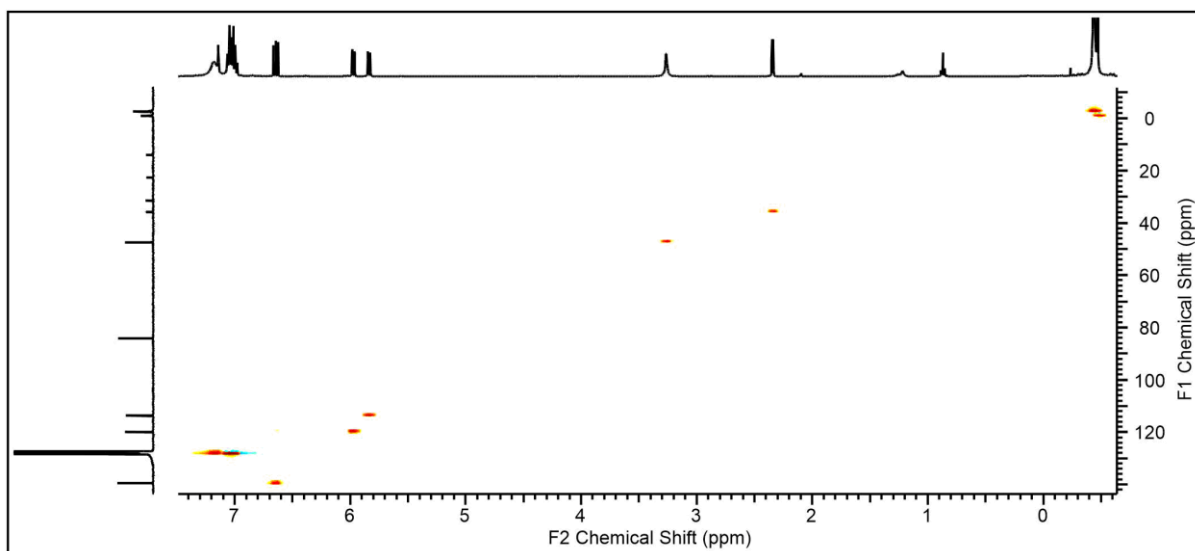


**Figure S10.**  $^1\text{H}^{13}\text{C}$ -HSQC NMR spectrum (400/101 MHz) of  $[\text{ONCH}]\text{Y}(\text{AlMe}_3)_3$  ( $3^{\text{Y}}$ ) in  $\text{C}_6\text{D}_6$  at  $26^\circ\text{C}$ .

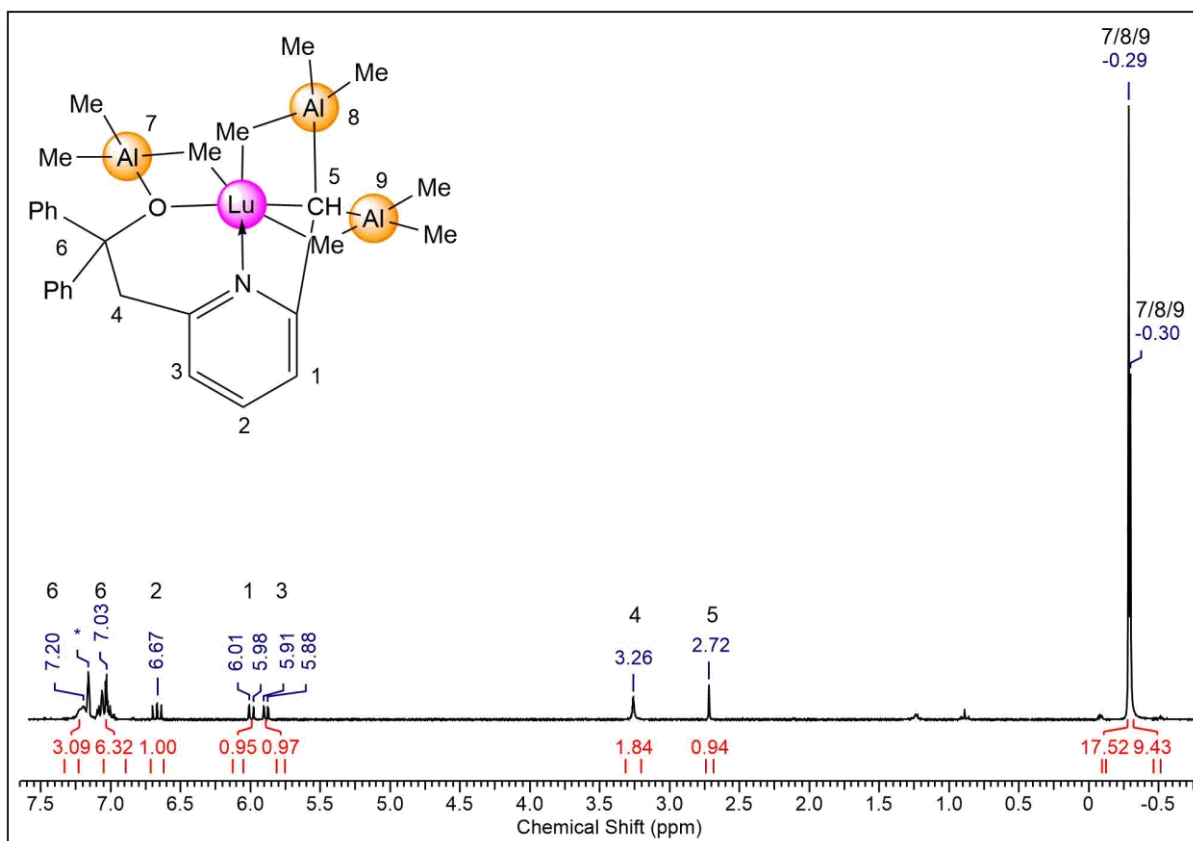


**Figure S11.**  $^1\text{H}$  NMR spectrum (400 MHz) of  $[\text{ONCH}]\text{Lu}(\text{AlMe}_3)_3$  ( $3^{\text{Lu}}$ ) in  $\text{C}_6\text{D}_6$  at  $26^\circ\text{C}$ .

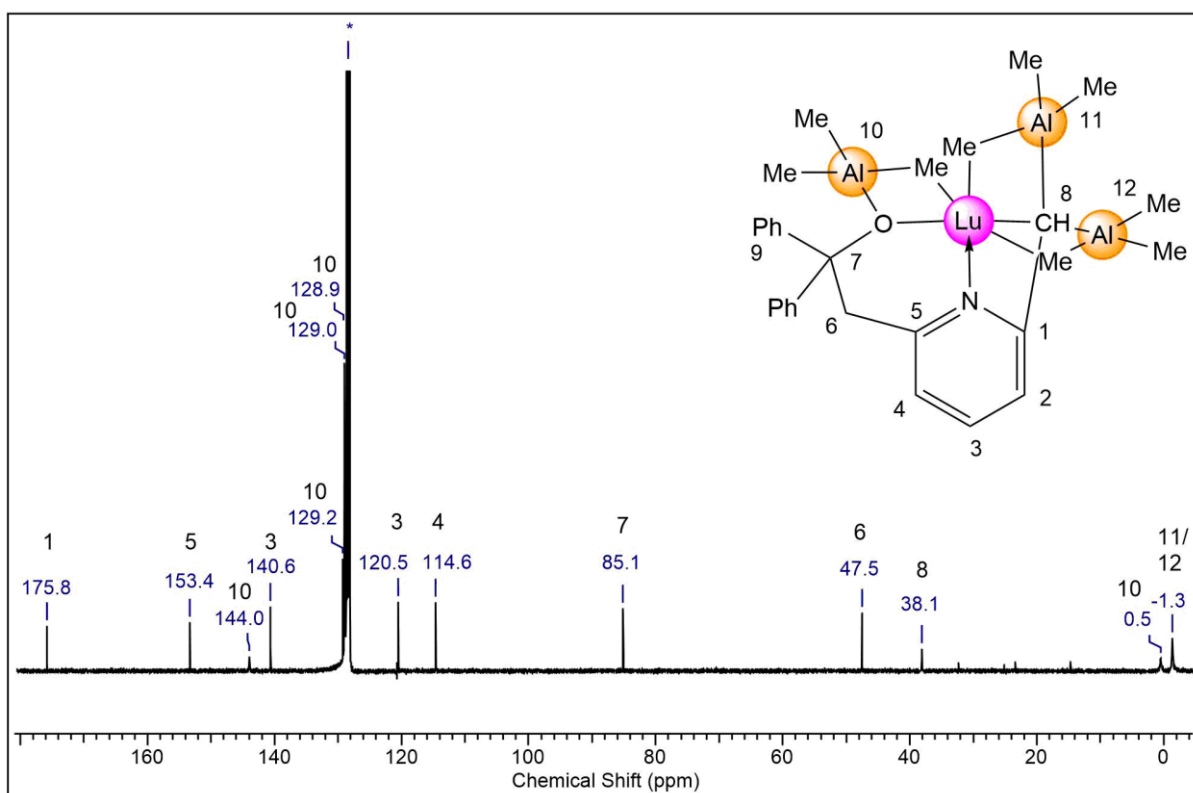


**Figure S12.**  $^{13}\text{C}\{^1\text{H}\}$  NMR spectrum (101 MHz) of  $[\text{ONCH}]\text{Lu}(\text{AlMe}_3)_3$  ( $3^{\text{Lu}}$ ) in  $\text{C}_6\text{D}_6$  at  $26^\circ\text{C}$ .

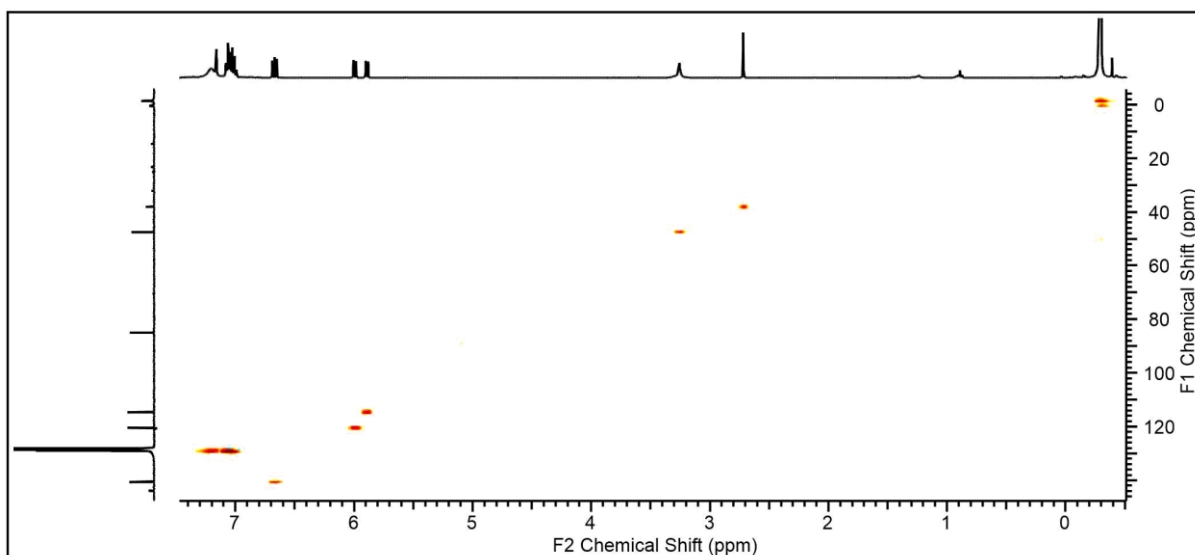


**Figure S13.**  $^1\text{H}^{13}\text{C}$ -HSQC NMR spectrum (400/101 MHz) of  $[\text{ONCH}]\text{Lu}(\text{AlMe}_3)_3$  ( $3^{\text{Lu}}$ ) in  $\text{C}_6\text{D}_6$  at  $26\text{ }^\circ\text{C}$ .

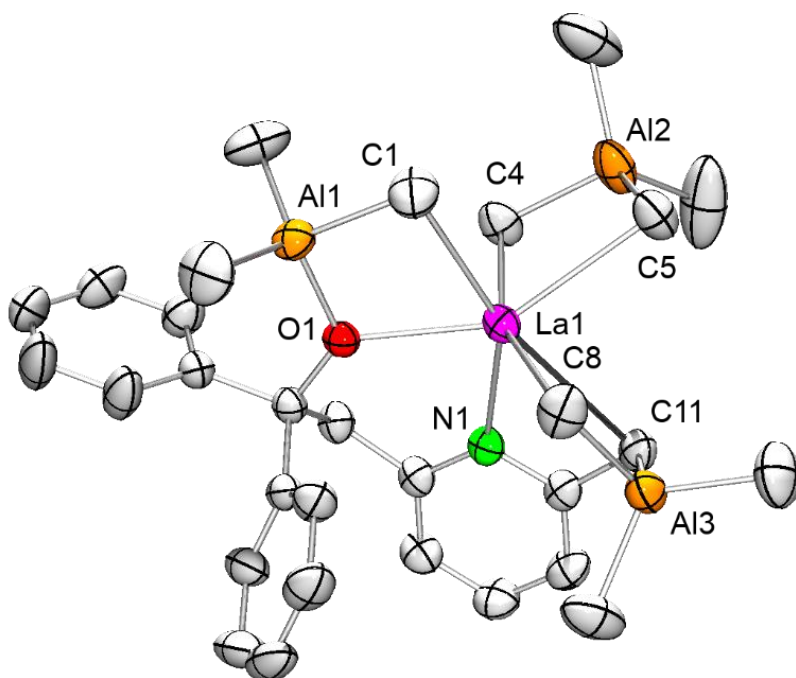


**Figure S 14.** Molecular structure of  $[\text{ONCH}_2]\text{La}(\text{AlMe}_3)_2(\text{AlMe}_4)$  ( $2^{\text{La}}$ ). Hydrogen atoms are omitted for clarity. The asymmetric unit contains 0.5 toluene which is omitted for clarity. Atomic displacement parameters set at the 50% probability level. Selected bond lengths [ $\text{\AA}$ ] and angles [ $^\circ$ ]:  $\text{La1}-\text{C1}$  2.726(2),  $\text{La1}-\text{C4}$  2.687(2),  $\text{La1}-\text{C5}$  2.787(2),  $\text{La1}-\text{C8}$  2.719(2),  $\text{La1}-\text{C11}$  2.949(2),  $\text{La1}\cdots\text{Al1}$  3.3508(5),  $\text{La1}\cdots\text{Al2}$  3.2829(5),  $\text{La1}\cdots\text{Al3}$  3.4012(5),  $\text{La1}-\text{N1}$  2.516(1),  $\text{La1}-\text{O1}$  2.4114(9),  $\text{Al1}-\text{O1}$  1.862(1),  $\text{Al3}-\text{C11}$  2.091(2),  $\text{O1}-\text{La1}-\text{C11}$  126.22(4),  $\text{O1}-\text{La1}-\text{N1}$  76.38(3),  $\text{N1}-\text{La1}-\text{C11}$  51.40(4),  $\text{N1}-\text{La1}-\text{Al2}$  107.21(3).

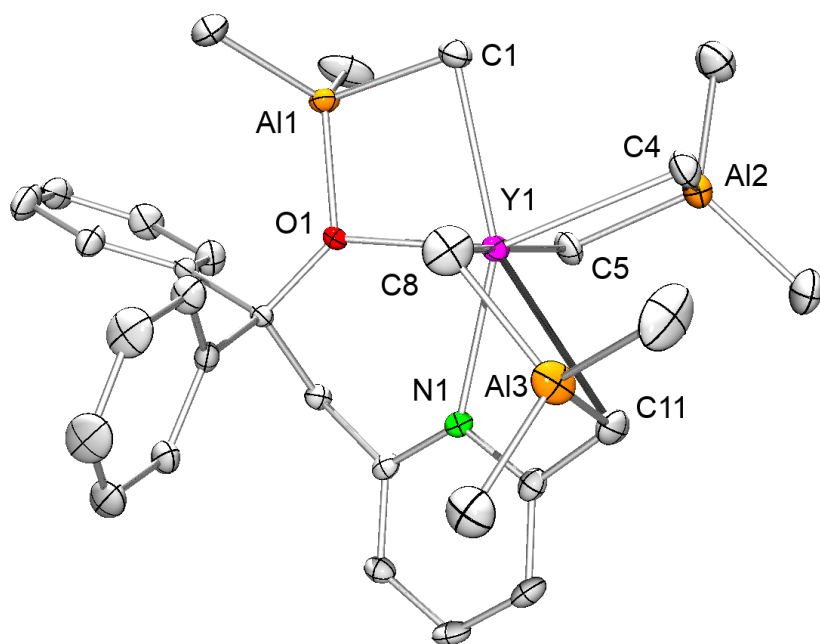


**Figure S 15.** Molecular structure of  $[\text{ONCH}_2]\text{Y}(\text{AlMe}_3)_2(\text{AlMe}_4)$  ( $2^{\text{Y}}$ ). Hydrogen atoms are omitted for clarity. The asymmetric unit contains 0.5 toluene which is omitted for clarity. Atomic displacement parameters set at the 50% probability level. Selected bond lengths [ $\text{\AA}$ ] and angles [ $^\circ$ ]: Y1–C1 2.583(3), Y1–C4 2.518(3), Y1–C5 2.677(3), Y1–C8 2.513(4), Y1–C11 2.848(3), Y1 $\cdots$ Al1 3.1934(8), Y1 $\cdots$ Al2 3.1390(9), Y1 $\cdots$ Al3 3.251(1), Y1–N1 2.386(2), Y1–O1 2.270(2), Al1–O1 1.851(2), Al3–C11 2.070(3), O1–Y1–C11 130.21(7), O1–Y1–N1 78.70(6), N1–Y1–C11 53.16(8), N1–Y1–Al2 108.75(5).

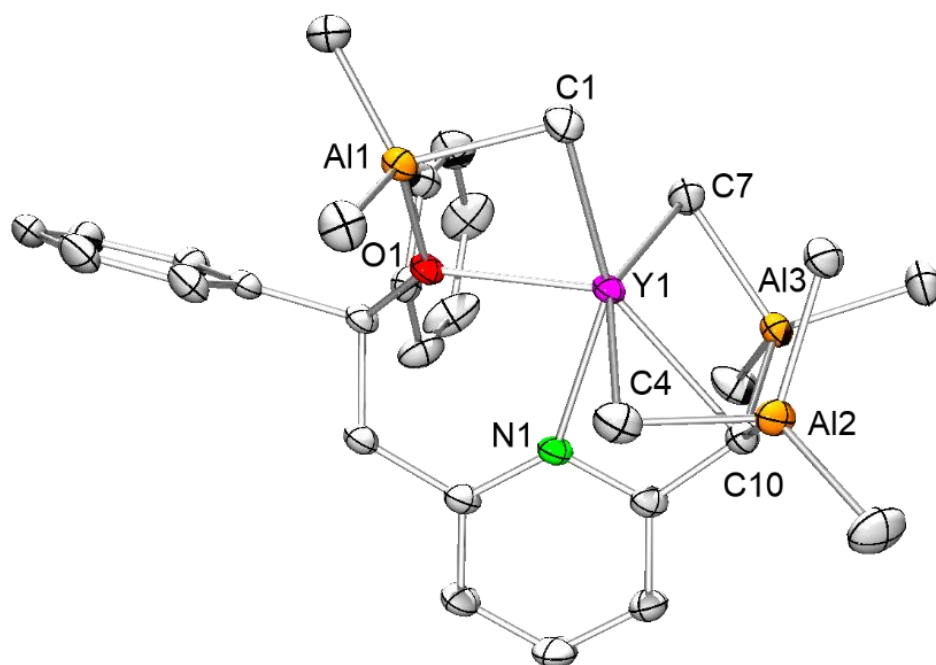


**Figure S 16.** Molecular structure of  $[\text{ONCH}]\text{Y}(\text{AlMe}_3)_3$  ( $3^{\text{Y}}$ ). Hydrogen atoms are omitted for clarity. The asymmetric unit contains one toluene which was omitted for clarity. Atomic displacement parameters set at the 50% probability level. Selected bond lengths [ $\text{\AA}$ ] and angles [ $^\circ$ ]: Y1–C1 2.568(2), Y1–C4 2.640(2), Y1–C7 2.483(2), Y1–C10 2.611(2), Y1 $\cdots$ Al1 3.1899(6), Y1 $\cdots$ Al2 2.8420(6), Y1 $\cdots$ Al3 3.1295(6), Y1–N1 2.325(1), Y1–O1 2.270(1), Al1–O1 1.849(1), Al2–C10 2.052(2), Al3–C10 2.063(2), O1–Y1–C10 134.96(5), O1–Y1–N1 75.10(5), N1–Y1–C10 56.92(5).

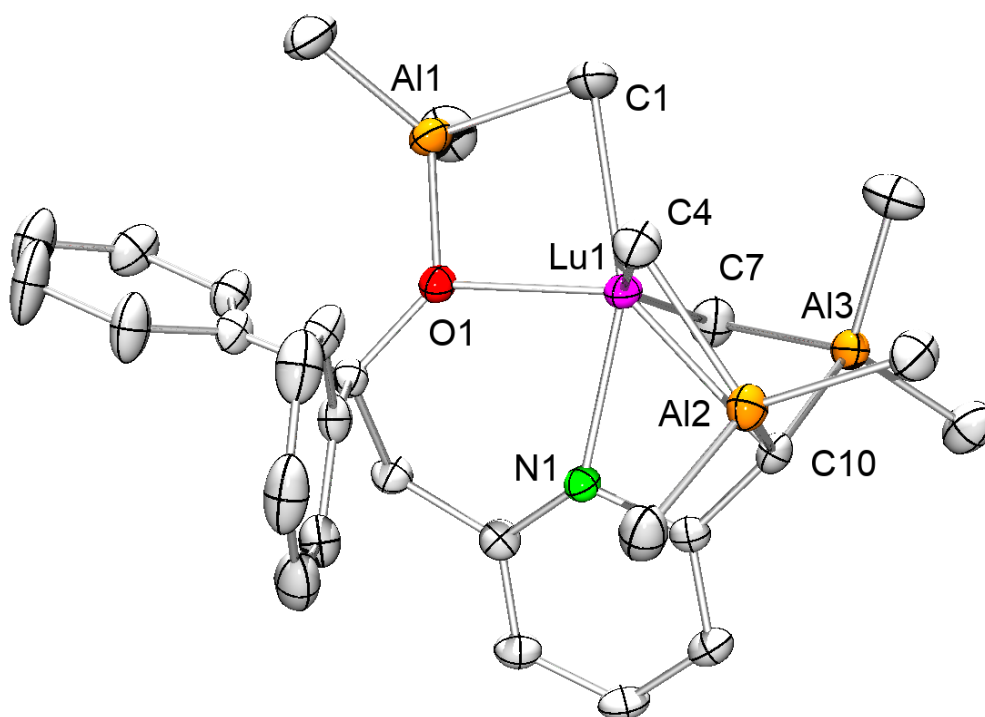


**Figure S 17.** Molecular structure of [ONCH]Lu(AlMe<sub>3</sub>)<sub>3</sub> (**3<sup>Lu</sup>**). Hydrogen atoms are omitted for clarity. Atomic displacement parameters set at the 50% probability level. Selected bond lengths [Å] and angles [°]: Lu1–C1 2.511(3), Lu1–C4 2.580(3), Lu1–C7 2.436(3), Lu1–C10 2.524(3), Lu1···Al1 3.1221(9), Lu1···Al2 2.8623(8), Lu1···Al3 3.0575(9), Lu1–N1 2.281(2), Lu1–O1 2.193(2), Al1–O1 1.848(2), Al2–C10 2.076(3), Al3–C10 2.073(3), O1–Lu1–C10 136.27(8), O1–Lu1–N1 78.38(7), N1–Lu1–C10 58.33(9).

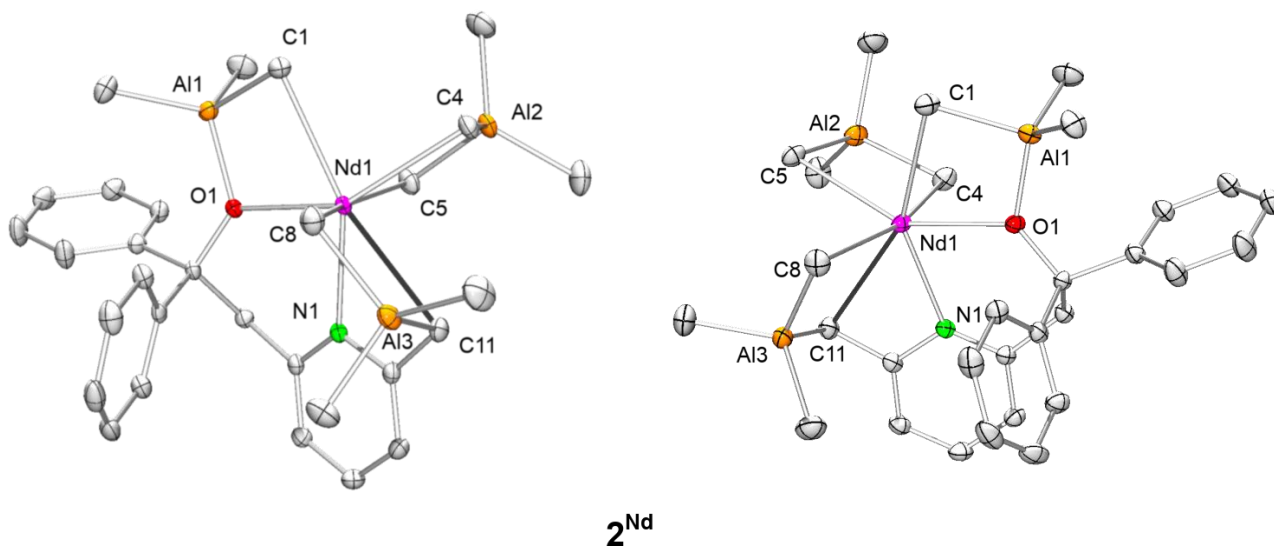


**Figure S18.** Comparison of both enantiomers of **2<sup>Nd</sup>**.

**Table S1.** Crystallographic data for compounds **2<sup>La</sup>**, **2<sup>Nd</sup>**, and **2<sup>Y</sup>**

	<b>2<sup>La</sup></b>	<b>2<sup>Nd</sup></b>	<b>2<sup>Y</sup></b>
CCDC number	XX	XX	XX
formula	C <sub>33.5</sub> H <sub>51</sub> Al <sub>3</sub> LaNO	C <sub>33.5</sub> H <sub>51</sub> Al <sub>3</sub> NdNO	C <sub>33.5</sub> H <sub>51</sub> Al <sub>3</sub> YNO
M [g·mol <sup>-1</sup> ]	703.60	708.93	653.60
Color	yellow	blue/green	yellow
Crystal dimensions [mm]	0.52 x 0.45 x 0.28	0.242 x 0.214 x 0.165	0.197 x 0.183 x 0.070
Crystal system	triclinic	triclinic	monoclinic
space group	P1	P1	P21/c
a [Å]	10.3933(4)	10.6177(3)	17.8953(13)
b [Å]	11.9336(4)	11.4277(4)	10.0184(8)
c [Å]	15.6945(6)	16.3857(4)	20.9266(15)
α [°]	87.3861(4)	93.045(2)	90
β [°]	85.6753(4)	99.2350(10)	109.621(3)
γ [°]	72.0755(4)	112.8170(10)	90
V [Å <sup>3</sup> ]	1846.32(12)	1794.24(9)	3533.9(5)
Z	2	2	4
T [K]	200(2)	100(2)	100(2)
ρ <sub>calcd</sub> [g·cm <sup>-3</sup> ]	1.266	1.312	1.228
μ [mm <sup>-1</sup> ]	1.252	1.545	1.749
F(000)	726	732	1380
Unique reflns	10787	8887	7791
Observed reflns (I>2σ)	31465	31707	56238
R1/wR2 (I>2σ)	0.0252/0.0723	0.0233/0.0580	0.0450/0.0980
R1/wR2 (all data)	0.0279/0.0749	0.0260/0.0596	0.0566/0.1017
Goodness of fit	1.076	1.034	1.121



**Table S2.** Crystallographic data for compounds **3<sup>Y</sup>** and **3<sup>Lu</sup>**.

	<b>3<sup>Y</sup>B</b>	<b>3<sup>Lu</sup>A</b>
CCDC number	XX	XX
formula	C <sub>35</sub> H <sub>55</sub> Al <sub>3</sub> YNO	C <sub>29</sub> H <sub>43</sub> Al <sub>3</sub> LuNO
M [g·mol <sup>-1</sup> ]	675.65	677.55
Color	yellow	yellow
Crystal dimensions [mm]	0.425 x 0.348 x 0.238	0.132 x 0.124 x 0.104
cell	triclinic	monoclinic
space group	P1	P21/n
a [Å]	10.3672(4)	11.1015(9)
b [Å]	12.9566(5)	21.7863(18)
c [Å]	14.9981(6)	13.0879(10)
α [°]	99.106(2)	90
β [°]	95.286(2)	104.7510(10)
γ [°]	109.956(2)	90
V [Å <sup>3</sup> ]	1846.44(13)	3061.1(4)
Z	2	4
T [K]	100(2)	150(2)
ρ <sub>calcd</sub> [g·cm <sup>-3</sup> ]	1.215	1.470
μ [mm <sup>-1</sup> ]	1.676	3.332
F(000)	716	1368
Unique reflns	8139	9386
Observed reflns (I>2σ)	74275	48629
R1/wR2 (I>2σ)	0.0307/0.0798	0.0303/0.0545
R1/wR2 (all data)	0.0333/0.0817	0.0488/0.0612
Goodness of fit	1.028	1.019

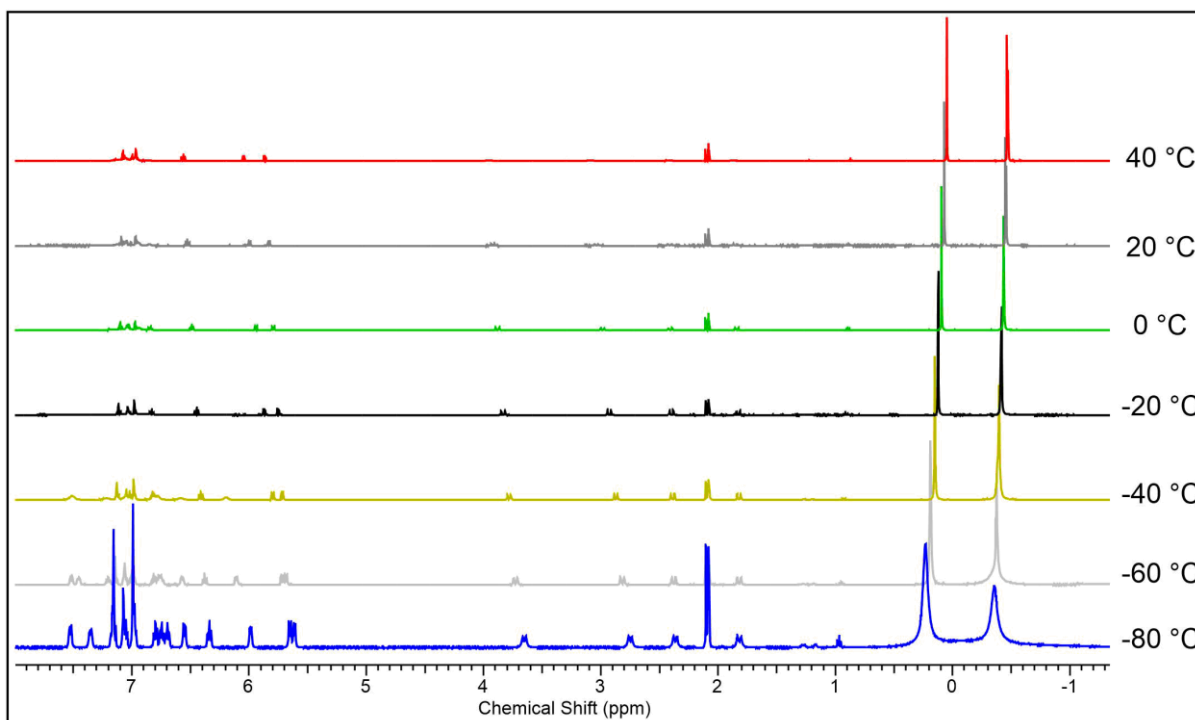


**Figure S19.** VT  $^1\text{H}$  NMR spectrum (500 MHz) of  $[\text{ONCH}_2]\text{La}(\text{AIme}_3)_2(\text{AIme}_4)$  ( $2^{\text{La}}$ ) in toluene- $d_8$ . From  $-80\text{ }^\circ\text{C}$  to  $40\text{ }^\circ\text{C}$ .

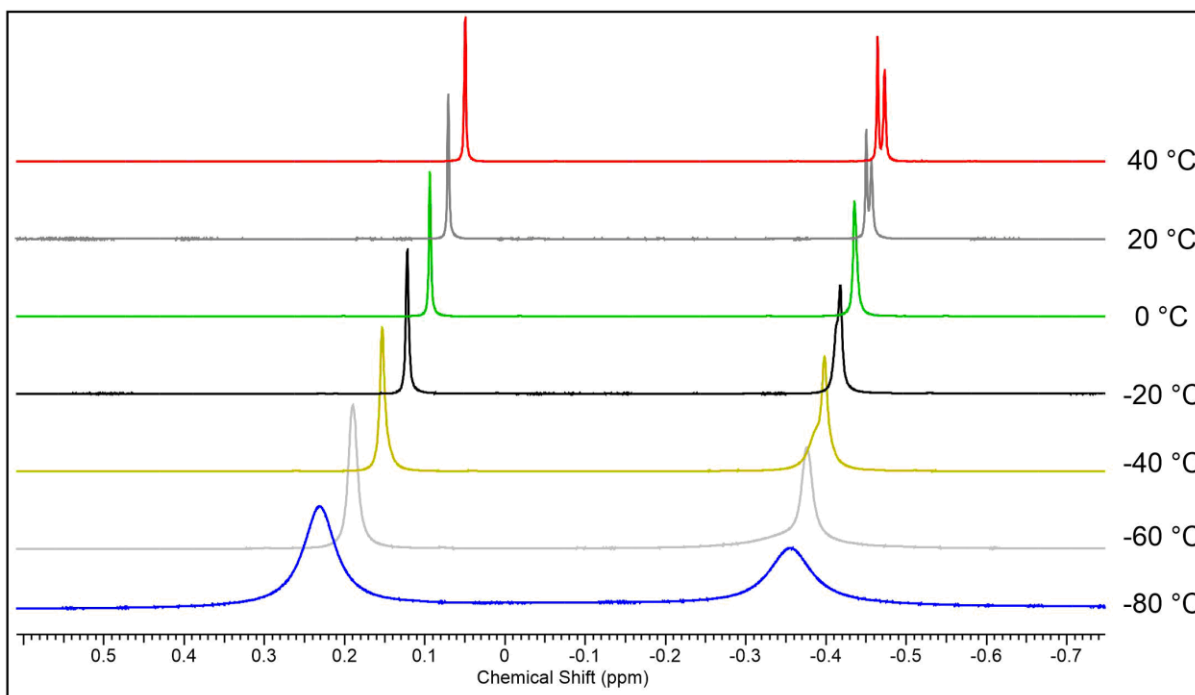


**Figure S20.** Detailed view of the VT  $^1\text{H}$  NMR spectrum (500 MHz) of  $[\text{ONCH}_2]\text{La}(\text{AIme}_3)_2(\text{AIme}_4)$  ( $2^{\text{La}}$ ) in toluene- $d_8$ . From  $-80\text{ }^\circ\text{C}$  to  $40\text{ }^\circ\text{C}$ .

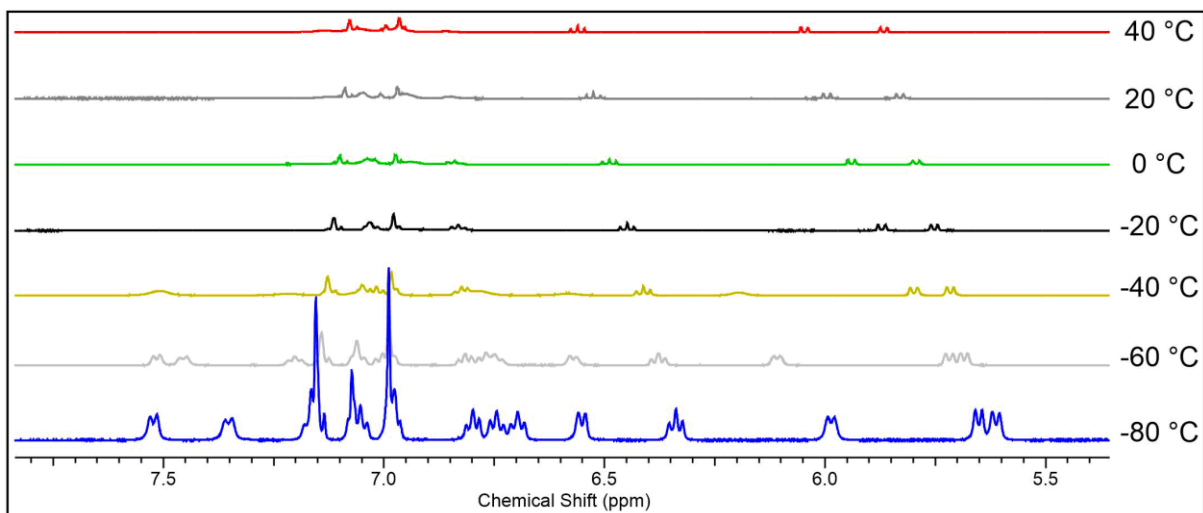


**Figure S21.** Detailed view of VT <sup>1</sup>H NMR spectrum (500 MHz) of [ONCH<sub>2</sub>]La(AIme<sub>3</sub>)<sub>2</sub>(AIme<sub>4</sub>) (**2<sup>La</sup>**) in toluene-*d*<sub>8</sub>. From -80 °C to 40 °C.

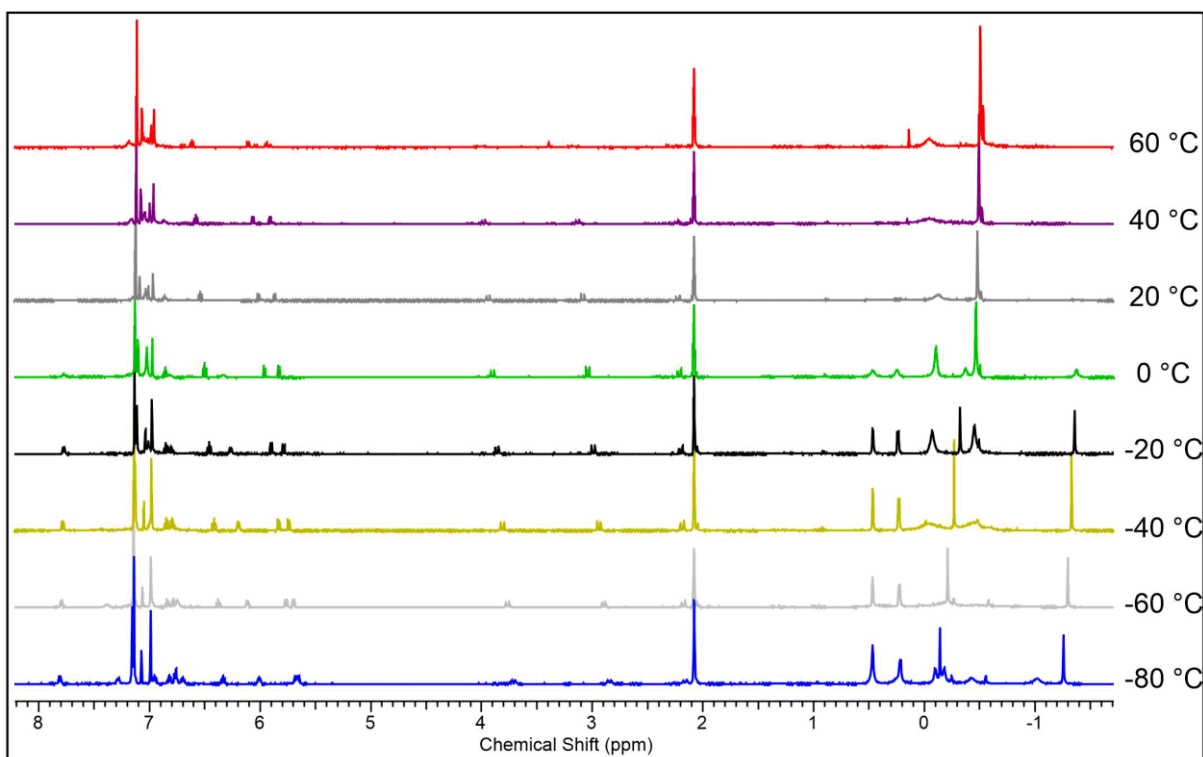


**Figure S22.** VT <sup>1</sup>H NMR spectrum (500 MHz) of [ONCH<sub>2</sub>]Y(AIme<sub>3</sub>)<sub>2</sub>(AIme<sub>4</sub>) (**2<sup>Y</sup>**) in toluene-*d*<sub>8</sub>. From -80 °C to 60 °C.

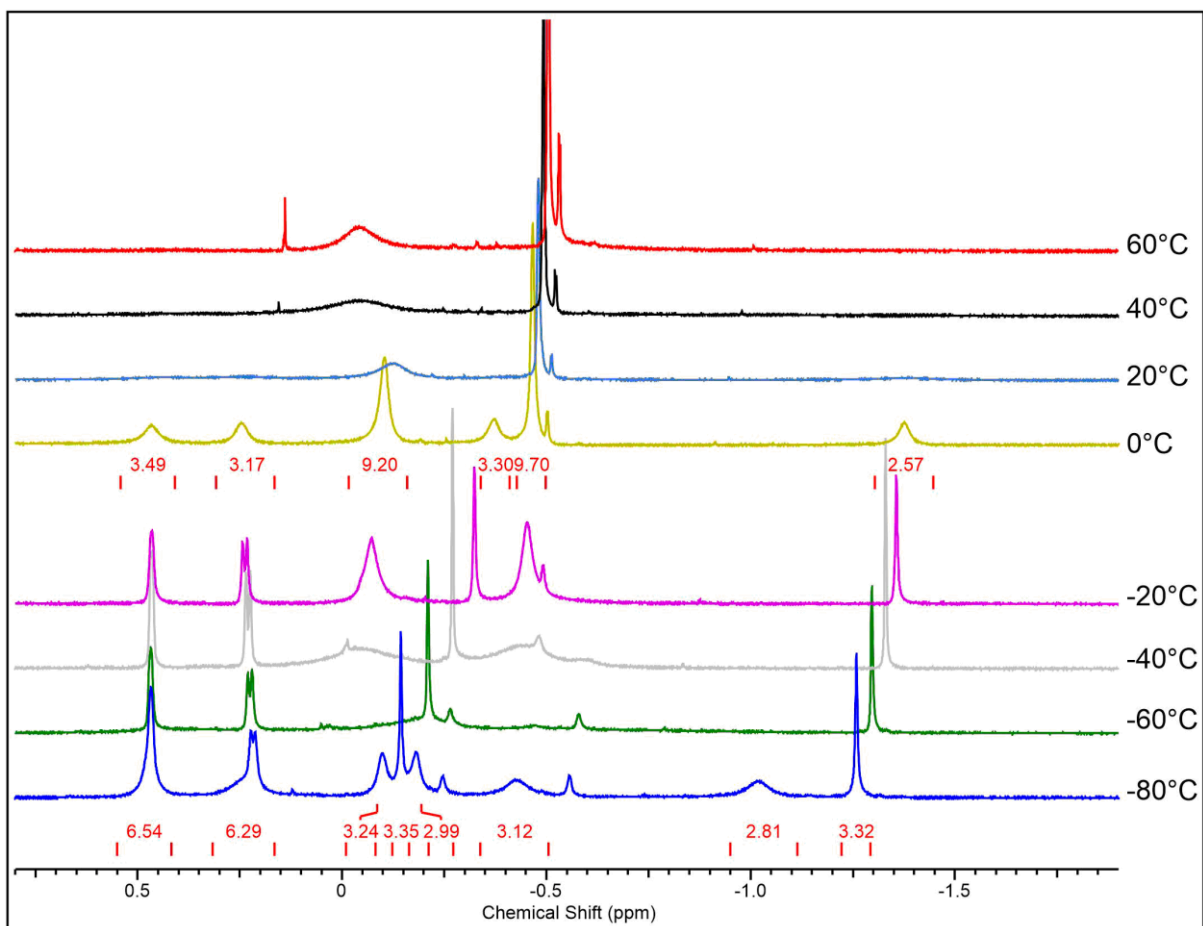


**Figure S23.** Detailed view of VT  $^1\text{H}$  NMR spectrum (500 MHz) of  $[\text{ONCH}_2]\text{Y}(\text{AlMe}_3)_2(\text{AlMe}_4)$  ( $2^{\text{Y}}$ ) in  $\text{toluene-}d_8$ . From  $-80^\circ\text{C}$  to  $60^\circ\text{C}$ .

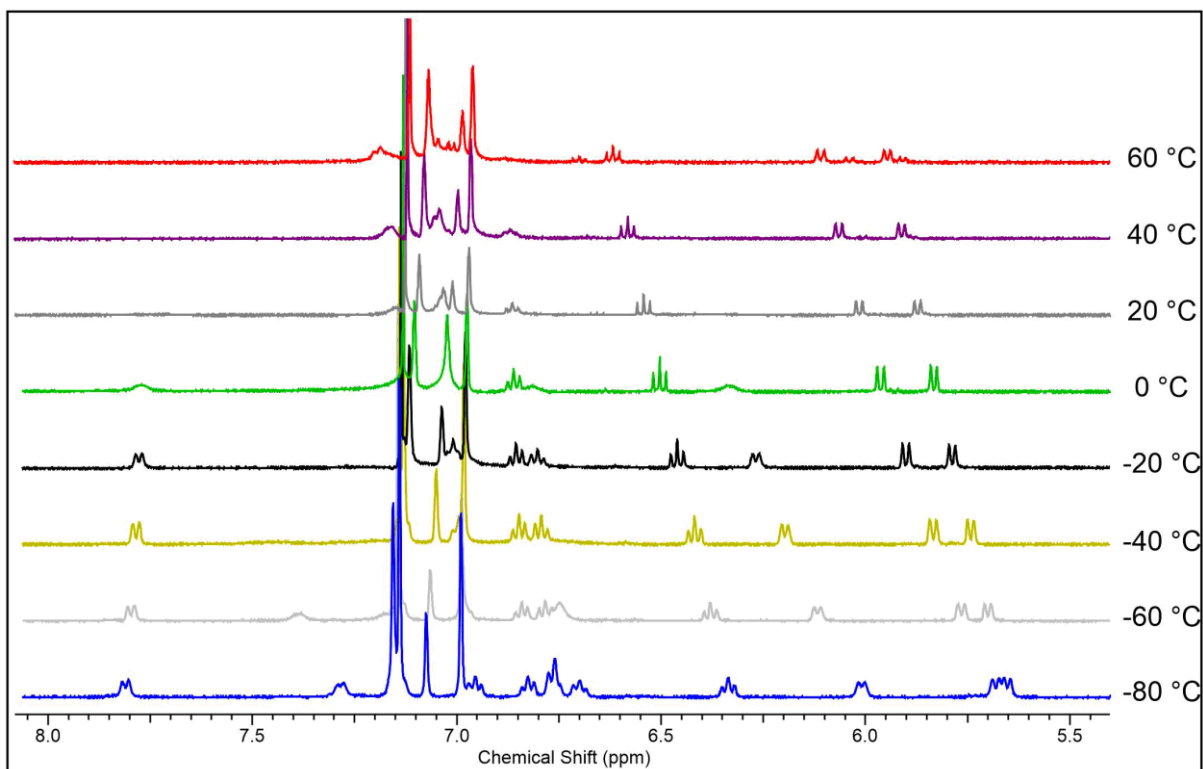


**Figure S24.** Detailed view of VT <sup>1</sup>H NMR spectrum (500 MHz) of [ONCH<sub>2</sub>]Y(AlMe<sub>3</sub>)<sub>2</sub>(AlMe<sub>4</sub>) (**2<sup>Y</sup>**) in toluene-*d*<sub>8</sub>. From -80 °C to 60 °C.

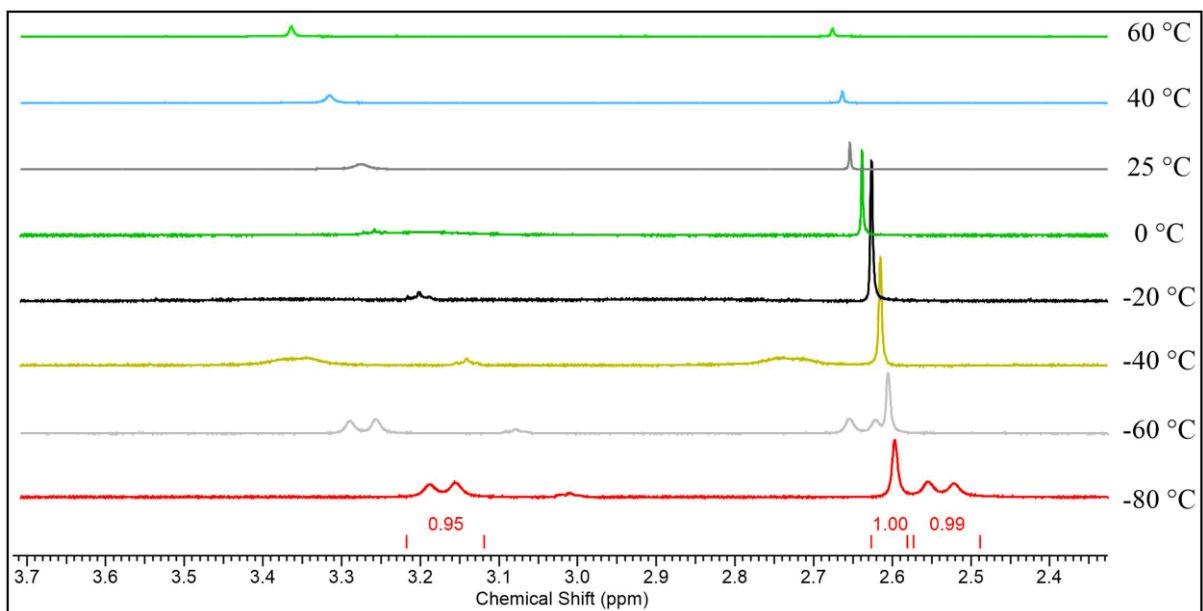


**Figure S25:** Detailed view of VT <sup>1</sup>H NMR spectrum (500 MHz) of [ONCH]Y(AlMe<sub>3</sub>)<sub>3</sub> (**3<sup>Y</sup>**) in toluene-*d*<sub>8</sub>. From -80 °C to 60 °C.

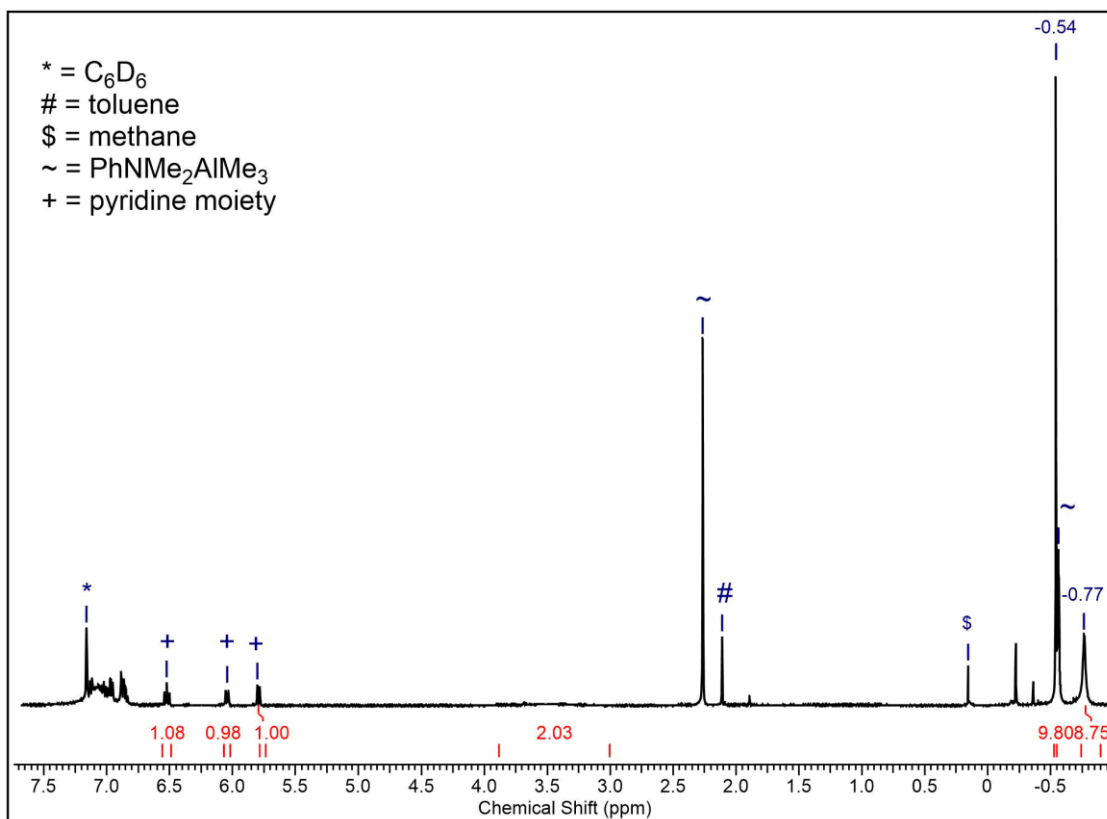


**Figure S26.** <sup>1</sup>H NMR spectrum (400 MHz) of the reaction of [ONCH<sub>2</sub>]La(AlMe<sub>3</sub>)<sub>2</sub>(AlMe<sub>4</sub>) (**2**<sup>L<sub>a</sub></sup>) with [Ph<sub>3</sub>C][B(C<sub>6</sub>F<sub>5</sub>)<sub>4</sub>] in C<sub>6</sub>D<sub>6</sub> at 26 °C.

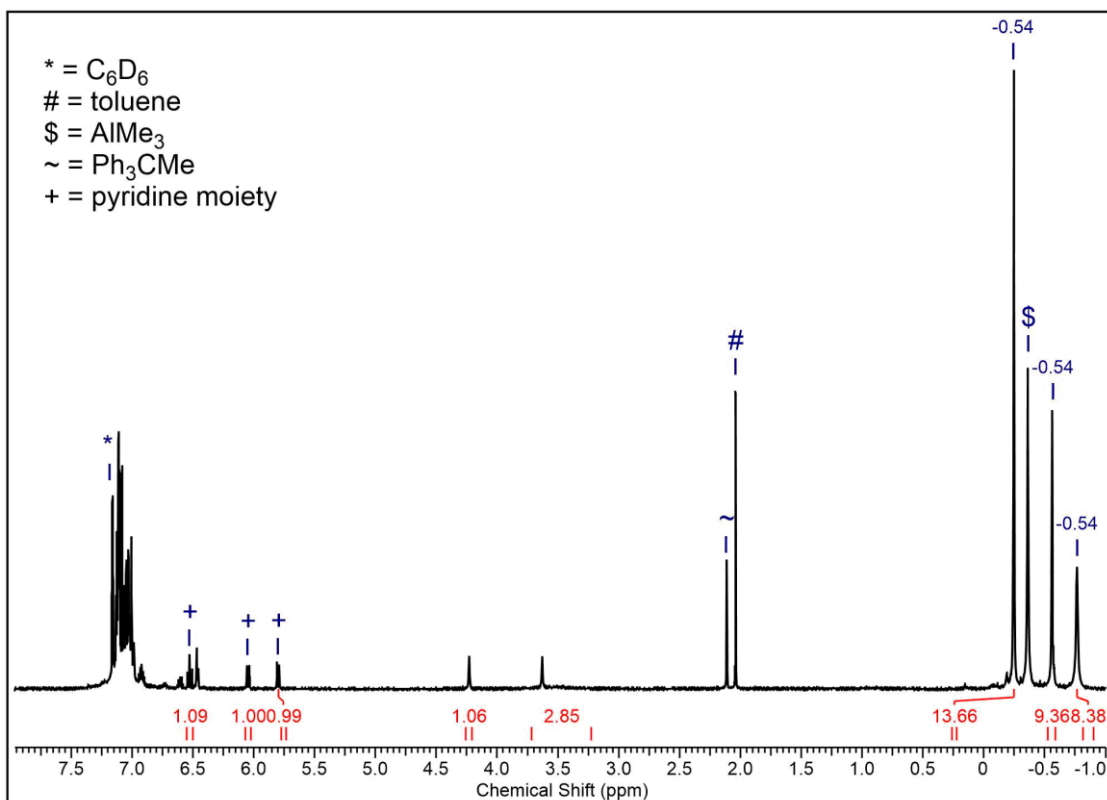


**Figure S 27.** <sup>1</sup>H NMR spectrum (400 MHz) of the reaction of [ONCH<sub>2</sub>]La(AlMe<sub>3</sub>)<sub>2</sub>(AlMe<sub>4</sub>) (**2**<sup>L<sub>a</sub></sup>) with [PhNMe<sub>2</sub>H][B(C<sub>6</sub>F<sub>5</sub>)<sub>4</sub>] in C<sub>6</sub>D<sub>6</sub> at 26 °C

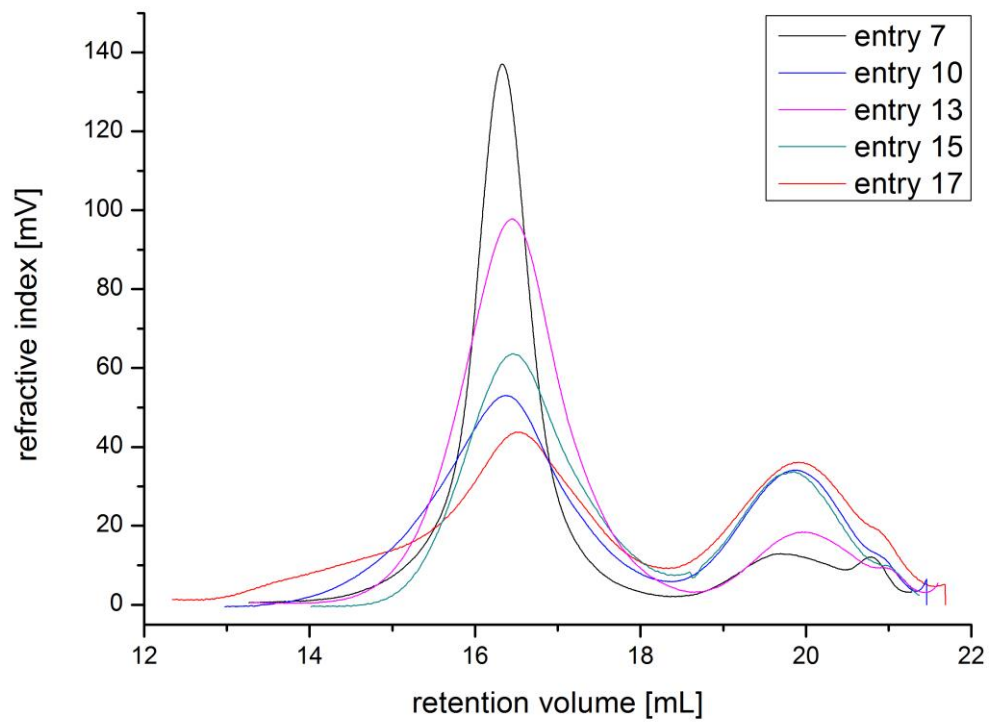


**Figure S28.** Refractive index (RI) of bimodal polyisoprenes (entry 7, 10, 13, 15, and 17).





# Appendix



## **Poster Presentations**

Structural Motifs of Fluorenyl and Indenyl Rare-Earth-Metal Half-Sandwich Complexes

Dominic Diether, Cäcilia Maichle-Mössmer, Reiner Anwander, XXVIII Tage Der Seltenen Erden Terrae Rarae, Tübingen (Germany), 4-6/10/2017.

## **Oral Presentations**

Fluorenyl and Indenyl Rare-Earth-Metal Half-Sandwich Complexes

Dominic Diether, Cäcilia Maichle-Mössmer, Reiner Anwander, XXVIII International Conference on Organometallic Chemistry (ICOMC), Florence (Italy), 15-20/7/2018.



# Curriculum Vitae

## Personal Details

Name: Dominic Diether  
Date of Birth: June 11, 1989  
Place of Birth: Reutlingen, Germany  
Nationality: German

## Education

Aug. 2015 – Sep. 2019	PhD studies Eberhard Karls Universität Tübingen, Germany Supervisor: Prof. Dr. R. Anwänder
Oct. 2018 – Nov. 2018	Research scientist at the University of Oxford, UK “Fabrication of Biodegradable Polymers” Supervisor: Prof. Dr. C. Williams
Feb. 2015 – Aug. 2015	Diploma thesis: “Yttrium Fluorenyl and Indenyl Tetramethylaluminates” Supervisor: Prof. Dr. R. Anwänder
Oct. 2008 – Aug. 2015	Study of chemistry (Diploma), Eberhard Karls Universität Tübingen, Germany
Sept. 2005 – Jul. 2008	Abitur at Technisches Gymnasium, Derendingen

